Dissertation zur Erlangung des Doktorgrades

der Fakultät für Chemie und Pharmazie

der Ludwig-Maximilians-Universität München

# Photopharmacology of Enzymatic Activity and Transmembrane Protein Function

Johannes Broichhagen

aus

Würzburg, Deutschland

2014

**Erklärung**

Diese Dissertation wurde im Sinne von § 7 der Promotionsordnung vom 28. November 2011 von Herrn Prof. Dr. Dirk Trauner betreut.

**Eidesstattliche Versicherung**

Diese Dissertation wurde eigenständig und ohne unerlaubte Hilfe erarbeitet.

München, den 4. September 2014

Johannes Broichhagen

Dissertation eingereicht am 5. September 2014

1. Gutachter: Prof. Dr. Dirk Trauner

2. Gutachterin: Prof. Dr. Anja Hoffmann-Röder

Mündliche Prüfung am 7. Oktober 2014

**Danksagung**

Über vier Jahre Promotionsstudium gibt es soviel zu erzählen und berichten, dass eine eigene Arbeit darüber angefertigt werden kann. Infolgedessen fasse ich mich kurz und halte die besonderen, individuellen Momente und Erlebnisse in persönlicher Erinnerung.

Mein Dank gilt in erster Linie meinem Doktorvater, Prof. Dr. Dirk Trauner, für die Möglichkeit unter seiner Leitung meine Doktorwürde zu erlangen. Weiterhin für das Bereitstellen von Verbrauchsmaterialien und vor allem für seine Erlaubnis und Unterstützung des Öfteren auch andere Forschungseinrichtungen über einen längeren Zeitraum besuchen zu dürfen. Letzteres hat mich wissenschaftlich und menschlich positiv entwickelt und in gleicher Weise geprägt.

Ich danke meiner Prüfungskommision, voran der Zweitgutachterin Prof. Dr. Anja Hoffmann-Röder, Prof Dr. Harald Janovjak, Prof. Dr. Franz Bracher, Prof. Dr. Klaus T. Wanner und Prof. Dr. Michael Groll.

Desweiteren gilt mein Dank meinen Kollaborationspartner, von denen ich sehr viel gelernt und profitiert habe: Prof. Dr. Harald Janovjak, Dr. David Hodson, Dr. Colette Dissous, Dr. Jerome Vicogne, Dr. Robert Torka und Innokentij Jurastow.

Für finanzielle und ideelle Unterstützung danke ich der Studienstiftung des deutschen Volkes für ein Promotionsstipendium (und namentlich meinem Vertrauensdozenten Prof. Dr. Wilhelm Heizmann), der European Molecular Biology Organization (EMBO) für ein “short-term visiting fellowship” und der

European Association for the Study of Diabetes (EASD) für ein “Albert-Renold Young Investigator Travel Fellowship”.

Ich danke allen (auch ehemaligen) Mitgliedern des Arbeitskreis Trauner sowie die Praktikanten die ich betreuen durfte für eine spannende und intensive Zeit. Den Mitarbeitern der LMU im analytischen Department (insbesondere Dr. Peter Mayer) und Dr. Anja Haniel in der Administration danke ich für ihre Hilfe.

Eine weiterer Dank geht an Henning, Veronika und Josephine: ihr seid super; weitermachen!

Shushu, vielen Dank für den immerwährenden Rückhalt, den ständigen Zuspruch und dein Verständnis. – ich habe dich wahnsinnig lieb!

Zuletzt danke ich meiner Familie für die uneingeschränkte Unterstützung. Jederzeit. Danke Gabriele, Helmut und Caroline.

“Complexity is the problem that any theory of biology has to solve.”

Richard Dawkins

**Parts of this work has been published in peer-reviewed journals**

1. Optical control of insulin release using a photoswitchable sulfonylurea, Broichhagen, J.; Schönberger, M.; Cork, S. C.; Frank, J. A.; Marchetti, P.; Bugliani, A. M.; Shapiro, A. M. J.; Trapp, S.; Rutter, G. A.; Hodson, D. J.; Trauner, D., *Nature Communications* **2014**, *5*:5116.

2. Optical Control of Acetylcholinesterase with a Tacrine Switch, Broichhagen, J.; Jurastow, I.; Iwan, K.; Kummer, W.; Trauner, D., *Angewandte Chemie International Edition* **2014**, *53*, 7657-7660; Optische Kontrolle der Acetylcholinesterase mit einem schaltbaren Tacrin, Broichhagen, J.; Jurastow, I.; Iwan, K.; Kummer, W.; Trauner, D., *Angewandte Chemie* **2014**, *126*, 7788-7792.

**Further publications in peer-reviewed journals include**

1. The *in vivo* chemistry of photochromic tethered ligands, Broichhagen, J.; Trauner, D., Current Opinion in Chemical Biology **2014**, *21*, 121-127.

2. Bilirubin in a New Light, Broichhagen, J.; Trauner, D., Angewandte Chemie International Edition 2013, 52, 13868-13870; Bilirubin in einem neuen Licht, Broichhagen, J.; Trauner, D., Angewandte Chemie **2013**, *125*, 14112-14114.

## Forschungszusammenfassung

Die optische Kontrolle biologischer Funktionen ist mittlerweile gut erforscht und dokumentiert. Zur Untersuchung von biologischen Zusammenhängen kann somit Licht als Inputsignal verwendet werden, das eine hohe räumliche und zeitliche Auflösung besitzt und desweiteren nicht invasiv ist.

Im Jahre 2004 zeigten Trauner und Kramer die Möglichkeit auf mit Hilfe von Azobenzol-basierten quartären Ammoniumsalzen Kaliumkanäle unter Bestrahlung mit Licht zu öffnen und zu schließen. Seitdem ist dieser optochemisch-genetische Ansatz auf weitere Proteine ausgeweitet worden, vor allem auf Ionenkanäle und G-protein-gekoppelte Rezeptoren. In dieser Arbeit wurde das optochemisch-genetische Prinzip weiter ausgebaut.

Eine weitere grosse Klasse von Proteinen, die Enzyme, wurden zum Ziel optochemischer Kontrolle erklärt. Außerdem wurde der ATP-gesteuerte Kaliumkanal Kir6.2/SUR1 mit Hilfe von Photopharmazeutika reguliert. Das Konzept der "Azologisierung" von bekannten Medikamenten oder "research tools" wurde angewandt auf eine Vielzahl von weiteren Molekülen, beispielweise die Acetylcholinrezeptoren.

Kapitel 1-3 führt thematisch in die Arbeit ein mit je einem Abstract auf englisch und deutsch sowie einer ausführlichen Einleitung. Kapitel 4 führt Mitwirkende und Kollaborationspartner auf, die an den verschiedenen Projekten beteiligt waren.

Kapitel 5 beschreibt den Ansatz einer lichtgesteuerten Rezeptor-Tyrosin-Kinase (RTK). Ausgehend von Proteinen aus Insekten, die unter Aktivierung mit Aminosäuren Tyrosin-Kinase-Aktivität zeigen, wurden viele Proteinchimären kloniert. Eine Chimäre, zusammengesetzt aus der Ligandenbindungsdomäne des metabotropen Glutamatrezptors und des Insulinrezeptors zeigt Tyrosinphosphorylierung nach der Stimulation mit Glutamat (Abbildung 1). Dies

ist das erste Mal, dass RTK-Aktivität mit einem Neurotransmitter ausgelöst werden konnte.

Weitere Enzyme können mit Licht kontrolliert warden: die Acetylcholinesterase mit einem löslichen Azobenzol-Liganden (**AzoTHA**) (Kapitel 6) und das Isozym II der Carboanhydrase mit einem kovalent and das Enzym verknüpftem lichtschaltbarem Arylsulfonamid (**SA-2** an verschiedenen Carboanhydrase Mutanten) (Kapitel 7). In beiden Fällen war das reversible Schalten von Enzymaktivität über mehrere Zyklen möglich.

Ein weiteres "Target" war der ATP-gesteuerte Kaliumkanal Kir6.2/SUR1, der in der Bauspeicheldrüse im Zusammenspiel mit anderen Proteinen für die Insulinausschüttung verantwortlich ist. Mit einem azobenzolbasierten Sulfonylharnstoff, **JB253**, konnte die Depolarisation von Beta-Zellen optisch manipuliert werden. Das Resultat ist eine lichtabhängige Insulinsekretion, die auch Anwendung in der medizinischen Forschung finden kann. Diese Erfindung wird momentan einer Patentprüfung unterzogen.

Die Verwendung von kovalent verküpften Photopharmazeutika in einem genetisch enkodierten System wird in Kapitel 9 beschrieben. So können mit sogenannten SNAP-tags Fusionsproteine erzeugt werden, die eine saubere und fast quantitative Reaktion mit dem Photoschalter ermöglichte. Somit konnten metabotrope Glutamatrezeptoren reversibel aktiviert werden, deren Aktivität elektrophysiologisch ausgelesen wurde.

Weitere Photopharmazeutika werden beschrieben, die beispielsweise selektiv die nicotinischen und muscarinischen Acetylcholinrezeptoren ansprechen. Diese spielen eine wichtige Rolle im cholinergen System (in verschiedensten Geweben von der Trachea bis hin zum Gehirn, Kapitel 10). Synthesebeispiele für die weitere Derivatisierungen von Azobenzolen werden aufgeführt (Kapitel 11)

Zusammenfassend wird das Design und die Synthese von azobenzolbasierten und damit lichtabhängigen Pharmazeutika aufgezeigt. Die biologische Evalution reicht von *in vitro* und *in cellulo* Studien bis hin zu explantierten Organen (bspw. Luftröhre und Bauchspeicheldrüse). Klinische Studien für die Anwendung in der Humanmedizin erwartet weitere Tests.

*Table of Contents*

# 1 Abstract

The control of biological function with light is a rapidly growing research frontier in today's biochemical and medicinal research. The advantage to precisely control protein function and their interactions selectively in a temporal and spatial manner gains deep insight into the complicated orchestra of cell (network) and animal behavior. The effort to implement photoresponsive molecules to achieve photocontrol over every endogenous protein is called "optome" and is being pursued by the Trauner group and others. Ultimately, there should be enough tools in hand for researchers all over the world to address biological questions in every field of expertise. Accordingly, the complexity of cell communication can be trivialized to a level that makes it more clear-cut to understand.

In this work, the photocontrol over a variety of different targets is presented, starting with the conceptual idea, over the rational design of photopharmaceuticals (including their synthesis and characterization) ultimately leading to their application. Particular targets described herein are enzymes, such as human carbonic anhydrase II and human acetylcholinesterase. Furthermore, all families of transmembrane receptors, such as ion channels, G-protein coupled receptors and receptor-linked enzymes, are in the scope of this work. More precisely, the inward-rectifying ATP-gated potassium channel 6.2 and nicotinic acetylcholine receptors as examples for ion channels. In addition, the muscarinic acetylcholine receptor and the $GABA_B$ receptor are described as targets for G-protein coupled receptors. In the case of receptor-linked enzymes, receptor tyrosine kinases were investigated with the aim to achieve photocontrol.

The logic of photopharmacology is demonstrated in vitro and in vivo, proving the global applicability of this concept. For instance, photocontrol over acetylcholinesterase is achieved in explanted mouse trachea: the muscle relaxation kinetics can be controlled with light. Even more, optical control over the ATP-gated potassium channel Kir6.2/SUR1 was achieved, which is mainly

responsible for insulin release from the pancreas. Consequently, insulin secretion was dependent on light. It can be envisioned that blood glucose levels can therefore be controlled with, having an impact in translational medicine. For instance, this might contribute to the treatment of patients suffering from type 2 diabetes mellitus.

## 2 *Abstract (deutsch)*

Kontrolle über biologische Funktion mit Licht ist ein schnell wachsendes Forschungsfeld in der heutigen biochemischen und medizinischen Forschung. Proteinfunktion und –interaktion präzise in zeitlicher und räumlicher Auflösung zu kontrollieren hat den Vorteil tiefer Einsicht in das komplexe Orchester von Zell (und deren ausgebildeten Netzwerken) und Tierverhalten zu gewähren.

Die Methode photoresponsive Moleküle zu implementieren um Photokontrolle über jedes endogene Protein zu erhalten wird "Optom" genannt und wird unter anderem von der Trauner Forschungsgruppe verfolgt. Es sollten in der Zukunft genügend Methoden ("Tools") für Wissenschaftler auf der ganzen Welt zur Verfügung stehen, um biologische Fragestellungen im jeweiligen Feld der Expertise zu adressieren, und schließlich Proteininteraktionen und Antworten mit den zuvor beschriebenen Vorteilen untersuchen zu können. Demnach sollte komplexes Zellverhalten vereinfacht werden können, sodass dieses leichter zu verstehen ist.

In dieser Arbeit wird die Photokontrolle über mehrere verschiedene biologische "Targets" präsentiert. Beginnend mit der konzeptionellen Idee der Photopharmakologie über das rationale Design von Photopharmazeutika bis hin zu deren Synthese, Charakterisierung und deren Anwendung. Die beschriebenen "Targets" reichen von Enzymen, wie die Acetylcholinesterase und humane Carboanhydrase hin zu Transmembranproteinen, wie etwa Ionenkanäle, G-Protein gekoppelte Rezeptoren und rezeptorgelinkten Enzymen. Die Logik und Funktionsweise der Photopharmakologie wurde sowohl in vitro als auch in vivo angewandt und demonstriert die globale Applizierbarkeit dieses Konzepts. Als Beispiel wurde die Acetylcholinesterase in explantierten Mausluftröhren kontrolliert: die Muskelrelaxation kann hierbei mit Licht gesteuert werden. Weiterhin wurde die optische Kontrolle über den ATP-gesteuerten Kaliumkanal Kir6.2/SUR1 erreicht, einem Kanal der hauptsächlich für die Insulinausschüttung aus der Bauchspeicheldrüse verantwortlich ist. Demnach war die Insulinsekretion aus Langerhansschen Inseln lichtabhängig. Mit

lichtgesteuerter Hormonesekretion, das der oszillativen, physiologischen Wirkung entspricht kann Photopharmakologie zum Beispiel in der Behandlung von Diabetes mellitus Typ 2 eingesetzt werden und zur Behandlung dieser Krankheit beitragen.

# *3 Introduction to Photopharmacology*

The ultimate goal to understand complex biological function and behaviour is tackled by manipulating certain biomolecules selectively and reversibly in a temporal and spatial manner.[1] Therefore, a biological target can be turned "on" and "off" with high precision in all four dimensions, which gives insight into its role together with other biomolecules and responses.

"Photopharmacology" is the control over biological function with light utilizing drug-like small molecules.[2,3] Together with "Optogenetics",[4] which describes the introduction of light-sensitive proteins on a genetic level, it has become a major frontier in scientific research.[3,5,6]

Even more, biological behavior and/or responses often show oscillative characteristics.[7] The cardiac rhythm, day/night cycles, the release of hormones or the rhythmic activity of electric fluctuations in the brain, for instance, are tightly controlled to fulfill their physiological purpose in health. The malfunction of these periodically reoccurring physiological events can result in pathologies, such as cardiac dysrhythmia, insomnia, metabolic or neural diseases.

When treating a patient with modern drugs, they are applied globally and at a given time point. As good as modern pharmacology has emerged to be there are still disadvantages that occur in the treatment of diseases. For instance, drugs are utilizing their pharmacological power to off-targets and get cleared over time; the consequence being a decreasing efficacy after a high concentration in the beginning time point.

This issue can be overcome if drugs can be controlled from the outside with an input signal. Therefore, they can become active or inactive in a repeated manner while only acting in the tissues or organs where they are required. In order to trigger this, light is a beneficial input signal. It bears the exquisite characteristic of being non-invasive, non-toxic and repeatedly applicable with high temporal

precision. Consequently, off-target effects in other tissues can be excluded as spatial control can be achieved in the same manner as time-dependent actions.

In the course of basic research,[8-13] as well as treating and healing diseases, the photopharmacological approach using photopharmaceuticals can provide a major leap forward.[14] Even more, non-invasiveness and non-phototoxicity can be achieved with red-shifted photopharmaceuticals[15] or two-photon[16] photopharmacology, which helps deep tissue penetration and has been exemplified recently on glutamate receptors.

With the power of synthetic chemists, who can design and synthesize photopharmaceuticals based on known and established drugs,[17] biologists and medical doctors can benefit from this idea to ultimately understand and deduce complex biological networks. With light-delivery systems that are beyond the proof-of-principle state for animal (including human) applications,[18,19] a sufficient and precise delivery of a drug can be envisioned to a specific region on peak-demand.

# *4 Project Affiliation Disclosure*

"*Da wird ein uebersummatives System nach den Teilen gefragt. Das ist so absurd, als ob man ein einzelnes Pixel auf einem Bild nach seinem Beitrag zu dem Gemalten befragen wuerde. Das Gemalte entsteht erst in der Summe aller Teile; und ist dann noch dazu mehr als die Summe der Teile.*"

Peter Kruse

With this quote from Prof. Dr. Peter Kruse, I want to disclaim and enclose that all projects described herein have been an intellectual and practical process involving more people than myself. More importantly, the work was considerably influenced by a lot of people and is essentially more than the sum of everyone's sole opinion and input. Therefore, I mainly write about findings, results and discussions *we* made. In particular, I list the people involved in every project in this chapter and their specific contributions.

- Chapter 5: Prof. Dr. Harald Janovjak (Supervision), Dr. Colette Dissous (Supervision), Dr. Jerome Vicogne (Supervision), Dr. Robert Torka (Supervision), Prof. Dr. Axel Ullrich (Supervision).
- Chapter 6: Prof. Dr. Wolfgang Kummer (Supervision), Innokentij Jurastow (*ex vivo* mouse tracheal tensometry), Katharina Iwan (Synthesis).
- Chapter 7: Dr. Kateri H. DuBay (Calculations), Prof. Dr. Michael Groll (Protein X-ray diffractometry), Dr. Laura Osorio (Synthesis), Leander Runtsch (Synthesis), Katharina Iwan (Synthesis), Michael Gattner (Protein Mass Spectrometry), Dr. David Eisen (Protein Mass Spectrometry), Prof. Dr. Thomas Carell (Protein Mass Spectrometry and Supervision).
- Chapter 8: Dr. David J. Hodson (Supervision), Prof. Dr. Guy A. Rutter (Supervision), James Frank (Electrophysiology), Dr. Simon C. Cork

(Electrophysiology), Dr. Stefan Trapp (Electrophysiology), Dr. Matthias Schönberger (Electrophysiology), Silke Duensing-Kropp ([3H]-Assay), Dr. Georg Höfner ([3H]-Assay), Prof. Dr. Klaus T. Wanner ([3H]-Assay).

- Chapter 9: Simon Nadal (Synthesis), Kevin R. Sokol (Synthesis), Philipp Leippe (Synthesis), Arunas Damijonaitis (Electrophysiology).
- Chapter 10: Dr. Matthias Schönberger (Electrophysiology), Arunas Damijonaitis (Electrophysiology), Jonas Hertl (Synthesis), Prof. Dr. Philipp Sasse (*ex vivo* heart physiology).
- Chapter 11: Kevin R. Sokol (Synthesis).

I am again grateful to have met and learned from these people, ultimately enabling me to write this thesis. Nevertheless, this dissertation is my own work and I alone am fully responsible for any mistakes or errors.

# *5 Receptor Tyrosine Kinases*

## 5.1 Introduction

How do cells communicate? How do they sense and process signals and information from the environment to produce directed responses? Where do they sense and direct their response? When and for how long do they respond to stimuli? These are the central questions that need to be answered in order to gain an understanding of the complex sequence of events connecting a stimulus from the 'outside world' with its effect at the end of signaling pathways. First messengers, such as hormones, growth factors, neurotransmitters or cytokines bind to receptors on the cell surface and trigger a second messenger response in the cytosol, often *via* a tightly controlled cascade.[20] To examine cellular signaling, various approaches have been explored.[21] For example, molecular components of the pathways can be withheld through genetic manipulation while monitoring different cellular responses. Alternatively, proteins and enzymes can be engineered through replacement or deletion of one or more amino acids, with the goal of understanding their basic activity. Furthermore, a large body of data obtained from pharmacological studies complements these genetic techniques. However, these pharmacological approaches are intrinsically rather slow, because they are diffusion limited; and non-specific, since they affect entire organisms or large populations of cells at the same time. While we now have a deep understanding of individual components and basic communication steps, we still require novel technologies that allow us to arrange them temporally and spatially to gain an understanding of the dynamics of signaling pathways.

Dynamic control of biological functions can be achieved using synthetic photoswitches, which have the advantages that they can be switched on and off with a very fast response time (in the millisecond range) and with high spatial precision (in the micrometer range).[2,3] In this manner, signals can be generated locally (by directing light) and at different levels (by controlling its intensity). All

these properties individually or combined provide a new, variable and powerful approach for the investigation of signaling. Photosensitive compounds that contain a reversibly photoswitchable moiety were developed, and together with the hijacking of nature's photoreceptors formed the start of the optogenetic era (*vide supra*).[4] Two major classes of cell surface receptors, namely ionotropic and metabotropic receptors were successfully controlled using these light-dependent ligands.[6] However, the third class of cell surface receptors, receptor-linked enzymes (RLEs) – which mediate essential information for cell regulation and survival – have not yet been photocontrolled.

A wide variety of so-called venus-flytrap receptors, classified by their ligands or their structural assembly, are known.[22] The nomenclature of venus-flytrap (VFT) receptors is an allegory to the animal eating plant *Dionaea muscipula* (Figure 1a). The receptor's ligand binding domain (LBD) consists of two lobes that bind the ligand between them (Figure 1b) and resemble the plant when it has captured its prey.

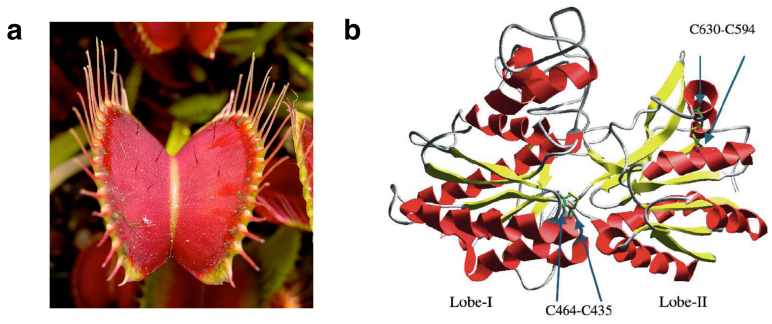


**Figure 1: The VFT receptor. a)** The venus-flytrap plant *Dionaea muscipula*; photo by Noah Elhardt, licensed under the Creative Commons Attribution-Share Alike 2.5 Generic; **b)** modeled LBD in a VFT receptor, taken and modified from Vicogne *et al.*[23]

The VFT domain is a structural motif found in receptors among all animals. VFT receptors sense first messengers, such as glutamate, γ-amino butyric acid (GABA) and cyclic peptides.[24] They have been utilized in the light-control of ionotropic glutamate receptors[25] (though in these cases they are named

clamshell receptors) which control ion flow across a membrane and in the light-control of metabotropic glutamate receptors[26], which control G-protein activity as described above. Cyclic peptides, such as the atrial natriuretic peptide (ANP) are agonists for receptor-linked guanylate cyclases (RGCs), which cyclize guanosine triphosphate (GTP) to cyclic guanosine monophosphate (cGMP).[27] Notably, the VFT domain was also found in receptor tyrosine kinases (RTKs) from invertebrates, particularly insects.[28] Interestingly, the extracellular domain of this particular RTK is responsive to arginine and thus resembles the metabotropic VFT receptors that have been photocontrolled recently with glutamate-derived PCLs and PTLs. Since the cytosolic tyrosine kinase (TK) domain resembles that of the insulin receptor[23], it is capable of activating kinase cellular signaling pathways.[28] These proteins are interesting targets for generating light-controlled kinases.

Receptor tyrosine kinases (RTKs) belong to the family of receptor-linked enzymes (RLE) and sense growth factors, cytokines and hormones.[20] RTKs usually consist of a receptor domain on the extracellular side (the ligand binding domain, LBD) that is connected by a single-pass transmembrane (TM) domain to a tyrosine kinase (TK) domain (Figure 2a). When activated by a first-messenger, the protein oligomerizes and triggers cytosolic enzyme activity, initially autophosphorylating itself (Figure 2b) followed by further signaling. One important class of RTKs comprises of epidermal growth factor receptors (EGFR/Erb1 and ErbB2-4), which play key roles in cell proliferation, differentiation and cancer. Here they will serve to introduce functional principles shared by many RTKs.[29] Among others, ErbB receptors utilize the Ras/Erk signaling pathway (Figure 2f).[20] In this pathway, adaptor proteins like Shc (SH2-domain-containing transforming protein C) and Grb2 (growth factor receptor-bound protein 2) assemble signaling complexes on activated RTKs. Binding of Sos1 (son of sevenless 1) to Grb2 translocates Sos1 to the membrane and activates a GTPase and kinase cascade consisting of Ras, Raf, MEK (*i.e.* the mitogen-activated protein kinase, MAPK pathway) and Erk (extracellular signal-regulated kinase). Active Erk is then translocated to the nucleus and stimulates gene transcription (Figure 2g). Signals may also be transmitted in parallel

pathways, *e.g. via* Rac/Cdc42 or phospholipase C. Negative feedback loops control the amplitude and duration of the signal. Erk activates antagonists (such as Sprty) and prevents Sos1 from activating Ras. Activated receptors are internalized into early endosomes (Figure 2c) followed either by recycling to the membrane (Figure 2d) or destruction in lysosomes (Figure 2e). Internalized receptors trigger signaling pathways distinct from those at the cell surface. Importantly, a dynamic and complex network ensures fidelity of both RTK signaling and internalization.[30]

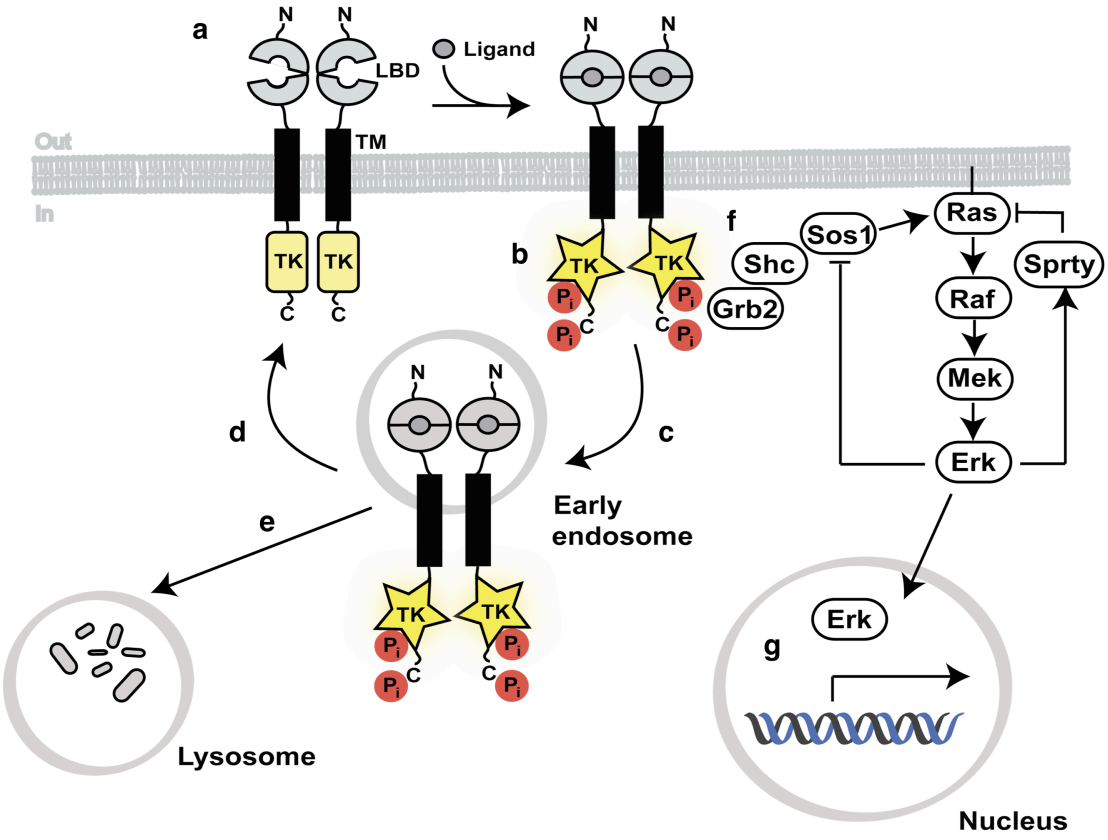


**Figure 2: Ras/Erk mitogen activated protein kinase (MAPK) pathway. a)** Receptor tyrosine kinases are single transmembrane bound proteins that dimerize and cross- or autophosophorylate (**b**) themselves once activated. The receptor is then internalized (**c**) and either reincorporated in the membrane once dephosphorylated (**d**) or degraded in the lysosome (**e**). The phosphorylation of the C-terminal domain leads to the assembly of adapter proteins (**f**), which triggers a signaling pathway ultimately influencing the transcriptional level (**g**). N: N-terminus, LBD: ligand-binding domain, TM: transmembrane domain, TK: tyrosine kinase, C: C-terminus.

RTK mutations usually affect its activity, abundance, distribution or regulation, which in turn are linked with several severe diseases, such as diabetes, inflammation and cancer.[31] Furthermore, it is known that approximately 30% of human tumors exhibit a hyperactive Ras-mutation, which is activated by RTKs utilizing the Ras/Erk pathway guiding cell proliferation and growth.[32]

Cancer is one of the major diseases of the civilized world and has a great impact on society in terms of suffering and socio-economics.[33] Much effort has been expended in understanding this disease in its biomedical detail; however, as of today it is not described fully. Drugs targeting RTKs have been designed to alter RTK activity by allosteric or oligomerization inhibition, but a switchable drug that can be utilized to repeatedly probe RTK activation and investigate this kind of stimulation is not yet available.

## 5.2 Results and Discussion

The first described receptor tyrosine kinases that bear venus-flytrap domains (*i.e.* venus kinase receptors, VKRs) from the nematode *Schistosoma mansoni* (SmVKR1 and SmVKR2) are not known to express in mammalian cells.[23] Therefore, the VKR from the honeybee *Apis mellifera* (AmVKR)[28] was chosen to be the first investigated fundamentally with a complete characterization. This choice was based on the little knowledge to date about AmVKR and its behaviour in mammalian cells aside from the observation that AmVKR can be phosphorylated by L-arginine (Arg). The initial idea was to show that AmVKR, once stimulated, is able to initiate signaling cascades in mammalian cell lines, because its intracellular tyrosine kinase domain is homologous to the human insulin receptor (hIR). Furthermore, there was some discrepancy in the literature concerning the amino acid sequence of AmVKR: while full sequencing (for sequencing primer see Table 1) determined amino acid 1050 as a glycine residue ($^{1050}$G), the deposited structure in uniprot.org depicts an arginine residue ($^{1050}$R) at this particular position. When aligned with AmVKR, the hIR has a glycine at this position, and consulting X-ray structures of the tyrosine kinase (TK) domain reveals the importance of this position, as it is at the turn of a loop, where a replacement of glycine could have a tremendous impact on folding and therefore activity.[34] Consequently, AmVKR activity was tested for both, a wild-type glycine (wt, $^{1050}$G) and an arginine ($^{1050}$R) construct.

Given the limited knowledge about this particular enzyme, proof is necessary that it is able to exhibit activity in mammalian cells. More possibilities should be taken into consideration than solely focusing on known hIR activating pathways, such as one of the mitogen-activated protein kinase (MAPK) pathways, Ras/Erk (Figure 2). On one hand, crosstalk has to be ruled out between possible pathways, gaining insight into primary activated pathways – on the other hand other possible pathways that could have been overlooked due to the exotic nature of this particular receptor should not be missed.

For this purpose, a novel *L*-arginine (Arg)-free media was prepared, to starve the cells in order to get a good signal to noise ratio and even more importantly to avoid densensitization and/or internalization during expression and starvation. This was possible by using SILAC medium (PAA, #E15-086), supplemented with *L*-glutamine, *L*-lysine, antibiotics (penicillin and streptomycin) and 0.5% of dialyzed (*i.e.* amino acid free) fetal bovine serum (FBS) (PAA, #A11-507). The next step was to test cell survival in this medium, as there was no precedence found in the literature for the cultivation of HEK293 cells without Arg. Indeed, the cells survived in this medium up to 24 hours without any visually perceivable changes in their morphology. Supplying the medium with an *L*-arginine-*O*-ethyl ester, in order to supply Arg for the cell after cytosolic ester hydrolysis while not activating AmVKR, caused cell death over a couple of hours, maybe due to too high generation of ethanol *in vivo*. Finally, expression of AmVKR on the cell surface was validated by primary HA epitope and secondary mouse antibody staining (Alexa488) imaged by confocal microscopy (Figure 3a). Live cells were nuclei stained with 4',6-diamidino-2-phenylindole (DAPI) and dead cells with propidium iodide (PI) and both also imaged by confocal microscopy. An overlay of images aquired with all three filters shows the distribution of AmVKR on the cell surface, while cells were alive and not apoptotic (according to no PI stained cells observed) (Figure 3b).

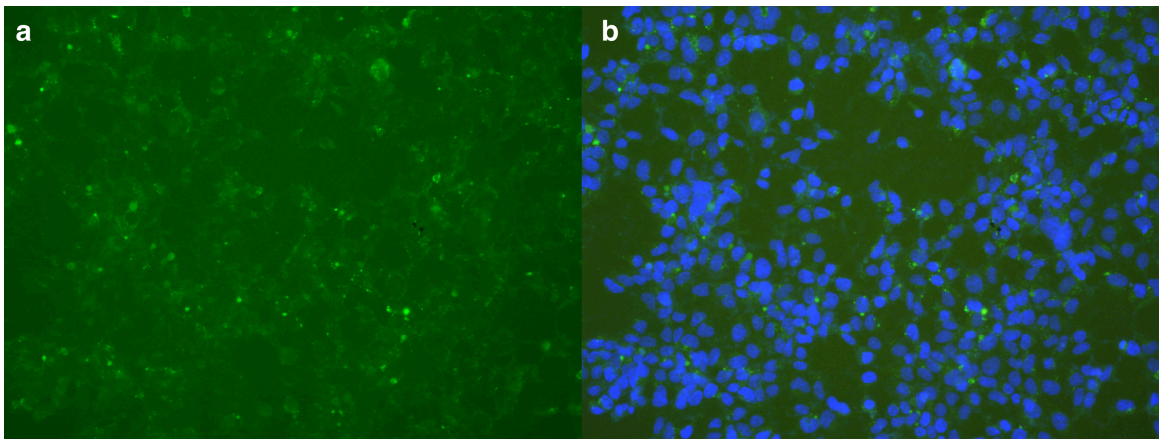


**Figure 3: Heterologous expression of AmVKR in HEK293t cells. a)** anti-HA-epitope and secondary Alexa488 staining imaged by confocal microscopy proves

AmVKR expression. **b)** Overlay of **a)** with DAPI and PI staining to prove cell survival.

Given that AmVKR expresses in HEK293 cells and that these cells can be grown in the absence of its proposed activating ligand *L*-arginine, first testing by Western Blotting (WB) and ELISA was performed for both wt $^{1050}$G and $^{1050}$R, while a mutant (YY$^{1043}$FF) that cannot be phosphorylated served as a control for expression and background activity (for primers used to obtain mutants see Table 2). Results from immunoblotting with p-Tyr antibodies clearly showed expression of all three constructs, with a more pronounced band of the wt-AmVKR construct (Figure 4a). ELISA confirmed this observation, after blocking with either fetal calf serum (FCS) or probumin, as wt-AmVKR resulted in a higher fluorescence under both blocking conditions (Figure 4b). Consequently, wt-AmVKR ($^{1050}$G) was the protein to be tested further, rendering the $^{1050}$R mutant irrelevant for ongoing studies.

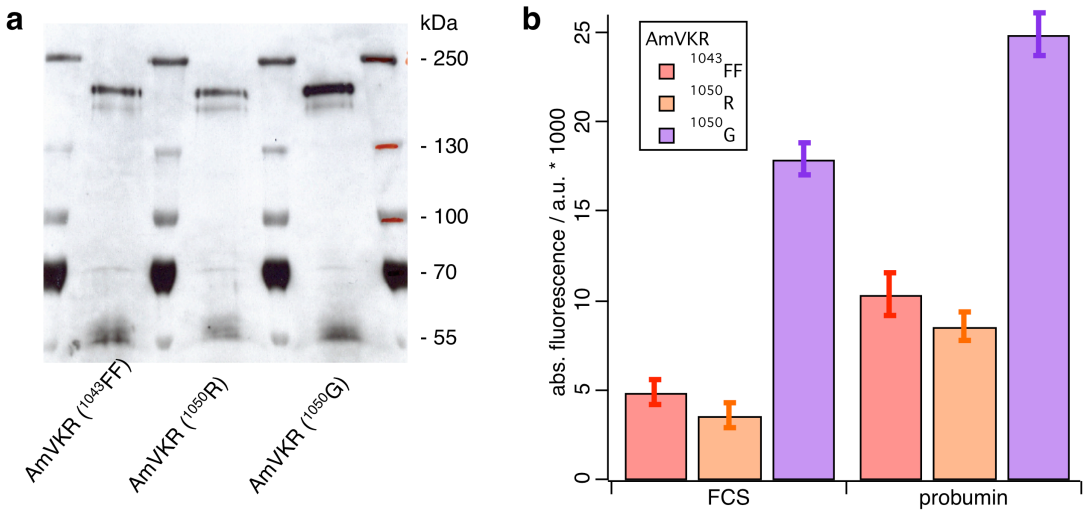


**Figure 4: Phosphorylation of AmVKR confirmed by WB and ELISA. a)** WB of three AmVKRs (dead kinase $^{1043}$FF that cannot be phosphorylated, and both $^{1050}$R/G polymorphs) after stimulation with arginine shows thicker band of $^{1050}$G-AmVKR. **b)** ELISA with the plasmids used in **a)** quantifies phosphorylation levels of AmVKRs. FCS (left) and probumin (right) have been screened as blocking solutions and gave similar results.

With the upstream activation observed, the next step is to further elucidate the next steps in cellular signaling. In order to ultimately gain a more detailed understanding of which signaling pathway is triggered, AmVKR in adherent HEK293t cells was tested with a Cignal™ 45-pathway kit (SA Bioscience, #CCA-901L). With this fast and high-throughput screen based on a DualGlo luciferase system, it is possible to screen 45 main cell signaling pathways, while the normalization of cell number is achieved intrinsically by measuring two different luciferases (firefly and renilla) (see Experimental for detailed pathway description). The bioluminescent photons emitted are counted and plotted as relative luciferase units (RLU) in arbitrary units (a.u.). However, when wt-AmVKR was transfected and stimulated as before, no pathway was triggered according to luciferase expression and subsequent bioluminescence readout (Figure 5). Because the expression of a large plasmid can cause cell stress and therefore activate certain signaling pathways, *i.e.* transcription factors, a dead kinase mutant (K909A) was chosen to obtain a plausible normalization as control. This mutation abolishes ATP binding and therefore cannot cross- or autophophorylate the intracellular C-terminal domain. With respect to the dead kinase mutant, AmVKR does not trigger a signaling pathway observable with this kit when stimulated with 400 µM *L*-arginine. Note that positive and negative control give the same magnitude of signals as expected when divided by a second measurement of the same kind.

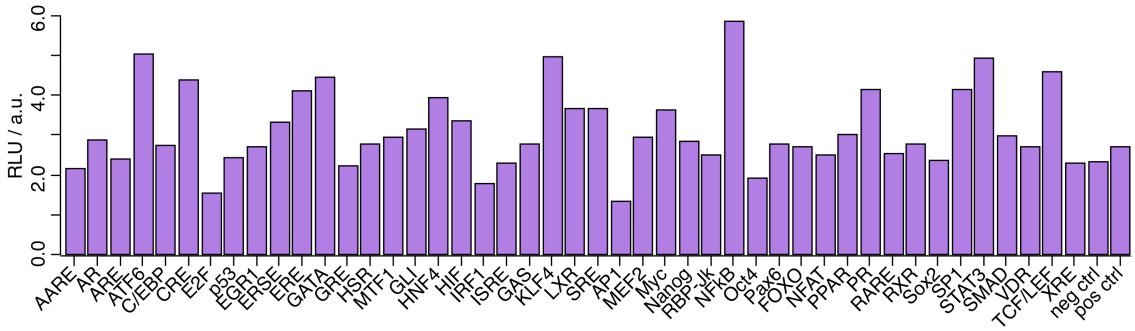


**Figure 5: Initial 45-pathway test with AmVKR in HEK293t cells.** After stimulation with 400 µM *L*-arginine, no pathway is triggered significantly.

With the hypothesis of MAPK activation, a closer examination of the intracellular domain revealed no mammalian docking site for *e.g.* Shc binding proteins, which are essentials adapters for Erk activation (Figure 2). Therefore, a Shc docking site needed to be introduced. The mammalian sequence for binding to Shc is YxxM,[28] leaving two random amino acids in between the necessary tyrosine and methionine random. After aligment of the intracellular domain of AmVKR with Shc, the tyrosine residue ($^{1278}$Y) is conserved, while the methionine residue ($^{1281}$M) is replaced with an aspartate amino acid in wt-AmVKR. Therefore, two more mutants were built, the first with the sequence $^{1278}$YSSM, which leaves the two native serine residues intact, and a second one $^{1278}$YTHM, which renders this site as the exact same amino acid sequence found in the hIR. These complicated mutations were achieved with only one primer pair (for primers used to obtain mutants see Table 2) and correct mutation was confirmed by full sequencing. When utilizing the 45 pathway kit again to screen for pathway activation, NFκB was found to be activated for both Shc docking mutants (*i.e.* $^{1278}$YSSD and $^{1278}$YTHM) when normalized to another dead kinase version of AmVKR, a K$^{909}$A mutant (Figure 6a and b). This mutation was used instead of the $^{1043}$FF mutant for two main reasons: first, the $^{1043}$FF mutant will not be phosphorylated only on these residues, which could leave other tyrosines on the intracellular side still active. Secondly, Before mutating several tyrosines to non-phosphorylatable phenyalanines, the K$^{909}$A mutant is a small change; the lysine is required for ATP binding in order to transfer the phosphate group. As this is not present anymore, auto- and/or cross-phosphorylation cannot take place. This experiment was performed with 400 µM of Arg as a stimulant.

NFκB (nuclear factor kappa-light-chain-enhancer of activated B cells) is a transcription factor that is activated when the cell is under stress, such as UV irradiation, radicals, etc.[35,36] However, as this was only observed with the Shc docking domain in place, we reasoned that this is the cause for NFκB activation, although cell signal streaming from Shc to NFκB is not a classical signaling pathway.[20] Even more, NFκB has not been described to cross-talk with Erk transcription.

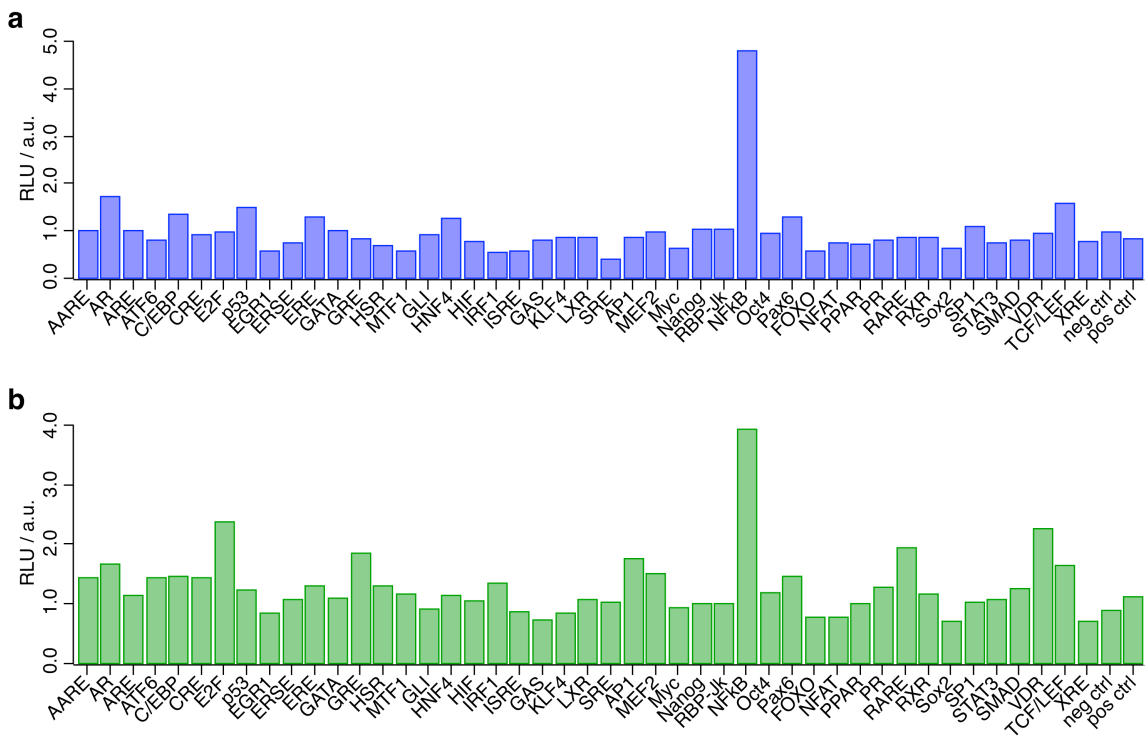


**Figure 6: 45-Pathway screen with YSSM (a, blue) and YTHM (b, green) introduced Shc2 binding domains in AmVKR.** For both mutants NFKB stands out after normalization with a dead kinase version ($K^{909}A$) of AmVKR.

This finding opened the door for more detailed studies on both AmVKR_YxxM mutants. For this, exclusively NFκB reported plasmids based on the DualGlo luciferase system were used (SA Bioscience, #CLS-013L) and different conditions could be screened with wt-AmVKR and the kinase-dead version serving as controls. Standard stimulation was performed with 4 mM Arg. To obtain a dose-response, different Arg concentrations were used for receptor stimulation (Figure 7a) and several other amino acid ligands (*i.e.* *L*-Lys, *L*-Glu, GABA, NMDA, and *L*-ornithine), which are known to activate VFT receptors (*L*-Glu, GABA, NMDA) or are similar to arginine (*L*-Lys, *L*-ornithine) were screened (Figure 7b). However, when the experiments were redone, no NFκB activation was observed when the Arg concentration was increased stepwise from 20 µM to 4 mM. Furthermore, other ligands also seemed not to activate this particular transcription factor. This leaves the results obtained from the 45 pathway screen inconclusive and could indicate for an artifact. Notably, all obtained signals were

higher than cells transfected with sole reporter plasmid (RP). This observation can be attributed to cell stress caused by expression of large proteins including their shuttling, for which NFκB is also activated (*vide supra*).

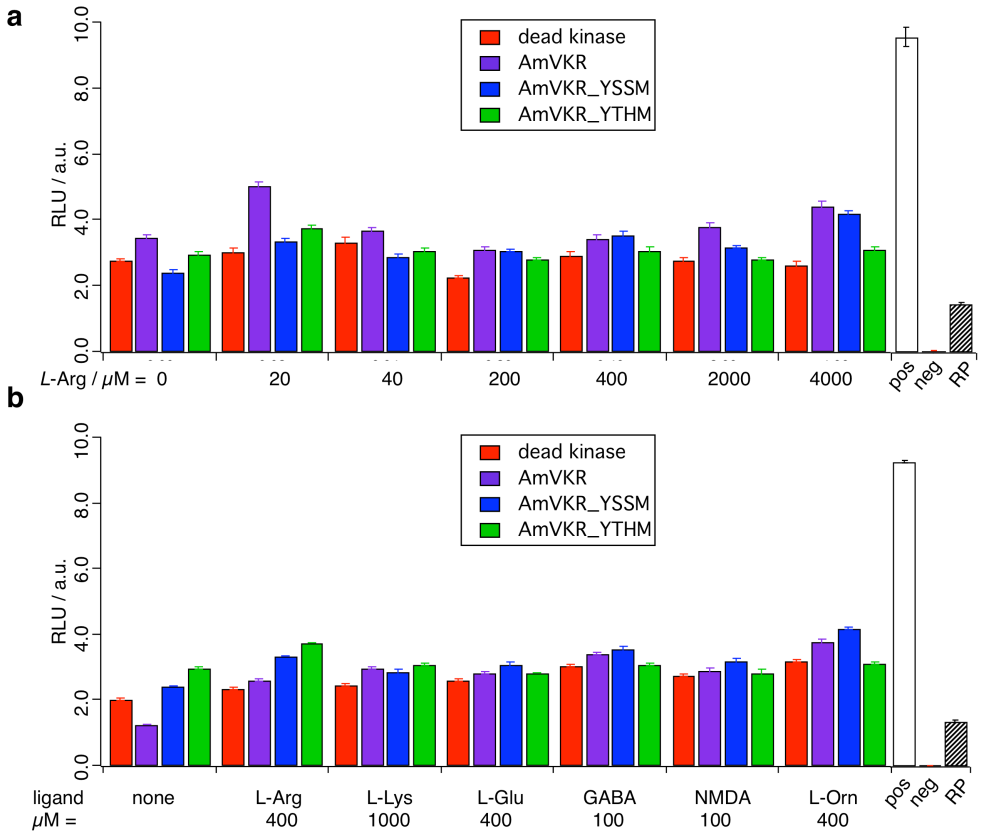


**Figure 7: Arginine concentration and ligand screen of AmVKR (purple) and AmVKR mutants (dead kinase $K^{909}A$, red; YSSM, blue; YTHM, green) towards NFKB. a)** Concentration study with *L*-arginine stimulation did not show an activating effect. **b)** Ligand study of various amino acids showed no activation of NFKB. pos = positive control, neg = negative control, RP = reported plasmid.

After these efforts, a different approach was taken mainly due to the concern that a protein from an insect might not be the best system for probing function in mammalian cells. Looking again at the homology of AmVKR to mammalian proteins, its ligand binding domain is close to glutamate receptors and its intracellular part resembles the insulin receptor (*vide supra*). By constructing novel chimeras based on the domain structure of AmVKR, new proteins were

designed and cloned. Firstly, the AmVKR-LBD was displaced by the mGluR2-LBD. However, some structural characteristics had to be considered: the mGluR2-LBD is connected to the 7TM-domain via a cysteine rich domain (CRD). On the other hand, the AmVKR-LBD is connected to the single TM-helix *via* a peptide linker (L1). As a possible activation mechanism remains elusive, four chimeras were cloned with scrambled linker characteristics (Figure 8a) according to the protocol from Gibson *et al.*,[37] which allows restriction enzyme free cloning of large fragments (for "Gibson" primers see Table 3). This yielded the chimeras A-D that are all linked differently from the LBD to the TM domain: chimera A lacks any of the connecting structural features, chimera B is connected *via* linker L1 from AmVKR, chimera C is connected *via* the cysteine rich domain (CRD) from mGluR2, while chimera C bears the CRD and the L1 peptide as a connective (Figure 8b) (see Experimental for full sequences of all chimeras). Furthermore, the Shc-binding sites were also engineered into all chimeras, containing either the YSSM or the YTHM motif yielding another eight chimeras P315-322 (see Figure 9b and Experimental for details).

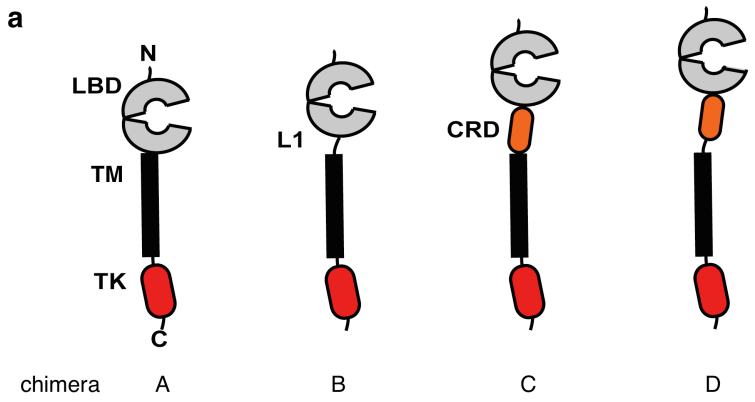


| domain | origin |
|---|---|
| N | mGluR2 |
| LBD | mGluR2 |
| CRD | mGluR2 |
| L1 | AmVKR |
| TM | AmVKR |
| TK | AmVKR |
| C | AmVKR |

**Figure 8: Cloned chimeras A-D between mGluR2 and AmVKR. a)** Schematic represenation of four chimeras and their connection between the ligand-binding domain (LBD) and transmembrane domain (TM). While A is directly connected, B bears a linker (L1) from the native AmVKR protein, C bears the cysteine-rich domain (CRD) from the mGluR2 and D contains both L1 and CRD domains. **b)** Origin of the domains that can be found in the chimeras A-D. N = N-terminus, TK = tyrosine kinase, C = C-terminus.

Aiming at Erk activation testing was again performed using a DualGlo Luciferase readout (SA Bioscience, #CSS-010L). After transfection of all eight constructs P315-P322 into HEK293t cells and expression over night, however, they did not show a stimulatory response to *L*-glutamate (400 µM) streaming on Erk (Figure 9a). Figure 9b depicts amino acid composition of chimeras used. The protocol used, was that after outgrow followed by starvation in DMEM with 0.1% dialyzed FBS (which contains no glutamate) the stimulation period was over night and subsequent measured with the DualGlo luciferase plasmids. While control experiments showed expected results, AmVKR transfected cells also showed a slight increase in luciferase expression. Solely transfected reporter plasmid (RP) gave signals in the same range as all expressed chimeras. Therefore, and activation by glutamate can be clearly ruled out.

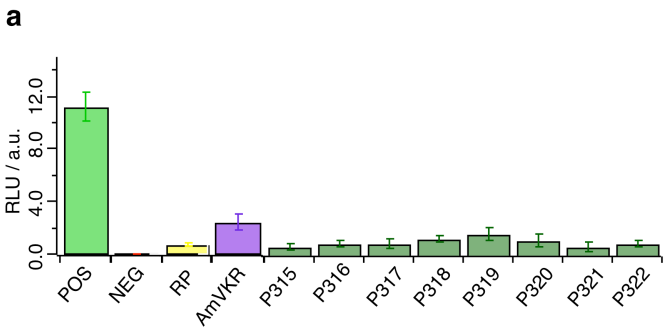


b

| | L1 | CRD | Shc2 |
|---|---|---|---|
| P315 | no | no | YSSM |
| P316 | no | no | YTHM |
| P317 | yes | no | YSSM |
| P318 | yes | no | YTHM |
| P319 | no | yes | YSSM |
| P320 | no | yes | YTHM |
| P321 | yes | yes | YSSM |
| P322 | yes | yes | YTHM |

**Figure 9: Glutamate screen of YSSM and YTHM containing chimeras A-D. a)** None of the Shc2 binding domain containing chimeras responded to glutamate towards Erk-activation. AmVKR and sole reporter plasmid (RP) served as control. POS = positive control, NEG = negative control. **b)** Composition of mutants P315-322 including the mutated Shc docking domain.

Another step was taken based on the domains from AmVKR. One construct was a kind gift from Dr. Colette Dissous and Dr. Jerome Vicogne and consisted of the LBD from the mGluR2 connected to the tyrosine kinase domain from Met, *i.e.* the TK domain of the HGF (hepatocyte growth factor) receptor. This resulted in the chimera mGluR2_Met (see Experimental for full sequence). Met is known to

stimulate MAPK pathway ultimately leading to Erk activation.[38] This construct showed constitutive activity towards MAPK pathways, also evaluated by a 45-pathway kit as before (Figure 10) with no stimulating ligands and in the absence of glutamate. Finally, Erk activation stands out as the primary transcription factor activated (serum response element, SRE) among others, such ATF6, GLI, AP1 and STAT3. While ATF6 (activating transcription factor 6) can be appointed to cellular stress and hedgehog (GLI) is also known to be activated by Met[39], AP1 (activator protein 1) and STAT3 (Signal transducer and activator of transcription 3) are stress and mitogen activated protein kinase pathways (SAPK and MAPK), respectively, and therefore the results are as expected. Nevertheless, studies continued with Erk screening fort wo reasons: first, Erk showed to be the most activated, and second it is known to be streamed to by Met.

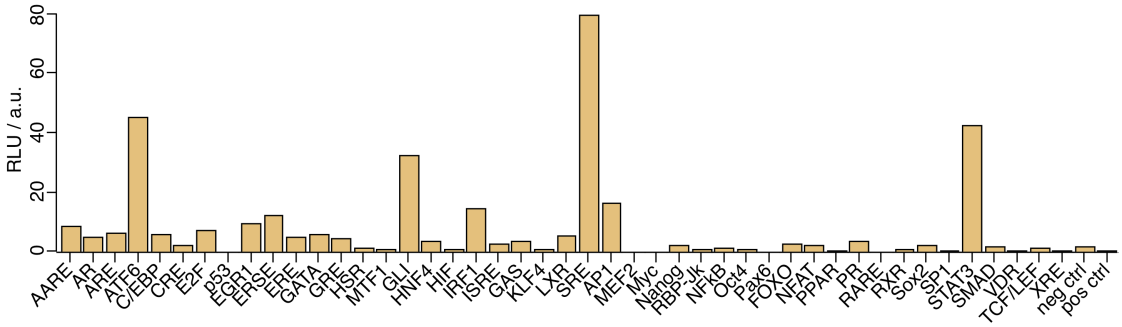


**Figure 10: 45-Pathway screen for the mGluR2_Met construct.** Activation is observed towards ATF6, GLI, SRE, AP1 and STAT3, the three latter being S/MAPK pathway triggered transcription factors.

As Erk was activated even without the stimulant glutamate for the mGluR2_Met construct concerns were that this construct cannot be activated further as it exhibits constant phosphorylation resulting in constant Erk activation. In order to lower this activity to obtain stimulatory responses, the cysteine 121 was mutated to a serine residue (C121S). As mGluR2s function as covalently connected dimers through a disulfide bond resulting from the oxidation of the C121,[40] a possibility was that this also triggers continuous activation by close

proximity due to covalent connection. Indeed, the C121S mutant exhibited lower basal activity (Figure 11, brown) with respect to the cysteine containing "wt" construct (Figure 11, ochre) when tested towards Erk phosphorylation. However, activity was still increased when compared to AmVKR (Figure 11, purple) or mock cells (Figure 11, gray) if not stimulated (left bars of each plasmid). Furthermore, when stimulated with glutamate (0.4 and 1.0 mM) or with the addition of 10% FBS, Erk levels decreased for both mGluR2_Met constructs (Figure 11) although this had no effect on AmVKR expressing cells. Consequently, these constructs were not feasible for further elucidation and activation of a TK with glutamate.

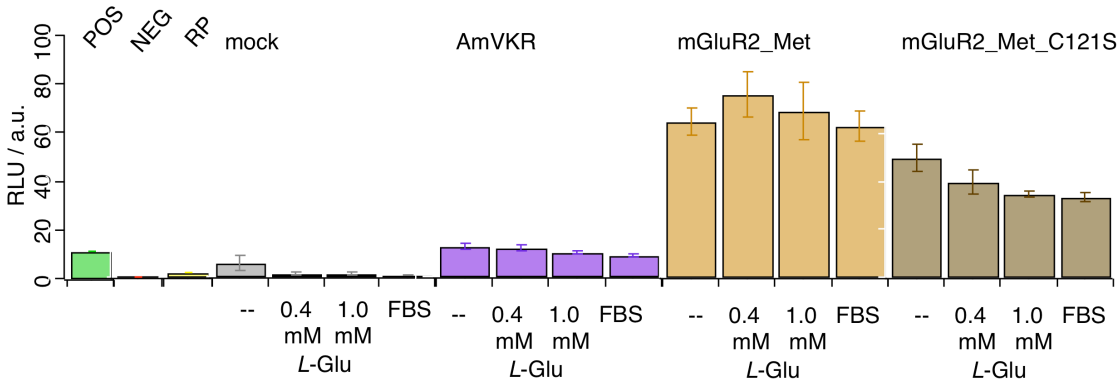


**Figure 11: Erk-activation of "wt" mGluR2_Met and mGluR2_Met C121S mutant.** mGluR2_Met (ochre) does activate Erk independent from stimulating reagents (0.4 mM and 1.0 mM Glu and FBS). Erk phosphorylation is diminished (with no activating ligand effect) for its C121S mutant (brown) and further reduced with the addition of glutamate (0.4 mM and 1.0 mM) or FBS. Mock cells (gray), AmVKR (purple) and reporter plasmid (RP) transfected cells served as control. POS = positive control, NEG = negative control.

In a last attempt still based on the domain composition of AmVKR, a chimera was cloned with the TK domain from the human insulin receptor (hIR) and the mGluR2 LBD by TOPO® cloning (see Experimental for primer and cloning details), *viz* LL1-3 (see Experimental for full sequence). LL1, LL2 and LL3 proved to be the same clones by full sequencing, therefore only LL1 was used only in later experiments. This construct unites all the domain features from AmVKR by

engineering mammalian protein domains together, *i.e.* the VFT-LBD with a intracellular TK domain. As activity testing described above was usually performed at the end of a signaling cascade, the aim was now to observe earlier activation. This could give a clearer signal because after tyrosine phosphorylation, the measure transcription and translation of luciferase might be "diluted" through the signaling pathway. Therefore, phosphotyrosine WB was performed, which measures signals at the top of the signaling cascade.

In first experiments, expression of LL1-3 in HEK293t cells was validated by HA-immunoprecipitation together with HA-mGluR2 and the HA-mGluR2_Met construct (Figure 12, top). Furthermore, phosphorylation of Akt (p-Akt) and Erk (p-Erk) was measured. Akt was chosen because Shc is known to also activate Akt/PI3K (phosphoinositide-3 kinase, also known as protein kinase B, PKB) signaling pathways.[20] However, p-Akt remained on a constant level for all transfections (Figure 12, middle). Regarding p-Erk, the mGluR2_Met construct proved to be constitutive active under normal expression conditions, *i.e.* DMEM supplied with 10% FBS thereby validating the luciferase experiments performed before. On the other hand, p-Erk levels were lower for control experiments (mock cells) as well as for mGluR2 and LL1-3 transfected cells (Figure 12, bottom).

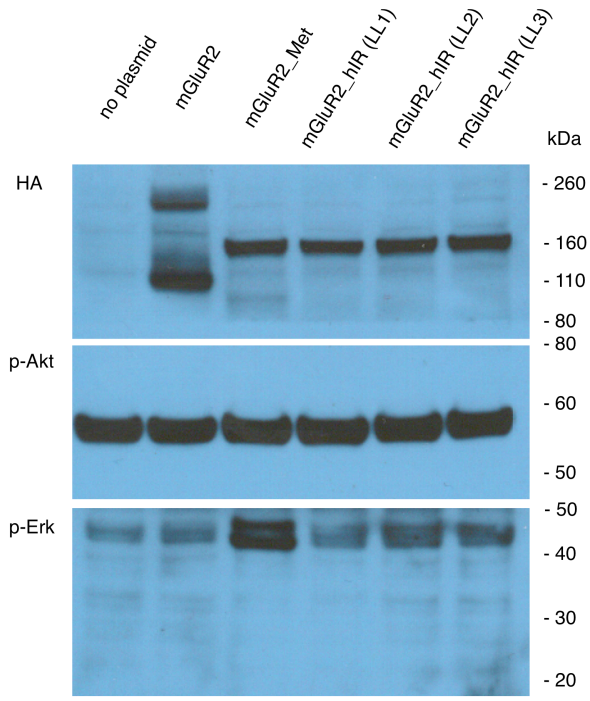


**Figure 12: Expression validation and HA-antibody testing of mGluR2_hIR construct together with p-Akt and p-Erk in HEK293t cells.** top: HEK293t cells transfected with mGluR2, mGluR2_Met construct and mGluR2_hIR construct (LL1-3) showed all expression measured by HA-antibody staining. No transfection served as negative control. Middle: p-Akt levels stayed constant for all testings. Bottom: p-Erk levels proved constitutive mGluR2_Met activity towards Erk (see Figure 13 for total Akt and total Erk levels), while mock cells, and mGluR2 and LL1-3 transfected cells showed lower phosphorylation.

Another antibody was tested against the intracellular domain of the mGluR2 (cell signal, #12056) in order to quantify the basal expression of this receptor in HEK293t cells. This is a necessary control step as otherwise glutamate stimulation might give positive results based in endogenously expressed proteins (Figure 13, top). The WB clearly shows that mGluR2 is not natively expressed in HEK293t cells. Furthermore, the antibody did not show background activity, as lanes of untransfected cells (no plasmid) as well as LL1-LL3 transfected cells showed no binding towards the antibody. Even more, total Akt (t-Akt) (Figure 13, middle) and total Erk (t-Erk) (Figure 13, bottom) levels remained unaffected in mock cells and in plasmid transfected cells. Total protein quantification is necessary to determine the ratio between total protein

abundance and phosphorylated protein. These results were promising indications en route to achieving a glutamate activated tyrosine kinase.

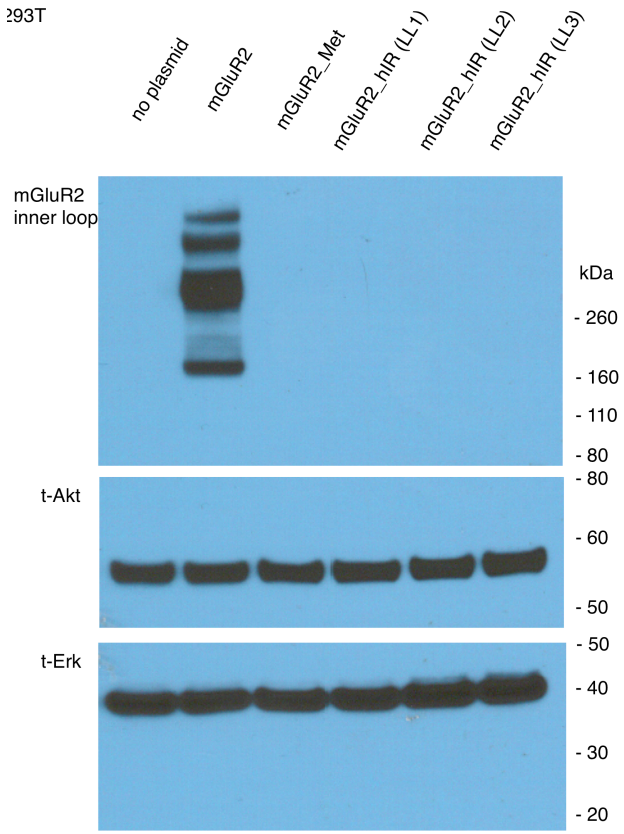


**Figure 13: anti-mGluR2 antibody (inner loop) testing.** Same membrane as in Figure 12 was subjected to mGluR2 antibody staining (top). Total Akt (middle) and total Erk (bottom) levels remained constant in all experiments.

In the next step, the measurement of h_IR TK phosphorylation had to be tested to validate the functionality of the new constructs, so p-Tyr antibodies that bind to the tyrosine phosphorylated protein backbone were tested. Antibodies against β-IR and tyrosine phosphorylation (p-Tyr1361) were tested (Figure 14) by transfection of the full length insulin receptor (Figure 14, right) and subsequent stimulation with glutamate and insulin (ins) (Figure 14) while mock cells served as control (Figure 14, left).

Control experiments, with either no stimulation, or stimulated by 5 mM glutamate (G5) or 100 nM insulin (Ins) revealed no detectable expression of endogenous h_IR in HEK293t cells by β-IR antibodies, accordingly no phosphorylation has been detected either (Figure 14, left). Akt levels remained constant with respect to total amount and phosphorylated amount no matter what stimulation protocol was performed. Erk levels, however, remained constant in total amounts, but an increase in phosphorylated Erk was detected. This can be accounted to the very low expression of h_IR, which is not detectable but nevertheless gives a signal on the transcription factor level when activated.

More importantly, cells transfected with h_IR proved the IR antibodies working (*vide infra*). Akt levels also remained unaffected no matter which stimulant was used the same way as for mock cells. Even more, Erk was phosphorylated significantly when transfected with h_IR. Phosphorylation was observed for unstimulated cells as well as stimulated ones with 100 nM Ins. Conversly, and against expectations, stimulation with G5 decreased p-Erk levels. To date, an explanation for this is lacking, however, one reason can be imagined, *i.e.* the activation of phophatases with G5, which dephosphorylate p-Erk.

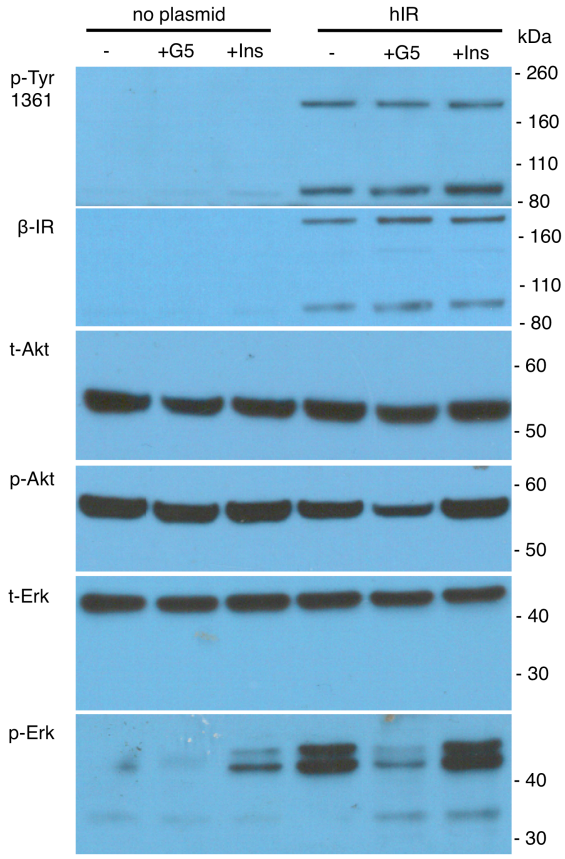


**Figure 14: Testing of phosho-tyrosine 1361 (p-Tyr 1361) and β-IR antibodies.** HEK293t cells were transfected with human insulin receptor (right) (non- transfected cells served as control, left). p-Tyr1361 and β-IR antibodies showed both two bands at 180 and 90 kDa accounting for the undenaturated hIR and the denaturated beta-chain, respectively. Total and phopshporylated Akt and Erk was measured. A decrease in p-Erk can be clearly observed by treatment of hIR transfected cells with 5 mM glutamate (G5).

With antibodies being validated and tested in control studies, the mGluR2_hIR contruct LL1 could be further evaluated. Therefore, HEK293t cells were transfected with LL1 and stimulated with different concetrations of glutamate (0, 0.5, 1.0, 2.5, and 5.0 mM, *i.e.* -, G0.5, G1, G2.5 and G5) as well as with Ins. Expression was proved by HA- and β-IR-antibodies (Figure 15). Phosphorylation of LL1 was tested with p-Tyr1361 Abs and as before Akt and Erk. In an inital experiment results remained inconclusive as they did not show the same behaviour as before (e.g. Erk phosphorylation with Ins). Together with the scrambling of glutamate stimulated cells by loading, it cannot be ruled out that a mix-up in samples occured. However, as a first test, the expression of the LL1

construct was demonstrated again together with the validation of the IR-antibodies towards this chimera, which is important for further screens.

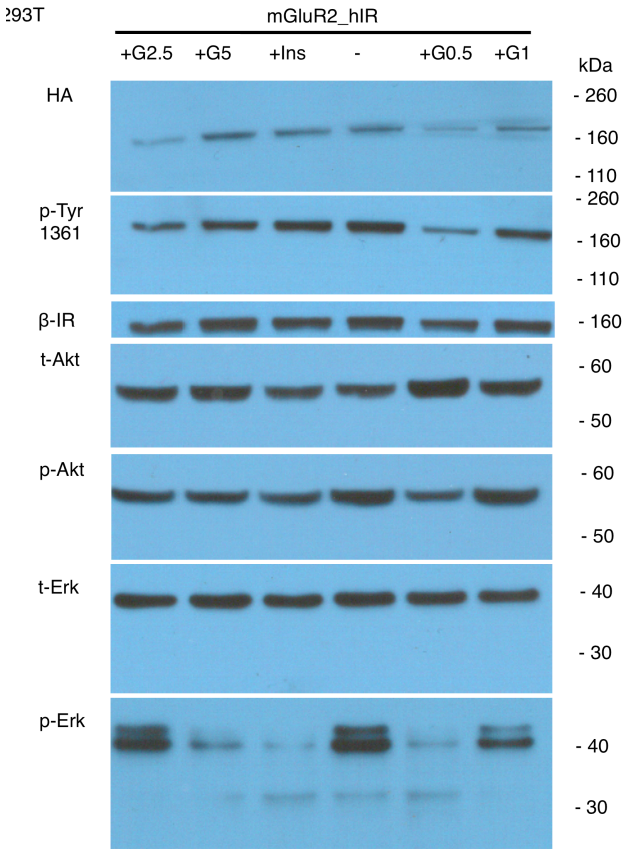


**Figure 15: WB evaluation of mGluR2_hIR construct with increasing glutamate concentrations in HEK293 cells.** HA, p-Tyr1361 and β-IR antibodies prove functional expression of mGluR2_hIR (LL1). Akt and t-Erk levels remain unaffected towards stimulation while p-Erk gives a stronger signal in two samples.

The mGluR2_hIR construct LL1 was expressed again in HEK293t cells, this time with h_IR and mock cells as controls with better results (Figure 16) as obtained before. Phosphorylated levels were integrated and divided by total protein levels of the corresponding antibody (Figure 17). Experiments concerning mock cells and h_IR transfected cells resemble the results from before (Figure 13 and Figure 14) and will not be discussed in detail. It should be noted, however, that this time

the endogenous h_IR in mock cells was detected with antibody beta-IR and pTyr1361.

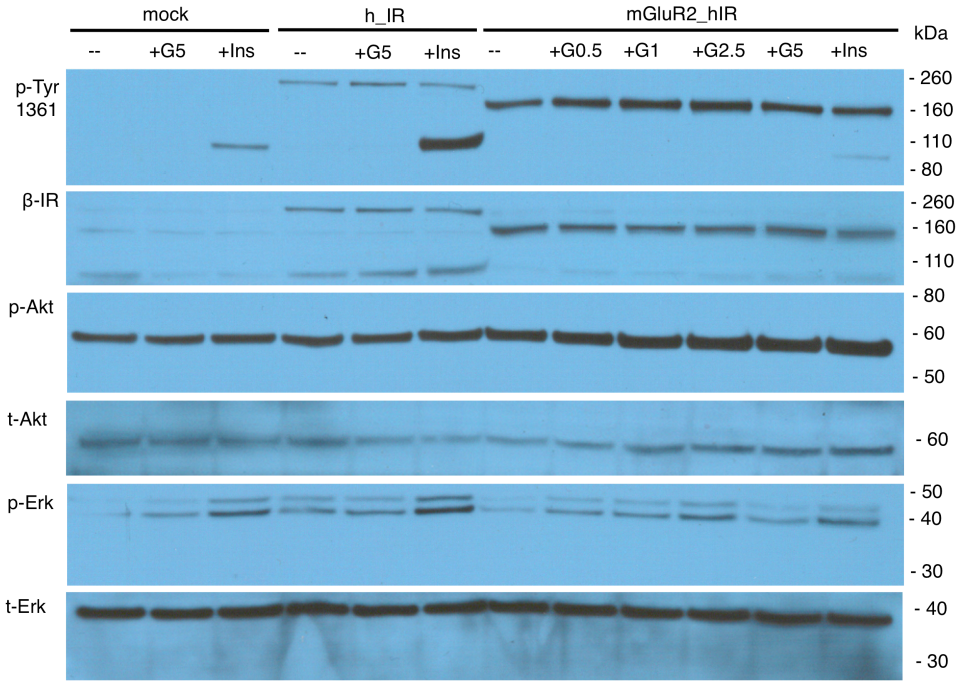


**Figure 16: WB of mock HEK293t cells or expressing h_IR or mGluR2_hIR including glutamate concentration dependent phosphorylation studies of β_IR domain, Akt and Erk.**

The right side of Figure 16 resembles the same experiment as performed before with respect to transfection and stimulation (Figure 15). Integrated and relative phosphorylation levels of LL1, Akt and Erk are shown in Figure 17 (right). Phosphorylation of the receptor is increasing with increasing concentrations of glutamate up to 1.0 mM and is decreasing again with higher concentrations (2.5 and 5.0 mM) (Figure 17, red). p-Akt/t-Akt remained stable (Figure 17, black) and p-Erk/t-Erk follows the same trend as receptor phosphorylation, only with a peak at 2.5 mM glutamate stimulation. The fact that p-levels are decreasing with 5.0 mM glutamate resemble the trend observed from h_IR transfected cells stimulated with the same concentration (*vide supra*). Taken together, these results set the working concentration of glutamate stimulation to 2 mM and

time-course experiments would have to be performed to gain an understanding about the kinetics of activation.

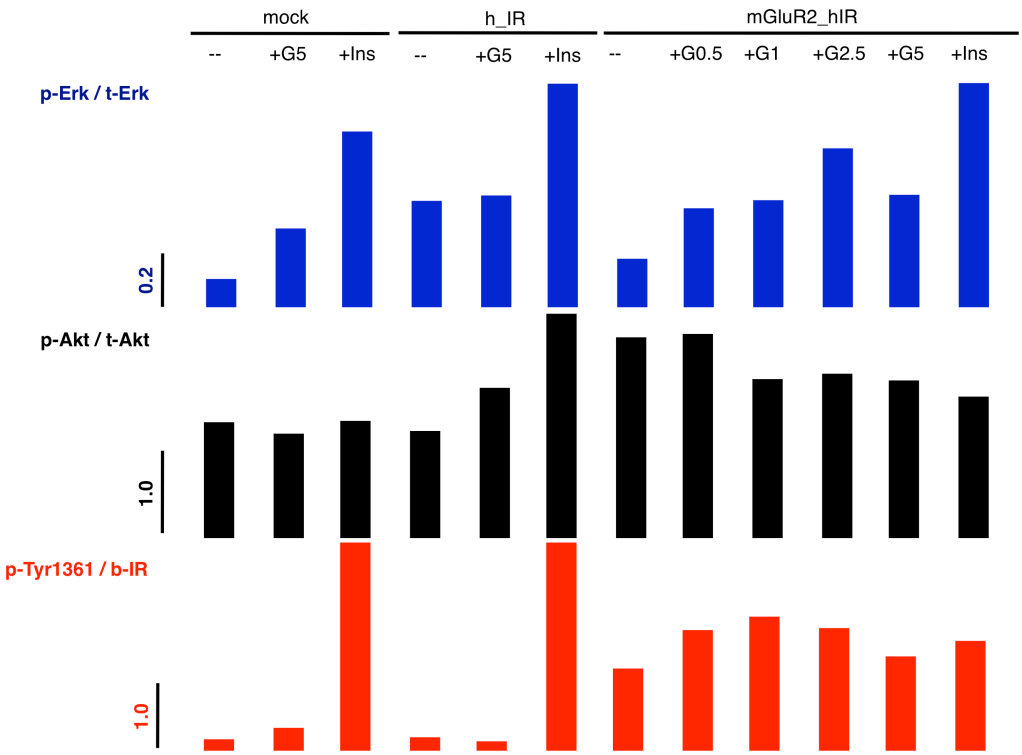


**Figure 17: Evaluation of WB from Figure 16 by integrating signals from phophorylated bands divided by integrated total signals (p/t).** p-Erk/t-Erk (blue), p-Akt/t-Akt (black) and p-Tyr1361/β-IR (red). A peak for mGlur2_hIR construct (LL1) for p-Erk/t-Erk was observed for a stimulation with 2.5 mM gluatamate.

The kinetics of protein activation are crucial for possible later light-activating experiments. With the observation that 2.5 mM glutamate stimulated the LL1 construct towards phosphorylation, 2 mM glutamate was chosen as a working concentration and stimulation was performed for different time points (*i.e.* 0, 2, 5, 10, 15, and 20 minutes) in duplicates (Figure 18). p- and t-Akt levels were not measured, as they proved to be independent towards stimulation in previous testings. Integrated levels of phosphorylated and total protein levels were

divided and plotted agains time as seen in Figure 19. The same experiment was performed for hIR (WB not shown, but evaluated in Figure 19).

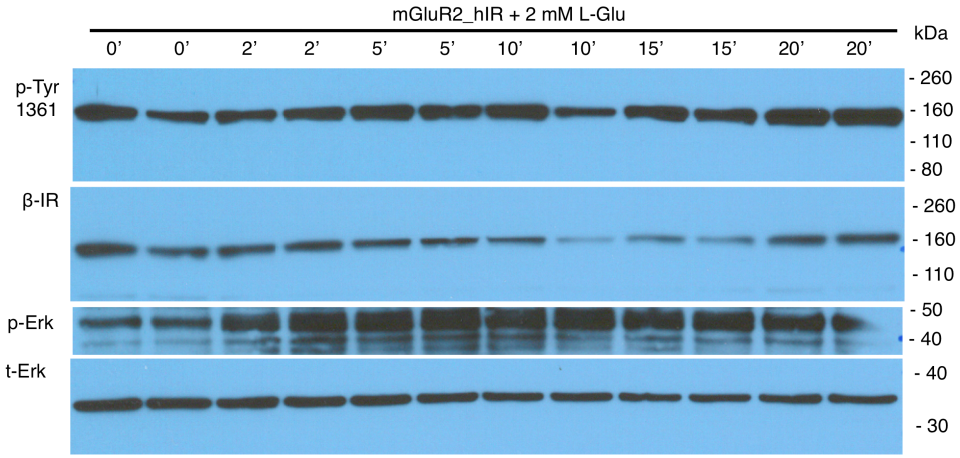


**Figure 18: Time dependent study of mGluR2_hIR activation with 2 mM glutamate.** mGluR2_hIR transfected HEK293t cells were treated in duplicated with 2 mM Glu over the course of 0, 2, 5, 10, 15 and 20 min.

The WB seen in Figure 18 was evaluated and shows interesting findings (Figure 19). h_IR transfected cells exhibit a peak of phosphorylation after 2 minutes (Figure 19, green). However, this experiment was not performed in duplicates and might be an artifact that has to be reexamined. More importantly, phosphorylation levels of both mGluR2_hIR duplicates showed an increase in signal. This was observed for both, the IR-phosphorylation (Figure 19, light and dark blue) and p-Erk (Figure 19, light and dark red, expanded on the right) after 10 minutes of stimulation.

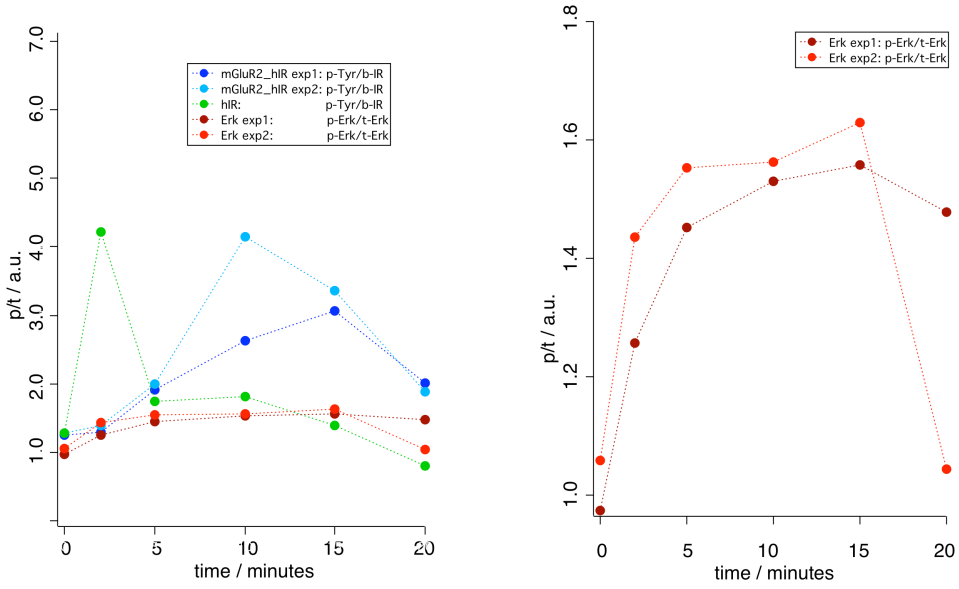


**Figure 19: Evaluation of WB from Figure 18 by integrating signals from phophorylated bands divided by integrated total signals.** Maximal stimulation was achieved for p-Tyr (blue) and Erk (red) after 10 min. hIR transfected cells served as control and show peak activation at 2 min.

In order to prove the function of the mGluR2_hIR chimera LL1 in a variety of biological context, the experiments from HEK293t cells were also conducted in HeLa cells. HeLa cells were chosen as they exhibit a lower endogenous Akt activity, therefore it was possible to observe activation of PKB as well (*vide supra*). In an experiment similar to before in HEK293t cells, mGluR2_hIR was transfected and mock cells served as controls while stimulation was achieved with no ligand, 2.0 mM glutamate (G2) and insulin (Ins) and visualized by WB (Figure 20).

Indeed, mock HeLa cells responded to 100 nM insulin by phosphorylation of Akt and Erk (Figure 20, left). More importantly, the LL1 construct responded to 2.0 mM gluatamate by Erk phosphorylation (Figure 20, right).

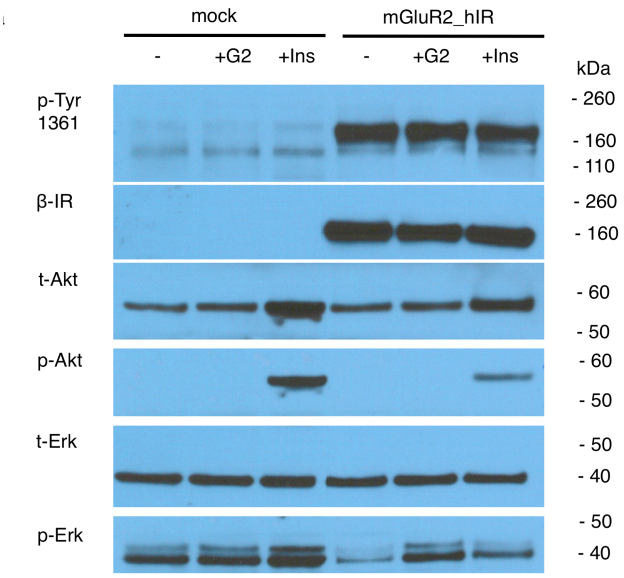


**Figure 20: WB evaluation of mGluR2_hIR construct LL1 in HeLa cells.** Same experimental setup as for HEK293t cells (Figure 14) only with 2.0 mM glutamate.

Again, signals detected in WB from Figure 20 were integrated and the phosphorylation signals were divided by signals occuring from total protein measurement (Figure 21). While mock cells and transfected cells responded to insulin stimulation by Akt phosphorylation (blue), only transfected cells exhibit an increase in the p-Erk/t-Erk signal (gray). Interestingly, no increased signals were detected with p-Tyr1361 ABs. However, this can be attributed to several effects, such as the action of phosphatases, which dephosphorylate the receptor or just receptor clearing by internalization.

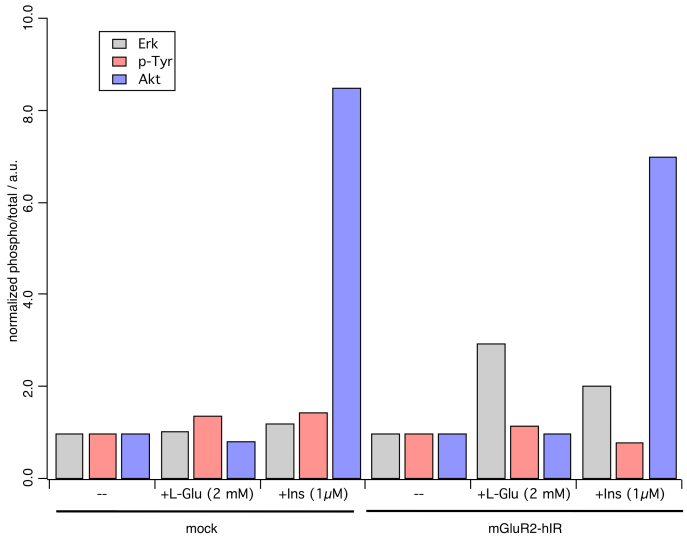


**Figure 21: Evaluation of WB from Figure 20 by integrating signals from phophorylated bands divided by integrated total signals.** Mock cells served as controls and showed Akt-phosphorylation (blue) only by treatment with insulin. mGluR2_hIR transfected cells showed Erk-phosphorylation (gray) by treatment with 2 mM Glu or insulin, while p-Akt-levels showed the same behaviour as for mock cells. Tyrosine-phosphorylation (red) remained stable in all experiments.

In a last experiment, the stimulating effect of glutamate was to be shown in HeLa cells by alpha-screening, which is a method with very high signal accuracy.[41] Briefly, this method can be used in cell lysates and contains two antibodies of interest that both are linked to different beads and bind to the analyte protein. Once they are bound and therefore in close proximity, one bead can be activated with 680 nm light to generate singlet oxygen, which is sensed by the second bead resulting in an emission at 615 nm. The emitted photons can be counted and used for the determination of how much (phosphorylated) protein is present.

With mock cells serving as control, a significant increase in both p-Tyr and p-Akt could only be observed by treatment with insulin. As expected, this trend is also observed from mGluR2_hIR transfected cells.

In this final tests, Erk phosphorylation was again triggered with a peak of 2.0 mM glutamate, while lower concentrations did not manage to give that signal.

Furthermore, as in HEK293t cells, higher concentration of glutamate (G5) give a decreased signal.

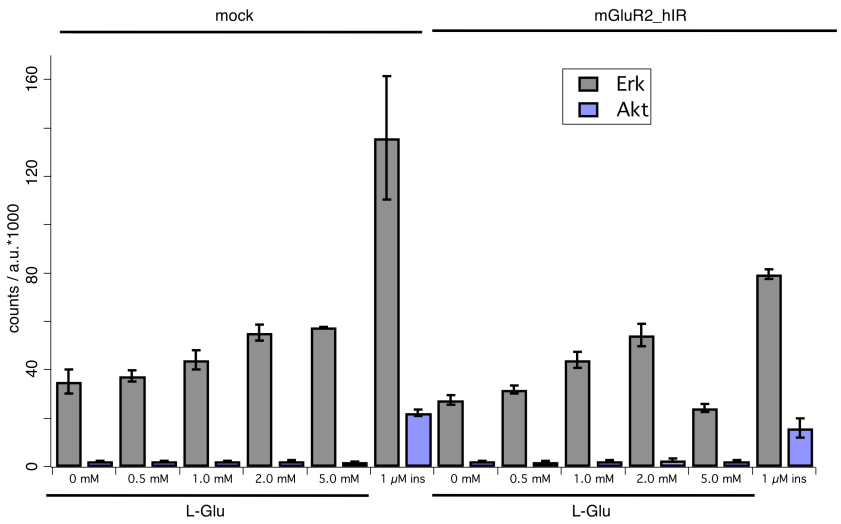


**Figure 22: alpha screen of Erk- and Akt-phosphorylation in HeLa cells by increasing concentration of glutamate.** Mock cells served as control (left) and both Erk and Akt were significantly phosphorylated only by treatment with insulin. mGluR2_hIR transfected cells showed an increase in p-Erk up to 2 mM, while 5 mM decreased the signal. Akt was only activated by insulin treatment.

All these findings taken together point out the mGluR2_hIR chimera LL1 is working best in HeLa cells with a stimulating concentration of 2.0 mM glutamate for Erk phosphorylation. To the best of our knowledge, this is the first time a RTK has been stimulated with a small molecule neurotransmitter.

## 5.3 Summary and Outlook

Several attempts have been made towards a light-activated receptor tyrosine kinase. Starting with the testing of a venusflytrap tyrosine kinase receptor from the honeybee *apis mellifera* (AmVKR), moving to mGluR2 venusflytrap chimeras that are fused to the tyrosine kinase domain of AmVKR and mGluR2_Met constructs, the study closes with a novel fusion protein between the mGluR2-LBD and hIR-TK domain. The latter is inspired by the domain homologs of AmVKR. These proteins have been evaluated in terms of heterologous expression and have been assayed by a variety of methods, such as DualGlo luciferase systems, Western Blotting and alpha-screening, in HEK293t and HeLa cells towards multiple ligands with different concentrations and time-points.

After intensive focus on native AmVKR and fusion chimeras A-D as well as mGluR2_Met, the final and most promising testing has been performed on the mGluR2_hIR construct LL1 in HeLa cells with 2.0 mM glutamate as a stimulant.

To conclude finally, and after multiple attempts to activate tyrosine kinase activity with an amino acid neurotransmitter, the LL1 construct showed concentration dependent Erk-phosphorylation with 2.0 mM glutamate in both HEK293t and HeLa cells, both immortalized cell lines used extensively in heterologous expression and testing. The next step towards light control would be the mutation to the cysteine mutant to attach *D*-MAG0 (see Experimental), which was used to light-control the mGluR2. So far, all PCRs using the primers listed in Table 5 failed to date. Nevertheless, with the L300C mutant, which is necessary for PTL labeling introduced in the future, experiments can be conducted towards a light control of RTK function. Furthermore, primers have been designed for the truncation and expansion of the transmembrane domain of LL1 (see Table 6). By inserting or deleting an amino acid from the helix, the intracellular domains will have a twist in their molecular assembly. This could also affect tyrosine phosphorylation and/or downstream signals but has to be evaluated empirically.

Another congener was synthesized from a *D*-MAG0 precursor, *viz.* ***D*-AG0** (see Experimental) that lacks the maleimide and might serve as a PCL. Taken together, the construction, expression and stimulation of the mGluR2_hIR construct LL1 can ultimately lead to a LiVKR, a light-activated receptor tyrosine kinase.

## 5.4 Experimental

### 5.4.1 (2*S*,4*S*)-2-amino-4-(4-((4-((*E*)-(4-(2-(2,5-dioxo-2,5-dihydro-1*H*-pyrrol-1-yl)acetamido)phenyl)diazenyl)phenyl)amino)-4-oxobutyl)-pentanedioic acid, *D*-MAG0

*D*-MAG0 has been synthesized in a multistep procedure as previously described and spectra matched those reported.[42]

### 5.4.2 (2*S*,4*S*)-2-amino-4-(4-((4-((*E*)-(4-(2-aminoacetamido)phenyl)diazen-yl)phenyl)amino)-4-oxobutyl)pentanedioic acid TFA salt, *D*-AG0 x TFA

#### 5.4.2.1 Synthesis

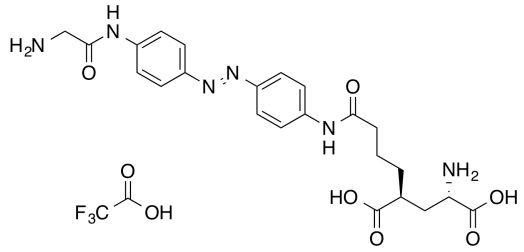

The PCL ***D*-AG0** derived from a *D*-MAG0 precursor **5.1** has been synthesized for the first time (Supplementary Scheme 1). Briefly, 17.4 mg (29.7 µmol) of **5.1** was dissolved in 4 mL of neat TFA at 0 °C and stirred for 10 min. The product was precipitated by the addition of 100 mL $Et_2O$ and collected by sedimentation (4,000 rpm, 10 min). After decantation and another washing step with $Et_2O$ and subsequent sedimentation as before, 17.0 mg (28.4 µmol) of ***D*-AG0** were obtained in 96% yield as its TFA salt.

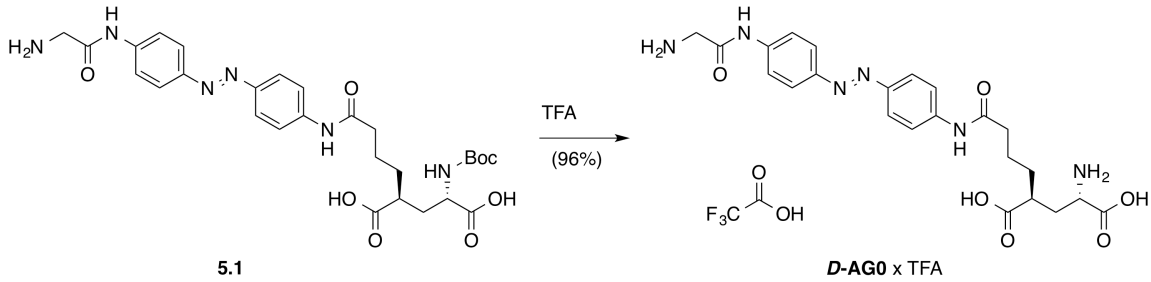


**Supplementary Scheme 1: Synthesis of *D*-AG0.**

**$^1$H NMR** (400 MHz, DMSO-$d_6$): $\delta$ [ppm] = 7.91 – 7.86 (m, 4H), 7.79 – 7.75 m, 4H), 3.90 (s, 3H), 2.83 – 2.79 (m, 1H), 2.48–2.45 (m, 2H), 2.22–2.11 (m, 1H), 2.11–1.99 (m, 1H), 1.75 (m, 4H).

**$^{13}$C NMR** (101 MHz, DMSO-$d_6$): $\delta$ [ppm] = 177.9, 174.2, 172.1, 165.7, 150.5, 150.1, 142.7, 141.7, 124.7, 124.6, 121.1, 121.0, 52.7, 42.7, 42.3, 37.5, 33.7, 32.9, 23.8.

**HRMS (ESI)**: calc. for $C_{23}H_{29}N_6O_6^+$ $(M+H)^+$: 485.2143, found: 485.2143.

**UV/Vis** (LCMS): $\lambda$ ($\pi \rightarrow \pi^*$) = 366 nm.

**$R_t$** (LCMS; MeCN/$H_2O$/formic acid = 10/90/0.1 → 90/10/0.1 over 7 min) = 1.682 min.

### 5.4.2.2 Spectral Data

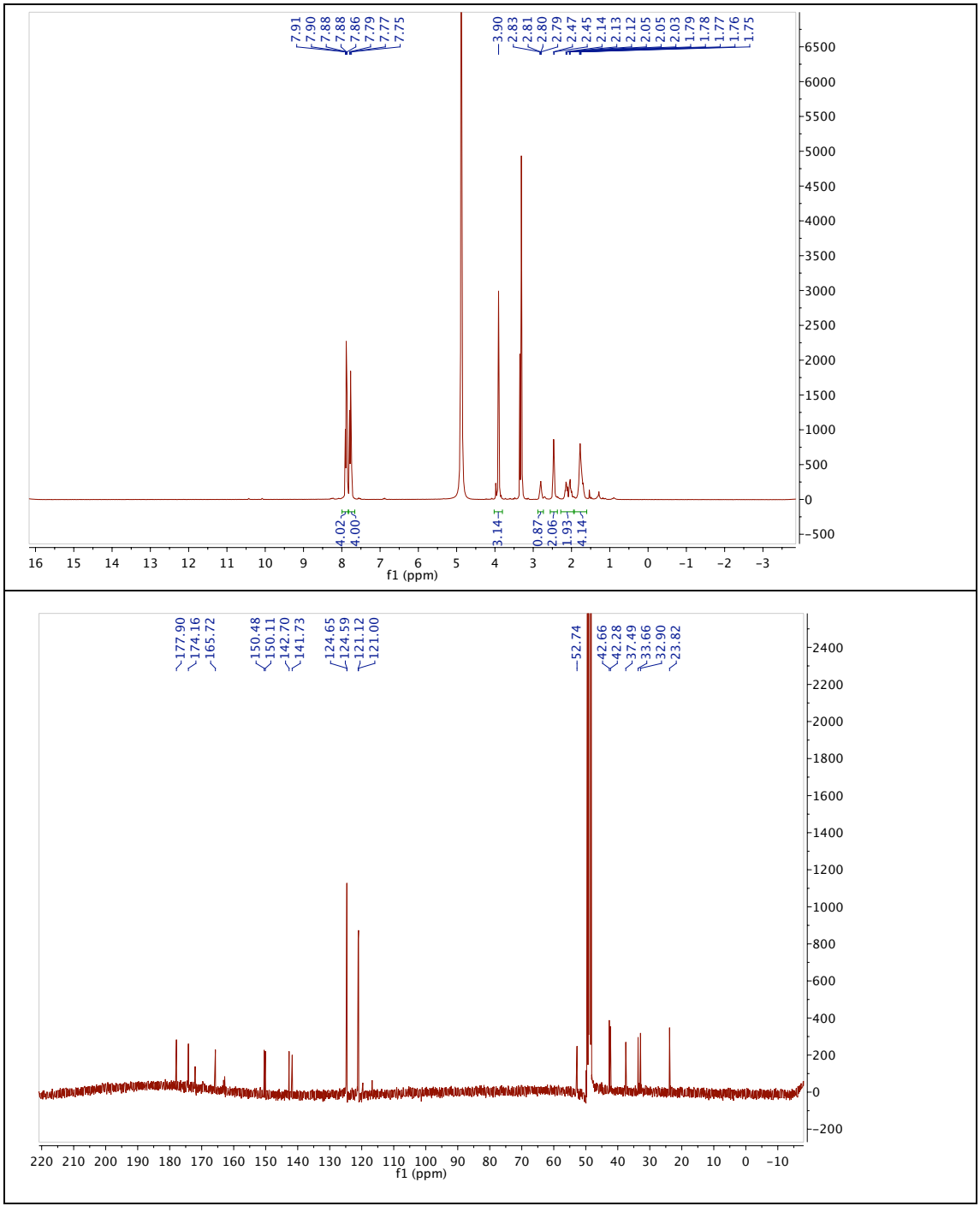

### 5.4.3 AmVKR Mutants and Cloning of VFT$^{mGluR2}$-TK$^{AmVKR}$ Chimeras

Plasmid containing AmVKR was a gift kindly provided by Colette Dissous, PhD. The plasmid was transformed and amplified from *E. coli* and submitted to full sequencing (primer are listed in Table 1).

**Table 1: Sequencing primer for AmVKR.**

| name | sequence (5'-3') |
|---|---|
| SNAP_end | GTGAAAGAGTGGCTGCTG |
| 1F | AGATCGTTGGTATTTCTGC |
| 2F | GAAATACACCGAGTACATAT |
| 3F | CGAAAAGCATGCCAGAC |
| 4F | ATGCTACCTGTAAGATGG |

Site-directed mutagenesis in order to yield a constitutively active mimic ($^{1043}$YYEE), kinase dead constructs ($^{909}$A and $^{1031}$DNA) to introduce mammalian Shc-2 binding motifs ($^{1284}$YSSM and $^{1284}$YTHM) and to scramble position 1050 between an arginine and a glycine residue was performed. Primers used for PCR site-directed mutagensis are shown in Table 2.

**Table 2: Primer for site-directed mutagenesis AmVKR and later constructs**

| name | sequence (5'-3') |
|---|---|
| $^{1284}$YTHM_F | TTACACGCACATGAACGGCGGTGGCAGCATTC |
| $^{1284}$YTHM_R | CGTTCATGTGCGTGTAATCGCAATTATTCGATATCCCCG |
| $^{1284}$YSSM_F | TCGAGCATGAACGGCGGTGGCAGCATTC |
| $^{1284}$YSSM_R | GCCGTTCATGCTCGAGTAATCGCAATTATTCGATAT |
| $^{1031}$DNA_F | GTGAAGCTTGGAGACAATGCTATGACGAGGTTG |
| $^{1031}$DNA_R | CAACCTCGTCATAGCATTGTCTCCAAGCTTCAC |
| $^{1043}$FF_F | GTACGAGAACGATTACTACGAGGAGAATCGAAGAGGTATGC |
| $^{1043}$FF_R | GCATTACCTCTTCGATTGACTTGAAGAAATCGTTCTCGTAC |

| | |
|---|---|
| $^{1043}$YYEE_F | GTACGAGAACGATTACTACGAGGAGAATCGAAGAGGTATGC |
| $^{1043}$YYEE_R | GCATACCTCTTCGATTCTCCTCGTAGTAATCGTTCTCGTAC |
| $^{909}$A_F | GTTGGCTAGCCGTGGCCGTGGCGACTCTGAAGATTGGAAGTTC |
| $^{909}$A_R | GAACTTCCAATCTTCAGAGTCGCCACGGCCACGGCTAGCCAAC |
| $^{1050}$R_F | CAAGTTCAATCGAAGACGTATGCTACCTGTAAG |
| $^{1050}$R_R | CTTACAGGTAGCATACGTCTTCGATTGAACTTG |
| $^{1050}$G_F | TCAATCGAAGAGGTATGCTACCTGTAAGATGGATGG |
| $^{1050}$G_R | AGGTAGCATACCTCTTCGATTGAACTTGTAGTAATCGTTC |

VFT$^{mGluR2}$-TK$^{AmVKR}$ chimeras were cloned according to the method by Gibson *et al.* for large fragment DNA cloning[37] (vide infra). First, fragments were amplified by PCR using the Pfu-X core kit (Jena Bioscience, #PCR-237L) with primer used from Table 3.

**Table 3: Primers for Gibson-Cloning of chimeras A-D.**

| name | sequence (5'-3') |
|---|---|
| pF_mGluR2 | AGACTGGGCAAGCCTGGGCTGGGCACCGGTGAGGGCCCGGCCAAGAAGGT |
| pR_mGluR2_A (CRD/L1$^{-/-}$) | TGTGAAACCAATGATATTGACGATCACGAAGCGAGAGGCAGGAAGAGGTC |
| pR_mGluR2_B (CRD/L1$^{-/+}$) | GGGGTAAAAATTACCGACCAATCGAGTTTCGCGAGAGGCAGGAAGAGGTC |
| pR_mGluR2_C (CRD/L1$^{+/-}$) | TGTGAAACCAATGATATTGACGATCACGAACCAGGCATCACCCCAGCGGA |
| pR_mGluR2_D (CRD/L1$^{+/+}$) | GGGGTAAAAATTACCGACCAATCGAGTTTCCCAGGCATCACCCCAGCGGA |
| pR_AmVKR (CRD/L1$^{+/-}$) | CAGGGTCAGCACCTTCTTGGCCGGGCCCTCACCGGTGCCCAGCCCAGG |
| pF_AmVKR_A (CRD/L1$^{-/-}$) | CCATCAGCCGGACCTCTTCCTGCCTCTCGCTTCGTGATCGTCAATATCATTGGTT |
| pF_AmVKR_B | CCATCAGCCGGACCTCTTCCTGCCTCTCGCGAAACTCGATTGGTCG |

| | |
|---|---|
| (CRD/L1$^{-/+}$) | GTAATTTTTAC |
| pF_AmVKR_C (CRD/L1$^{+/-}$) | CAGGAGTACATCCGCTGGGGTGATGCCTGGTTCGTGATCGTCAATATCATTGGTT |
| pF_AmVKR_D (CRD/L1$^{+/+}$) | CAGGAGTACATCCGCTGGGGTGATGCCTGGGAAACTCGATTGGTCGGTAATTTTTAC |

The PCR reaction was subjected to DpnI (NEB, #R0176S) digestion for 2 hours at 37 °C and DNA-fragments were purified using the QIAquick PCR purification (Qiagen, #28104). Gibson master mix and assembly buffer was prepared according to Gibson et al., and the corresponding fragments were incubated for 1 hour at 50 °C, before transforming into competent *E. coli* cells. Cells were plated on Amp-resistant agar plates and colonies were picked the next day for outgrow in 5 mL LB/Amp medium. DNA extraction and purification was performed using a DNA purification kit (Jena Bioscience, #PP-201L), and constructs were characterized first by gel electrophoresis and further by didesoxy-PCR full sequencing by using primers depicted in Table 4. Full sequences of all constructs can be found in the Appendix.

**Table 4: Sequencing primers for VFT$^{mGluR2}$-TK$^{AmVKR}$ chimeras A-D.**

| name | sequence (5'-3') |
|---|---|
| SNAP_end | GTGAAAGAGTGGCTGCTG |
| v2.1 | ACATCTGCGTGGCCACTT |
| v2.2 | CGCTACCAGAAGGTAGGC |
| v2.3 | ATCGTCAATATCATTGGT |
| 4F | ATGCTACCTGTAAGATGG |

### 5.4.4 Cloning of VFT$^{mGluR2}$-TK$^{hIR}$ Chimeras and Mutants

Tyrosine kinase domain was amplified by PCR using the GoTaq® HotStart (Promega, #M5001) kit according to the manufacturer's instructions. Primers

used were forward 5'-AGCGGCCGCGCCCGTCAAATATTGCAAAAAT-3' and reverse 5'-ATCTAGATTAGGAAGGATTGGACCGAGGCAAG-3'. The desired 1.2 kB-fragment was isolated and purified (Qiagen, #28704) by gel electrophoresis. The fragment was subcloned into a TOPO®-vector (Invitrogen, #KA4510-20) and transformed into T1 phage resistant chemically competent *E. coli* cells according to the manufacturer's instructions and plated on Kan-resistant agar plates. Colonies were picked and grown for 16 hours o.n. in LB/Kan medium. After mini-preparation of the DNA from 4 mL of cell culture (Macherey-Nagel, #740588.250), the insert was cut with NotI (NEB, #R0189S) and XbaI (Roche, #674 257) restriction enzymes in buffer H (Roche, #11417991001) for 1 hour at 37 °C and purified by gel electrophoresis (~1.2 kB-fragment). In parallel, $VFT^{mGluR2}$-$TK^{Met}$ construct was cut with the same restriction enzymes under the same conditions and also purified by gel electrophoresis (~8 kB-fragment). Ligation was performed by using the TAKARA ligation kit (Clontech, #6023) and following the 30 minute/16 °C manufacturer's protocol with subsequent transformation into T1 phage resistant chemically competent *E. coli* cells, plated on Amp-containing agar plates. Colonies were picked and grown for 16 hours at 37 °C o.n. in LB/Amp medium and DNA purification was achieved as described above. The final construct was characterized by didesoxy-PCR sequencing.

Further site-directed mutagenesis was performed using the QuikChange Lightning Site-Directed Mutagenesis Kit (Agilent Technologies, #210509) according to the manufacturer's instructions. Primer for the creation of the L300C mutant and for the transmembrane domain elongation/truncation are shown in Table 6.

**Table 5:Primer for creating the L300C mutant**

| name | sequence (5'-3') |
|---|---|
| L300C_v1_F | CGGCTGGGGGGCCTGCGAGA |
| L300C_v1_R | CCACCACGCTCTCGCAGGCCC |
| L300C_v2_F | GGCCTGCGAGAGCGTGGTGG |
| L300C_v2_R | CCACCACGCTCTCGCAGGCC |
| L300C_v3_F | GATCTGCGAGAGCGTGGTGGCAGGCAGTG |

| | |
|---|---|
| L300C_v3_R | GATCGCAGGCCCCCCAGCCGTCGCT |

**Table 6: Primer for transmembrane domain extension/truncation of the mGluR2_hIR construct.**

| name | sequence (5'-3') |
|---|---|
| LL1_TMext_F | GCAAAAATTATCATCATTGGCCCCCTCATCTTT |
| LL1_TMext_R | AAAGATGAGGGGGCCAATGATGATAATTTTTGC |
| LL1_TMtrun_F | ATTGCAAAAATTATCGGCCCCCTCATCTTT |
| LL1_TMtrun_R | AAAGATGAGGGGGCCGATAATTTTTGCAAT |

### 5.4.5 45-Pathway Kit Signaling Pathway Description

**Table 7: 45-Pathway kit abbreviations and according transcription factor.**

| Reporter | Pathway | Transcription Factor |
|---|---|---|
| AARE | Amino Acid Deprivation Response | ATF4/ATF3/ATF2 |
| AR | Androgen Receptor | Androgen Receptor |
| ARE | Antioxidant Response | Nrf2 & Nrf1 |
| ATF6 | ATF6 | ATF6 |
| C/EBP | C/EBP | C/EBP |
| CRE | cAMP/PKA | CREB |
| E2F | Cell Cycle | E2F/DP1 |
| p53 | p53/DNA Damage | p53 |
| EGR1 | EGR1 | EGR1 |
| ERSE | Endoplasmic Reticulum Stress | CBF/NF-Y/YY1 |
| ERE | Estrogen Receptor | Estrogen Receptor |
| GATA | GATA | GATA |
| GRE | Glucocorticoid Receptor | Glucocorticoid Receptor |
| HSR | Heat Shock Response | HSF |
| MTF1 | Heavy Metal Stress | MTF1 |

| | | |
|---|---|---|
| GLI | Hedgehog | GLI |
| HNF4 | Hepatocyte Nuclear Factor 4 | HNF4 |
| HIF | Hypoxia | HIF-1 |
| IRF1 | Interferon Regulation | IRF1 |
| ISRE | Type I Interferon | STAT1/STAT2 |
| GAS | Interferon Gamma | STAT1/STAT1 |
| KLF4 | KLF4 | KLF4 |
| LXR | Liver X Receptor | LXRa |
| SRE | MAPK/ERK | Elk-1/SRF |
| AP1 | MAPK/JNK | AP-1 |
| MEF2 | MEF2 | MEF2 |
| Myc | c-myc | Myc/Max |
| Nanog | Nanog | Nanog |
| RBP-Jk | Notch | RBP-Jk |
| NFκB | NFκB | NFκB |
| Oct4 | Oct4 | Oct4 |
| Pax6 | Pax6 | Pax6 |
| FOXO | PI3K/AKT | FOXO |
| NFAT | PKC/Ca++ | NFAT |
| PPAR | PPAR | PPAR |
| PR | Progesterone Receptor | Progesterone Receptor |
| RARE | Retinoic Acid Receptor | Retinoic Acid Receptor |
| RXR | Retinoid X Receptor | Retinoid X Receptor |
| Sox2 | Sox2 | Sox2 |
| SP1 | SP1 | SP1 |
| STAT3 | STAT3 | STAT3 |
| SMAD | TGFβ | SMAD2/SMAD3/SMAD4 |
| VDR | Vitamin D Receptor | Vitamin D Receptor |
| TCF/LEF | Wnt | TCF/LEF |
| XRE | Xenobiotic | AhR |

# *6 Acetylcholinesterase*

Parts of this work have been published in *Angewandte Chemie International Edition* **2014**, *53*, 7657-60.[43]

## 6.1 Introduction

Synaptic communication is largely based on small diffusible molecules (neurotransmitters) that translate electrical signals into chemicals ones.[44] Once released from presynaptic vesicles, these neurotransmitters cross the synaptic cleft in order to stimulate receptors, *i.e.* ligand-gated ion channels and G-protein coupled receptors, on the postsynaptic side. A third essential component of synaptic transmission consists of transporters or enzymes that remove or inactivate the neurotransmitter, respectively, to prevent tonic stimulation and allow for the meaningful integration of signals.

Among the diverse set of neurotransmitters that mediate chemical communication in humans, acetylcholine (ACh) is especially important. When released into the synapse, it stimulates nicotinic and muscarinic acetylcholine receptors to modulate cellular excitability. Fast inactivation is achieved by acetylcholinesterase (AChE), which hydrolyzes ACh to acetate and choline with diffusion-controlled kinetics (Figure 23a).[45] A large number of AChE inhibitors are known, which range from drugs, such as tacrine (**THA**), to research tools, such as decamethonium (**DECA**), and nerve gases, such as sarin (Figure 23b). Many of these have been co-crystallized with AChE, providing detailed insights into the mode of action of this enzyme and its inhibitors.[46] Some of these are also clinically relevant, since they raise acetylcholine levels, which has beneficial effects to patients suffering from, for instance, Alzheimer, myasthenia gravis and glaucoma.[47]

In recent years, the control of neural systems with light has become a major scientific frontier. Light is non-invasive and can be applied with very high temporal and spatial control. It can interact with genetically encoded photoreceptors ("Optogenetics")[48] or with photoswitchable drugs that target native receptors and change their efficacy upon photoisomerization (Figure 23c). We call the latter approach "photopharmacology",[2] and it has been applied to: the optical control of ion channels[9,25] and GPCRs,[42] the restoration of visual response in blind mice[49] and the control of nociception mediated by DRG-neurons.[50]

Enzymes, such as AChE, that have fast kinetics and a large influence on the activity of neural networks are also a prime target for photopharmacology. Indeed, AChE has been investigated in this respect form early in the development of the field. Pioneering studies from the late 1960's and early 1970's by Erlanger and colleagues show that photoregulation of AChE could be achieved with azobenzene-based quaternary ammonium ions that mimic ACh, such as *p*-phenylazophenyl-trimethylammonium and *N*-*p*-phenylazophenylcarbamylcholine (Figure 23d).[51-53] Photocontrol of an AChE isolated from the scorpion *Heterometus fulvipes* was achieved by exposure to sunlight.[52] Activity was measured by a reaction between non-hydrolyzed ACh and hydroxylamine, followed by photometric quantification of an iron-complex,[54] thus providing a proof of concept for a photoswitchable enzyme inhibitor.

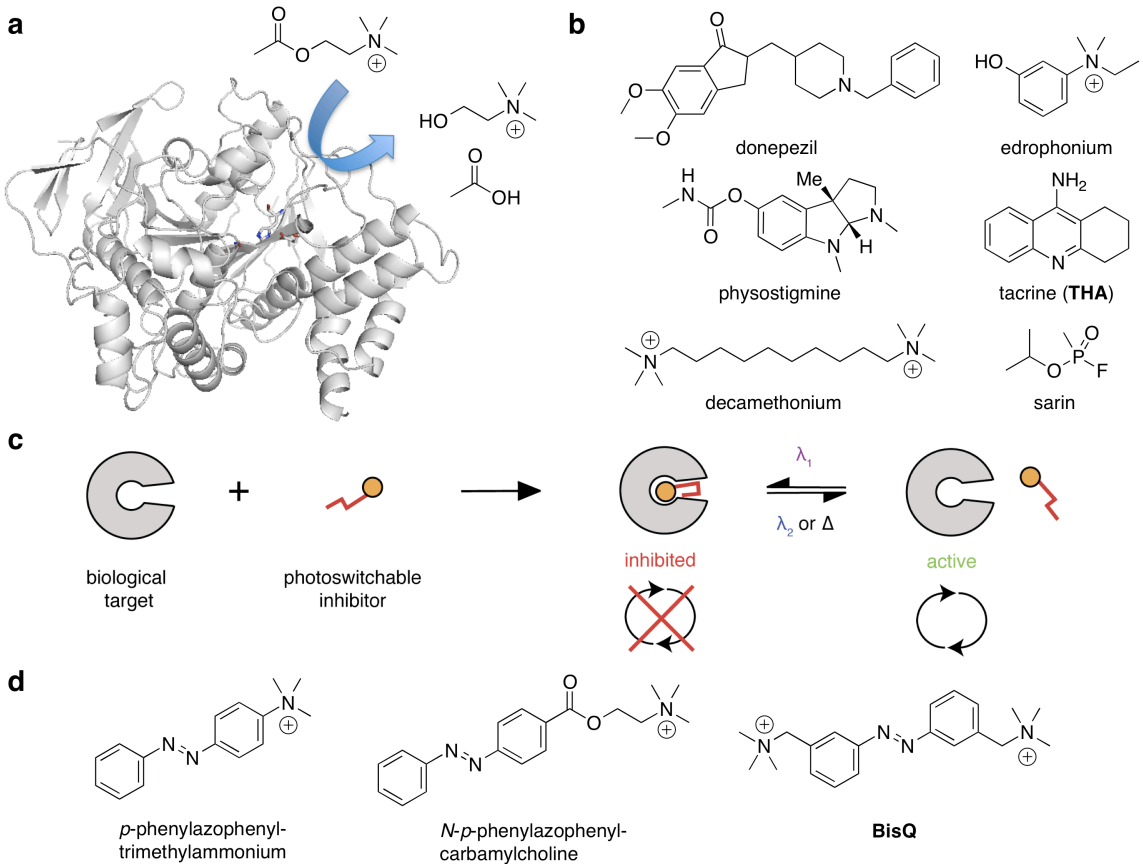


**Figure 23: AChE function and inhibition. a)** AChE (pdb: 1ACJ)[55] catalyzes the hydrolysis of acetylcholine (ACh) with water to acetate and choline. **b)** Ligands for AChE inhibition. **c)** Photopharmacological control of an enzyme with a photochromic inhibitor. **d)** Photochromic molecules used to control the cholinergic system.

## 6.2 Results and Discussion

Since Erlanger's pioneering studies, the ability to heterologously express enzymes, reliably assay them, study them with X-ray crystallography, and rationally design ligands has much improved. In addition, the precise delivery of light of a given wavelength and intensity has become more practical, recently driven by the rapid development of Optogenetics. Given the longstanding interest in the optical control of neural systems in the Trauner group, a reinvestigation of photochromic blockers of mammalian, *i.e.* human acetylcholine esterase was envisioned in order to explore new chemotypes that could prove to be useful in neuroscience.

In order to quickly assay human AChE activity in the presence of a photoswitchable inhibitor, a commercially available kit that is offered to measure AChE content in a variety of biological samples was modified.[56] It utilizes the intrinsic ability of AChE to cleave acetyl*thio*choline, which subsequently reacts with Ellman's reagent to liberate a colored thiolate (Figure 24a). Using a UV/Vis spectrometer, it is possible to photometrically follow the appearance of the thiolate at $\lambda$ = 410 nm, while alternately irradiating with an orthogonal light beam of different wavelengths, to reversibly trigger photoswitching (Figure 24b).

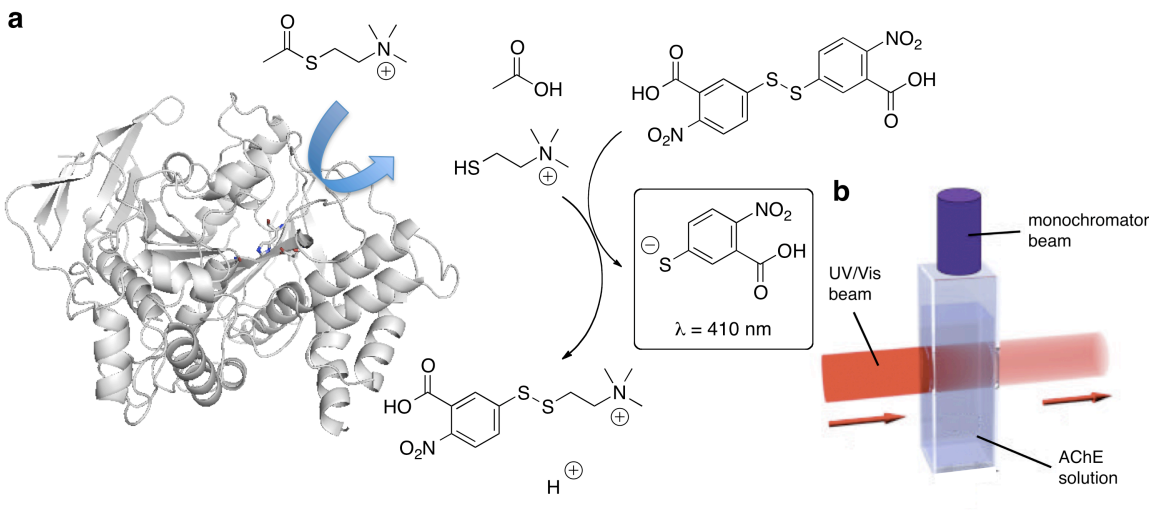


**Figure 24: Colorimetric assay for measuring AChE activity in the presence of a photoswitchable blocker. a)** Hydrolysis of acetylthiocholine yields thiocholine, which reacts with Ellman's reagent to yield a colored thiolate ($\lambda_{max}$ = 410 nm). **b)** Schematic representation of the experimental configuration.

Initial efforts were directed towards the doubly charged ACh mimic **BisQ** (Figure 23d), which was developed by Erlanger and Lester as a photoswitchable agonist for the nicotinic acetylcholine receptor,[57] but had not been described as photoswitchable inhibitor of AChE. Given its resemblance with decamethonium, it was hypothesized that it could also act as a photochromic inhibitor of the enzyme as well. **BisQ** is indeed a blocker of human AChE in the dark ($K_i$ = 3.13 μM, Table 8) but one which does not significantly change its activity upon photoisomerization. This result and an inspection of the X-ray structure of decamethonium bound to AChE (pdb: 1ACL)[55] imply that **BisQ** does not simultaneously occupy both cationic binding sites when blocking the enzyme. Thus, one can hypothesize that both isomeric forms of **BisQ** exhibit comparable blocking characteristics.

A systematic exploration of AChE X-ray structures showed that the inhibitors tacrine (**THA**) (pdb: 1ACJ)[55] and 9-benzyl **THA** (pdb: 1DX4)[58] occupy the catalytic site of the enzyme while being partially solvent-exposed. The knowledge that substitution in the 9-position of **THA** is tolerated enabled the design of several azobenzene derivatives that are termed **AzoTHA**s (Scheme 1a).

The small series includes a minimally substituted azobenzene (**AzoTHA**), an ester derivative thereof (**AzoTHA-2**) and a triazole (**AzoTHA-3**), which was made by "click-chemistry" to pave the way for rapid diversification. Furthermore, a red-shifted version was obtained by the introduction of an electron-donating diethyl amine moiety (**AzoTHA-4**). The synthesis of **AzoTHA** started with the condensation of anthranilic acid (**6.1**) and cyclohexanone (**6.2**) in refluxing phosphoryl chloride to yield 9-chloro-**THA** (**6.3**).[59] After recrystallization from acetone, single crystals of **6.3** were obtained suitable for X-ray diffractometry (see Experimental). Aromatic substitution of the chloride with 4-(2-aminoethyl)aniline (**6.4**) enabled by catalytic amounts of sodium iodide in refluxing phenol yielded phenethylamine derivative **6.5**. This transformation might proceed *via* a Finkelstein-type halogen exchange, with the iodide being a better leaving group with respect to the chloride. However, the reaction has not been carried out without the addition of NaI due to substantial amounts of product obtained for further synthesis, therefore no conclusions can be made. Finally, the azobenzene moiety was installed *via* Mills reaction using nitrosobenzene (**6.6**) (Scheme 1b). As a "regular" azobenzene, **AzoTHA** could be switched to its *cis*-form with UV-light ($\lambda$ = 350 nm) and back to its *trans*-form using blue light ($\lambda$ = 440 nm) (Scheme 1b, c). The small change in the $\pi$-$\pi^*$-band upon irradiation can be partly attributed to the underlying absorption of the quinoline chromophore of **THA** (black line, Scheme 1c).

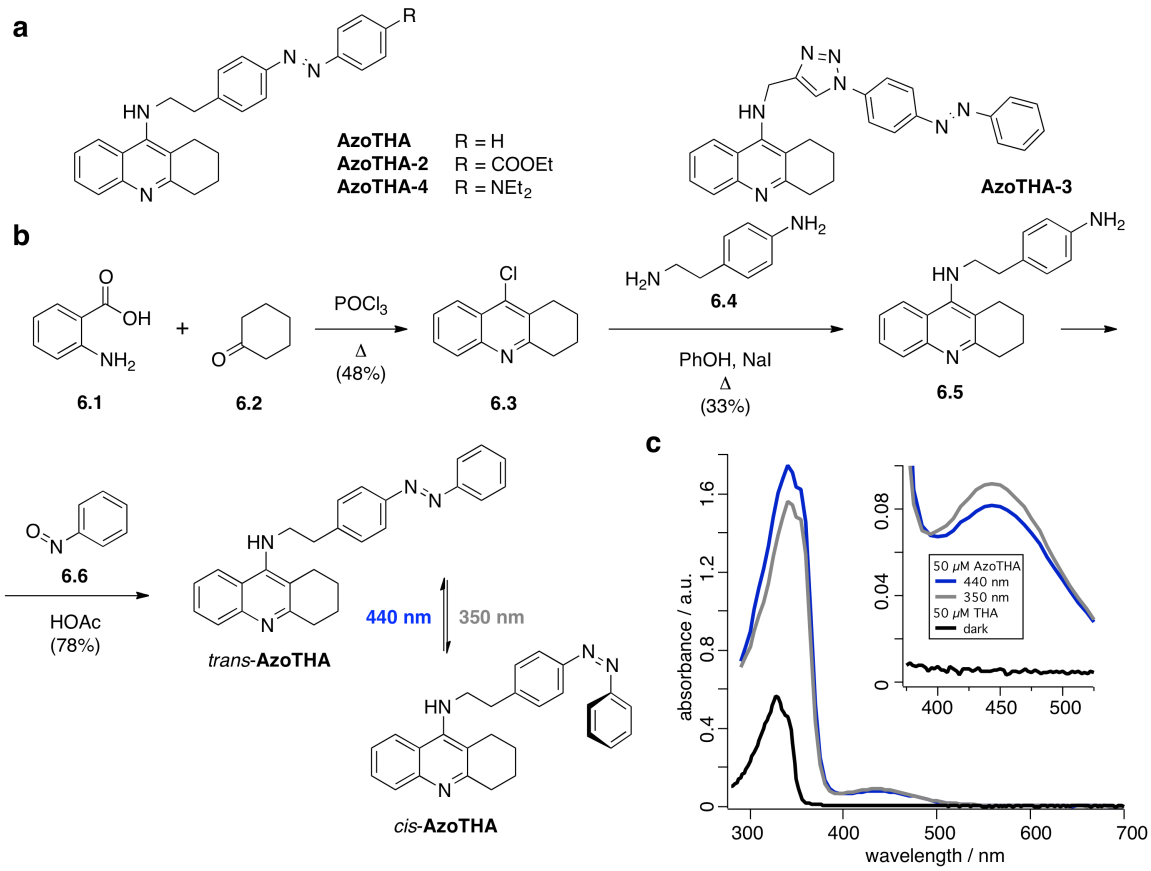


**Scheme 1: Design, synthesis and spectroscopy of AzoTHAs. a)** A three compound library of tacrine-derived photoswitches. **b)** Three step synthesis yields the photochromic AChE blocker **AzoTHA**, which exhibits reversible *cis*-/*trans*-isomerisation using UV light (λ = 350 nm) and blue light (λ = 440 nm). **c)** UV/Vis spectra of the *cis*- (gray) and *trans*-isomer (blue) of **AzoTHA** (insert: expansion of the n-π* band) and **THA** (black).

**AzoTHA-2** was synthesized by submitting **6.5** to a Mills reaction with nitroso compound **6.7** in acetic acid and was isolated in 31% yield (Scheme 2a). The spectral characteristics are shown in Scheme 2b in the same manner as for **AzoTHA**.

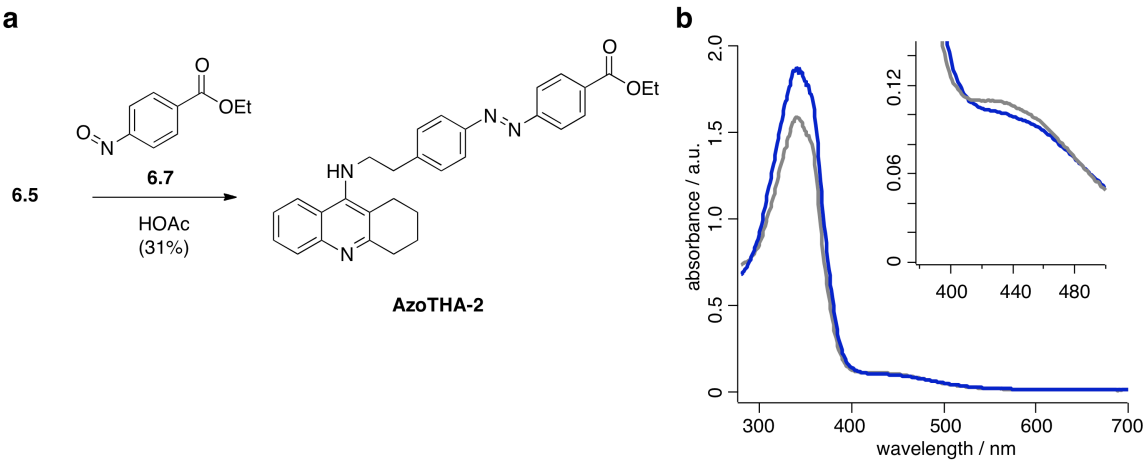


**Scheme 2: Synthesis of AzoTHA-2. a)** Synthesis of **AzoTHA-2** via a Mills reaction between aniline **6.5** and nitroso compound **6.7**. **b)** UV/Vis spectra of *trans*- (blue) and *cis*- state (gray) (insert: expansion of the n-π* band).

In order to obtain **AzoTHA-3** *via* alkyne-azide click chemistry, the precursors had to be synthesized. Propargyl tacrine **6.9** was obtained by aromatic substitution of chlorotacrine **6.3** by propargylamine (**6.8**) in refluxing phenol with the addition of catalytic amounts of sodium iodide (Scheme 3a). The corresponding azide-containing azobenzene **6.11** was synthesized from amino azobenzene **6.10** by diazoation with a nitrite source and subsequent [3+2]- and retro-[3+2] cycloadition with TMS-azide in 91% yield (Scheme 3b). Final "click" was performed with a copper(II) source and sodium ascorbate as an *in situ* reductant to give **AzoTHA-3** in 41% yield (Scheme 3c). Spectral characteristics of the *cis*- and *trans*-isomer are depicted in Scheme 3d in the same manner as for **AzoTHA**.

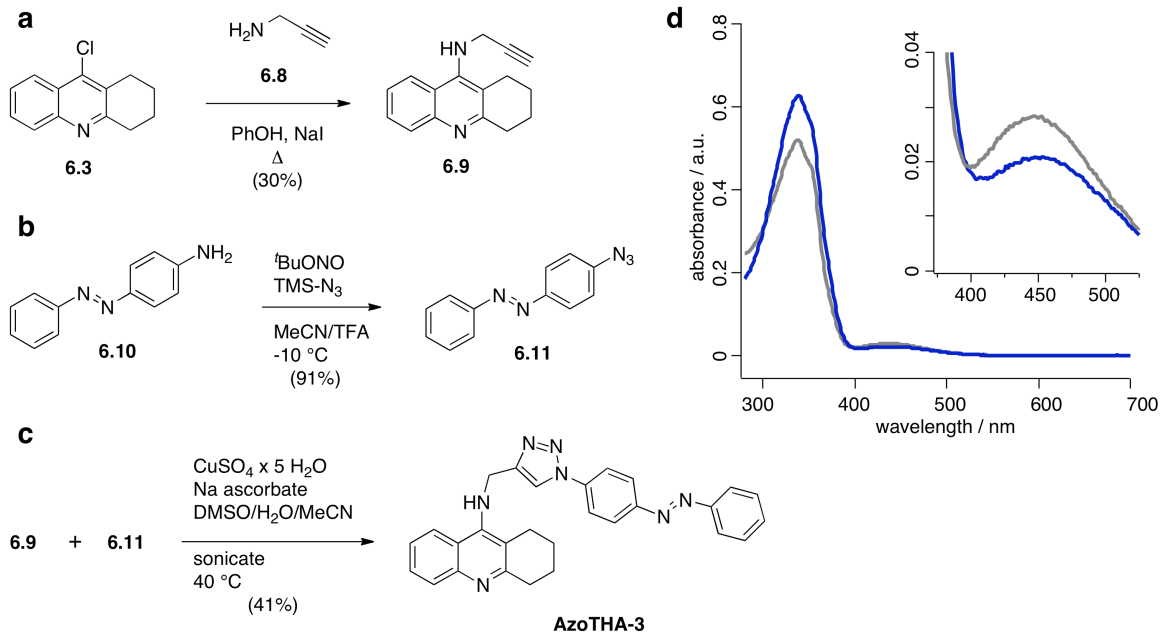


**Scheme 3: Synthesis of AzoTHA-3. a)** 9-chloro-THA (**6.3**) was subjected to aromatic substitution with propargyl amine (**6.8**) to yield 9-propargyl-THA (**6.9**). **b)** 4-azido azobenzene (**6.11**) was obtained from 4-amino azobenzene (**6.10**). **c)** Click reaction between alkyne **6.9** and azide **6.11** to yield **AzoTHA-3**. **d)** UV/Vis spectra of *trans*- (blue) and *cis*- (grey) state (insert: expansion of the n-π* band).

A red-shifted version of **AzoTHA** was also obtained starting from amine **6.5**. By diazotation and trapping the resulting diazonium salt with *N*,*N*-diethylaniline yielded **AzoTHA-4** in 49% yield (Scheme 4a). This transformation showcases the synthetic variability of aniline **6.5**, which can subjected to Mills reactions or diazonium couplings to obtain further derivatized tacrine containing PCLs with different substitution patterns and spectral characteristics. Even more, crystals of **AzoTHA-4** suitable for X-ray diffractometry were obtained by letting a concentrated solution in DMSO stand at room temperature open to the atmosphere. The solved structure can be seen in Scheme 4b. **AzoTHA-4** shows a red-shift in its π-π*-band resulting in a $\lambda_{max}$ = 440 nm. Consequently, **AzoTHA-4** can be switched with visible blue light (Scheme 4c, blue) while it relaxes in the dark (Scheme 4c, black).

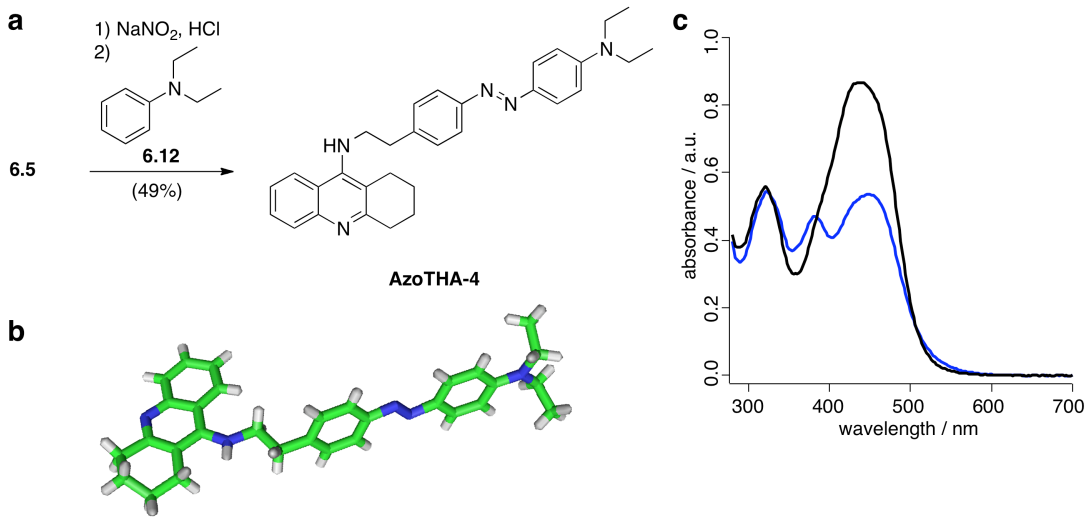


**Scheme 4: Synthesis of AzoTHA-4. a)** Synthesis of **AzoTHA-4** *via* diazotation and azo-coupling by again employing intermediate **6.5**. **b)** Crystal structure of **AzoTHA-4**. **c)** UV/Vis spectra of *trans*- (black) and *cis*- (blue) state in the dark and under illumination with λ = 440 nm, respectively (insert: expansion of the n-π* band).

Last, but not neast, **AzoTHA-5** was synthesized based on a different structural approach where the diazene unit is directly linked to the quinoline core. Initial studies commencing with **THA** proved to be unsuccessful by either employing diazotization (although the diazonium salt can presumably be formed, based on observed color change) or by a Mills reaction (Scheme 5a, data not shown). However, by adapting the synthetic approach of **AzoTHA**s mentioned above, **6.3** was reacted with phenylhydrazine (**6.13**) to give the quinoline hydrazine **6.14**, which was prone to oxidation when exposed to air. Therefore, **6.14** was only characterized briefly (*i.e.* LCMS and HRMS) in order to be oxidized completely to obtain **AzoTHA-5** (Scheme 5b). Interestingly, a side-reaction was observed probably by a radical mechanism that links the hydrazine nitrogen to the benzylic carbon to form the pyrazole **6.15**. The UV/Vis spectrum of **AzoTHA-5** was acquired (Scheme 5c), but no spectral changes were observable upon reversible illumination with 360 and 460 nm. Due to this fact further evaluation of **AzoTHA-5** was postponed and to be carried out in the future.

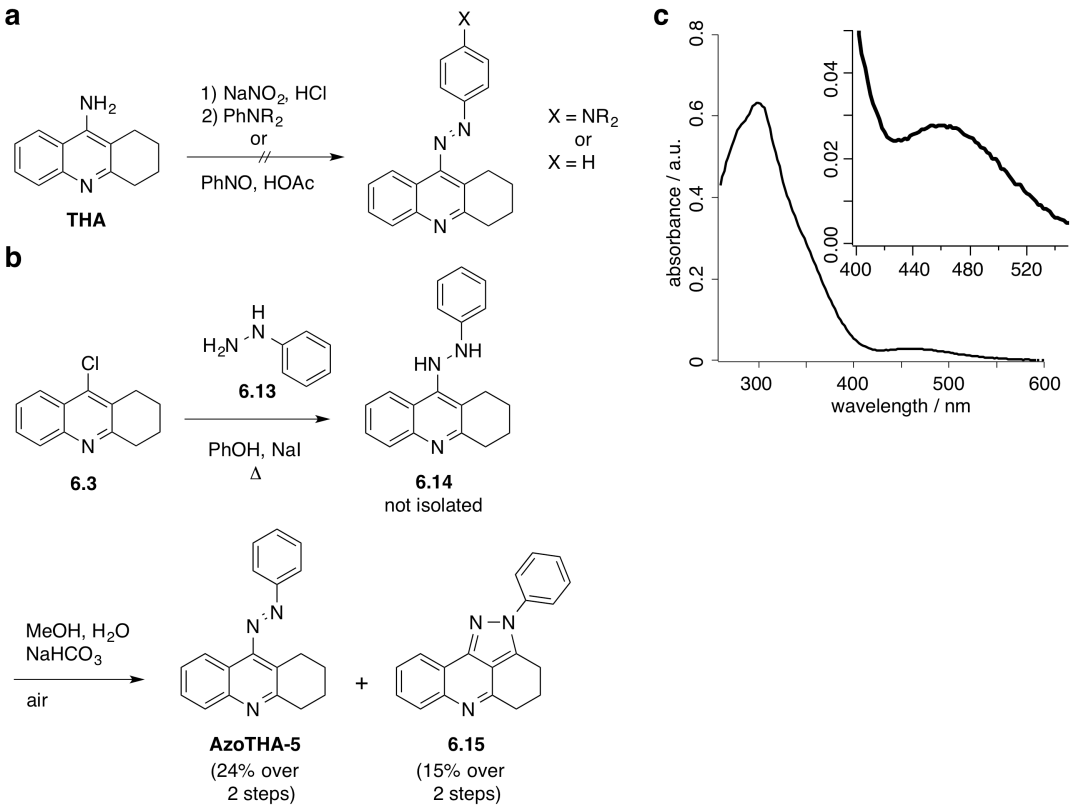


**Scheme 5: Synthesis of AzoTHA-5. a)** The diazene unit could not be installed starting from **THA** neither with a diazotation nor with a Mills reaction. **b) 6.3** was reacted with phenylhydrazine (**6.13**) in an nucleophilic aromatic substitution to give **6.14** that was directly oxidized under aerobic conditions to **AzoTHA-5** and pyrazole **6.15** in a side reaction. **c)** UV/Vis spectra of **AzoTHA-5** (insert: expansion of the n-π* band).

Switching kinetics of **AzoTHA** were measured with the assay setup described in Figure 24. Dark-adapted **AzoTHA** in PBS buffer showed a different spectrum than in DMSO (Figure 25a), and switching (*i.e.* change of the π-π*- and the n-π*-band) was not observable in aqueous solvents. Therefore, kinetic experiments were conducted in DMSO and fitted the according slopes exponentially (Figure 25b). Cycles were 9 minutes long and started with the dark-adapted state and irradiation of λ = 350 nm while observing the absorbance change at both the π-π*-band (Figure 25c) at λ = 350 nm and the n-π*-band (Figure 25d) at λ = 440 nm. Exposure to λ = 440 nm led to the *trans*-isomer but not in yields comparable to the dark-adapted state. Furthermore, after another cycle of λ = 350 nm and

subsequent shutting the light off, **AzoTHA** showed bi-stability in the measured minute timeframe (the relevant timeframe for our biological experiments).

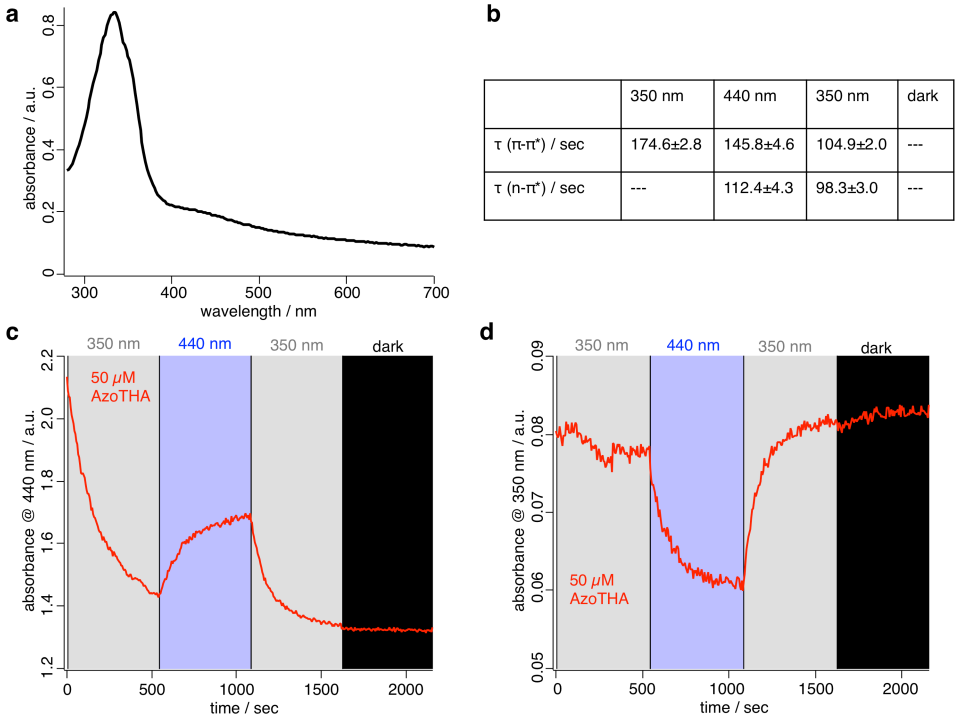


| | 350 nm | 440 nm | 350 nm | dark |
|---|---|---|---|---|
| τ (π-π*) / sec | 174.6±2.8 | 145.8±4.6 | 104.9±2.0 | --- |
| τ (n-π*) / sec | --- | 112.4±4.3 | 98.3±3.0 | --- |

**Figure 25: Switching kinetics of AzoTHA. a)** UV/Vis spectra of 50 µM **AzoTHA** in PBS buffer, **b)** τ-values for **AzoTHA**, observed in change of absorbance at the π-π*- and the n-π*-band in seconds, **c)** kinetic trace of **AzoTHA** followed at λ = 350 nm and **d)** λ = 440 nm.

**AzoTHA** in its dark-adapted form inhibits AChE with a $K_i$ of approximately 100 nM, while **AzoTHA-2**, **AzoTHA-3** and **AzoTHA-4** showed significantly lower affinities (Figure 26, Table 8). As such *trans*-**AzoTHA** is about tenfold less active than **THA**, but more active than decamethonium (**DECA**) and **BisQ** (See Experimental for the synthesis and characterization of **THA**).

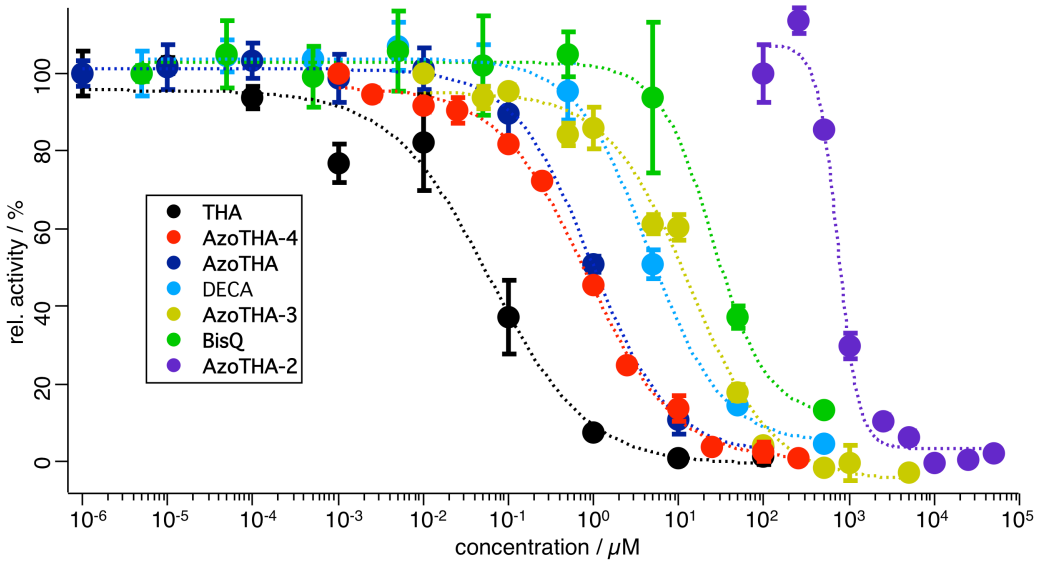


**Figure 26: Colorimetric endpoint measurement to determine $IC_{50}$ values for various AChE blockers. THA** (black), **AzoTHA** (dark blue), **AzoTHA-2** (purple), **AzoTHA-3** (yellow), **AzoTHA-4** (red), **BisQ** (green) and **DECA** (cyan).

**Table 8: Inhibitory constants ($K_i$) of AChE blockers (N=3, mean±S.D.).**

| | THA | Azo THA | Azo THA-2 | Azo THA-3 | Azo THA-4 | DECA | BisQ |
|---|---|---|---|---|---|---|---|
| $K_i$ | 6.40 | 95.35 | 78400 | 10807 | 76500 | 457.8 | 3130 |
| (nM) | ±3.20 | ±12.39 | ±3600 | ±1070 | ±3230 | ±52.0 | ±1180 |

Having determined the $K_i$ of **AzoTHA**, the photo-dependent activity of this particular enzyme inhibitor at this concentration was assessed. In photopharmacology, it is generally advisable to employ concentrations close to the $K_i$ (or $EC_{50}$) of the dark-adapted state, since the largest dynamic change can be expected in this region. When 0.05 U/mL of AChE was incubated with 1.0 µM of **AzoTHA**, photodependent activity could be induced (Figure 27a). By contrast, **AzoTHA-2** and **AzoTHA-4** exhibited no photodependent activity, while **AzoTHA-3** activity was low. The subsequent investigations were therefore focused on **AzoTHA** (Fig. 27). Activity was reduced to 17% compared with unblocked AChE when the sample was irradiated with blue light (λ = 440 nm) and was almost abolished (4% activity) when the light was switched to UV (λ =

350 nm). Thus, **AzoTHA** is more active as an inhibitor in its *cis*-state and becomes less active in the dark-adapted *trans*-state. This effect could be repeated over many cycles with no apparent loss of activity (Figure 27b, c). Fitting the off- and on-sets-slopes of photoswitching exponentially, the $\tau_{on/off}$ values remain stable (Figure 27d) over the cycles and their average can be determined as $\tau_{off}$ = 4.74 ± 1.81 seconds and $\tau_{on}$ = 4.17 ± 1.09 seconds, which represents a benchmark point into enzymatic photopharmacology.

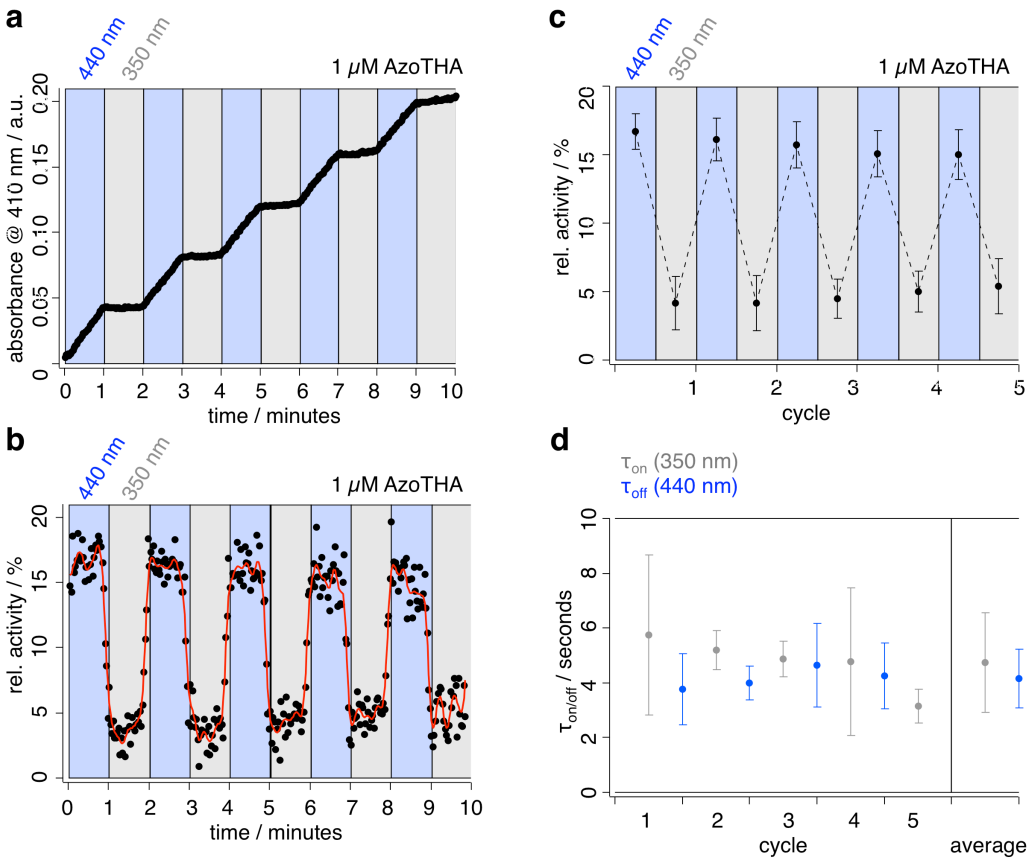


**Figure 27: *In vitro* photocontrol of AChE with AzoTHA. a)** Hydrolysis of acetylthiocholine in the presence of AChE (0.05 U/mL), **AzoTHA** (1 µM) and irradiated with either blue light (λ = 440 nm, blue bars) or UV-light (λ = 350 nm, grey bars). **b)** Reversible photocontrol of AChE (0.05 U/mL) with 1 µM **AzoTHA** controlled by blue light (λ = 440 nm, blue bars) and UV-light (λ = 350 nm, grey bars). Black dots show data points derived from the initially recorded slope (see a) of catalytic activity, red line shows binomial fit. **c)** Average light-dependent activity calculated from b over 5 cycles. **d)** $\tau_{off}$ (gray) and $\tau_{on}$ (blue) values for the

repeated deactivation and activation over several cycles (left side) and their averaged values (right side). Error bars show S.D.; N=3 for all experiments.

To establish that **AzoTHA** can be used to control physiological responses with light *in vitro*, the next experiments were aimed at *in vivo* evaluation of **AzoTHA** in the mouse trachea. The smooth muscle of this airway constricts in response to ACh, which is an effect that can be recorded by force transducers, an assay known as tracheal tensometry.[60] Electrical field stimulation (EFS) leads to the release of ACh at the neuromuscular endplate, in an experimental setting similar to the classical Loewi experiment.[1] When the electrical stimulation is shut off, ACh release from nerve fibers ceases and the relaxation kinetics of the trachea reflect AChE activity as the enzyme is degrading ACh. The high affinity AChE blocker physostigmine was used as reference in the conducted experiments. At 10 μM, physostigmine induced a constriction of the preparation even without further EFS (Figure 28a) which is attributed to a direct activation of acetylcholine receptors in addition to AChE inhibition.[61] In contrast, 50 μM **AzoTHA** in the dark did not evoke an increase in the basal tone (Figure 28a), thus providing a pharmacologically cleaner tool to study cholinergic systems. When **AzoTHA** treated (50 μM) tracheas were stimulated by EFS (100 Hz, 10 V, 2 ms) different relaxation kinetics were observed when irradiated with UV-light *versus* blue light (Figure 28b). The observed kinetics ($\tau_{off}$) are in agreement with our previously performed *in vitro* experiments: in the presence of *cis*-**AzoTHA** (UV irradiation), AChE is inhibited to a larger extent and ACh clearance kinetics are significantly slower ($\tau_{off,\ cis}$ = 15.25 ± 1.48 seconds) when compared to *trans*-**AzoTHA** (blue light, $\tau_{off,\ trans}$ = 11.29 ± 0.77 seconds). In the absence of an inhibitor ACh is cleared even faster ($\tau_{off}$ = 4.81 ± 0.95 seconds) (Figure 28c). These results demonstrate an increase in inhibition of 61% under UV light irradiation when background is subtracted.

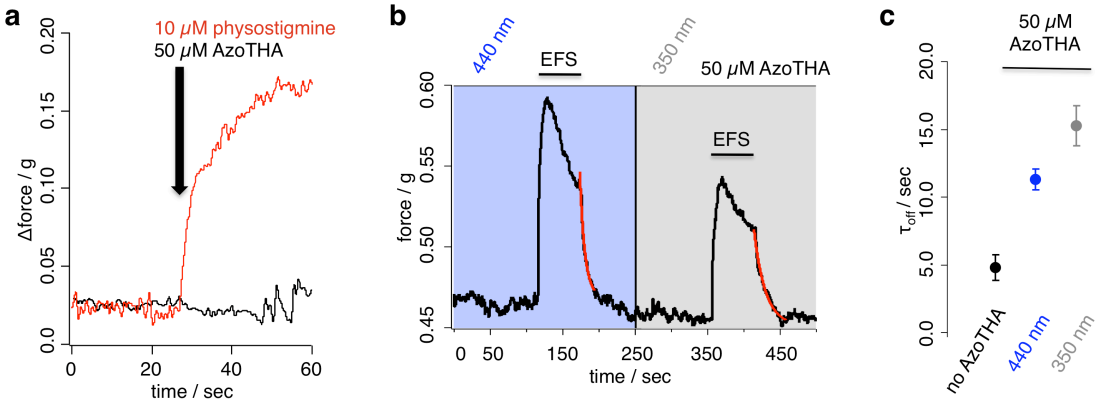


**Figure 28: *In vivo* photocontrol of AChE with AzoTHA. a)** Basal tonus is not affected by **AzoTHA** (50 µM, black) but with physostigmine (10 µM, red) in mouse trachea preparations. **b)** Relaxation kinetics are slower under irradiation with UV light (350 nm) than with blue light (440 nm) in mouse trachea preparations (50 µM **AzoTHA**, EFS, 100 Hz, 10 V, 2 ms). **c)** $\tau_{off}$ values fitted from **b)** with no blocker (black) and with **AzoTHA** (50 µM) under blue (λ = 440 nm, blue) and UV light (λ = 350 nm, gray); (N=3, mean±SD, t-test: $p$=0.02).

Control experiments included repetitive EFS without any drug, and in the presence of physostigmine instead of **AzoTHA**. Figure 29a shows a decrease in amplitude after consecutively applied EFS as was also observed in AzoTHA incubated trachea. The AChE blocker physostigmine increased basal tonus (Figure 29b) and had a more pronounced effect on relaxation kinetics (Figure 29c, d).

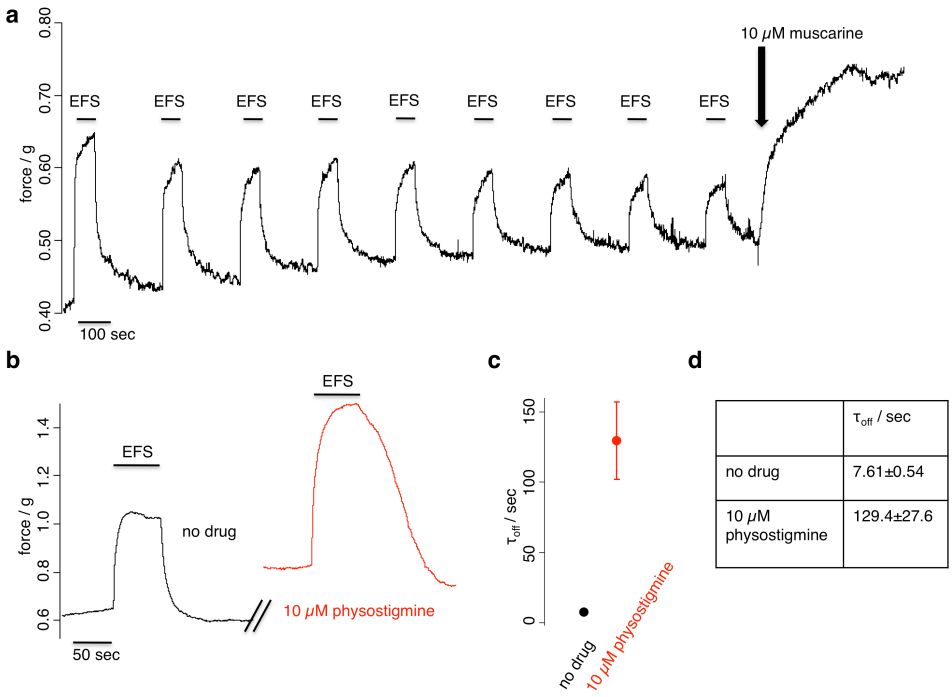


| | $\tau_{off}$ / sec |
|---|---|
| no drug | 7.61±0.54 |
| 10 μM physostigmine | 129.4±27.6 |

**Figure 29: Tracheal tensometry control experiments. a)** Repetitive trains (1 min each) of EFS (100 Hz, 10 V, 2ms) result in a gradual decrease of the constrictory response; still, the trachea remains responsive to 10 µM muscarine. **b)** Basal tone and time to return to relaxation after cessation of EFS are increased in the presence of physostigmine (10 µM) (red). Relaxation kinetics are shown in **c)** and in numbers in **d)** (mean±S.D.; N=4 tracheas).

Nevertheless, kinetics under UV- and blue light followed consistend trends (see Experimental), irrespective of the order in which they were applied and EFS was conducted.

## 6.3 Summary and Outlook

In summary, several novel photochromic inhibitors of AChE, one of the most important enzymes involved in synaptic transmission have been rationally designed and synthesized. Starting with a commercially available AChE assay kit, a generally applicable method to monitor photochromic AChE inhibitors was developed. Using this *in vitro* assay, it was found that one of the molecules, **AzoTHA**, can reversibly switch enzymatic activity using light in a fast manner. **BisQ**, a known photochromic agonist of acetylcholine receptors, was also determined as a blocker that has no photodependent effect on AChE activity. Further biological evaluation showed that **AzoTHA** does have a light-dependent effect on AChE kinetics in mouse trachea preparations with improved characteristics (such as not increasing the basal tonus) compared to physostigmine. In accordance with *in vitro* data, AChE activity can be inhibited to a greater extent with UV light.

A different publication from Decker and co-workers demonstrates control of AChE activity with a diarylethene photoswitch resulting in optical control of β-amyloid aggregation.[62] However, due to the long irradiation times necessary to achieve photoswitching and the different biological goal, this tool is not comparable to **AzoTHA**, which works on a timescale of seconds and on the neuromuscular endplate. This study remains the first example of manipulating neural communication *via* optical control of an enzyme that clears a neurotransmitter from the active zone.

In the future, **AzoTHA-5** needs to be tested towards AChE photodependent activity and, in a more general perspective, **AzoTHA**s could be improved by making them more water-soluble. This could be achieved by adding, for instance, hydrophilic groups, such as PEG-chains. For this purpose one can envision modifying alkyne tacrine **6.9** by clicking a more polar azide-containing azobenzene to it. Albeit its lower photodependent activity, further derivatizing **AzoTHA-3** seems the most promising, as the pharmacological space is rather limited for the other **AzoTHA**s. These improvements could be realized with the

building blocks already available in order to create a second generation of **AzoTHA**s.

## 6.4 Experimental

### 6.4.1 Synthesis

#### 6.4.1.1 9-Chloro-5,6,7,8-tetrahydroacridine (6.3)

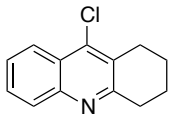


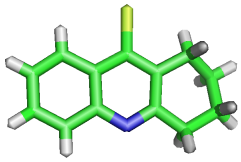

9-Chloro-5,6,7,8-tetrahydroacridine was synthesized as reported before.[59]

Briefly, anthranilic acid (**6.1**) (3.70 g, 26.95 mmol, 1.04 eq.) and cyclohexanone (**6.2**) (2.86 g, 25.85 mmol, 1.00 eq.) were combined and cooled to 0 °C. $POCl_3$ (12.5 mL) was added dropwise by an addition funnel under ice cooling and vigorous stirring to the reaction mixture before it was heated to reflux for 2 h. The solution was allowed to cool to r.t., before being diluted with EtOAc (100 mL) and carefully neutralized with $K_2CO_3$ under ice-cooling. The organic layer was washed with brine, dried ($K_2CO_3$) and the solvent was removed *in vacuo.* The crude product was recrystallized from acetone to afford 2.68 g of **6.3** (12.32 mmol) as pale yellow crystals suitable for X-ray diffractometry in 48% yield.

**$^1$H NMR** (300 MHz, $CDCl_3$): $\delta$ [ppm] = 8.42 (ddd, $J$ = 8.4, 1.5, 0.6 Hz, 1H), 8.27 (ddd, $J$ = 8.4, 1.3, 0.6 Hz, 1H), 7.94 (ddd, $J$ = 8.4, 6.9, 1.5 Hz, 1H), 7.80 (ddd, $J$ = 8.3, 6.8, 1.2 Hz, 1H), 3.41 (td, $J$ = 6.0, 5.5, 1.1 Hz, 2H), 3.34–3.22 (m, 2H), 2.30–2.17 (m, 4H).

**$^{13}$C NMR** (75 MHz, $CDCl_3$): $\delta$ [ppm] = 159.3, 146.5, 141.2, 129.0, 128.6, 128.5, 126.3, 125.2, 123.5, 34.1, 27.3, 22.5, 22.5.

**HRMS (EI)**: calc. for $C_{13}H_{12}ClN^+$ $(M)^{\bullet+}$: 217.0635, found: 217.0643.

**UV/Vis** (LCMS): $\lambda_{max1}$ = 238 nm, $\lambda_{max2}$ = 324 nm.

**$R_t$** (LCMS; MeCN/$H_2O$/formic acid = 10/90/0.1 → 90/10/0.1 over 7 min) = 2.984 min.

### 6.4.1.2 *N*-(4-Aminophenethyl)-1,2,3,4-tetrahydroacridin-9-amine (6.5)

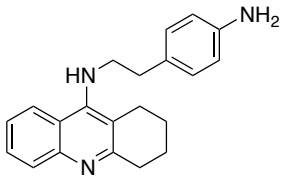


9-Chloro-5,6,7,8-tetrahydroacridine (**6.3**) (163 mg, 0.75 mmol, 1.0 eq.), phenol (1.00 g) and NaI (37 mg, 0.25 mmol, 0.33 eq.) were combined under a nitrogen atmosphere and the reaction mixture was heated to 80 °C. 4-(2-aminoethyl)aniline (**6.4**) (100 mg, 0.75 mmol, 1.0 eq.) was added and the reaction mixture was refluxed for 1 h. The resulting mixture was allowed to cool to approximately 50 °C and EtOAc (50 mL) was added to precipitate the crude product. The resulting solid was collected (pore III frit) and washed with EtOAc before it was redissolved in MeOH (50 mL) and subjected to flash column chromatography (DCM/MeOH = 9/1 → 8/2) to afford 79 mg (0.25 mmol) of **6.5** as a pale yellow solid in 33% yield.

**$^1$H NMR** (400 MHz, DMSO-$d_6$): $\delta$ [ppm] = 8.30 (s, 1H), 8.16 (d, $J$ = 8.5 Hz, 1H), 7.76 (d, $J$ = 8.4 Hz, 1H), 7.62 (dd, $J$ = 8.5, 6.7 Hz, 1H), 7.40 (dd, $J$ = 8.6, 6.8 Hz, 1H), 6.83 (d, $J$ = 8.5 Hz, 2H), 6.46 (d, $J$ = 8.5 Hz, 2H), 6.14 (br s, 1H), 3.71 (t, $J$ = 7.5 Hz, 2H), 2.93–2.90 (m, 2H), 2.72 (t, $J$ = 7.5 Hz, 2H), 2.61–2.58 (m, 2H), 1.81–1.76 (m , 4H).

**$^{13}$C NMR** (101 MHz, DMSO-$d_6$): $\delta$ [ppm] = 150.9, 146.7, 145.2, 129.6, 128.6, 128.0, 127.8, 123.7, 122.9, 119.9, 116.7, 115.8, 115.4, 50.2, 36.4, 33.5, 24.4, 22.9, 22.6.

**HRMS (ESI)**: calc. for $C_{21}H_{24}N_3^+$ $(M+H)^+$: 318.1965, found: 318.1967.

**UV/Vis** (LCMS): $\lambda_{max1}$ = 348 nm, $\lambda_{max2}$ = 357 nm.

**$R_t$** (LCMS; MeCN/$H_2O$/formic acid = 10/90/0.1 → 90/10/0.1 over 7 min) = 1.775 min.

### 6.4.1.3 (*E*)-*N*-(4-(Phenyldiazenyl)phenethyl)-1,2,3,4-tetrahydroacridin-9-amine (AzoTHA)

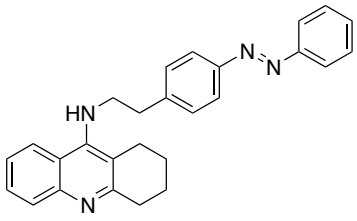


A round-bottom flask was charged with *N*-(4-aminophenethyl)-1,2,3,4-tetrahydroacridin-9-amine (**6.5**) (50 mg, 0.16 mmol, 1.0 eq.) in glacial acetic acid (4 mL) and nitrosobenzene (**6.6**) (20 mg, 0.19 mmol, 1.2 eq.) was added in one portion. The reaction mixture was stirred o.n. before it was neutralized with sat. $NaHCO_3$ and extracted with EtOAc (3 x 25 mL). The combined organic layers were washed with sat. $NaHCO_3$, water and brine before the solvent was removed in vacuo to yield a crude product, which was further purified by flash column chromatography (DCM/MeOH = 9/1) to yield 50.2 mg (0.123 mmol) of **AzoTHA** in 78% yield.

**$^1$H NMR** (400 MHz, $CDCl_3$): $\delta$ [ppm] = 8.18 (d, *J* = 8.5 Hz, 1H), 8.11–7.99 (m, *J* = 8.4 Hz 1H), 7.98–7.79 (m, 4H), 7.59 (ddd, *J* = 8.3, 6.9, 1.2 Hz, 1H), 7.56–7.44 (m, 3H), 7.44–7.32 (m, 3H), 4.01 (t, *J* = 6.9 Hz, 2H), 3.12 (t, *J* = 6.7 Hz, 4H), 2.66–2.43 (m, 2H), 1.83 (t, *J* = 3.3 Hz, 4H).

**$^{13}$C NMR** (101 MHz, $CDCl_3$): $\delta$ [ppm] = 152.5, 151.6, 141.0, 131.1, 130.1, 129.5, 129.1, 128.7, 127.4, 125.2, 124.5, 123.3, 122.8, 121.2, 120.3, 118.4, 114.3, 49.4, 37.0, 31.4, 24.2, 22.4, 21.7.

**HRMS (EI)**: calc. for $C_{27}H_{26}N_4^{\cdot+}$ $(M)^{\cdot+}$: 406.2152, found: 406.2144.

**UV/Vis** (50 µM in DMSO): $\lambda_{max}$ (trans, $\pi \rightarrow \pi^*$) = 348 nm; $\lambda_{max}$ (cis, $\pi \rightarrow \pi^*$) = 348 nm; $\lambda_{max}$ (cis, $n \rightarrow \pi^*$) = 440 nm.

**$R_t$** (LCMS; MeCN/$H_2O$/formic acid = 10/90/0.1 → 90/10/0.1 over 7 min) = 4.093 min.

#### 6.4.1.4 1,2,3,4-Tetrahydroacridin-9-amine (tacrine, THA)

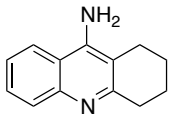


A Dean-Stark apparatus was charged with 2-aminobenzonitrile (0.75 g, 6.35 mmol, 1.0 eq.) in xylene (7.5 mL) and *p*-toluenesulfonic acid (24 mg, 0.02 eq.). Cyclohexanone (2.11 g, 21.4 mmol, 3.3 eq.) dissolved in 2 mL xylene was added drop-wise and the solution was refluxed for 3 h before another 24 mg of *p*-toluenesulfonic acid was added and refluxing was continued o.n.. The dark red solution was allowed to cool to r.t., the solvent was decanted off and the remaining red viscous oil was taken up in warm DCM, which was then cooled and the precipitate was collected, and further washed with DCM. The product was extracted with DCM after basifying with 10 mL of 1M NaOH. The organic layer was stirred over $K_2CO_3$ and activated charcoal before filtering the suspension over Celite. Removal of all volatiles afforded 0.60 g (3.03 mmol) of **THA** as a pale yellow powder in 48% yield.

**$^1$H NMR** (300 MHz, $CDCl_3$): $\delta$ [ppm] = 7.90–7.80 (m, 1H), 7.68–7.58 (m, 1H), 7.44 (ddd, *J* = 8.3, 6.8, 1.3 Hz, 1H), 7.20 (ddd, *J* = 8.2, 6.8, 1.3 Hz, 1H), 4.84 (s, 2H), 2.95 (td, *J* = 5.3, 4.1, 2.3 Hz, 2H), 2.50–2.35 (m, 2H), 1.80 (td, *J* = 4.0, 2.1 Hz, 4H).

**$^{13}$C NMR** (75 MHz, $CDCl_3$): $\delta$ [ppm] = 158.4, 146.7, 146.4, 128.4, 128.2, 123.5, 120.0, 117.1, 110.1, 34.0, 23.5, 22.7, 22.6.

**LRMS (ESI)**: calc. for $C_{13}H_{15}N_2^+$ $(M+H)^+$: 199.1, found: 199.1.

**UV/Vis** (LCMS): $\lambda_{max1}$ = 241 nm, $\lambda_{max2}$ = 324 nm, $\lambda_{max3}$ = 336 nm.

**$R_t$** (LCMS; MeCN/$H_2O$/formic acid = 10/90/0.1 → 90/10/0.1 over 7 min) = 1.973 min.

### 6.4.1.5 Ethyl 4-nitrosobenzoate (6.7)

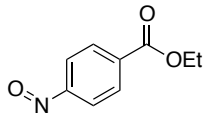

A round bottom flask was charged with ethyl 4-aminobenzoate (1.0 eq.) in a mixture of DCM/$H_2O$ = 1/1. Oxone® (2.0 eq.) was added and the biphasic system was stirred vigorously for 3 h. The layers were separated and the green organic layer was washed with 1 M HCl (2 x), water and brine before it was dried over $MgSO_4$. After removal of all volatiles, the crude nitroso compound was isolated as a yellow solid, which was used without further purification.

### 6.4.1.6 Ethyl (*E*)-4-((4-(2-((1,2,3,4-tetrahydroacridin-9-yl)amino)ethyl)-phenyl)diazenyl)benzoate (AzoTHA-2)

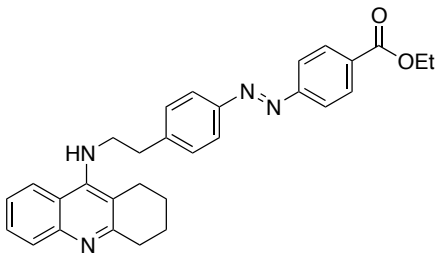

A round-bottom flask was charged with **6.5** (26.6 mg, 0.08 mmol, 1.0 eq.) in glacial acetic acid (5 mL) and ethyl 4-nitrosobenzoate (**6.7**) (~60% pure, 45.0 mg, ~3.0 eq.) was added in one portion. The reaction mixture was stirred for o.n. before it was neutralized with sat. $NaHCO_3$ and extracted with EtOAc (2 x). The combined organic layers were dried over $MgSO_4$ and after filtration and removal of all volatiles the crude product was further purified by RP-HPLC (MeCN/$H_2O$/formic acid = 10/90/0.1 → 80/20/0.1) to yield 12.5 mg (0.026 mmol) of **AzoTHA-2** as an orange solid in 31% yield.

**$^1$H NMR** (400 MHz, $CDCl_3$): $\delta$ [ppm] = 8.18 (s, 1H), 8.09 (d, *J* = 8.5 Hz, 2H), 8.02 (d, *J* = 8.5 Hz, 1H), 7.89 (d, *J* = 8.5 Hz, 2H), 7.76 (d, *J* = 8.1 Hz, 2H), 7.65 (dd, *J* = 8.5, 1.3

Hz, 1H), 7.47 (ddd, *J* = 8.3, 6.6, 1.3 Hz, 1H), 7.36 (d, *J* = 8.1 Hz, 2H), 7.28 (ddd, *J* = 8.3, 6.7, 1.3 Hz, 1H), 4.29 (q, *J* = 7.1 Hz, 2H), 3.67 (d, *J* = 6.7 Hz, 2H), 2.92 (t, *J* = 7.3 Hz, 2H), 2.83 (t, *J* = 6.3 Hz, 2H), 2.59 (t, *J* = 6.2 Hz, 2H), 1.83–1.64 (m, 4H), 1.29 (t, *J* = 7.1 Hz, 3H).

**$^{13}$C NMR** (101 MHz, $CDCl_3$): $\delta$ [ppm] = 165.1, 157.6, 154.5, 150.5, 150.2, 146.4, 144.3, 131.7, 130.5, 130.0, 128.1, 127.9, 123.4, 123.1, 122.9, 122.6, 120.1, 116.1, 61.1, 49.1, 36.5, 33.2, 25.0, 22.6, 22.3, 14.2.

**HRMS (ESI)**: calc. for $C_{30}H_{31}N_4O_2^+$ $(M+H)^+$: 479.2442, found: 479.2443.

**UV/Vis** (LCMS): $\lambda_{max}$ = 338 nm.

**$R_t$** (LCMS; MeCN/$H_2O$/formic acid = 10/90/0.1 → 90/10/0.1 over 7 min) = 3.755 min.

### 6.4.1.7 *N*-(Prop-2-yn-1-yl)-1,2,3,4-tetrahydroacridin-9-amine (6.9)

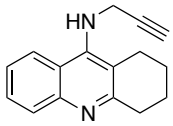


In a round-bottom flask, **6.3** (163 mg, 0.75 mmol, 1.0 eq.), phenol (1 g) and NaI (37 mg, 0.25 mmol, 0.33 eq.) were combined under a nitrogen atmosphere. The reaction mixture was heated up to 80 °C and propagylamine (**6.8**) (41.3 mg, 0.75 mmol, 1.0 eq.) was added drop-wise. The reaction mixture was refluxed for 1 h and after cooling a crude product was precipitated by the addition of EtOAc, which was collected with a pore III frit and washed with EtOAc before redissolving in MeOH (50 mL). The solvent was removed *in vacuo* and the crude product was filtered over a plug of silica (MeOH/DCM = 2/8) to yield a crude product of **6.9**, which was briefly characterized by proton NMR and LRMS and used without further purification for click chemistry.

**$^1$H NMR** (200 MHz, MeOD-$d_4$): $\delta$ [ppm] = 8.59 (d, $J$ = 8.7 Hz, 1H), 8.34–8.08 (m, 1H), 7.95–7.73 (m, 1H), 7.68–7.55 (m, 1H), 4.66 (d, $J$ = 2.5 Hz, 2H), 3.05 (m, 2H), 2.96 (t, $J$ = 2.5 Hz, 1H), 2.76 (m, 2H), 1.97 (m, 4H).

**LRMS (ESI)**: calc. for $C_{20}H_{23}N_4^+$ $(M+2MeCN+H)^+$: 319.2, found: 319.2.

**UV/Vis** (LCMS): $\lambda_{max1}$ = 208 nm, $\lambda_{max2}$ = 216 nm, $\lambda_{max3}$ = 234 nm, $\lambda_{max4}$ = 319 nm, $\lambda_{max5}$ = 376 nm.

**$R_t$** (LCMS; MeCN/$H_2O$/formic acid = 10/90/0.1 → 90/10/0.1 over 7 min) = 2.108 min.

### 6.4.1.8 (*E*)-1-(4-Azidophenyl)-2-phenyldiazene (6.11)

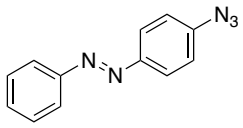


A solution of 100 mg (1.0 eq., 0.50 mmol) (*E*)-4-(phenyldiazenyl)aniline (**6.10**) in 10 mL MeCN was cooled to -10 °C, and 77 mg (1.5 eq., 0.75 mmol, 89 µL) of $^t$BuONO was added, followed by 10 drops of TFA. The reaction mixture immediately turned into a deep red color. After stirring for 5 minutes, 69 mg (1.2 eq., 0.60 mmol, 78 µL) of TMS azide was added drop-wise to the solution and it was stirred for another hour until it was allowed to warm to r.t.. The reaction was diluted with 25 mL of $H_2O$ and extracted with EtOAc (2 x). The combined organic layers were washed with $H_2O$ (3 x 50 mL) and brine and finally dried over $MgSO_4$. After removal of the drying agent by filtration, the crude solution was concentrated *in vacuo* and submitted to flash column chromatography on silica gel (pentane/DCM = 9/1) to yield 102.0 mg (0.46 mmol) of the desired product as a red solid in 91% yield.

**$^1$H NMR** (300 MHz, $CDCl_3$): $\delta$ [ppm] = 7.97–7.89 (m, 4H), 7.55–7.47 (m, 3H), 7.16 (d, $J$ = 9.0 Hz, 2H).

**$^{13}$C NMR** (75 MHz, $CDCl_3$): $\delta$ [ppm] = 152.6, 149.8, 142.6, 131.0, 129.1, 124.6, 122.8, 119.6.

**HRMS (EI)**: calc. for $C_{12}H_9N_5^{\cdot+}$ $(M)^{\cdot+}$: 223.0858, found: 223.0850 (4.2% rel. intensity); calc. for $C_{12}H_9N_3^{\cdot+}$ $(M\text{-}N_2)^{\cdot+}$: 195.0791, found: 195.0791 (14.9% rel. intensity).

**UV/Vis** (LCMS): $\lambda_{max}$ = 349 nm.

**$R_t$** (LCMS; MeCN/$H_2O$/formic acid = 10/90/0.1 → 90/10/0.1 over 7 min) = 5.518 min.

### 6.4.1.9 (*E*)-*N*-((1-(4-(Phenyldiazenyl)phenyl)-1*H*-1,2,3-triazol-4-yl)methyl)-1,2,3,4-tetrahydroacridin-9-amine (AzoTHA-3)

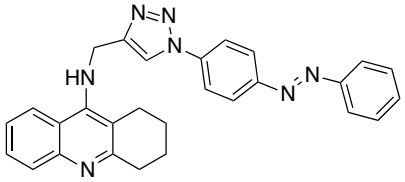


Propargyl tacrine **6.9** (47.3 mg, 0.20 mmol, 1.0 eq.) and 4-azido azobenzene **6.11** (58.1 mg, 0.26 mmol, 1.3 eq.) were dissolved in DMSO (9 mL) in a round bottom flask under a nitrogen atmosphere. A degassed stock solution of the catalyst was made: $CuSO_4$ x 5 $H_2O$ (10.0 mg, 0.040 mmol, 0.2 eq.) was dissolved in water (7.6 mL) and sodium ascorbate (10.0 mg, 0.050 mmol, 0.25 eq.) was added under a nitrogen stream. This stock solution was poured into the reaction mixture. Another 9 mL of DMSO was added to the mixture to obtain a homogeneous solution. The reaction vessel was sonicated at 40 °C for 45 min before MeCN (5 mL) was added and the reaction vessel was sonicated again at 40 °C for another 30 min. Afterwards, the reaction was quenched by addition of sat. $NaHCO_3$-solution (50 mL) and was extracted with EtOAc (2 x 50 mL). The combined organic layers were washed with brine (50 mL) and dried over $MgSO_4$ before all volatiles were removed *in vacuo*. The crude product was purified by flash column chromatography on deactivated (with $NEt_3$) silica gel (DCM/MeOH = 9.5/0.5 →

9.2/0.8) to afford 37.2 mg of **AzoTHA-3** (0.083 mmol) as an orange solid in 41% yield.

**$^1$H NMR** (400 MHz, $CDCl_3$): $\delta$ [ppm] = 8.77 (s, 1H), 8.14 (dd, *J* = 8.6, 1.4 Hz, 1H), 8.07 (d, *J* = 9.0 Hz, 2H), 8.02 (d, *J* = 9.0 Hz, 2H), 7.92–7.83 (m, 1H), 7.67 (dd, *J* = 8.5, 1.3 Hz, 1H), 7.62 – 7.51 (m, 3H), 7.48 (ddd, *J* = 8.4, 6.8, 1.3 Hz, 1H), 7.31 (ddd, *J* = 8.2, 6.8, 1.3 Hz, 1H), 5.91 (t, *J* = 7.0 Hz, 1H), 4.67 (d, *J* = 6.6 Hz, 2H), 2.86 (t, *J* = 6.3 Hz, 2H), 2.75 (t, *J* = 6.1 Hz, 2H), 1.83–1.70 (m, 4H).

**$^{13}$C NMR** (101 MHz, $CDCl_3$): $\delta$ [ppm] = 157.8, 151.7, 150.9, 149.6, 147.4, 146.4, 138.1, 131.7, 129.4, 127.9, 124.0, 123.5, 122.9, 122.5, 121.0, 120.4, 120.3, 119.8, 117.0, 42.8, 33.2, 24.8, 22.5, 22.2.

**HRMS (ESI)**: calc. for $C_{28}H_{26}N_7^+$ $(M+H)^+$: 460.2244, found: 460.2244.

**UV/Vis** (LCMS): $\lambda_{max}$ = 336 nm.

**$R_t$** (LCMS; MeCN/$H_2O$/formic acid = 10/90/0.1 → 90/10/0.1 over 7 min) = 2.774 min.

### 6.4.1.10 (*E*)-*N*-(4-((4-(Diethylamino)phenyl)diazenyl)phenethyl)-1,2,3,4-tetrahydroacridin-9-amine (AzoTHA-4)

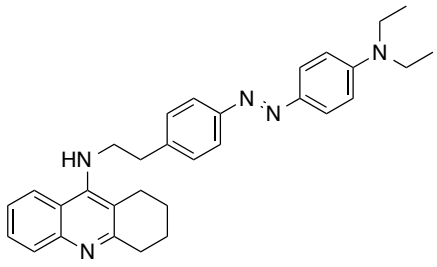


A round-bottom flask was charged with **6.5** (31.0 mg, 0.098 mmol, 1.0 eq.) in 10 mL 2.4 M HCl and cooled to 0 °C. An aqueous solution of $NaNO_2$ (8.1 mg, 0.117 mmol, 1.2 eq.) in 10 mL water was added drop-wise. The reaction mixture turned pale yellow, was stirred for 10 minutes at 0 °C before it was transferred to a pre-cooled flask containing *N*,*N*-diethylaniline (**6.12**) dissolved in 10 mL of 3 M NaOAc (water/MeOH = 1/1). The reaction mixture turned red and was

allowed to warm to r.t. before it was extracted three times with EtOAc with the help of sat. $NaHCO_3$. The combined organic layers were dried over $MgSO_4$ and after filtration and removal of all volatiles the crude product was further purified by flash column chromatography on $NEt_3$ deactivated silica (100% EtOAc) to yield 22.9 mg (0.048 mmol) of **AzoTHA-4** as an orange solid in 49% yield.

**$^1$H NMR** (400 MHz, $CDCl_3$): $\delta$ [ppm] = 7.99–7.73 (m, 6H), 7.55 (ddd, $J$ = 8.3, 6.8, 1.4 Hz, 1H), 7.36–7.28 (m, 3H), 6.73 (d, $J$ = 9.2 Hz, 1H), 3.79 (t, $J$ = 6.8 Hz, 2H), 3.45 (q, $J$ = 7.1 Hz, 4H), 3.02 (m, 4H), 2.53 (t, $J$ = 6.3 Hz, 2H), 1.90–1.81 (m, 4H), 1.23 (t, $J$ = 7.1 Hz, 6H).

**$^{13}$C NMR** (101 MHz, $CDCl_3$): $\delta$ [ppm] = 158.6, 152.2, 150.2, 150.1, 147.4, 143.0, 139.6, 129.3, 128.8, 128.3, 125.3, 123.8, 122.7, 122.4, 120.4, 116.7, 110.9, 50.0, 44.7, 37.1, 34.1, 24.6, 23.0, 22.7, 12.6.

**HRMS (ESI)**: calc. for $C_{31}H_{36}N_5^+$ $(M+H)^+$: 478.2965, found: 478.2961.

**UV/Vis** (50 µM in DMSO): $\lambda_{max}$ (trans)= 438 nm, $\lambda_{max1}$ (cis)= 446 nm, $\lambda_{max2}$ (cis)= 378 nm.

**UV/Vis** (LCMS): $\lambda_{max}$ = 440 nm.

**$R_t$** (LCMS; MeCN/$H_2O$/formic acid = 10/90/0.1 → 90/10/0.1 over 7 min) = 4.033 min.

### 6.4.1.11 (*E*)-9-(phenyldiazenyl)-1,2,3,4-tetrahydroacridine (AzoTHA-5) and 2-phenyl-2,3,4,5-tetrahydropyrazolo[3,4,5-*kl*]acridine (6.15) *via* 6.14

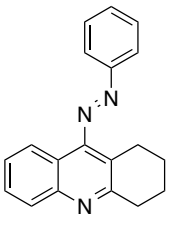


and

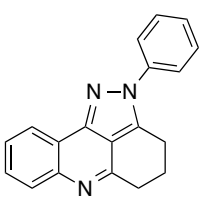


*via*

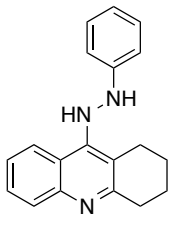

9-Chloro-5,6,7,8-tetrahydroacridine (**6.3**) (70 mg, 0.353 mmol, 1.0 eq.), phenol (500 mg) and NaI (17.6 mg, 0.117 mmol, 0.33 eq.) were combined under a nitrogen atmosphere and the reaction mixture was heated to 80 °C. Phenylhydrazine (**6.13**) (38.3 mg, 0.353 mmol, 1.0 eq.) was added and the reaction mixture was refluxed for 1 h. The resulting mixture was allowed to cool to approximately 50 °C and EtOAc (50 mL) was added to precipitate the product. The resulting solid was collected (pore III frit) and washed with EtOAc and filtered over a plug of silica (10% MeOH in DCM) before it was characterized briefly to be the desired hydrazine **6.14** (yellow powder, 40.1 mg) and used without further purification.

**$^1$H NMR** (400 MHz, DMSO-$d_6$): $\delta$ [ppm] = 9.88 (br s, 1H), 9.07 (d, $J$ = 8.8 Hz, 1H), 8.71 (s, 1H), 7.87–7.75 (m, 2H), 7.44 (ddd, $J$ = 8.5, 6.2, 2.0 Hz, 1H), 7.23 (t, $J$ = 7.8 Hz, 2H), 6.91–6.77 (m, 3H), 3.04–3.00 (m, 2H), 2.73–2.71 (m, 2H), 1.84–1.82 (m, 4H).

**HRMS (ESI)**: calc. for $C_{19}H_{20}N_3^+$ $(M+H)^+$: 290.1652, found: 290.1650.

**UV/Vis** (LCMS): $\lambda_{max1}$ = 240 nm, $\lambda_{max2}$ = 338 nm.

**$R_t$** (LCMS; MeCN/$H_2O$/formic acid = 10/90/0.1 → 90/10/0.1 over 7 min) = 3.054 min.

**6.14** (30.0 mg) was dissolved in MeOH (4 mL) and 1 M $NaHCO_3$ (1 mL) and the mixture was stirred o.n. exposed to the atmosphere. The resulting precipitate was extracted in DCM (3 x) and the combined organic layers were washed with water and brine. The crude material was subjected to flash column chromatography (100% DCM) to obtain 18.4 mg (0.064 mmol) of **AzoTHA-5** as a red solid and 11.0 mg (0.038 mmol) of **6.15** as a brownish solid in 24% and 15% yield, respectively.

Spectral data for **AzoTHA-5**:

**$^1$H NMR** (400 MHz, $CDCl_3$): $\delta$ [ppm] = 8.06–7.99 (m, 3H), 7.77 (dd, *J* = 8.4, 1.3 Hz, 1H), 7.68–7.57 (m, 4H), 7.42 (dd, *J* = 8.4, 6.8 Hz, 1H), 3.21 (t, *J* = 6.5 Hz, 2H), 2.88 (t, *J* = 6.5 Hz, 2H), 2.07–1.96 (m, 2H), 1.92–1.83 (m, 2H).

**$^{13}$C NMR** (101 MHz, $CDCl_3$): $\delta$ [ppm] = 159.9, 153.8, 152.5, 147.1, 132.3, 129.3, 128.9, 128.4, 126.1, 123.0, 122.7, 120.3, 119.2, 34.1, 24.9, 22.8, 22.7.

**HRMS (ESI)**: calc. for $C_{19}H_{18}N_3^+$ $(M+H)^+$: 288.1495, found: 288.1494.

**UV/Vis** (LCMS): $\lambda_{max1}$ = 254 nm, $\lambda_{max2}$ = 316 nm, $\lambda_{max3}$ = 455 nm.

**$R_t$** (LCMS; MeCN/$H_2O$/formic acid = 10/90/0.1 → 90/10/0.1 over 7 min) = 3.605 min.

Spectral data for **6.15**:

**$^1$H NMR** (400 MHz, $CDCl_3$): $\delta$ [ppm] = 8.50–8.44 (m, 1H), 8.07 (d, *J* = 8.2 Hz, 1H), 7.76 (d, *J* = 7.9 Hz, 2H), 7.72–7.62 (m, 1H), 7.61–7.52 (m, 3H), 7.45 (t, *J* = 7.4 Hz, 1H), 3.27 (t, *J* = 6.0 Hz, 2H), 3.14 (t, *J* = 6.2 Hz, 2H), 2.39 (p, *J* = 6.1 Hz, 2H).

**$^{13}$C NMR** (101 MHz, $CDCl_3$): $\delta$ [ppm] = 159.6, 146.8, 146.3, 140.1, 139.6, 129.6, 129.4, 128.9, 128.1, 125.8, 123.2, 122.7, 120.2, 116.9, 30.3, 25.1, 24.0.

**LRMS (ESI)**: calc. for $C_{19}H_{16}N_3^+$ $(M+H)^+$: 286.1, found: 286.1.

**UV/Vis** (LCMS): $\lambda_{max1}$ = 200 nm, $\lambda_{max1}$ = 234 nm, $\lambda_{max1}$ = 324 nm.

**$R_t$** (LCMS; MeCN/$H_2O$/formic acid = 10/90/0.1 → 90/10/0.1 over 7 min) = 2.928 min.

### 6.4.2 Mouse Tracheal Tensometry

#### 6.4.2.1 General

Mice (strain 129S6/SvEvTac) were killed by inhalation of an overdose of isoflurane (Abbott, Wiesbaden, Germany) and exsanguination. The trachea was removed and a segment of 5 cartilage rings was cut and mounted between two

stainless hooks. The lower hook was fixed at the bottom of the organ bath and upper one was connected to an isometric transducer (PowerLAb 8/30; ADInstruments, Bella Vista, Australia) connected to a PC with the recorder software (Labchart, ADInstruments, Bella Vista, Australia). The organ bath (15 ml) contained phenolred-free minimal essential medium (Invitrogen, Darmstadt, Germany) with 100 U/ml penicillin and 100 g/ml streptomycin, which was bubbled with 21% $O_2$/79% $N_2$. Tissue was then maintained under ~400 mN (mg) base tension. After a 20 min equilibrium period, the tracheal segments were stimulated with electrical field stimulation (EFS) with the following settings: 100 Hz, 10 V and 2 ms for 1 min. These stimulations were performed in untreated and treated (AzoTHA or physostigmine) tracheal segments. At the end of the experiment, viability of the preparation was tested by pharmacological activation of tracheal muscle constriction with muscarine (10 µM). Physostigmine (*E8625*) and muscarine (*M107*) were purchased from Aldrich, freshly dissolved in DMSO and aliquoted to stock solutions prior to use. All used reagents were pipetted directly into the bath solutions.

#### 6.4.2.2 AzoTHA effect upon kinetics of EFS-induced changes in tracheal tone

EFS experiments were conducted on three tracheas. First, tracheas were stimulated with three trains of EFS in the absence of a drug. Then, 50 µM **AzoTHA** was added to the organ bath, and EFS trains were applied while illuminating with alternating wavelengths. Data was exported into Igor Pro v6.22a and the off-slope was exponentially fitted to obtain τ-values (Table 9). The absolute amplitude of increase in tracheal tone gradually decreased during repetitive EFS (9 trains per trachea: 3 without drug, 3 with **AzoTHA** at both wavelengths each), which was also observed in control experiments without drug (Figure 29a) and, therefore, not related to AChE inhibition.

**Table 9: $\tau_{off}$-values of EFS trachea (mean±S.D.).**

| $\tau_{off}$(sec) | Exp #1 | Exp #2 | Exp #3 |
|---|---|---|---|
| No **AzoTHA** | 4.81±0.95 | 3.36±0.08 | 4.03±0.94 |
| 50 μM **AzoTHA** (440 nm) | 11.29±0.77 | 5.13±0.18 | 4.85±0.83 |
| 50 μM **AzoTHA** (350 nm) | 15.25±1.49 | 6.13±0.65 | 8.02±1.57 |

## 6.5 Spectral Data

### 6.5.1 9-Chloro-5,6,7,8-tetrahydroacridine (6.3)

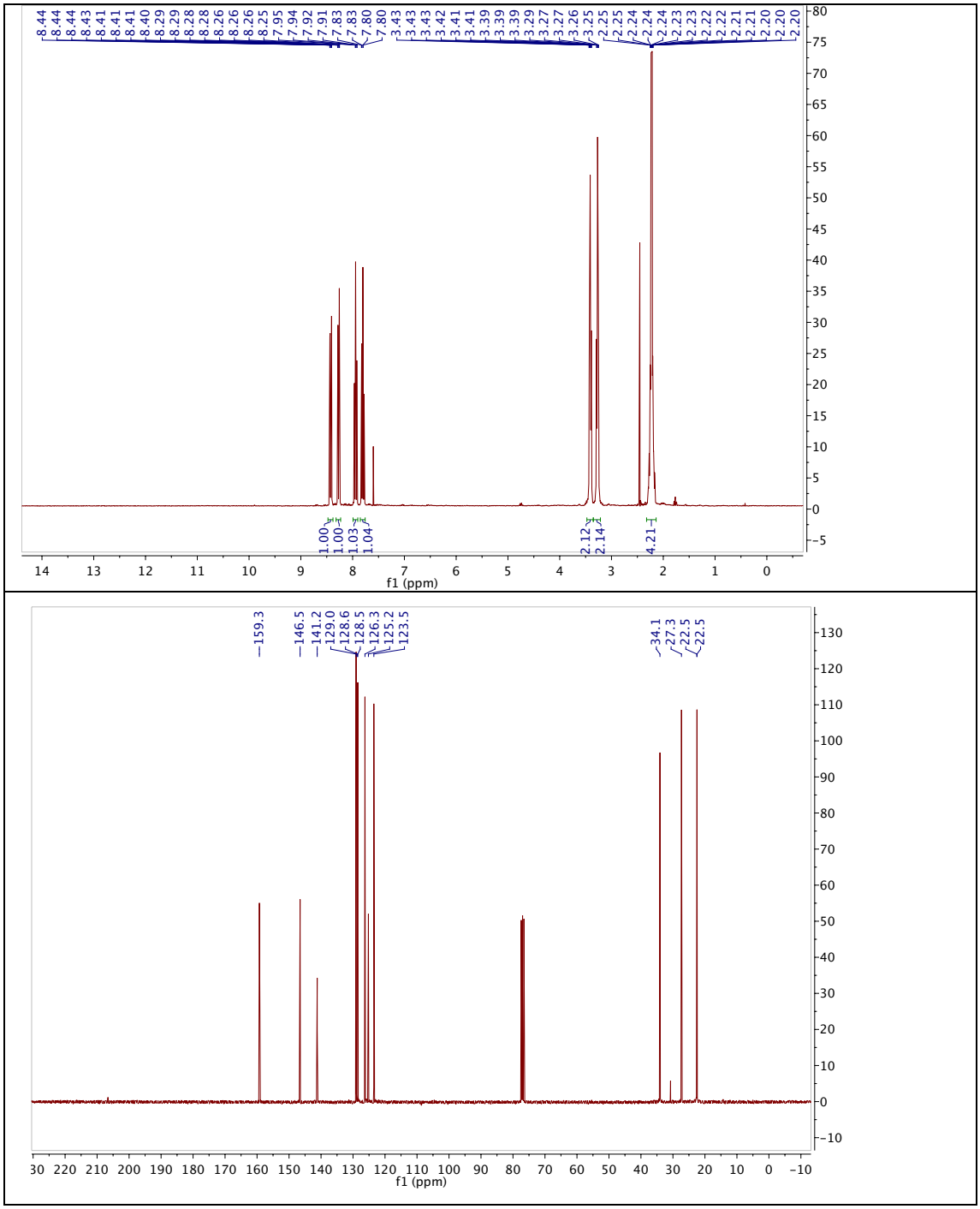

### 6.5.2 *N*-(4-Aminophenethyl)-1,2,3,4-tetrahydroacridin-9-amine (6.5)

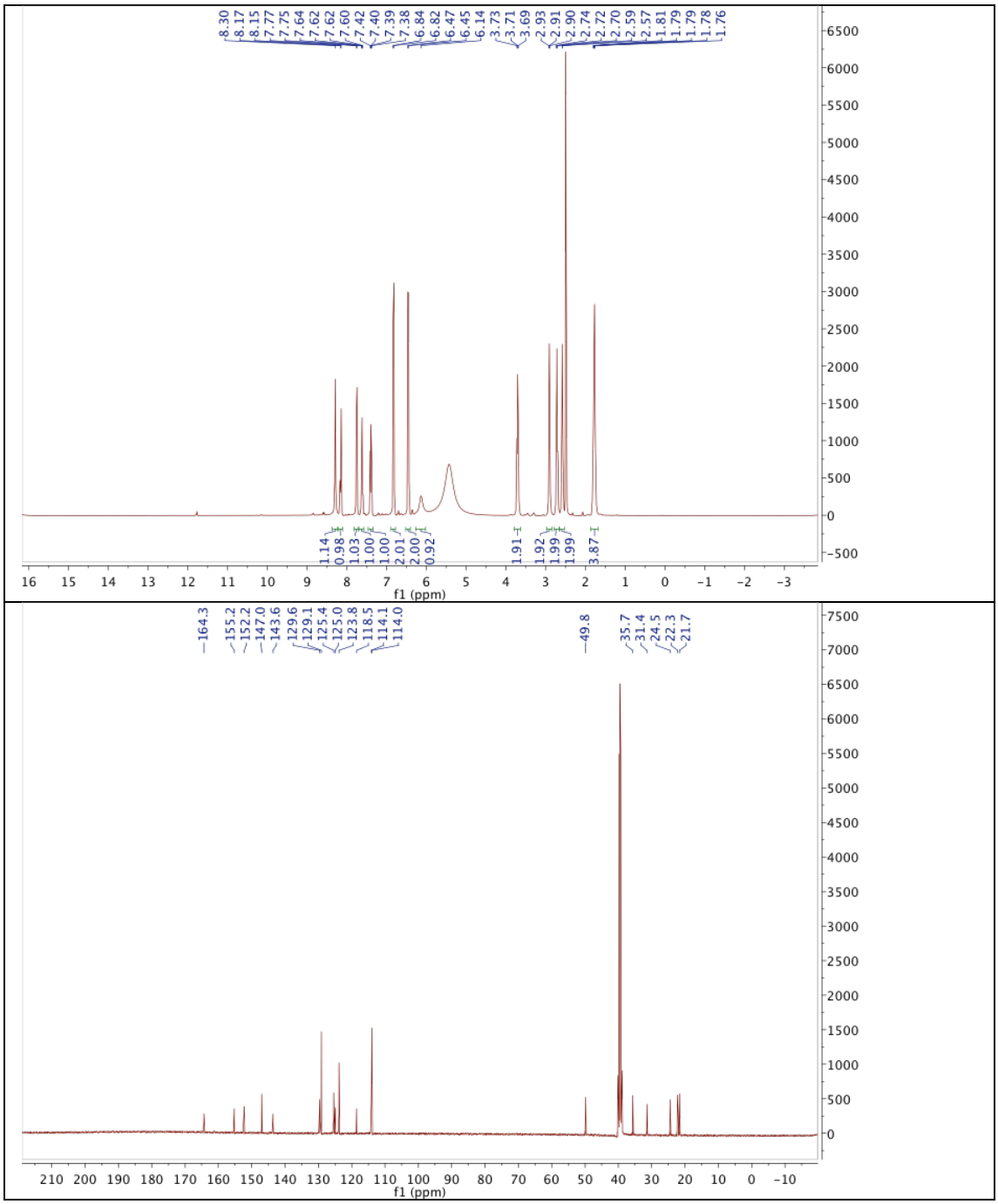

### 6.5.3 (*E*)-*N*-(4-(Phenyldiazenyl)phenethyl)-1,2,3,4-tetrahydroacridin-9-amine (AzoTHA)

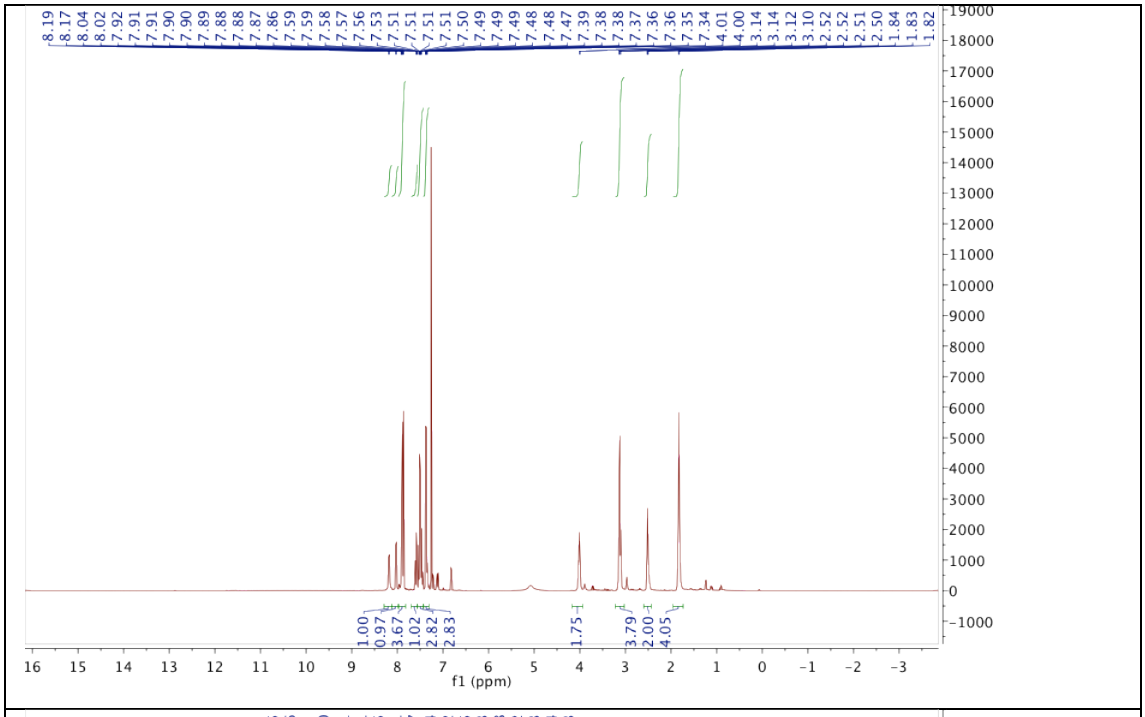


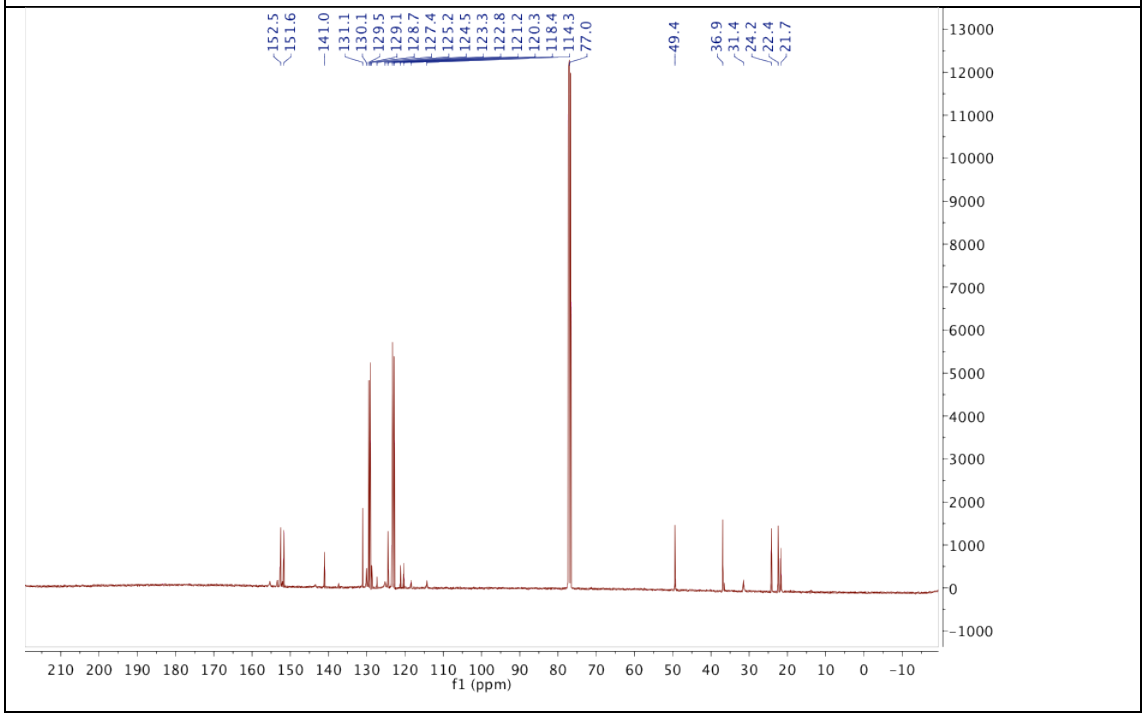

### 6.5.4 1,2,3,4-Tetrahydroacridin-9-amine (THA)

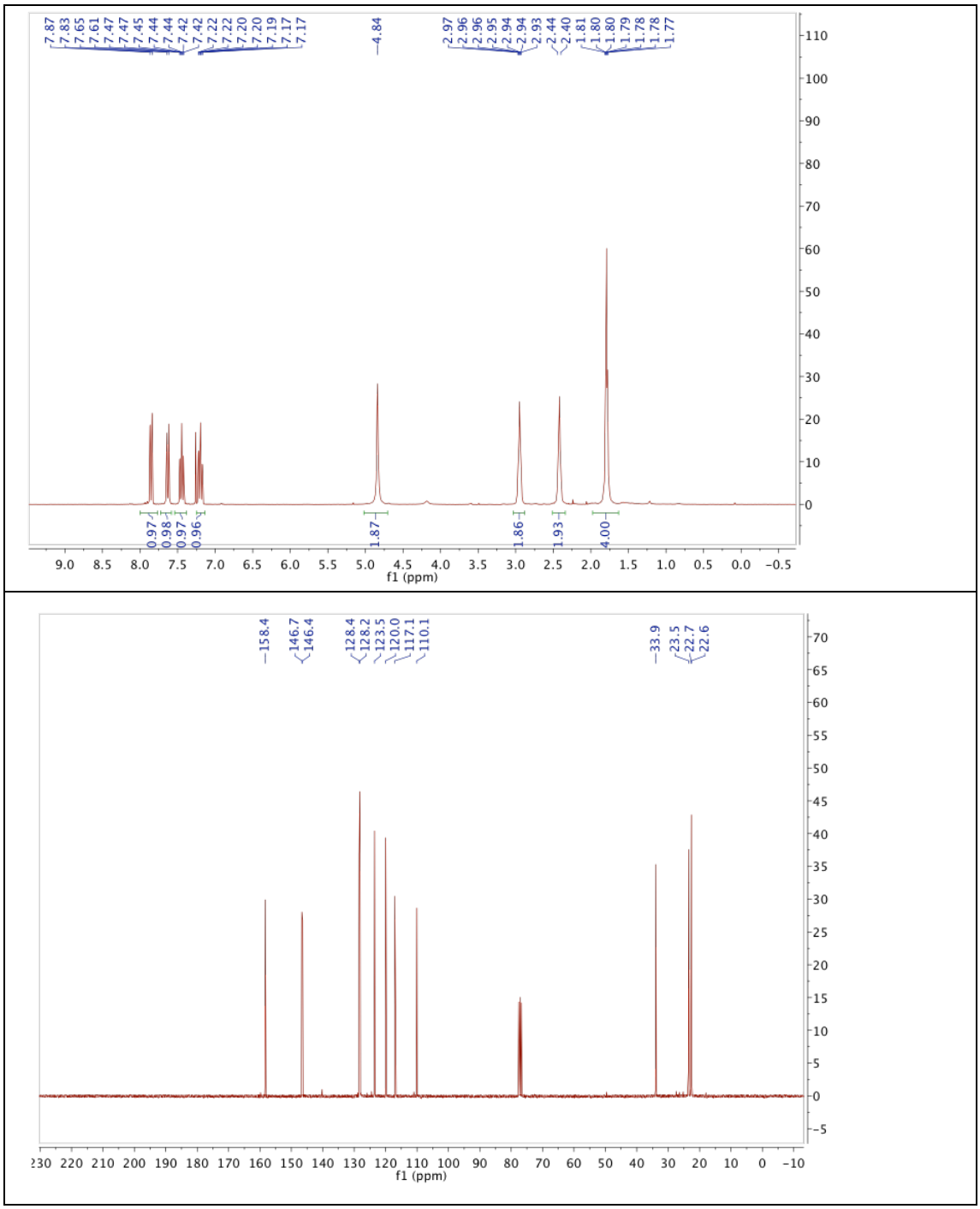

### 6.5.5 Ethyl (*E*)-4-((4-(2-((1,2,3,4-tetrahydroacridin-9-yl)amino)ethyl)-phenyl) diazenyl)benzoate (AzoTHA-2)

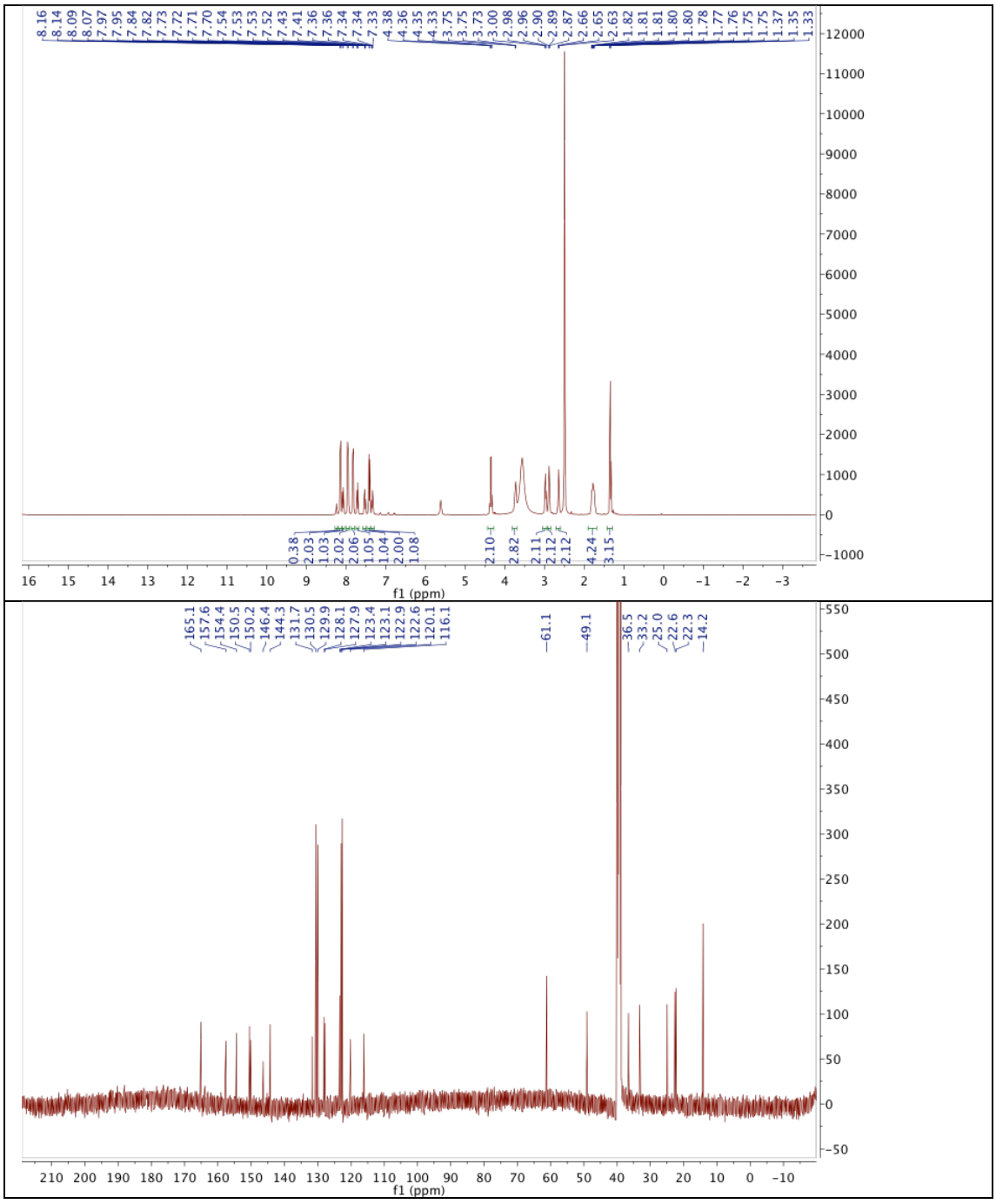

### 6.5.6 (*E*)-1-(4-Azidophenyl)-2-phenyldiazene (6.11)

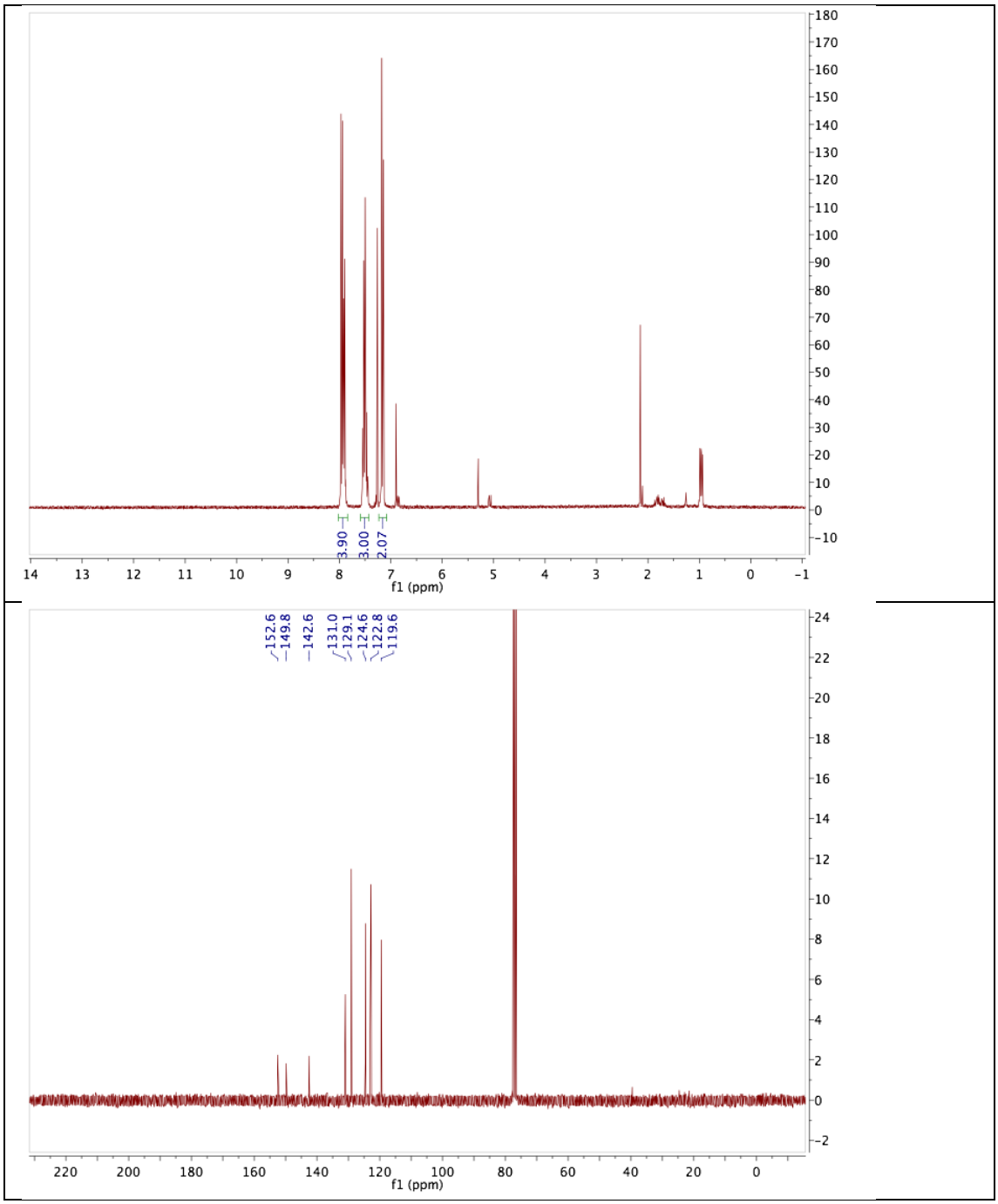

### 6.5.7 (*E*)-*N*-((1-(4-(Phenyldiazenyl)phenyl)-1*H*-1,2,3-triazol-4-yl)methyl)-1,2,3,4-tetrahydroacridin-9-amine (AzoTHA-3)

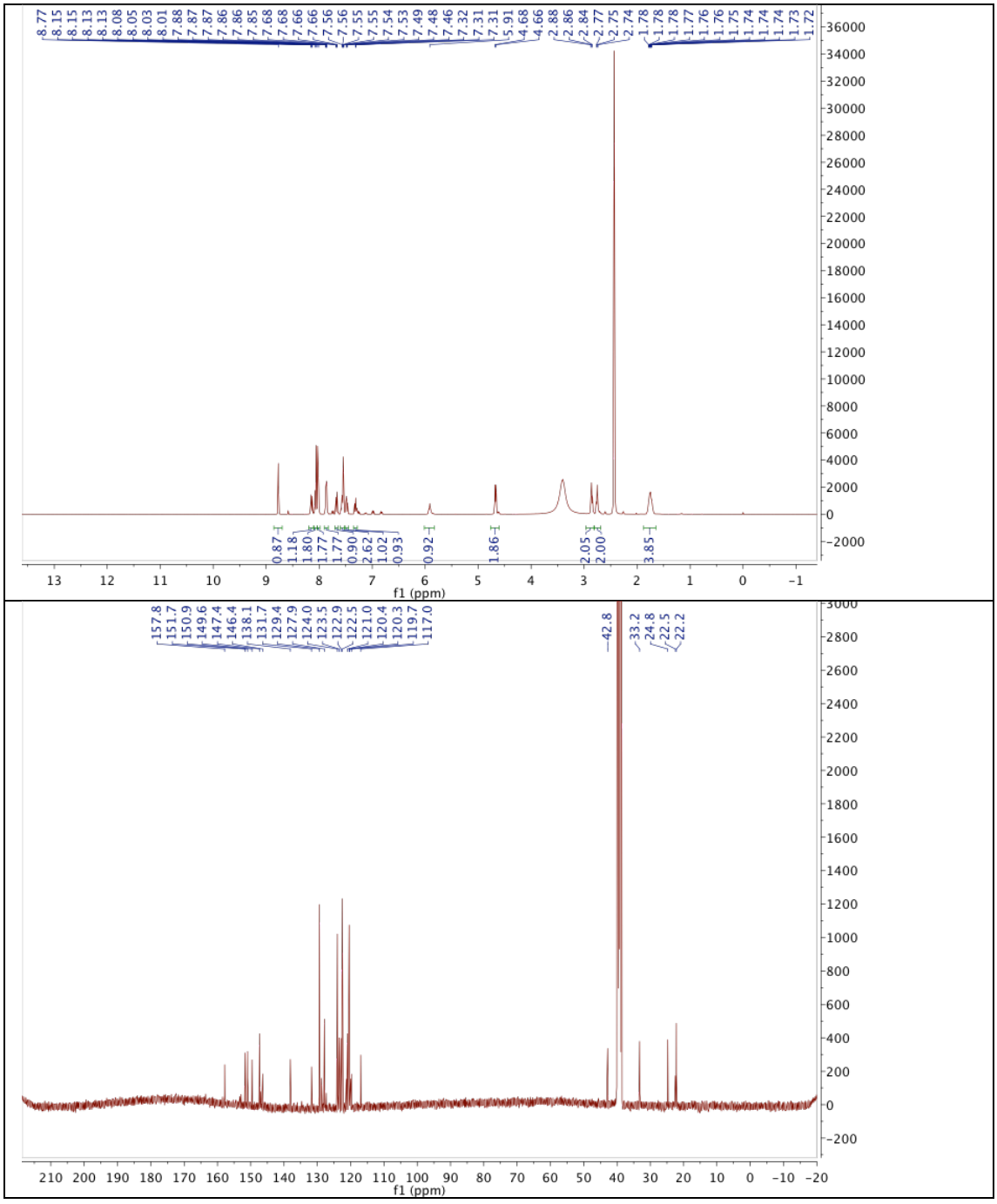

### 6.5.8 (*E*)-*N*-(4-((4-(Diethylamino)phenyl)diazenyl)phenethyl)-1,2,3,4-tetrahydroacridin-9-amine (AzoTHA-4)

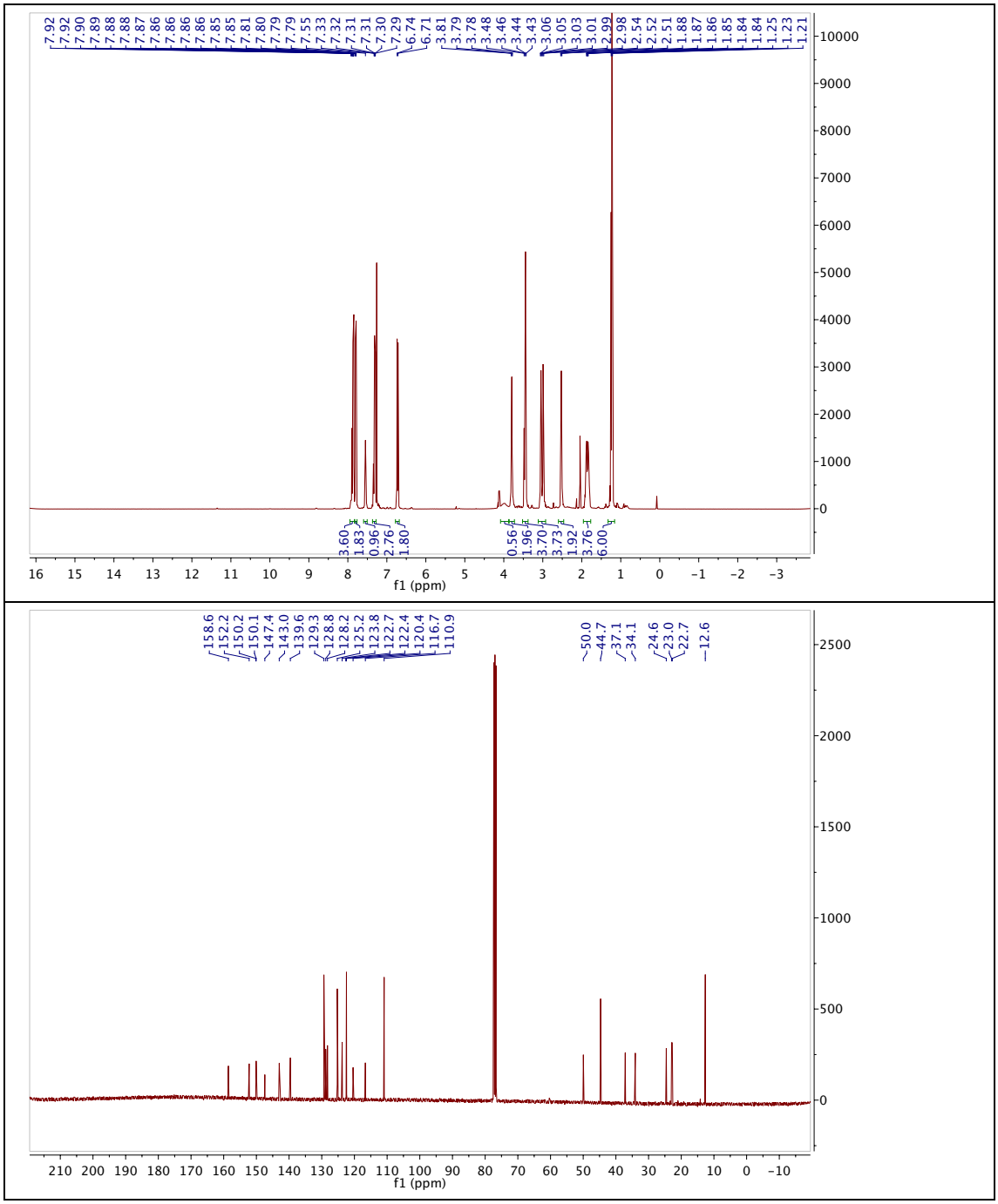

### 6.5.9 9-(2-Phenylhydrazinyl)-1,2,3,4-tetrahydroacridine (6.14)

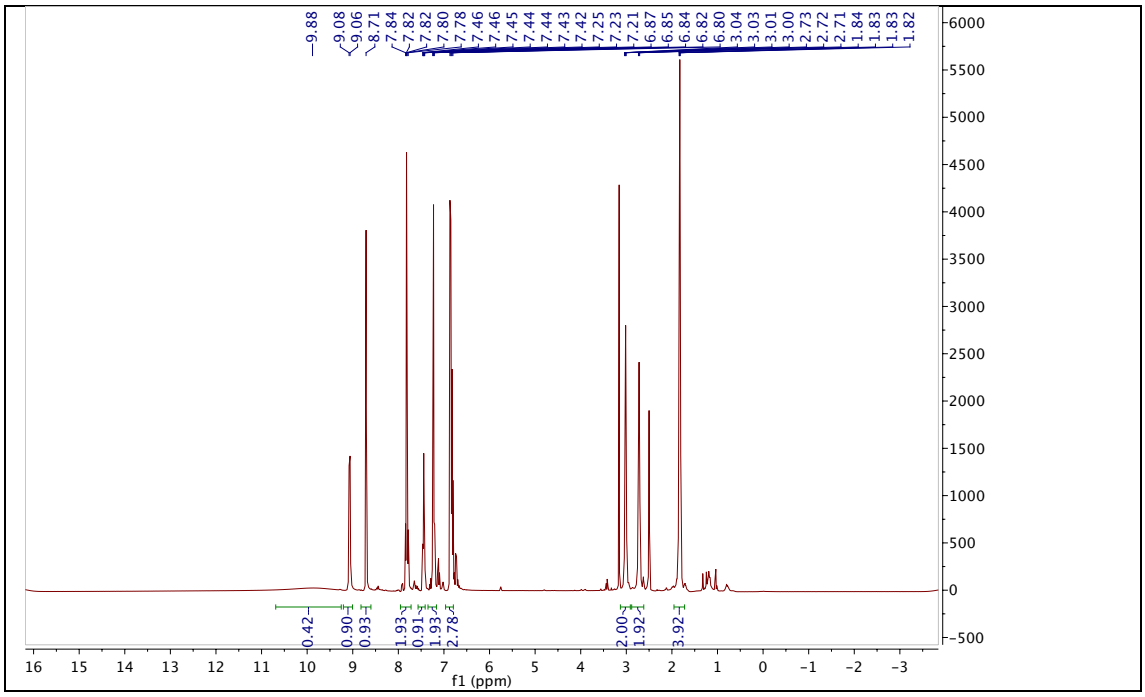

## 6.5.10 (*E*)-9-(Phenyldiazenyl)-1,2,3,4-tetrahydroacridine (AzoTHA-5)

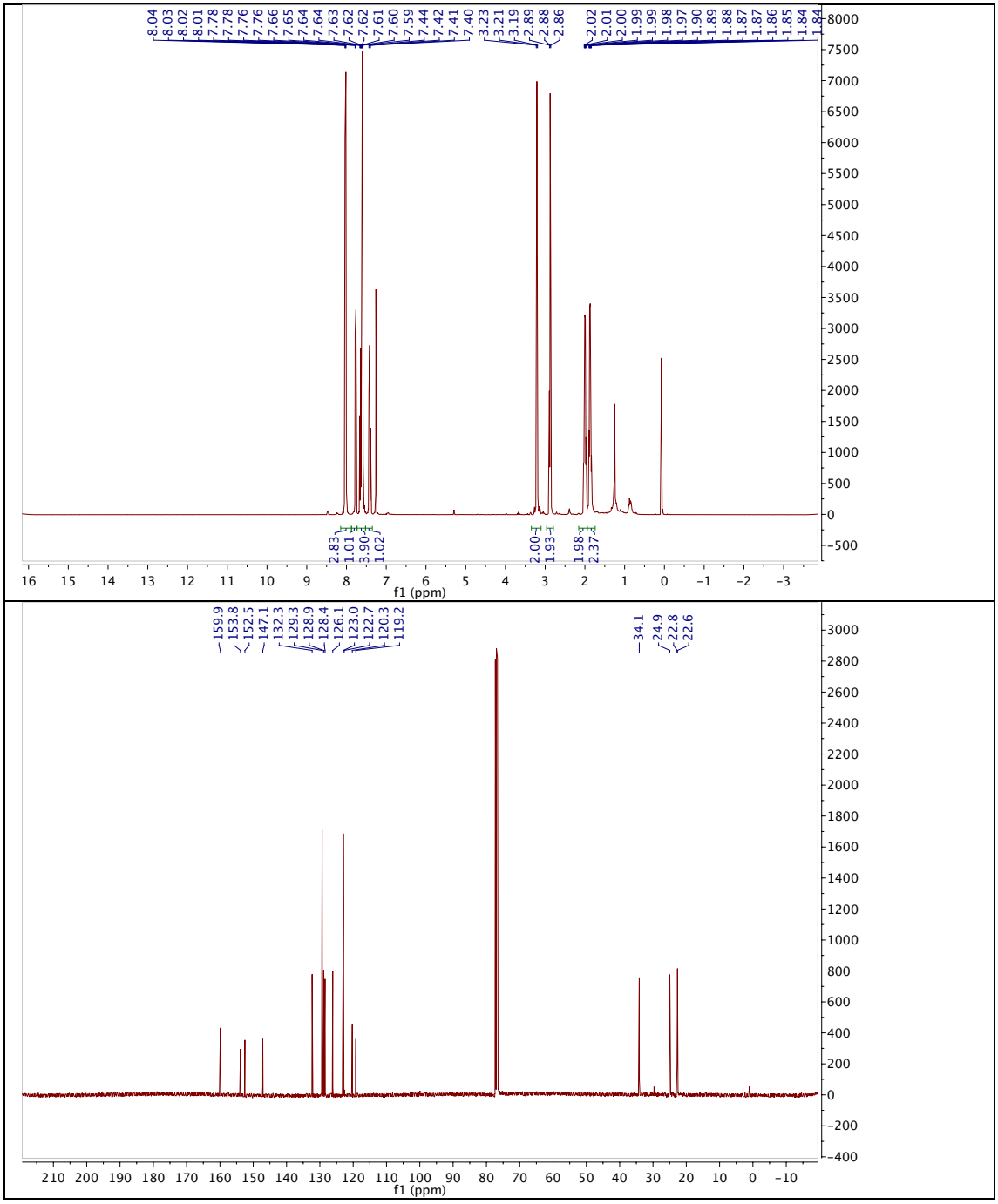

### 6.5.11 2-Phenyl-2,3,4,5-tetrahydropyrazolo[3,4,5-*kl*]acridine (6.15)

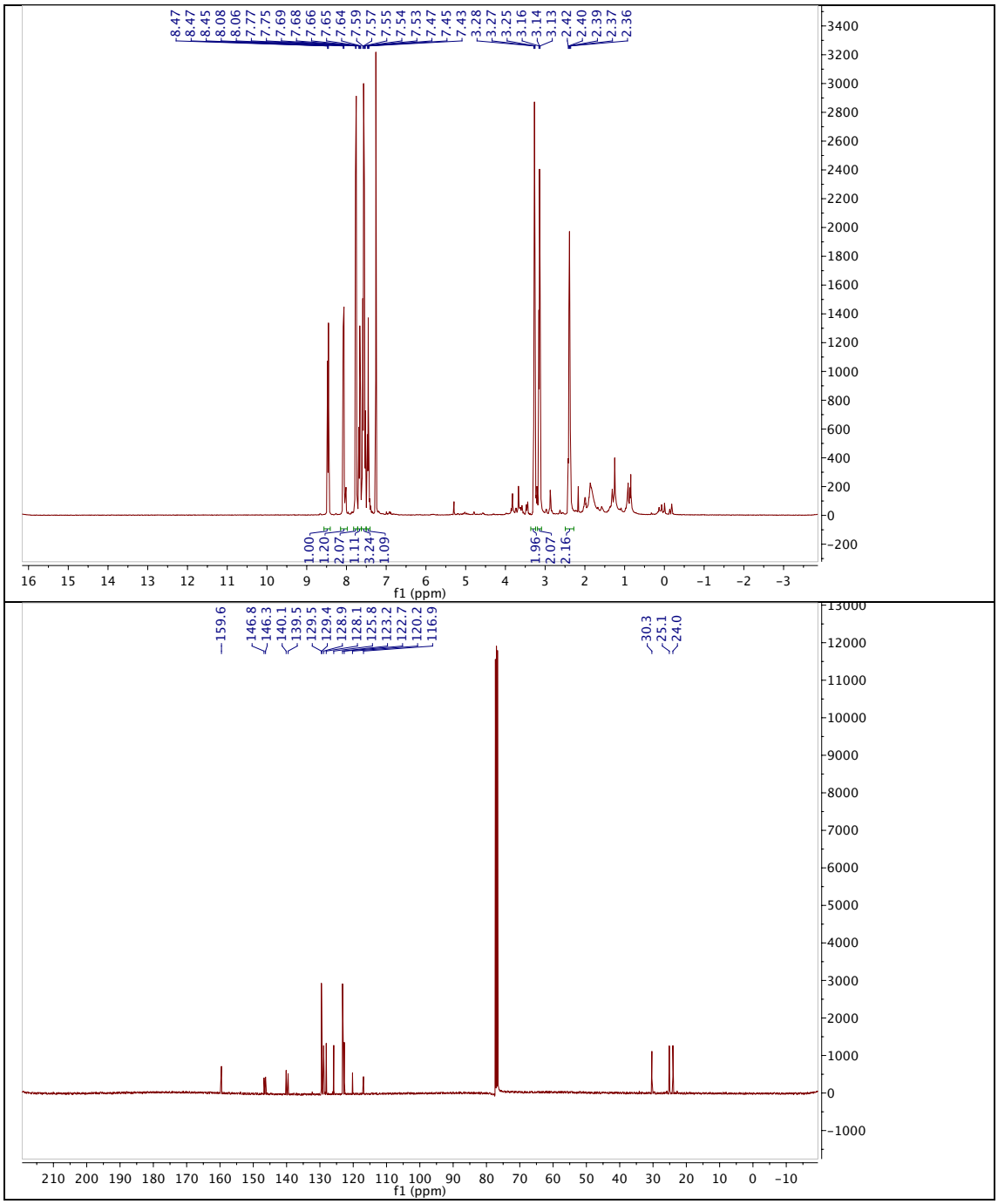

## 6.6 X-ray Crystallographic Data

### 6.6.1 9-Chloro-5,6,7,8-tetrahydroacridine (6.3)

**Supplementary Table 1: Crystallographic data of 6.3.**

| | **6.3** |
|---|---|
| net formula | $C_{13}H_{12}ClN$ |
| $M_r$/g mol$^{-1}$ | 217.694 |
| crystal size/mm | 0.512 × 0.344 × 0.234 |
| $T$/K | 173(2) |
| radiation | MoKα |
| diffractometer | 'Oxford XCalibur' |
| crystal system | triclinic |
| space group | $P$1bar |
| $a$/Å | 15.7176(5) |
| $b$/Å | 15.8055(5) |
| $c$/Å | 22.8646(7) |
| α/° | 73.014(3) |
| β/° | 77.980(3) |
| γ/° | 60.271(3) |
| $V$/Å$^3$ | 4703.6(3) |
| $Z$ | 18 |
| calc. density/g cm$^{-3}$ | 1.38339(9) |
| μ/mm$^{-1}$ | 0.327 |
| absorption correction | 'multi-scan' |
| transmission factor range | 0.94684–1.00000 |
| refls. measured | 27969 |
| $R_{int}$ | 0.0254 |
| mean σ($I$)/$I$ | 0.0554 |
| θ range | 4.21–26.37 |
| observed refls. | 13094 |
| $x$, $y$ (weighting scheme) | 0.0522, 1.2561 |

| | |
|---|---|
| hydrogen refinement | constr |
| refls in refinement | 18998 |
| parameters | 1243 |
| restraints | 0 |
| $R(F_{obs})$ | 0.0521 |
| $R_w(F^2)$ | 0.1385 |
| $S$ | 1.037 |
| shift/error$_{max}$ | 0.001 |
| max electron density/e Å$^{-3}$ | 0.521 |
| min electron density/e Å$^{-3}$ | −0.310 |

### 6.6.2 (*E*)-*N*-(4-((4-(Diethylamino)phenyl)diazenyl)phenethyl)-1,2,3,4-tetrahydroacridin-9-amine (AzoTHA-4)

**Supplementary Table 2: Crystallographic data of AzoTHA-4.**

| | **AzoTHA-4** |
|---|---|
| net formula | $C_{31}H_{35}N_5$ |
| $M_r$/g mol$^{-1}$ | 477.643 |
| crystal size/mm | 0.150 × 0.100 × 0.020 |
| $T$/K | 173(2) |
| radiation | 'Mo Kα |
| diffractometer | 'Bruker D8Venture' |
| crystal system | monoclinic |
| space group | $P2_1/c$ |
| $a$/Å | 17.199(3) |
| $b$/Å | 7.1538(12) |
| $c$/Å | 20.583(3) |
| α/° | 90 |
| β/° | 90.490(5) |
| γ/° | 90 |
| $V$/Å$^3$ | 2532.3(7) |
| $Z$ | 4 |

| | |
|---|---|
| calc. density/g cm$^{-3}$ | 1.2529(3) |
| μ/mm$^{-1}$ | 0.075 |
| absorption correction | multi-scan |
| transmission factor range | 0.9069–0.9580 |
| refls. measured | 45456 |
| $R_{int}$ | 0.0520 |
| mean σ($I$)/$I$ | 0.0243 |
| θ range | 3.01–25.38 |
| observed refls. | 3657 |
| $x$, $y$ (weighting scheme) | 0.0491, 1.1619 |
| hydrogen refinement | mixed |
| refls in refinement | 4664 |
| parameters | 331 |
| restraints | 0 |
| $R(F_{obs})$ | 0.0426 |
| $R_w(F^2)$ | 0.1135 |
| $S$ | 1.046 |
| shift/error$_{max}$ | 0.001 |
| max electron density/e Å$^{-3}$ | 0.476 |
| min electron density/e Å$^{-3}$ | −0.268 |

# *7 Human Carbonic Anhydrase II*

## 7.1 Introduction

In this chapter, a rational approach to the design of a photocontrollable enzyme, based on the photopharmacological PTL logic alongside inhibitory studies of PCLs is described. As a proof-of-concept system the ubiquitous enzyme Carbonic Anhydrase (CA) was chosen, which has previously been a target for photocontrol using different strategies, such as the photoswitchable affinity labeling (PAL) concept[63] and the complexation of a photoresponsive 1,2-dithienylethene via a copper(II) iminodiacetate moiety.[64] However, these studies were limited in the control of CAs by either or the lack of a structurally guided approach for well-defined labeling; unknown labeling yields; non-covalent linkage and long-irradiation times. The goal in this work was to rationally design a structurally well-defined, quantitatively-labeled covalent enzyme, that would enable robust *in vitro* studies on this enzymatic system, whilst laying the groundwork for *in vivo* measurements in more complicated catalytic systems. Consequently, and with respect to the light-controlled AChE with a photochromic ligand (PCL, see Chapter 6), it would expand the photopharmacological photochromic tethered ligand (PTL) concept to enzymatic systems, proving its global application to the most important system of life: controlling catalysis.

Carbonic anhydrase (CA) is a ubiquitously found zinc containing metallo-enzyme with many isoforms, which all catalyze the conversion of carbon dioxide and water to bicarbonate and a proton (Figure 30a, left).[65] Despite its native purpose of pH and pressure regulation, its intrinsic esterase activity can be utilized to measure its activity by hydrolysis of *para*-nitrophenyl actetate (*p*NPA) to a phenolate, of which the product appearance can be observed colorimetrically (Figure 30a, right).[66] For this purpose, pNPA was synthesized by the acylation of 4-nitrophenol with acetyl chloride in DCM. A crystal structure was obtained and is depicted in Figure 30a. In humans, isoform II (human Carbonic Anhydrase II; hCAII) is found in many tissues, and among other regulatory tasks it is responsible for maintaining the inner eye pressure. Failure of hCAII is associated

with glaucoma.[65,67] Treatment of this severe disease that results in blindness is achieved with the application of arylsulfonamides.[67] Being a transition-state analogue,[68] this functional group exhibits excellent blocking characteristics of hCAII and culminates its power in many modern marketed drugs, such as sulfanilamide (**7.1**), acetazolamide (**AAZ**) and dorzolamide.[69] Furthermore, sulfonamide-containing azobenzenes exhibit affinity and blocking capability for hCAII (Figure 30b).[70]

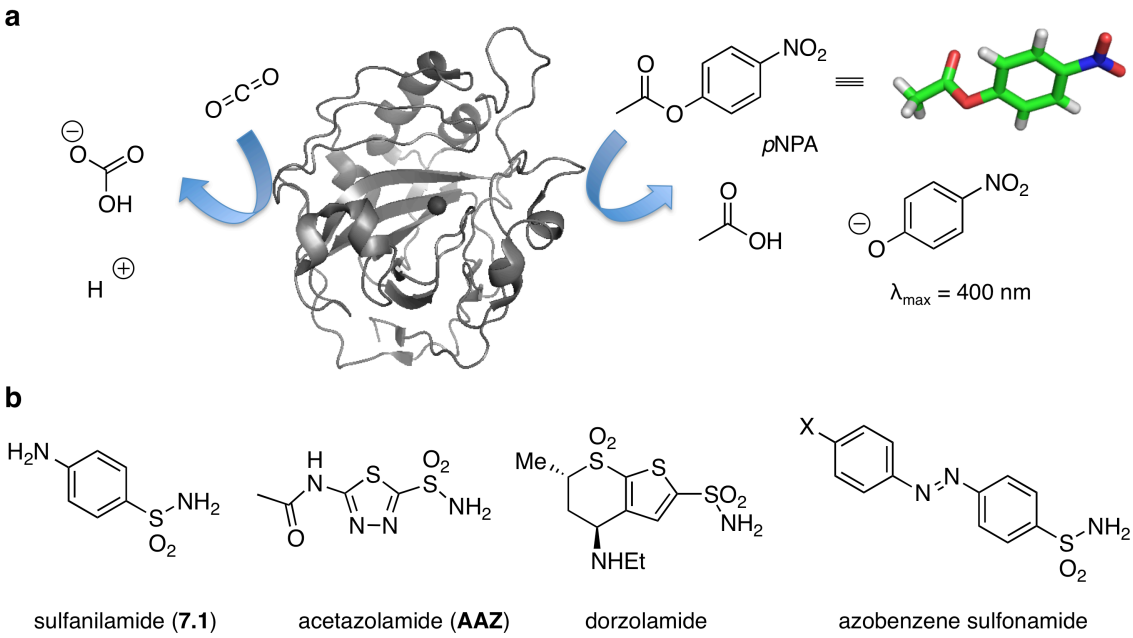


**Figure 30: Function and inhibition of hCAII. a)** hCAII (pdb: 2vva)[71] catalyzes the hydration of carbon dioxide to bicarbonate and a proton (left) and the hydrolysis of *p*NPA to acetate and a colored phenolate ($\lambda_{max}$ = 400 nm). **b)** Known aryl sulfonamide containing pharmacophores of hCAII, including one merged to an azobenzene (right).

Starting with PCLs and characterizing them towards wild-type human Carbonic Anhydrase isozyme II (hCAII), the synthesis of a library of nine sulfonamide-containing azobenzene molecules is described. As none of these molecules showed photoresponsive catalytic behaviour towards hCAII, a PTL approach follows outlined in six sections. In Section I, a strategy to apply optochemical genetic controls to the enzymatic activity of the hCAII is explained. In Section II, the design and synthesis of the necessary PTLs is discussed. Using a novel computational approach outlined in Section III, several potential hCAII mutation

sites that would be likely to facilitate the covalent labeling and photo-reponsive behavior of the designed PTLs are found. The design culminates in the development of the Light-controlled human Carbonic Anhydrase II (LihCAII) and its reversible photocontrol as demonstrated in Section IV including proof of labeling by full protein mass spectrometry. Additional X-ray crystallographic studies are described in Section V, where hCAII crystal structures (in 1.15–1.50 Å resolution) together with photochromic ligands are presented. Section VI describes an attempt to label the native cysteine (C206) in hCAII by mutational and crystallographic studies. Last but not least, another technique is introduced for the labeling of hCAII *via* tetrazine-norbornene click chemistry on engineered unnatural amino acids.

## 7.2 Results and Discussion

### 7.2.1 PCL Approach

Azobenzenes can be synthesized by a variety of known chemical transformations.[72] Among the most widely used is the diazotization of aniline, followed by trapping the diazonium salt with an electron rich aromatic compound (such as anilines and phenols). For electron-poor azobenzenes a condensation reaction between an aryl nitroso and aniline can be employed, known as the Mills reaction. We synthesized nine 4'-substituted sulfonamide containing azobenzenes **7.2-7.10**, as this substitution pattern will have the biggest impact on the electronics of the sulfonamide group due to communication *via* the conjugated π-system of the aromatic units and the diazene unit. Diazotization of sulfanilamide and subsequent reaction with phenol, *N*,*N*-diethylaniline and *N*-phenylmorpholine lead to azobenzenes **7.2**, **7.3** and **7.4**, in moderate to low yields (43%, 38% and 25%, respectively) (Scheme 7a). Employing a methylene-protected aniline according to the procedure from Supuran and co-workers,[70] it is possible to obtain amine azobenzene **7.5** in a one-pot reaction over three steps in 25%. By diazotization and trapping the salt with TMS-azide, azide azobenzene **7.6** is obtained in 75% *via* a [3+2] and retro-[3+2] cycloaddition (Scheme 7b) according to the methodology of Barral *et al.*.[73] The mechanism proceeds *via* a pentazole that is formed by reaction between the created diazonium salt and and the azide. Upon collapse of the pentazole with the extrusion of nitrogen, the aromatic azide is formed as described above and not *via* an aromatic substitution, which seems intuitive. For the Mills reaction, different nitroso compounds were generated that were all used without further purification for the following condensation reactions. For example, sulfanilamide reacted with Oxone® in a biphasic DCM/water-mixture to its nitroso counterpart, which was condensed with 4-toluidine to give methyl azobenzene **7.7** (Scheme 7c) in 49% yield over two steps. Additionally, several *in situ* generated nitroso compounds bearing a nitro and a carboxyl ester were reacted with sulfanilamide to obtain nitro azobenzene **7.8** and ethyl ester azobenzene **7.10**, respectively. Commercially available nitrosobenzene gave rise to the

unsubstituted sulfonamide **7.9** (Scheme 7d). The yield was poor for nitro azobenzene **7.8** (9%). However, reaction of nitrosobenzene was accomplished in low yield to obtain **7.9** (38%), while **7.10** was isolated in quantitative yield (99%).

Crystals suitable for X-ray diffractometry were obtained for azobenzenes **7.2**, **7.3**, **7.4**, **7.5**, **7.6**, **7.7**, **7.8** and **7.10** by (crystallization conditions can be found in the Experimental section). Interestingly, compounds with a strong +M effect (**7.3** and **7.4**) show a $sp^2$-hybridized S-N-bond, while the other molecules (i.e. **7.2**, **7.6**, **7.7**, **7.8** and **7.10**) exhibit an $sp^3$-hybridized S-N-bond.

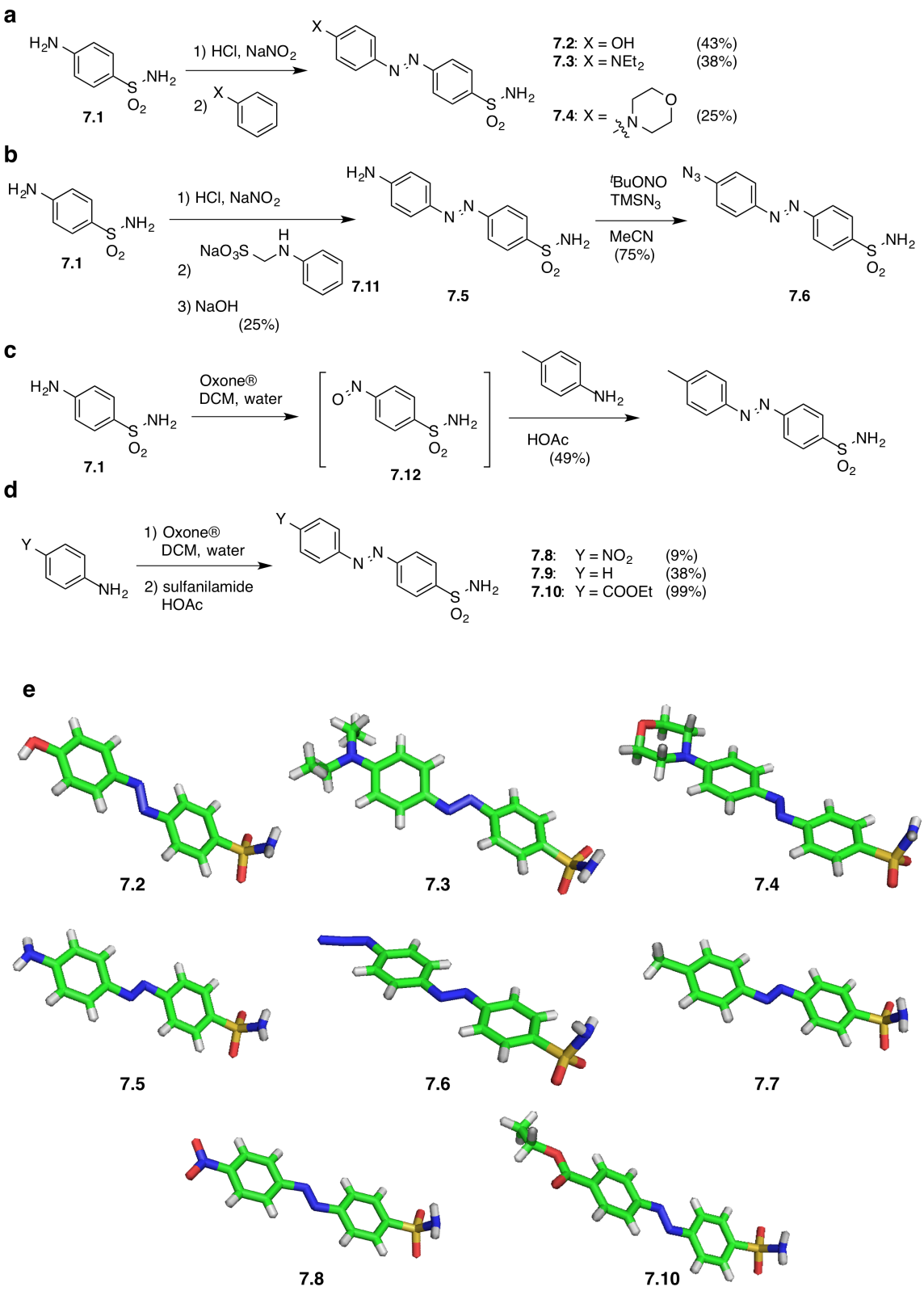


**Scheme 6: Synthesis of azobenzene-containing aryl sulfonamides by different strategies. a)** Diazotation and trapping of the diazonium salt with an electron-rich aromatic compound yields azobenzenes **7.2**–**7.4**. **b)** Reaction of a methylene-protected aniline and one-pot deprotection yields **7.5**, which can be further derivatized to **7.6**. **c)** Formation of the nitroso species of sulfanilamide

for subsequent Mills condensation to give **7.7**. **d)** Formation of the nitroso derivative of anilines, which are reacted with sulfanilamide in a Mills reaction to obtain **7.8**– **7.10**. **e)** Crystal structures were obtained for compounds **7.3**, **7.4**, **7.5**, **7.6**, **7.7**, **7.8** and **7.10** (cosolvents and/or multiple molecules in the asymmetric cell are omitted for clarity).

The substitution pattern on the aromatic core together with their electronic characteristics determines the absorption spectra (the most dominant being the π-π*-band) of the individual azobenzene.[74] The wavelength of maximal absorption ($\lambda_{max}$) was assessed by RP-LCMS equipped with a UV/Vis diode array detector, when determining the purity of the library. Therefore, $\lambda_{max}$ is determined in a water/acetonitrile mixture, which mimics aqueous conditions also used for biological assaying. The results are given in Table 10. While the "naked" azobenzene **7.9** has the absorption maximum in the bluest part of the spectrum ($\lambda_{max}$ = 322 nm), substitution on the azobenzene in the 4'-position leads to a bathochromic shift, which is smaller for electron-withdrawing groups ($\lambda_{max}$ = 328 nm for **7.8**; $\lambda_{max}$ = 342 nm for **7.10**) and more pronounced for electron-donating groups (($\lambda_{max}$ = 338 nm for **7.7**, $\lambda_{max}$ = 358 nm for **7.2**, $\lambda_{max}$ = 404 nm for **7.5**, $\lambda_{max}$ = 414 nm for **7.4**, and $\lambda_{max}$ = 460 nm for **7.3**). Interestingly, azide **7.6** with a Hammett constant of $\sigma$ = 0.08,[75] exhibits a bathochromic shift ($\lambda_{max}$ = 356) close to hydroxy azobenzene **7.2** although it can be considered neither electron-withdrawing, nor electron-donating.

In order to determine the half-maximal inhibitory constants ($IC_{50}$s) for the library, a colorimetric endpoint measurement of the catalyzed *p*NPA hydrolysis (Figure 30a) was employed. Usually, a dansyl competition assay is employed fur this purpose,[65,76] however, as this assay is based on fluorescence and azobenzenes can quench fluorescence,[77] this might cause a distortion of the obtained data. Furthermore, irradiation with UV-light can result in azobenzene-*cis*-isomerization, which could lead to different binding characteristics. Therefore, this system was not used as a first choice. By using the benchmark blocker **AAZ**, an $IC_{50}$ of 55 nM was obtained, which is in accordance with previously reported inhibition constants.[70] Consequently, this assay can assess the inhibitory characteristics of our library in a robust and reliable manner.

By using the Cheng-Prusoff equation[78] with a Michaelis-Menten constant of $K_M$ = 1092.5 µM for *p*NPA (Supplementary Figure 2), the inhibitory constant $K_i$ (Table 10) was calculated for each compound from the $IC_{50}$s obtained from fitting the activity *versus* concentration sigmoidal curve (Figure 31a). Azobenzenes **7.2** and **7.5** have been synthesized and tested previously, and the $K_i$s determined in the previous work are about an order of magnitude higher than in the findings described herein ($K_i$ (**7.2**) = 665 nM or 29.7; $K_i$ (**7.5**) = 106 nM or 30.7).[70] However, these data were recorded using a $CO_2$-hydration assay, which differs in substrate and kinetics from the endpoint system. Interestingly, the most efficient blocker turned out to be **7.3** ($K_i$ = 25.0 nM), which also shows the greatest shift in its UV/Vis spectra. Another electron donating blocker with a methyl group substituent (**7.4**), however, has the lowest affinity ($K_i$ = 65.1 nM) of the library. **7.4** offers the second-lowest affinity ($K_i$ = 55.4 nM), which seems counter-intuitive, as the only difference with respect to **7.3** is the connection of the ethyl chains by an oxygen atom to a morpholine ring. This does not only affect the binding properties, but also the π-π*-band, which is 46 nm blue shifted relative to **7.3**. The inhibitors with the proton and azide substituents (**7.9** and **7.6**, respectively) show very similar affinity towards hCAII with a $K_i$ = 44.8 nM and $K_i$ = 46.1 nM. Sterics are also restrained, but should not affect binding, as the 4'-position is solvent-exposed. Taken all these findings into account, it can be concluded that the sulfonamide-zinc interaction dominates the binding affinity.

**Table 10: Maximal absorbance wavelength ($\lambda_{max}$), Hammett constants ($\sigma$) and inhibitory characteristics ($IC_{50}$ and $K_i$) of 7.2-7.10 including AAZ.**

| | substitution pattern | $\lambda_{max}$ (nm) | Hammett constant $\sigma^{75}$ | $IC_{50}$ (nM) | $K_i$ (nM) |
|---|---|---|---|---|---|
| **7.2** | OH | 358 | -0.37 | 165.6 | 29.7 |
| **7.3** | $NEt_2$ | 460 | -0.83 | 139.6 | 25.0 |
| **7.4** | $N(CH_2CH_2)_2O$ | 414 | -0.83[a] | 309.2 | 55.4 |
| **7.5** | $NH_2$ | 404 | -0.66 | 171.4 | 30.7 |
| **7.6** | $N_3$ | 356 | 0.08 | 257.1 | 46.1 |
| **7.7** | Me | 338 | -0.17 | 363.2 | 65.1 |
| **7.8** | $NO_2$ | 328 | 0.78 | 159.4 | 28.6 |
| **7.9** | H | 322 | 0.00 | 249.7 | 44.8 |
| **7.10** | COOEt | 342 | 0.45 | 167.9 | 30.1 |
| **AAZ** | --- | --- | --- | 55.5 | 10.0 |

[a] To the best of our knowledge, the Hammett constant for morpholine has not been determine, therefore we use the parameter for alkylated amines due to its similar electronic nature.

The electronic difference of the azobenene library can be expressed by their absorption spectra or in their Hammett constants. When plotted against each other a trend can be observed, which is reflected by a more bathochromic shift when the Hammett constant becomes more negative (Figure 31b). However, when plotting the Hammett constants or the maximal absorbance wavelength versus the $IC_{50}$ (Figure 31c and 31d, respectively), no overall correlation can be hypothesized. In both cases, morpholine **7.4**, azide **7.6**, methyl **7.7** and unsubstituted azobenzene sulfonamide **7.9** are in one region (250-300 µM), while all other inhibitors (phenol **7.2**, alkyl aniline **7.3**, aniline **7.5**, nitro **7.8** and ethyl carboxylate **7.10**) show higher affinity around 150 µM. The latter also

shows a distribution from UV- to blue maximal absorbance. It can therefore be speculated that electronics do not have a primary effect on binding properties towards hCAII, but rather the sole presence of an aryl sulfonamide is enough. It should be pointed out that "naked" azobenzene **7.9** does not follow the trend when correlating its by definition Hammett constant of σ = 0.00 to its $\lambda_{max}$ = 322 nm. As the plots from Figure 31c and 31d can be considered mirror images of each other, as a consequence **7.9** does not fit into this picture.

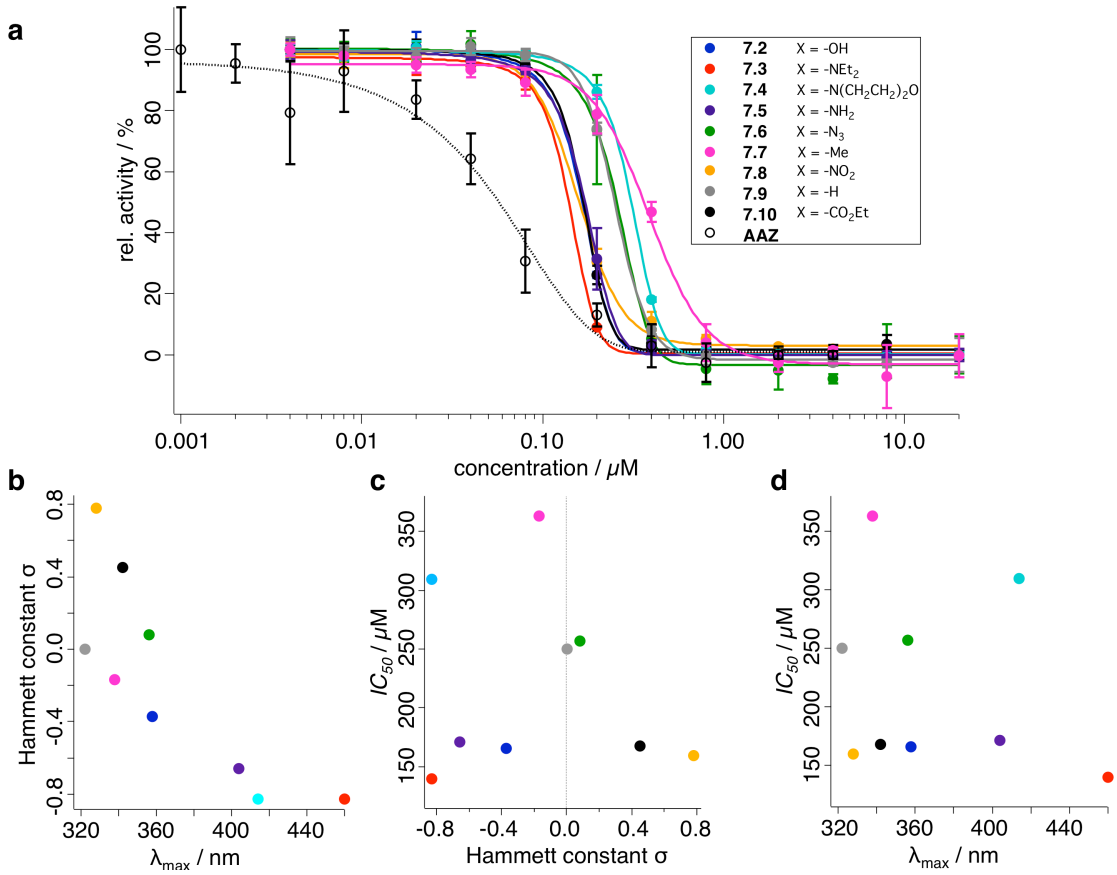


**Figure 31: Inhibition of hCAII by electronically different azobenzene sulfonamides and AZZ. a)** End point measurement for the determination of $IC_{50}$ for compounds **7.2-7.10**. **b)** Hammett constants versus maximal absorbance wavelength shows decreasing trend. **c)** $IC_{50}$ *versus* Hammett constants. **d)** $IC_{50}$ *versus* $\lambda_{max}$.

Concerning steric reasons, and as the functional groups employed are small modifications in size, steric effects contributing to blocking characteristics can be excluded, as the moieties are exposed to the surrounding. However, interactions in these regions can contribute to the binding of a blocker by for instance

hydrogen bonding, a fact that has not been explored and can not be ruled out in the study described herein.

### 7.2.2 PTL Approach using Thiol-Maleimide Chemistry

#### 7.2.2.1 Section I: Photopharmacological Control of hCAII

The idea behind the photochromic tethered ligand (PTL) approach of photopharmacology unites the strengths of molecular biology and chemical synthesis to yield a photocontrollable protein *via* covalent labeling. If an appropriate attachment site is not present in the native protein, tools from molecular biology are used to create and introduce PTL-binding reactive groups (usually a reduced thiol from a cysteine) into the amino acid backbones *via* site-directed mutagenesis PCR and heterologous expression systems. Chemical synthesis is then used to make well-defined and fully–characterized photoresponsive ligands. Designing a functional PTL requires four basic components: (i) a chemical moiety (*i.e.* a ligand with inhibitory, agonistic or antagonistic properties) which binds to the active site of its target with sufficient affinity; (ii) a photoswitchable unit which undergoes a reversible conformational change upon irradiation with orthogonal and discrete wavelengths of light; (iii) a reactive functional group, which tethers the PTL to the protein *via* the (introduced) PTL-binding site; and (iv) appropriately-structured linkers between these components which enable the photo-responsive behavior of the switch to alter the active-site binding of component (i). With the PTL covalently attached to its target, the ligand's local concentration is always quite high, however due to the introduced photoswitchable moiety, in one photostationary state the ligand is able to reach the active site, while in the other it is not (Figure 32).

In this chapter, an established model system was chosen that is well-known, plays a key role in opthamologic disease, and is therefore an essential component of the vision restoration program in the Trauner research group. Being an ubiquitous zinc-containing metalloprotein, human Carbonic Anhydrase

II (hCAII) catalyzes the reversible conversion of carbon dioxide and water into a proton and bicarbonate (Figure 30a).[65] Among other regulatory tasks in the body, hCAII plays a crucial role in maintaining the inner pressure of the eyeball, and its failure is associated with glaucoma.[67] It has been used extensively as a model system for enzymology for several reasons[65]: firstly, other approaches have been successful at introducing photoreponsivity into hCA (*vide infra*). Secondly, its mode of action is well understood, inhibitors are known and well-characterized (Figure 30b), crystal structures are available, assays (such as the colorimetric *p*NPA assay, Figure 30a) are well-established, and, being a monomeric, single amino acid strand protein with no disulfide bonds, it is stable and easy to handle.

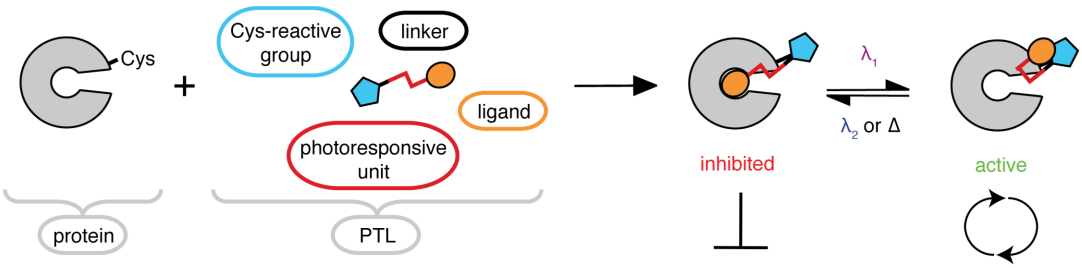


**Figure 32: The logic of a PTL approach for light-controlled enzymes.** A target protein bearing a reduced, free cysteine on the surface can be covalently labeled with a PTL. A PTL consists of four major features: a cysteine-reactive group (usually a maleimide), a linker, a photoresponsive unit (usually an azobenzene) and a pharmacophore (ligand). Once attached, the PTL can reach the catalytic active site thereby blocking it or is unable to reach it depending on the light-induced geometry.

#### 7.2.2.2 Section II: Design and Synthesis of PTLs SA-1 to SA-3

In order to design a functional PTL, the aforemetioned four components must be developed in concert, and the final choices are discussed in detail in this section:

i) *Inhibitor*. Acting as transition state analogues, arylsulfonamides are known pharmacophores that block the enzymatic activity of CAs with a dissociation constant ($K_d$) from the picomolar to the micromolar range.[65] As they are commercially available and the structure–activity relationship allows permutation in the 4-position of the aromatic unit, aryl sulfonamides served as a scaffold for further design, sulfanilamide (**7.1**) being a prime example (Figure 33a). This structural feature is used commonly in the research and development of novel CA blockers.

ii) *Photoresponsive unit*. The Trauner group has frequently utilized azobenzenes as photoswitches.[2] Their reversible conformational *cis-trans*-isomerism results in a change of d(*trans*) = 1.3 nm to d(*cis*) = 0.8 nm with respect to the distance between their 4- and 4'-functionalized position (Figure 33b). Switching is robust and fast over many cycles, and switching wavelengths can be red-shifted by increasing the electron density of the azobenzene moiety. *cis*-Isomerization is usually achieved with UV-light, while *trans*-isomerization can be triggered with visible light (typically blue light). Furthermore, relaxation to the *trans*-state can occur in the dark, which is usually slower than applying light. Together, these properties make azobenzenes the photoswitchable unit of choice for the reversible and especially for the fast photocontrol of biological function with light from the UV-A to visible range.

iii) *Cysteine-reactive group*. Maleimides readily react with the thiol group of cysteines, anchoring the PTL to the protein in a 1,4-Michael-Addition, a so-called "click-reaction."[79] The reaction is sufficiently fast and has been utilized extensively to label proteins as it can be performed at room temperature in aqueous conditions. The resulting succinimide is able to be hydrolysed by the addition of one water molecule to any of the two non-equivalent carbonyl groups to give the corresponding free acid (Figure 33c).[80,81] Depending on whether

hydrolysis occurs at the α-CO or at the β-CO, different degrees of freedom are liberated with respect to the attached R moiety. By losing strain and rotational restriction from the succinimide ring, the end-to-end-distance of the opened PTL is increased. It is believed that with the generated negative charge the retro-Michael-Addition is surpressed due to the increased $pK_a$ of the α-hydrogen atom.

iv) *Linker*. The distance between the cysteine reactive group and the inhibitory group is crucial as the latter should be able to reach the active site in one conformation but not in the other; too short a linker could prevent binding in both *cis*- and *trans*-states, while too long a linker could result in binding regardless of the azobenzene conformation. Theoretically, a linker could also be installed between the inhibitor and the azobenzene group. However, and with respect to the design described herein, this possibility was not considered as sulfonamide containing azobenzenes were already known to block hCAII activity. Furthermore, merging the arylsulfonamide pharmacophore with the azobenzene's aromatic ring adds more strain to the PTL, resulting in a more substantial conformational change when photoswitched.

Combining these components, one can come up with three PTLs (**SA-1** to **SA-3**, Figure 33d), all of them containing a maleimide end group, an azobenzene, and an arylsulfonamide on the opposite end of the PTL molecule. However, the linker between the maleimide and azobenzene differs: **SA-1** bears a glycine linker; **SA-2** is extended to a bis-glycine; and **SA-3** contains a methylene triazole specifically designed to increase the rotational strain. With these permutations, different degrees of length and flexibility were implemented in our potential PTLs, providing the variety necessary to develop a set of suitable cysteine attachment sites.

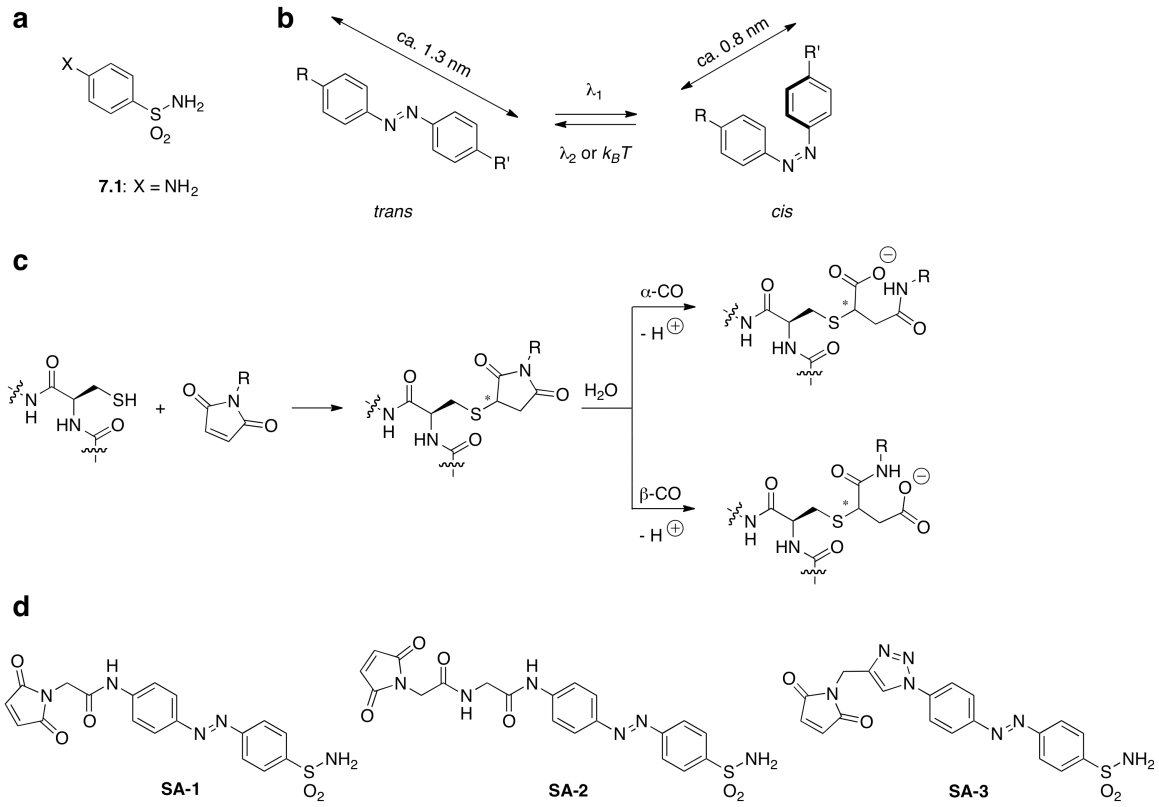


**Figure 33: The logic of our PTL design, based on: a)** an arylsulfonamide as a hCAII inhibitor; **b)** the photoresponsive azobenzene unit with its wavelength-dependent *cis-trans*-isomerism; **c)** the maleimide which undergoes "click chemistry" with a reduced thiol creating a stereocenter with subsequent water hydrolysis (that occurs unregioselective) of the corresponding succinimide; and **d)** our resulting PTL*s* **SA-1** to **SA-3** with different linkers between the azobezenzene and the maleimide.

The synthesis of the PTLs was achieved in multistep sequences and detailed procedures including full characterization can be found in the Experimental section. Starting with several precursors for the final photochromic tethered ligands (PTLs), 4-((4-aminophenyl)diazenyl)benzenesulfonamide[82] (**7.5**) was obtained in a three step sequence in 25% yield and subsequently connected to the maleimide-containing acid **7.13** with the coupling reagents EDCI and HOBt and DIPEA as a base and proton transferring reagent in order to obtain **SA-1** in 29% yield after RP-HPLC purification. Several conditions were screened as coupling conditions (not shown), proving the aromatic amine to be very unreactive. It should be noted, that the addition of 4 Å molecular sieves to the reaction mixture improved the yield by roughly 10% (Scheme 6a).

**SA-2** was synthesized differently from **SA-1** in order to bypass the low yielding amide coupling and to avoid the time consuming work-up procedure. Firstly, the nitroso species **7.11** was obtained by oxidation of sulfanilamide (**7.1**) with Oxone® in a DCM/water mixture, which was used without further purification and subsequently condensed with aromatic amine **7.14**[83] in a Mills reaction to yield carbamate **7.15**. Deprotection of the Boc-group with TFA in DCM then yielded the free amine as its corresponding TFA salt **7.16**. In order to attach the maleimide moiety, acyl chloride **7.17**[9] was prepared as previously reported[84] and used for the acylation of **7.16** to obtain **SA-2** in 19% yield in the final step (Scheme 6b).

The last PTL (**SA-3**) was prepared through alkyne azide "click chemistry." Starting from maleic anhydride (**7.18**) and propargyl amine (**7.19**), the ring-opened (*Z*)-4-oxo-4-(prop-2-yn-1-ylamino)but-2-enoic acid (**7.20**) was obtained as a crude product and subsequently ring-closed to *N*-propargylmaleimide (**7.21**) through the addition of $ZnBr_2$ as a Lewis acid and HHMDS as a Brønsted base as described in past work from our group.[85] Following the synthetic protocol from Barral *et al.*, azide **7.6** was obtained from **7.5** by diazotation with *tert*-butyl nitrite in TFA-acidic acetonitrile and subsequent reaction with TMS-azide (*vide supra*).[86] After the *in-situ* formation of pentazole via a 1,3-dipolar cycloaddition and following a retro Huisgen reaction with extrusion of nitrogen, the desired azide was obtained in 75% yield. The azide then underwent a 1,4-regioselective Cu(I)-catalyzed Huisgen cycloaddition with alkyne **7.21** to yield the title compound **SA-3** in 65% (Scheme 6c).

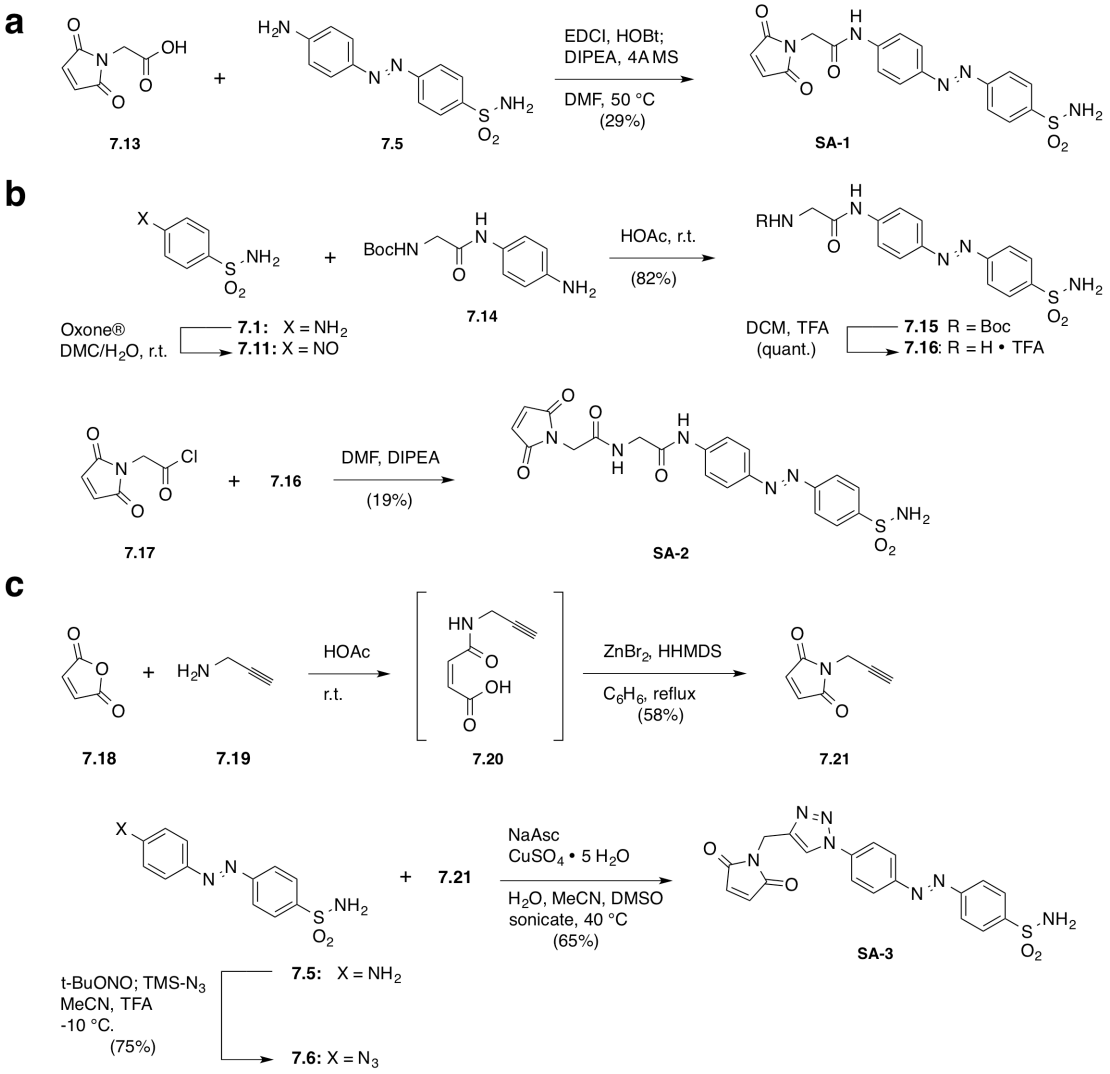


Scheme 7: **PTL-Synthesis. a) SA-1** by HOBt/DCC mediated amide coupling; **b) SA-2** by acylation and **c) SA-3** by alkyne-azide click chemistry.

In Summary, the three PTLs **SA-1**, **SA-2** and **SA-3** were prepared in multistep procedures from commercially available or previously described compounds in overall yields of 29%, 17% and 28%, respectively. Optimization of the synthetic protocols is a future goal, but was not neccessary for this study as sufficient quantities (milligrams) of the PTLs were obtained in pure form. In addition, the inhibitory capacity of each PTL was tested on wild-type (wt) hCAII to confirm that blocking can be achieved before moving to hCAII mutants. Indeed, all PTLs were strong blockers of wt hCAII with half-maximal inhibitory constants ($IC_{50}$s) of 5.36, 0.31 and 0.24 μM for **SA-1**, **SA-2** and **SA-3**, respectively (see Supporting Figure 2).

#### 7.2.2.3 Section III: Computational Modeling to Determine Candidate PTL Attachment Sites

Once the **SA-1** to **SA-3** PTLs were designed and prepared, the next step was to determine the optimal site on the hCAII backbone to introduce the cysteine residue, providing a reaction site for the thiol-maleimide "click–chemistry". In the hCAII structure, there are greater than 200 possible mutation sites to consider, far more than can feasibly be explored experimentally. In order to reduce this number to a handful of likely sites, a computational screening approach was developed that aimed at identifying a small number of optimal candidates for testing.

Good candidate sites in the protein structure are positions where a cysteine mutation would allow EITHER the *cis* structure OR the *trans* structure (but not both) of the PTL to fit in such a way that the maleimide would be able to bind to the cysteine residue in that site while the sulfonamide sits in the binding pocket. To determine these sites, two known crystal structures of hCAII (pdb: 2cba[87] and 1bnt[68]) provided invaluable information, allowing to start each calculation with the sulfonamide appropriately coordinated to the zinc ion in the binding pocket (see Experimental: Computational Methods). Since the computation is largely a geometric problem, a simple united atom model was used for the protein and considered only Lennard-Jones (LJ) interactions with a cut-off implemented for too-close steric contacts (see Experimental: Computational Methods). During the

calculation, the sulfonamide end remained coordinated to the zinc ion while the rest of the PTL was allowed to rotate around its single bonds in order to explore the physical space available to it. Potential maleimide binding sites were then identified whenever the maleimide moiety came close enough to an $\alpha$-carbon position of a given site's residue to bind (were that residue is a cysteine).

Within the simulation, the PTL could be made to interact with different subsets of the protein: the backbone alone, the backbone plus a subset of the side-chains, etc... In order to minimize the number of computations needed while still getting a comprehensive picture of the good candidate sites for cysteine mutation, the calculation was progressed through the following three steps: (1) consideration of the LJ interactions of the PTL with just the backbone atoms; (2) consideration of the LJ interactions of the PTL with the backbone atoms and the subset of all side-chains that were determined not to be potential maleimide-binding sites in step 1; and (3) consideration of the LJ interactions of the PTL with the backbone and all side-chains atoms except those of each potential maleimide-binding site determined in step 2 (so that the wt residue would not interfer with the assessment of its binding potential were it to become a cysteine) (Figure 34a). See Experimental: Computational Methods for more details.

An optimal cysteine mutation site is one that is detected as a potential maleimide-binding site when tested individually with all other side-chains present in their crystallographic positions for the *cis* or *trans* isomer (as in step 3), but is not detected as a potential binding site even when using the backbone-only analysis with the other isomer (as in step 1). With this criteria in mind, four cysteine mutants were identified as providing optimal maleimide-binding sites: D130C (with **SA-2**), F131C (with **SA-2**), G132C (with **SA-1**, **SA-2**, and **SA-3**), and K133C (with **SA-2**) (Figure 34b). See Experimental for the full set of results.

Having identified these optimal PTL-hCAII mutant combinations computationally, the next step was to experimentally test how well these combinations would be able to function as a photocontrollable enzyme.

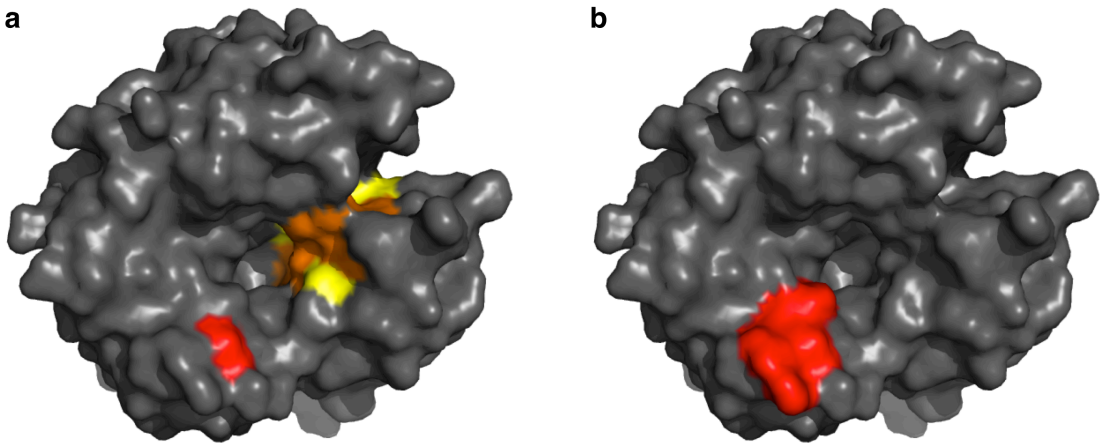


**Figure 34: Results of Computational Screening. a)** Shows the results of screening steps 1, 2, and 3 for **SA-1**, where the yellow indicates the residues that resulted from step 1, orange indicates those that remained of interest after step 2, and red indicates the only residue, G132, that remained after the screening in step 3. **b)** Shows the predicted optimal cysteine mutation sites for **SA-1**, **SA-2**, and **SA-3**.

#### 7.2.2.4 Section IV: LihCAII: Light-Controlled human Carbonic Anhydrase II

hCAII hydrolyzes the ester bond of *para*-nitrophenyl acetate (*p*NPA) with water to acetate and *p*-nitrophenol, whose deprotonated form at physiological pH has an absorbance maximum around 400 nm. This intrinsic esterase activity can be employed to measure enzyme activity[65] (Figure 30a) and therefore report on the photoresponsive behaviour of the enzyme. The appearance of this band can be measured using a UV-spectrophotometer and follows pseudo-first order kinetics. The resulting data can be fit to a linear wave to obtain the activity.[88] Rate constants are reported in units of absorbance change per time, which neglects its conversion into the moles per minute unit by the law of Lambert-Beer by its direct proportional relationship. With this, the obtained data is clearer and neglects further assumptions, such as different extinction coefficients that differ in the literature.[63,65,88,89] The studies were performed at final concentrations of 0.5 µM of the labeled hCAII mutant of interest and 5 mM of *p*NPA in 50 mM Tris buffer at a physiological pH (7.4) with a setup previously reported from the Trauner group.[63] With a large *p*NPA excess pseudo-first order kinetics are given.

Looking at the primary sequence, hCAII bears one native cysteine (C206). In crystal structures, where hCAII was crystallized with the help of mercury salts

this cysteine has access to the periphery and is therefore solvent exposed. Although when this cysteine is mutated to a serine so that the affinity to mercury is abolished, the oxygen atom in the crystal structure points into the proteins hydrophobic core. Therefore, concerns were possible cross reactivity, double labeling of the mutants as well as intramolecular oxidation to form a disulfide bond, which could alter the proteins shape and function. As work-up difficulities with the C206 present were experienced, and furthermore previous reports mention a C206S mutant having the same catalytic activity,[90] an additional mutation for all our candidates was introduced, making them double-mutants. Mutations were introduced by site-directed mutagenesis and hCAII was expressed in and purified from BL21 (DE3) *E. coli* cells (see Experimental). The purity was determined to be >95% by SDS-PAGE and the mutants were further purified by gel filtration for crystallographic studies (see Experimental and Supporting Figure 1 for details and *vide infra*).

Furthermore, another mutant that was not predicted from the computational approach was expressed and testes: G129C, which lies next to the amino acid residues that should give photoresponse according to the code. In the following, all the double mutants are referred to only their PTL attachment site with a given number: mutant I (G129C), mutant II (D130C), mutant III (F131C), mutant IV (G132C) and mutant V (K133C).

All free enzymes were active towards *p*NPA hydrolysis but exhibited different activities (Figure 35a). This allowed the proceeding with our studies and means that mutations in these positions are tolerated. The observed rate constants, $k_{obs}$, were obtained by a linear fit of the respective slope. By subtraction of the background hydrolysis ($k_{bkgr}$ = 0.024±0.008 $A_{400}$/min for 5 mM and $k_{bkgr}$ = 0.009±0.001 $A_{400}$/min for 1 mM *p*NPA, respectively), the absolute velocity $k_{hCAII}$ of each mutant was obtained (Table 11). While mutants I, II, IV and V gave similar rate constants, mutant III showed significantly lower activity. Every mutant was labeled with PTL **SA-1**, **SA-2** and **SA-3** by a novel protocol developed in our laboratories to remove the excess PTL (see below for detailed protocols). The attachment of the PTLs was confirmed by full protein mass spectrometry (see Experimental). Unfortunately, and albeit multiple attempts, labeling of mutant III with any of the PTLs proved to be unsuccessful (see crystal structure

section V for further discussion). Furthermore, some mutants showed an additional mass of m/z = 18, which we assume is the hydrolyzed succinimide species (Figure 33c) of the respective combination system (see Experimental and *vide infra*).

In general, and as expected, PTL labeling lowers the activity of the remaining mutants. This is an indication that the predicted amino acids for cysteine introduction are correct at this point. Attachment of **SA-1**, **SA-2** and **SA-3** to mutant I, II and IV decreases their rate constant $k_{obs}$, while mutant III keep a steady rate constant (rate constants are depicted in Figure 35b and listed in Table 11). This is in accordance with the unsuccessful labeling of this particular mutant, and furthermore proves that our incubation protocol with subsequent removal of the PTL is clean and does not alter enzymatic activity by left-over diffusable sulfonamides in solution. Mutant V, however, could not be labeled with **SA-1** and **SA-3** but stills exhibits lower activity.

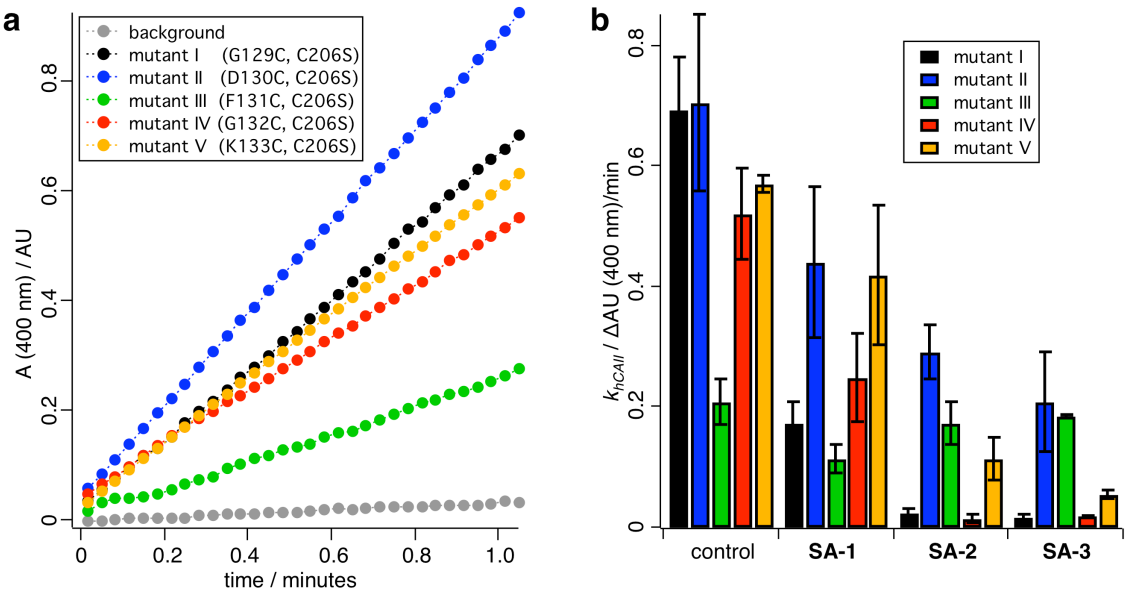


**Figure 35: *p*NPA assay of hCAII and kinetics. a)** Kinetic traces from free, unlabeled enzyme obtained with the *p*NPA assay, and **b)** when linearly fitted and background subtracted rate constants $k_{obs}$ of labeled enzymes in the dark (bars represent S.D., N=3-4).

**Table 11: Rate constants $k_{hCAII}$ [ΔmA (400 nm)/min] of mutants I-IV unlabeled and labeled with SA-1, SA-2 and SA-3 in the dark (mean±S.D., N=3-4).**

| $k_{hCAII}$ [ΔmAU / min] | mutant I (G129C, C206S) | mutant II (D130C, C206S) | mutant III (F131C, C206S) | mutant IV (G132C, C206S) | mutant V (K133C, C206S) |
|---|---|---|---|---|---|
| control | 693.3±86.7 | 705.0±146.2 | 209.1±39.0 | 520.5±75.0 | 568.9±15.0 |
| **SA-1** | 172.1±35.0 | 440.7±126.3 | 114.1±22.6 | 248.5±73.2 | 419.6±115.0 |
| **SA-2** | 22.8±4.5 | 290.4±44.9 | 171.7±35.0 | 14.4±7.3 | 114.6±36.6 |
| **SA-3** | 17.3±4.1 | 209.2±82.3 | 184.7±1.3 | 18.3±0.4 | 53.4±6.5 |

In order to measure the photoresponse, the enzymes were incubated as described above and irradiated with the appropriate wavelengths $\lambda_1$ and $\lambda_2$ for the reversible switching of **SA-1** and **SA-2** labeled samples ($\lambda_1$ (*trans*) = 440 nm and $\lambda_2$ (*cis*) = 370 nm) and for **SA-3** ($\lambda_1$ = 440 nm and $\lambda_2$ = 335 nm) to achieve photoisomerization of the azobenzene. One experiment was performed over a period of 12 minutes, with changing wavelenghts of applied light every 2 minutes. From all possible combinations only **SA-2** attached to mutants I, IV and V were able to perform light-dependent kinetics (Figure 36a). For the latter two, the combination is in accordance with the calculated versions. Mutant I, however, was also able to give photoresponsive behaviour even though the calculations did not predict this very mutant. Interestingly, the kinetic traces show an induction period until the conversion of the substrate is kinetically stable. Therefore, rate constants were obtained by fitting the last 30 seconds before the light was switched to a different wavelength to obtain the highest velocity. Derived and background subtracted rate constants are shown in Figure 36b at important time points (after 2, 4, 6, 8, 10 and 12 minutes) before the enzyme activity was switched again culminating in the reversible photocontrol of hCAII over three cycles. Exact values are given in Table 12 and are represented in Figure 36c. The change in velocity is highly significant for all **SA-2** labeled mutants I (***$p$=0.002), IV (***$p$=0.004) and V (***$p$=0.002) and are accelerated under UV-irradiation by 2.6-, 5.5- and 1.4-fold, respectively.

Furthermore, the on- and off-sets-slopes were fitted exponentially (see Experimental for further details) to obtain the $\tau_{on,\ cis}$- and $\tau_{off,\ trans}$-values (Figure 36d). Catalytic activity of mutant I can be switched with $\tau_{on,\ cis,\ MutI}$ = 0.80 ± 0.12 min and $\tau_{off,\ trans,\ MutI}$ = 0.90 ± 0.24 min, while mutant IV can be switched on in a faster manner ($\tau_{on,\ cis,\ MutIV}$ = 0.33 ± 0.07 min) but off-switching occurs slower ($\tau_{off,\ trans,\ MutIV}$ = 1.71 ± 0.49 min) both also with respect to mutant I. Mutant V shows switching in the range of mutant I ($\tau_{on,\ cis,\ MutV}$ = 0.74 ± 0.12 min and $\tau_{off,\ trans,\ MutV}$ = 0.66 ± 0.03 min).

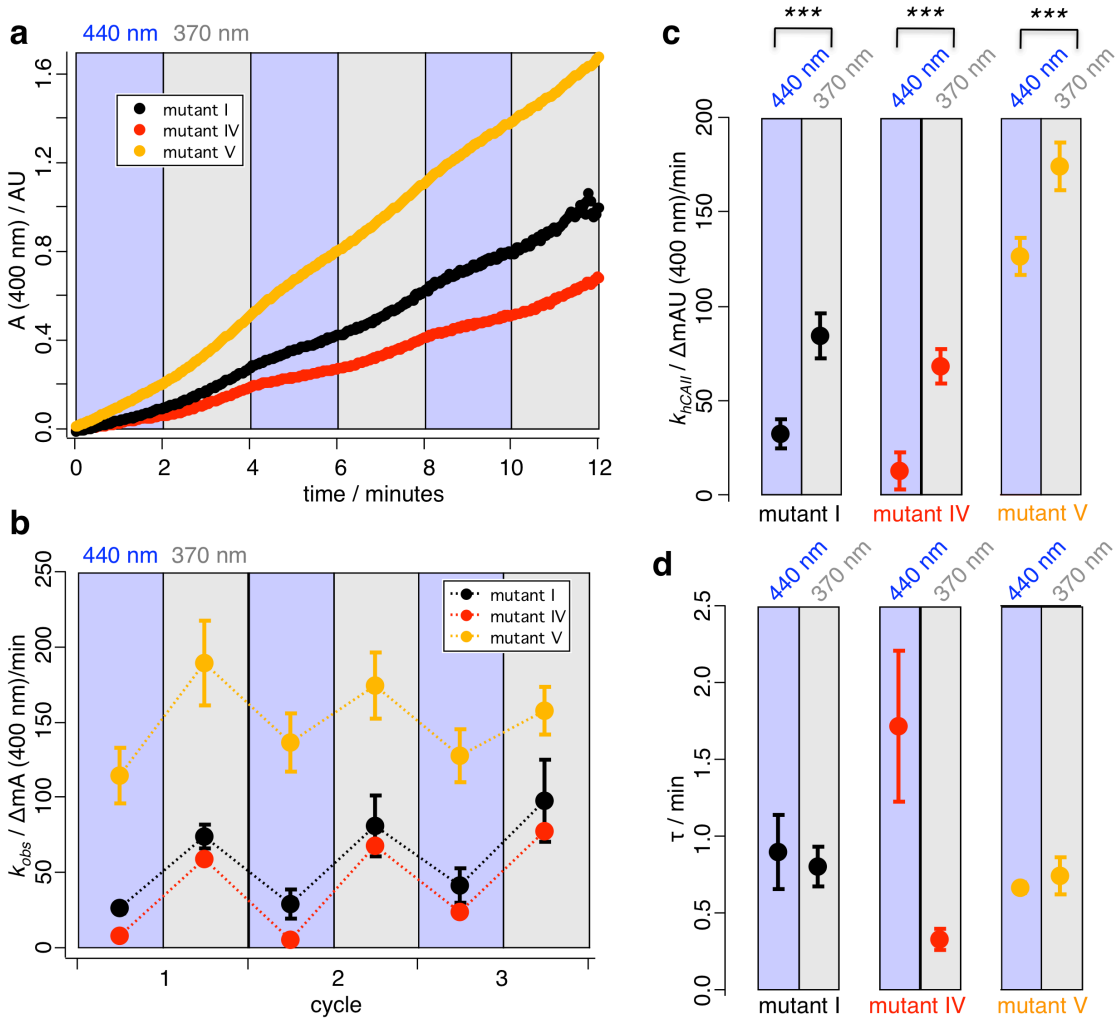


**Figure 36: UV-traces for LihCAII activity: a)** photodependent traces of mutant I, IV and V with attached **SA-2** when irradiated with 440 nm (blue background) and 370 nm (gray background), **b)** calculated rate constants of photodependent kinetics for the timepoints with maximal velocity show reversibility of enzymatic activity, which **c)** proved to be highly significant (T-test for all: ***$p$<0.004) when averaged, **d)** exponentially derived τ-values for on- and off-kinetics (bars represent SEM, N=6-8).

**Table 12: Rate constants $k_{hCAII}$ [ΔmAU (400 nm)/min] of mutants I, IV and V under irradiation with $\lambda_1$ (*trans*)= 440 nm and $\lambda_2$ (*cis*) = 370 nm for each cycle including mean value thereof.**

| cycle | mutant I (G129C, C206S) $k_{hCAII}$ [ΔmAU/min] | | mutant IV (G132C, C206S) $k_{hCAII}$ [ΔmAU/min] | | mutant V (K133C, C206S) $k_{hCAII}$ [ΔmAU/min] | |
|---|---|---|---|---|---|---|
| | $\lambda_1$ = 440 nm | $\lambda_1$ = 370 nm | $\lambda_1$ = 440 nm | $\lambda_1$ = 370 nm | $\lambda_1$ = 440 nm | $\lambda_1$ = 370 nm |
| 1 | 26.6±3.8 | 73.7±8.3 | 8.3±5.4 | 59.1±3.9 | 114.6±18.3 | 189.3±28.1 |
| 2 | 29.3±1.0 | 81.1±20.0 | 5.3±1.8 | 67.9±3.8 | 137±19.0 | 174.4±22.1 |
| 3 | 41.6±11.1 | 97.4±27.1 | 23.6±5.7 | 77.6±2.7 | 127.2±16.2 | 157.5±16.2 |
| mean ±S.D. | 32.5±8.0 | 84.1±12.1 | 12.4±9.8 | 68.2±9.2 | 126.2±11.0 | 173.7±15.9 |

### 7.2.2.5 Section V: Crystallographic Studies

X-Ray crystallography was furthermore employed to obtain atom coordinates in order to render a three-dimensional picture of the investigated structure and determine absolute stereochemical relationships of the labeled cysteines to the maleimides. To do so, chosen hCAII structures were co-crystallized with various photochromic ligands. Firstly, information about mutant III should be obtained, in order to understand its failure to bind the maleimide group. Secondly, more structural information about the labeling of G132C with **SA-2** should be elucidated. As already proven by mass spectrometry this combination yields full labeling, so it was a suitable candidate to gain knowledge about the absolute stereochemistry of the attachment site in its bound state.

The first attempts at crystallization used the photochromic ligand **7.5**, which was co-crystallized with the wild-type enzyme (Figure 37a) and mutant III (Figure 37b). Interestingly, the ligand adopts the trans-isomer when bound to the wild-type protein, but shows *cis*/*trans*-isomerism when bound to mutany III (detailed

view in Figure 37c, d). Furthermore, the cysteine replacing the phenylalanine (F131C) is buried inside the hydrophobic core of the enzyme. It can therefore be concluded that this is the reason why this particular mutant was not prone to labeling with a maleimide ligand. Interestingly, the computational screening technique relies on the placement of the α-carbons of the proposed mutation site, and does not consider the orientation of its side-chains. In this case, the α-carbon is solvent exposed (Figure 37b), but the introduced cysteine is not, illustrating one limitation of the screening algorithm. To confirm this, mutant III was co-crystallized with **SA-2**, which showed similar results: parts of the azobenzene, its linker and the maleimide could not be resolved in this structure (Figure 38a), leading to the conclusion that the maleimide end of the ligand is not attached to the introduced cysteine due to various degrees of freedom. As the calculations suggested mutant III would work with **SA-2** for the photoresponsive design, and labeling of this mutant was not possible so far, a more flexible model compound **7.22** was designed and synthesized (Figure 38b). **7.22** lacks the azobenzene unit and consists only of the sulfonamide for binding to the active site and a maleimide for attachment. The model compound **7.22** was obtained by amide bond formation between sulfanilamide (**7.1**) and previously described acyl chloride **7.17** in poor yield (9%). The co-crystallization of mutant III and **7.22** could circumvent the non-resolvable and flexible part of **SA-2**, therefore providing detailed information on thiol-maleimide binding. Although this ligand binds to the active site and can be resolved with high accuracy, mutant III still did not react to bind with **7.22** (Figure 38c). Conclusively, efforts for successful labeling of mutant III were ended due to the evidence for its cysteine non-accessibility.

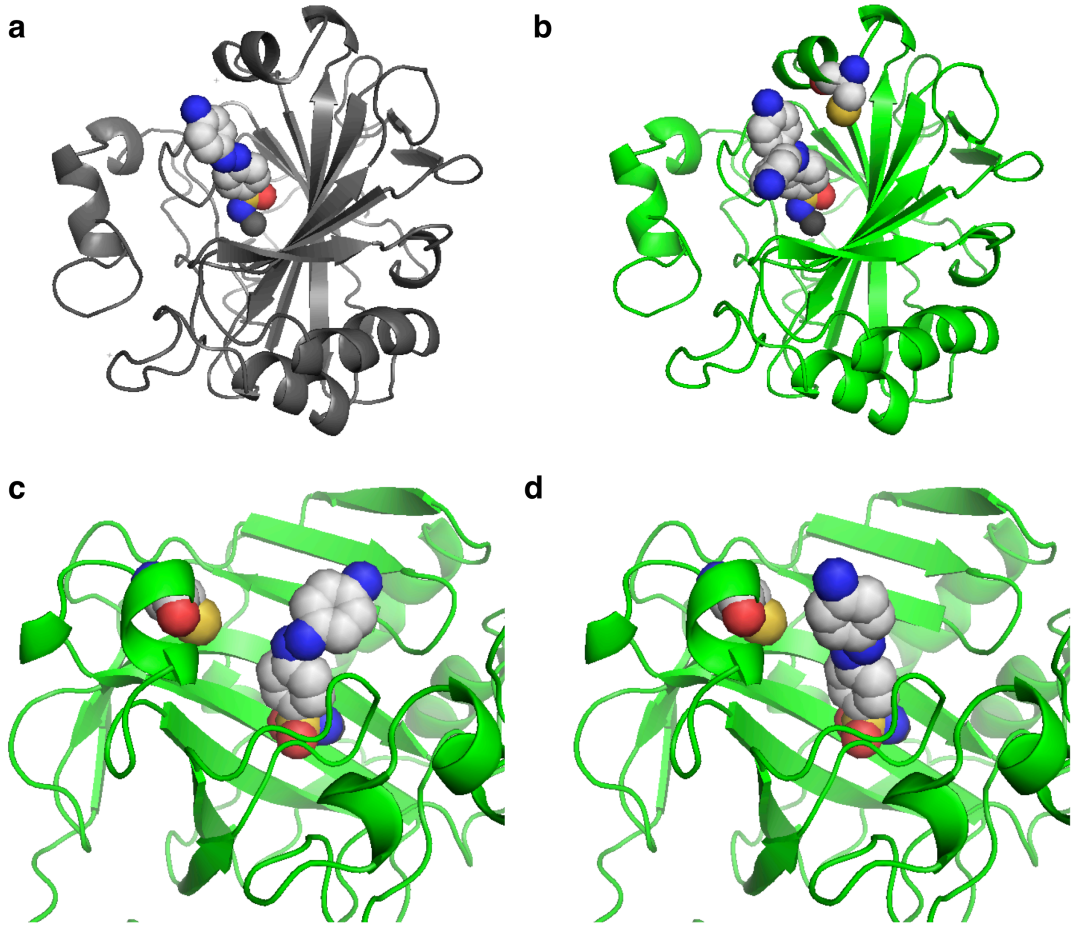


**Figure 37: X-ray structures of wild-type hCAII (gray) and mutant III (green) with photochromic ligands. a)** Wild-type structure of hCAII bound to **7.5** shows the binding of sulfonamide-containing azobenzenes in its *trans*-state. **b)** mutant IV bound to **7.5**, which is found in its *cis*- and *trans*-isomer. Zoom-in for the binding of **c)** *cis*-**7.5** and **d)** *trans*-**7.5**.

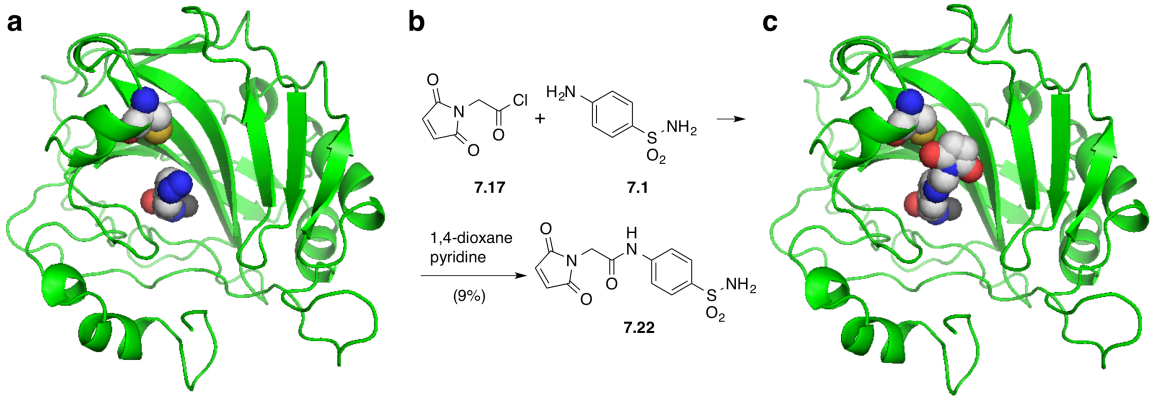


**Figure 38: Cysteine labeling studies of mutant III (green). a)** Mutant III bound with **SA-2**: the crystal structure cannot be resolved beyond the diazene

unit. **b)** Synthesis of the non-photochromic sulfonamide inhibitor **7.22**. **c)** Mutant III is not prone to labeling with flexible maleimide **7.22**, which proves the inaccessibility of this particular cysteine mutant.

In order to investigate the stereochemistry of the hydrolyzed succinimide structure mutant IV was co-crystallized with **SA-2**. Unfortunately, it was not possible to resolve the electron density around the introduced cysteine (Figure 39). Therefore, it can be assumed that neither the resulting stereochemistry of the 1,4-Michael-Addition, nor the regiochemistry of the succinimide ring–opening is selective. Consequently, the resulting isomers would adopt various structural states, which would account for the observed disorder in electron density.

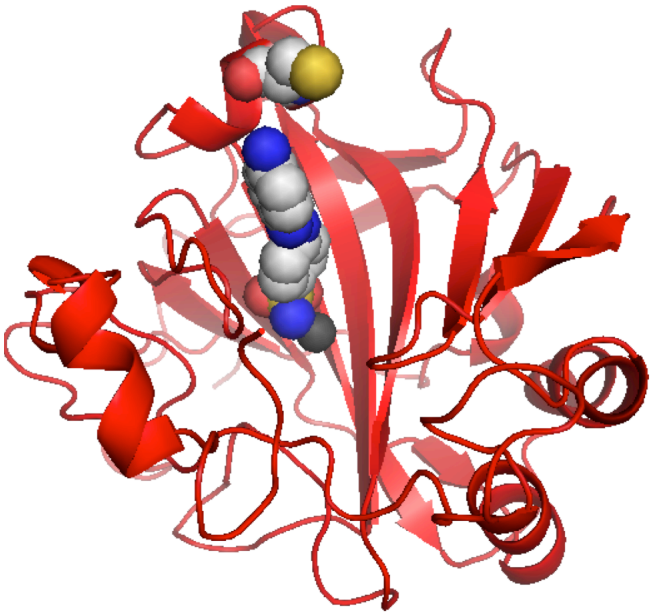

**Figure 39: Cysteine labeling studies of mutant IV (red) in complex with SA-2**. Although labeling has been proved by mass spectrometry with the addition of one water molecule, the extact attachment configuration cannot be resolved, leading to the hypothesis that thiol-maleimide addition is not stereoselective and the subsequent water hydrolysis is not regioselective.

The results from the crystal structures explain the lack of reactivity of mutant III towards a maleimide and provided deeper insight into the *cis*/*trans*

configuration when a photochromic ligand is bound to the central zinc ion. These findings will help to refine the modeling approach in future studies by providing the atomic coordinates of the bound PTL **SA-2** as well as motivation to take into account the solvent-accessibility of any mutated cysteine residues. Interestingly, the aim to resolve the water adduct of the succinimide lead us to the hypothesis that Michael-Addition and subsequent water-addition is neither stereoselective nor regioselective in this particular protein environment.

#### 7.2.2.6 Section VI: Attempts to label C206 with Maleimides

In the previous sections, a double-mutant was used to create LihCAII. One mutation was the introduction of a cysteine, which could be labeled with PTLs, the second mutation was the replacement of the native cysteine by a serine residue (C206S). The second mutation was chosen mainly for two reasons: firstly, changing the native cysteine to a serine residue helps the purification, and secondly it solves the issue of possible overlabeling. However, and as mentioned before, this cysteine points towards the catalytic center, but is shielded from the zinc-ion by a leucine (L198) residue. The resulting question surfaces, if this cysteine can be harvested for maleimide labeling by replacing the leucine with an alanine (L198A). Even more, this mutant has been described before and proved to have impaired activity nevertheless being still active towards *p*NPA catalytic hydrolysis.[91]

After mutation from the wild-type enzyme (see Experimental for further details), the L198A mutant was co-crystallized with **SA-2** to see if C206 is accessible. Similar results as previous crystallization attempts were obtained with this PTL as before: the PTL was not completely resolvable and the electron density diminished beyond the rigid azobenzene (Figure 40a and b). Again, this issue might be circumvented by using maleimide containing sulfonamide **7.22** (Figure 40c and d).

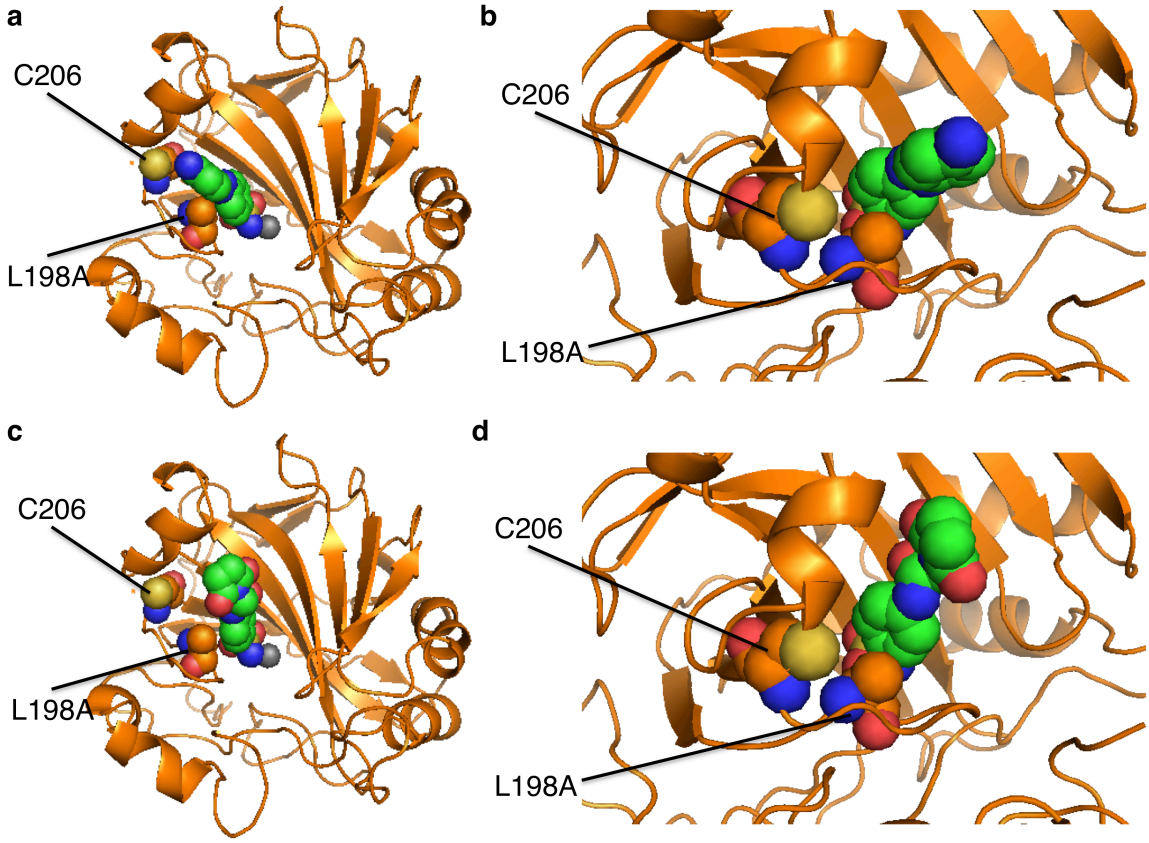


**Figure 40: L198A hCAII mutant studies towards native C206 labeling with SA-2 and 7.22. a)** L198A mutant in complex with **SA-2** and zoom-in depicted in **b)**. **c)** L198A mutant in complex with **7.22** and zoom-in depicted in **d)**.

However, after solving the X-ray structure it became clear that the maleimide functional group is too large to fit in the exposed space that was created. Therefore, labeling of C206 would need further engineering of hCAII, which does not seem feasible with respect to maintain enzymatic function.

### 7.2.3 PTL Approach using incorporated Unnatural Amino Acids

An approach to overcome maleimide-cysteine labeling and its mentioned drawbacks can be envisioned by the use of fusion proteins that bear domains for covalent attachment or by the incorporation of unnatural amino acids (UAA). For the latter, the so-called amber-supression technique exists.[92] Briefly, an amber codon (TAG) is mutated in the DNA sequence at an appropriate position, which will be translated into a non-naturally occurring amino acid.[93] This UAA can bear

different chemical moieties, which can be subjected to chemical transformations in the presence of aqueous solutions under mild conditions.[93] In this respect, "click chemistry" follows the guidelines of being a covalent modification under mild conditions, furthermore high-yielding and bioorthogonal.[94] The most prominent click-reaction is the Cu(I)-catalyzed alkyne-azide [3+2]-reaction resulting in a triazole, which has been proven to work for protein labeling.[95,96] However, copper is cytotoxic and therefore not desirable when working with biological systems.[97,98] Another click-reaction is the inverse-electron demand Diels-Alder (IDDA) between a double bond and a tetrazine. Initial [4+2] reaction between these functional groups yields a tetraaza-bicyclic structure that collapses in a retro-[4+2] reaction with the extrusion of nitrogen to a 4,5-dihydropyridazine.[99] Ultimately, after 1,3-H shift, a 1,4-dihydropyridazine is obtained that undergoes oxidation to the diazine (Figure 41a). Indeed, (*endo*- and *exo*-) norbornene-containing amino acids can be expressed and are tolerated and was chosen as an entry point in this study (Figure 41b).[93]

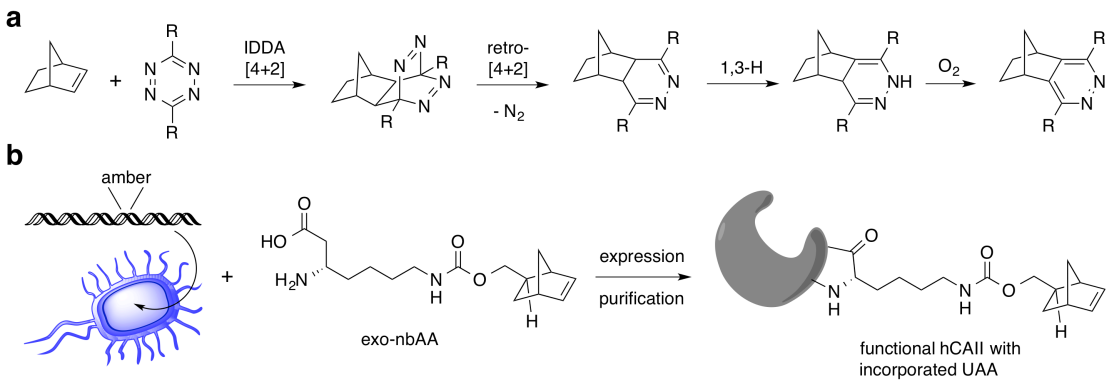


**Figure 41: Tetrazine norbornene "click chemistry" with protein incorporated unnatural amino acids (UAAs). a)** Tetrazine/norbornene click reaction proceeds via an inverse-electron demand Diels-Alder (IDDA) reaction followed by a retro-[4+2] reaction to release nitrogen. The resulting dihydropyridazine undergoes a 1,3-H shift and may be oxidized under ambient conditions to the pyridazine by molecular oxygen. **b)** Amber-codon containing plasmid is transformed into bacterial cells prone for amber-supression for protein expression and is cultivated in the presence of a norbornene-containing amino acid (exo-nbAA) to give the incorporated UAA in the protein backbone.

The mutation site known to be tolerated was chosen for different amino acids in terms of sustained catalytic activity, according to our results described above and an *exo*-norbornene-containing amino acid was translated into the position G132nb of human Carbonic Anhydrase II (hCAII) by methods previously reported.[93] This was based on the observation that *exo*-norbornenes react faster than their endo-isomers.[99] The synthesis of a PTL for this system was based on the design for thiol-maleimide labeling of hCAII and therefore had to bear a sulfonamide, an azobenzene and a linker that connects the photoswitchable pharmacophore to the tetrazine. The tetrazine itself is substituted with pyridine heterocycles to improve its stability and accelerate labeling.[100] Accordingly, a tetrazine with a free amino group was synthesized as previously reported.[101] Starting with 2-cyano pyridine (**7.23**), 5-amino-2-cyanopyridine (**7.25**) and hydrazine (**7.24**) the dihydrotetrazine **7.26** was obtained (Scheme 8a). As a side product the homopyridine **7.27** was also obtained in a crystalline form suitable for X-ray diffractometry and adopts an interesting structure with an angle of 113° between the two pyridine rings. In order to obtain the tetrazine **7.28**, **7.26** was oxidized with DDQ in refluxing PhMe, which was subjected to ring-opening of glutaric anhydride (**7.29**) to access a carboxylic acid functional group bearing tetrazine (**7.30**). Final coupling with sulfonamide-azobenzene-containing free amine **7.16** using HBTU as a coupling agent gave access to the desired PTL **JB369** in 70% yield (Scheme 8b).

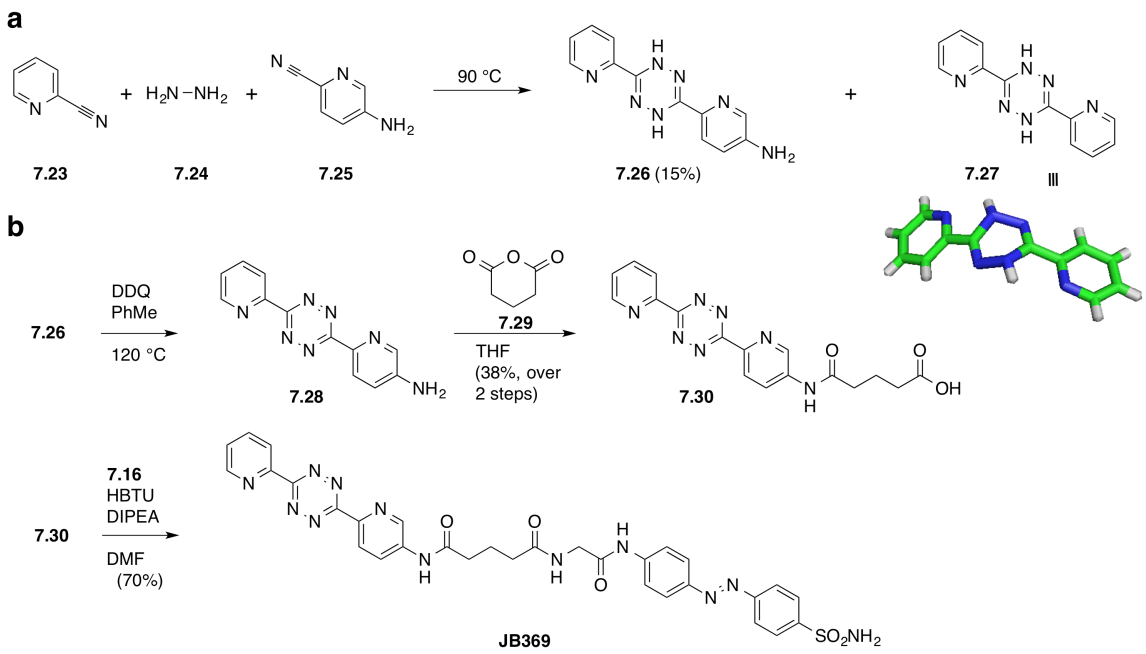


**Scheme 8: Synthesis of a tetrazine-containing PTL. a)** Free amine dihydrotetrazine (**7.26**) is obtained from stochastic reaction between two cyanopyridines **7.23** and **7.25** and hydrazine (**7.24**). A statistical mixture is obtained and a crystal structure was solved for the isolated dihydrotetrazine **7.27**. **b)** Oxidation of **7.26** with DDQ yields tetrazine **7.28**, which can be subjected to anhydride opening of gluaric anhydride (**7.29**) to give free acid **7.30**. The final PTL **JB369** is obtained by HBTU-mediated peptide coupling between **7.30** and **7.16** (*vide supra*).

Click reaction with the G132nb hCAII was completed within minutes (with both 5 and 25 equivalents of **JB369**) and full labeling was confirmed by full protein mass spectrometry (see Experimental) after utilizing the same work-up procedure as with the maleimide containing PTLs. Catalytic activity was measured by *p*NPA catalyzed hydrolysis and proved to be completely abolished, *i.e.* showing same rate constants as background hydrolysis (Figure 42). Furthermore, the catalytic activity could not be rescued by application of UV and blue light. This might be the result of the close proximity of the attachment site to the catalytically active center together with the rather long linker length of the PTL resulting in the constant inhibition of hCAII.

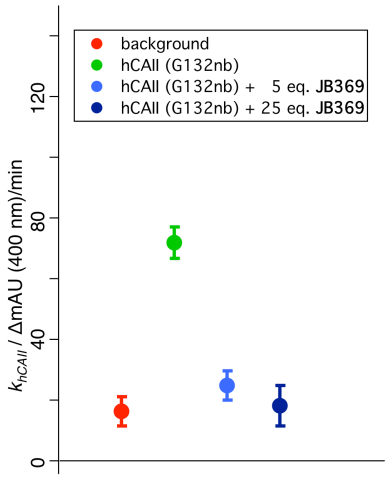


**Figure 42: Catalytic *p*NPA hydrolysis activity of (non-) labeled norbornene-containing hCAII.** The mutant is catalytically active (green) when compared to background hydrolysis (red). When exposed to 5 eq. (light blue) or 25 eq. (dark blue) **JB369** activity is reduced to background levels therefore rendering the mutant inactive. Catalytic activities have been measured after removal of excess **JB369**.

## 7.3 Summary and Outlook

Herein, it is demonstrated for the first time the rational design of a light-switchable enzyme utilizing the concept of Optochemical Genetics to obtain three Light-controlled human Carbonic Anhydrases II (LihCAIIs).

Beginning with the synthesis, characterization and inhibition of photochromic ligands (PTLs) towards wt hCAII the experimental setups were chosen to be a *p*NPA assay. Inhibition did not rely on applied light and azobenzene-isomers. Furthermore, the idea of correlating electron density of the sulfonamide by plotting the Hammett constants of substituents in the 4'-position to the inhibition characteristics did not give a linear relationship. Nevertheless, the synthesis of nine azobenzene-containing sulfonamides, eight of them with crystal structures, which served as precursors for PTL studies is described.

Based on the novel use of computational modelling, six photoresponsive and six non-photoresponsive combinations from three designed PTLs and four different hCAII mutants were predicted. Ultimately, two predicted working combinations, mutant VI (G132C, C206) and mutant V (K133C, C206S) with PTL **SA-2** were found. Even more, an unpredicted mutant I (G129C, C206) was also photoresponsive when labeled with **SA-2**. Mutant III (F131C, C206S), however, could not be labeled with maleimides following the protocol developed in our laboratory. Consequently, this particular predicted site can not be confirmed with the PTLs described herein. The huge quantity of available hCAII mutants together with the abundance of easily synthesized PTLs by chemical synthesis serves as a good basis for further investigations. Attachment conformation with Full Protein Mass Spectrometry is a fast and reliable method to determine the labeling efficiency. This was important to the above-mentioned aims, and is novel in the photocontrol of proteins, where unconfirmed labeling and overlabeling was usually an issue which could not be addressed. Furthermore, crystal structures with resolutions between 1.15–1.50 Å were obtained, which show the labeled mutant IV and the unlabeled mutant III. Unfortunately, resolving the attachment site to gain insight into the stereochemical preference for binding, as well as regioselectivity for succinimide opening was not possible.

It can therefore be assumed that the chemical surrounding is not very well defined and a mixture of possible stereoisomers and ring-opened products are present. Nevertheless, this question will be addressed in ongoing studies. The crystallographic studies furthermore showcase a photochromic ligand in its *cis*- and *trans*-state, which will be the iterative entry point for further PTL designs.

Additionally, a tetrazine based PTL **JB369** was designed and synthesized to be attached successfully to an *exo*-norbornene unnatural amino acid (UAA) expressing hCAII mutant. Although labeling was fast and quantitative, catalytic activity was completely blocked and could not be rescued under irradiation with light.

In summary and to conclude, a novel, rationally-designed and photoresponsive protein system for the studies of enzymatic activity was developed, which natively plays a key role of the physiology of the eye, where research for vision restoration is also present in the Trauner group.

## 7.4 Experimental

### 7.4.1 Synthesis

#### 7.4.1.1 Mills reaction procedure (A) for azobenzene formation

A round bottom flask was charged with aniline (1.0 eq.), dissolved in HOAc (and if necessary an organic co-solvent) and nitrosobenzene (1.2–3.0 eq.) was added in one portion. The mixture was stirred at r.t. or 60 °C o.n. and then neutralized with the addition of aqueous sat. $NaHCO_3$ and extracted with EtOAc (3x). The combined organic layers were washed with aqueous sat. $NaHCO_3$ and brine before it was dried over $MgSO_4$ and subjected to flash column chromatography.

#### 7.4.1.2 Diazonium coupling procedure (B) for azobenzene formation

A round bottom flask was charged with aniline (1.0 eq.), dissolved in 2.4 M HCl and cooled to 0 °C. 1.2 eq of an aqueous 2.3 M $NaNO_2$ solution was added dropwise to form the diazonium salt, which resulted in a yellow color. The mixture was stirred for 5-10 min at 0 °C before it was transferred to a solution of the corresponding coupling partner in aqueous 1 M NaOAc (with the addition of methanol until everything was dissolved). The solution turned red immediately and was allowed to warm to r.t.. Workup procedure depended on the azobenzene formed and can be found listed under the appropriate compound below.

#### 7.4.1.3 Aniline oxidation procedure (C) for nitroso formation

A round bottom flask was charged with aniline (1.0 eq.) in DCM and water was added. Oxone® (2.0 eq.) was added and the biphasic system was stirred vigorously for 3 h. The layers were separated and the green organic layer was washed with 1 M HCl (2x), water and brine before it was dried over $MgSO_4$. After

removal of all volatiles, the crude nitroso compound was isolated as a solid, which was used without further purification.

#### 7.4.1.4 4-Nitrophenylacetate (*p*NPA)

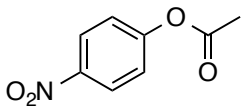

A round bottom flask was charged with 4-nitrophenol (1.0 eq.) dissolved in DCM. $Ac_2O$ (20 eq.) was added dropwise and the solution was stirred at r.t. for 1 h. The reaction was quenched by the addition of sat. aqueous $NaHCO_3$ and the layers were seperated. After drying the organic layer over $MgSO_4$ and removal of all volatiles and desired product was obtained in a crystalline form.

#### 7.4.1.5 4-Nitrosobenzenesulfonamide (7.12)

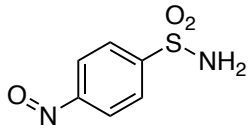

4-Nitrosobenzenesulfonamide was synthesized *via* procedure C.

Amounts: sulfanilamide (4.00 g, 23.2 mmol), Oxone® (14.2 g, 46.4 mmol), DCM/water = 75/150 mL

#### 7.4.1.6 Ethyl 4-nitrosobenzoate

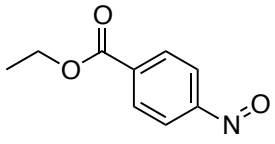

Ethyl 4-nitrosobenzoate was synthesized *via* procedure C.

Amounts: 4-amino ethylbenzoate (4.00 g, 24.2 mmol), Oxone® (14.9 g, 48.4 mmol), DCM/water = 75/150 mL

### 7.4.1.7 1-Nitro-4-nitrosobenzene

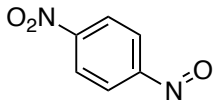

1-Nitro-4-nitrosobenzene was synthesized *via* procedure C.

Amounts: 4-nitroaniline (6.00 g, 46.8 mmol), Oxone® (28.8 g, 93.6 mmol), DCM/water = 150/150 mL.

### 7.4.1.8 (*E*)-4-(4-Hydroxyphenyldiazenyl)benzenesulfonamide (7.2)

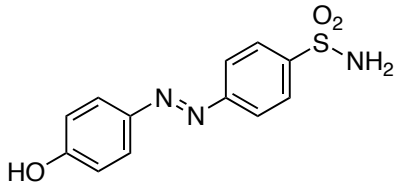

(*E*)-4-(4-Hydroxyphenyldiazenyl)benzenesulfonamide was prepared according to procedure B. After completion of the reaction, the product was precipitated by the addition of 2 M HCl and extracted with EtOAc. The organic layer was washed with brine, dried over $MgSO_4$ and filtered. After removal of all volatiles, the solid was recrystallized from hot acetone o.n. to obtain 3.47 g (12.5 mmol, 43%) of the desired product as a red solid.

Amounts: sulfanilamide (1.0 eq., 5.00 g, 29.0 mmol), phenol (1.0 eq., 2.73 g, 29.0 mmol), $NaNO_2$ (1.2 eq., 2.4 g, 34.8 mmol).

**$^1$H NMR** (400 MHz, DMSO-$d_6$): $\delta$ [ppm] = 10.48 (br s, 1H), 8.01 (d, $J$ = 8.6 Hz, 2H), 7.96 (d, $J$ = 8.7 Hz, 2H), 7.86 (d, $J$ = 8.8 Hz, 2H), 7.51 (br s, 2H), 6.98 (d, $J$ = 8.9 Hz, 2H).

**$^{13}$C NMR** (101 MHz, DMSO-$d_6$): $\delta$ [ppm] = 161.8, 153.7, 145.3, 145.0, 127.0, 125.4, 122.5, 116.2.

**HRMS (ESI)**: calc. for $C_{12}H_{10}N_3O_3S^-$ $(M-H)^-$: 276.0448, found: 276.0447.

**UV/Vis** (LCMS): $\lambda_{max}$ = 358 nm.

**$R_t$** (LCMS; MeCN/$H_2O$/formic acid = 10/90/0.1 → 90/10/0.1 over 7 min) = 3.067 min.

**IR** (ATR): wave number/$cm^{-1}$ = 3345, 3241, 1595, 1502, 1427, 1300, 1266, 1156, 1138, 1089, 901, 848, 796, 709.

**m.p.** = decomposition >250 °C

### 7.4.1.9 (*E*)-4-((4-(Diethylamino)phenyl)diazenyl)benzenesulfonamide (7.3)

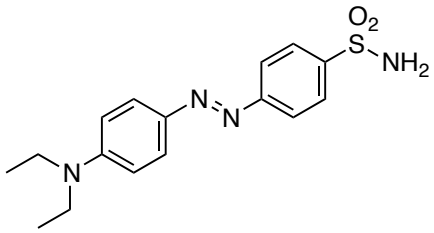


(*E*)-4-((4-(Diethylamino)phenyl)diazenyl)benzenesulfonamide was prepared according to procedure A. Flash column chromatography (25% EtOAc/*i*-hexanes) was performed to obtain 1.45 g (4.37 mmol, 38%) of the desired product as a red solid.

Amounts: sulfanilamide (2.00 g, 11.6 mmol, 1.0 eq.), $NaNO_2$ (0.96 g, 13.9 mmol, 1.2 eq.), *N*,*N*-diethylaniline (1.73 g, 11.6 mmol, 1.84 mL, 1.0 eq).

**$^1$H NMR** (400 MHz, DMSO-$d_6$): $\delta$ [ppm] = 7.95 (d, *J* = 8.6 Hz, 2H), 7.88 (d, *J* = 8.6 Hz, 2H), 7.81 (d, *J* = 9.2 Hz, 2H), 7.45 (s, 2H), 6.82 (d, *J* = 9.3 Hz, 2H), 3.47 (q, *J* = 7.0 Hz, 4H), 1.15 (t, *J* = 7.0 Hz, 6H).

**$^{13}$C NMR** (101 MHz, DMSO-$d_6$): $\delta$ [ppm] = 154.2, 150.8, 143.8, 142.2, 126.9, 125.8, 121.9, 111.1, 44.2, 12.5.

**HRMS (ESI)**: calc. for $C_{16}H_{21}N_4O_2S^+$ $(M+H)^+$: 333.1380, found: 333.1377.

**UV/Vis** (LCMS): $\lambda_{max}$ = 460 nm.

**$R_t$** (LCMS; MeCN/$H_2O$/formic acid = 10/90/0.1 → 90/10/0.1 over 7 min) = 4.364 min.

**IR** (ATR): wave number/$cm^{-1}$ = 3364, 3261, 2978, 1603, 1585, 1513, 1404, 1386, 1353, 1331, 1313, 1302, 1277, 1195, 1164, 1138, 1102, 1083, 1015, 884, 848, 821, 738, 681.

**m.p.** = 190-195 °C

### 7.4.1.10 (*E*)-4-((4-Morpholinophenyl)diazenyl)benzenesulfonamide (7.4)

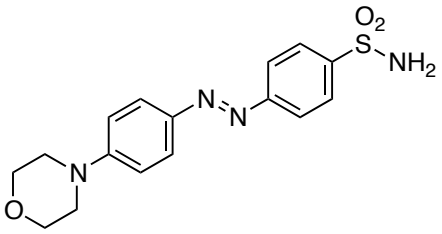


(*E*)-4-((4-Morpholinophenyl)diazenyl)benzenesulfonamide was prepared according to procedure B. After completion of the reaction, the resulting solid was filtered off and washed twice with water and finally recrystallized from acetone to to obtain 991 mg (2.86 mmol, 25%) of the desired product as a red solid.

Amounts: sulfanilamide (1.0 eq., 2.00 g, 11.6 mmol), *N*-phenylmorpholine (1.0 eq., 1.89 g, 11.6 mmol), $NaNO_2$ (1.2 eq., 0.96 g, 13.9 mmol).

**$^1$H NMR** (400 MHz, DMSO-$d_6$): $\delta$ [ppm] = 7.98 (d, $J$ = 8.7 Hz, 2H), 7.94 (d, $J$ = 8.7 Hz, 2H), 7.85 (d, $J$ = 9.1 Hz, 2H), 7.49 (br s, 2H), 7.10 (d, $J$ = 9.2 Hz, 2H), 3.75 (m, 4H), 3.35 (m, 4H).

**$^{13}$C NMR** (101 MHz, DMSO-$d_6$): $\delta$ [ppm] = 153.9, 153.6, 144.6, 144.1, 127.0, 125.0, 122.3, 113.8, 65.9, 46.9.

**HRMS (ESI)**: calc. for $C_{16}H_{17}N_4O_3S^-$ $(M-H)^-$: 345.1027, found: 345.1026.

**UV/Vis** (LCMS): $\lambda_{max}$ = 414 nm.

**$R_t$** (LCMS; MeCN/$H_2O$/formic acid = 10/90/0.1 → 90/10/0.1 over 7 min) = 3.612 min.

**IR** (ATR): wave number/$cm^{-1}$ = 3197, 3081, 2859, 1600, 1506, 1448, 1380, 1336, 1301, 1269, 1234, 1160, 1141, 1110, 1089, 1068, 1051, 917, 852, 826, 740, 698.

**m.p.** = decomposition 220 °C

### 7.4.1.11 (*E*)-4-(4-Aminophenyldiazenyl)benzenesulfonamide (7.5)

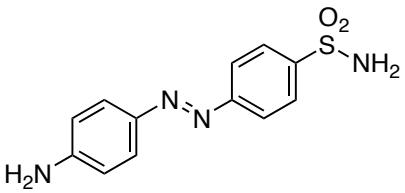


(*E*)-4-(4-Aminophenyldiazenyl)benzenesulfonamide was prepared according to a published procedure and the spectral data matched that reported.[102]

**$^1$H NMR** (400 MHz, DMSO-$d_6$): $\delta$ [ppm] = 7.94 (d, *J* = 8.6 Hz, 2H), 7.87 (d, *J* = 8.6 Hz, 2H), 7.71 (d, *J* = 8.8 Hz, 2H), 7.45 (s, 2H), 6.69 (d, *J* = 8.8 Hz, 2H), 6.33 (br s, 2H).

**$^{13}$C NMR** (101 MHz, DMSO-$d_6$): $\delta$ [ppm] = 154.2, 153.8, 143.8, 142.8, 126.9, 125.9, 122.0, 113.5.

**HRMS (ESI)**: calc. for $C_{12}H_{13}N_4O_2S^+$ $(M+H)^+$: 277.0754, found: 277.0753.

**UV/Vis** (LCMS): $\lambda_{max}$ = 404 nm.

**$R_t$** (LCMS; MeCN/$H_2O$/formic acid = 10/90/0.1 → 90/10/0.1 over 7 min) = 3.000 min.

**IR** (ATR): wave number/$cm^{-1}$ = 3378, 3347, 3256, 3046, 1620, 1600, 1503, 1424, 1394, 1330, 1300, 1235, 1162, 1137, 1089, 1010, 901, 849, 839, 706.

**m.p.** = 240 °C

### 7.4.1.12 (*E*)-4-(4-Azidophenyldiazenyl)benzenesulfonamide (7.6)

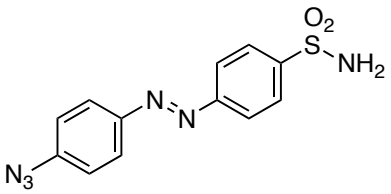

A solution of 126 mg (0.46 mmol, 1.0 eq.) 4-((4-aminophenyl)-diazenyl)benzenesulfonamide (**7.5**) in 20 mL MeCN was cooled to -10 °C and 72 mg (0.70 mmol, 82 µL, 1.5 eq.) of *t*-BuONO was added, followed by 10 drops of TFA. The reation mixture turned a deep red color. After stirring for 5 min, 64 mg (0.56 mmol, 74 µL, 1.2 eq.) of $TMSN_3$ was added drop-wise to the solution and it was stirred for another hour after which it was allowed to warm to r.t.. The reaction was diluted with 25 mL of $H_2O$ and extracted with EtOAc. The organic layer was separated, washed with $H_2O$ (3 x 50 mL) and brine and finally dried over $MgSO_4$. Flash column chromatography (50% EtOAc/pentane) was performed to obtain 88.0 mg (0.29 mmol, 63%) of the desired product as a red solid.

**$^1$H NMR** (400 MHz, MeCN-$d_3$) $\delta$ [ppm] = 8.06–7.98 (m, 6H), 7.27 (d, $J$ = 8.9 Hz, 2H), 5.79 (br s, 2H).

**$^{13}$C NMR** (101 MHz, MeCN-$d_3$): $\delta$ [ppm] = 154.3, 149.5, 144.8, 143.9, 127.3, 124.8, 123.0, 120.0.

**HRMS (ESI)**: calc. for $C_{12}H_9N_6O_2S^-$ $(M-H)^-$: 301.0513, found: 301.0519.

**UV/Vis** (LCMS): λ (π → π*) = 356 nm; λ (n → π*) = 443 nm.

**$R_t$** (LCMS; MeCN/$H_2O$/formic acid = 10/90/0.1 → 90/10/0.1 over 7 min) = 4.190 min.

**IR** (ATR): wave number/$cm^{-1}$ = 3365, 3266, 2117, 1595, 1496, 1335, 1302, 1276, 1162, 1144, 1126, 1104, 1092, 1012, 894, 849, 718, 661.

**m.p.** = decomposition >175 °C

### 7.4.1.13 (*E*)-4-(*p*-Tolyldiazenyl)benzenesulfonamide (7.7)

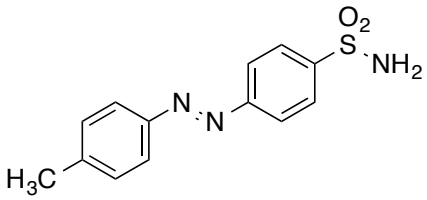


(*E*)-4-(*p*-Tolyldiazenyl)benzenesulfonamide was prepared according to procedure A. Flash column chromatography (100% DCM) was performed to obtain 22.6 mg (0.08 mmol, 45%) of the desired product as a red solid.

Amounts: nitroso sulfanilamide (3.0 eq., 100.9 mg, 0.54 mmol), *p*-toluidine (1.0 eq., 19.5 mg, 0.18 mmol), HOAc (10 mL).

**$^{1}$H NMR** (400 MHz, DMSO-$d_6$): $\delta$ [ppm] = 8.02 (s, 4H), 7.85 (d, $J$ = 8.3 Hz, 2H), 7.55 (s, 2H), 7.44 (d, $J$ = 8.3 Hz, 2H), 2.42 (s, 3H).

**$^{13}$C NMR** (101 MHz, DMSO-$d_6$): $\delta$ [ppm] = 153.4, 150.0, 145.8, 142.8, 130.1, 127.1, 123.0, 122.9, 21.2.

**HRMS (ESI)**: calc. for $C_{13}H_{14}N_3O_2S^+$ $(M+H)^+$: 276.0801, found: 276.0799.

**UV/Vis** (LCMS): $\lambda_{max}$ ($\pi \rightarrow \pi^*$) = 334 nm; $\lambda_{max}$ ($n \rightarrow \pi^*$) = 448 nm.

**$R_t$** (LCMS; MeCN/$H_2O$/formic acid = 10/90/0.1 → 90/10/0.1 over 7 min) = 3.355 min (*cis*); 4.133 min (*trans*).

**IR** (ATR): wave number/$cm^{-1}$ = 3355, 3261, 1602, 1548, 1500, 1452, 1399, 1382, 1342, 1302, 1226, 1175, 1162, 1144, 1105, 1090, 1012, 905, 851, 826, 782, 749, 726, 704.

**m.p.** = 215-220 °C

### 7.4.1.14 (*E*)-4-((4-Nitrophenyl)diazenyl)benzenesulfonamide (7.8)

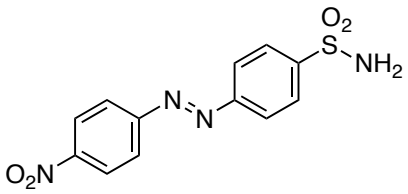

(*E*)-4-((4-Nitrophenyl)diazenyl)benzenesulfonamide was prepared according to procedure A. Flash column chromatography (acetone/*i*-hexanes = 3/7 → 1/1) was performed to obtain 448 mg (1.46 mmol, 9%) of the desired product as a red solid.

Amounts: sulfanilamide (1.0 eq., 2.80 g, 16.3 mmol), 1-nitro-4-nitrosobenzene (1.0 eq., 2.48 g, 16.3 mmol), HOAc/DCM (1/1, 40 mL).

**$^{1}$H NMR** (400 MHz, DMSO-$d_6$): $\delta$ [ppm] = 8.47 (d, $J$ = 9.0 Hz, 2H), 8.17–8.11 (m, 4H), 8.07 (d, $J$ = 8.6 Hz, 2H), 7.60 (br s, 2H).

**$^{13}$C NMR** (101 MHz, DMSO-$d_6$): $\delta$ [ppm] = 154.9, 153.1, 148.9, 147.0, 127.2, 125.2, 123.8, 123.6.

**HRMS (ESI)**: calc. for $C_{12}H_9N_4O_4S^-$ $(M-H)^-$: 305.0350, found: 305.0349.

**UV/Vis** (LCMS): λ (π → π*) = 328 nm; λ (n → π*) = 459 nm.

**$R_t$** (LCMS; MeCN/$H_2O$/formic acid = 10/90/0.1 → 90/10/0.1 over 7 min) = 3.871 min.

**IR** (ATR): wave number/$cm^{-1}$ = 3346, 3261, 3101, 1609, 1540, 1479, 1345, 1323, 1301, 1215, 1156, 1108, 1089, 1004, 896, 858, 842, 754, 730, 718, 683.

**m.p.** = 215 °C

### 7.4.1.15 (*E*)-4-(Phenyldiazenyl)benzenesulfonamide (7.9)

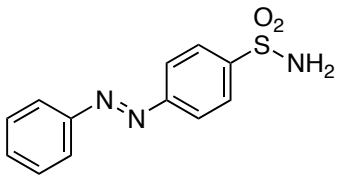

(*E*)-4-(Phenyldiazenyl)benzenesulfonamide was prepared according to procedure A. Flash column chromatography (DCM/MeOH = 100/0 → 100/5) was performed to obtain 291 mg (1.11 mmol, 38%) of the desired product as a red solid.

Amounts: sulfanilamide (1.0 eq., 0.50 g, 2.90 mmol), nitrosobenzene (1.0 eq., 311 mg, 2.90 mmol), HOAc (20 mL).

**$^{1}$H NMR** (400 MHz, acetone-$d_6$): $\delta$ [ppm] = 8.11–8.05 (m, 2H), 8.05–8.00 (m, 2H), 7.98–7.89 (m, 2H), 7.65–7.51 (m, 2H), 6.71 (br s, 2H).

**$^{13}$C NMR** (101 MHz, acetone-$d_6$): $\delta$ [ppm] = 155.0, 153.3, 147.0, 133.0, 130.3, 128.2, 123.9, 123.9.

**HRMS (ESI)**: calc. for $C_{12}H_{10}N_3O_2S^-$ $(M-H)^-$: 260.0499, found: 260.0498.

**UV/Vis** (LCMS): λ (π → π*) = 322 nm; λ (n → π*) = 446 nm.

**$R_t$** (LCMS; MeCN/$H_2O$/formic acid = 10/90/0.1 → 90/10/0.1 over 7 min) = 3.852 min.

**IR** (ATR): wave number/$cm^{-1}$ = 3353, 3258, 1649, 1583, 1550, 1479, 1439, 1400, 1157, 1143, 1088, 1070, 1020, 1009, 999, 907, 848, 767, 722, 683.

**m.p.** = 205-207 °C

### 7.4.1.16 (*E*)-Ethyl 4-((4-sulfamoylphenyl)diazenyl)benzoate (7.10)

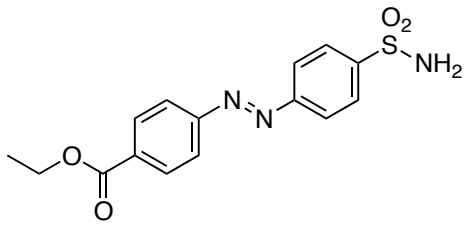

(*E*)-Ethyl 4-((4-sulfamoylphenyl)diazenyl)benzoate was prepared according to procedure A. Flash column chromatography (DCM/MeOH = 100/0 → 100/2) was performed to obtain 46.5 mg (0.14 mmol, quant.) of the desired product as a red solid.

Amounts: sulfanilamide (1.0 eq., 24.7 mg, 0.14 mmol), ethyl 4-nitrosobenzoate (3.0 eq., 77.0 mg, 0.43 mmol), HOAc (10 mL).

**$^{1}$H NMR** (400 MHz, $CD_3OD$): $\delta$ [ppm] = 8.22 (d, $J$ = 8.6 Hz, 2H), 8.14–8.04 (m, 4H), 8.04 (d, $J$ = 8.6 Hz, 2H), 4.42 (q, $J$ = 7.1 Hz, 2H), 1.43 (t, $J$ = 7.1 Hz, 3H).

**$^{13}$C NMR** (101 MHz, $CD_3OD$): $\delta$ [ppm] = 167.2, 156.3, 155.5, 147.5, 134.3, 131.7, 128.5, 124.4, 124.0, 62.6, 14.6.

**HRMS (ESI)**: calc. for $C_{15}H_{14}N_3O_4S^-$ $(M-H)^-$: 332.0711, found: 332.0710.

**UV/Vis** (LCMS): λ (π → π*) = 342 nm; λ (n → π*) = 455 nm.

**$R_t$** (LCMS; MeCN/$H_2O$/formic acid = 10/90/0.1 → 90/10/0.1 over 7 min) = 4.157 min.

**IR** (ATR): wave number/$cm^{-1}$ = 3339, 3250, 1708, 1603, 1558, 1408, 1337, 1273, 1216, 1164, 1126, 1105, 1093, 1025, 1008, 901, 864, 847, 830, 772, 726, 717, 691, 654.

**m.p.** = 190 °C

### 7.4.1.17 2-(2,5-Dioxo-2,5-dihydro-1*H*-pyrrol-1-yl)-acetic acid (7.13)

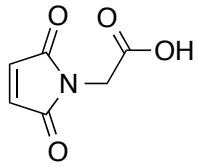

The compound was prepared as reported previously[84] and the spectral data matched that reported.

**$^1$H NMR** (400 MHz, DMSO-$d_6$): $\delta$ [ppm] = 8.13 (br s, 2H), 6.07 (s, 2H), 3.65 (s, 2H).

**$^{13}$C NMR** (101 MHz, DMSO-$d_6$): $\delta$ [ppm] = 169.2, 167.3, 135.2, 39.9.

### 7.4.1.18 2-(2,5-Dioxo-2,5-dihydro-1*H*-pyrrol-1-yl)-*N*-(4-((4-sulfamoylphenyl)diazenyl)phenyl)acetamide (SA-1)

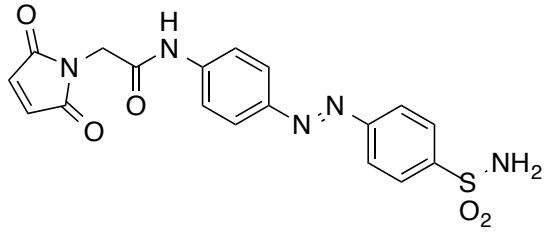

In a 100 mL round bottom flask maleimide containing acid **7.13** (55.8 mg, 0.36 mmol, 1.1 eq.), HOBt (48.6 mg, 0.36 mmol, 1.1 eq.), and EDCI (111.6 mg, 126 µL, 0.65 mmol, 2.0 eq.) were dissolved in DMF (20 mL) with the addition of 4Å molecular sieves. The mixture was cooled to 0 °C and stirred for 20 min. Aminoazobenzene **7.5** (123.0 mg, 0.33 mmol, 1.0 eq.) was dissolved in DMF (10 mL) and was added drop-wise to the reaction mixture. After the drop-wise addition of DIPEA (127 mg, 0.17 mL, 0.98 mmol, 3.0 eq.) the reaction mixture was heated to 50 °C and stirred o.n.. After completion of the reaction the solvent was removed *in vacuo* and filtered through a plug of C18-functionalized silica. The crude product was finally purified by RP-HPLC to afford 40 mg of **SA-1** in 29% yield as a red solid.

**$^1$H NMR** (400 MHz, DMSO-$d_6$): $\delta$ [ppm] = 8.00 (d, $J$ = 8.9 Hz, 1H), 7.88 (d, $J$ = 8.9 Hz, 1H), 7.72 (d, $J$ = 8.9 Hz, 1H), 7.08 (s, 1H), 6.69 (d, $J$ = 8.9 Hz, 1H), 4.17 (s, 1H).

**$^{13}$C NMR** (101 MHz, DMSO-$d_6$): $\delta$ [ppm] = 170.3, 166.0, 155.4, 154.1, 142.9, 138.4, 134.9, 128.9, 126.2, 122.0, 113.5, 30.7.

**HRMS (ESI)**: calc. for $C_{18}H_{14}N_5O_5S^-$ $(M-H)^-$: 412.0721, found: 412.0720.

**UV/Vis** (40 µM in DMSO): $\lambda_{max}$ = 440 nm.

**$R_t$** (LCMS; MeCN/$H_2O$/formic acid = 10/90/0.1 → 90/10/0.1 over 7 min) = 3.378 min.

**IR** (ATR): wave number/$cm^{-1}$ = 3479, 3378, 2360, 2340, 1704, 1621, 1599, 1588, 1506, 1459, 1428, 1395, 1374, 1352, 1292, 1192, 1158, 1137, 1084, 845, 828, 781, 717, 696.

**m.p.** = decomposition >215 °C

### 7.4.1.19 *tert*-Butyl (2-((4-aminophenyl)amino)-2-oxoethyl)carbamate (7.14)

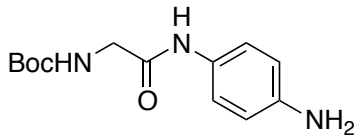


The compound was prepared as reported previously and the spectral data matched the one reported.[83]

**$^1$H NMR** (300 MHz, MeCN-$d_3$) $\delta$ [ppm] = 8.11 (br s, 1H), 7.21 (d, *J* = 8.7 Hz, 2H), 6.59 (d, *J* = 8.7 Hz, 2H), 4.02 (br s, 2H), 3.72 (d, *J* = 6.0 Hz, 2H), 1.43 (s, 9H).

**$^{13}$C NMR** (75 MHz, MeCN-$d_3$) $\delta$ [ppm] = 168.6, 157.1, 145.7, 129.6, 122.7, 115.4, 80.0, 45.1, 28.6.

**HRMS (ESI)**: calc. for $C_{13}H_{19}N_3NaO_3^+$ $(M+Na)^+$: 288.1319, found: 288.1318.

**UV/Vis** (LCMS): $\lambda_{max}$ = 242 nm.

**$R_t$** (LCMS; MeCN/$H_2O$/formic acid = 10/90/0.1 → 90/10/0.1 over 7 min) = 1.660 min.

**m.p.:** 145-148 °C.

### 7.4.1.20 *tert*-Butyl (2-oxo-2-((4-((4-sulfamoylphenyl)diazenyl)phenyl) amino) ethyl) carbamate (7.15)

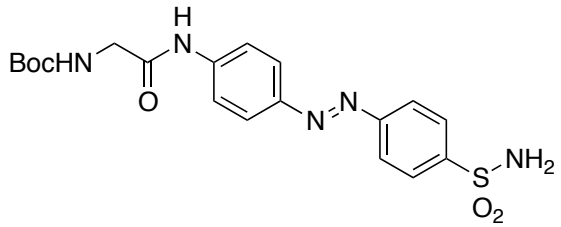


4-Nitrosobenzene sulfonamide **7.14** (0.10 g, 0.38 mmol, 1.0 eq.) was dissolved in 3 ml of AcOH and amine **5** (0.11 g, 0.57 mmol, 1.5 eq.) was added to it. The reaction mixture was stirred at room temperature over night before it was neutralized by the addition of saturated aqueous solution of $NaHCO_3$ and extracted three times with EtOAc. The combined organic layers were washed with water and brine and finally dried over $MgSO_4$. The crude was purified by flash column chromatography on silica gel (EtOAc/MeOH = 10/1) and the desired product was obtained in 82 % yield as a red solid.

**$^1$H NMR** (400 MHz, DMSO-$d_6$) $\delta$ [ppm] = 10.36 (br s, 1H), 8.04 – 7.98 (m, 2H), 7.94 (d, $J$ = 9.0 Hz, 2H), 7.84 (d, $J$ = 9.0 Hz, 2H), 7.52 (br s, 2H), 7.10 (t, $J$ = 6.0 Hz, 1H), 3.78 (d, $J$ = 6.1 Hz, 2H), 1.40 (s, 9H).

**$^{13}$C NMR** (101 MHz, DMSO-$d_6$) $\delta$ [ppm] = 168.9, 156.0, 153.6, 147.5, 145.5, 142.8, 127.1, 124.2, 122.7, 119.3, 78.2, 44.0, 28.2.

**HRMS (ESI)**: calc. for $C_{19}H_{23}N_5NaO_5S^+$ $(M+Na)^+$: 456.1312, found: 456.1309.

**UV/Vis** (LCMS): $\lambda_{max}$ = 356 nm.

**$R_t$** (LCMS; MeCN/$H_2O$/formic acid = 10/90/0.1 → 90/10/0.1 over 7 min) = 3.501 min.

### 7.4.1.21 2-Amino-N-(4-((4-sulfamoylphenyl)diazenyl)phenyl)acetamide (TFA salt) (7.16)

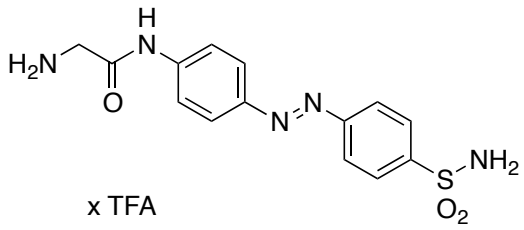


Boc-protected amine **7.15** (0.68 g, 1.57 mmol) was suspended in DCM (20 mL) and TFA (6.5 mL) was added. The reaction mixture was stirred at room temperature for 1.5 h and the volatiles evaporated to dryness. The title compound was obtained in quantitative yield as a yellow solid.

**$^{1}$H NMR** (400 MHz, DMSO-$d_6$) $\delta$ [ppm] = 10.85 (s, 1H), 8.17 (br s, 3H), 8.04–7.96 (m, 6H), 7.84 (d, *J* = 9.0 Hz, 2H), 7.54 (s, 2H), 3.86 (d, *J* = 4.6 Hz, 2H).

**$^{13}$C NMR** (101 MHz, DMSO-$d_6$) $\delta$ [ppm] = 165.5, 153.5, 147.9, 145.7, 141.8, 127.1, 124.4, 122.8, 119.5, 41.3.

**$^{19}$F NMR** (376 MHz, DMSO-$d_6$) *$\delta$ [ppm] =* -73.84.

**HRMS (ESI)**: calc. for $C_{14}H_{16}N_5O_3S^+$ $(M+H)^+$: 334.0968, found: 334.0965.

**UV/Vis** (LCMS): $\lambda_{max}$ = 352 nm.

**$R_t$** (LCMS; MeCN/$H_2O$/formic acid = 10/90/0.1 → 90/10/0.1 over 7 min) = 1.789 min.

### 7.4.1.22 2-(2,5-Dioxo-2,5-dihydro-1*H*-pyrrol-1-yl)-acetyl chloride (7.17)

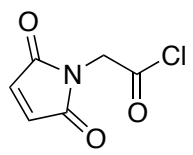

2-(2,5-Dioxo-2,5-dihydro-1*H*-pyrrol-1-yl)acetyl chloride was prepared by refluxing 2-(2,5-dioxo-2,5-dihydro-1*H*-pyrrol-1-yl)acetic acid (**7.13**) (1.0 eq., 300 mg, 1.93 mmol) in 4 mL of thionyl chloride for 5 hours under a nitrogen atmosphere. The leftover thionyl chloride was removed by co-evaporation with toluene, the remaining crude acyl chloride was taken up in DCM and used immediately without further purification.

### 7.4.1.23 2-(2,5-Dioxo-2,5-dihydro-1*H*-pyrrol-1-yl)-*N*-(2-oxo-2-((4-((4-sulfamoylphenyl)diazenyl)phenyl) amino)ethyl)acetamide (SA-2)

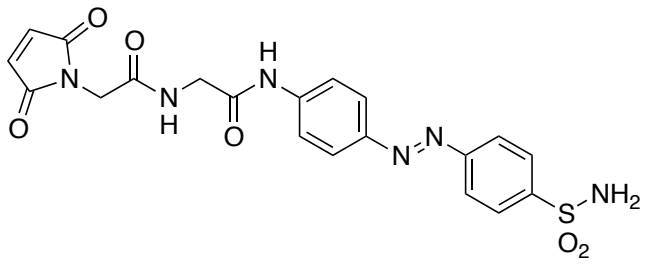

Compound **7.16** was dissolved in 4 mL anhydrous DMF and DIPEA (5.0 eq., 129 mg, 1 mmol, 0.17 mL) was added drop-wise. The mixture was stirred for 30 min and freshly prepared 2-(2,5-dioxo-2,5-dihydro-1*H*-pyrrol-1-yl)acetyl chloride **7.17** in 1 mL DCM was carefully added drop-wise and the mixture was allowed to stir o.n. at r.t.. DMF was removed by taking up the crude reaction mixture in EtOAc and subsequent washing of the organic layer with water. Final purification by flash column chromatography on silica gel (100% EtOAc → 10% MeOH / EtOAc) yielded 18 mg (19%) of the title compound as a red powder.

**$^1$H NMR** (400 MHz, DMSO-$d_6$) $\delta$ [ppm] = 10.42 (s, 1H), 8.60 (t, $J$ = 5.7 Hz, 1H), 8.04–7.98 (m, 4H), 7.95 (d, $J$ = 8.9 Hz, 2H), 7.84 (d, $J$ = 9.0 Hz, 2H), 7.52 (s, 2H), 7.11 (s, 2H), 4.14 (s, 2H), 3.98 (d, $J$ = 5.7 Hz, 2H).

**$^{13}$C NMR** (101 MHz, DMSO-$d_6$) $\delta$ [ppm] = 171.1, 168.4, 167.1, 154.0, 148.0, 145.9, 143.0, 135.3, 127.5, 124.6, 123.1, 119.8, 43.3, 39.2 (under solvent signal, found by HSQC).

**HRMS (ESI)**: calc. for $C_{20}H_{19}N_6O_6S^+$ $(M+H)^+$: 471.1081, found: 471.1079.

**UV/Vis** (50 µM in DMSO): $\lambda_{max}$ (trans, π → π*) = 367 nm; $\lambda_{max}$ (cis, π → π*) = 332 nm; $\lambda_{max}$ (cis, n → π*) = 440 nm.

**UV/Vis** (LCMS): $\lambda_{max}$ (trans, π → π*) = 356 nm; $\lambda_{max}$ (cis, π → π*) = 332 nm; $\lambda_{max}$ (cis, n → π*) = 435 nm.

**$R_t$** (LCMS; MeCN/$H_2O$/formic acid = 10/90/0.1 → 90/10/0.1 over 7 min) = 2.468 min (*cis*), 2.805 min (*trans*).

**IR** (ATR)**:** wave number/$cm^{-1}$ **=** 3372, 3294, 1710, 1669, 1344, 1172, 850, 836.

**m.p.:** decomposition >250 °C.

### 7.4.1.24 (*Z*)-4-Oxo-4-(prop-2-yn-1-ylamino)but-2-enoic acid (7.20)

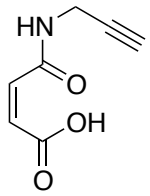


The compound was prepared as previously described in our group.[85]

Maleic anhydride (**7.18**, 178 mg, 1.82 mmol, 1.0 eq.) and propargyl amine (**7.19**, 100 mg, 1.82 mmol, 1.0 eq.) were dissolved in 2 mL glacial acetic acid and stirred for 16 h at r.t.. The solution was neutralized with aqueous sat. $NaHCO_3$, extracted with EtOAc and successively washed with aqueous sat. $NaHCO_3$, water and brine before drying over $MgSO_4$. After removal of all solvents the crude product was obtained, which was used without further purification.

### 7.4.1.25 1-(Prop-2-yn-1-yl)-1*H*-pyrrole-2,5-dione (7.21)

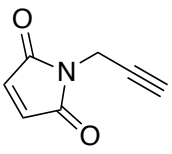

The compound was prepared as previously described in our group and the spectral data matched the one reported.[85]

(*Z*)-4-Oxo-4-(prop-2-ynylamino)but-2-enoic acid (**7.20**, 0.802 g, 5.24 mmol, 1.0 eq.) was dissolved in benzene (150 mL) and HHMDS (1.27 g, 7.86 mmol, 1.5 eq.) and $ZnBr_2$ (1.18 g, 5.24 mmol, 1.0 eq.) were added to the solution and the reaction mixture was refluxed for 2 h. Afterwards, the cooled reaction mixture was poured into distilled water (222 mL) and subsequently extracted with EtOAc (2 x 222 mL). The combined organic layers were washed with HCl (0.1 M, 445 mL), Brine (445 mL) and dried over $MgSO_4$. The solvent was removed *in vacuo.* The crude product was purified by flash column chromatography (DCM) to afford **7.21** (0.413 g, 3.06 mmol, 58 %) as a colorless oil.

**$^1$H NMR** (300 MHz, $CDCl_3$): $\delta$ [ppm] = 6.75 (s, 2H), 4.29 (d, $J$ = 2.5 Hz, 2H), 2.21 (t, $J$ = 2.5 Hz, 1H).

**$^{13}$C NMR** (75 MHz, $CDCl_3$): $\delta$ [ppm] = 169.4, 134.6, 77.1, 71.7, 27.0.

**HRMS (EI)**: calc. for $(M)^{\bullet+}$: 135.0315, found: 135.0316.

**UV/Vis** (LCMS): $\lambda_{max1}$ = 228 nm, $\lambda_{max2}$ = 290 nm.

**$R_t$** (LCMS; MeCN/$H_2O$/formic acid = 10/90/0.1 → 90/10/0.1 over 7 min) = 2.218 min.

### 7.4.1.26 4-((4-(4-((2,5-Dioxo-2,5-dihydro-1*H*-pyrrol-1-yl)methyl)-1*H*-1,2,3-triazol-1-yl)phenyl)diazenyl)benzenesulfonamide (SA-3)

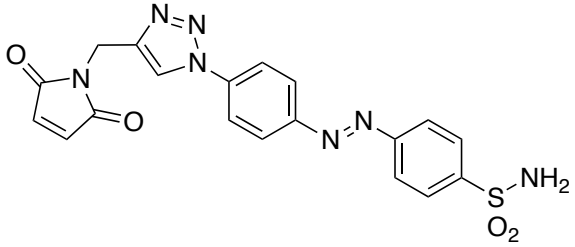

*N*-Propargyl maleimide **7.21** (17.2 mg, 0.039 mmol, 1.3 eq.) and azide **7.6** (9.0 mg, 0.030 mmol, 1.0 eq.) were combined in a round bottom flask und purged

with nitrogen. A degassed solution of $CuSO_4 \cdot 5\ H_2O$ (1.5 mg, 0.006 mmol, 0.2 eq.) and sodium ascorbate (1.5 mg, 0.007 mmol, 0.25 eq.) in water (1.32 mL) and MeCN (1.98 mL) was added. In order to obtain a homogeneous solution 3.3 mL of DMSO was added to the mixture and the resulting solution was sonicated at 40 °C for 15 min. Afterwards, the reaction was quenched by addition of sat. $NaHCO_3$-solution (30 mL) and was extracted with EtOAc (2 x 30 mL). The combined organic layers were washed with brine (30 mL) and dried over $MgSO_4$. The solvent was removed *in vacuo* and the crude product was purified by flash column chromatography (DCM/MeOH = 9/1) to afford **SA-3** (8.5 mg, 0.019 mmol, 65%) as a red solid.

**$^1$H NMR** (400 MHz, acetone-$d_6$): $\delta$ [ppm] = 8.63 (s, 1H), 8.18 (br s, 4H), 8.14–8.09 (m, 6H), 6.97 (s, 2H), 4.88 (d, $J$ = 0.6 Hz, 2H).

**$^{13}$C NMR** (101 MHz, acetone-$d_6$): $\delta$ [ppm] = 171.0, 154.9, 152.6, 147.2, 145.3, 140.2, 135.5, 128.3, 125.4, 124.1, 121.9, 121.7, 33.5.

**HRMS (ESI)**: calc. for $C_{19}H_{16}N_7O_4S^+$ $(M+H)^+$: 438.0979, found: 438.0980.

**UV/Vis** (80 µM in DMSO): $\lambda_{max}$ (trans, $\pi \rightarrow \pi^*$) = 354 nm; $\lambda_{max}$ (cis, $\pi \rightarrow \pi^*$) = 348 nm; $\lambda_{max}$ (cis, $n \rightarrow \pi^*$) = 440 nm.

**UV/Vis** (LCMS): $\lambda_{max}$ (trans, $\pi \rightarrow \pi^*$) = 334 nm.

**$R_t$** (LCMS; MeCN/$H_2O$/formic acid = 10/90/0.1 → 90/10/0.1 over 7 min) = 3.341 min.

### 7.4.1.27 2-(2,5-Dioxo-2,5-dihydro-1*H*-pyrrol-1-yl)-*N*-(4-sulfamoyl-phenyl)acetamide (7.22)

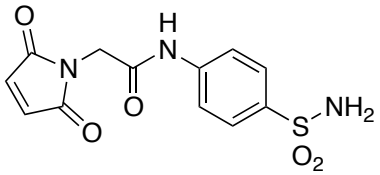

In a round bottom flask, 1.00 g (1.0 eq., 5.81 mmol) of sulfanilamide (**7.1**) was dissolved in a mixture of 30 mL of 1,4-dioxane and 1.4 mL of pyridine under a nitrogen atmosphere. 2-(2,5-Dioxo-2,5-dihydro-1*H*-pyrrol-1-yl)acetyl chloride (**7.17**, ~1.0 g in 10 mL 1,4-dioxane) was added drop-wise at r.t. under vigorous stirring. After 5 min, the reaction was diluted with EtOAc (100 mL) and quenched by the addition of 1 M HCl (100 mL). The organic layer was separated, washed with brine and dried over $MgSO_4$. The crude was concentrated *in vacuo* and submitted to flash column chromatography (pentane/EtOAc = 1/4) to yield 155 mg (0.50 mmol) of the desired product in 9% yield as a white solid.

**$^1$H NMR** (600 MHz, DMSO-$d_6$) $\delta$ [ppm] = 10.61 (s, 1H), 7.77 (d, $J$ = 8.8 Hz, 2H), 7.70 (d, $J$ = 8.8 Hz, 2H), 7.26 (s, 2H), 7.15 (s, 2H), 4.31 (s, 2H).

**$^{13}$C NMR** (101 MHz, DMSO-$d_6$) $\delta$ [ppm] = 170.6, 165.5, 141.3, 138.7, 135.0, 126.8, 118.8, 40.4.

**HRMS (ESI)**: calc. for $C_{12}H_{10}N_3O_5S^-$ $(M-H)^-$: 308.0347, found: 308.0349.

**UV/Vis** (LCMS): $\lambda_{max}$ = 257 nm.

**$R_t$** (LCMS; MeCN/$H_2O$/formic acid = 10/90/0.1 → 90/10/0.1 over 7 min) = 2.037 min.

**IR** (ATR)**:** wave number/$cm^{-1}$ = 3337, 3273, 3098, 1708, 1693, 1592, 1535, 1423, 1400, 1309, 1151, 1093, 904, 832, 821, 696.

**m.p.:** decomposition >250 °C.

### 7.4.1.28 6-(6-(Pyridin-2-yl)-1,4-dihydro-1,2,4,5-tetrazin-3-yl)pyridin-3-amine (7.26)

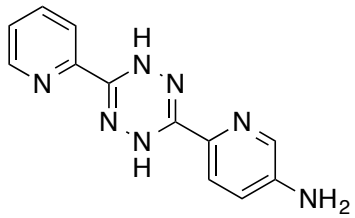

6-(6-(Pyridin-2-yl)-1,4-dihydro-1,2,4,5-tetrazin-3-yl)pyridin-3-amine was prepared as previously reported.[101]

Briefly, 2-cyanopyridine (**7.23**) (3.00 g, 28.8 mmol, 1.0 eq.) and 5-amino-2-cyanopyridine (**7.25**) (3.40 g, 28.8 mmol, 1.0 eq.) were dissolved in hydrazine hydrate (**7.24**) (5.60 mL, 120 mmol, 4.2 eq.) and heated to 90 °C for 12 h. The precipitate was collected and subjected to flash column chromatography (pentane/acetone = 1/1; $R_f$ = 0.2–0.4). The final product was recrystallized from chloroform to obtain 1.10 g (4.36 mmol) of the title compound in 15% yield as a yellow solid.

3,6-Di(pyridin-2-yl)-1,4-dihydro-1,2,4,5-tetrazine (**7.27**) was isolated as a side product in crystalline form suitable for X-ray diffractometry (see below).

**$^1$H NMR** (400 MHz, DMSO-$d_6$) $\delta$ [ppm] = 8.70 (br s, 1H), 8.65 (br s, 1H), 8.63–8.61 (m, 1H), 7.99–7.88 (m, 3H), 7.68–7.63 (m, 1H), 7.51 (dddd, $J$ = 7.3, 4.9, 1.4, 0.4 Hz, 1H), 7.00 (ddd, $J$ = 8.6, 2.7, 0.4 Hz, 1H), 5.87 (s, 2H).

**$^{13}$C NMR** (101 MHz, DMSO-$d_6$) $\delta$ [ppm] = 148.5, 147.5, 146.7, 146.6, 146.6, 137.3, 134.2, 134.1, 125.1, 121.8, 120.8, 120.3.

**HRMS (ESI)**: calc. for $C_{12}H_{10}N_7^+$ $(M\text{-}H_2+H)^+$: 252.0992, found: 252.0992.

**UV/Vis** (LCMS): $\lambda_{max}$ = 298 nm.

**$R_t$** (LCMS; MeCN/$H_2O$/formic acid = 10/90/0.1 → 90/10/0.1 over 7 min) = 2.759 min.

### 7.4.1.29 6-(6-(Pyridin-2-yl)-1,2,4,5-tetrazin-3-yl)pyridin-3-amine (7.28)

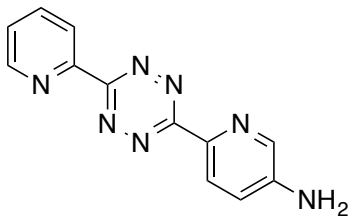

6-(6-(Pyridin-2-yl)-1,2,4,5-tetrazin-3-yl)pyridin-3-amine was prepared as previously reported[101] with brief characterization by LCMS and $^1$H NMR (200 MHz).

Briefly, a round-bottom flask was charged with **7.26** (791 mg, 3.12 mmol, 1.0 eq.) in 30 mL degassed PhMe under a nitrogen atmosphere and DDQ (1.42 g, 6.24 mmol, 2.0 eq.) was added. The resulting suspension was refluxed for 12 hours before all volatiles were removed *in vacuo* and the crude product was subjected to flash column chromatography on deactivated silica gel (acetone/pentane = 0/100 → 5/95 → 10/90 → 20/80) to yield 135 mg (0.53 mmol) of **7.28** in 17% yield, which was used in the next step without further characterization.

### 7.4.1.30 5-Oxo-5-((6-(6-(pyridin-2-yl)-1,2,4,5-tetrazin-3-yl)pyridin-3-yl)amino)pentanoic acid (7.30)

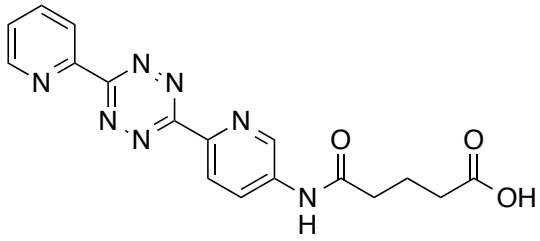


5-Oxo-5-((6-(6-(pyridin-2-yl)-1,2,4,5-tetrazin-3-yl)pyridin-3-yl)amino)pentanoic acid was prepared as previously reported[101] with brief characterization by LCMS and $^1$H NMR (200 MHz).

Briefly, 135 mg (0.54 mmol, 1.0 eq.) of **7.28** was dissolved in 40 mL dry THF and glutaric anhydride (**7.29**) was added portion wise (total amount = 1.0 g over 6 h). All volatiles were removed *in vacuo* and the crude product was sonicated in $Et_2O$. The suspension was centrifuged (4,000 rpm) and the precipitate was collected by filtration to yield 52.4 mg (0.134 mmol) of **7.30** in 25% yield.

**LRMS (ESI):** calc. for $C_{17}H_{16}N_7O_3^+$ $(M+H)^+$: 366.1, found: 366.2.

**UV/Vis** (LCMS): $\lambda_{max}$ = 324 nm.

**$R_t$** (LCMS; MeCN/$H_2O$/formic acid = 10/90/0.1 → 90/10/0.1 over 7 min) = 2.393 min.

### 7.4.1.31 (*E*)-$N^1$-(2-Oxo-2-((4-((4-sulfamoylphenyl)diazenyl)phenyl)-amino) ethyl)-$N^5$-(6-(6-(pyridin-2-yl)-1,2,4,5-tetrazin-3-yl)pyridin-3-yl)glutaramide (JB369)

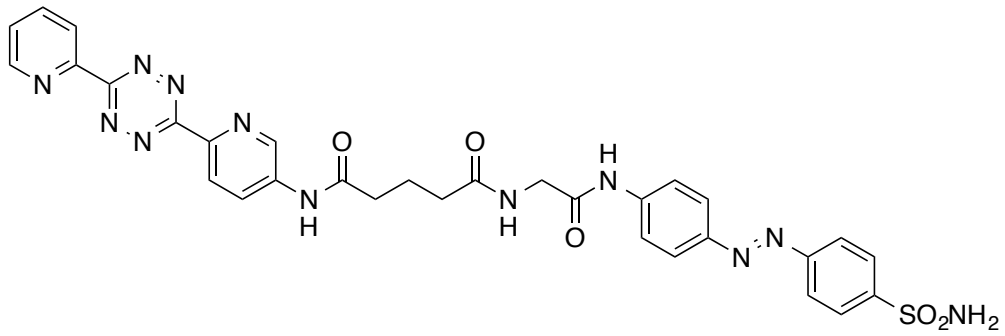

A round-bottom flask was charged with 5-oxo-5-((6-(6-(pyridin-2-yl)-1,2,4,5-tetrazin-3-yl)pyridin-3-yl)amino)pentanoic acid (**7.30**) (16.2 mg, 0.044 mmol, 1.0 eq.), 2-amino-*N*-(4-((4-sulfamoylphenyl)diazenyl)phenyl)acetamide (**7.16**) (22.7 mg, 0.053 mmol, 1.2 eq.) and HBTU (17.5 mg, 0.046 mmol, 1.05 eq.) dissolved in 600 µL DMSO. The reaction mixture was cooled to 0 °C and DIPEA was added (56.9 mg, 77 µL, 0.440 mmol, 10.0 eq.) in one portion. The resulting solution was stirred at r.t. o.n. and then subjected to C18 RP column chromatography (MeCN/$H_2O$/FA/DMF = 15/85/0.1/0 → 30/70/0.1/0 → 50/50/0.1/0 → 70/30/0.1/0 → 100/0/0.1/0 → 0/0/0/100) to yield 21.0 mg (0.031 mmol) of **JB369** as a red solid in 70% yield.

**$^1$H NMR** (400 MHz, DMSO-$d_6$) $\delta$ [ppm] = 10.82 (s, 1H), 10.64 (s, 1H), 9.30 (dd, *J* = 2.5, 0.7 Hz, 1H), 9.10 (ddd, *J* = 4.7, 1.8, 0.9 Hz, 1H), 8.86–8.76 (m, 2H), 8.69 (dd, *J* = 8.7, 2.5 Hz, 1H), 8.42 (t, *J* = 5.9 Hz, 1H), 8.34 (td, *J* = 7.8, 1.8 Hz, 1H), 8.26 (d, *J* = 8.8 Hz, 2H), 8.22–8.14 (m, 3H), 7.89 (ddd, *J* = 7.6, 4.7, 1.2 Hz, 1H), 7.68 (s, 2H), 4.28 (d, *J* = 5.8 Hz, 2H), 3.62 (s, 3H), 2.76 (t, *J* = 7.3 Hz, 2H), 2.58 (t, *J* = 7.3 Hz, 2H), 2.19 (qu, *J* = 7.3 Hz, 2H).

**$^{13}$C NMR** (101 MHz, DMSO-$d_6$) $\delta$ [ppm] = 173.3, 173.0, 169.5, 164.3, 164.0, 154.7, 151.4, 151.3, 148.7, 146.6, 144.9, 143.8, 142.1, 139.6, 138.2, 127.8, 127.1, 126.7, 125.4, 124.8, 124.8, 123.4, 120.1, 43.8, 36.5, 34.9 (HMBC), 21.9.

**HRMS (ESI)**: calc. for $C_{31}H_{29}N_{12}O_5S^+$ $(M+H)^+$: 681.2099, found: 681.2092.

**UV/Vis** (50 µM in DMSO): $\lambda_{max}$ = 370 nm.

**$R_t$** (LCMS; MeCN/$H_2O$/formic acid = 10/90/0.1 → 90/10/0.1 over 7 min) = 5.131 min.

### 7.4.2 hCAII encoding Plasmids

Plasmids (pACA) coding for hCAII mutants D130C, F131C, G132C and K133C were a genrous gift from Prof. Dr. Carol A Fierke, Michigan. All full sequences including the mutated ones can be found in the Appendix.

### 7.4.3 Site-Directed Mutagenesis

Site-Directed Mutagenesis was performed according to the manufacturer's instructions using the Pfu-X three-step protocol (Jena Bioscience, #PCR-207L).

**Table 13: Primer for site-directed mutagenesis of hCAII.**

| name | sequence (5'-3') |
|---|---|
| wt_132_F1 | GAACAAAGCTGTGCAGCAACCTGATG |
| wt_132_R1 | GAACTTTCCCAAAATCCCCATATTTGGT |
| wt_132_F2 | AAATATGGGGATTTTGGGAAAGCTGTGCAGCAACCTGATG |
| wt_132_R2 | ATCAGGTTGCTGCACAGCTTTCCCAAAATCCCCATATTTGGT |
| G129C_F | ACTGGAACACCAAATATTGTGATTTTGGGAAAGC |
| G129C_R | GCTTTCCCAAAATCACAATATTTGGTGTTCCAGT |
| C206S_F | CTCCTCTTCTGGAATCTGTGACCTGGATTG |
| C206S_R | CAATCCAGGTCACAGATTCCAGAAGAGGAG |

| | |
|---|---|
| L198A_F | CAGGCTCAGCGACCACCCCTCCTCTTCTG |
| L198A_R | GGGTGGTCGCTGAGCCTGGGTAGGTCCAG |

After PCR, the template was digested for 2 h at 37 °C by the addition of DpnI (NEB, #R0176), before plating on Amp resistant agar plates. Colonies were picked and grown in 5 mL LB medium (Amp). All constructs were validated by sequencing (SEQLAB Göttingen; sequencing primer: 5'-CACTATAGGGAGACCACA -3').

### 7.4.4 Protein Expression in and Purification from *E. coli* Cells

DNA (1 uL of 20 ng/uL) was transformed into *E. coli* BL21 (DE3) cells to express the desired protein. After incubation for 30 minutes on ice the cells were heat-shocked for precisely 30 seconds at 42 °C. Afterwards the sample was put on ice again for 2 minuntes before a preculture in 400 µL LB medium (pH = 7.4) for 1 h at 37 °C was started. Finally, the complete sample was plated on an agar plate (Amp) and incubated at 37 °C overnight. One colony was picked and transferred into a 20 mL test tube, 20 mL LB medium (100 µg/L Amp) was added and the sample was shaken overnight at 37 °C at 180 rpm to obtain a pre-culture. The total amount of the pre-culture was added to 5 L of LB medium (100 µg/L Amp) and incubated at 37 °C in a shaker at 180 rpm. Cells grew for 5.25 h until an $OD_{600}$ ~ 0.9-1 was reached. Protein expression was induced by the addition of IPTG (1 mM final concentration) followed by the addition of $ZnSO_4$ (10 mL of sterile filtered 0.5 M stock). The culture was incubated for another 9 h at 37 °C with shaking at 180 rpm. Finally, cells were harvested by centrifuging at 4 °C for 8 min at 8,000 rpm. The resulting, decanted supernatant was deactivated with bleach and discarded, the cell pellets were frozen and stored at -20 °C until further use.

The frozen cell pellet was lysed by the addition of 50 mL lysis buffer at 0 °C until the solution was homogeneous. Cell rupture was performed using a French-press ($p_{max}$ = 1500 psi). The lysate was centrifuged at 4 °C at 18,000 rpm for 30 min

before the supernatant was collected and dialyzed against 5 L of a solution of 50 mM Tris (pH = 8.0) and 0.5 mM $ZnSO_4$ at 4 °C o.n.. Further precipitate was removed by centrifugation at 4 °C and 18,000 rpm for 30 min.

The lysate was finally purified by affinity chromatography using an AEKTA purifier with a sulfonamide-based agarose resin (Sigma, #A0796). The column was flushed with 2 column volumes of activation buffer A before it was charged with the lysate. The bound protein was washed with 4 column volumes of washing buffer B before it was eluted with 2 column volumes of elution buffer C. The enzyme was dialysed twice against 5 L of $dH_2O$ and then freeze-dried to yield 100-250 mg of pure protein as a white fluffy powder in sufficient purity for assaying.

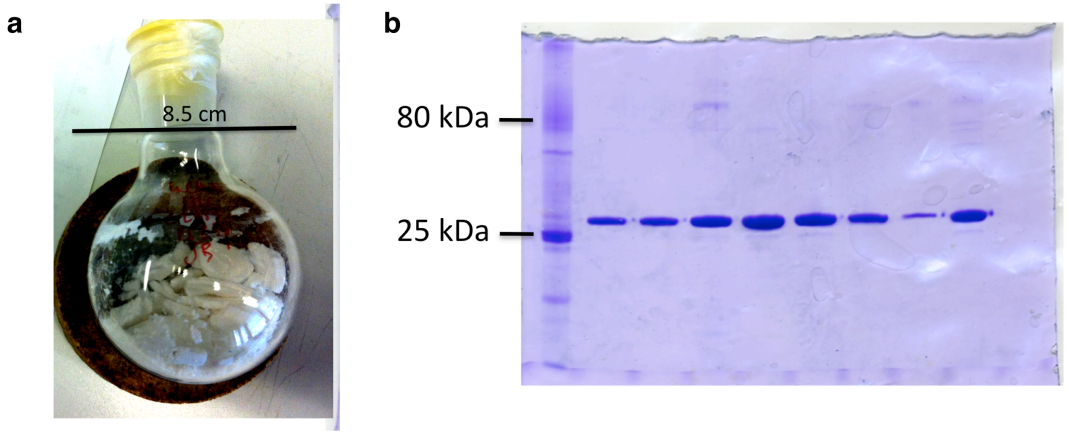


**Supplementary Figure 1: Quantity and purity of hCAII expression from *E. coli* BL21 (DE3) cells. a)** 150-200 mg of enzyme were obtained from a 5 L culture. **b)** Representative SDS-PAGE after coomassie staining proves purity to be >95%.

### 7.4.5 Protein Crystallization

Prior to crystallization, hCAII was further purified by gel filtration using an AEKTA purifier with gel filtration buffer as an eluent. Pure hCAII was dissolved in $dH_2O$ (10 mg / mL) and centrifuged for 25 min at 13,500 rpm at 4 °C. The supernatant was separated into 49 µL aliquots and 1 µL of ligand (69 mM in DMSO) was added. After sufficient incubation at r.t., the resulting suspension was

centrifuged for 25 min at 13,500 rpm at 4 °C, and 2 µL of the final supernatant was mixed with 2 µL of reservoir solution onto a coverslip in order to crystallize by the hanging drop method, the reservoir solution being as previously reported (3 M $(NH_4)_2SO_4$, Aldrich, #A2939; 50 mM Tris, pH = 8.5; 2 mM PCMB, Sigma, #55540).[103] Crystals were harvested using a Nylon loop after growing for 5-7 days and frozen in liquid nitrogen after soaking for 5-10 seconds in 25-30% glycerol in 2 M $(NH_4)_2SO_4$ serving as a cryoprotectant.

### 7.4.6 Protein X-ray Crystallographic Data Collection

Datasets were collected using either synchrotron radiation at the X06SA-beamline, SLS (Villigen, Switzerland) or on a Bruker Microstar/X8 Proteum with a Cu rotating anode (λ = 1.54 Å) (Bruker AXS, Fitchburg, WI, USA). Synchrotron datasets were processed using the program package XDS and in-house datasets with the Proteum software suit from Bruker (Bruker AXS, Fitchburg, WI, USA). For structure determination of the various domains, molecular replacement was performed in Phaser[104] by using the coordinates of suitable starting models. The models were completed either using the interactive three-dimensional graphic program MAIN[105] or with the program COOT[106]. Stereochemically restrained refinement of the models was carried out in REFMAC5[105] using maximum-likelihood targets. Water molecules were located with ARP/wARP[107] solvent within the CCP4i GUI and verified manually in COOT. The stereochemical quality of the models was assessed with PROCHECK[108]. Structures were solved by Prof. Dr. Michael Groll, TU Munich, by molecular replacement with the hCAII (pdb: 2vva[71]) crystal structure serving as a model. Molecular illustrations were prepared in PyMOL (DeLano Scientific, Palo Alto, CA, USA).

### 7.4.7 Protein X-ray Crystallographic Data

#### 7.4.7.1 Annotation for Crystallographic Tables

[a] Asymmetric unit.

[b] The values in parentheses of resolution range, completeness, $R_{merge}$ and I/s (I) correspond to the last resolution shell.

[c] Friedel pairs were treated as identical reflections.

[d] $R_{merge}(I) = \Sigma_{hkl}\Sigma_j \mid [I(hkl)_j - I(hkl)] \mid \Sigma_{hkl} I_{hkl}$ , where $I(hkl)_j$ is the $j^{th}$ measurement of the intensity of reflection hkl and <I(hkl)> is the average intensity.

[e] $R = \Sigma_{hkl} \mid |F_{obs}| - |F_{calc}| \mid / \Sigma_{hkl} |F_{obs}|$, where $R_{free}$ is calculated for a randomly chosen 5 % of reflections, which were not used for structure refinement, and $R_{work}$ is calculated for the remaining reflections.

[f] Deviations from ideal bond lengths/angles.

[g] Number of residues in favoured, allowed or outlier region.

### 7.4.7.2 hCAII*7.22

**Crystallographic Table 1: hCAII*7.22**

| | **hCAII*7.22** |
|---|---|
| **Crystal parameters** | |
| Space group | $P2_1$ |
| Cell constants | a= 42.2 Å |
| | b= 41.3 Å |
| | c= 72.2 Å |
| | β= 104.3 ° |
| AU[a] | 1 |
| **Data collection** | |
| Beam line | X06SA, SLS |
| Wavelength (Å) | 1.0 |
| Resolution range (Å)[b] | 30 – 1.2 |
| | (1.3 – 1.2) |
| No. observations | 236329 |
| No. unique reflections[c] | 71499 |
| Completeness (%)[b] | 94.8 (91.2) |

| | |
|---|---|
| $R_{merge}$ (%)[b, d] | 5.9 (38.7) |
| I/s (I)[b] | 10.4 (3.5) |
| **Refinement (REFMAC5)** | |
| Resolution range (Å) | 10 – 1.2 |
| No. refl. working set | 67924 |
| No. refl. test set | 3575 |
| No. non hydrogen | 2402 |
| No. of ligand atoms | 21 |
| Solvent ($H_2O$, $Zn^{2+}$, $Hg^{2+}$) | 332 |
| $R_{work}$ / $R_{free}$ (%)[e] | 14.8 / 16.7 |
| r.m.s.d. bond (Å) / (°)[f] | 0.009 / 1.39 |
| Average B-factor (Å$^2$) | 16.1 |
| Ramachandran Plot (%)[g] | 96.9 / 3.1 / 0 |
| PDB accession code | xxxx |

### 7.4.7.3 hCAII(L198A)*7.22

**Crystallographic Table 2: hCAII(L198A)*7.22**

| | **hCAII(L198A)*7.22** |
|---|---|
| **Crystal parameters** | |
| Space group | $P2_1$ |
| Cell constants | a= 42.2 Å |
| | b= 41.5 Å |
| | c= 72.0 Å |
| | β= 104.4 ° |
| AU[a] | 1 |
| **Data collection** | |
| Beam line | X06SA, SLS |

| | |
|---|---|
| Wavelength (Å) | 1.0 |
| Resolution range (Å)[b] | 30 – 1.15 |
| | (1.25 – 1.15) |
| No. observations | 278311 |
| No. unique reflections[c] | 83065 |
| Completeness (%)[b] | 95.0 (96.4) |
| $R_{merge}$ (%)[b, d] | 4.6 (13.9) |
| I/s (I)[b] | 14.3 (6.5) |
| **Refinement (REFMAC5)** | |
| Resolution range (Å) | 10 – 1.15 |
| No. refl. working set | 78910 |
| No. refl. test set | 4154 |
| No. non hydrogen | 2504 |
| No. of ligand atoms | 47 |
| Solvent ($H_2O$, $Zn^{2+}$, $Hg^{2+}$) | 411 |
| $R_{work}$ / $R_{free}$ (%)[e] | 13.7 / 16.1 |
| r.m.s.d. bond (Å) / (°)[f] | 0.015 / 1.89 |
| Average B-factor (Å$^2$) | 15.2 |
| Ramachandran Plot (%)[g] | 96.9 / 3.1 / 0 |
| PDB accession code | xxxx |

### 7.4.7.4 hCAII(F131C, C206S)*7.22

**Crystallographic Table 3: hCAII(F131C, C206S)*7.22**

| | **hCAII(F131C, C206S)*7.22** |
|---|---|
| **Crystal parameters** | |
| Space group | $P2_1$ |

| | |
|---|---|
| Cell constants | a= 42.4 Å |
| | b= 41.4 Å |
| | c= 72.0 Å |
| | β= 104.1 ° |
| AU[a] | 1 |
| **Data collection** | |
| Beam line | X06SA, SLS |
| Wavelength (Å) | 1.0 |
| Resolution range (Å)[b] | 30 – 1.2 |
| | (1.3 – 1.2) |
| No. observations | 205559 |
| No. unique reflections[c] | 73965 |
| Completeness (%)[b] | 97.4 (96.9) |
| $R_{merge}$ (%)[b, d] | 6.3 (22.2) |
| I/s (I)[b] | 11.2 (5.3) |
| **Refinement (REFMAC5)** | |
| Resolution range (Å) | 10 – 1.2 |
| No. refl. working set | 70266 |
| No. refl. test set | 3699 |
| No. non hydrogen | 2453 |
| No. of ligand atoms | 21 |
| Solvent ($H_2O$, $Zn^{2+}$, $Hg^{2+}$) | 380 |
| $R_{work}$ / $R_{free}$ (%)[e] | 14.9 / 16.8 |
| r.m.s.d. bond (Å) / (°)[f] | 0.009 / 1.35 |
| Average B-factor (Å$^2$) | 12.7 |
| Ramachandran Plot (%)[g] | 96.9 / 3.1 / 0 |
| PDB accession code | xxxx |

### 7.4.7.5 hCAII(L198A)*SA-2

**Crystallographic Table 4: hCAII(L198A)*SA-2**

| | **hCAII(L198A)*SA-2** |
|---|---|
| **Crystal parameters** | |
| Space group | $P2_1$ |
| Cell constants | a= 42.4 Å |
| | b= 41.4 Å |
| | c= 72.0 Å |
| | β= 104.1 ° |
| AU[a] | 1 |
| **Data collection** | |
| Beam line | X06SA, SLS |
| Wavelength (Å) | 1.0 |
| Resolution range (Å)[b] | 30 – 1.2 |
| | (1.3 – 1.2) |
| No. observations | 212859 |
| No. unique reflections[c] | 74298 |
| Completeness (%)[b] | 97.9 (99.0) |
| $R_{merge}$ (%)[b, d] | 6.5 (15.8) |
| I/s (I)[b] | 12.6 (7.8) |
| **Refinement (REFMAC5)** | |
| Resolution range (Å) | 10 – 1.2 |
| No. refl. working set | 70467 |
| No. refl. test set | 3709 |
| No. non hydrogen | 2770 |
| No. of ligand atoms | 30 |
| Solvent ($H_2O$, $Zn^{2+}$, $Hg^{2+}$) | 294 |

| | |
|---|---|
| $R_{work}$ / $R_{free}$ (%)[e] | 15.3 / 16.7 |
| r.m.s.d. bond (Å) / (°)[f] | 0.009 / 1.28 |
| Average B-factor (Å$^2$) | 12.4 |
| Ramachandran Plot (%)[g] | 96.5 / 3.5 / 0 |
| PDB accession code | xxxx |

### 7.4.7.6 hCAII(G132C_C206S)*SA-2

**Crystallographic Table 5: hCAII(G132C_C206S)*SA-2**

| | **hCAII(G132C_C206S)*SA-2** |
|---|---|
| **Crystal parameters** | |
| Space group | $P2_1$ |
| Cell constants | a= 42.5 Å |
| | b= 41.5 Å |
| | c= 72.3 Å |
| | β= 104.3 ° |
| CPs / AU[a] | 1 |
| **Data collection** | |
| Beam line | X06SA, SLS |
| Wavelength (Å) | 1.0 |
| Resolution range (Å)[b] | 30 – 1.5 |
| | (1.6 – 1.5) |
| No. observations | 108912 |
| No. unique reflections[c] | 37834 |
| Completeness (%)[b] | 95.9 (98.7) |
| $R_{merge}$ (%)[b, d] | 7.0 (54.7) |

| | |
|---|---|
| I/s (I)[b] | 10.5 (2.2) |
| **Refinement (REFMAC5)** | |
| Resolution range (Å) | 10 – 1.5 |
| No. refl. working set | 35941 |
| No. refl. test set | 1892 |
| No. non hydrogen | 2332 |
| No. of ligand atoms | 30 |
| Solvent ($H_2O$, $Zn^{2+}$, $Hg^{2+}$) | 251 |
| $R_{work}/R_{free}$ (%)[e] | 15.8 / 18.9 |
| r.m.s.d. bond (Å) / (°)[f] | 0.007 / 1.16 |
| Average B-factor (Å$^2$) | 16.7 |
| Ramachandran Plot (%)[g] | 96.9 / 3.1 / 0 |
| PDB accession code | xxxx |

### 7.4.7.7 hCAII(F131C_C206S)*SA-2

**Crystallographic Table 6: hCAII(F131C_C206S)*SA-2**

| | **hCAII(F131C_C206S)*SA-2** |
|---|---|
| **Crystal parameters** | |
| Space group | $P2_1$ |
| Cell constants | a= 42.5 Å |
| | b= 41.5 Å |
| | c= 72.5 Å |
| | β= 104.3 ° |
| CPs / AU[a] | 1 |
| **Data collection** | |
| Beam line | X06SA, SLS |
| Wavelength (Å) | 1.0 |

| | |
|---|---|
| Resolution range (Å)[b] | 30 – 1.3 |
| | (1.4 – 1.3) |
| No. observations | 170333 |
| No. unique reflections[c] | 58813 |
| Completeness (%)[b] | 97.7 (98.4) |
| $R_{merge}$ (%)[b, d] | 7.1 (44.2) |
| I/s (I)[b] | 10.1 (4.2) |
| **Refinement (REFMAC5)** | |
| Resolution range (Å) | 10 – 1.3 |
| No. refl. working set | 55870 |
| No. refl. test set | 2941 |
| No. non hydrogen | 2504 |
| No. of ligand atoms | 12 |
| Solvent ($H_2O$, $Zn^{2+}$, $Hg^{2+}$) | 336 |
| $R_{work}/R_{free}$ (%)[e] | 14.7 / 17.8 |
| r.m.s.d. bond (Å) / (°)[f] | 0.009 / 1.39 |
| Average B-factor (Å$^2$) | 15.9 |
| Ramachandran Plot (%)[g] | 96.9 / 3.1 / 0 |
| PDB accession code | xxxx |

### 7.4.7.8 hCAII(F131C, C206S)*7.5

**Crystallographic Table 7: hCAII(F131C, C206S)*7.5**

| | **hCAII(F131C, C206S)*7.5** |
|---|---|
| **Crystal parameters** | |
| Space group | $P2_1$ |
| Cell constants | a= 42.4 Å |
| | b= 41.2 Å |

| | |
|---|---|
| | c= 72.2 Å |
| | β= 104.1 ° |
| CPs / AU[a] | 1 |
| **Data collection** | |
| Beam line | X06SA, SLS |
| Wavelength (Å) | 1.0 |
| Resolution range (Å)[b] | 30 – 1.3 |
| | (1.4 – 1.3) |
| No. observations | 187541 |
| No. unique reflections[c] | 53275 |
| Completeness (%)[b] | 94.3 (93.0) |
| $R_{merge}$ (%)[b, d] | 5.8 (37.3) |
| I/s (I)[b] | 12.7 (3.4) |
| **Refinement (REFMAC5)** | |
| Resolution range (Å) | 10 – 1.3 |
| No. refl. working set | 50611 |
| No. refl. test set | 2664 |
| No. non hydrogen | 2472 |
| No. of ligand atoms | 38 |
| Solvent ($H_2O$, $Zn^{2+}$, $Hg^{2+}$) | 390 |
| $R_{work}/R_{free}$ (%)[e] | 16.5 / 17.8 |
| r.m.s.d. bond (Å) / (°)[f] | 0.005 / 1.14 |
| Average B-factor (Å$^2$) | 14.9 |
| Ramachandran Plot (%)[g] | 96.9 / 3.1 / 0 |
| PDB accession code | xxxx |

### 7.4.8 PTL-Labeling

Lyophilized hCAII was dissolved in 50 mM Tris buffer (pH = 7.4) at a concentration of 10 mg/mL and centrifuged for 25 min at 13,500 rpm at r.t.. The supernatant was separated to aliquots of 48 µL and 1 µL of PTL (32-100 mM in DMSO) and 1 µL of TCEP (0.1 M in $dH_2O$) was added. Solely DMSO instead of maleimide solution was added to hCAII aliquots to serve as controls. The resulting suspension was incubated for 20 h under shaking at 50 rpm at r.t.. The suspension was centrifuged and the clear supernatant collected, diluted with 450 µL of elution buffer (pH = 5.6, 0.1 M NaOAc, 0.2 M $NaClO_4$) and transferred to a microcentrifuge filter (Sartorius, Vivacon 500, MWCO 10 kDA, #VN01H01). Excess of maleimide was removed by repeated centrifugation (5 x 10 min, 13,500 rpm, 4 °C) of concentrated (~50 µL) and subsequently diluted (~500 µL) solution with elution buffer. Finally, the buffer was replaced to 50 mM Tris (pH = 7.4) by the same protocol for final assaying and the enzyme concentration was measured with a nanodrop.

### 7.4.9 Determination of half-maximal Inhibitory Concentration ($IC_{50}$)

Approximately 1.0 mg of hCAII was dissolved in 100 µL of 50 mM Tris (pH=7.4) and diluted to a final concentration of 500 nM (concentration was determined in duplicates by absorbance spectroscopy) and mixed with the appropriate amount of blocker. The enzyme-blocker solution was then pipetted into a 96 well plate (white, clear flat bottom) containing *p*NPA for a final concentration of 5 mM. This was added simultaneously with a multi-well-pipette. After 20-30 min of incubation in the dark, the absorbance was measured using a plate-reader at λ = 400 nm. Obtained data was background substracted and divided by data points of non-inhibited hCAII in order to obtain relative activity. The data points were fitted sigmoidal (eq. 1) or using the Hill equation (eq. 2) using IgorPro (version 6.22A) and the resulting equation was solved to obtain the $IC_{50}$ by using y = 0.5. All experiments were performed at least in triplicates.

$$y = base + [max / (1 + \exp[(xhalf - x)/rate)]] \quad \text{(eq. 1)}$$

$$y = base + (max - base)/(1 + (xhalf / x)^{rate}) \quad \text{(eq. 2)}$$

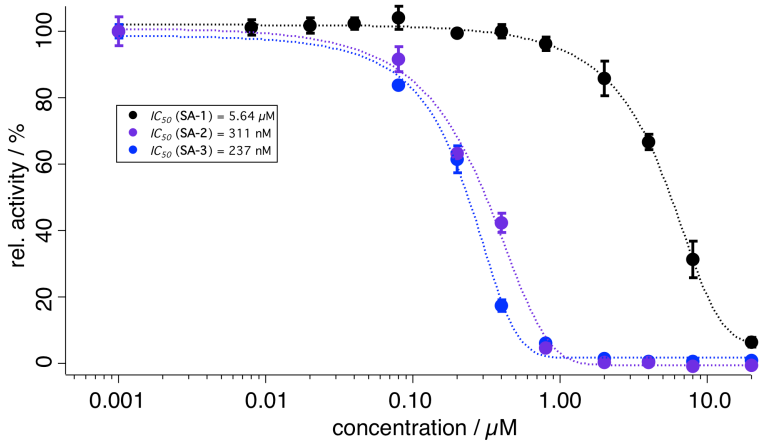


**Supplementary Figure 2: $IC_{50}$s of PTLs SA-1, SA-2 and SA-3 towards wt hCAII proved to be 5.36, 0.31 and 0.24 µM, respectively.**

### 7.4.10 Determination of Inhibitory Constants ($K_i$)

Inhibitory constants were determined using the Cheng-Prussow equation (eq. 3)[78] with the obtained half-maximal inibitory constants ($IC_{50}$) and with [$S$] = 5.0 mM.

$$K_i = IC_{50} / (1 + [S]/K_M) \quad \text{(eq. 3)}$$

The Michaelis-Menten constant $K_M$ was obtained for this assay system independently by measuring the initial catalytic velocities of hCAII catalyzed *p*NPA hydrolysis at various concentrations and was determined to be 1092.5 µM (Supplementary Figure 3).

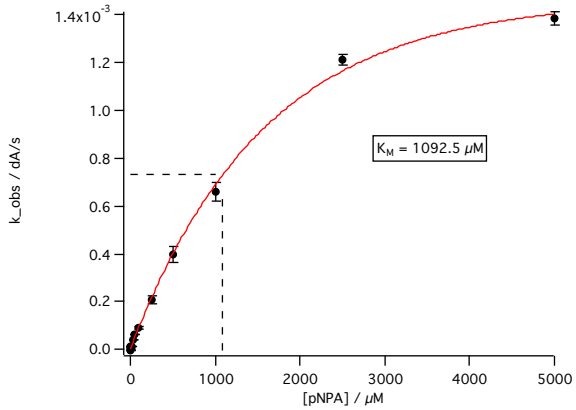


**Supplementary Figure 3: Determination of the Michaelis-Menten constant $K_M$ for hCAII and *p*NPA as a model system.**

### 7.4.11 Kinetic hCAII Assay

Kinetic assays were performed using the intrinsic esterase activity of hCAII as previously reported.[63] Briefly, 1 µL of *p*NPA (0.5 M in DMSO) was added to a 99 µL solution of the corresponding (non-)labeled enzyme (0.5 µM in 50 mM Tris buffer, pH = 7.4) in a 100 µL cuvette (HELLMA Quartzglas SUPRASIL®, #105.201-QS) and mixed vigorously by up-and-down pipetting. The appearance of the hydrolysed phenolate was observed at an absorbance of λ = 400 nm at 2 second intervals.

## 7.5 Full Protein Mass Spectrometry

### 7.5.1 hCAII Mutant I (G129C, C206S)

No PTL

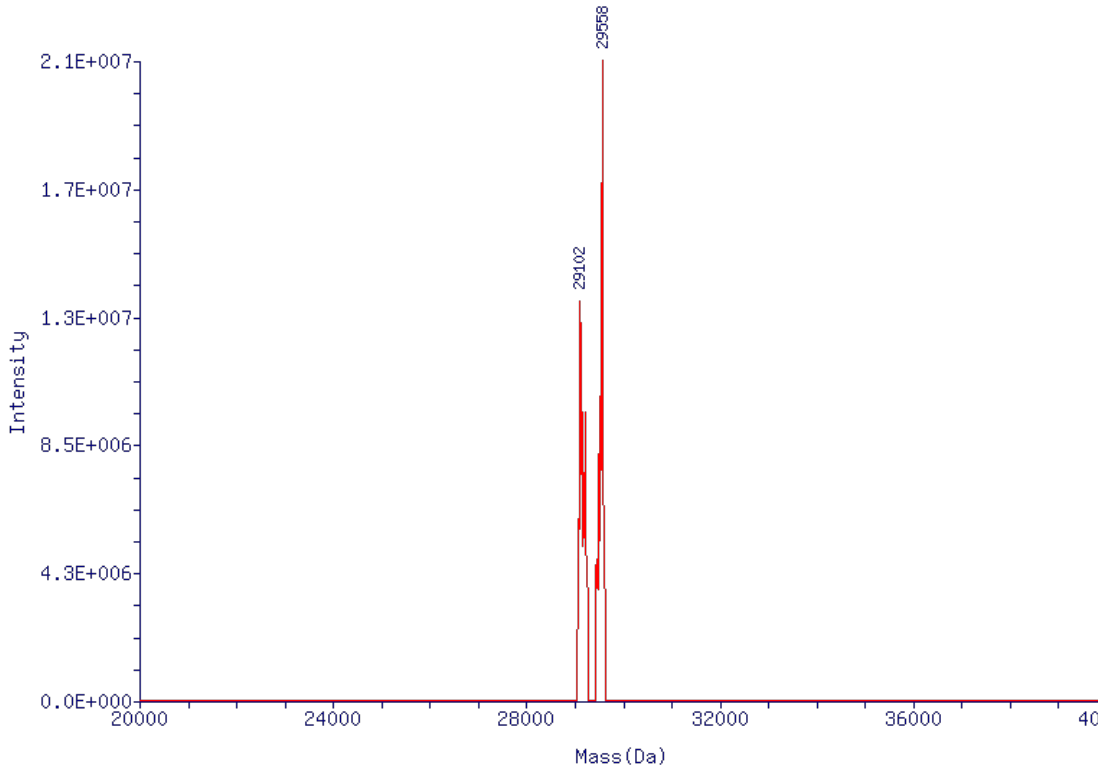


| Mass (Da) | Intensity | Score | Δ Mass | %Relative | %Total |
|---|---|---|---|---|---|
| 29557.6 | 2.13E+007 | 13.43 | 0.0 | 100.00 | 40.66 |
| 29101.7 | 1.33E+007 | 5.27 | -455.9 | 62.41 | 25.38 |
| 29204.2 | 9.62E+006 | 3.27 | -353.4 | 45.06 | 18.32 |
| 29483.8 | 8.21E+006 | 2.52 | -73.8 | 38.48 | 15.64 |

**+ SA-1**

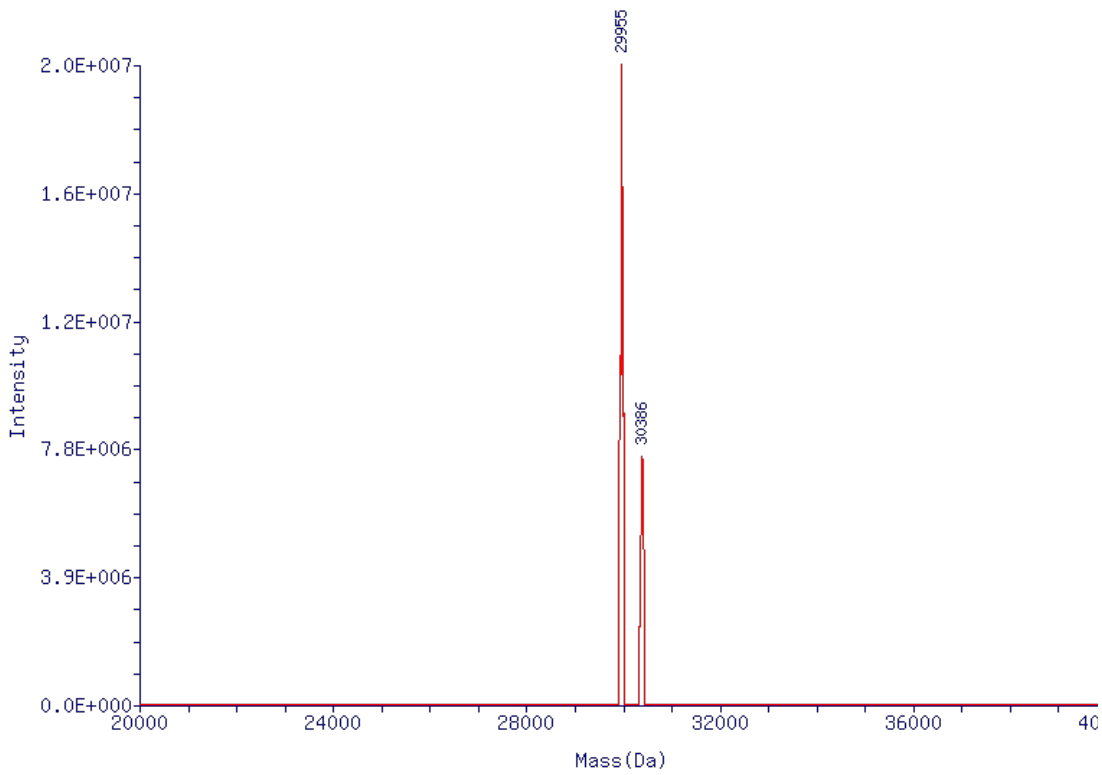


| Mass (Da) | Intensity | Score | Δ Mass | %Relative | %Total |
|---|---|---|---|---|---|
| 29955.4 | 1.96E+007 | 4.78 | 0.0 | 100.00 | 72.13 |
| 30384.0 | 7.55E+006 | 2.05 | 428.6 | 38.63 | 27.87 |

**+ SA-2**

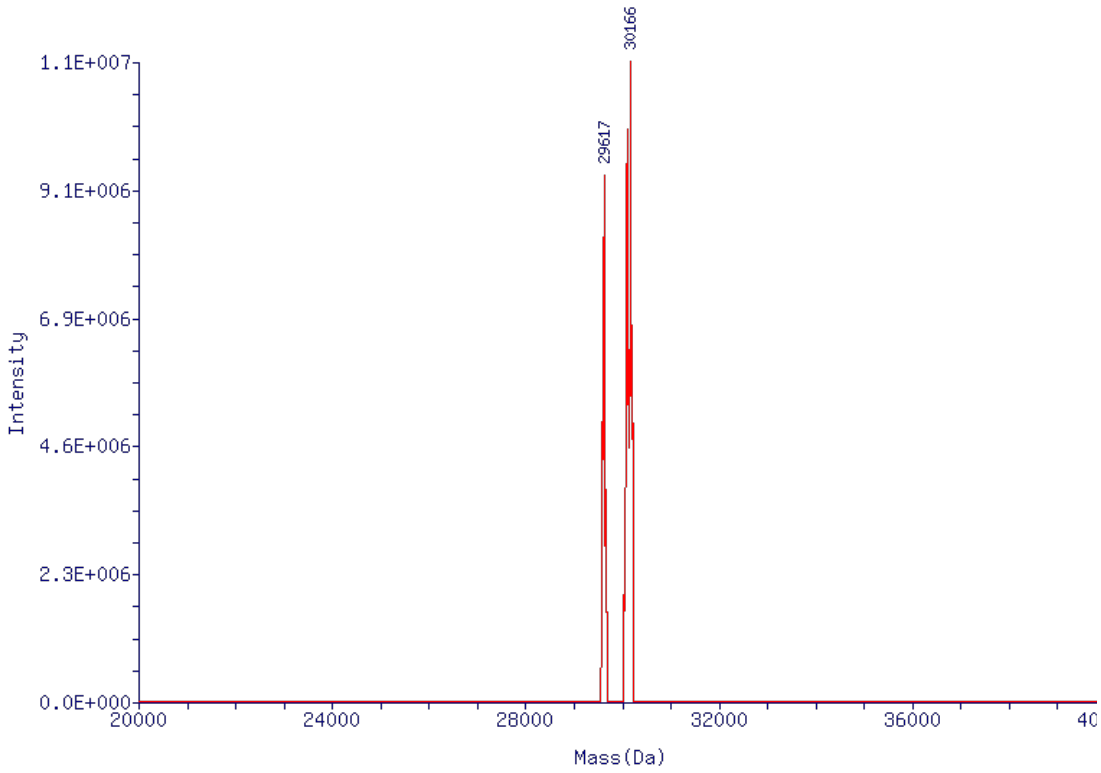


| Mass (Da) | Intensity | Score | Δ Mass | %Relative | %Total |
|---|---|---|---|---|---|
| 30166.5 | 1.14E+007 | 11.18 | 0.0 | 100.00 | 36.81 |
| 30104.0 | 1.02E+007 | 7.28 | -62.5 | 89.35 | 32.89 |
| 29616.0 | 9.40E+006 | 6.74 | -550.5 | 82.29 | 30.29 |

**+ SA-3**

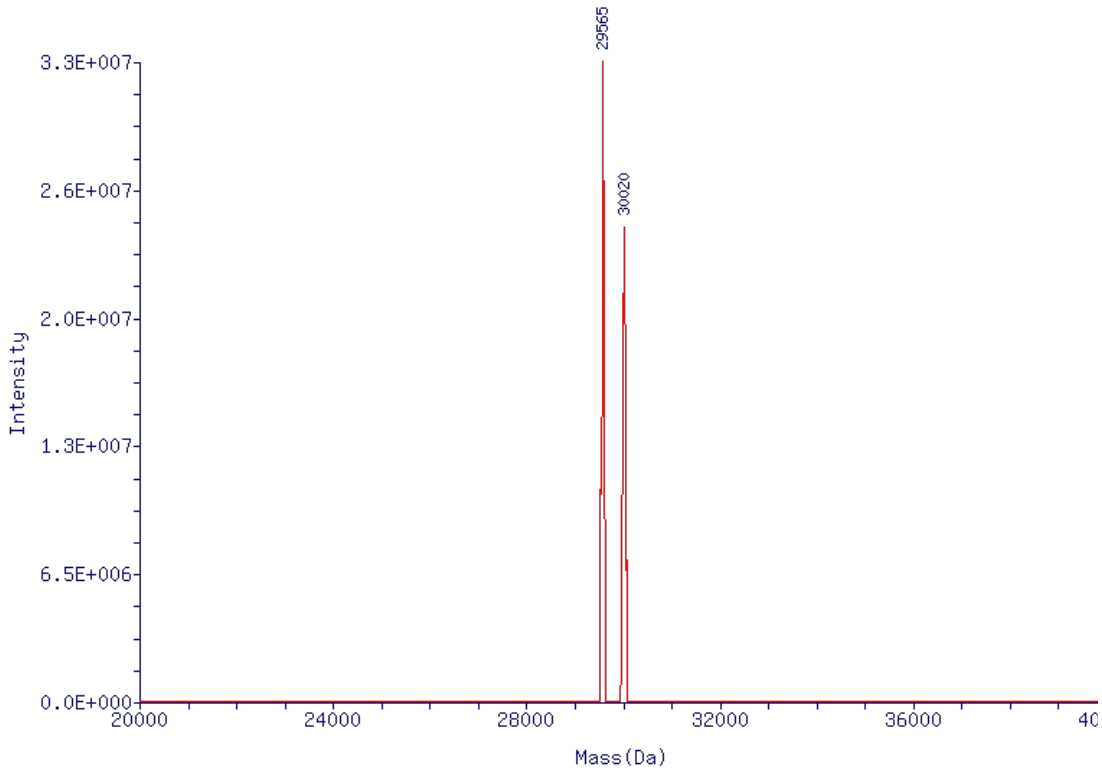


| Mass (Da) | Intensity | Score | Δ Mass | %Relative | %Total |
|---|---|---|---|---|---|
| 29565.3 | 3.26E+007 | 10.02 | 0.0 | 100.00 | 57.45 |
| 30018.9 | 2.41E+007 | 4.96 | 453.6 | 74.06 | 42.55 |

### 7.5.2 hCAII Mutant II (D130C, C206S)

No PTL

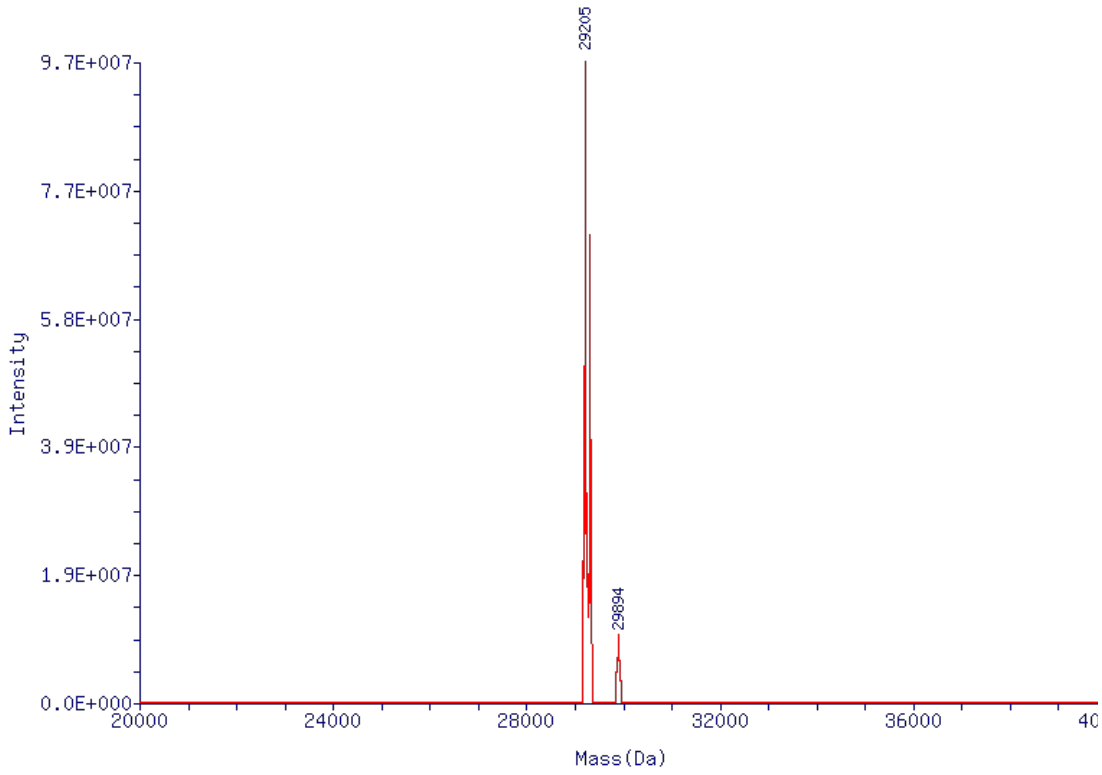


| Mass (Da) | Intensity | Score | Δ Mass | %Relative | %Total |
|---|---|---|---|---|---|
| 29204.5 | 9.67E+007 | 18.09 | 0.0 | 100.00 | 54.49 |
| 29304.0 | 7.06E+007 | 14.41 | 99.5 | 73.00 | 39.77 |
| 29893.9 | 1.02E+007 | 2.47 | 689.4 | 10.54 | 5.74 |

**+ SA-1**

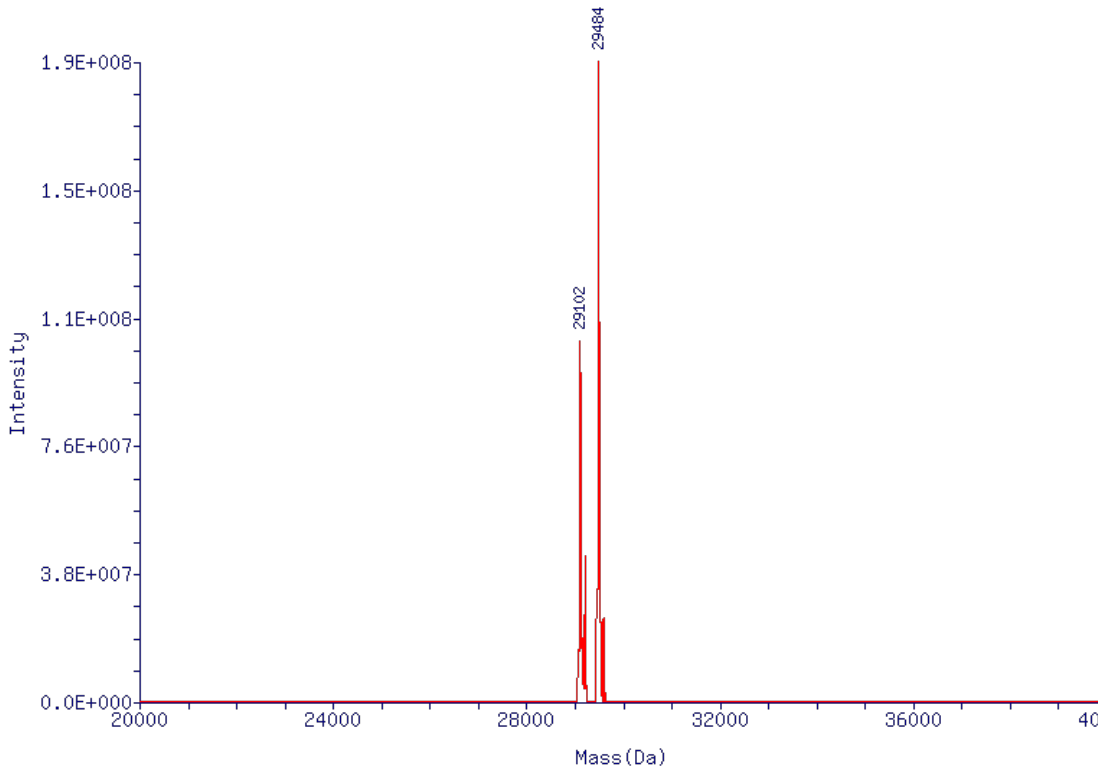


| Mass (Da) | Intensity | Score | Δ Mass | %Relative | %Total |
|---|---|---|---|---|---|
| 29484.0 | 1.90E+008 | 22.94 | 0.0 | 100.00 | 52.03 |
| 29102.1 | 1.07E+008 | 16.14 | -381.9 | 56.26 | 29.27 |
| 29203.1 | 4.32E+007 | 6.86 | -280.9 | 22.78 | 11.85 |
| 29583.6 | 2.50E+007 | 4.50 | 99.6 | 13.16 | 6.85 |

**+ SA-2**

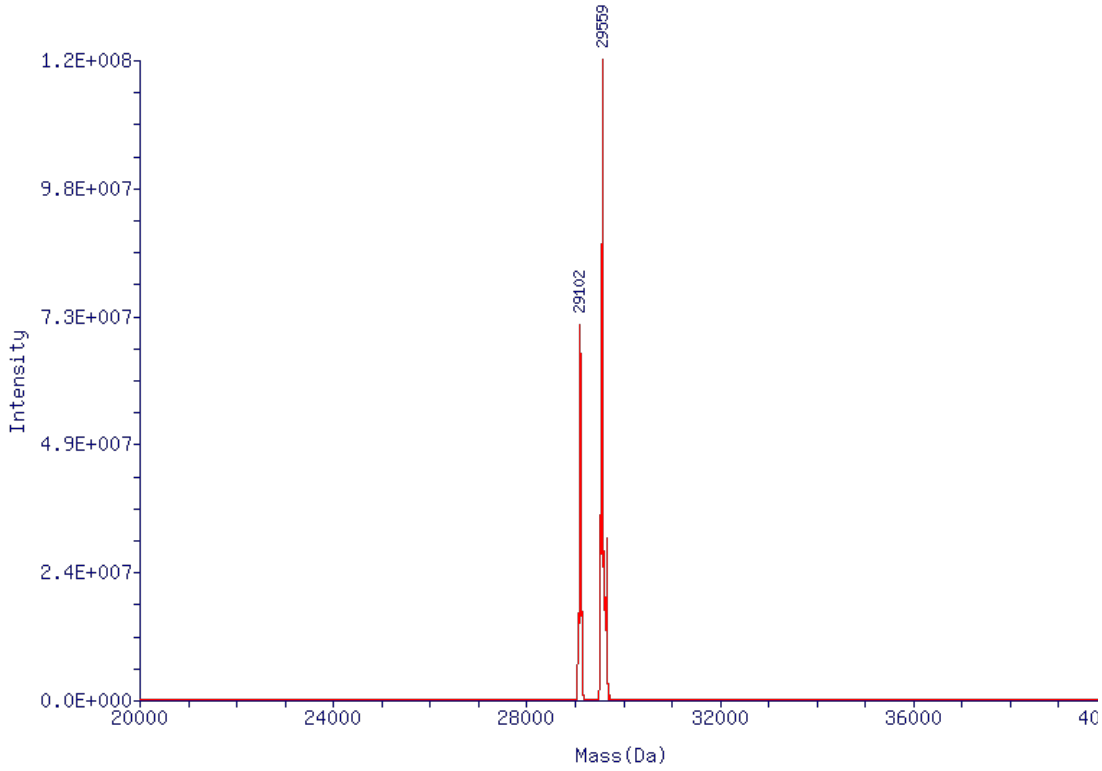


| Mass (Da) | Intensity | Score | Δ Mass | %Relative | %Total |
|---|---|---|---|---|---|
| 29558.5 | 1.22E+008 | 20.26 | 0.0 | 100.00 | 54.40 |
| 29101.9 | 7.14E+007 | 14.04 | -456.6 | 58.55 | 31.85 |
| 29655.2 | 3.08E+007 | 3.36 | 96.7 | 25.26 | 13.74 |

**+ SA-3**

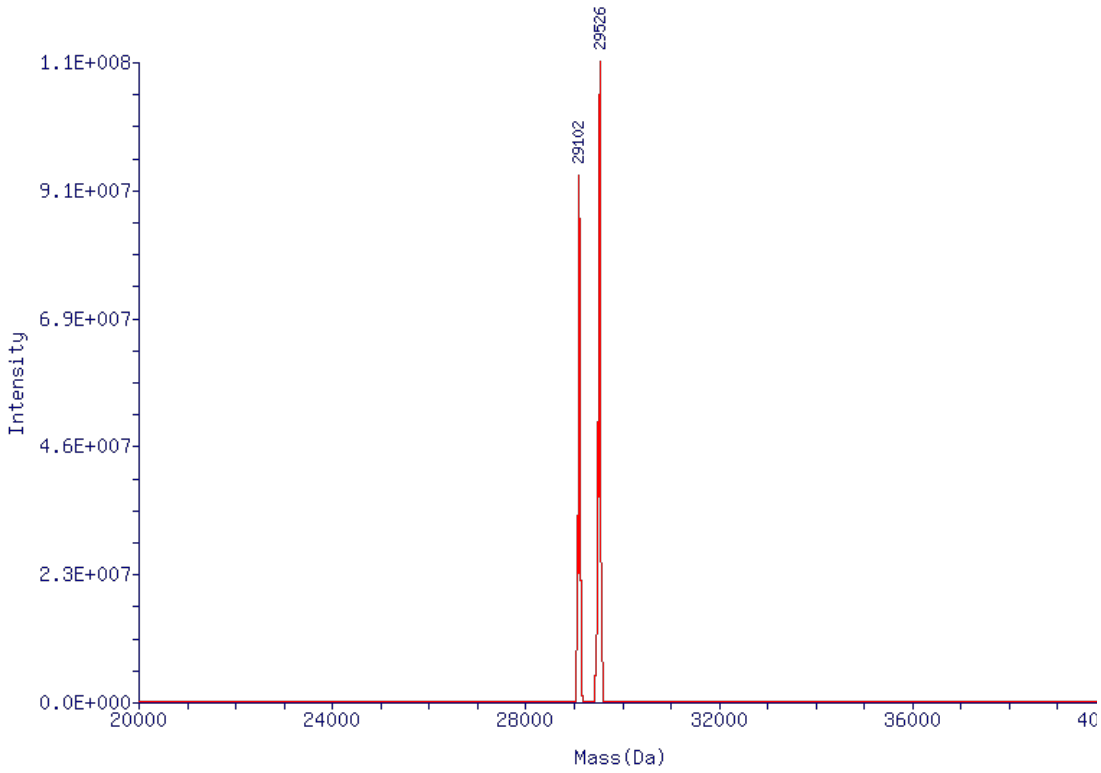


| Mass (Da) | Intensity | Score | Δ Mass | %Relative | %Total |
|---|---|---|---|---|---|
| 29525.1 | 1.14E+008 | 18.71 | 0.0 | 100.00 | 46.42 |
| 29101.9 | 9.40E+007 | 16.25 | -423.2 | 82.29 | 38.20 |
| 29473.2 | 3.78E+007 | 4.55 | -51.9 | 33.13 | 15.38 |

### 7.5.3 hCAII Mutant III (F131C, C206S)

No PTL

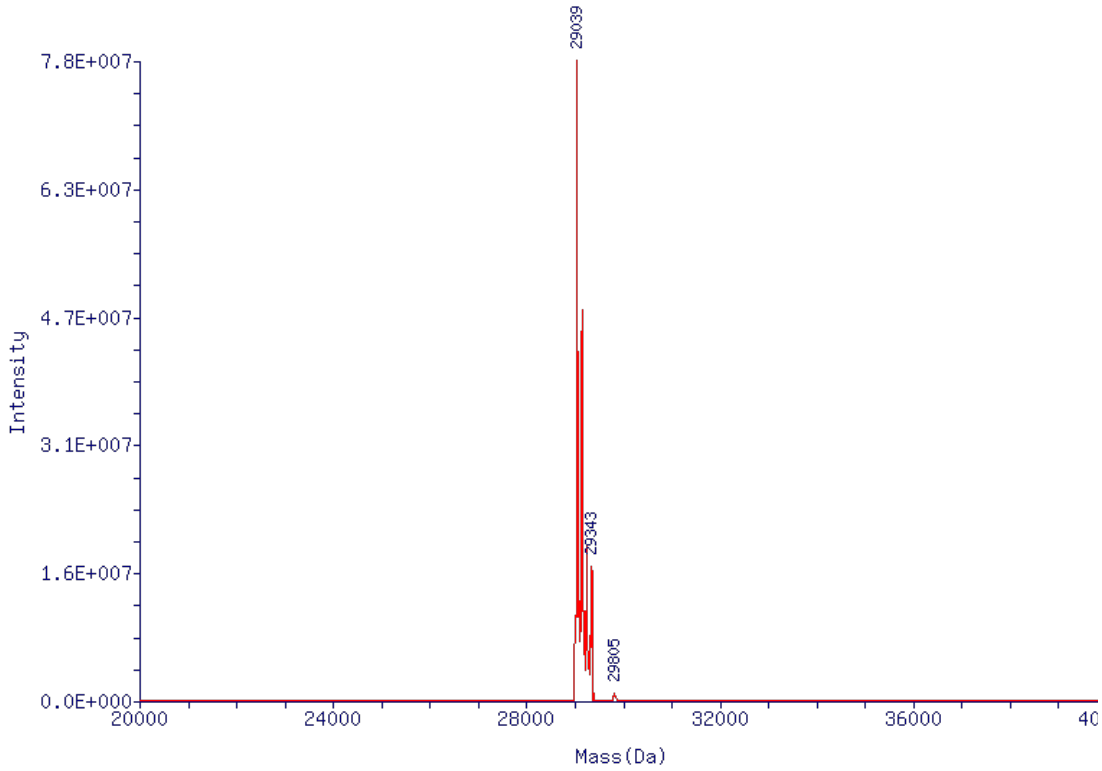


| Mass (Da) | Intensity | Score | Δ Mass | %Relative | %Total |
|---|---|---|---|---|---|
| 29038.2 | 7.83E+007 | 21.27 | 0.0 | 100.00 | 48.27 |
| 29137.3 | 4.79E+007 | 17.43 | 99.1 | 61.10 | 29.49 |
| 29237.1 | 1.89E+007 | 8.85 | 198.9 | 24.06 | 11.62 |
| 29341.5 | 1.64E+007 | 5.20 | 303.3 | 20.87 | 10.07 |
| 29803.3 | 8.89E+005 | 2.29 | 765.1 | 1.14 | 0.55 |

**+ SA-1**

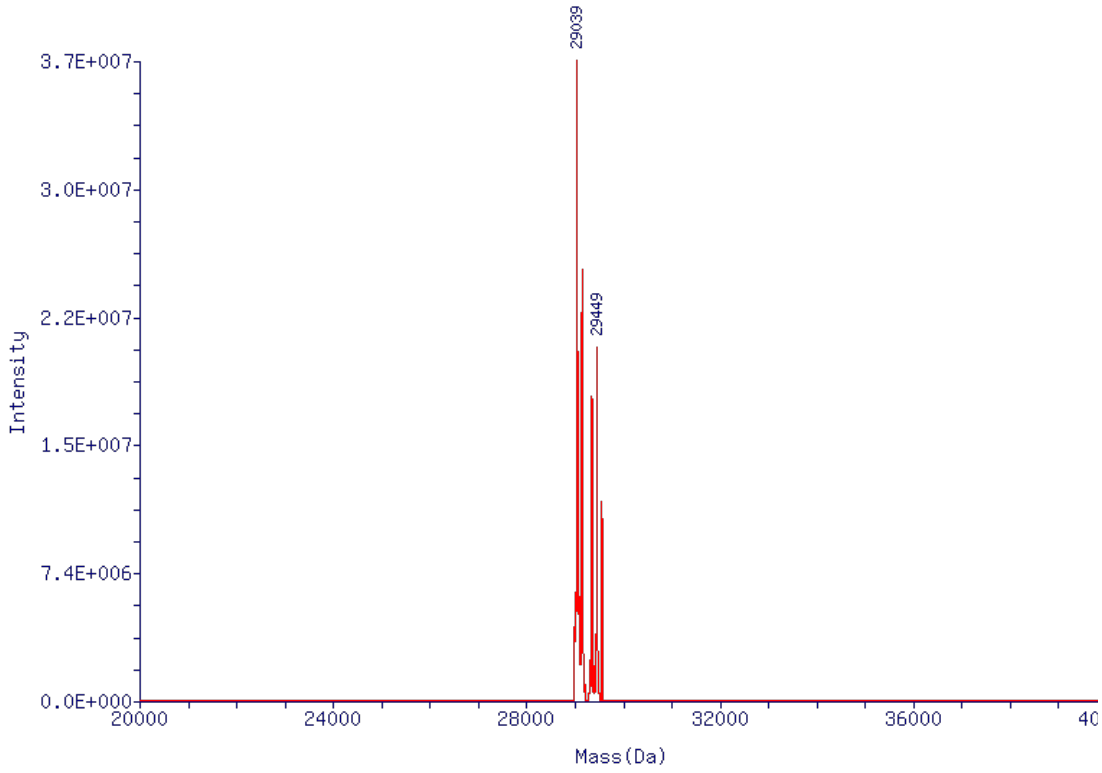


| Mass (Da) | Intensity | Score | Δ Mass | %Relative | %Total |
|---|---|---|---|---|---|
| 29038.2 | 3.70E+007 | 12.71 | 0.0 | 100.00 | 33.19 |
| 29138.4 | 2.50E+007 | 9.44 | 100.2 | 67.45 | 22.39 |
| 29448.0 | 2.04E+007 | 6.28 | 409.8 | 55.10 | 18.29 |
| 29343.2 | 1.76E+007 | 4.64 | 305.0 | 47.60 | 15.80 |
| 29548.0 | 1.15E+007 | 2.05 | 509.8 | 31.13 | 10.33 |

**+ SA-2**

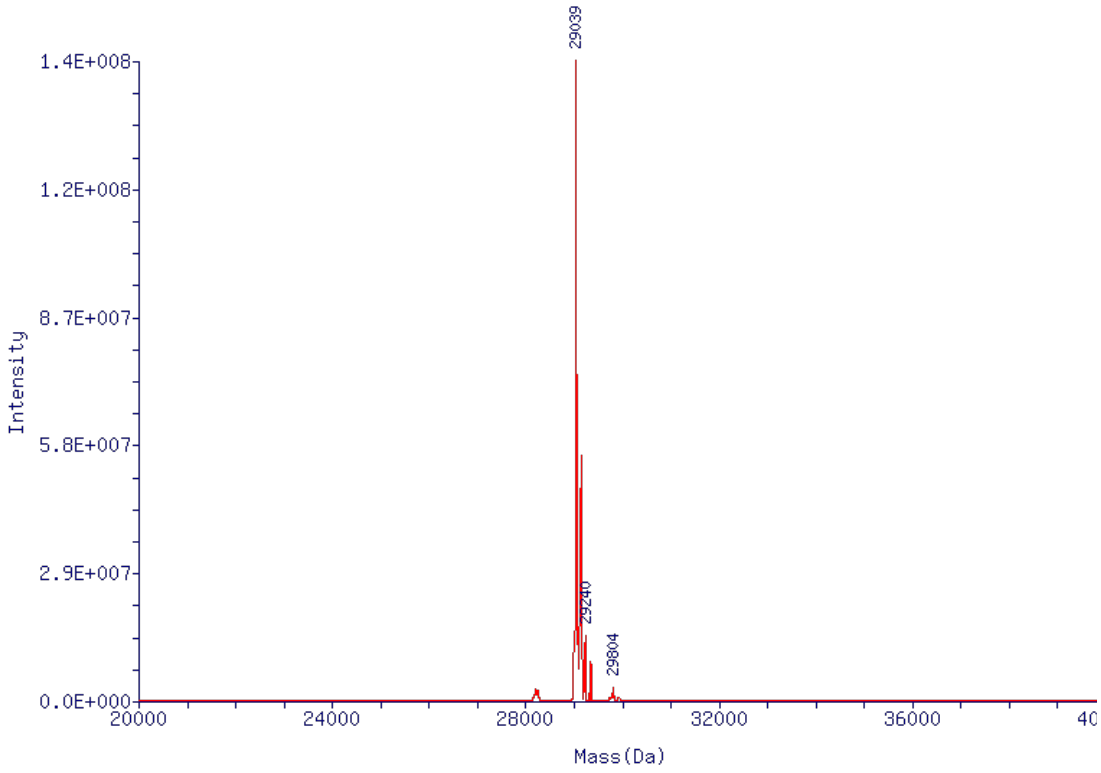


| Mass (Da) | Intensity | Score | Δ Mass | %Relative | %Total |
|---|---|---|---|---|---|
| 29038.3 | 1.45E+008 | 29.82 | 0.0 | 100.00 | 62.84 |
| 29138.5 | 5.53E+007 | 19.75 | 100.2 | 38.20 | 24.01 |
| 29239.3 | 1.45E+007 | 5.83 | 201.0 | 10.05 | 6.31 |
| 29342.7 | 8.77E+006 | 2.44 | 304.4 | 6.06 | 3.81 |
| 29804.1 | 3.05E+006 | 3.17 | 765.8 | 2.10 | 1.32 |
| 28193.8 | 2.45E+006 | 2.48 | -844.5 | 1.69 | 1.06 |
| 28265.9 | 1.50E+006 | 3.07 | -772.4 | 1.04 | 0.65 |

**+ SA-3**

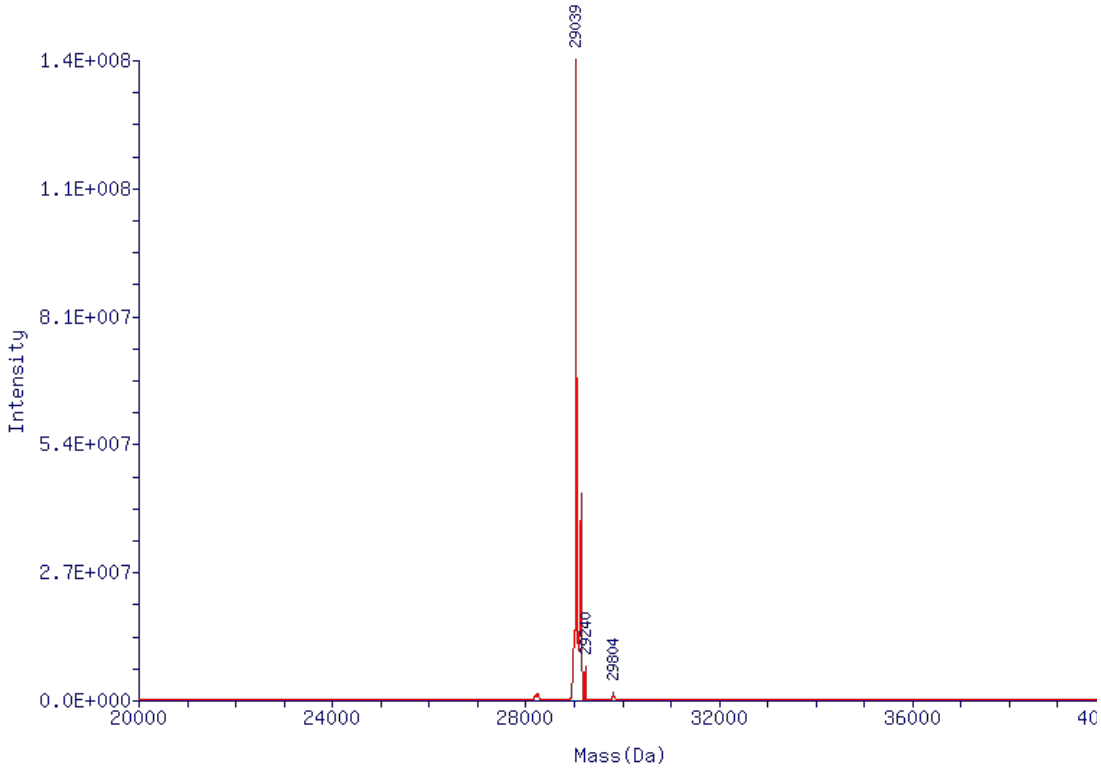


| Mass (Da) | Intensity | Score | Δ Mass | %Relative | %Total |
|---|---|---|---|---|---|
| 29038.3 | 1.36E+008 | 30.44 | 0.0 | 100.00 | 64.24 |
| 29138.5 | 4.37E+007 | 18.13 | 100.2 | 32.15 | 20.65 |
| 29093.5 | 1.39E+007 | 4.11 | 55.2 | 10.24 | 6.58 |
| 28977.3 | 9.46E+006 | 2.37 | -61.0 | 6.97 | 4.48 |
| 29239.1 | 6.92E+006 | 2.32 | 200.8 | 5.09 | 3.27 |
| 29805.3 | 1.65E+006 | 2.88 | 767.0 | 1.22 | 0.78 |

### 7.5.4 hCAII Mutant IV (G132C, C206S)

No PTL

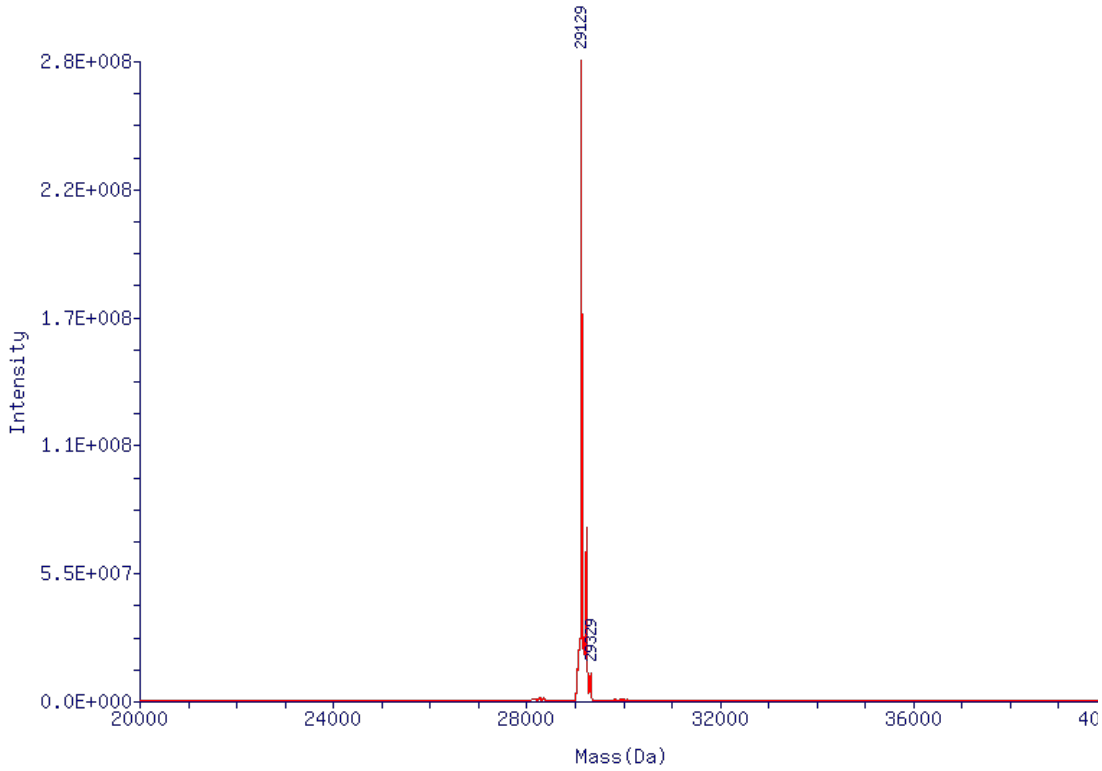


| Mass (Da) | Intensity | Score | Δ Mass | %Relative | %Total |
|---|---|---|---|---|---|
| 29128.4 | 2.75E+008 | 38.18 | 0.0 | 100.00 | 71.06 |
| 29228.7 | 7.45E+007 | 23.63 | 100.3 | 27.03 | 19.21 |
| 29076.9 | 2.59E+007 | 11.13 | -51.5 | 9.39 | 6.67 |
| 29328.8 | 1.19E+007 | 4.80 | 200.4 | 4.32 | 3.07 |

**+ SA-1**

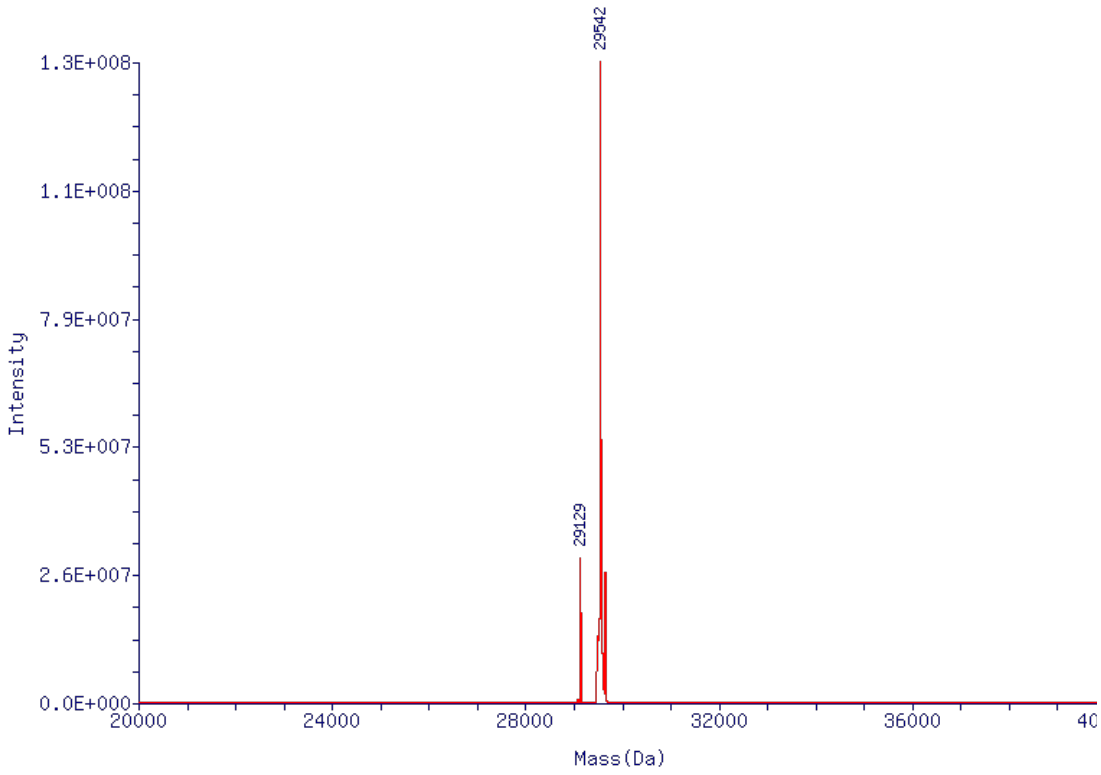


| Mass (Da) | Intensity | Score | Δ Mass | %Relative | %Total |
|---|---|---|---|---|---|
| 29542.0 | 1.31E+008 | 29.96 | 0.0 | 100.00 | 65.52 |
| 29128.5 | 2.95E+007 | 12.73 | -413.5 | 22.45 | 14.71 |
| 29642.2 | 2.65E+007 | 13.09 | 100.2 | 20.21 | 13.24 |
| 29483.6 | 1.31E+007 | 2.99 | -58.4 | 9.97 | 6.53 |

**+ SA-2**

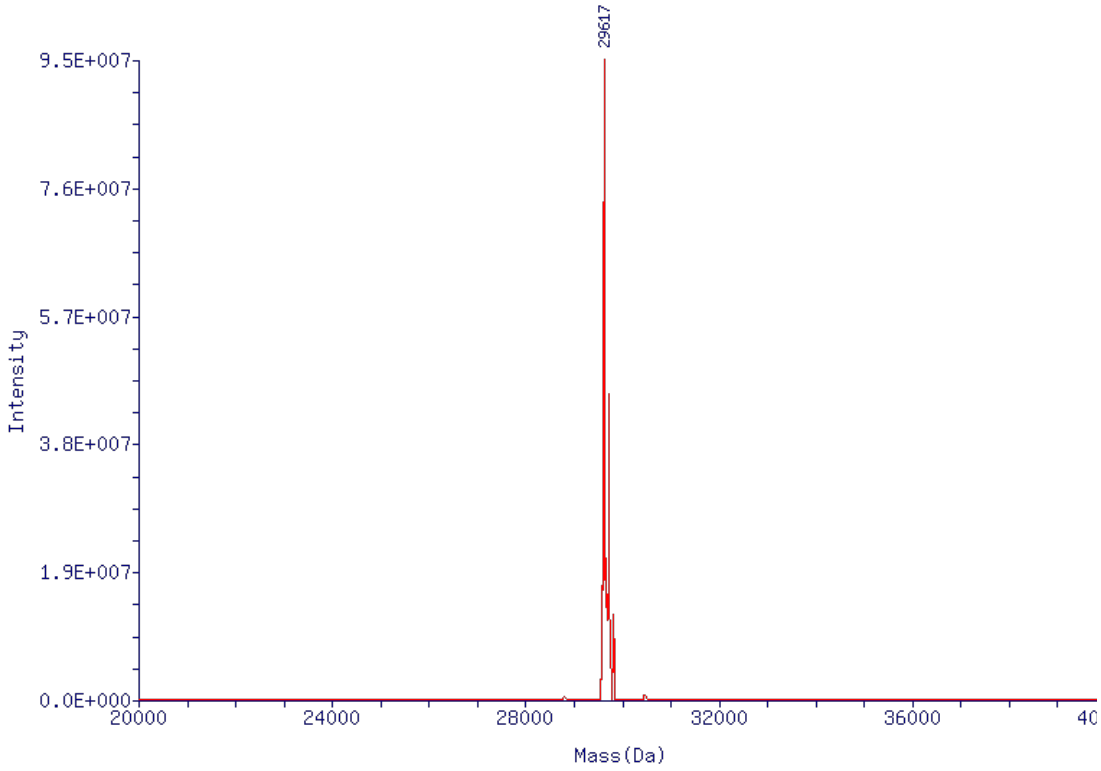


| Mass (Da) | Intensity | Score | Δ Mass | %Relative | %Total |
|---|---|---|---|---|---|
| 29616.9 | 9.47E+007 | 25.68 | 0.0 | 100.00 | 50.51 |
| 29715.4 | 4.52E+007 | 17.74 | 98.5 | 47.72 | 24.10 |
| 29660.5 | 2.09E+007 | 7.84 | 43.6 | 22.02 | 11.12 |
| 29570.5 | 1.41E+007 | 3.92 | -46.4 | 14.91 | 7.53 |
| 29814.8 | 1.26E+007 | 4.76 | 197.9 | 13.34 | 6.74 |

**+ SA-3**

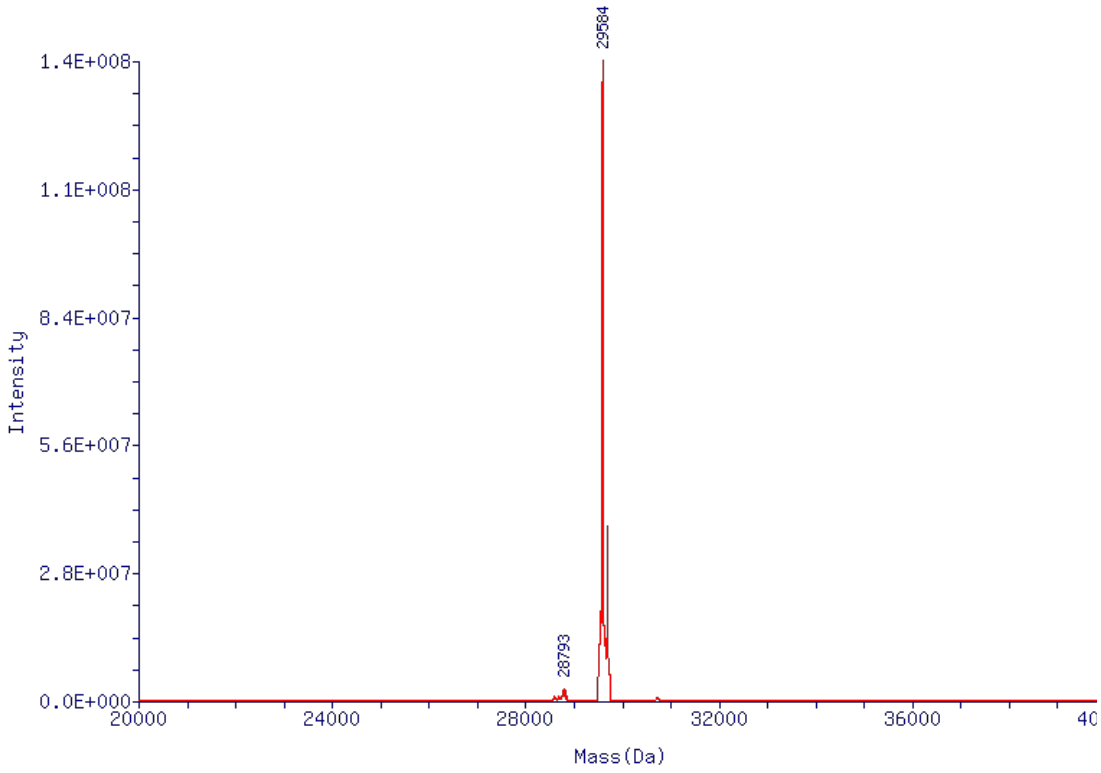


| Mass (Da) | Intensity | Score | Δ Mass | %Relative | %Total |
|---|---|---|---|---|---|
| 29583.7 | 1.39E+008 | 32.69 | 0.0 | 100.00 | 65.20 |
| 29684.2 | 3.79E+007 | 18.42 | 100.5 | 27.23 | 17.75 |
| 29539.5 | 1.96E+007 | 10.63 | -44.2 | 14.03 | 9.15 |
| 29635.0 | 1.44E+007 | 8.71 | 51.3 | 10.36 | 6.76 |
| 28795.3 | 2.45E+006 | 4.99 | -788.4 | 1.76 | 1.15 |

### 7.5.5 hCAII Mutant V (K133C, C206S)

No PTL

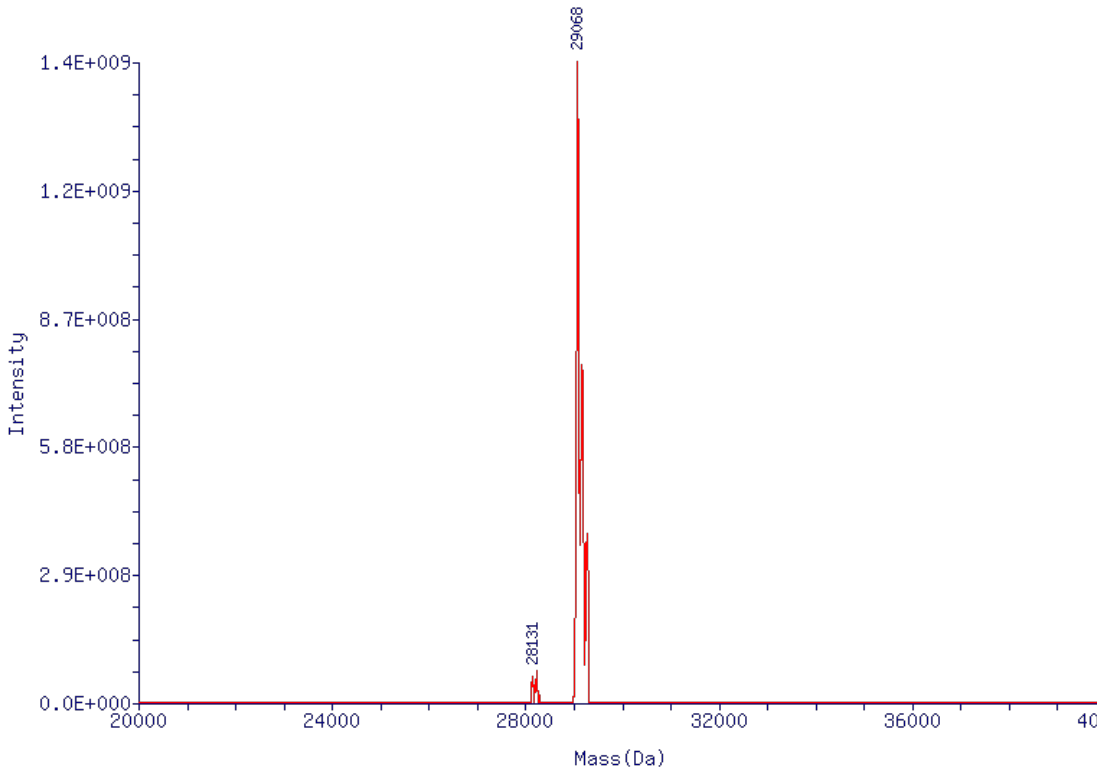


| Mass (Da) | Intensity | Score | Δ Mass | %Relative | %Total |
|---|---|---|---|---|---|
| 29067.9 | 1.44E+009 | 15.22 | 0.0 | 100.00 | 40.08 |
| 29165.3 | 7.60E+008 | 8.94 | 97.4 | 52.64 | 21.09 |
| 29111.1 | 5.05E+008 | 5.98 | 43.2 | 34.98 | 14.02 |
| 29264.4 | 3.82E+008 | 3.30 | 196.5 | 26.46 | 10.60 |
| 29024.4 | 3.77E+008 | 2.97 | -43.5 | 26.11 | 10.46 |

**+ SA-1**

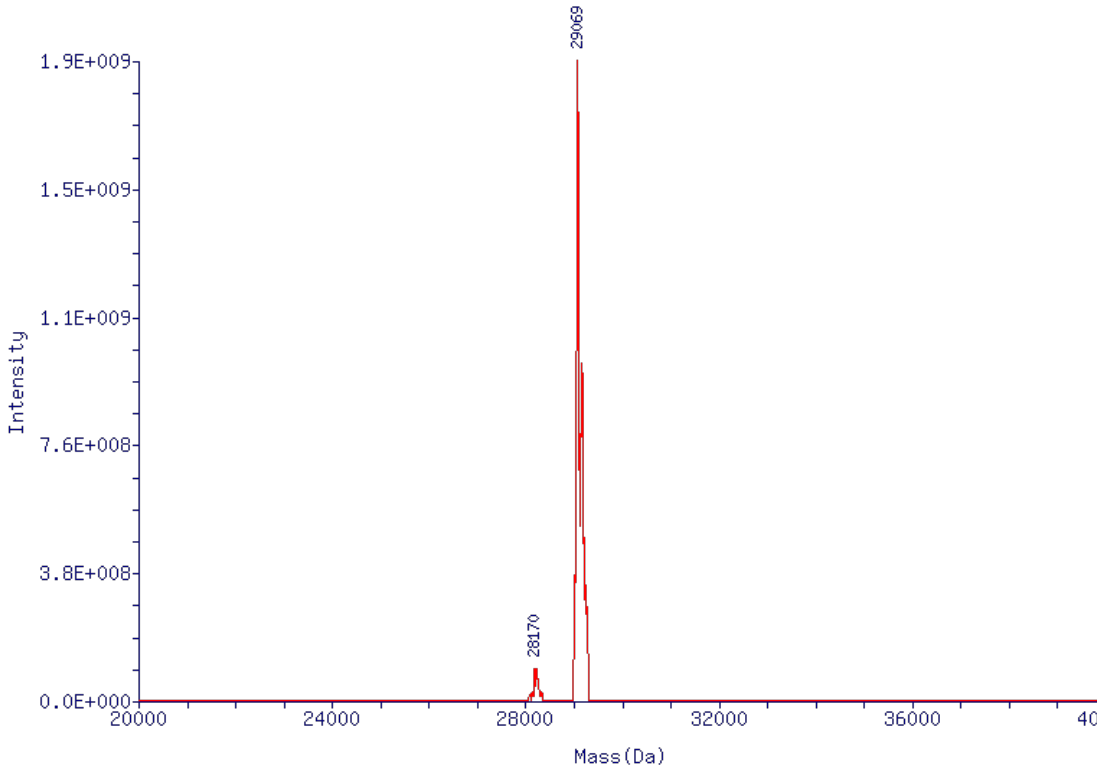


| Mass (Da) | Intensity | Score | Δ Mass | %Relative | %Total |
|---|---|---|---|---|---|
| 29070.0 | 1.91E+009 | 17.64 | 0.0 | 100.00 | 43.69 |
| 29157.9 | 1.00E+009 | 11.90 | 87.9 | 52.74 | 23.04 |
| 29201.6 | 4.79E+008 | 5.04 | 131.6 | 25.12 | 10.97 |
| 29013.3 | 3.76E+008 | 3.82 | -56.7 | 19.73 | 8.62 |
| 29251.2 | 2.96E+008 | 3.34 | 181.2 | 15.53 | 6.78 |

**+ SA-2**

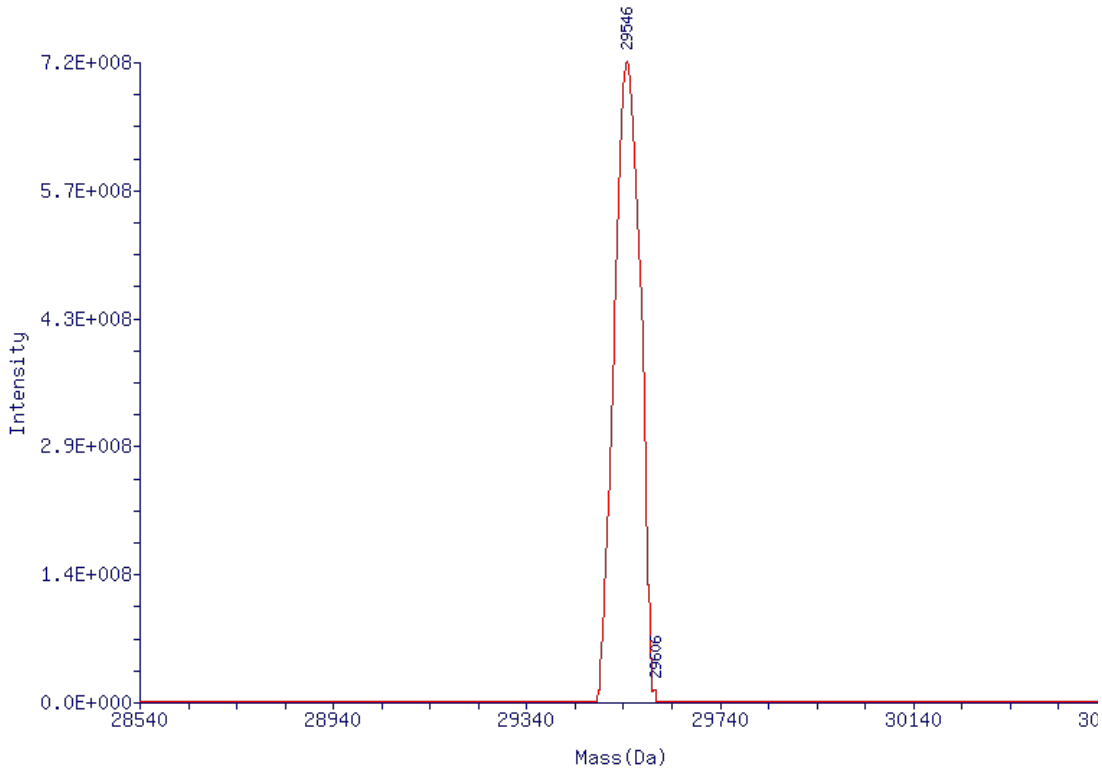


| Mass (Da) | Intensity | Score | Δ Mass | %Relative | %Total |
|---|---|---|---|---|---|
| 29545.0 | 7.16E+008 | 6.10 | 0.0 | 100.00 | 100.00 |

**+ SA-3**

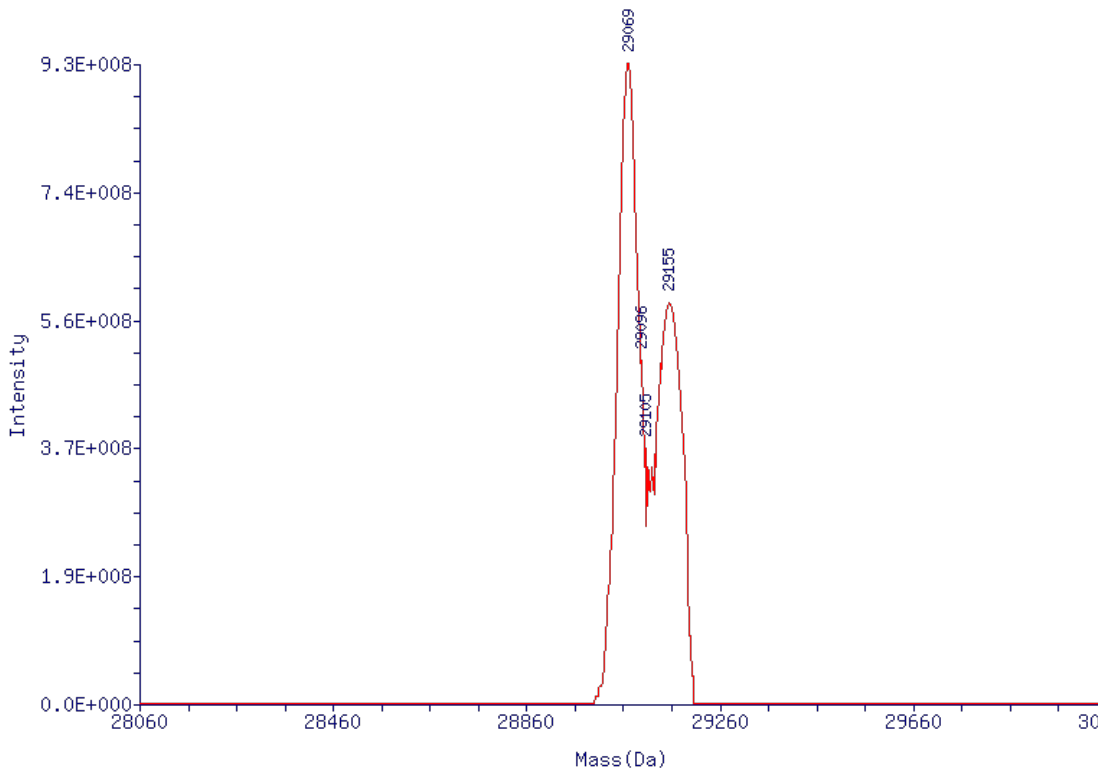


| Mass (Da) | Intensity | Score | Δ Mass | %Relative | %Total |
|---|---|---|---|---|---|
| 29069.4 | 9.27E+008 | 9.14 | 0.0 | 100.00 | 61.53 |
| 29153.7 | 5.80E+008 | 5.26 | 84.3 | 62.53 | 38.47 |

## 7.6 Computational Methods

Computation has been performed by Kateri H. DuBay, PhD, and is enclosed herein for clarification.

In order to model the PTL-hCAII system appropriately, the sulfonamide was placed in the binding pocket according to a crystal structure of bound hCAII (1BNT).[68] The PTL structures were then generated using the program Maestro.[109] No minimizations were done to refine the idealized structures that were initially generated in this program. In addition, although a twist is known to be present in the *cis* conformation of the azobenzene, the *cis* structures were modeled without the twist, since it introduces a stereocenter into the structure. Instead, the idealized (untwisted) structure was used as a proxy for the average between the two possible twisted conformations.

The physical interactions in the PTL-protein system were modeled using a united atom approximation where hydrogen atoms are not considered separately from their neighboring heavy atoms. In order to simplify the calculation, only the steric interactions and van der Waals attractions between atoms were considered in this screening, implemented through a Lennard-Jones potential as well as a cut-off at 0.75 times the van der Waals radius, beyond which point steric overlaps were forbidden, as described in Ref[110]. Sampling proceeded through a series of randomly-proposed rotations around single bonds, and moves were accepted or rejected using the Metropolis criteria.[111] Potential maleimide-binding sites were recorded if a residue's $C_\alpha$ atom was within 2.6 - 4.6 Å of one of the two potential cysteine-binding carbons on the maleimide ring of the PTL.

Step 1 of the screening process consisted of sampling the possible single-bond rotations of the PTL while only considering the sterics and van der Waals interactions of the PTL with itself and with the backbone atoms of the protein. If the *cis* or *trans* PTL was not able to get close enough to bind to one of the $C_\alpha$ atoms in this case, with no side-chains to get in the way, then we could consider it as inaccessible to that isomer of the PTL.

Step 2 of the screening process consisted of sampling while considering the interactions of the PTL with itself and with the backbone atoms of the protein plus those of the side-chains that had been ruled out as potentially accessible sites for either the *cis* or the *trans* isomer in Step 1. Since these side-chains had been ruled out in Step 1, they would be present even in the final mutated version of hCAII, and therefore, even in their presence, the PTL would need to be able to come within binding distance of the $C_\alpha$ atoms of any remaining mutation site candidates.

Step 3 of the screening process consisted of sampling while considering the interactions of the PTL with itself and all backbone and side-chain atoms except the side-chain atoms of the remaining candidate maleimide-binding mutation sites, each considered on their own (i.e., unlike Steps 1 & 2, this step required a different run for each site considered). In this case, we wanted to ensure that, even with all other side-chains present, the PTL would still be able to get within the appropriate proximity of the $C_\alpha$ atom of that residue to bind, were it converted to a cysteine residue.

It is important to note that Steps 2 & 3 above could be performed either while keeping the protein's side-chains static or while allowing them to rotate. Allowing the side-chains to rotate yields more information regarding potential maleimide binding sites, but is significantly more expensive computationally. Since the aim here was to not only determine which PTL structures are best suited to yield photo-switchable responses in HCAII, but also to determine the fastest approaches to screening for appropriate cysteine mutation sites, both rotating and static side-chains were tested. Runs where the side-chains were frozen consisted of approximately 500,000 proposed rotations and took between 30 and 50 minutes of computational time. Runs where the side-chains were allowed to rotate consisted of approximately 5,000,000 proposed rotations and took between 2 to 12 hours of computational time; in these runs, rotations of the PTL were proposed one out of every five Monte Carlo steps.

**Supplementary Table 3: This table lists the residues that were identified as potential maleimide-binding sites in Steps 1-3 for PTLs SA-1, SA-2, SA-3 in both their *cis* and *trans* conformations.** The main results are shown for when the protein's side-chains are held constant, with any additional residues identified during side-chain rotations indicated in parentheses. (Note: There was only one remaining potential maleimide-binding site to test after Step 1 for the *trans* isomers of **SA-1** and **SA-3**, thus we skipped directly to Step 3 in those cases.)

| | ***Step 1*** | ***Step 2*** | ***Step 3*** |
|---|---|---|---|
| **SA-1** | | | |
| ***cis*** | 5-7, 13, 64, 65, 96, 199-201, 244-246 | 5, 6, 64, 65, 199, 200, 244-246 *(side-chain rotations add: 7, 96, 201)* | none *(side-chain rotations add: 64, 65, 96, 200, 244-246)* |
| ***trans*** | 132 | *n/a* | 132 *(same for side-chain rotations)* |
| **SA-2** | | | |
| ***cis*** | 5-7, 11-13, 15, 16, 20, 23, 62-65, 94-96, 106, 199-203, 231, 241-246 | 5-7, 11-13, 15, 16, 20, 23, 62-65, 95, 96, 199-203, 231, 241, 244-246 *(side-chain rotations add 94, 106, 242, 243)* | none *(side-chain rotations add 64, 200)* |
| ***trans*** | 62, 130-133, 171 | 62, 130-133 *(same for side-chain rotations)* | 62, 130-133 *(same for side-chain rotations)* |
| **SA-3** | | | |
| ***cis*** | 5-7, 12, 13, 16, 64, 199-201, 244-246 | 5-7, 12, 13, 16, 64, 199-201, 244-246 *(same for side-chain rotations)* | none *(side-chain rotations add: 64, 200)* |
| ***trans*** | 132 | *n/a* | 132 *(same for side-chain rotations)* |

The full results for **SA-1**, **SA-2**, and **SA-3** are shown in Supplementary Table 3. The optimal cysteine mutation site is one that is identified in all three steps of the screening process as a potential maleimide-binding site for either the *cis* or the *trans* isomer, but does not show up even in Step 1 of the opposite isomer.

This criteria maximizes the likelihood of the PTL being able to reach the binding pocket in one configuration, but not in the other -- which is the basis for the desired photoswitchable behavior. Ideally, such a site would be accessible to one isomer even when all other side-chains are considered in their crystalline configuration. Fortunately, in this particular PTL-protein system, that criteria yielded six optimal mutant-PTL combinations, a very good number to implement experimentally.

In this system, the *cis* structures of the proposed PTLs cannot exit the binding pocket of hCAII through the main tunnel without any adjustments in side-chain positions, while the *trans* structures can. Thus most of the initial *cis*-accessible potential binding sites identified in Step 1 are actually occluded by neighboring side-chains once they are taken into account in Step 2 and Step 3, whereas the *trans*-accessible maleimide binding sites are less likely to be occluded by neighboring side-chains. It turns out that several potential binding sites can be identified for the *cis* structure when the protein's side-chains are allowed to rotate, whereas the potential binding sites identified for the *trans* structure are the same whether or not the side-chains are allowed to rotate. It is therefore possible in looking at Supplementary Table S1 to find potential maleimide binding sites where the *cis* isomer allows the sulfonamide to complex with the zinc ion but the *trans* isomer does not, but these are less optimal. Given the promising number of optimal mutant-PTL combinations found in this system even with static side-chains we conclude that considering the degrees of freedom of the protein's side-chains is not necessary here -- and significantly more costly, computationally. However, were such static-side-chain screenings fail in identifying a reasonable number of optimal mutation sites in other systems, rotations of the side-chains should also be considered.

## 7.7 Spectral Data

### 7.7.1 (*E*)-4-(4-Hydroxyphenyldiazenyl)benzenesulfonamide (7.2)

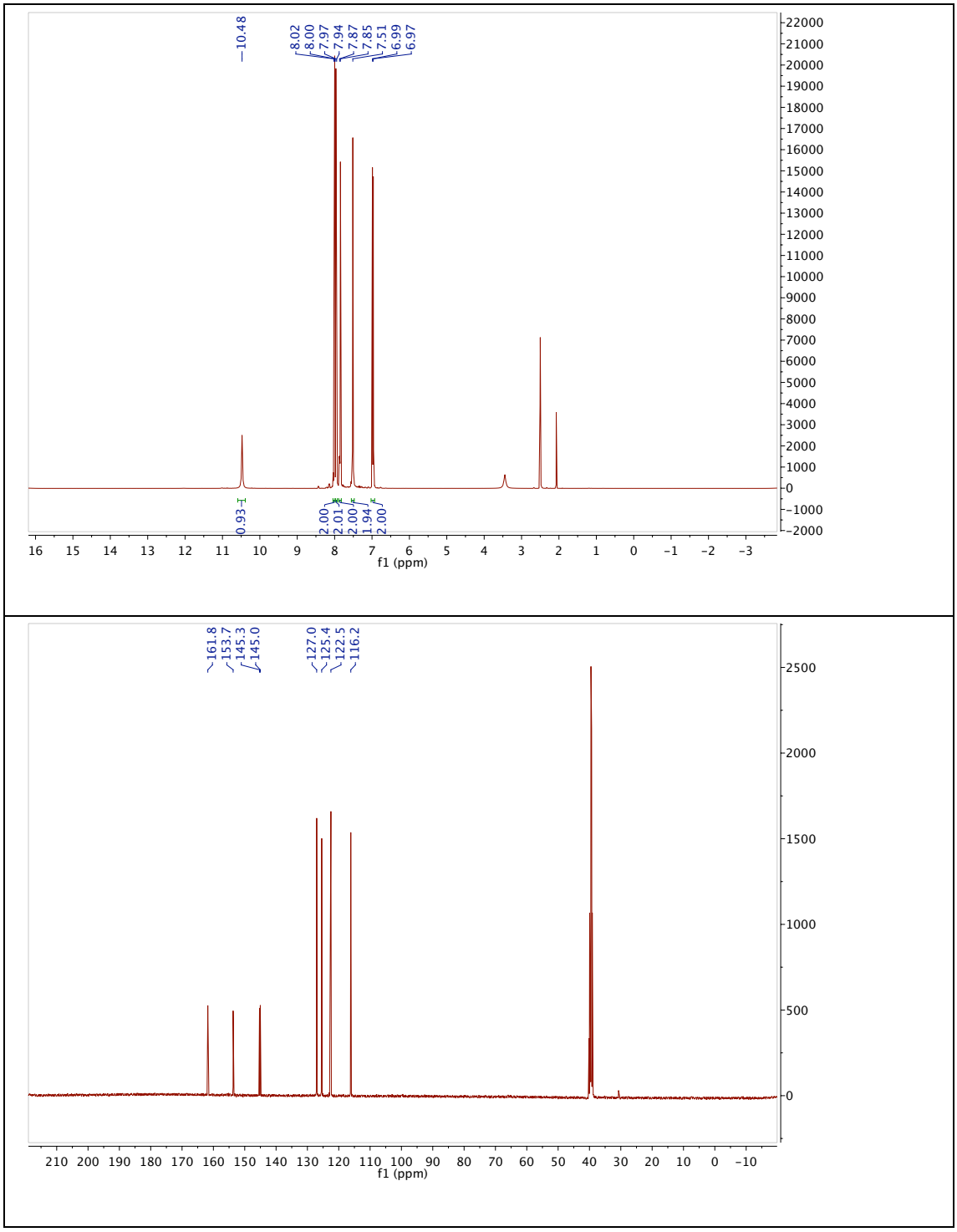

### 7.7.2 (*E*)-4-((4-(Diethylamino)phenyl)diazenyl)benzenesulfonamide (7.3)

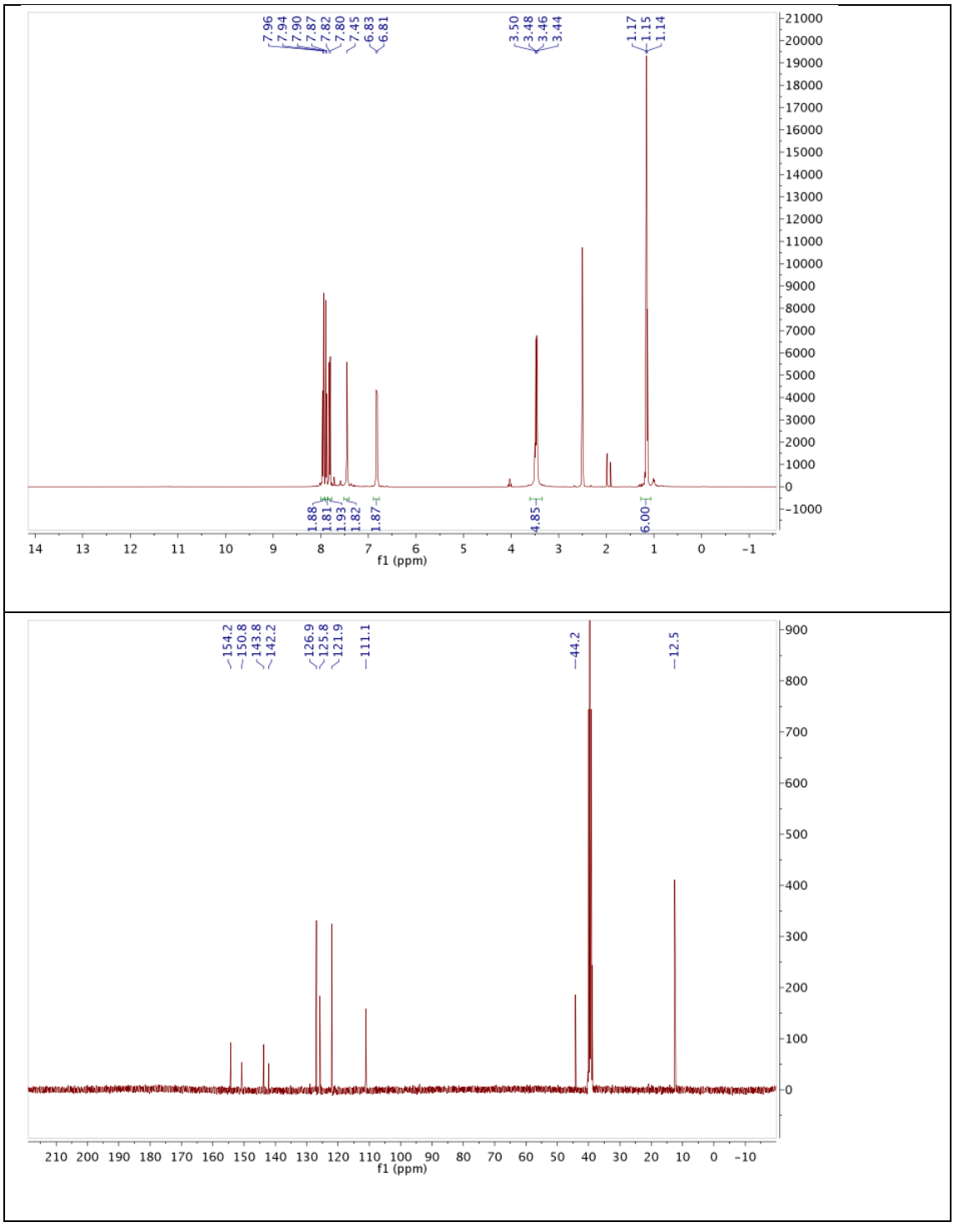

### 7.7.3 (*E*)-4-((4-Morpholinophenyl)diazenyl)benzenesulfonamide (7.4)

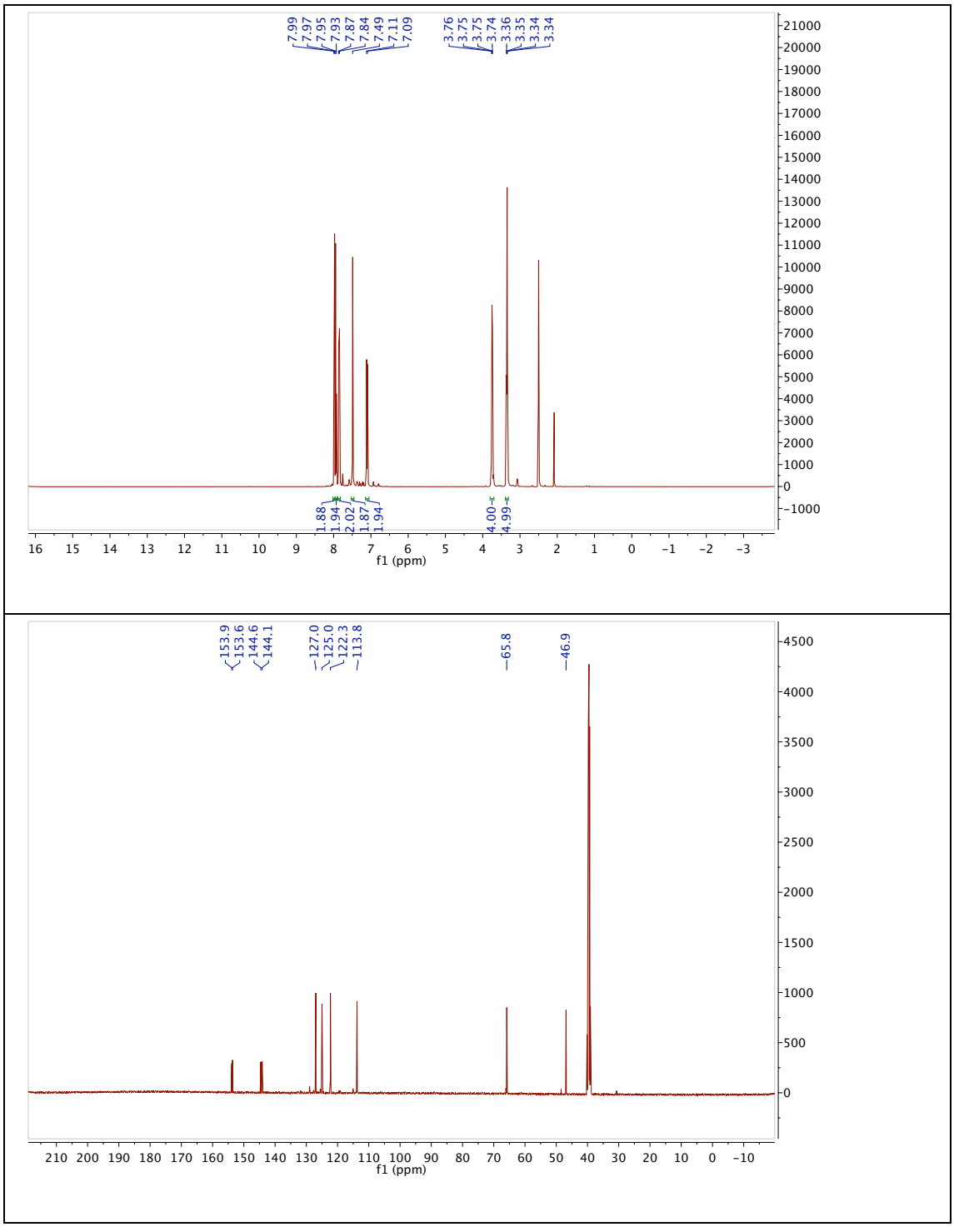

### 7.7.4 (*E*)-4-(4-Azidophenyldiazenyl)benzenesulfonamide (7.6)

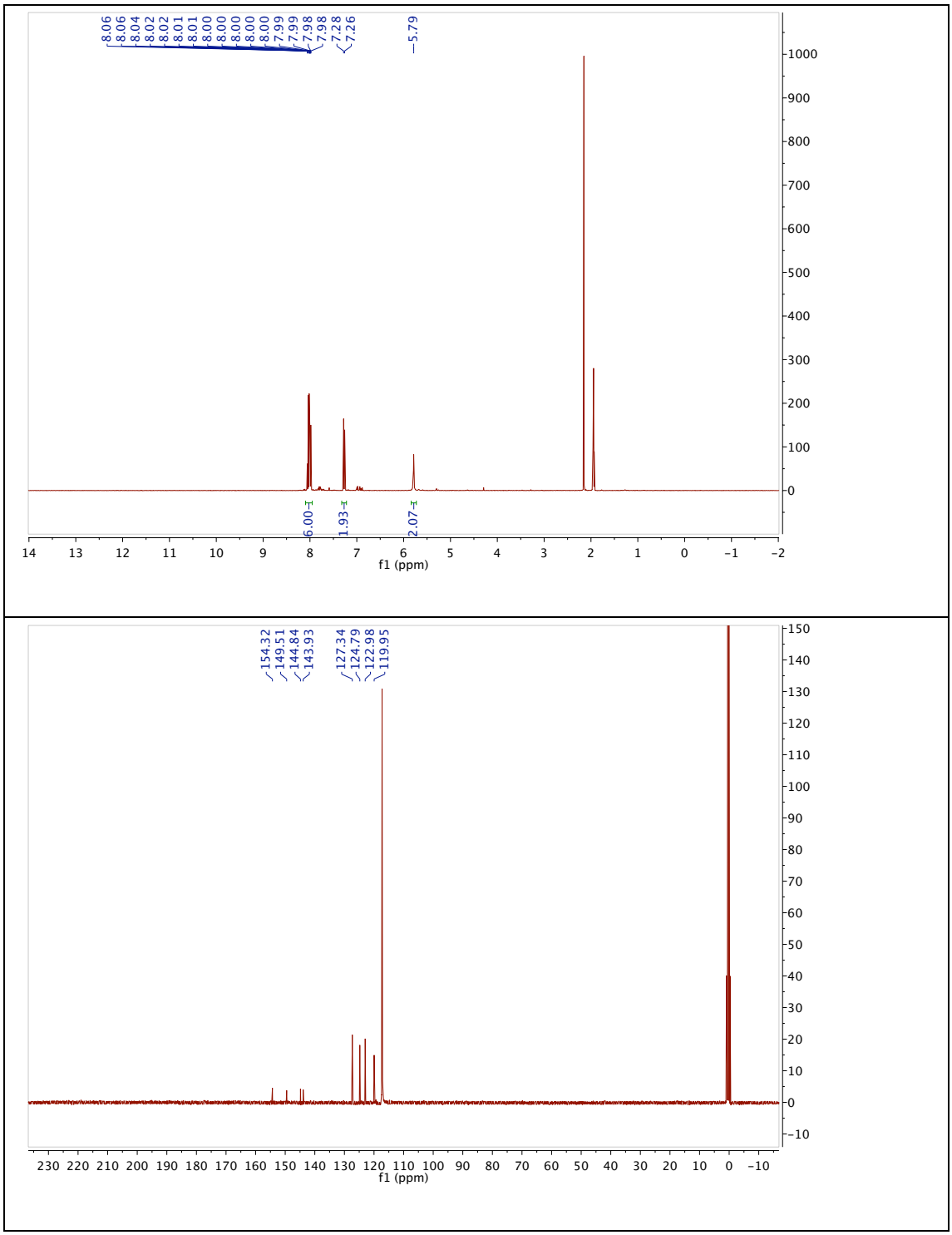

## 7.7.5 (*E*)-4-(*p*-Tolyldiazenyl)benzenesulfonamide (7.7)

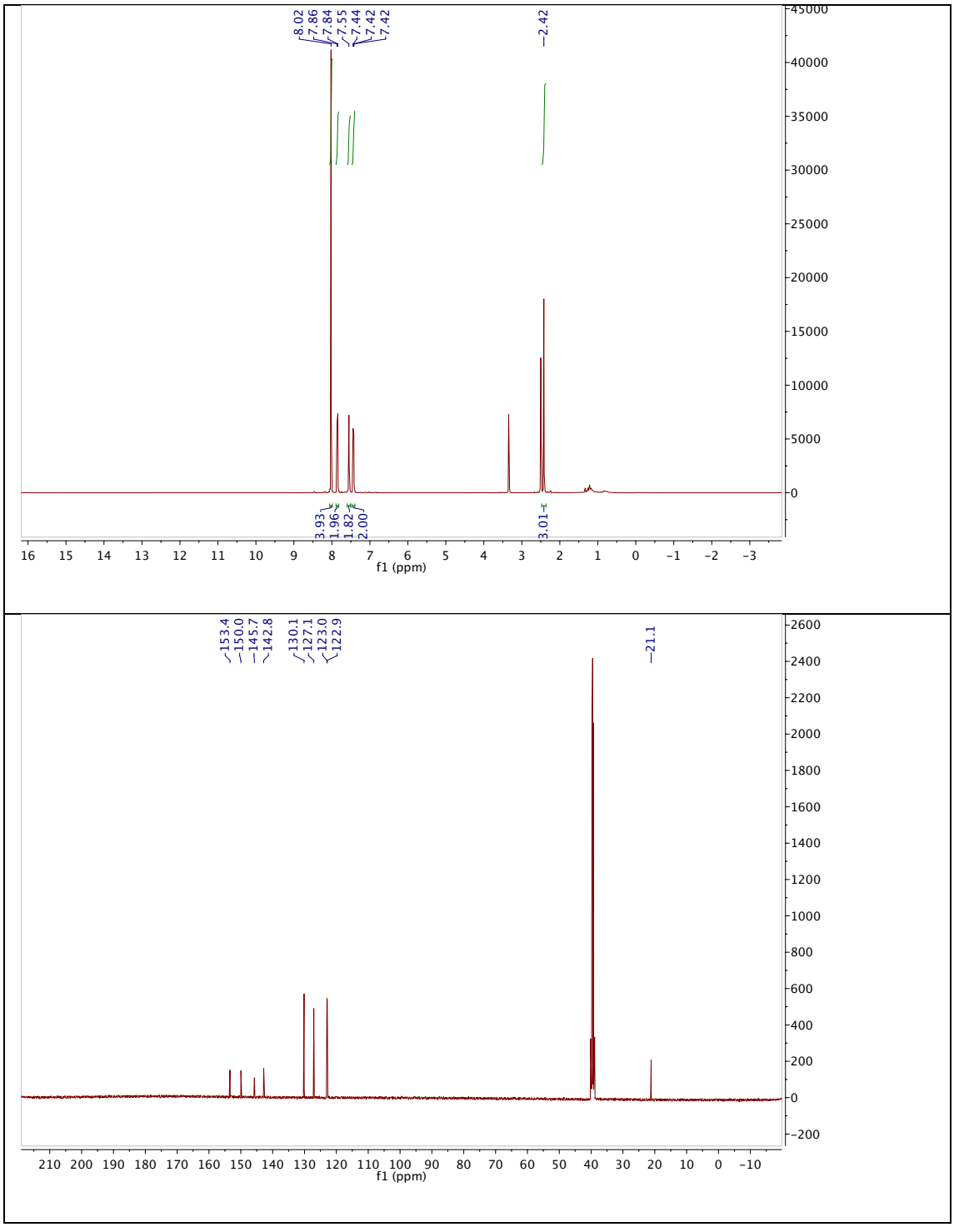

### 7.7.6 (*E*)-4-((4-Nitrophenyl)diazenyl)benzenesulfonamide (7.8)

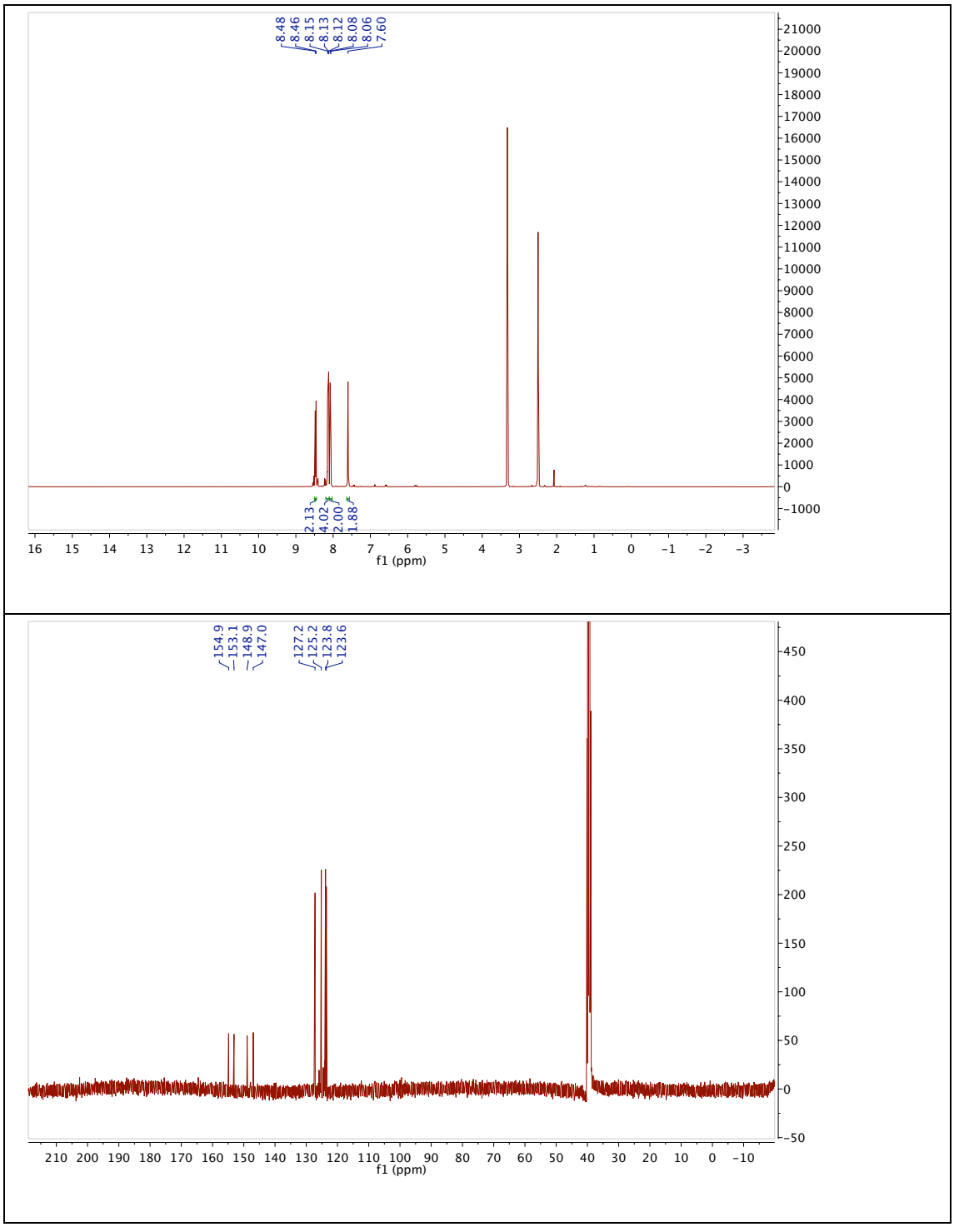

### 7.7.7 (*E*)-4-(Phenyldiazenyl)benzenesulfonamide (7.9)

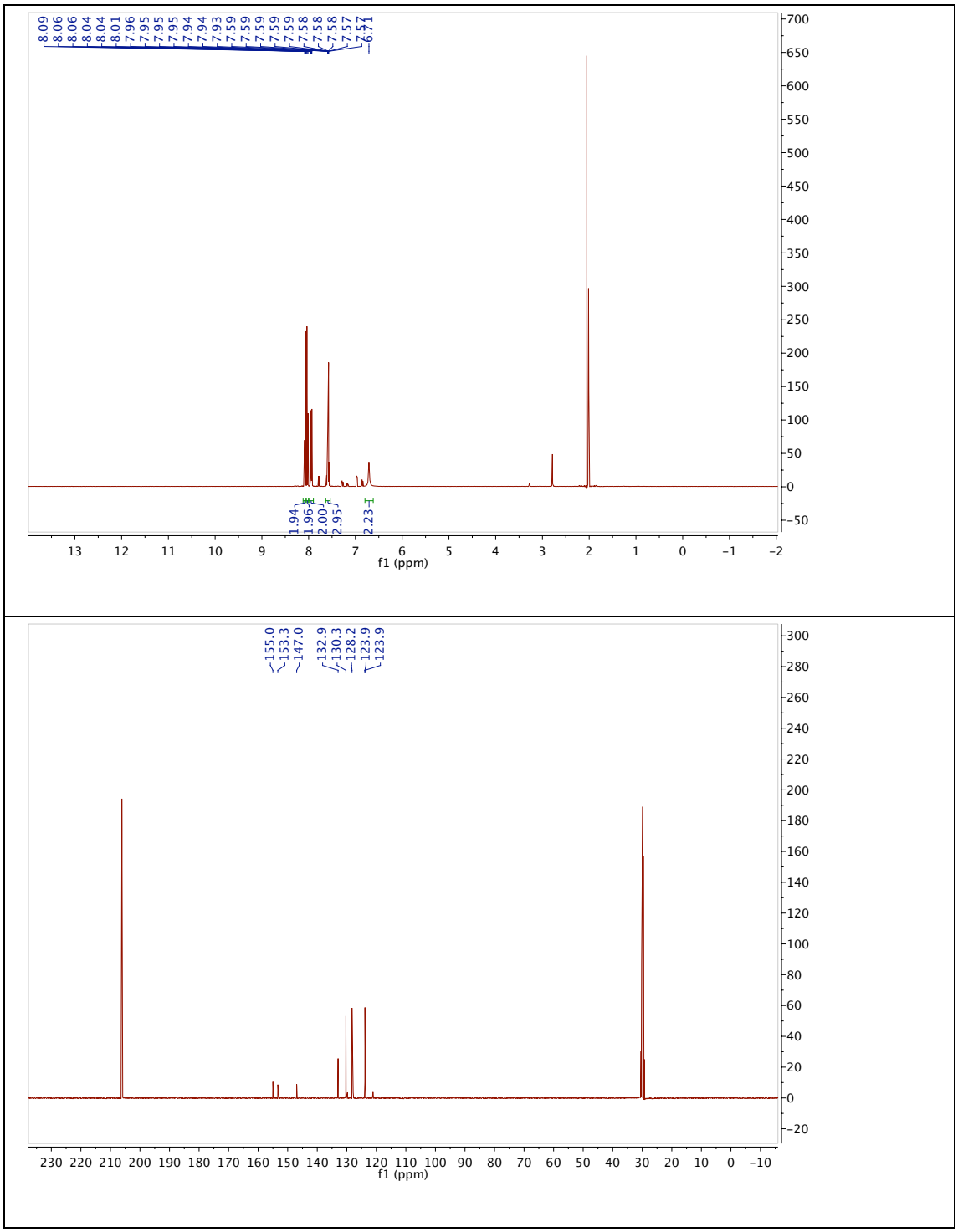

### 7.7.8 (*E*)-Ethyl 4-((4-sulfamoylphenyl)diazenyl)benzoate (7.10)

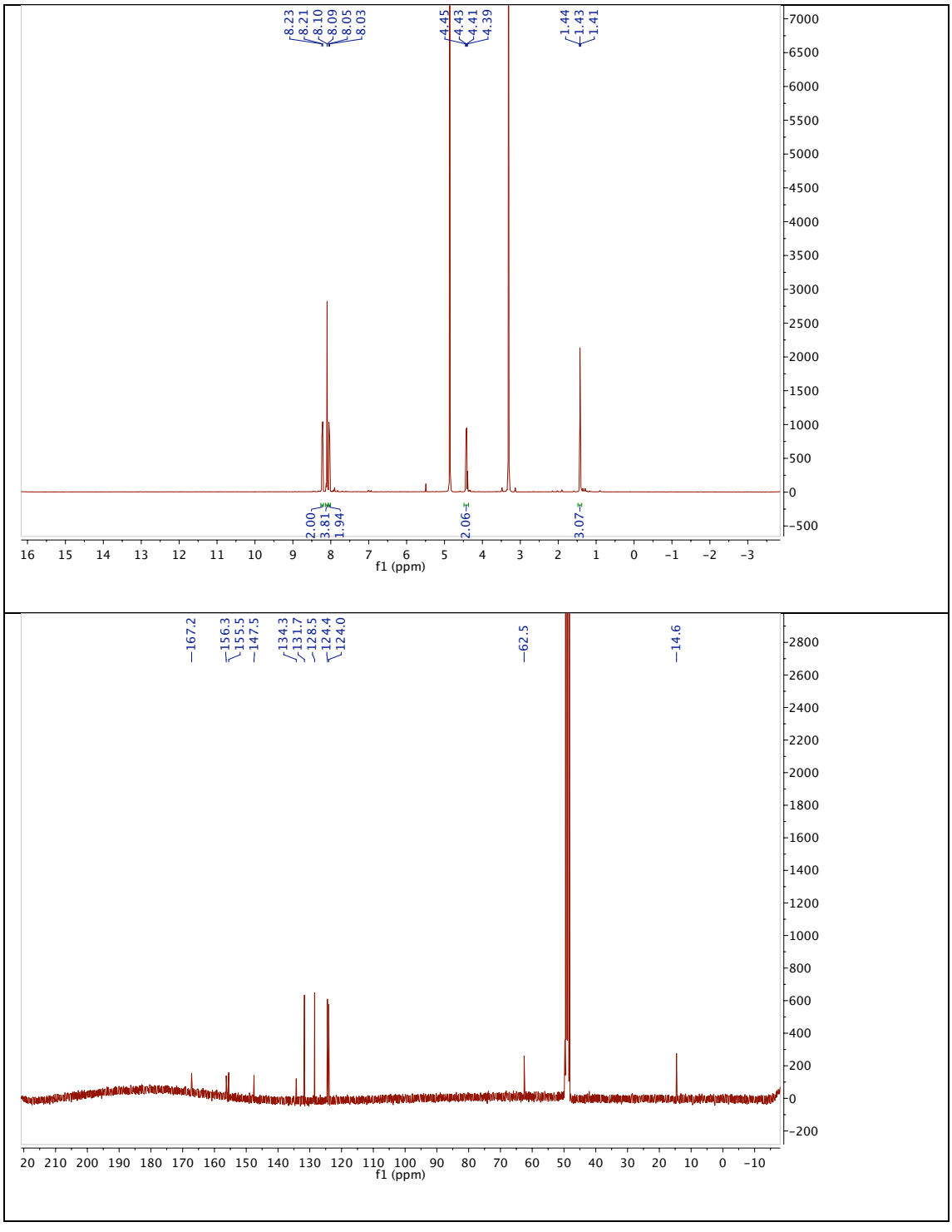

### 7.7.9 2-(2,5-Dioxo-2,5-dihydro-1*H*-pyrrol-1-yl)-acetic acid (7.13)

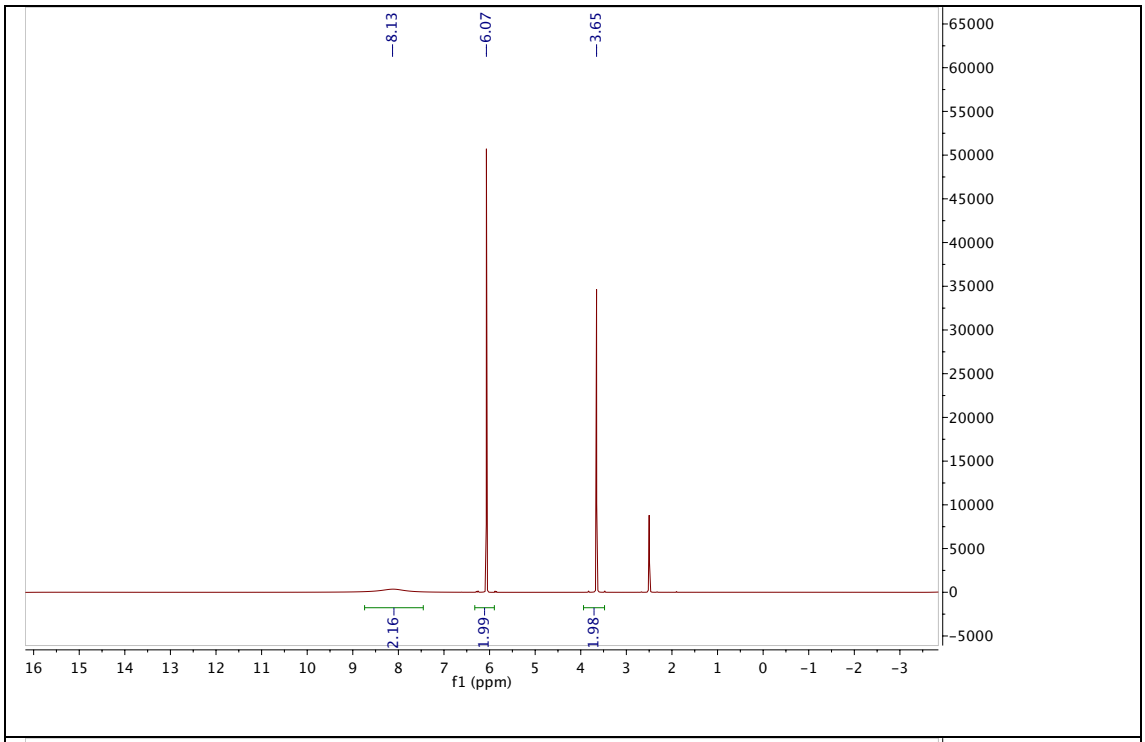


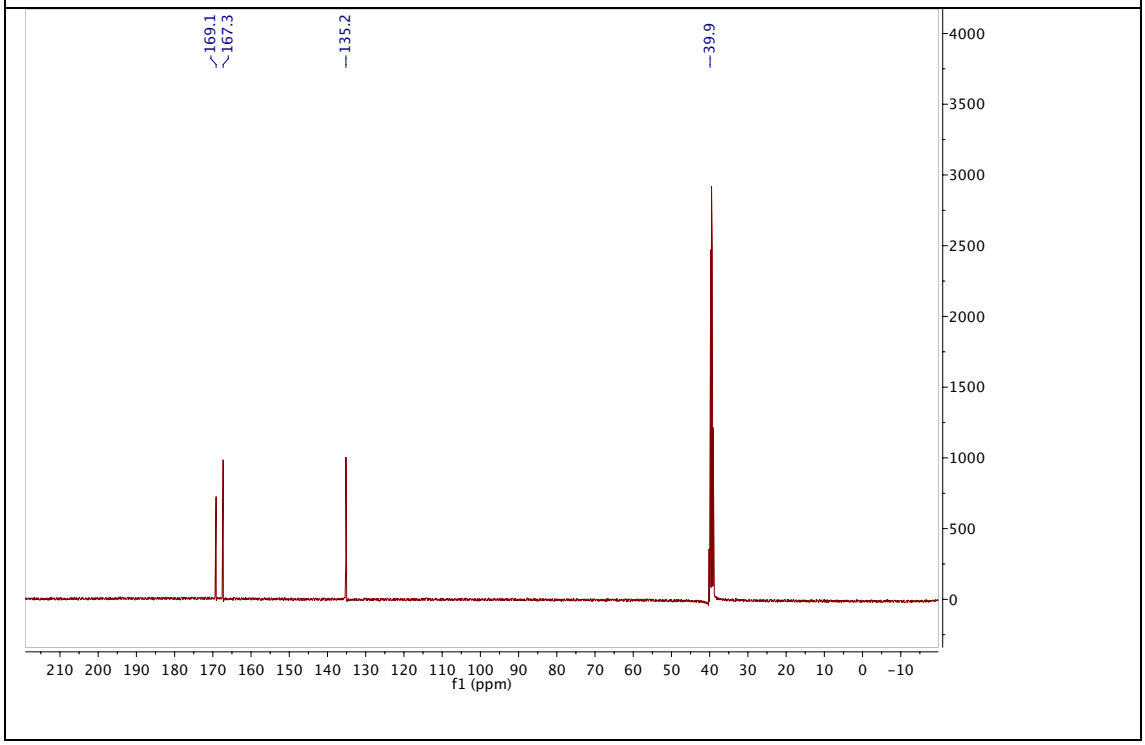

### 7.7.10 2-(2,5-Dioxo-2,5-dihydro-1*H*-pyrrol-1-yl)-*N*-(4-((4-sulfamoylphenyl)diazenyl)phenyl)acetamide (SA-1)

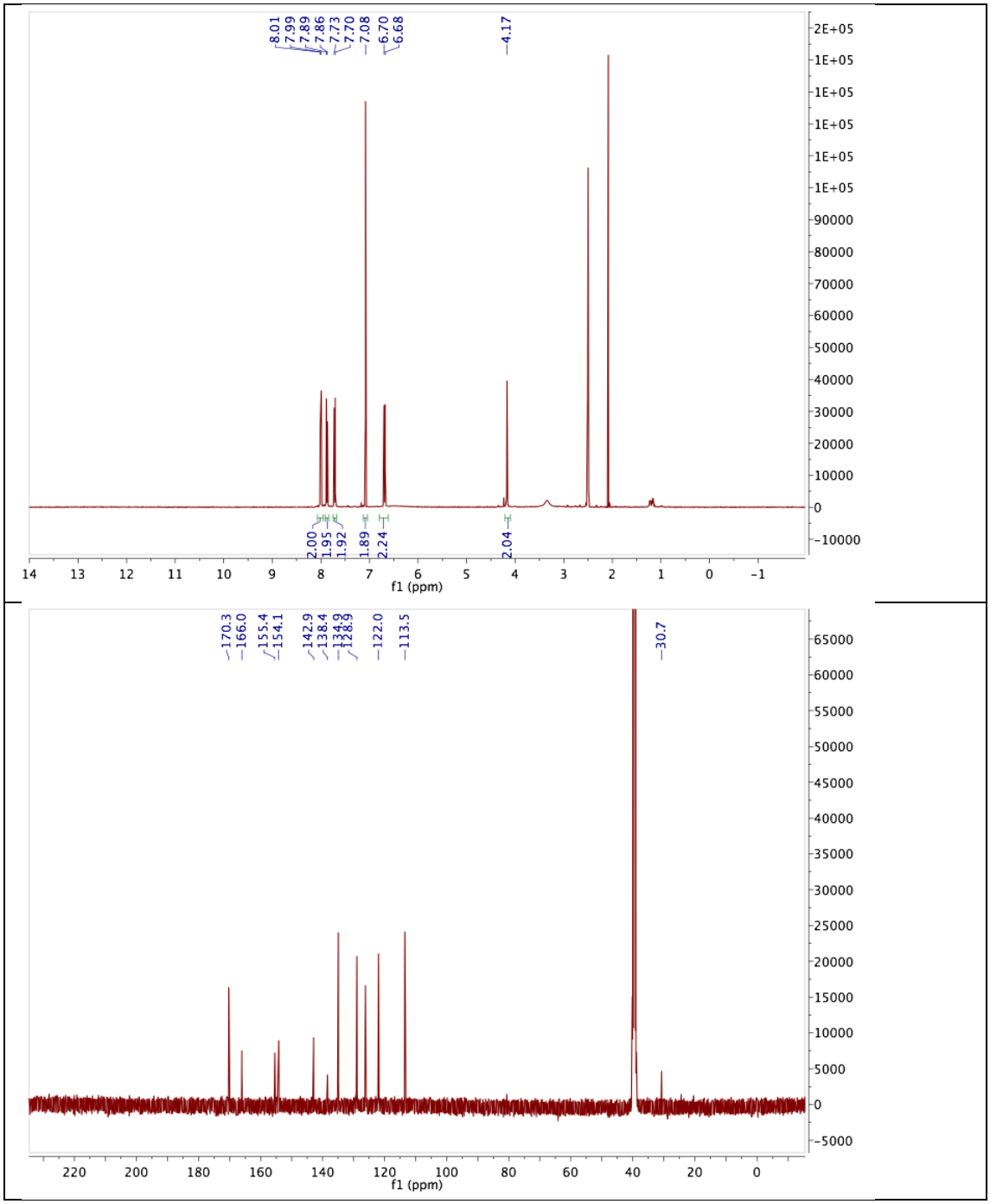

### 7.7.11 1-(Prop-2-yn-1-yl)-1*H*-pyrrole-2,5-dione (7.21)

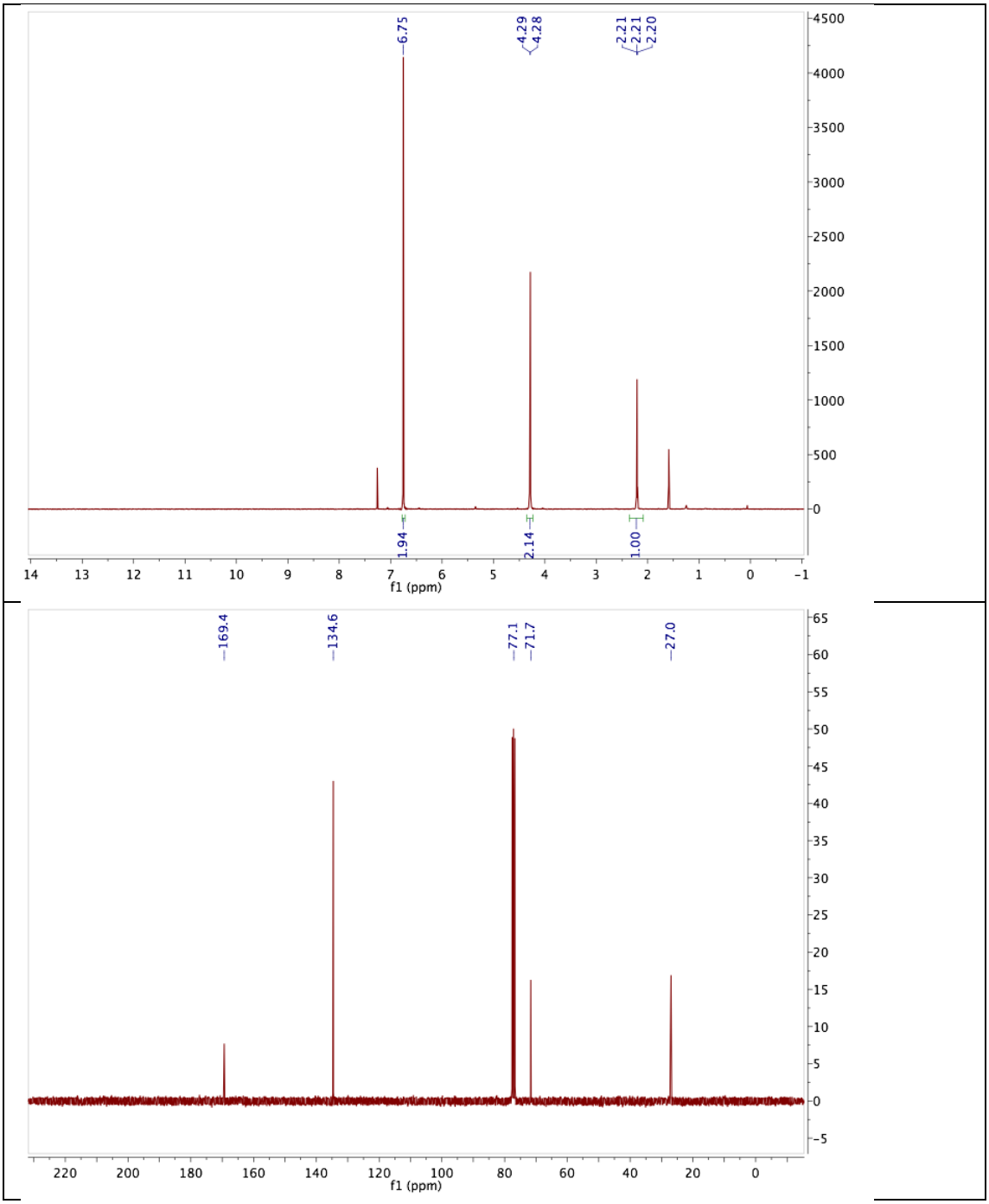

### 7.7.12 4-((4-(4-((2,5-Dioxo-2,5-dihydro-1*H*-pyrrol-1-yl)methyl)-1*H*-1,2,3-triazol-1-yl)phenyl)diazenyl)benzenesulfonamide (SA-3)

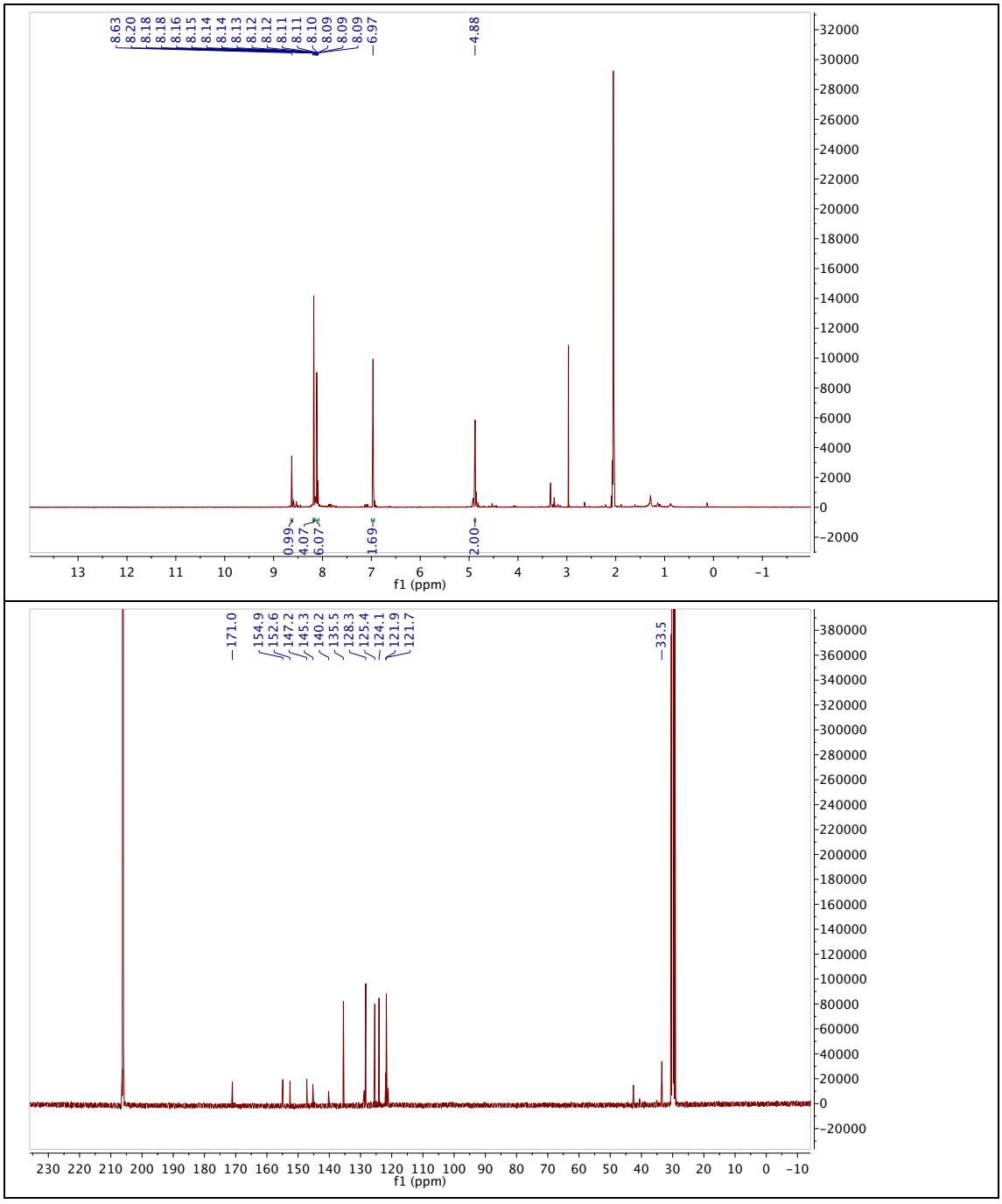

**7.7.13 *tert*-Butyl (2-oxo-2-((4-((4-sulfamoylphenyl)diazenyl)phenyl)amino)-ethyl) carbamate (7.15)**

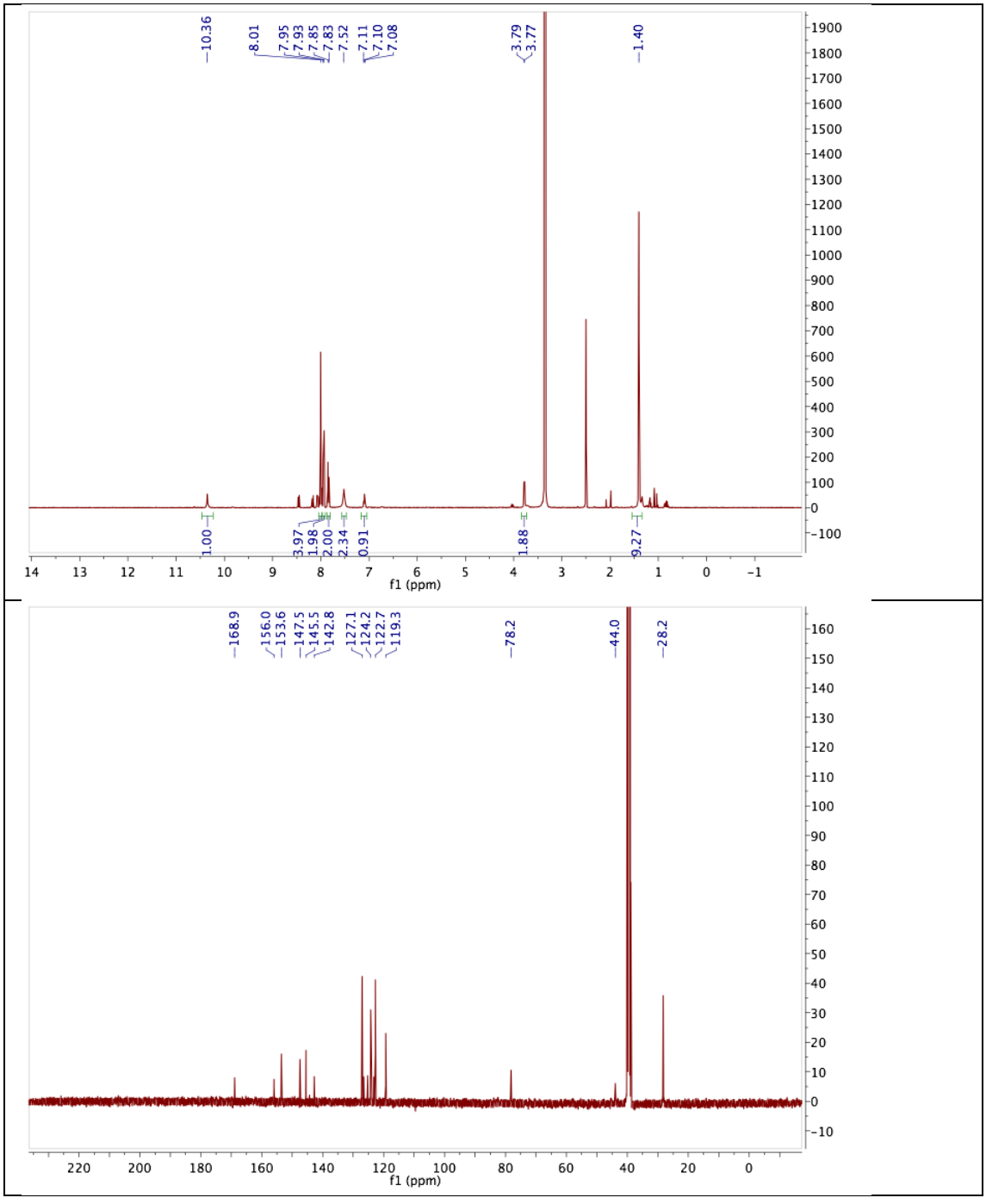

### 7.7.14 2-Amino-*N*-(4-((4-sulfamoylphenyl)diazenyl)phenyl)acetamide (TFA salt) (7.16)

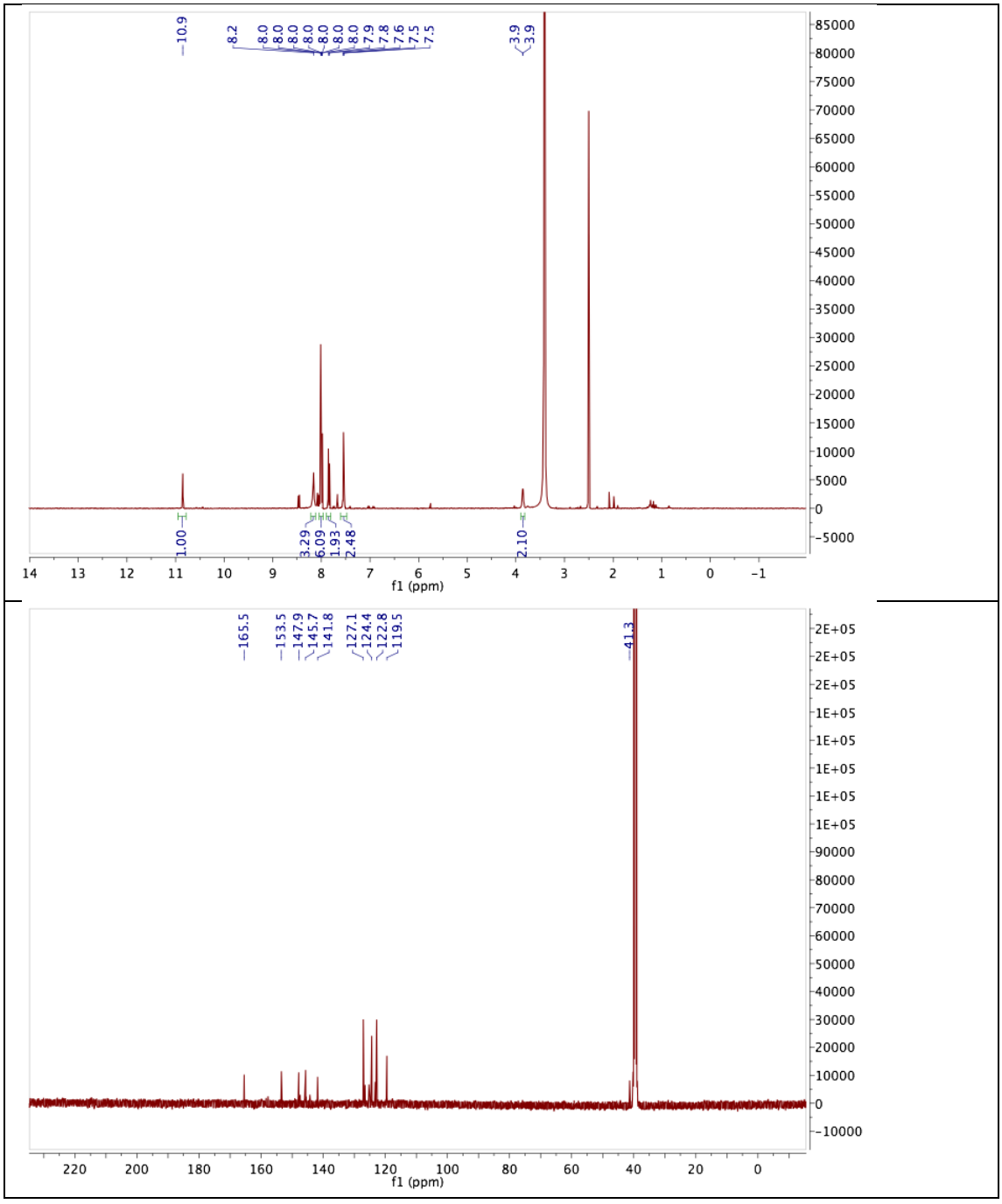

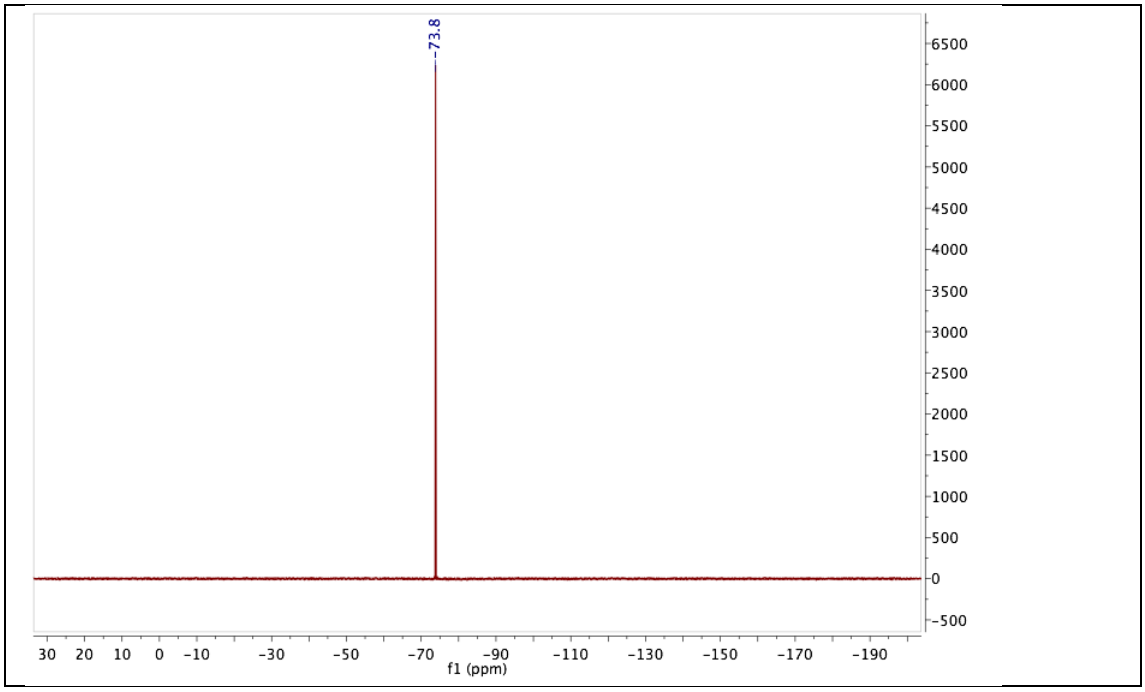
-73.8
6500
6000
5500
5000
4500
4000
3500
3000
2500
2000
1500
1000
500
0
-500
30 20 10 0 -10 -30 -50 -70 -90 -110 -130 -150 -170 -190
f1 (ppm)

### 7.7.15 2-(2,5-Dioxo-2,5-dihydro-1*H*-pyrrol-1-yl)-*N*-(2-oxo-2-((4-((4-sulfamoylphenyl)diazenyl)phenyl) amino)ethyl)acetamide (SA-2)

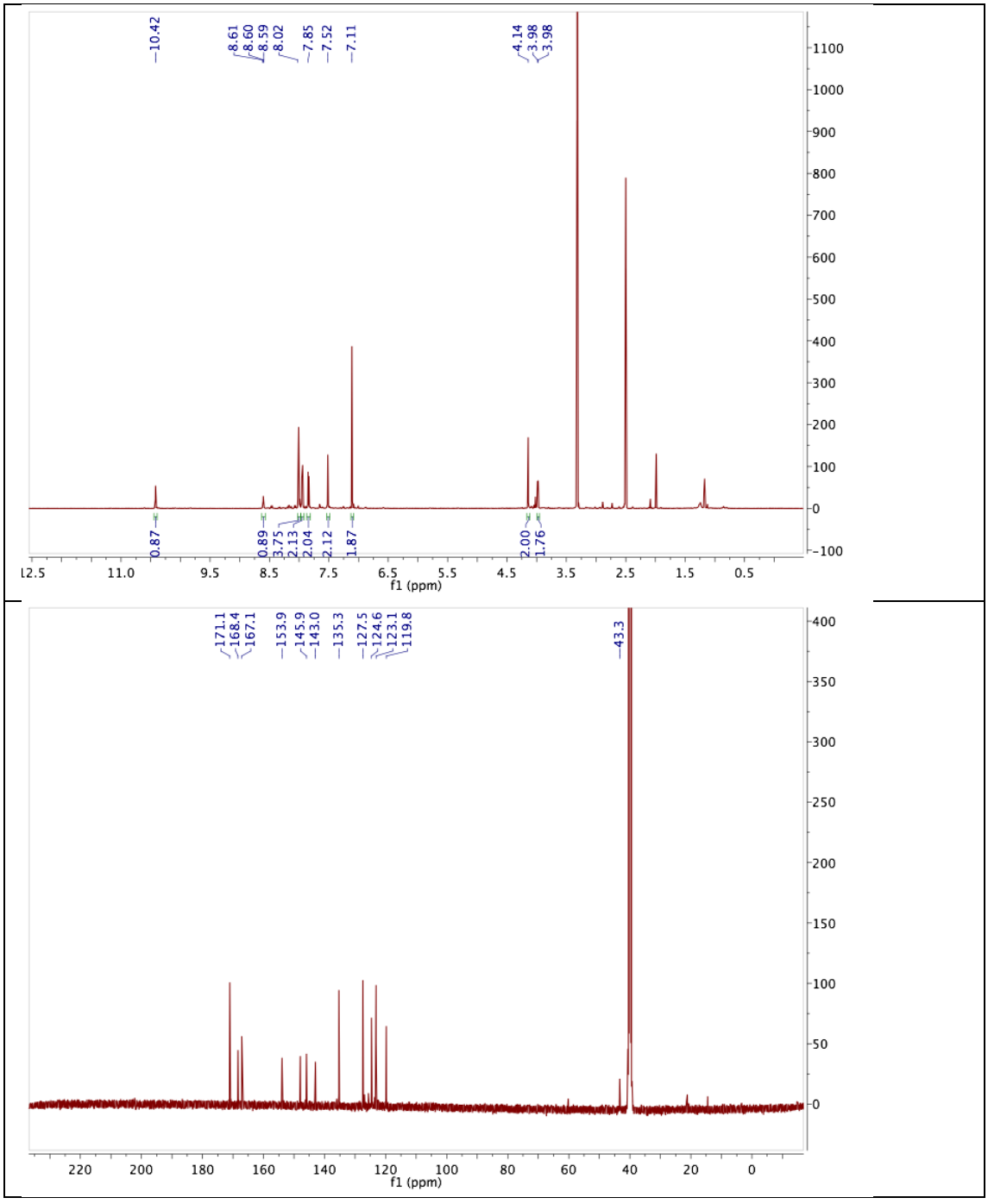

### 7.7.16 2-(2,5-Dioxo-2,5-dihydro-1*H*-pyrrol-1-yl)-*N*-(4-sulfamoylphenyl) acetamide (7.22)

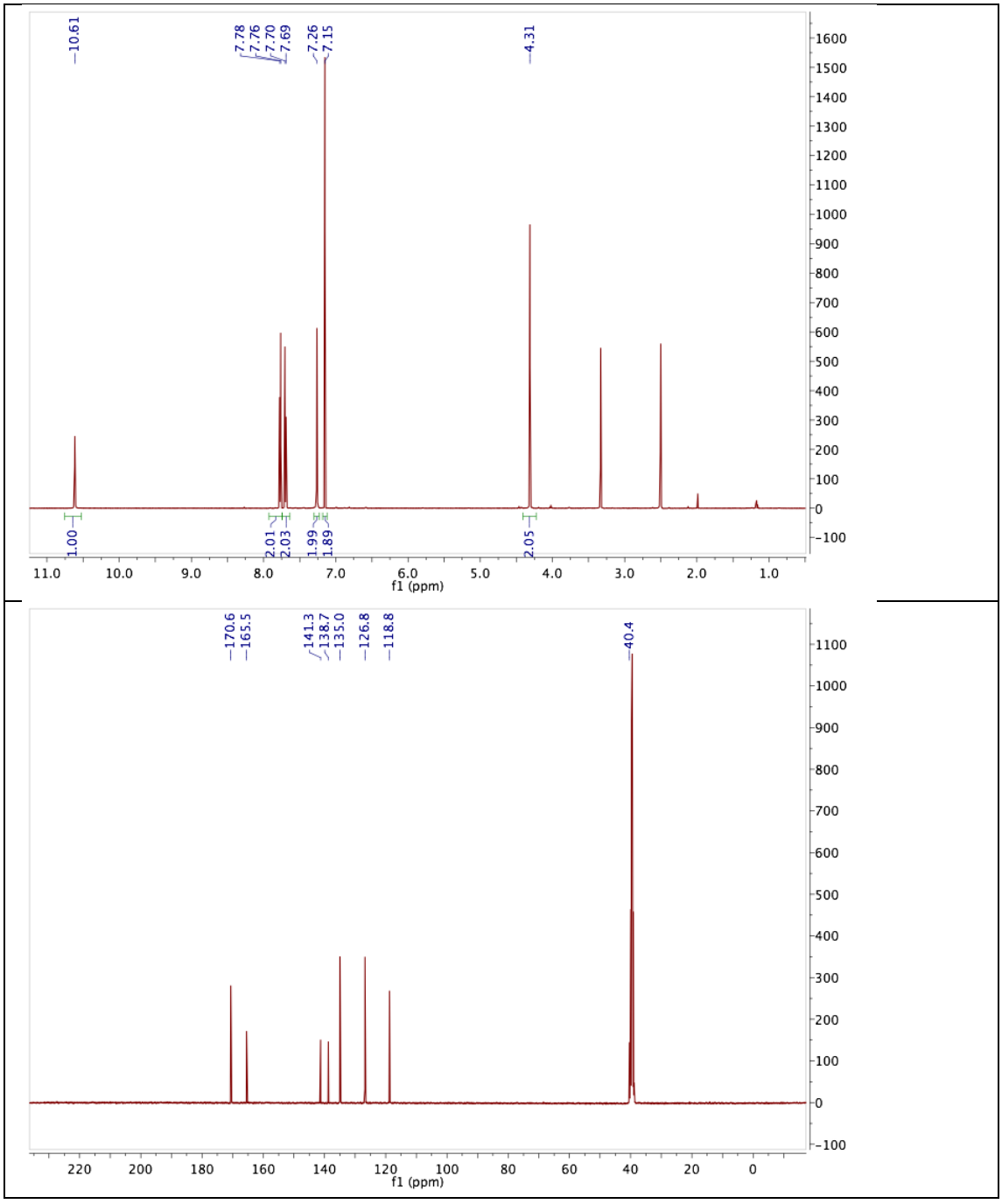

## 7.7.17 (*E*)-$N^1$-(2-Oxo-2-((4-((4-sulfamoylphenyl)diazenyl)phenyl)amino) ethyl)-$N^5$-(6-(6-(pyridin-2-yl)-1,2,4,5-tetrazin-3-yl)pyridin-3-yl)glutaramide (JB369)

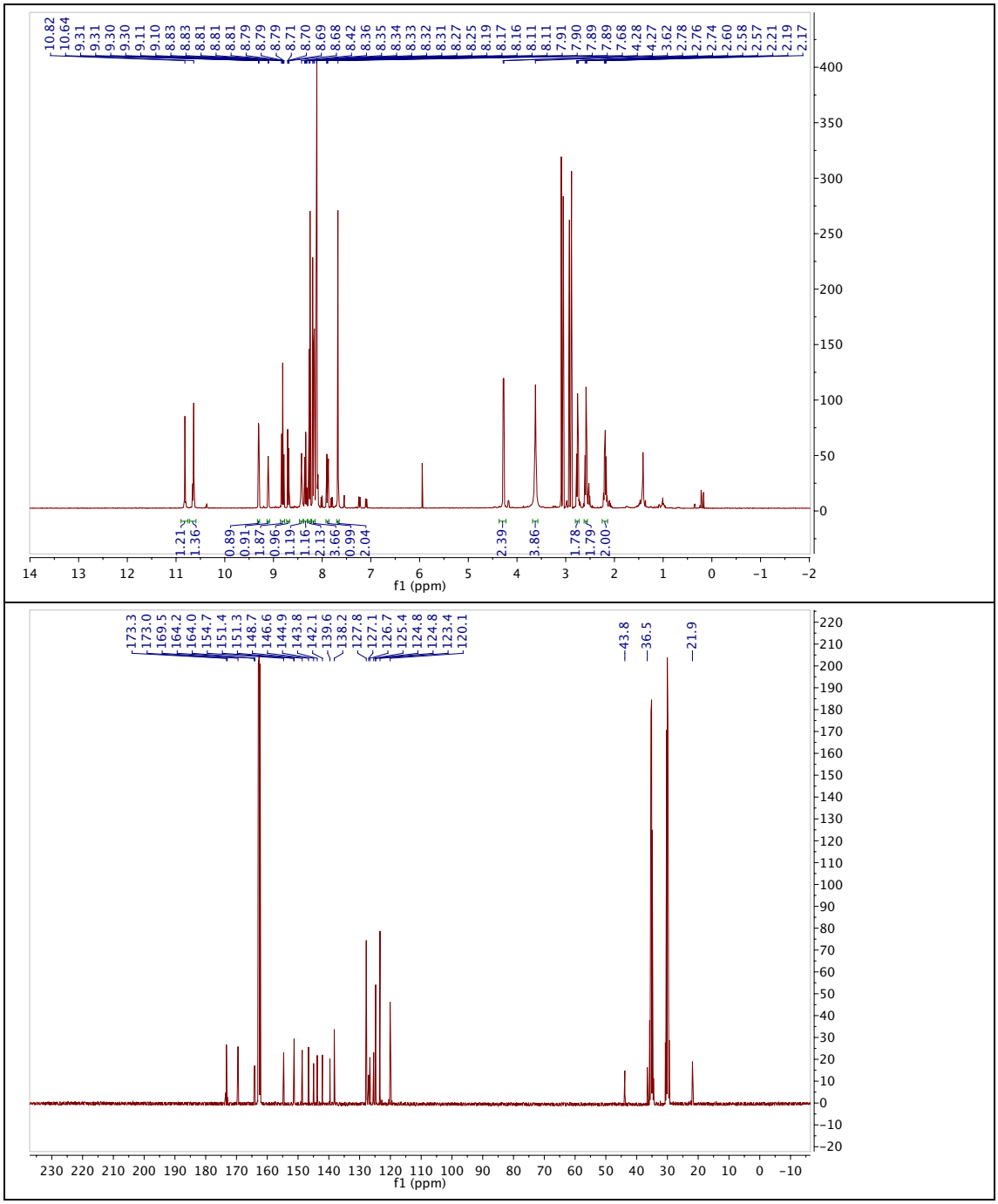

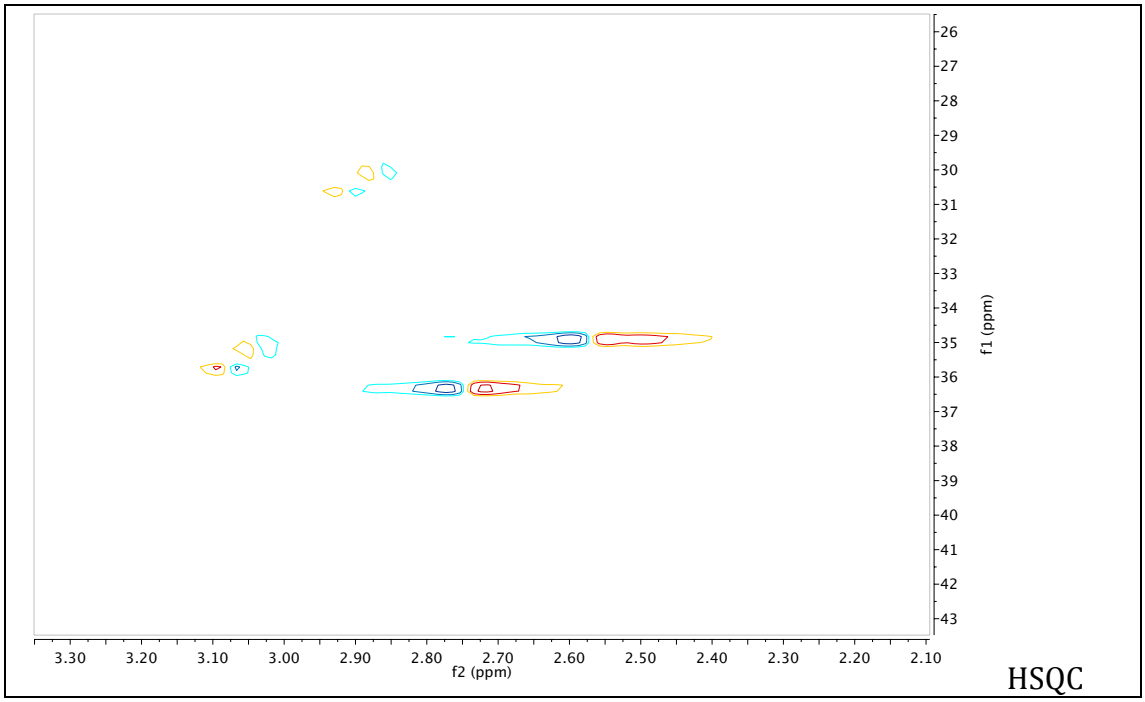
26
27
28
29
30
31
32
33
34
35
36
37
38
39
40
41
42
43
f1 (ppm)
3.30
3.20
3.10
3.00
2.90
2.80
2.70
2.60
2.50
2.40
2.30
2.20
2.10
f2 (ppm)

HSQC

## 7.8 X-ray Crystallographic Data

Crystals suitable for X-ray diffractometry of **7.2** were obtained from a DMSO/water solution. Crystals suitable for X-ray diffractometry of **7.3**, **7.4**, **7.6**, **7.7** and **7.8** were obtained by allowing a concentrated solution of the azobenzene in DMSO stand open to the atmosphere for 2-10 days. Crystals suitable for X-ray diffractometry of **7.5** were obtained from a 1 M HCl/EtOH solution. Crystals suitable for X-ray diffractometry of **7.9** were obtained from a hot solution of EtOH.

Crystals suitable for X-ray diffractometry of (3,6-di(pyridin-2-yl)-1,4-dihydro-1,2,4,5-tetrazine were obtained from the fraction collection after flash column chromatography by allowing the solution to stand open to the atmosphere o.n..

Crystals suitable for X-ray diffractometry of hCAII and its mutants were obtained as described in the Experimental section.

### 7.8.1 *para*-Nitrophenylacetate (*p*NPA)

**Supplementary Table 4: Crystallographic data of *p*NPA.**

| | ***p*NPA** |
|---|---|
| net formula | $C_8H_7NO_4$ |
| $M_r$/g mol$^{-1}$ | 181.146 |
| crystal size/mm | 0.374 × 0.332 × 0.175 |
| $T$/K | 173(2) |
| radiation | MoKα |
| diffractometer | 'Oxford XCalibur' |
| crystal system | monoclinic |
| space group | 'P 21/c' |
| $a$/Å | 13.9255(6) |
| $b$/Å | 7.3676(3) |

| | |
|---|---|
| $c$/Å | 16.0440(7) |
| α/° | 90 |
| β/° | 91.030(4) |
| γ/° | 90 |
| $V$/Å$^3$ | 1645.81(12) |
| $Z$ | 8 |
| calc. density/g cm$^{-3}$ | 1.46215(11) |
| μ/mm$^{-1}$ | 0.120 |
| absorption correction | 'multi-scan' |
| transmission factor range | 0.97321–1.00000 |
| refls. measured | 8944 |
| $R_{\mathrm{int}}$ | 0.0291 |
| mean σ($I$)/$I$ | 0.0366 |
| θ range | 4.239–26.367 |
| observed refls. | 2477 |
| $x$, $y$ (weighting scheme) | 0.0391, 0.2890 |
| hydrogen refinement | constr |
| refls in refinement | 3340 |
| parameters | 237 |
| restraints | 0 |
| $R(F_{\mathrm{obs}})$ | 0.0398 |
| $R_{\mathrm{w}}(F^2)$ | 0.1007 |
| $S$ | 1.044 |
| shift/error$_{\mathrm{max}}$ | 0.001 |
| max electron density/e Å$^{-3}$ | 0.206 |
| min electron density/e Å$^{-3}$ | −0.232 |

### 7.8.2 (*E*)-4-(4-Hydroxyphenyldiazenyl)benzenesulfonamide (7.2)

**Supplementary Table 5: Crystallographic data of 7.2**

| | **7.2** |
|---|---|
| net formula | $C_{12}H_{11}N_3O_3S$ |
| $M_r$/g mol$^{-1}$ | 277.300 |
| crystal size/mm | 0.090 × 0.060 × 0.040 |
| $T$/K | 173(2) |
| radiation | 'Mo Kα |
| diffractometer | 'Bruker D8Venture' |
| crystal system | triclinic |
| space group | $P1$ |
| $a$/Å | 5.9930(2) |
| $b$/Å | 7.7671(3) |
| $c$/Å | 26.2903(11) |
| α/° | 81.8058(13) |
| β/° | 83.7090(13) |
| γ/° | 89.4342(12) |
| $V$/Å$^3$ | 1203.96(8) |
| $Z$ | 4 |
| calc. density/g cm$^{-3}$ | 1.52987(10) |
| μ/mm$^{-1}$ | 0.277 |
| absorption correction | multi-scan |
| transmission factor range | 0.9074–0.9585 |
| refls. measured | 21464 |
| $R_{int}$ | 0.0273 |
| mean σ($I$)/$I$ | 0.0377 |
| θ range | 2.36–26.40 |
| observed refls. | 7359 |
| *x, y* (weighting scheme) | 0.0457, 0.2288 |
| hydrogen refinement | mixed |
| Flack parameter | 0.02(4) |
| refls in refinement | 8998 |

| | |
|---|---|
| parameters | 733 |
| restraints | 15 |
| $R(F_{obs})$ | 0.0374 |
| $R_w(F^2)$ | 0.0929 |
| $S$ | 1.045 |
| shift/error$_{max}$ | 0.001 |
| max electron density/e Å$^{-3}$ | 0.250 |
| min electron density/e Å$^{-3}$ | −0.258 |

C-H: constr, N-H und O-H: refall, wobei alle Bindngen mit DFIX fixiert wurden.

### 7.8.3 (*E*)-4-((4-(Diethylamino)phenyl)diazenyl)benzenesulfonamide (7.3)

**Supplementary Table 6: Crystallographic data of 7.3.**

| | **7.3** |
|---|---|
| net formula | $C_{18}H_{26}N_4O_3S_2$ |
| $M_r$/g mol$^{-1}$ | 410.556 |
| crystal size/mm | 0.060 × 0.050 × 0.040 |
| $T$/K | 100(2) |
| radiation | 'Mo Kα |
| diffractometer | 'Bruker D8Venture' |
| crystal system | monoclinic |
| space group | $P2_1$ |
| $a$/Å | 7.5368(3) |
| $b$/Å | 8.1064(3) |
| $c$/Å | 16.7424(7) |
| α/° | 90 |
| β/° | 94.6119(14) |
| γ/° | 90 |
| $V$/Å$^3$ | 1019.59(7) |
| $Z$ | 2 |
| calc. density/g cm$^{-3}$ | 1.33731(9) |

| | |
|---|---|
| μ/mm$^{-1}$ | 0.287 |
| absorption correction | multi-scan |
| transmission factor range | 0.8939–0.9585 |
| refls. measured | 12699 |
| $R_{int}$ | 0.0255 |
| mean σ($I$)/$I$ | 0.0283 |
| θ range | 3.06–26.49 |
| observed refls. | 3925 |
| *x, y* (weighting scheme) | 0.0312, 0.2439 |
| hydrogen refinement | mixed |
| Flack parameter | −0.01(4) |
| refls in refinement | 4138 |
| parameters | 256 |
| restraints | 1 |
| $R(F_{obs})$ | 0.0253 |
| $R_w(F^2)$ | 0.0623 |
| $S$ | 1.051 |
| shift/error$_{max}$ | 0.001 |
| max electron density/e Å$^{-3}$ | 0.310 |
| min electron density/e Å$^{-3}$ | −0.281 |

### 7.8.4 (*E*)-4-((4-Morpholinophenyl)diazenyl)benzenesulfonamide (7.4)

**Supplementary Table 7: Crystallographic data of 7.4.**

| | **7.4** |
|---|---|
| net formula | $C_{16}H_{18}N_4O_3S$ |
| $M_r$/g mol$^{-1}$ | 346.405 |
| crystal size/mm | 0.130 × 0.120 × 0.040 |
| $T$/K | 100(2) |
| radiation | 'Mo Kα |
| diffractometer | 'Bruker D8Venture' |
| crystal system | orthorhombic |

| | |
|---|---|
| space group | $Pna2_1$ |
| $a$/Å | 22.6988(7) |
| $b$/Å | 8.4921(3) |
| $c$/Å | 25.0001(8) |
| α/° | 90 |
| β/° | 90 |
| γ/° | 90 |
| $V$/Å$^3$ | 4819.0(3) |
| $Z$ | 12 |
| calc. density/g cm$^{-3}$ | 1.43240(9) |
| μ/mm$^{-1}$ | 0.225 |
| absorption correction | multi-scan |
| transmission factor range | 0.9040–0.9585 |
| refls. measured | 81173 |
| $R_{\mathrm{int}}$ | 0.0342 |
| mean σ($I$)/$I$ | 0.0198 |
| θ range | 3.00–26.41 |
| observed refls. | 9161 |
| $x$, $y$ (weighting scheme) | 0.0425, 1.4290 |
| hydrogen refinement | mixed |
| Flack parameter | 0.09(4) |
| refls in refinement | 9848 |
| parameters | 682 |
| restraints | 1 |
| $R(F_{\mathrm{obs}})$ | 0.0305 |
| $R_{\mathrm{w}}(F^2)$ | 0.0765 |
| $S$ | 1.033 |
| shift/error$_{\mathrm{max}}$ | 0.001 |
| max electron density/e Å$^{-3}$ | 0.328 |
| min electron density/e Å$^{-3}$ | −0.264 |

### 7.8.5 (*E*)-4-(4-Aminophenyldiazenyl)benzenesulfonamide (7.5)

**Supplementary Table 8: Crystallographic data of 7.5.**

| | **7.5** |
|---|---|
| net formula | $C_{12}H_{14}N_4O_3S$ |
| $M_r$/g mol$^{-1}$ | 294.331 |
| crystal size/mm | 0.120 × 0.080 × 0.040 |
| $T$/K | 173(2) |
| radiation | 'Mo Kα |
| diffractometer | 'Bruker D8Venture' |
| crystal system | orthorhombic |
| space group | $P2_12_12$ |
| $a$/Å | 7.2743(3) |
| $b$/Å | 30.3691(13) |
| $c$/Å | 6.0082(2) |
| α/° | 90 |
| β/° | 90 |
| γ/° | 90 |
| $V$/Å$^3$ | 1327.30(9) |
| $Z$ | 4 |
| calc. density/g cm$^{-3}$ | 1.47293(10) |
| μ/mm$^{-1}$ | 0.258 |
| absorption correction | multi-scan |
| transmission factor range | 0.9053–0.9585 |
| refls. measured | 14363 |
| $R_{int}$ | 0.0266 |
| mean σ($I$)/$I$ | 0.0211 |
| θ range | 3.10–26.44 |
| observed refls. | 2517 |
| *x, y* (weighting scheme) | 0.0467, 0.3027 |
| hydrogen refinement | mixed |

| | |
|---|---|
| Flack parameter | −0.01(8) |
| refls in refinement | 2716 |
| parameters | 205 |
| restraints | 0 |
| $R(F_{obs})$ | 0.0334 |
| $R_w(F^2)$ | 0.0841 |
| $S$ | 1.102 |
| shift/error$_{max}$ | 0.001 |
| max electron density/e Å$^{-3}$ | 0.302 |
| min electron density/e Å$^{-3}$ | −0.193 |

### 7.8.6 (*E*)-4-(4-Azidophenyldiazenyl)benzenesulfonamide (7.6)

**Supplementary Table 9: Crystallographic data of 7.6.**

| | **7.6** |
|---|---|
| net formula | $C_{14}H_{16}N_6O_3S_2$ |
| $M_r$/g mol$^{-1}$ | 380.448 |
| crystal size/mm | 0.130 × 0.110 × 0.090 |
| $T$/K | 173(2) |
| radiation | 'Mo Kα |
| diffractometer | 'Bruker D8Venture' |
| crystal system | monoclinic |
| space group | $P2_1/c$ |
| $a$/Å | 9.5471(3) |
| $b$/Å | 6.9479(3) |
| $c$/Å | 26.7173(10) |
| α/° | 90 |
| β/° | 97.7199(11) |
| γ/° | 90 |
| $V$/Å$^3$ | 1756.16(11) |
| $Z$ | 4 |
| calc. density/g cm$^{-3}$ | 1.43895(9) |

| | |
|---|---|
| μ/mm$^{-1}$ | 0.330 |
| absorption correction | multi-scan |
| transmission factor range | 0.8804–0.9590 |
| refls. measured | 21511 |
| $R_{int}$ | 0.0246 |
| mean σ($I$)/$I$ | 0.0201 |
| θ range | 3.03–27.55 |
| observed refls. | 3437 |
| $x$, $y$ (weighting scheme) | 0.0592, 1.1238 |
| hydrogen refinement | mixed |
| refls in refinement | 4019 |
| parameters | 236 |
| restraints | 0 |
| $R(F_{obs})$ | 0.0401 |
| $R_w(F^2)$ | 0.1118 |
| $S$ | 1.017 |
| shift/error$_{max}$ | 0.001 |
| max electron density/e Å$^{-3}$ | 0.967 |
| min electron density/e Å$^{-3}$ | −0.373 |

### 7.8.7 (*E*)-4-(*p*-Tolyldiazenyl)benzenesulfonamide (7.7)

**Supplementary Table 10: Crystallographic data of 7.7.**

| | **7.7** |
|---|---|
| net formula | $C_{14.70}H_{18.40}N_3O_3S_{1.85}$ |
| $M_r$/g mol$^{-1}$ | 344.444 |
| crystal size/mm | 0.090 × 0.060 × 0.010 |
| $T$/K | 173(2) |
| radiation | 'Mo Kα |
| diffractometer | 'Bruker D8Venture' |
| crystal system | monoclinic |
| space group | $P2_1/c$ |
| $a$/Å | 9.5107(4) |

| | |
|---|---|
| $b$/Å | 6.6459(3) |
| $c$/Å | 27.6033(11) |
| α/° | 90 |
| β/° | 95.6025(11) |
| γ/° | 90 |
| $V$/Å$^3$ | 1736.39(13) |
| $Z$ | 4 |
| calc. density/g cm$^{-3}$ | 1.31761(10) |
| μ/mm$^{-1}$ | 0.304 |
| absorption correction | multi-scan |
| transmission factor range | 0.9048–0.9585 |
| refls. measured | 28311 |
| $R_{int}$ | 0.0333 |
| mean σ($I$)/$I$ | 0.0215 |
| θ range | 2.97–26.40 |
| observed refls. | 2811 |
| $x$, $y$ (weighting scheme) | 0.0658, 1.0650 |
| hydrogen refinement | mixed |
| refls in refinement | 3563 |
| parameters | 220 |
| restraints | 0 |
| $R(F_{obs})$ | 0.0429 |
| $R_w(F^2)$ | 0.1345 |
| $S$ | 1.107 |
| shift/error$_{max}$ | 0.001 |
| max electron density/e Å$^{-3}$ | 0.600 |
| min electron density/e Å$^{-3}$ | −0.400 |

### 7.8.8 (*E*)-4-((4-Nitrophenyl)diazenyl)benzenesulfonamide (7.8)

**Supplementary Table 11: Crystallographic data of 7.8.**

| | **7.8** |
|---|---|

| | |
|---|---|
| net formula | $C_{14}H_{16}N_4O_5S_2$ |
| $M_r$/g mol$^{-1}$ | 384.433 |
| crystal size/mm | 0.120 × 0.080 × 0.050 |
| $T$/K | 173(2) |
| radiation | 'Mo Kα |
| diffractometer | 'Bruker D8Venture' |
| crystal system | monoclinic |
| space group | $P2_1/c$ |
| $a$/Å | 9.7420(5) |
| $b$/Å | 6.9706(3) |
| $c$/Å | 25.6450(13) |
| α/° | 90 |
| β/° | 95.7761(14) |
| γ/° | 90 |
| $V$/Å$^3$ | 1732.65(15) |
| $Z$ | 4 |
| calc. density/g cm$^{-3}$ | 1.47375(13) |
| μ/mm$^{-1}$ | 0.341 |
| absorption correction | multi-scan |
| transmission factor range | 0.9006–0.9585 |
| refls. measured | 17953 |
| $R_{int}$ | 0.0242 |
| mean σ($I$)/$I$ | 0.0216 |
| θ range | 2.76–26.40 |
| observed refls. | 2924 |
| *x, y* (weighting scheme) | 0.0667, 1.5179 |
| hydrogen refinement | mixed |
| refls in refinement | 3554 |
| parameters | 236 |
| restraints | 0 |
| $R(F_{obs})$ | 0.0501 |
| $R_w(F^2)$ | 0.1396 |
| $S$ | 1.054 |

| | |
|---|---|
| shift/error$_{max}$ | 0.001 |
| max electron density/e Å$^{-3}$ | 0.545 |
| min electron density/e Å$^{-3}$ | −0.306 |

### 7.8.9 (*E*)-Ethyl 4-((4-sulfamoylphenyl)diazenyl)benzoate (7.10)

**Supplementary Table 12: Crystallographic data of 7.10.**

| | **1i** |
|---|---|
| net formula | $C_{15}H_{15}N_3O_4S$ |
| $M_r$/g mol$^{-1}$ | 333.363 |
| crystal size/mm | 0.150 × 0.030 × 0.020 |
| $T$/K | 173(2) |
| radiation | 'Mo Kα |
| diffractometer | 'Bruker D8Venture' |
| crystal system | monoclinic |
| space group | $P2_1/n$ |
| $a$/Å | 16.4622(12) |
| $b$/Å | 4.9986(3) |
| $c$/Å | 18.5166(12) |
| α/° | 90 |
| β/° | 90.449(2) |
| γ/° | 90 |
| $V$/Å$^3$ | 1523.65(17) |
| $Z$ | 4 |
| calc. density/g cm$^{-3}$ | 1.45328(16) |
| μ/mm$^{-1}$ | 0.237 |
| absorption correction | multi-scan |
| transmission factor range | 0.8535–0.9585 |
| refls. measured | 17872 |
| $R_{int}$ | 0.0618 |
| mean σ($I$)/$I$ | 0.0485 |
| θ range | 3.30–26.40 |
| observed refls. | 2249 |

| | |
|---|---|
| $x, y$ (weighting scheme) | 0.0377, 0.9958 |
| hydrogen refinement | mixed |
| refls in refinement | 3115 |
| parameters | 217 |
| restraints | 0 |
| $R(F_{obs})$ | 0.0421 |
| $R_w(F^2)$ | 0.0988 |
| $S$ | 1.048 |
| shift/error$_{max}$ | 0.001 |
| max electron density/e Å$^{-3}$ | 0.530 |
| min electron density/e Å$^{-3}$ | −0.382 |

### 7.8.10 (3,6-Di(pyridin-2-yl)-1,4-dihydro-1,2,4,5-tetrazine (7.27)

**Supplementary Table 13: Crystallographic data of 7.27.**

| | **7.27** |
|---|---|
| net formula | $C_{12}H_{10}N_6$ |
| $M_r$/g mol$^{-1}$ | 238.248 |
| crystal size/mm | 0.158 × 0.133 × 0.118 |
| $T$/K | 100(2) |
| radiation | 'Mo Kα |
| diffractometer | 'Bruker D8Venture' |
| crystal system | triclinic |
| space group | $P$1bar |
| $a$/Å | 8.1962(3) |
| $b$/Å | 8.2748(3) |
| $c$/Å | 8.8576(3) |
| α/° | 102.0661(19) |
| β/° | 112.0420(17) |
| γ/° | 90.119(2) |
| $V$/Å$^3$ | 542.38(3) |
| $Z$ | 2 |

| | |
|---|---|
| calc. density/g cm$^{-3}$ | 1.45885(8) |
| μ/mm$^{-1}$ | 0.097 |
| absorption correction | multi-scan |
| transmission factor range | 0.9313–0.9590 |
| refls. measured | 10361 |
| $R_{int}$ | 0.0244 |
| mean σ($I$)/$I$ | 0.0204 |
| θ range | 3.16–27.54 |
| observed refls. | 2145 |
| $x$, $y$ (weighting scheme) | 0.0528, 0.1945 |
| hydrogen refinement | mixed |
| refls in refinement | 2487 |
| parameters | 171 |
| restraints | 0 |
| $R(F_{obs})$ | 0.0368 |
| $R_w(F^2)$ | 0.1029 |
| $S$ | 1.063 |
| shift/error$_{max}$ | 0.001 |
| max electron density/e Å$^{-3}$ | 0.367 |
| min electron density/e Å$^{-3}$ | −0.191 |

# *8 ATP-sensitive Potassium Channel Kir6.2/SUR1*

Parts of this work have been published in *Nature Communications* **2014**, *5*:5116.

## 8.1 Introduction

Type 2 diabetes mellitus (T2DM) is a global healthcare epidemic associated with life-changing sequelae ranging from blindness to cancer.[112,113] This endocrine disease, which currently affects 1 in 12 of the adult population worldwide, involves a disturbance of normal glucose homeostasis due to failure of the pancreatic beta cell mass to adequately compensate for increased peripheral insulin resistance.[114] As such, the rescue of insulin release through the coaxing of beta cell activity remains a therapeutically desirable approach for the long-term restoration of normal glucose levels.

Sulfonylureas, which target ATP-sensitive potassium ($K^+$) ($K_{ATP}$) channels, are a mainstay of diabetes therapy.[115-117] $K_{ATP}$ channels are hetero-octameric structures composed of four regulatory sulfonylurea receptor subunits (SUR1) and four Kir6.2 subunits, the latter forming a central ion pore that permits $K^+$ efflux.[118-120] By binding to SUR1, sulfonylureas block the Kir6.2 inward rectifier, leading to cell depolarization and opening of voltage-dependent $Ca^{2+}$ channels (VDCC).[121,122] The ensuing $Ca^{2+}$ influx,[123,124] along with $K_{ATP}$ channel-independent signals[125], drives various downstream processes which ultimately converge on the exocytosis of insulin.[126] Elevated circulating insulin can then act on target tissues to improve glucose uptake, hepatic glycogenesis and fatty acid synthesis[127] (Figure 43).

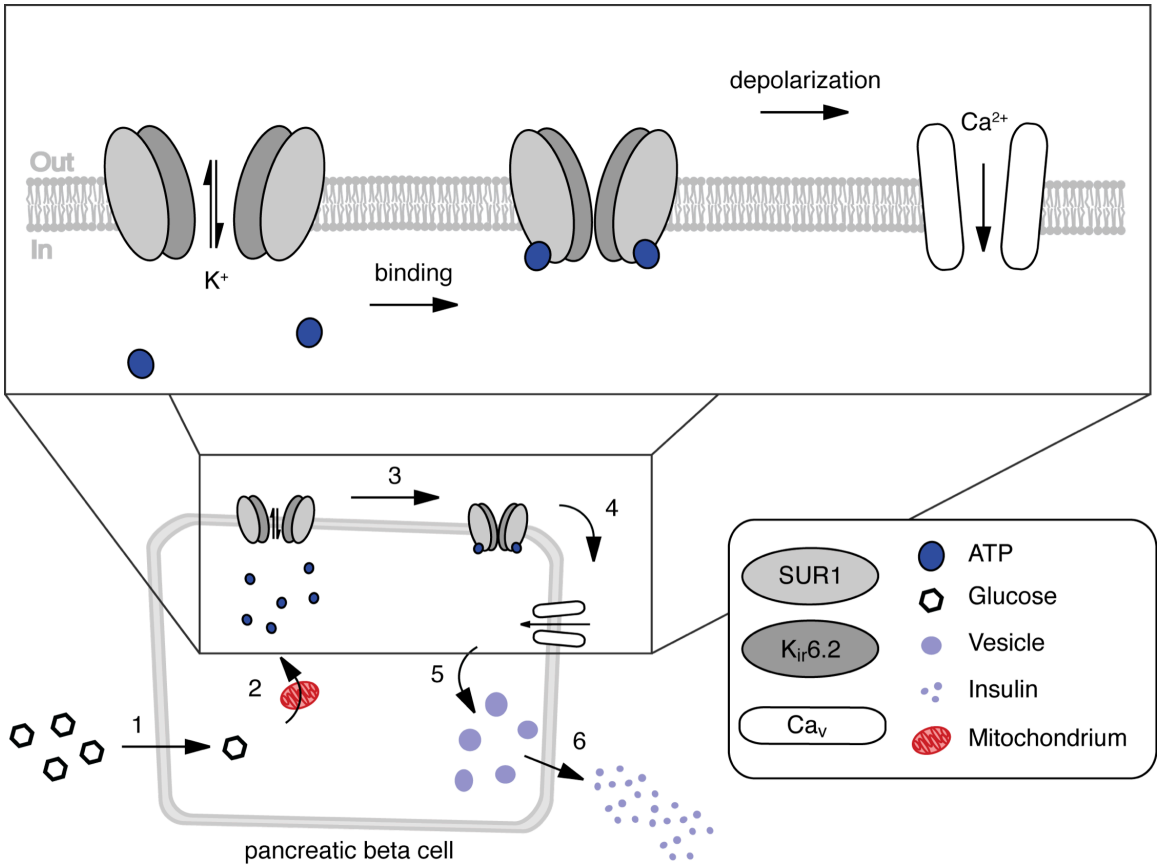


**Figure 43: Stimulation-secretion coupling in the pancreatic beta-cell.** Upper part: Zoom-in of $K_{ATP}$ channel function. Lower part: Glucose is transported into the cell and undergoes glycolysis followed by mitochondrial metabolism **(1).** The increase in ATP:ADP ratio **(2)** blocks hyperpolarizing $K_{ATP}$ channels. The resulting depolarization **(3)** of the cell membrane leads to $Ca^{2+}$ influx **(4)**, triggering exocytosis **(5)** and release of insulin into the circulation **(6)**.

While sulfonylureas are widely prescribed because of their effectiveness and relative inexpensiveness, they have a range of off-target effects which limits their therapeutic use. For example, sulfonylureas can provoke prolonged episodes of low blood glucose due to hyperinsulinemia,[128] elevate cardiovascular disease risk,[129] and induce weight gain.[130] Conversely, there is a lack of tools for the precise functional dissection of $K_{ATP}$ channels located not only in the pancreas, but also in the brain, heart and vascular smooth muscle.[131-134] With this in mind, this chapter describes an approach that is set out to combine the glucose-lowering attributes of sulfonylureas with the exquisite spatiotemporal control conferred by possession of photoresponsive elements.[2,135]

A “fourth-generation” sulfonylurea, *viz.* **JB253**, is showcased that based on glimepiride. **JB253** bears an azobenzene photoswitch, endowing $K_{ATP}$ channels with remarkable photocontrollable properties (Figure 44a). It is demonstrated that **JB253** offers sensitive, reversible and repeated manipulation of $K_{ATP}$ channel state and beta cell activity with visible light, yielding optical control over insulin release. Thus, **JB253** may allow the selective targeting of $K_{ATP}$ channels in the pancreas and elsewhere.

## 8.2 Results and Discussion

### 8.2.1 Design and Synthesis of JB253

Distinct substitution patterns are found within different classes of arylsulfonylurea drugs: while there may be a variety of moieties on the aryl-ring, ranging from a simple methyl group in tolbutamide to more complex structures like a linked pyrrolidinone in glimepiride (Figure 44b), the terminal nitrogen in sulfonylureas is usually substituted with an aliphatic group. It can be reasoned that, to generate a photoswitchable analogue, the aromatic core of the sulfonylurea drugs could be extended to an azobenzene. Furthermore, it was aimed for a cyclohexyl substituent on the urea moiety that mimics the corresponding substituent on glimepiride. Using a simple three-step procedure commencing with sulfanilamide, *N*,*N*-diethylaniline and cyclohexyl isocyanate, **JB253** could be synthesized rapidly and inexpensively in large quantities (Figure 44c). Initial photochromic characteristics of **JB253** were measured using a UV/Vis spectrophotometer equipped with a monochromator, affording a single broad band as expected for a push-pull azobenzene system ($\lambda_{max}$ = 472 nm) (Figure 44d).

Azobenzenes are known to be photoconverted between their *cis*- and *trans*-state by excitation with different wavelengths of light, or alternatively by illumination and dark relaxation. Indeed, **JB253** was readily converted to its *cis*-state by applying wavelengths ranging from λ = 400–500 nm (peak λ = 472 nm), while thermal relaxation to its *trans*-state occurred rapidly in the dark. X-Ray diffractometry revealed a high degree of structural similarity between *trans*-**JB253** and glimepiride crystals[136] (Figure 44e) (see Experimental). Whereas glimepiride in solution rotates freely around its ethylene carbon chain to adopt various possible binding conformations, **JB253** is rigid unless illuminated and so can only adopt two conformations depending on its isomeric state (*i.e. trans*- or *cis*-).

Attaching lipophilic azobenzene units normally renders molecules poorly soluble in water and aqueous buffers, an obvious drawback for their use in biological

systems. **JB253**, however, demonstrates excellent water solubility (≥ 0.1 mM) when diluted from a 50 mM stock solution in DMSO, presumably due to its acidity ($pK_a$ = 4.76, Supplementary Figure 4). These features were a promising entry point for the subsequent studies using mammalian cell lines and tissue.

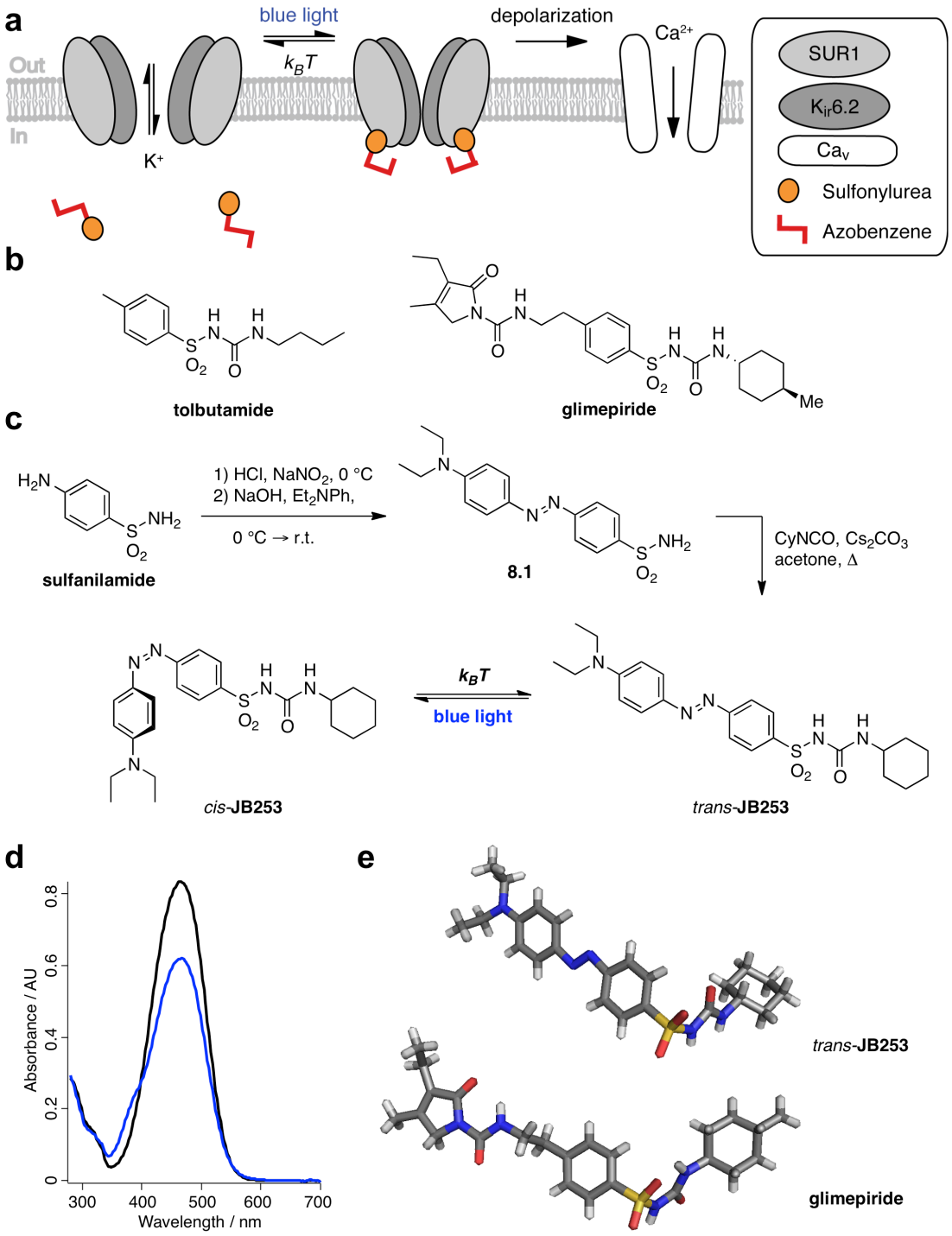


**Figure 44: Photopharmacology of $K_{ATP}$ channels: design, synthesis and characteristics of JB253. a)** The logic of a photoswitchable sulfonylurea: upon photoisomerization to the *cis*-state, **JB253** becomes more active, closing the $K_{ATP}$ channel. Thermal relaxation makes the compound less active or leads to dissociation, restoring the open form of the channel. Closure of $K_{ATP}$ channels leads to depolarization, promoting calcium influx and ultimately insulin release. **b)** Chemical structure of tolbutamide and glimepiride, which served as templates for **JB253**. **c)** Synthesis, structure and switching characteristics of **JB253**.

Sulfanilamide undergoes diazotization and is trapped with *N,N*-diethylaniline to yield an azobenzene-sulfonamide, which is converted to **JB253** by cyclohexyl isocyanate. *trans*-**JB253** can be reversibly switched to *cis*-**JB253** with blue light and relaxes thermally. **d)** UV/Vis spectra of **JB253** in the dark (black) and during constant illumination with 460 nm (blue). **e)** Crystal structure of *trans*-**JB253** (CCDC: 1014606) and glimepiride (CSD: TOHBUN01[136]) showing the structural similarity of both sulfonylureas.

Further congeners were synthesized with similar chemistry: **JB263** (Scheme 9a) and **JB386** (Scheme 9b) have different substitution patterns on the azobenzene and on the sulonylurea, respectively. A crystal structure was furthermore obtained from the crude reaction mixture of **JB386**, which is deprotonated and bound to a cesium cation (Scheme 9c). In the first substitution case (**JB263**), one can tune the maximal absorbance wavelength, while in the second case (**JB386**), the pharmacological unit represents tolbutamide with its *n*-butyl aliphatic chain (synthesized the same way as **JB253** using *n*-butyl isocyanate instead of cycloxyl isocyanate). **JB263** is prepared starting from sulfanilamide via diazotation and reaction with phenol to obtain sulfonamide **8.2**, which is converted to the sulfonylurea in the same way as **JB253**. **JB558** bears a diazathiophene aromatic ring (Scheme 9d), which results in a red-shift of its maximal absorbance wavelength ($\lambda_{max}$ = 530 nm) (Scheme 9e, green line). The synthesis of **JB558** begins with the deacylation of acetazolamide (**AAZ**) to the free amine **8.3**, which can be diazotized with sodium nitrite under strong acidic conditions. The diazonium salt is trapped with *N*,*N*-diethylaniline to yield sulfonamide **8.4**, which is converted to its sulfonylurea counterpart with cyclohexyl isocyanate. **JB263** and **JB386** exhibited their maximal absorbance at $\lambda_{max}$ = 370 nm (Scheme 9e, gray line) and $\lambda_{max}$ = 468 nm (Scheme 9e, purple line), respectively. Similar to **8.4**, a morpholine derived molecule **8.5** was synthesized (Scheme 9f) that was further converted to a sulfonylurea, *viz*. **JB541**. A crystal structure was obtained that showcases the diazathiophene ring in the hetero-azobenzene (Scheme 9g).

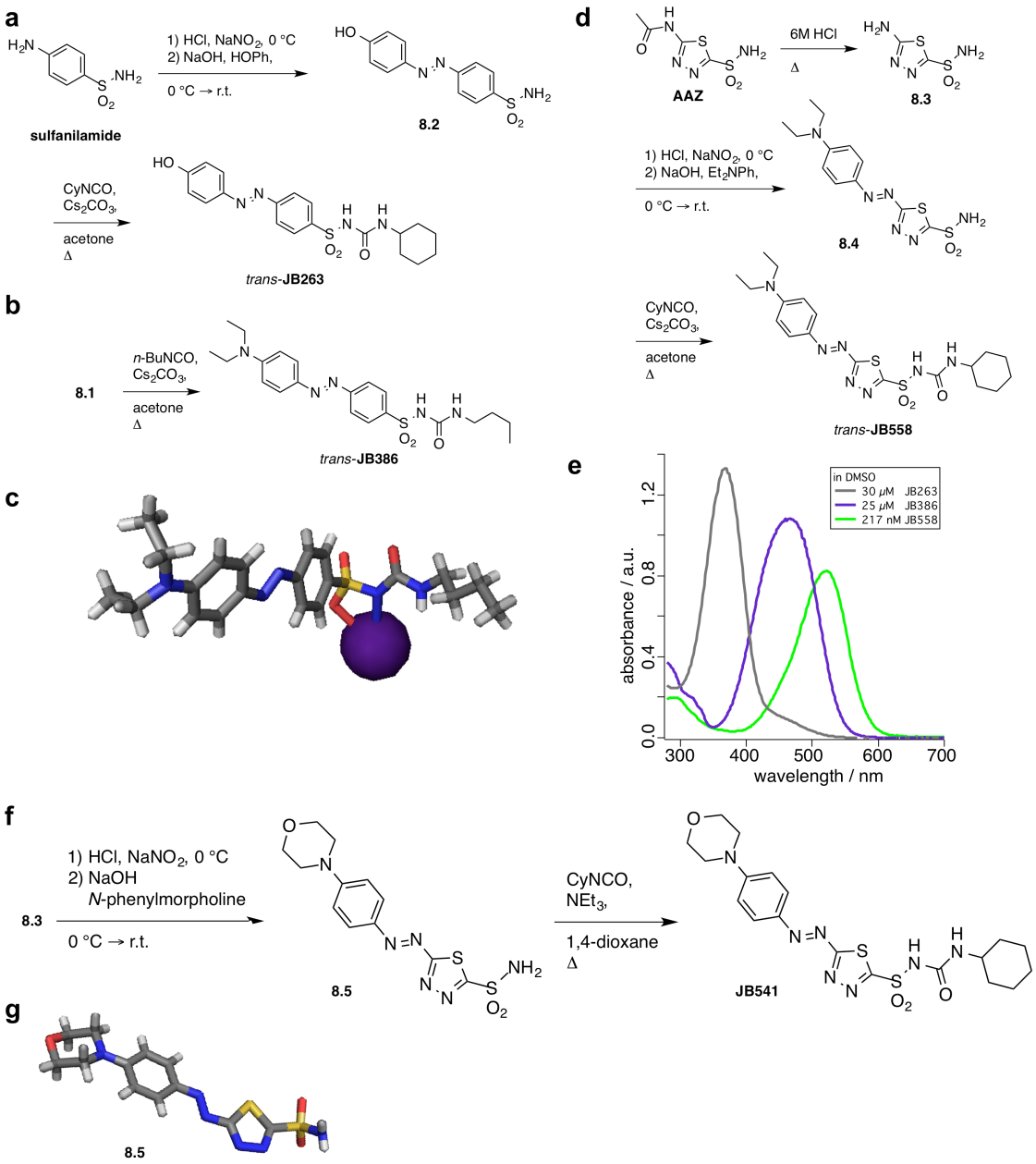


**Scheme 9: Synthesis and spectral characteristics of the JB253 congeners JB263, JB386 and JB558. a) JB263** was obtained by reaction of **8.2** and CyNCO; **b) JB386** was obtained by reaction from **8.1** with *n*-BuNCO and its crystal structure bound to cesium is depicted in **c)**; **d) JB558** was synthesized by deacylation of **AAZ** and subsequent installation of the sulfonylurea with CyNCO; **e)** UV-Vis spectra of **JB263** (gray), **JB386** (purple) and **JB558** (green) in DMSO. **f)** Synthesis of morpholine derivative **8.5** as a precursor for **JB541** including its crystal structure (**g**).

The synthetic route for the preparation of azosulfonylureas does not have to proceed *via* diazotization only but a Mills reaction can also be employed. Starting with the conversion of sulfanilamide to the sulfonylurea **8.6** leaves the aromatic amine in place that can be condensed with aryl nitroso compounds. Depicted in

Scheme 10, **8.6** is reacted with nitrosobenzene and 4-nitroso ethylbenzoate to give **JB030** and **JB243**, respectively. This proves the versatility of azosulfonylurea synthesis for tuning the characteristics of such compounds with respect to their wavelength and for structure activity relationships.

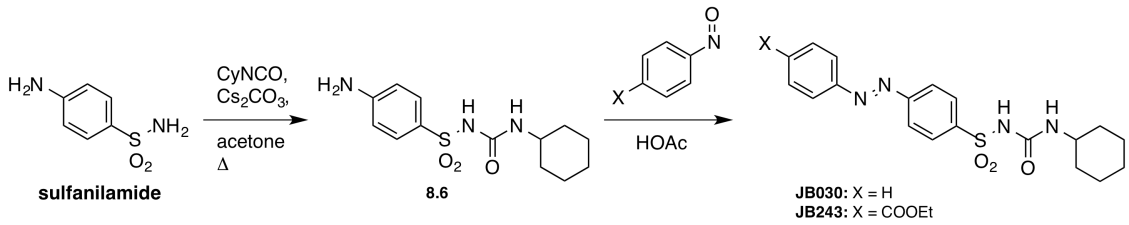


**Scheme 10: Mills reaction for azosulfonylurea synthesis.** Sulfanilamide is reacted with isocyanate to give **8.6** that can be condensed with aryl nitroso compounds to yield for instance **JB030** and **JB243**.

After all synthetic efforts, however, **JB253** exhibited the best results in preliminary electrophysiological testing, so the focus lies on this molecule in the studies described in this chapter.

### 8.2.2 JB253 Binding Studies

To determine the binding affinity of **JB253** to SUR1 relative to a known sulfonylurea (*i.e.* glimepiride), [3H]-glibenclamide displacement assays were performed. **JB253** bound SUR1 with a 1000-fold lower affinity compared to glimepiride, and this was unaffected by illumination ($IC_{50}$ = 8.3 nM *versus* 17.6 µM *versus* 14.8 µM for glimepiride *versus* *trans*-**JB253** *versus* *cis*-**JB253**, respectively) (Figure 45a). However, due to the potential for rapid thermal dark-relaxation during the wash cycles (see below), a role for *trans*- to *cis*-isomerization can not be excluded in strengthening **JB253** binding affinity. Therefore, to compare the activity profiles of *trans*-**JB253**, *cis*-**JB253** and glimepiride using a functionally-relevant readout, concentration-response experiments were conducted in mouse islets. The $EC_{50}$ of *cis*-**JB253** for cytosolic $Ca^{2+}$ rises was found to be 675 nM, similar to that obtained for glimepiride in the same system ($EC_{50}$ glimepiride = 399 nM) (Figure 45b). The concentration-response curve for glimepiride was right-shifted in the presence of a saturating

concentration of *trans*-**JB253**, demonstrating the presence of competitive agonism even under dark conditions (Figure 45b).

Since most sulfonlyureas have been reported to bind and activate Exchange Protein directly Activated by cAMP 2A (Epac2A),[137] an important mediator of insulin secretion,[138,139] the presence of interactions with **JB253** was assessed using a *Förster resonance energy transfer (*FRET)-based approach. To enable this, a full length Epac2-camps biosensor containing the sulfonylurea binding site was encoded in HEK293t cells.[138] Confirming the existence of sufonylurea-Epac2A interactions, application of either glimepiride (Figure 45c) or *cis*-**JB253** (Figure 45d) decreased FRET to a similar extent ($\Delta R/R_o$ = 0.052 *versus* 0.064 AU, glimepiride *versus cis*-**JB253**, respectively; NS, non-significant, Student's t-test).

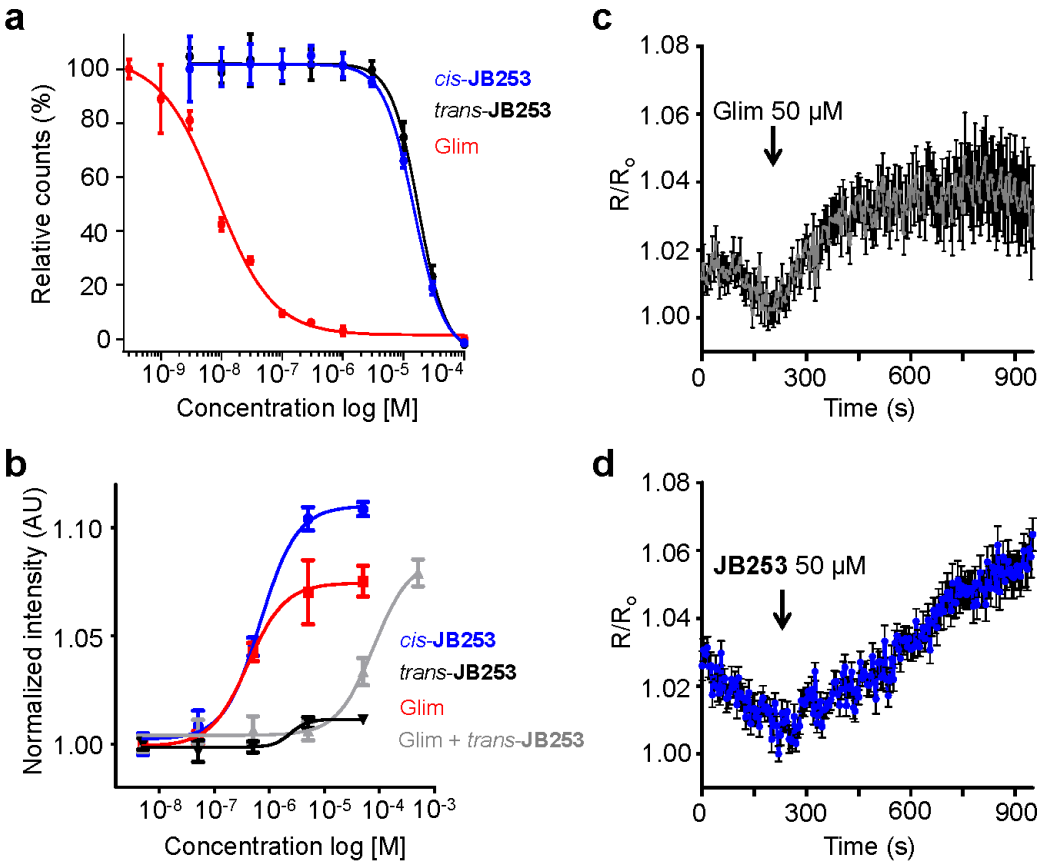


**Figure 45: JB253 binding and concentration-response studies. a)** Binding affinity of glimepiride (Glim) (red, $IC_{50}$ = 8.3 nM), *trans*-**JB253** (black, $IC_{50}$ = 17.6 µM) and *cis*-**JB253** (blue, $IC_{50}$ = 14.8 µM) were indirectly determined in SUR1-expressing HEK293t cells using displacement of [3H]-glibenclamide. Note that, due to the potential for thermal dark-relaxation during the harvesting and washing steps, effects of photoswitching on **JB253** binding affinity could not be excluded. Values represent the mean ± SD. **b)** *cis*-**JB253** and glimepiride (Glim) possess similar concentration-response curves for the stimulation of $[Ca^{2+}]_i$ in

mouse islets, while *trans*-**JB253** is largely ineffective. The concentration-response for glimepiride is right-shifted in the presence of a saturating concentration (100 μM) of trans-**JB253** (*n* = 3-5 recordings). **c)** HEK293t cells expressing a full length Epac2-camps probe respond to glimepiride with decreases in *Förster resonance energy transfer (*FRET) (represented here as an increase in $R/R_o$) (*n* = 28 cells from 4 recordings). **d)** As for **c)** but *cis*-**JB253**. Values represent the mean ± SEM for **c)-d)**.

### 8.2.3 JB253 allows Photoswitching of $K_{ATP}$ Channels

First investigations whether **JB253** could yield optical control over $K_{ATP}$ channel activity using a system free from confounding effects of glucose metabolism were conducted. To enable this, $K_{ATP}$ channels were heterologously expressed in HEK293t cells by transfection with plasmids encoding the Kir6.2 and SUR1 subunits along with GFP. Tolbutamide and diazoxide-sensitive inward-rectifying $K^+$ currents could be recorded in transfected cells, confirming the functional assembly of $K_{ATP}$ channels. In the dark state, **JB253** partly reduced $K^+$ current amplitude within a few seconds. This was however a fraction of that observed during 500 μM tolbutamide application (Supplementary Figure 5a and b). Subsequent illumination of **JB253** with wavelengths between 400-500 nm further closed the channel (Figure 46a), with ~45-72% block being achieved relative to that recorded using 500 μM tolbutamide (Supplementary Table 11). The reversal potential was close to the expected equilibrium potential for $K^+$, and this was unaffected by molecule orientation (-90.0 ± 1.8 *versus* -87.8 ± 1.6 mV, dark *versus* illuminated; non-significant) (Supplementary Figure 5c and d). As such, **JB253** possesses the advantageous property of becoming a high affinity $K_{ATP}$ channel blocker upon illumination.

Using a wavelength of 400 nm, heterologously-expressed $K_{ATP}$ channels could be repeatedly opened and closed in **JB253**-treated preparations without obvious desensitization (difference in ΔI [pA] between first and last switch = 14.9 ± 7.6 %) (Figure 46b and c) (Supplementary Tables 12 and 13). Upon switching to 400 nm, rapid block was observed ($\tau_{on}$ = 0.4 s) (Figure 46c). When the light source was shut off, thermal relaxation was fast, returning the $K_{ATP}$ channel to baseline levels within a couple of seconds ($\tau_{off}$ = 1.5 s) (Figure 46c) (Supplementary

Tables 11 and 12). While maximal photoblock of $K_{ATP}$ channels was observed at 460 nm, significant effects were also obtained with violet light (*i.e.* 405 nm), which was more compatible with fluorescence imaging of pancreatic beta cell function (see below). Confirming that **JB253** could photoswitch endogenous $K_{ATP}$ channels, hyperpolarizing currents were reversibly blocked in MIN6 beta cells following illumination (Supplementary Figure 6).

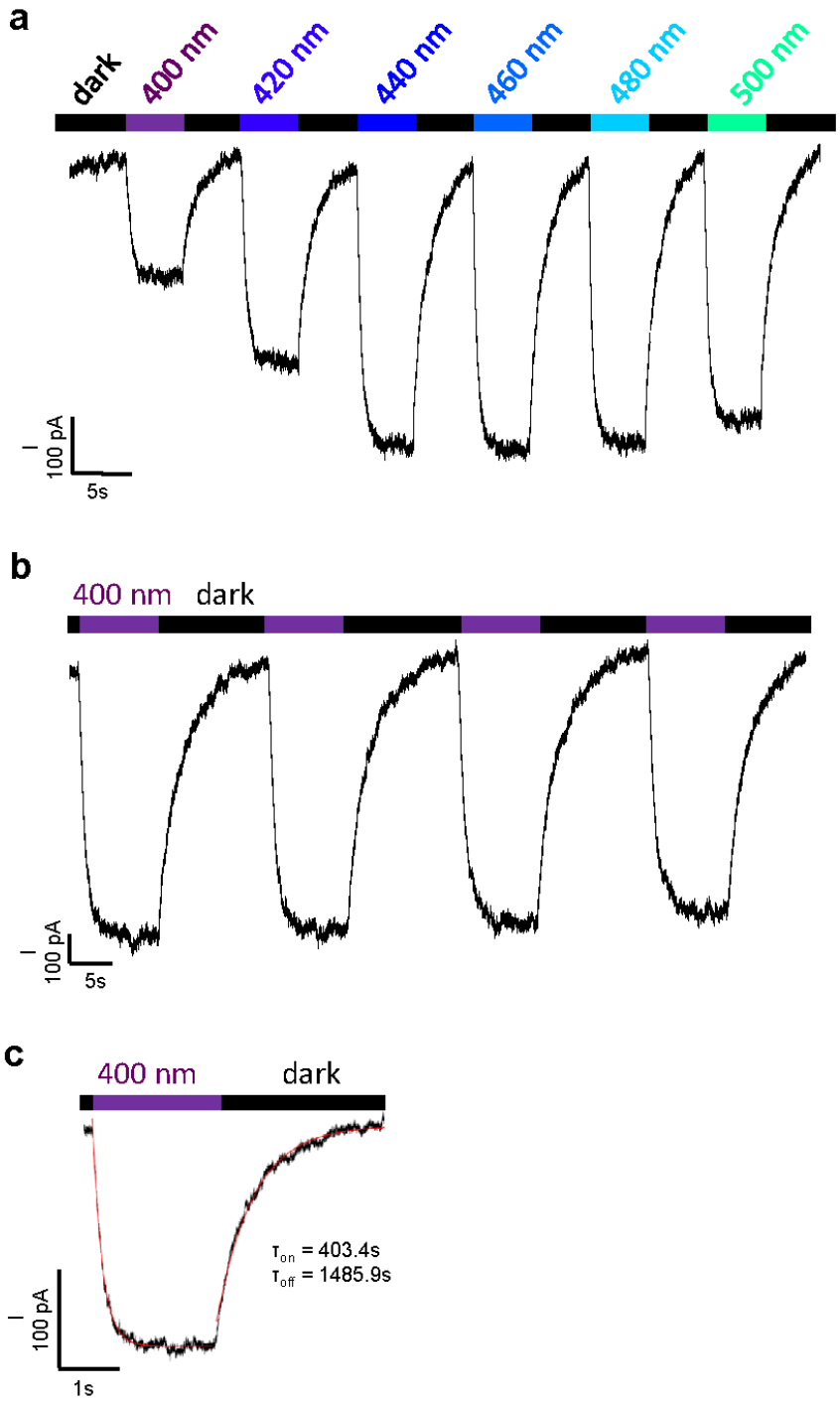


**Figure 46: JB253 confers photoswitching on $K_{ATP}$ channels: a)** Photocurrents recorded from HEK293t cells transfected with plasmids encoding Kir6.2 and SUR1 using the whole cell patch clamp configuration (holding potential -60 mV). **JB253**-treated cells respond to wavelengths between 400-500 nm with a reduction in the magnitude of the $K^+$ inward rectifier current. **b) JB253** allows reversible and repeated closure of $K_{ATP}$ channels in response to light-dark cycles using λ = 400 nm to induce *cis*-isomerization (purple) and relaxation in the dark (black). **c)** Kinetics of light-triggered block and thermal restoration of $K_{ATP}$ channel currents mediated by **JB253**.

### 8.2.4 Functional Interrogation of Beta Cell Activity within Intact Mouse Islets of Langerhans

Stimulus-secretion coupling in beta cells relies on the closure of $K_{ATP}$ channels, $Ca^{2+}$ influx through VDCC and release of insulin granules.[124] Therefore, attempts to manipulate beta cell activity by optically controlling $K_{ATP}$ channels with **JB253** were made.

Using functional multicellular $Ca^{2+}$ imaging (fMCI) to monitor cell activity directly *in situ* within intact islets,[140,141] increases in cytosolic free $Ca^{2+}$, assumed largely to emanate from beta cells under the conditions used here,[142] could be evoked following global illumination using a 405 nm laser (Figure 47a) ($n$ = 10 recordings). Just over half (54 %) of the fluo-2-loaded population responded to illumination with synchronous $Ca^{2+}$ rises (Figure 47a and b). Demonstrating the utility of **JB253** for the fine control of beta cell function, discrete $Ca^{2+}$ oscillations, thought to underlie generation of insulin pulses,[143,144] could be imposed using repeat exposure to 405 nm (Figure 47c). As anticipated, high doses of tolbutamide and diazoxide were able to augment and suppress, respectively, the effects of **JB253** (Figure 47d and e) ($n$ = 4-6 recordings).

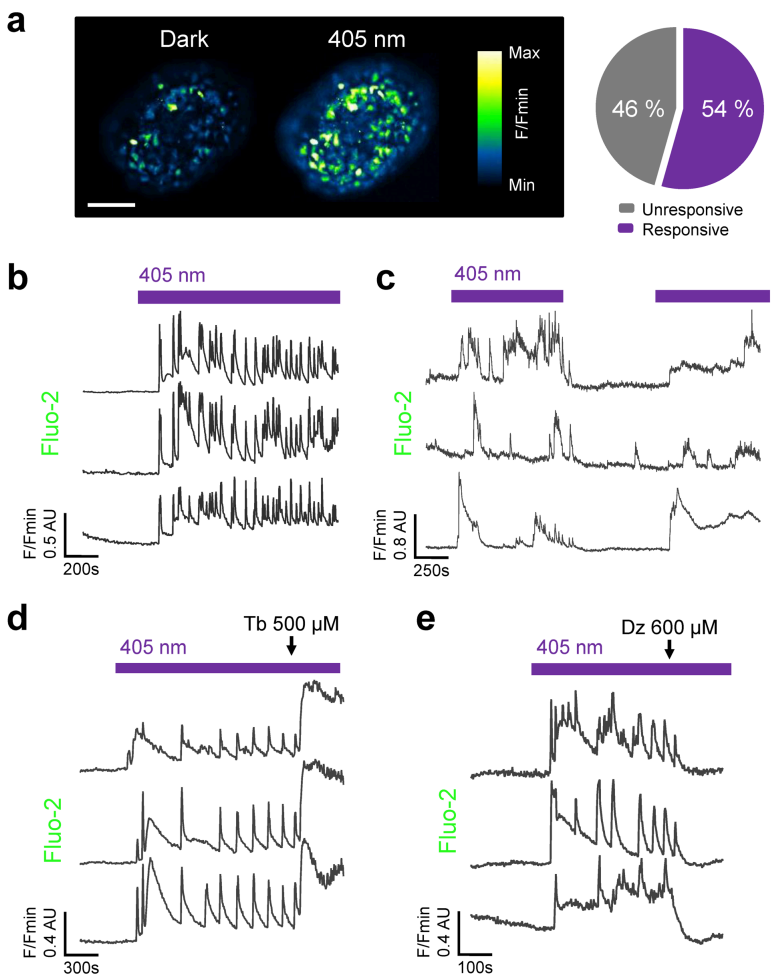


**Figure 47: JB253 allows optical manipulation of pancreatic beta cell activity. a)** Beta cells residing within **JB253**-treated islets display large increases in cytosolic $Ca^{2+}$ following exposure to 405 nm (purple) (scale bar, 110 µm). **b)** 405 nm illumination induces large and synchronous rises in $Ca^{2+}$ as indicated by Fluo-2. **c)** JB253 can be used to impose complex dynamics including $Ca^{2+}$ oscillations. **d)** High dose tolbutamide (Tb) augments the effects of **JB253** on $K_{ATP}$ channel blockade. **e)** Diazoxide (Dz) inhibits **JB253** effects by opening the $K_{ATP}$ channel ion pore. Traces represent *n* = 5-10 recordings.

The wavelength required to excite Fluo-2 (λ = 491 nm), a commonly used $Ca^{2+}$ indicator, could potentially lead to $K_{ATP}$ channel closure in **JB253**–treated islets due to *cis*-isomer formation. Therefore, the above experiments were repeated using the red (λ = 561 nm)-excited $Ca^{2+}$ indicator X-Rhod-1. Identical results were obtained to studies with Fluo-2 (Figure 48a and b) (63% responsive X-Rhod-1-loaded cells) (*n* = 3 recordings), confirming that the photostationary state of **JB253** during brief (263 ms) pulses of 491 nm light was alone

insufficient to close $K_{ATP}$ channels in the islet preparation. Likewise, global $Ca^{2+}$ oscillations could be induced in **JB253**–treated islets by more prolonged illumination with 440 nm and 491 nm laser lines and, as expected from the electrophysiological recordings, both wavelengths appeared to activate a slightly larger cell population (Figure 48c and d). These observations were unlikely due to $K_{ATP}$ channel closure at 561 nm, since **JB253** was unable to photoswitch $K^+$ currents at wavelengths > 560 nm (Supplementary Figure 7).

Demonstrating the spatial precision of **JB253**, a single islet from a doublet could be activated using a targeting laser without significantly stimulating its neighbor (~ 200 μm from center to center) (Figure 48e), in part aided by the high molecule extinction coefficient (38670 $mol^{-1}$ $cm^{-1}$ at 485 nm; see Experimental). Lastly, **JB253** did not appear to be cytotoxic to islets, as necrosis indices showed no significant differences in cell death *versus* DMSO-alone (Figure 48f).

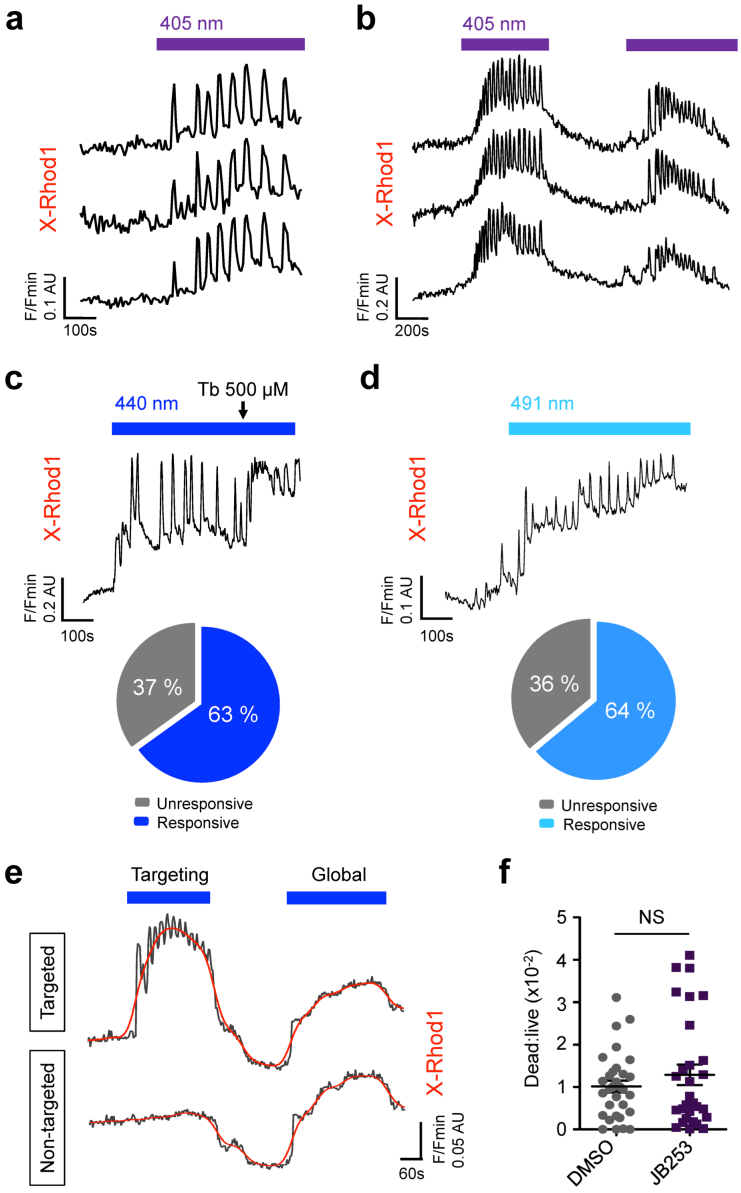


**Figure 48: Specific photoswitching of beta cell function in the violet-blue spectrum. a) JB253**-treated cells loaded with the red-shifted $Ca^{2+}$ indicator X-Rhod1 (λ excitation = 561 nm) similarly respond to 405 nm with $Ca^{2+}$ rises. **b)** As for **a)** but imposition of oscillations. **c) JB253**-treated beta cells display large increases in cytosolic $Ca^{2+}$ following exposure to 440 nm. **d)** As for **c)**, but following illumination with 491 nm (Tb, tolbutamide; positive control). **e)** A single islet can be photoswitched using a targeting laser while leaving its neighbor quiescent (~ 200 µm center-center). A global laser pulse evokes activity in both islets (grey, raw; red, smoothed). **f)** Incubation of islets with JB253 does not alter cell viability as assessed by calcein AM and propidium iodide incorporation (NS, non-significant *versus* DMSO-alone, Mann-Whitney U-test) (*n* = 28 islets from four animals). In all cases, traces represent *n* = 4-6 recordings. Values represent mean ± SEM.

### 8.2.5 Manipulation of human Islet Function using JB253

To underline the translational potential of **JB253** for use in man, $Ca^{2+}$-imaging experiments were repeated using isolated human islets of Langerhans. As observed for their mouse counterparts, beta cells within **JB253**-treated human islets responded to 440 nm and 491 nm with large intracellular $Ca^{2+}$ rises, and oscillations could be coaxed simply by turning the laser on and off (Figure 49a-c). **JB253** effects appeared to be due to $K_{ATP}$ blockade, as they could be mimicked and reversed using tolbutamide and diazoxide, respectively (Figure 49c and d).

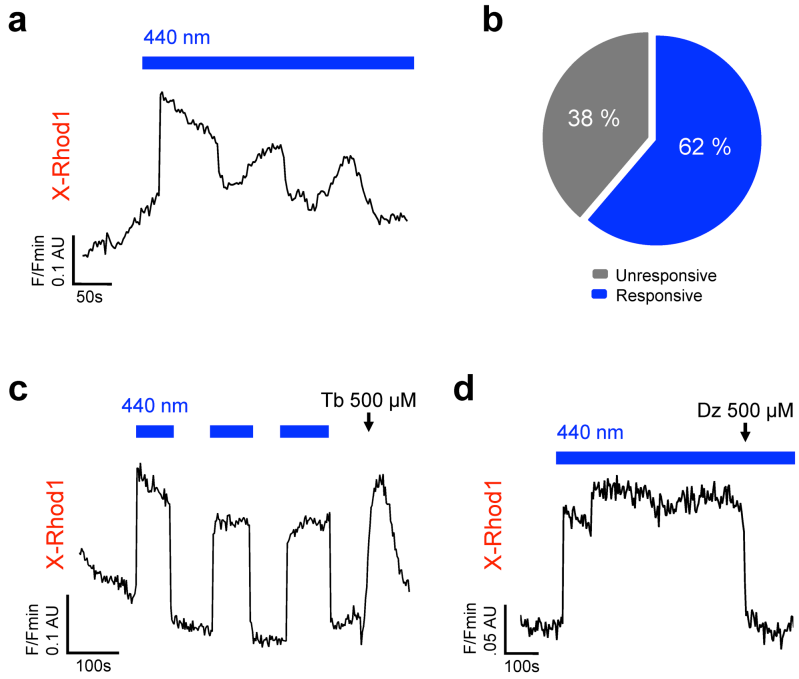


**Figure 49: Manipulation of human islet activity using JB253. a) JB253**-treated beta cells residing within intact human islets respond to 440 nm with rapid rises in cytosolic $Ca^{2+}$ levels. **b)** Almost 62% of X-Rhod1-loaded cells respond to **JB253** with $Ca^{2+}$ rises. **c)** As for a) but imposition of oscillations to demonstrate reversibility of **JB253** effects in human tissue (Tb, tolbutamide; positive control); **d)** Reversal of **JB253** action using diazoxide to open the $K_{ATP}$ channel ion pore (Dz, diazoxide; negative control). Traces represent $n$ = 6-7 islets from three donors.

### 8.2.6 Optical Stimulation of Insulin Release using JB253

To cement the link between photocontrol of $K_{ATP}$ channels, $[Ca^{2+}]_i$ and insulin secretion, islets (from $n$ = 10 mice) were incubated in the presence of **JB253** while being exposed to either dark, 405 nm or 485 nm. Insulin release was

similar in control experiments (5 mM glucose; shown to sensitize beta cells to sulfonylurea[145]) and **JB253**-treated islets in the dark, suggesting that any $K_{ATP}$ channel block and VDCC activity detected under these conditions was subthreshold for triggering $Ca^{2+}$-activated exocytosis (Figure 50). By contrast, **JB253**-treated islets secreted almost 4-8-fold more insulin following illumination, and this could be partially reversed using diazoxide (Figure 50). When exposed to 485 nm light, **JB253** was equipotent to glimepiride at stimulating insulin secretion (Figure 50).

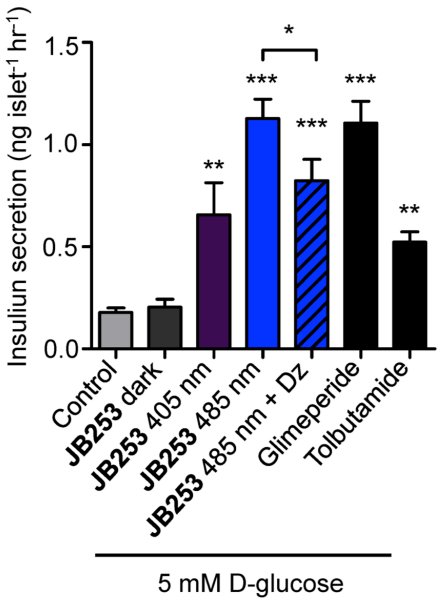


**Figure 50: JB253 yields optical control of insulin secretion. a)** Application of **JB253** under dark conditions is unable to influence insulin release *versus* control (5 mM glucose-alone) during static incubation of islets. By contrast, illumination with 405 nm and 485 nm significantly increases insulin secretion, and this is similar in magnitude to that achieved using glimepiride and tolbutamide (*n* = 9 mice) (*P<0.05 *versus* **JB253** 485 nm; **P<0.01 and ***P<0.001 *versus* G5; one-way ANOVA). Values represent mean ± SEM.

## 8.3 Discussion

In the present study, the development and testing of **JB253**, a chemical chimera of glimepiride and an azobenzene, which allows light-induced closure of $K_{ATP}$ channels is described. In the primary tissue employed here, *viz* islets of Langerhans, this translates to activated $Ca^{2+}$ flux and insulin release.

The principles of photopharmacology, *i.e.* the control of biological function with small molecule photoswitches, are now well-established.[2,3,146] In particular, azobenzene photoswitches have been employed as photochromic neurotransmitters and neuromodulators,[84,147] ion channel blockers,[50,135] covalently-bound ion channel gates[11] and enzyme inhibitors.[43,148] With respect to ion channels, however, they have mostly been used to optically control excitable cells in the mammalian nervous system, and none have directly targeted $K_{ATP}$ channels. These are ubiquitously-expressed channels that contribute to membrane potential in a number of cell types including hypothalamic and hippocampal neurons, cardiac myocytes, vascular smooth muscle and neuroendocrine cells.[122,131-134] Importantly, $K_{ATP}$ channels translate metabolic state to transmembrane potential and, in pancreatic beta cells, are central to glucose-stimulated insulin secretion.[121,122,124] Since electrical status is generally correlated to biological output in excitable tissues, **JB253** may provide a useful tool for investigating $K_{ATP}$ channel function under a range of normal and pathological states.

The prevailing view of sulfonylurea action is one of SUR1 binding, KATP channel closure and alterations to beta cell membrane potential.[118-120] However, recent studies have also invoked a K-ATP-independent signaling pathway whereby sulfonylurea may alter insulin release via Epac2A interactions.[137-139] Using radioactive displacement assays in combination with FRET experiments, **JB253** was found to interact with both SUR1 and Epac2A. While SUR1 affinity for **JB253** was much lower than glimepiride, the active *cis*-state due to rapid thermal back-relaxation could not be properly accessed. As such, a role for illumination in strengthening any interaction cannot be excluded *e.g.* by altering binding

conformation due to isomerization. Nonetheless, binding affinity does not necessarily predict sulfonylurea behavior.[149] Indeed, **JB253** and glimepiride possess similar $EC_{50}$ values for intracellular $Ca^{2+}$ rises and, when applied at the same concentration, both compounds stimulated almost identical levels of insulin secretion. Thus, **JB253** possesses a similar activity profile to glimepiride, most likely due to signaling via pathways generally acknowledged to underlie sulfonylurea action.

In addition to photopharmacology, optogenetic and artificial light-sensitive $K^+$ channels are equally applicable to the remote control of electrically-responsive cells, including beta cells.[150,151] However, therapeutic potential in humans is limited by the requirement for genetic manipulation, high activation irradiances and the hyperpolarizing effects of recombinantly-expressed Kir6.2. Alternatively, an implantable synthetic optogenetic transcription device has recently been shown to improve blood-glucose homeostasis in a mouse model of T2DM *via* the expression and secretion of incretin.[152] However, debate still exists as to whether incretin-based therapies are associated with increased risk of pancreatitis and pancreatic adenocarcinoma.[153,154] Nonetheless, similar concepts have recently been extended to designer fusion molecules and may in the future be adopted for insulin release.[155] By contrast, due to its favorable profile as an exogenously-applied sulfonylurea which is sensitive to light, **JB253** has advantages both as a research tool and as an anti-diabetic agent. It should be noted, however, that confirmation of glucose-lowering effects in rodents is required before studies using **JB253** can be extended to man.

In the context of photodynamic therapy, light penetration in human tissues has been studied in detail and is now well-understood.[156] Although the current activation wavelength of **JB253** (400-500 nm) limits deep tissue penetration, *e.g.* through the skin, the development of variants which can be switched at longer wavelengths has been carried out in parallel. For instance, **JB558** exhibits its maximal absorbance at 530 nm and will be tested in ongoing studies towards the targets described above. In addition, stimulated by the brisk development of optogenetics,[4] devices that can deliver light to target tissues with minimal

invasiveness and high spatial precision have emerged,[18,19] although their application to the pancreas is untested.

It can therefore speculated that **JB253** or related photoswitchable molecules that regulate $K_{ATP}$ channels may have an impact on human medicine and research. A long-standing challenge in endocrinology has been the inability to properly recreate the dynamics that underlie pulsatile hormone release, a prerequisite for proper downstream organ function.[157] Furthermore, disparate biological systems can use similar or identical molecular components. For example, $K_{ATP}$ channels are also expressed in the heart and brain, including in neuronal populations tasked with the central regulation of glucose homeostasis and counterregulatory responses.[133,158] Photopharmacology has the ability to target drug activity to the primary site of dysfunction with high spatial and temporal resolution.[3] **JB253** holds particular promise in this regard. It is non-cytotoxic and can be used to repeatedly modulate rodent and human beta cell activity, the basis for recreating the oscillatory activity known to orchestrate hormone pulses.[143,144] Its light-dependency means that **JB253** activity is spatially-restricted by illumination, potentially reducing extra-pancreatic effects. Finally, the ability to 'turn on' or 'turn off' **JB253** action would allow insulin secretion to be tailored to peak demand. Therefore, pending thorough *in vivo* validation, **JB253** and its congeners could potentially open up new avenues for the treatment of T2DM.

## 8.4 Summary and Outlook

In summary, a light-sensitive sulfonylurea, **JB253**, has been designed and synthesized that has a broad spectrum of application due to conferment of photoswitching on $K_{ATP}$ activity. Even more, **JB253** congeners have been synthesized with different characteristics. These include **JB263** (an hydroxy-substituted version of JB253 that results in blueshifting of its maximal absorbance wavelength), **JB386** (a *n*-butyl substituted version of **JB253** resembling tolbutamide) and **JB558** (a very red-shifted version of **JB253**). All these compounds will be tested for their photopharmacology in the same way as **JB253**. Furthermore, *in vivo* experiments will be performed in healthy and diabetic mice to evaluate a possible glucose-lowering effect in the body, which would mark the entry point into translational medicine.

## 8.5 Supplementary Figures and Tables

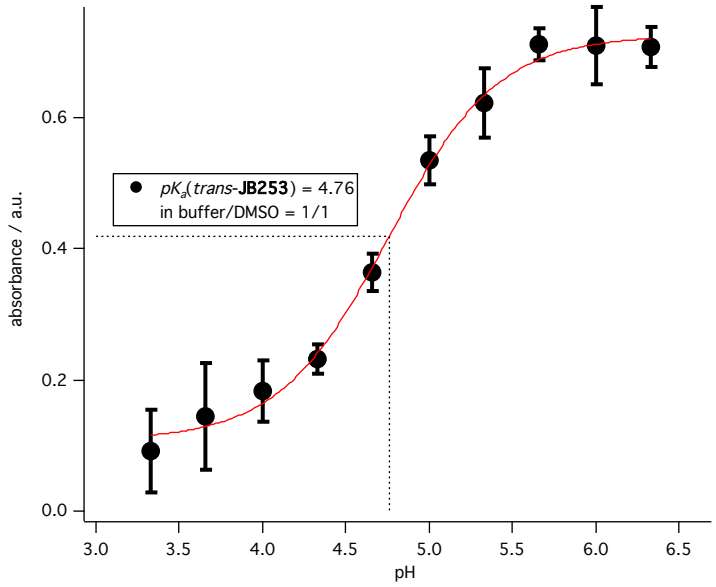


**Supplementary Figure 4: $pK_a$ of JB253 aquired according to Martinez *et al.*[159] utilizing a platereader assay.**

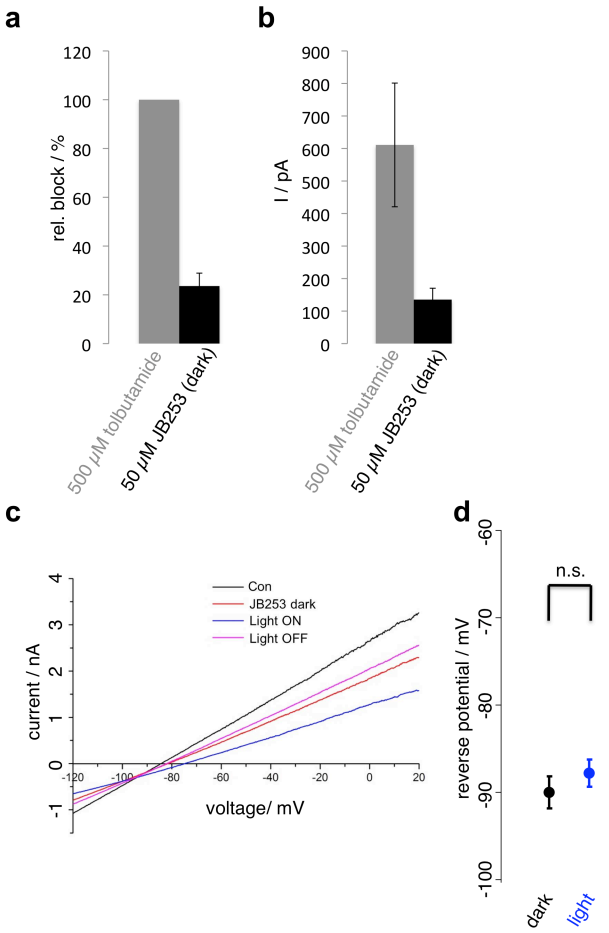


**Supplementary Figure 5: $K_{ATP}$ channel block characteristics of JB253 in the dark. a)** To account for cell-cell variation in current densities, magnitude block with **JB253** (dark) was calculated as a percentage *versus* that achieved with 500 µM tolbutamide in the same experiment (%± SEM; *n* = 3). **b)** Bar graph displaying the amplitude of the inward current (ΔI [pA]) at -60 mV elicited by application of either tolbutamide or **JB253** in the dark (current ± SEM, *n* = 3). **c)** Representative current-voltage (IV) relationships showing a minor decrease in membrane conductance upon application of JB253 in the dark (before drug = black; after drug = orange). This inhibition is reversibly enhanced by exposure to blue light (blue = ON; pink = OFF). **d)** Mean reversal potential ($E_{rev}$) before and after illumination of **JB253** measured in recordings as depicted in c). (NS, non-significant, *trans*-**JB253** *versus cis*-**JB253**; Student's paired t-test) (mV ± SEM, *n* = 5 independent recordings).

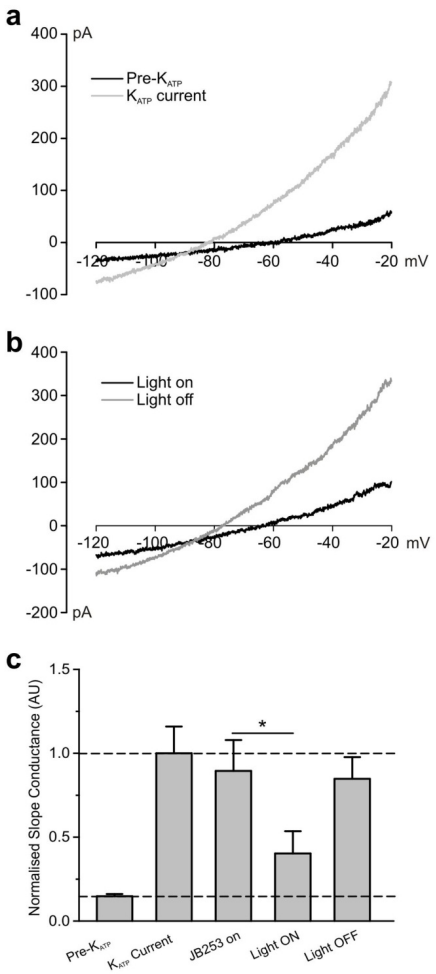


**Supplementary Figure 6: JB253 reversibly blocks $K_{ATP}$ currents in MIN6 beta cells. a)** Representative current-voltage (IV) relationships recorded straight after establishing the whole-cell configuration (Pre-$K_{ATP}$) and after development of the $K_{ATP}$ current due to wash-out of ATP from the cell (Peak $K_{ATP}$ current). **b)** IVs from the same cell as a) in the presence of either *trans*-**JB253** (light off) or *cis*-**JB253** (light on). **c)** Bar graph displaying mean data from experiments as shown in a) and b). Slope conductance was normalized to peak $K_{ATP}$ current. Note that at this concentration (10 μM) **JB253** only blocks the $K_{ATP}$ current during illumination and this is readily reversed when the light source is shut off (*P<0.05 *versus* **JB253** dark; one-way ANOVA) (*n* = 4 independent recordings).

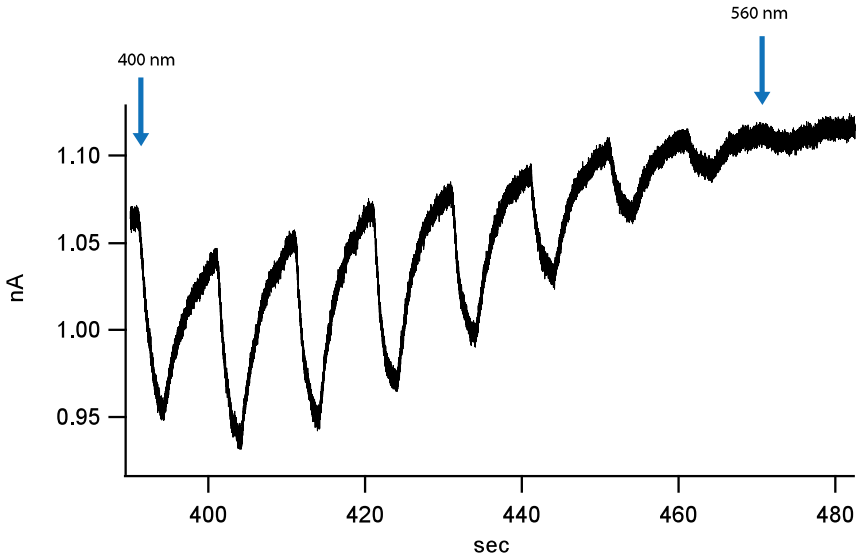


**Supplementary Figure 7: Extended JB253 action spectrum. JB253** is unable to photoswitch $K_{ATP}$ currents in HEK293t cells transfected with Kir6.2 and SUR1 at wavelengths > 560 nm (holding potential -60 mV).

**Supplementary Table 14: Wavelength-dependent kinetics and current change in JB253-treated cells.** On/off kinetics for various wavelengths are shown in ms ± SD (*n* = 3). Current change is expressed as percentage (% ± SD)-block *versus* that obtained with tolbutamide in the same experiment (*n* = 3). Current change (ΔI [pA]) for a single representative experiment is displayed. In all cases, cells were exposed to 500 µM tolbutamide before washout and application of 50 µM **JB253.**

| λ [nm] | $\tau_{on}$ [ms] | $\tau_{off}$ [ms] | % block | ΔI [pA] |
|---|---|---|---|---|
| 400 | 1176±385 | 2758±745 | 44.0±29.6 | 216 |
| 420 | 1309±438 | 2209±482 | 69.4±51.1 | 492 |
| 440 | 1246±421 | 2295±397 | 70.0±44.3 | 440 |
| 460 | 1181±447 | 1940±322 | 72.8±48.1 | 481 |
| 480 | 1163±434 | 2183±422 | 72.4±49.0 | 487 |
| 500 | 1244±462 | 2002±354 | 70.2±49.5 | 482 |

**Supplementary Table 15: Kinetics and current change during a repetitive illumination cycle.** On/off kinetics are shown as ms ± SEM and current change as pA ± SEM calculated following four dark/400 nm cycles. Values are from a single cell.

| $\tau_{on}$ [ms] | $\tau_{off}$ [ms] | ΔI [pA] |
|---|---|---|
| 477±26 | 1472±75 | 504.8±6.9 |

**Supplementary Table 16: Current change for first and last switch for all experiments.** The difference in current change (ΔI [pA]) between the first and last switch (400nm) is represented as a percentage (%).

| Experiment # | ΔI [pA] first switch | ΔI [pA] last switch | Cycles | Difference (%) |
|---|---|---|---|---|
| 1 | 136.5 | 89.5 | 12 | 34.4 |
| 2 | 438.8 | 423.8 | 9 | 3.4 |
| 3 | 200.0 | 161.0 | 5 | 19.5 |
| 4 | 521 | 510 | 4 | 2.1 |

## 8.6 Experimental

### 8.6.1 Synthesis

#### 8.6.1.1 (*E*)-4-((4-(Diethylamino)phenyl)diazenyl)benzenesulfonamide (8.1)

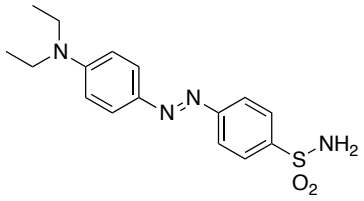

Sulfanilamide (2.00 g, 11.61 mmol, 1.0 eq.) was dissolved in 2.4 M HCl and cooled to 0 °C. Under vigorous stirring, a solution of $NaNO_2$ (0.96 g, 13.91 mmol, 1.2 eq.) in 6 mL water was added drop-wise until the solution turned pale yellow. The formed diazonium salt was stirred submerged in an icebath for an additional 10 minutes before it being transferred to a solution of *N*,*N*-diethylaniline (1.73 g, 11.61 mmol, 1.84 mL, 1.0 eq.) in a 1/1 mixture of 1 M NaOAc/MeOH. The solution turned to dark red and was allowed to warm to r.t. under stirring. The crude product was extracted with EtOAc (3x), and the combined organic layers were washed with brine and dried over $MgSO_4$. Flash column chromatography (25% EtOAc/*i*-hexanes) yielded 1.45 g (4.37 mmol) of **2** in 38% yield.

**$^1$H NMR** (400 MHz, DMSO-$d_6$): $\delta$ [ppm] = 7.95 (d, $J$ = 8.6 Hz, 2H), 7.88 (d, $J$ = 8.6 Hz, 2H), 7.81 (d, $J$ = 9.2 Hz, 2H), 7.45 (s, 2H), 6.82 (d, $J$ = 9.3 Hz, 2H), 3.47 (q, $J$ = 7.0 Hz, 4H), 1.15 (t, $J$ = 7.0 Hz, 6H).

**$^{13}$C NMR** (101 MHz, DMSO-$d_6$): $\delta$ [ppm] = 154.2, 150.8, 143.8, 142.2, 126.9, 125.8, 121.9, 111.1, 44.2, 12.5.

**HRMS** (ESI): calc. for $C_{16}H_{21}N_4O_2S^+$ $(M+H)^+$: 333.1380, found: 333.1377.

**$R_t$** (LCMS; MeCN/$H_2O$/formic acid = 10/90/0.1 → 90/10/0.1 over 7 min) = 4.364 min.

**UV/Vis** (LCMS): $\lambda_{max}$ = 460 nm.

### 8.6.1.2 (*E*)-*N*-(Cyclohexylcarbamoyl)-4-((4-(diethylamino)phenyl)-diazenyl)benzenesulfonamide (JB253)

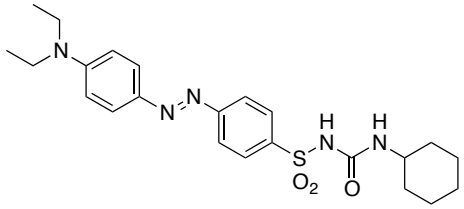

A mixture of (*E*)-4-((4-(diethylamino)phenyl)diazenyl)benzenesulfonamide (**8.1**) (332 mg, 1.0 mmol, 1.0 eq.) and $Cs_2CO_3$ (326 mg, 4.0 mmol, 4.0 eq.) in acetone (20 mL) was refluxed for 1 h before addition of cyclohexyl isocyanate (125 mg, 1.0 mmol, 119 µL, 1.0 eq.) diluted in acetone (20 mL). The reaction mixture was refluxed for an additional 3 h, before cooling to ~40 °C. The crude solid was filtered and washed with small amounts of acetone before being carefully dissolved in MeOH to yield 450 mg (0.98 mmol) of **JB253** in 98% yield.

**$^1$H NMR** (400 MHz, DMSO-$d_6$): $\delta$ [ppm] = 7.83 (d, *J* = 8.5 Hz, 2H), 7.78 (d, *J* = 9.1 Hz, 2H), 7.69 (d, *J* = 8.5 Hz, 2H), 6.80 (d, *J* = 9.3 Hz, 2H), 5.62 (br s, 2H), 3.46 (q, *J* = 7.0 Hz, 4H), 3.27 – 3.14 (br s, 1H), 1.86 – 1.38 (m, 5H), 1.33 – 0.92 (m, 11H).

**$^{13}$C NMR** (101 MHz, DMSO-$d_6$): $\delta$ [ppm] = 172.7 (HMBC, see spectra), 152.6, 150.2, 148.5, 142.2, 127.4, 125.3, 120.8, 111.0, 47.8, 44.1, 33.5, 25.5, 24.9, 12.5.

**HRMS** (ESI): calc. for $C_{23}H_{32}N_5O_3S^+$ $(M+H)^+$: 458.2220, found: 458.2219.

**$R_t$** (LCMS; MeCN/$H_2O$/formic acid = 10/90/0.1 → 90/10/0.1 over 7 min) = 5.285 min.

**UV/Vis** (100 µM in DMSO): $\lambda_{max}$ = 472 nm; (LCMS): $\lambda_{max}$ = 468 nm.

**Extinction coefficients** (Ringer solution): $\varepsilon_{405\ nm}$ = 18501 $mol^{-1}$ $cm^{-1}$; $\varepsilon_{485\ nm}$ = 38670 $mol^{-1}$ $cm^{-1}$.

**IR** (ATR): wavenumber/$cm^{-1}$ = 3331, 2928, 2851, 1652, 1626, 1602, 1576, 1537, 1514, 1390, 1349, 1174, 1130, 1086, 1042, 843, 820, 676.

**m.p.** = 190 °C

### 8.6.1.3 (*E*)-4-(Diethylamino)phenyl)diazenyl benzenesulfonamide (8.2)

This compound has been described and fully characterized as compound **7.3** in chapter 7.

### 8.6.1.4 (*E*)-*N*-(Butylcarbamoyl)-4-((4-(hydroxy)phenyl)diazenyl) benzenesulfonamide (JB263)

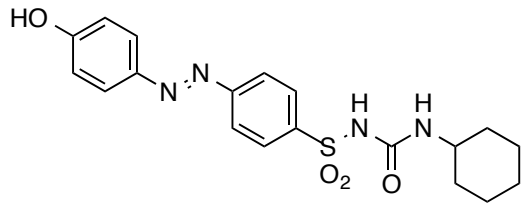


A mixture of (*E*)-4-((4-(hydroxy)phenyl)diazenyl)benzenesulfonamide (**8.2**) (500 mg, 1.80 mmol, 1.0 eq.) and $Cs_2CO_3$ (2.35 g, 7.20 mmol, 4.0 eq.) in acetonitrile (50 mL) was refluxed for 1 h before addition of cyclohexyl isocyanate (225 mg, 1.80 mmol, 215 µL, 1.0 eq.) diluted in acetonitrile (20 mL). The reaction mixture was refluxed for an additional 3 h, before cooling to ~40 °C. The crude solid was filtered and neutralized with aqueous HCl before it was extracted with EtOAc (3 x). Flash column chromatography (EtOAc/pentane = 1/1) yielded 644 mg (1.60 mmol) of **JB263** in 89% yield.

**$^1$H NMR** (400 MHz, DMSO-$d_6$): $\delta$ [ppm] = 10.53 (s, 1H), 8.06 (d, $J$ = 8.6 Hz, 2H), 7.95 (d, $J$ = 8.7 Hz, 2H), 7.86 (d, $J$ = 8.8 Hz, 2H), 6.97 (d, $J$ = 8.8 Hz, 2H), 6.42 (d, $J$ = 7.7 Hz, 1H), 3.44–3.20 (m, 3H, together with water), 1.78–1.39 (m, 5H), 1.39–0.97 (m, 5H).

**$^{13}$C NMR** (101 MHz, DMSO-$d_6$): $\delta$ [ppm] = 162.0, 154.4, 150.6, 145.3, 141.0, 128.7, 125.6, 122.4, 116.2, 48.2, 32.3, 25.0, 24.3.

**HRMS** (ESI): calc. for $C_{19}H_{22}N_4NaO_4S^+$ $(M+Na)^+$: 425.1254, found: 425.1250.

**$R_t$** (LCMS; MeCN/$H_2O$/formic acid = 10/90/0.1 → 90/10/0.1 over 7 min) = 4.007 min.

**UV/Vis** (LCMS): $\lambda_{max}$ = 362 nm.

### 8.6.1.5 (*E*)-*N*-(Butylcarbamoyl)-4-((4-(diethylamino)phenyl)diazenyl) benzenesulfonamide (JB386)

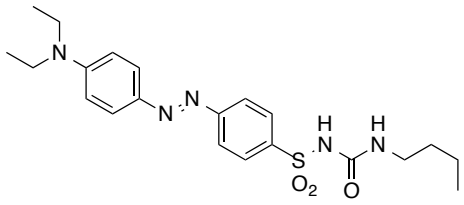

A round bottom flask was charged with **8.1** (332 mg, 1.0 mmol, 1.0 eq.) and $Cs_2CO_3$ (1.34 g, 4.0 mmol, 4.0 eq.) and refluxed in 20 mL acetone for 1 h. *n*-Butyl isocyanate (99 mg, 113 µL, 1.0 mmol, 1.0 eq.) dissolved in 20 mL acetone was added dropwise and the mixture was refluxed for another 3 h before it was allowed to warm to r.t.. The crude product was neutralized with aqueous HCl and extracted into EtOAC before it was subjected to flash column chromatography to obtain 360 mg (0.55 mmol) of **JB386** as its *N*-(bis(butylamino)methylene)butan-1-aminium salt in 55% yield.

**$^1$H NMR** (400 MHz, $CDCl_3$): $\delta$ [ppm] = 8.03 (d, *J* = 8.6 Hz, 2H), 7.94–7.81 (m, 4H), 6.70 (d, *J* = 9.2 Hz, 2H), 6.55 (t, *J* = 5.6 Hz, 1H), 5.12 (s, 2H), 3.45 (q, *J* = 7.1 Hz, 4H), 3.17–3.11 (m, 7H), 1.53–1.40 (m, 7H), 1.40 – 1.18 (m, 16H), 0.91–0.84 (m, 12H).

**$^{13}$C NMR** (101 MHz, $CDCl_3$): $\delta$ [ppm] = 159.1, 156.0, 152.2, 150.9, 143.1, 139.0, 128.3, 126.1, 122.3, 110.9, 44.7, 40.2, 39.7, 32.2, 31.6, 20.0, 19.8, 13.8, 13.6, 12.6.

**HRMS** (ESI): calc. for $C_{21}H_{30}N_5O_3S^+$ $(M+H)^+$: 432.2064, found: 432.2072.

**$R_t$** (LCMS; MeCN/$H_2O$/formic acid = 10/90/0.1 → 90/10/0.1 over 7 min) = 4.955 min.

**UV/Vis** (LCMS): $\lambda_{max}$ = 468 nm.

### 8.6.1.6 5-Amino-1,3,4-thiadiazole-2-sulfonamide (8.3)

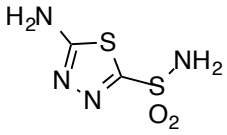


*N*-(5-sulfamoyl-1,3,4-thiadiazol-2-yl)acetamide (acetazolamide, **AAZ**) (3.00 g, 13.5 mmol, 1.0 eq.) was dissolved in 3 M HCl (23.4 mL) and refluxed at 110 °C for 3 h. The mixture was neutralized with 4 M NaOH (17.6 mL) and extracted with EtOAc (3 x 200 mL). The combined organic layers were washed with brine and concentrated *in vacuo*. 2.18 g (12.1 mmol) of the desired product were obtained in 90% yield.

**$^1$H NMR** (400 MHz, DMSO-$d_6$): $\delta$ [ppm] = 8.08 (br s, 2H), 7.90 (s, 2H).

**$^{13}$C NMR** (101 MHz, DMSO-$d_6$): $\delta$ [ppm] = 171.7, 157.9.

**LRMS** (LCMS): calc. for $C_2H_4N_4NaO_2S_2^+$ $(M+H)^+$: 203.2, found: 203.2.

**$R_t$** (LCMS; MeCN/$H_2O$/formic acid = 10/90/0.1 → 90/10/0.1 over 7 min) = 0.780 min.

**UV/Vis** (LCMS): $\lambda_{max}$ = 278 nm.

### 8.6.1.7 (*E*)-5-((4-(Diethylamino)phenyl)diazenyl)-1,3,4-thiadiazole-2-sulfonamide (8.4)

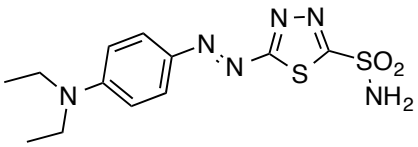

**8.3** (800 mg, 4.44 mmol, 1.0 eq.) was dissolved in $H_2O$ (32.0 mL) and cHCl (8.00 mL) at 0 °C. Sodium nitrate (738 mg, 10.7 mmol, 2.4 mmol) was added dropwise and the solution was stirred for 10 min at 0 °C. The prepared solution was added dropwise over 30 min to a solution of *N*,*N*-diethylaniline (748 µL, 4.88 mmol, 1.1 eq.) in MeOH/4 M NaOH (40.0 mL/10.0 mL) at 0 °C and stirred for 15 min at 0 °C. The reaction was allowed to warm up to r.t. and stirred o.n. at r.t.. The reaction mixture was acidified with 1 M HCl and extracted with EtOAc (3 x 250 mL), washed with brine and the crude product was filtered through a pore III frit with a plug of silica with EtOAc. 908 mg (2.67 mmol) of **8.4** were obtained in 60% yield.

**$^1$H NMR** (400 MHz, DMSO-$d_6$): $\delta$ [ppm] = 8.47 (br s, 2H), 7.86 (d, *J* = 9.2 Hz, 2H), 6.96 (d, *J* = 9.2, 2H), 3.59 (q, *J* = 6.8 Hz, 4H), 1.20 (t, *J* = 7.2 Hz, 6H).

**$^{13}$C NMR** (101 MHz, DMSO-$d_6$): $\delta$ [ppm] = 183.3, 167.3, 153.8, 142.0, 112.6, 79.2, 44.9, 12.6.

**HRMS (ESI)**: calc. for $C_{12}H_{17}N_6O_2S_2^+$ $(M+H)^+$: 341.0849, found: 341.0846.

**UV/Vis** (LCMS): $\lambda$ ($\pi \rightarrow \pi^*$) = 540 nm.

**$R_t$** (LCMS; MeCN/$H_2O$/formic acid = 10/90/0.1 → 90/10/0.1 over 7 min) = 3.845 min.

### 8.6.1.8 (*E*)-*N*-(Cyclohexylcarbamoyl)-5-((4-(diethylamino)phenyl)-diazenyl)-1,3,4-thiadiazole-2-sulfonamide (JB558)

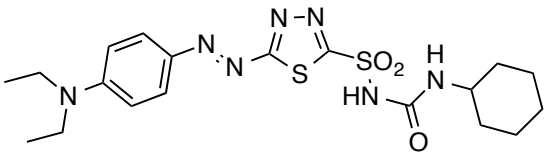

**8.4** (900 mg, 3.38 mmol, 1.0 eq.) was dissolved in dry 1,4-dioxane (10.0 mL) under a $N_2$-atmosphere. $NEt_3$ (300 µL, 2.17 mmol, 0.82 eq.) and cyclohexyl isocyanate (10.0 mL, 83.9 mmol, 32 eq.) were added and the mixture was refluxed for 2 h at 110 °C. The solution was acidified with 1 M HCl (50 mL) and extracted with EtOAc (3 x 50 mL), washed with brine, filtered through a PTFE filter (CHROMAFIL® Xtra PTFE 0.45) and subjected to RP-HPLC (MeCN/$H_2O$/formic acid = 10/80/0.1 → 80/20/0.1 over 30 min). 19.0 mg (40.9 µmol) of the desired product was obtained in 2% yield.

**$^1$H NMR** (400 MHz, DMSO-$d_6$): $\delta$ [ppm] = 7.86 (d, $J$ = 9.2 Hz, 2H), 6.97 (d, $J$ = 9.6 Hz, 2H), 6.68 (m, 1H), 3.60 (q, $J$ = 7.2 Hz, 4H), 3.54–3.47 (m, 1H), 1.75–1.6 (m, 4H), 1.55–1.45 (m, 2H), 1.25–1.14 (m, 10H).

**$^{13}$C NMR** (101 MHz, DMSO-$d_6$): $\delta$ [ppm] = 184.2, 164.4 (FA), 163.1, 158.2, 154.0, 150.6, 142.1, 112.8, 48.6, 45.0, 32.2, 24.3, 12.6.

**HRMS (ESI)**: calc. for $C_{19}H_{28}N_7O_3S_2^+$ $(M+H)^+$: 466.1690, found: 466.1690.

**UV/Vis** (LCMS): $\lambda$ ($\pi \rightarrow \pi^*$) = 545 nm.

**$R_t$** (LCMS; MeCN/$H_2O$/formic acid = 10/90/0.1 → 90/10/0.1 over 7 min) = 4.691 min.

**Extinction coefficient** (Ringer solution): $\varepsilon_{530\,nm}$ = 4,850,000 $mol^{-1}$ $cm^{-1}$.

### 8.6.1.9 (*E*)-5-((4-morpholinophenyl)diazenyl)-1,3,4-thiadiazole-2-sulfonamide (8.5)

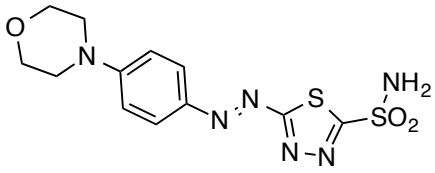

**8.3** (500 mg, 2.77 mmol, 1.0 eq.) was dissolved in 20 mL of a 2.4 M solution of HCl at 0 °C. $NaNO_2$ (230 mg, 3.33 mmol, 1.2 eq.) was dissolved in water (5 mL) and added drop wise to the cold solution to form the diazonium salt. The mixture was stirred for 15 minutes and then transferred into a pre-cooled solution of *N*-Phenyl morpholine (497 mg, 3.05 mmol, 1.1 eq.) in a mixture of MeOH and 4 M NaOH (20 mL / 5 mL). The solution turned to a deep purple color and was allowed to warm to r.t. under sturring for 3 hours. The reaction mixture was acidified with 1 M HCl and extracted with EtOAc. After concentrating the organic layer *in vacuo*, the crude was submitted to flash column chromatography on silica gel (100% EtOAc) to collect the red fraction, which was again concentrated and submitted again to flash column chromatography on silica gel (MeOH/DCM = 2/98) in order to obtain 70 mg (0.20 mmol) of the desired as a purple powder in 7% yield.

Crystals suitable for X-ray diffractometry were obtained as purple needles by letting a filtered and concentrated solution of the title compound stand in a DMSO/water mixture for four weeks.

**$^{1}$H NMR** (400 MHz, DMSO-d6) δ = 8.46 (s, 1H), 7.86 (d, *J* = 9.4 Hz, 2H), 7.13 (d, *J* = 9.5 Hz, 2H), 3.71 ($m_c$, 4H), 3.56 ($m_c$, 4H).

**$^{13}$C NMR** (101 MHz, DMSO-d6) δ = 183.3, 168.5, 156.0, 143.4, 128.4, 114.0, 66.2, 46.9.

**HRMS (ESI)**: calc. for $C_{12}H_{15}N_6O_3S_2$ $(M+H)^+$: 355.1, found: 355.1.

**UV/Vis** (LCMS): $\lambda_{max}$ = 522 nm

**$R_t$** (LCMS; MeCN/$H_2O$/formic acid = 10/90/0.1 → 90/10/0.1 over 7 min) = 4.155 min.

### 8.6.1.10 (*E*)-*N*-(Cyclohexylcarbamoyl)-5-((4-morpholinophenyl)-diazenyl)-1,3,4-thiadiazole-2-sulfonamide (JB541)

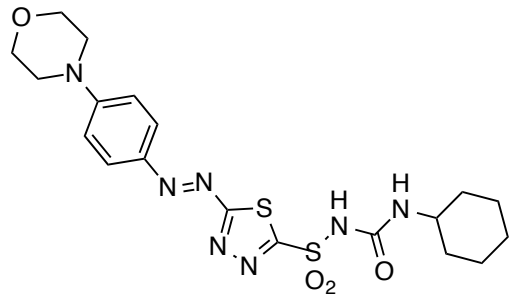

**8.5** (23.3 mg, 65.7 µmol, 1.0 eq.) was dissolved in dry 1,4-dioxane (10.0 mL) under a $N_2$-atmosphere. $NEt_3$ (100 µL, 7.23 mmol, 100 eq.) and cyclohexyl isocyanate (100 µL, 842 µmol, 12 eq.) were added and the mixture was refluxed for 2 h at 110 °C. The solution was acidified with 1 M HCl (50 mL) and extracted with EtOAc (3 x 50 mL), washed with brine, filtered through a PTFE filter (CHROMAFIL® Xtra PTFE 0.45) and subjected to flash column chromatography (MeOH/DCM = 0/100 → 1/100 → 2/100). 16.2 mg (33.8 µmol) of the desired product was obtained in 51% yield.

**$^1$H NMR** (400 MHz, DMSO-$d_6$): $\delta$ [ppm] = 8.13 (s, 1H), 7.90 (d, $J$ = 9.0 Hz, 2H), 7.18 (d, $J$ = 9.0 Hz, 2H), 6.52 (s, 1H), 3.83–3.70 (m, 4H), 3.59 (t, $J$ = 4.8 Hz, 4H), 1.79–1.43 (m, 5H), 1.31–1.02 (m, 5H).

**$^{13}$C NMR** (101 MHz, DMSO-$d_6$): $\delta$ [ppm] = 163.0, 155.5, 143.1, 127.9, 113.6, 107.9, 65.8, 48.4, 46.5, 32.4, 25.1, 24.5.

**LRMS (ESI)**: calc. for $C_{19}H_{28}N_7O_3S_2^+$ $(M+H)^+$: 480.1, found: 480.2.

**UV/Vis** (LCMS): $\lambda_{max}$ = 526 nm.

**$R_t$** (LCMS; MeCN/$H_2O$/formic acid = 10/90/0.1 → 90/10/0.1 over 7 min) = 4.313 min.

### 8.6.1.11 4-Amino-*N*-(cyclohexylcarbamoyl)benzenesulfonamide (8.6)

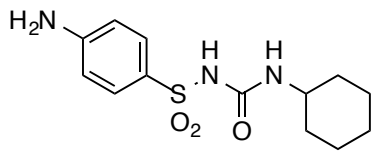

A round bottom flask was charged with 1.72 g sulfanilamide (10.0 mmol, 1.0 eq.) and 13.0 g $Cs_2CO_3$ (40.0 mmol, 4.0 eq.), suspended in 200 mL acetone and heated to reflux for 1 h before 1.25 g cyclohexyl isocyanate (1.19 mL, 10.0 mmol, 1.0 eq.) in 20 mL acetone was added dropwise. The mixture was heated to reflux for another 5 h before it was cooled to r.t. and quenched by the addition of water. Neutralization with cHCl and extraction with EtOAc (3 x) yielded a cude product that was dried under HV conditions and used without further purification.

### 8.6.1.12 (*E*)-*N*-(Cyclohexylcarbamoyl)-4-(phenyldiazenyl)benzene-sulfonamide (JB030)

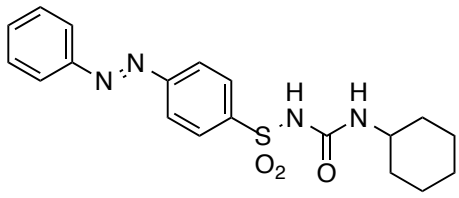

A round bottom flask was charged with 100 mg (0.34 mmol, 1.0 eq.) **8.6** and nitrosobenzene (1.2 eq.) dissolved in HOAc. The mixture was stirred at r.t. o.n. before it was quenched with sat. aqueous $NaHCO_3$, extracted in EtOAc and the crude material subjected to flash column chromatography (MeOH/DCM = 5/95) to yield 60.0 mg of the desired product in 46% yield.

**$^1$H NMR** (400 MHz, DMSO-$d_6$): $\delta$ [ppm] = 10.55 (s, 1H), 8.11 (d, $J$ = 8.5 Hz, 2H), 8.04 (d, $J$ = 8.5 Hz, 2H), 7.94 (dd, $J$ = 6.7, 3.0 Hz, 2H), 7.66–7.59 (m, 3H), 6.45 (d, $J$ = 7.9 Hz, 1H), 3.44–3.04 (m, 1H), 1.82–1.39 (m, 5H), 1.39–1.02 (m, 5H).

**$^{13}$C NMR** (101 MHz, DMSO-$d_6$): $\delta$ [ppm] = 154.1, 151.9, 150.4, 142.0, 132.5, 129.7, 128.9, 123.0, 122.9, 48.2, 32.3, 25.0, 24.3.

**HRMS (ESI)**: calc. for $C_{19}H_{22}N_4O_3S^-$ $(M-H)^-$: 385.1340, found: 385.1338.

**UV/Vis** (LCMS): $\lambda$ ($\pi \rightarrow \pi^*$) = 322 nm.

**$R_t$** (LCMS; MeCN/$H_2O$/formic acid = 10/90/0.1 → 90/10/0.1 over 7 min) = 4.952 min.

### 8.6.1.13 Ethyl (*E*)-4-((4-(*N*-(cyclohexylcarbamoyl)sulfamoyl)phenyl)-diazenyl)benzoate (JB243)

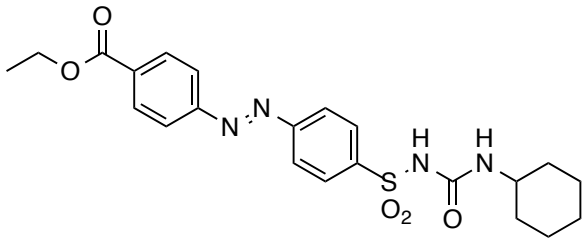

A round bottom flask was charged with 100 mg (0.34 mmol, 1.0 eq.) **8.6** andm90.4 mg (0.50 mmol) 4-nitroso ethylbenzoate (1.5 eq.) dissolved in HOAc. The mixture was stirred at 50 °C for 3 days before it was quenched with sat. aqueous $NaHCO_3$, extracted in EtOAc and the crude material subjected to flash column chromatography (100% DCM) to yield 62.2 mg (0.14 mmol) of the desired product in 40% yield.

**$^1$H NMR** (600 MHz, $CDCl_3$): $\delta$ [ppm] = 8.20 (d, *J* = 8.8 Hz, 2H), 8.10–8.02 (m, 4H), 7.99–7.95 (m, 2H), 6.50 (d, *J* = 8.0 Hz, 1H), 4.48–4.38 (m, 2H), 3.63 (dt, *J* = 7.5, 3.7 Hz, 1H), 1.92–1.84 (m, 2H), 1.70 (dt, *J* = 13.5, 4.1 Hz, 2H), 1.60 (dt, *J* = 12.9, 4.2 Hz, 1H), 1.44 (t, *J* = 7.1 Hz, 3H), 1.38–1.17 (m, 5H).

**$^{13}$C NMR** (151 MHz, $CDCl_3$): $\delta$ [ppm] = 165.6, 154.8, 154.3, 150.1, 141.1, 133.1, 130.4, 127.9, 127.4, 123.5, 122.9, 61.2, 49.1, 32.7, 25.1, 24.3, 14.1.

**LRMS (ESI)**: calc. for $C_{22}H_{27}N_4O_5S^+$ $(M+H)^+$: 459.2, found: 459.2.

**UV/Vis** (LCMS): λ (π → π*) = 324 nm.

**$R_t$** (LCMS; MeCN/$H_2O$/formic acid = 10/90/0.1 → 90/10/0.1 over 7 min) = 5.159 min.

### 8.6.2 Extinction Coefficients

#### 8.6.2.1 (*E*)-*N*-(Cyclohexylcarbamoyl)-4-((4-(diethylamino)phenyl)-diazenyl)benzenesulfonamide (JB253)

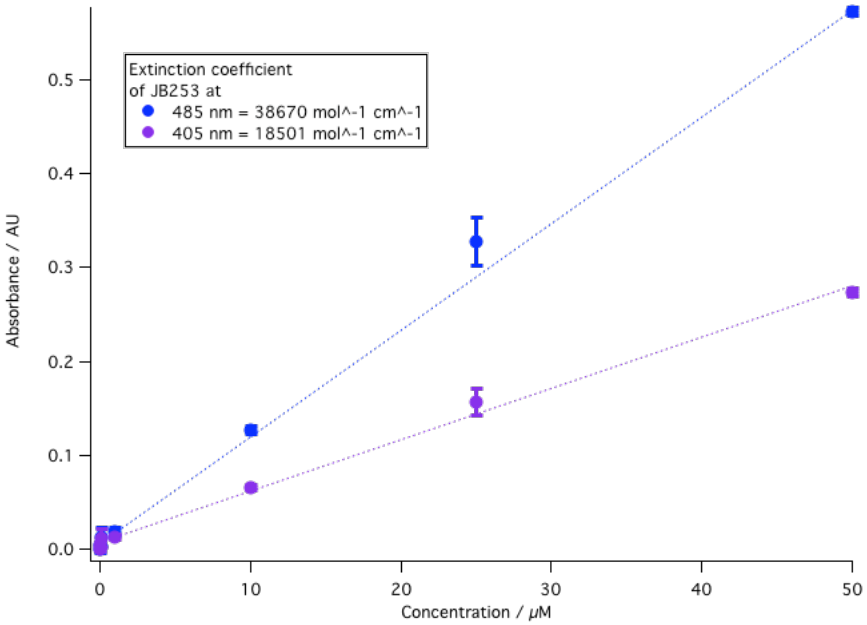

#### 8.6.2.2 (*E*)-*N*-(Cyclohexylcarbamoyl)-5-((4-(diethylamino)phenyl)-diazenyl)-1,3,4-thiadiazole-2-sulfonamide (JB558)

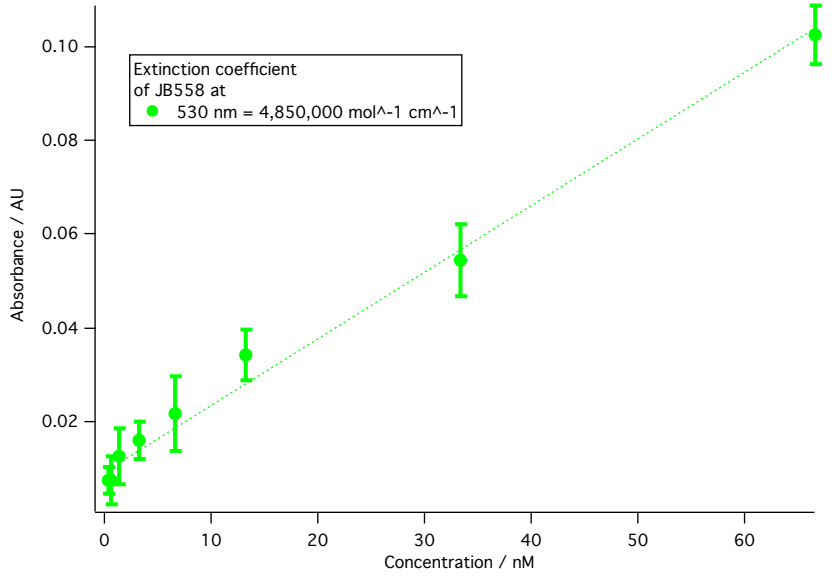


### 8.6.3 Biology

#### 8.6.3.1 Electrophysiology

HEK293t cells were incubated in Dulbecco´s Modified Eagle Medium (DMEM) + 10% FBS and used for electrophysiological recordings 24-48 hrs following Lipofectamine transfection with plasmids encoding Kir6.2 (Genbank D50581), rat SUR1 (Genbank L40624) and GFP. Whole cell patch clamp experiments were performed using a standard electrophysiology setup equipped with a HEKA Patch Clamp EPC10 USB amplifier and PatchMaster software (HEKA Electronik). Micropipettes were generated from "Science Products GB200-F-8P with filament" pipettes using a vertical puller. Resistance varied between 5-7 MΩ. Bath solution contained in mM: 3 KCl, 118 NaCl, 25 $NaHCO_3$, 2 $CaCl_2$, 1 $MgCl_2$, 10 HEPES (NaOH to pH 7.4). Pipette solution contained in mM: 90 K-gluconate, 10 NaCl, 10 KCl, 1 $MgCl_2$, 10 EGTA, 60 HEPES (KOH to pH 7.3), and the holding potential was -60 mV. Illumination during electrophysiology and UV/Vis experiments was performed using a TILL Photonics Polychrome 5000

monochromator. **JB253** was used at 50 μM as this concentration was found to be effective without quenching fluorescence in later experiments.

#### 8.6.3.2 [3H]-Glibenclamide Binding Studies

[3H]-Glibenclamide displacement assays were performed as previously described[139]. Briefly, SUR1-expressing HEK293t cells were harvested and washed twice in assaying buffer containing in mM: 119 NaCl, 4.7 KCl, mM $CaCl_2$, 1.2 $KH_2PO_4$, 1.2 $MgSO_4$, 5 $NaHCO_3$, and 20 HEPES, pH 7.4. In a 96-well plate, ~200,000 cells/well were incubated for 50 min with [3H]-glibenclamide (PerkinElmer) and different concentrations of glimepiride (Sigma-Aldrich) or **JB253**. Incubation was terminated by rapid filtration through Whatman GF/C filters by means of a Brandel MWXR-96 TI harvester and filters were washed 3 times with ice-cold assay buffer. Radioactivity was counted 6 h after cell and filter lysis in 200 μL Rotiszint EcoPlus (Roth) using a Packard microbeta scintillation counter (PerkinElmer).

#### 8.6.3.3 EPAC2 Imaging

EPAC2 imaging was performed similarly to that described previously. [160] Briefly, HEK293t were transfected with the full length construct for Epac2-camps containing the cAMP and sulfonylurea binding domains[138] (a kind gift from Prof. Jin Zhang, Johns Hopkins University) before imaging using a HEPES-bicarbonate buffer containing in mM: 120 NaCl, 4.8 KCl, 24 $NaHCO_3$, 0.5 $Na_2HPO_4$, 5 HEPES, 2.5 $CaCl_2$, 1.2 $MgCl_2$ and 5 D-glucose. Excitation was delivered at 440 nm and emitted signals captured using cerulean (530 nm) and citrine (470 nm) filters. FRET was calculated as the ratio of Cerulean (CFP):Venus (YFP) fluorescence. Signals were normalized using $R/R_o$ where R is the ratio at a given timepoint and $R_o$ is the minimum ratio.

#### 8.6.3.4 Islet Isolation

CD1 and C57BL6 mice were maintained in a specific pathogen-free facility under a 12h light–dark cycle with ad libitum access to water and food. Animals were euthanized using a schedule-1 method and pancreatic islets isolated by collagenase digestion, as described.[140] All procedures were approved by the Home Office according to the Animals (Scientific Procedures) Act 1986 of the United Kingdom (PPL 70/7349).

#### 8.6.3.5 Calcium Imaging

Islets were loaded for 30-45 mins in fluo2-AM (10 μM) diluted with a mixture of DMSO (0.01%, wt/vol) and pluronic acid (0.001%, wt/vol; all Invitrogen) in a bicarbonate buffer containing in mM: 120 NaCl, 4.8 KCl, 1.25 $NaH_2PO_4$, 24 $NaHCO_3$, 2.5 $CaCl_2$, 1.2 $MgCl_2$ and 3 D-glucose. fMCI was performed using a Zeiss Axiovert M200 fitted with a Nipkow spinning-disk head (Yokogawa CSU-10) and 10x/0.3NA objective adjusted for chromatic aberration (EC Plan-Neofluar, Zeiss). Pulsed (0.5 Hz for 263 ms) excitation was delivered at 491 nm and emitted signals recorded at 500-550 nm using a 16-bit EM-CCD camera (ImageEM 9100-13; Hamamatsu). During recording, islets were maintained at 35-36°C in the presence of 50 μM **JB253** using a custom-manufactured perfusion. Illumination was delivered using a 405 nm laser (Coherent) coupled to the side port of the microscope and configured to fill the back of the objective lens with light. Drugs were introduced through the perfusion system at the indicated time points and concentrations.

#### 8.6.3.6 Measurements of Insulin Secretion from Isolated Islets

Insulin secretion was measured from 6 islets per well, incubated at 37 °C for 30 min in 0.5 ml of Krebs-HEPES-bicarbonate (KHB) solution containing in mM: 130 NaCl, 3.6 KCl, 1.5 $CaCl_2$, 0.5 $MgSO_4$, 0.5 $NaH_2PO_4$, 2 $NaHCO_3$, 10 HEPES and 0.1 % (wt/vol) BSA, pH 7.4. [161] Illumination (λ = 405 nm) was performed using a Fluostar Optima microplate reader (BMG Labtech) and low intensity white light

was delivered using a transilluminator. Insulin concentrations were determined using specific radioimmunoassy (Millipore).

#### 8.6.3.7 Statistical Analysis

Data distribution was determined using the D'Agostino omnibus tests. Non-multifactorial pairwise comparisons were made using the Mann-Whitney U-test. Interactions between multiple treatments were assessed using Kruskal-Wallis test followed by pairwise comparisons using Dunn's post-hoc test. In all cases, analysis was performed using Graphpad Prism (Graphpad Software) and IgorPro, and results considered significant at $P<0.05$.

## 8.7 Spectral Data

### 8.7.1 (*E*)-4-((4-(Diethylamino)phenyl)diazenyl)benzenesulfonamide (8.1)

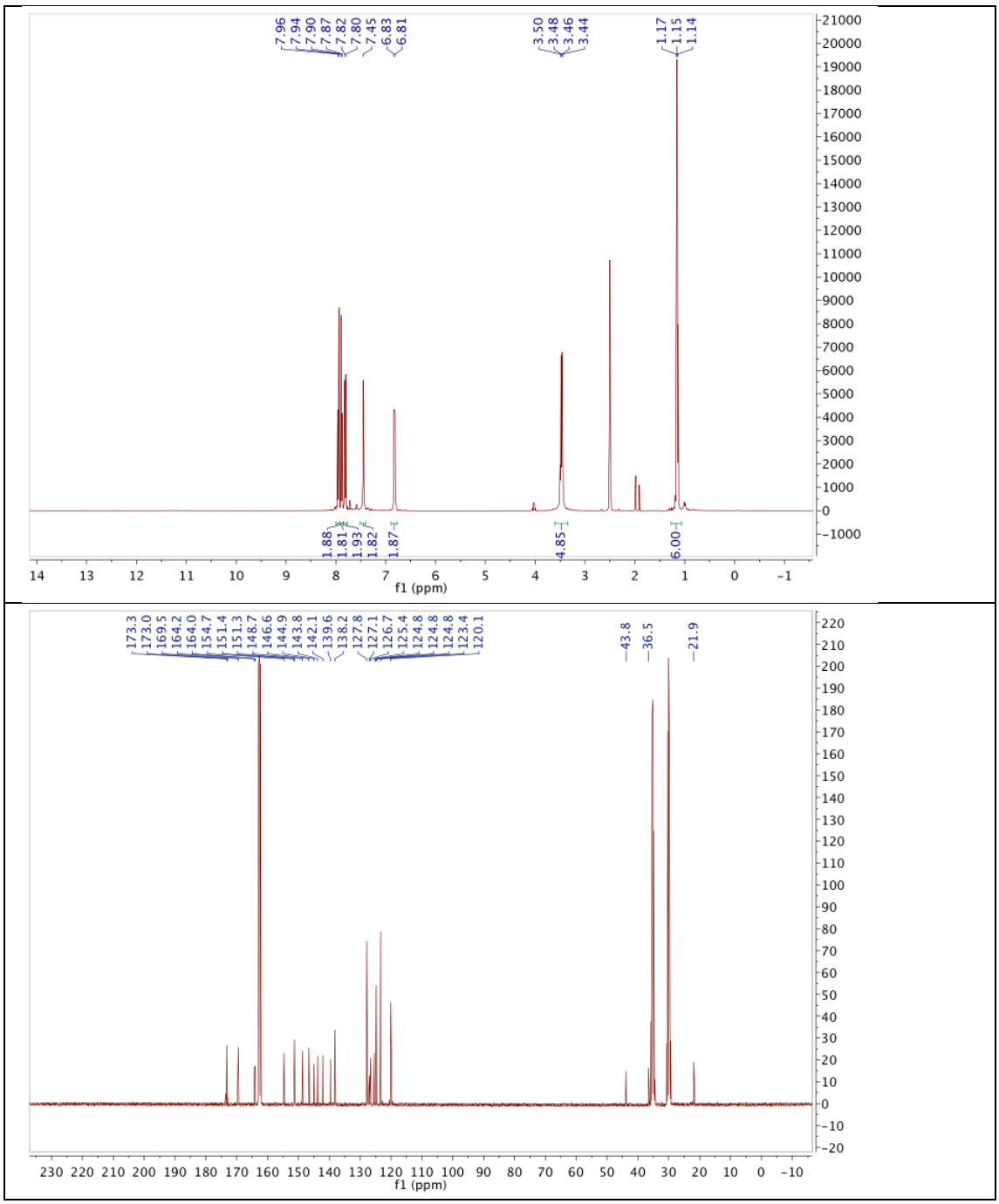

### 8.7.2 (*E*)-*N*-(Cyclohexylcarbamoyl)-4-((4-(diethylamino)phenyl)diazenyl)-benzenesulfonamide (JB253)

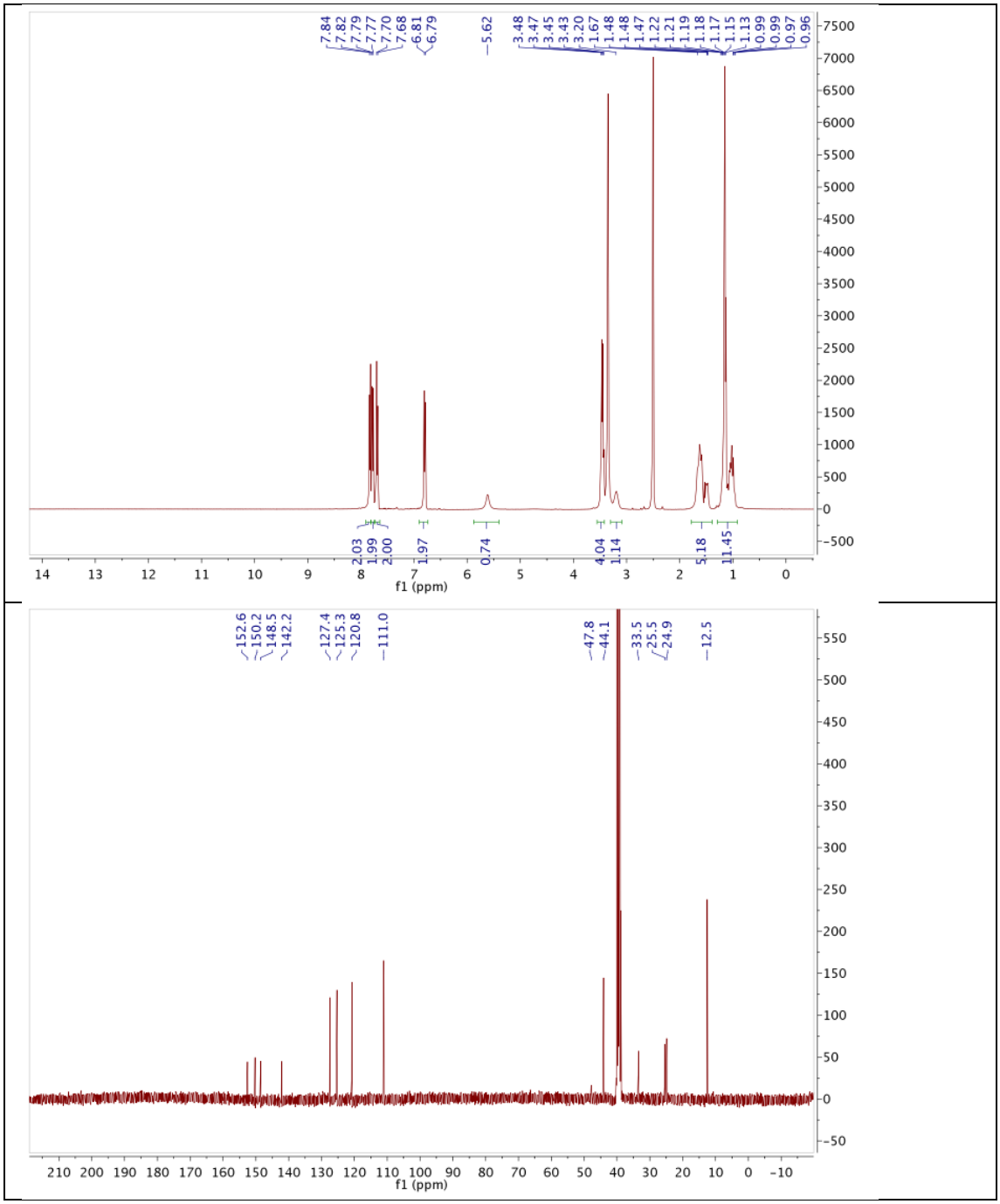

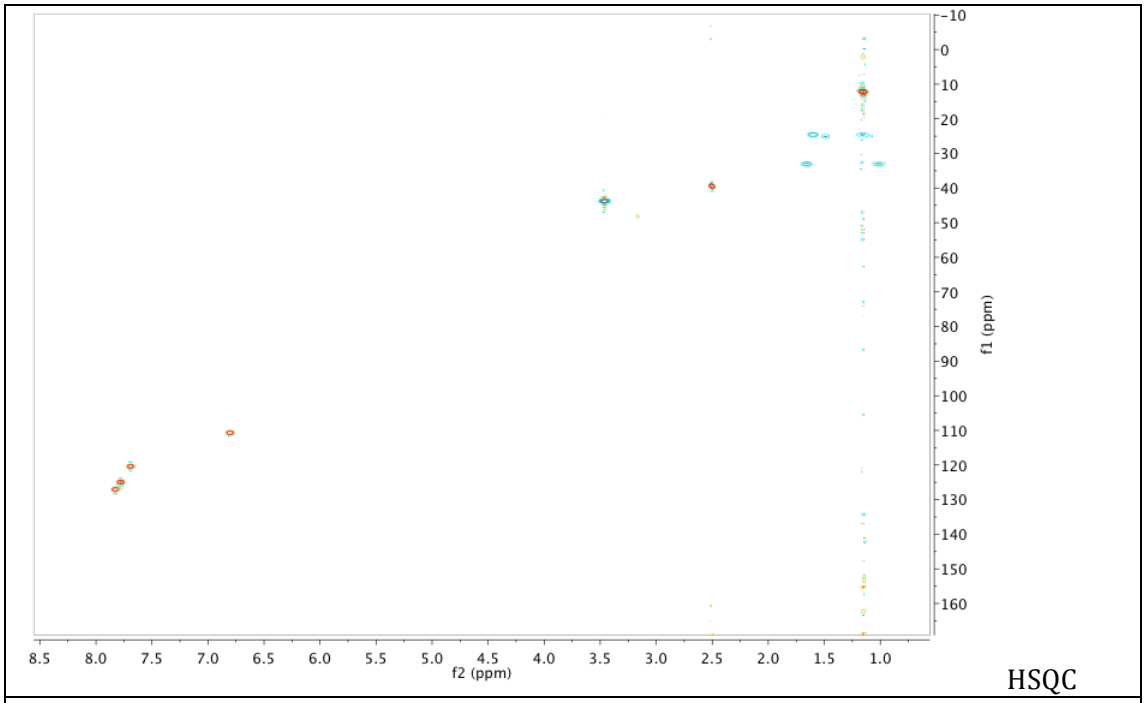


HSQC

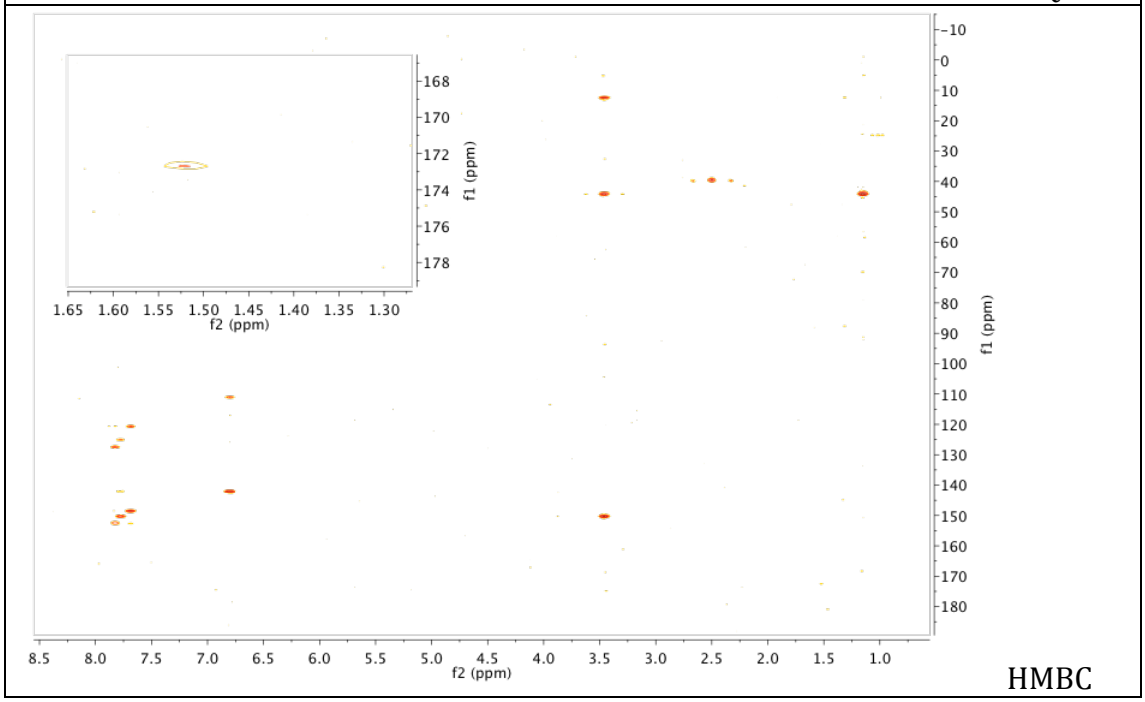


HMBC

### 8.7.3 (*E*)-*N*-(Cyclohexylcarbamoyl)-4-((4-(hydroxy)phenyl)diazenyl) benzenesulfonamide (JB263)

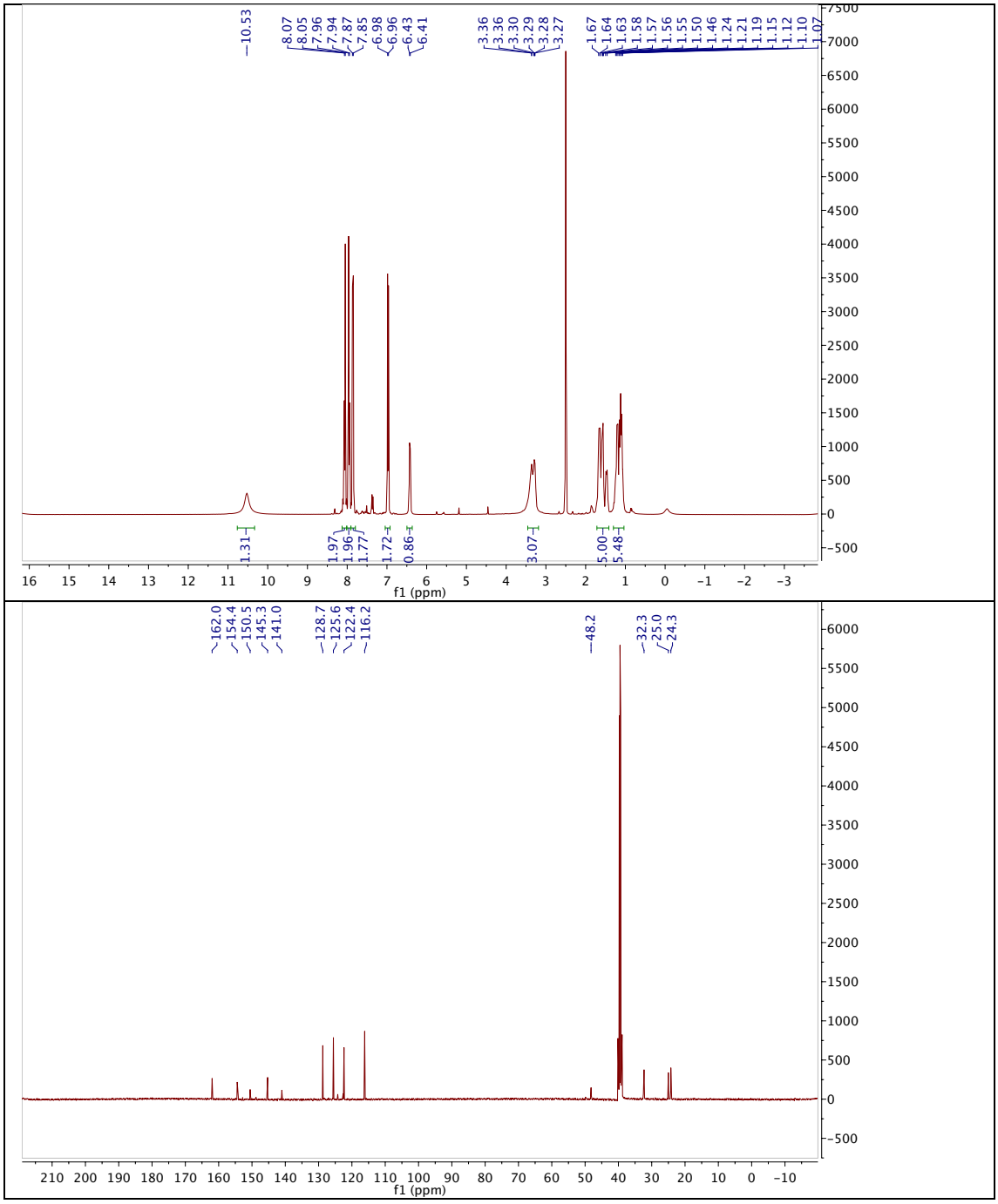

### 8.7.4 (*E*)-*N*-(Butylcarbamoyl)-4-((4-(diethylamino)phenyl)diazenyl) benzenesulfonamide (JB386)

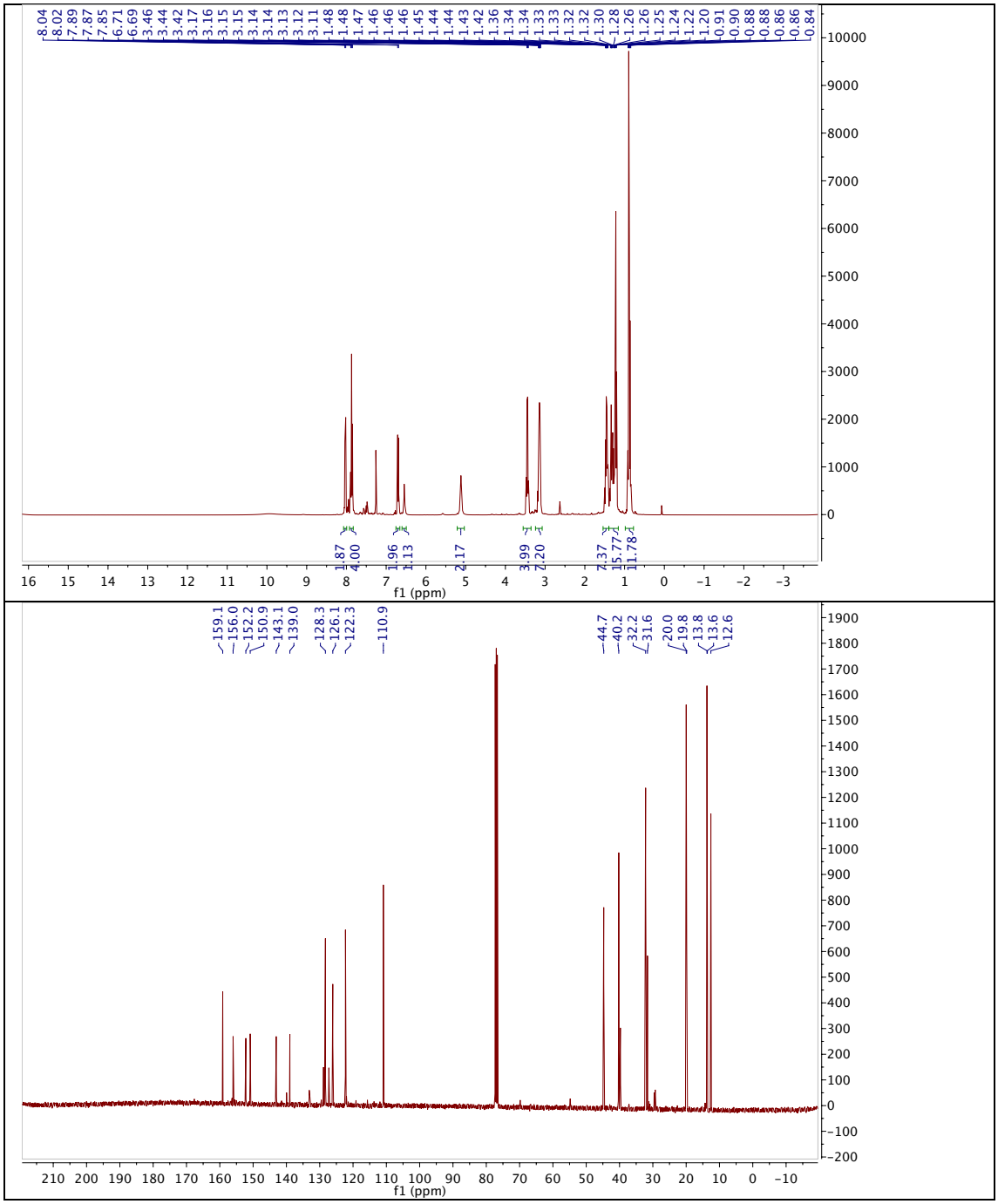

### 8.7.5 5-Amino-1,3,4-thiadiazole-2-sulfonamide (8.3)

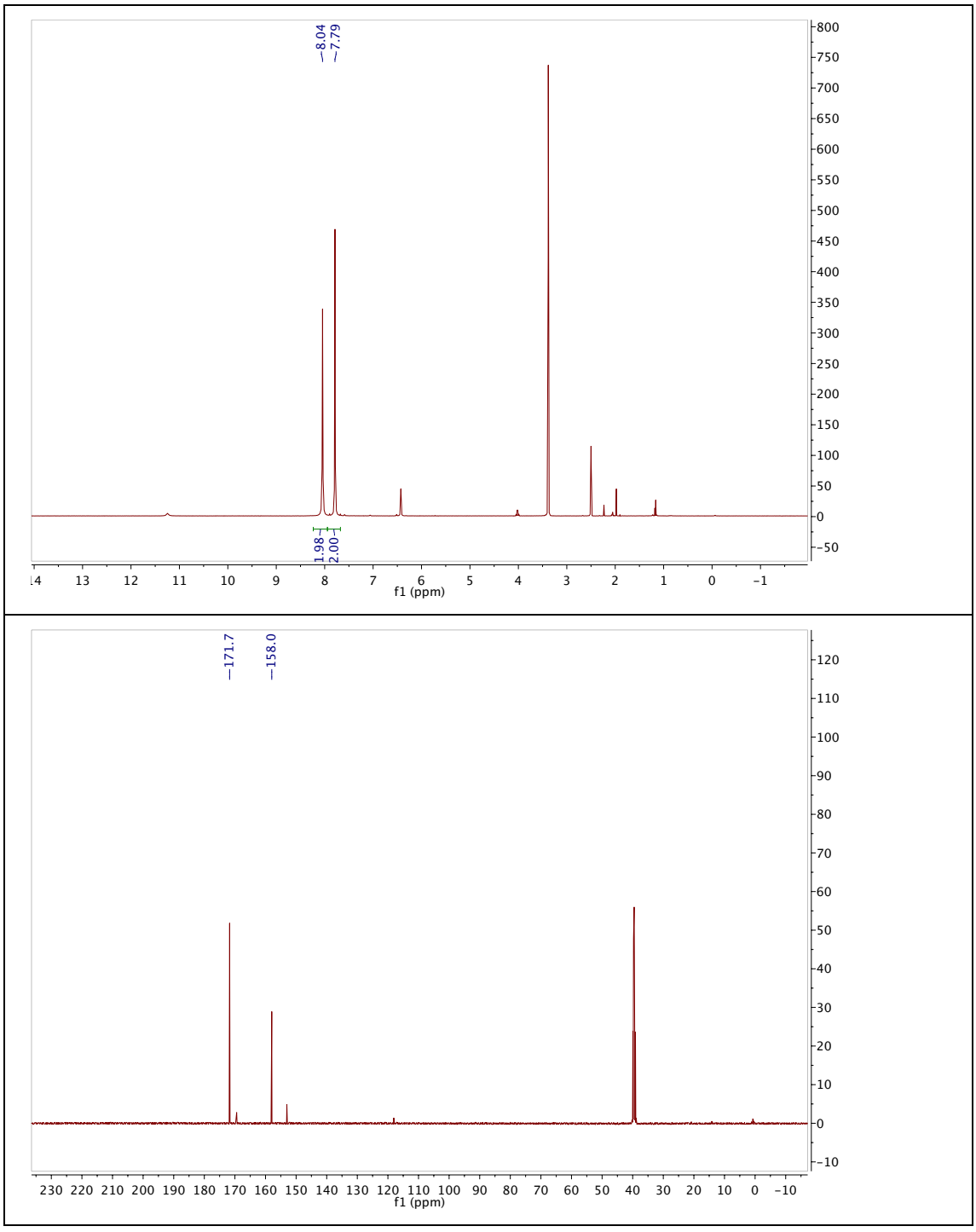

### 8.7.6 (*E*)-5-((4-(Diethylamino)phenyl)diazenyl)-1,3,4-thiadiazole-2-sulfonamide (8.4)

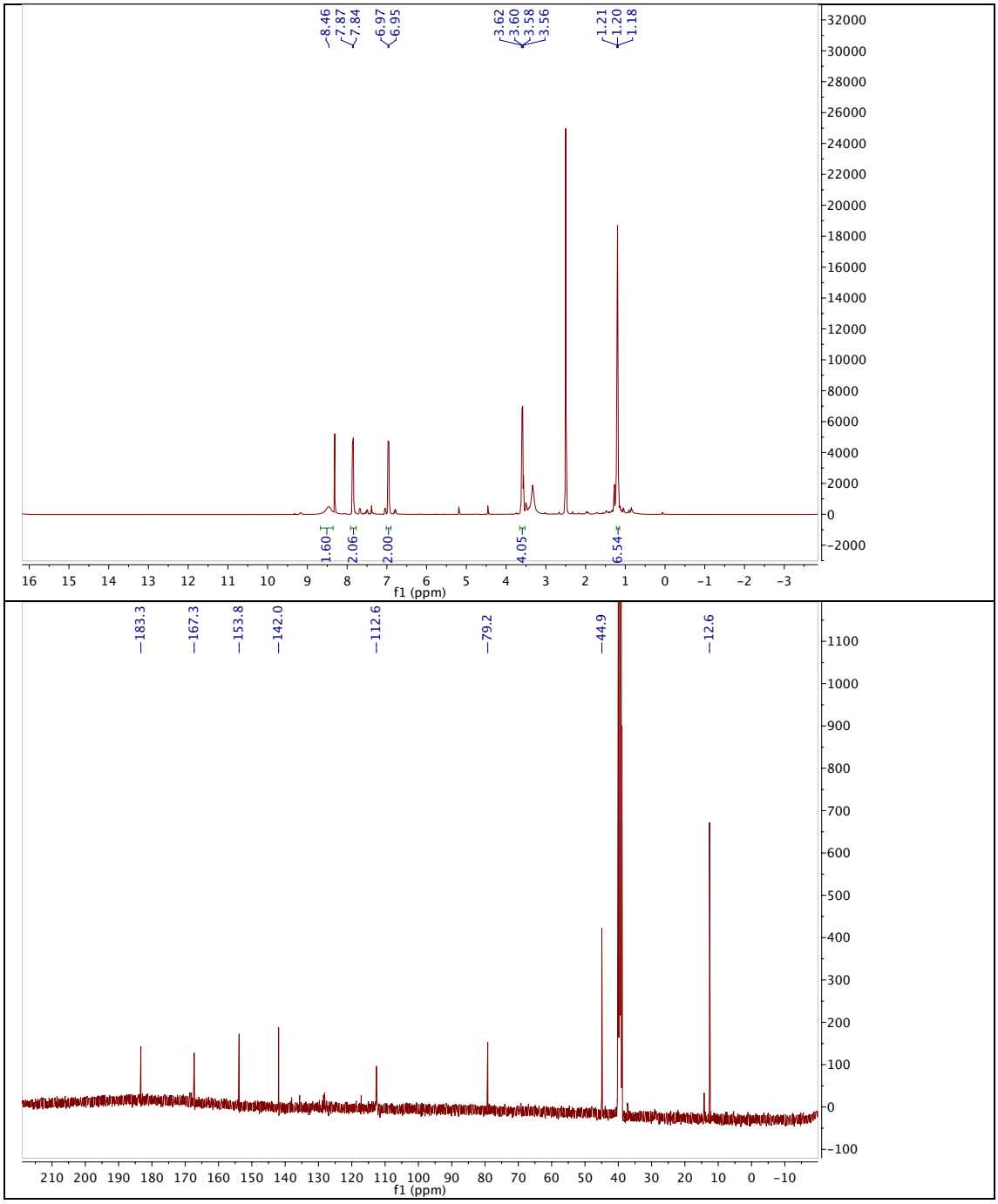

### 8.7.7 (*E*)-*N*-(Cyclohexylcarbamoyl)-5-((4-(diethylamino)phenyl)-diazenyl)-1,3,4-thiadiazole-2-sulfonamide (JB558)

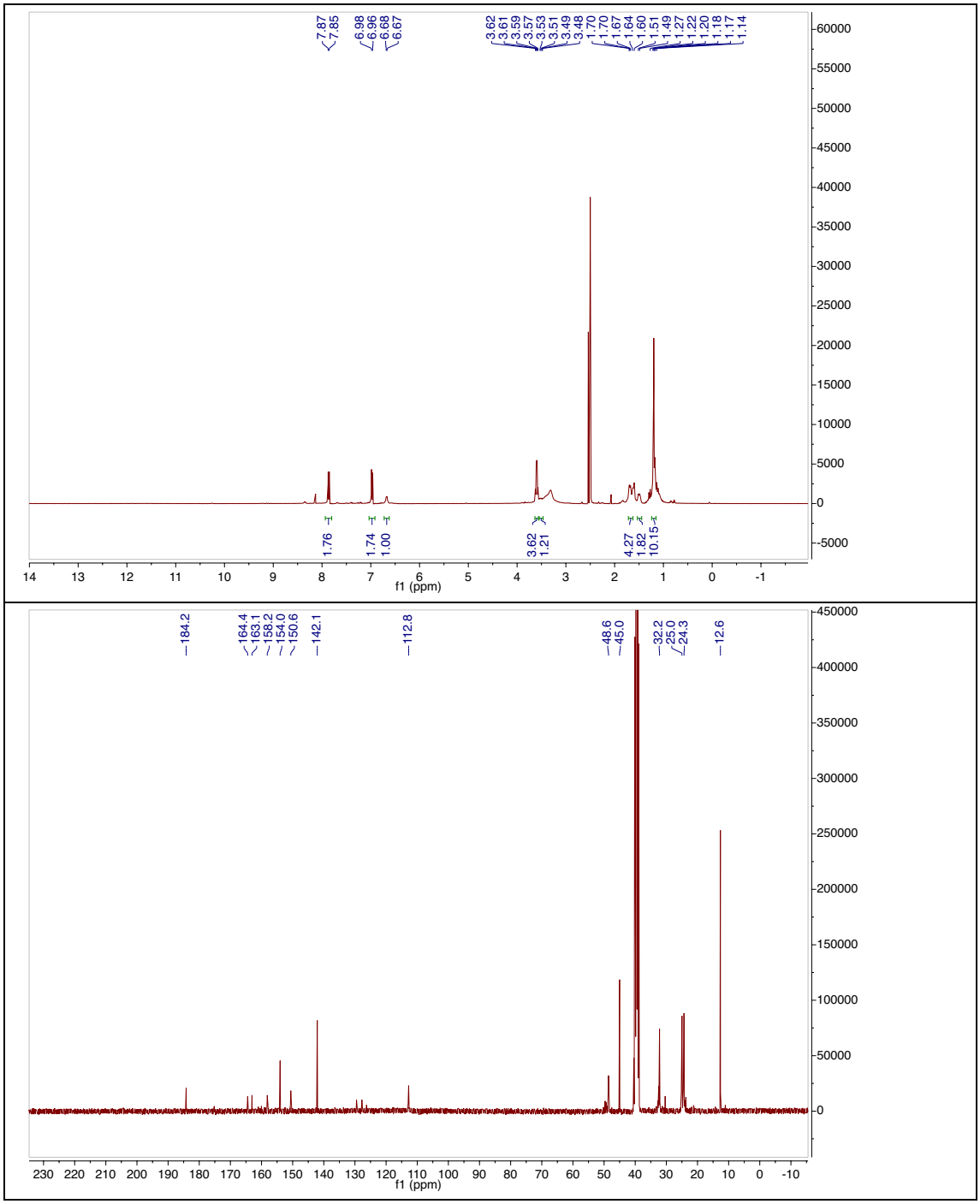

### 8.7.8 (*E*)-5-((4-morpholinophenyl)diazenyl)-1,3,4-thiadiazole-2-sulfonamide (8.5)

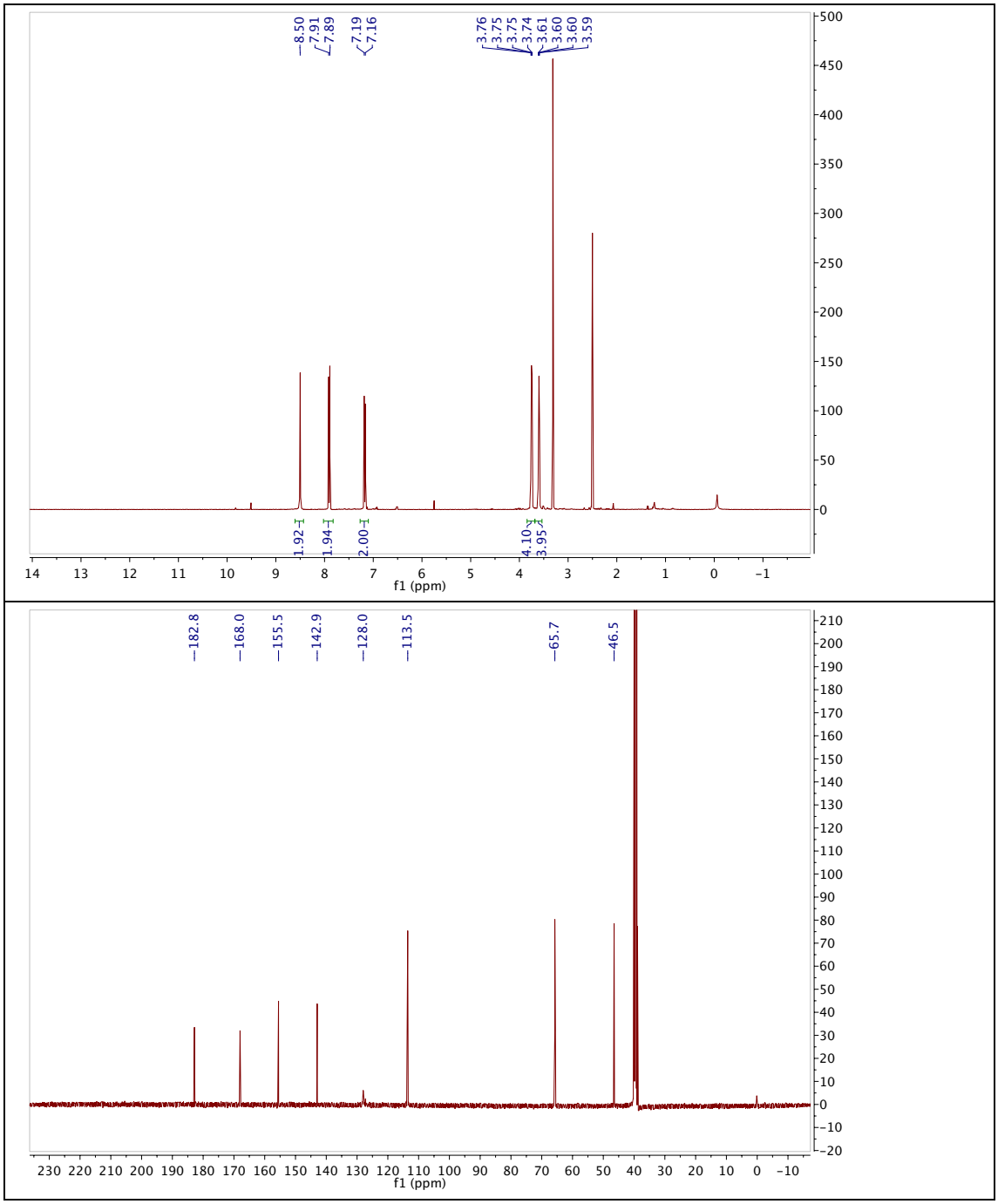

### 8.7.9 (*E*)-*N*-(Cyclohexylcarbamoyl)-5-((4-morpholinophenyl)-diazenyl)-1,3,4-thiadiazole-2-sulfonamide (JB541)

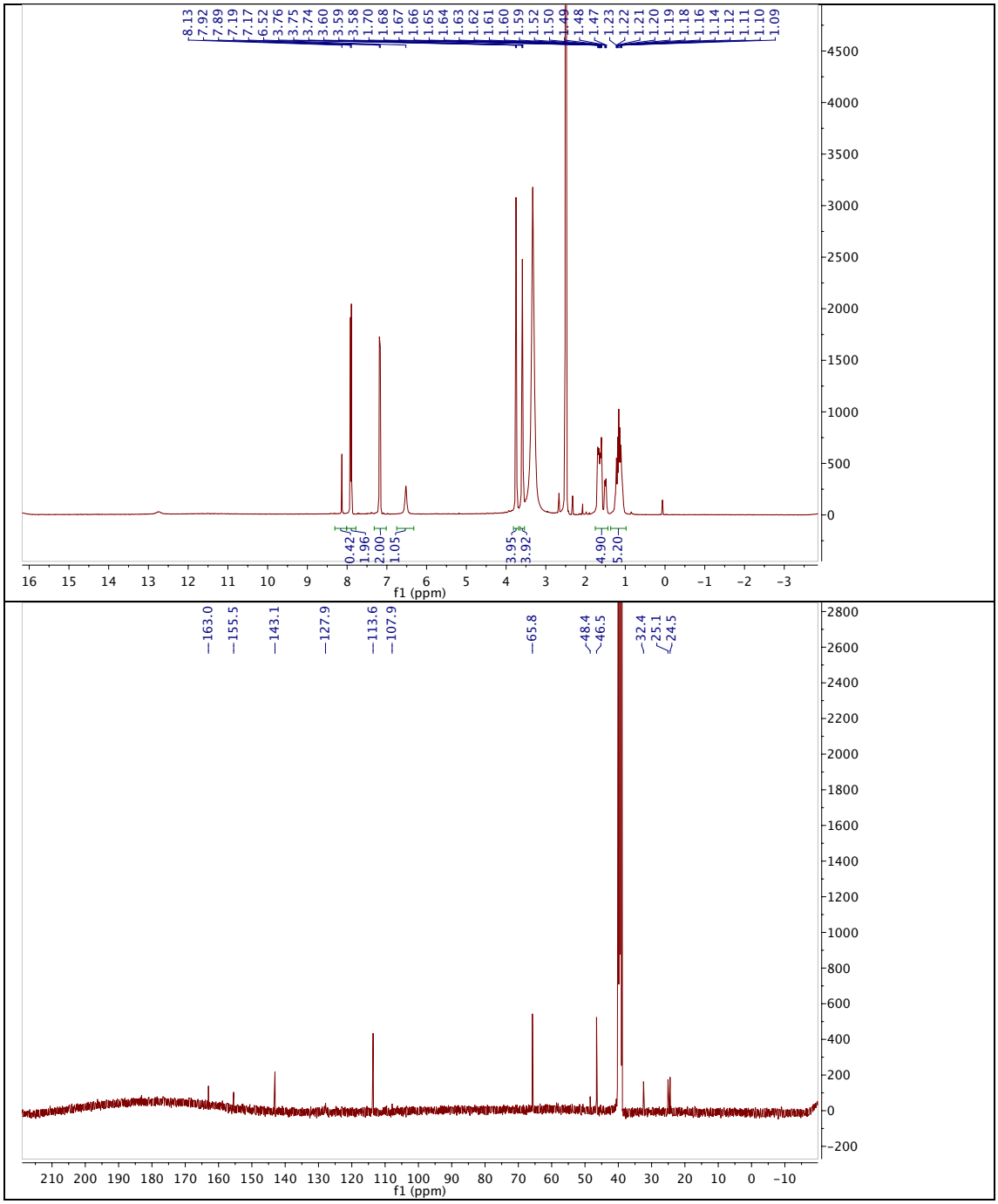

## 8.7.10 (*E*)-*N*-(Cyclohexylcarbamoyl)-4-(phenyldiazenyl)benzenesulfonamide (JB030)

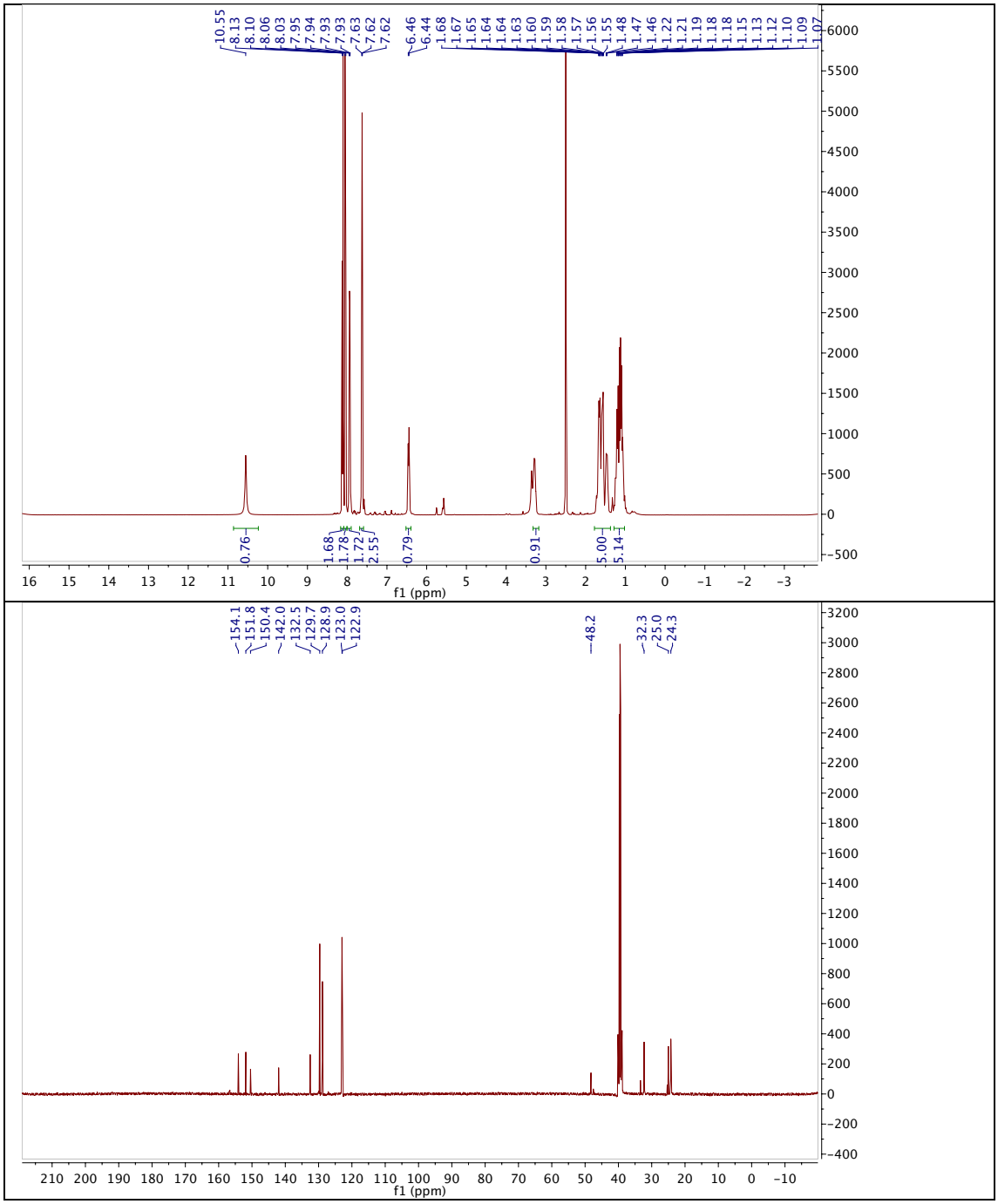

### 8.7.11 Ethyl (*E*)-4-((4-(*N*-(cyclohexylcarbamoyl)sulfamoyl)phenyl)diazenyl)-benzoate (JB243)

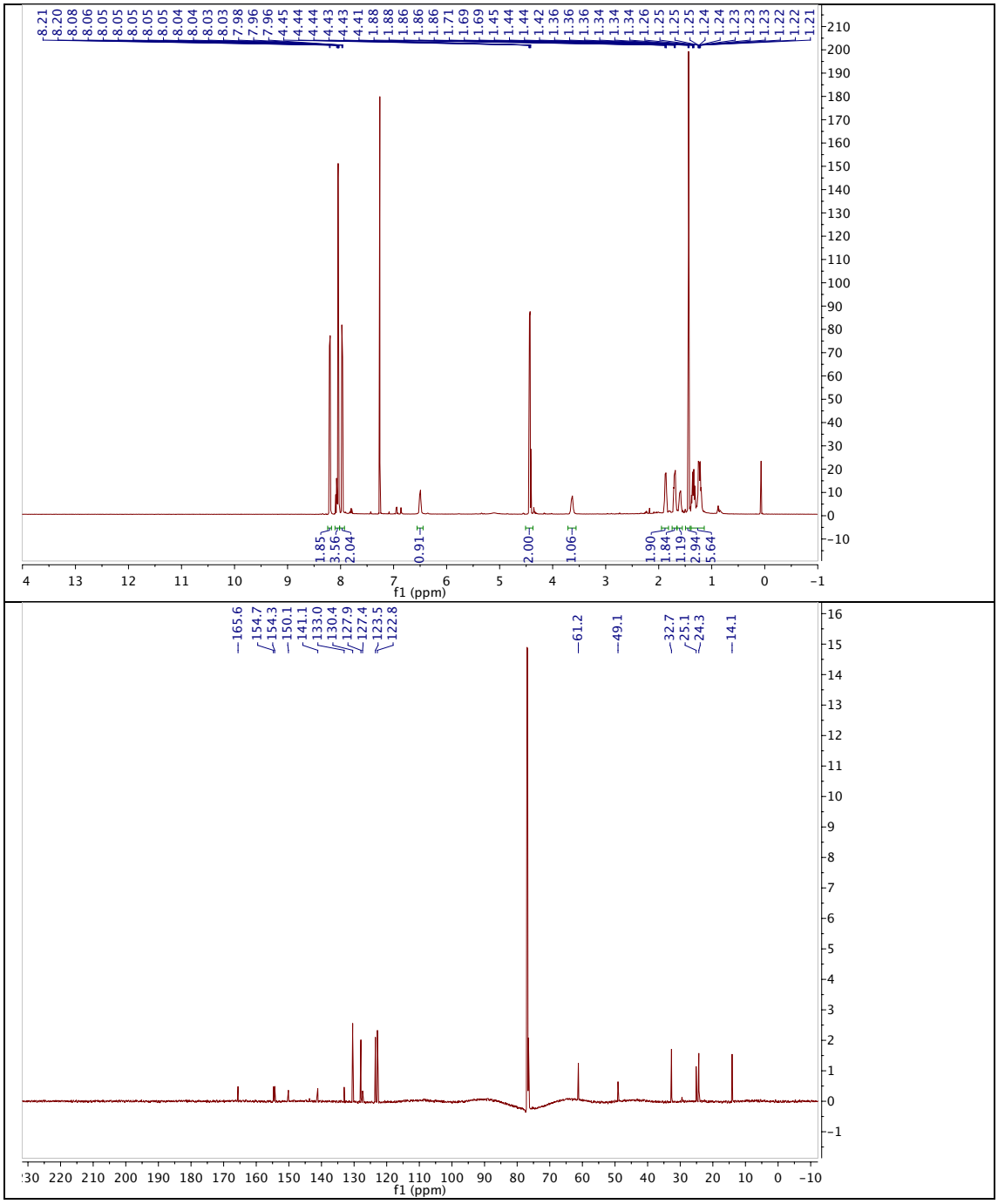

## 8.8 X-ray Crystallographic Data

### 8.8.1 (*E*)-*N*-(Cyclohexylcarbamoyl)-4-((4-(diethylamino)phenyl)diazenyl)-benzenesulfonamide (JB253)

**Supplementary Table 17: Crystallographic data of JB253.**

| | **JB253** |
|---|---|
| net formula | $C_{23}H_{31}N_5O_3S$ |
| $M_r$/g mol$^{-1}$ | 457.590 |
| crystal size/mm | 0.100 × 0.080 × 0.050 |
| $T$/K | 173(2) |
| radiation | 'Mo Kα |
| diffractometer | 'Bruker D8Venture' |
| crystal system | monoclinic |
| space group | $P2_1/n$ |
| $a$/Å | 15.8069(6) |
| $b$/Å | 9.0578(3) |
| $c$/Å | 17.1444(7) |
| α/° | 90 |
| β/° | 95.8298(13) |
| γ/° | 90 |
| $V$/Å$^3$ | 2441.97(16) |
| $Z$ | 4 |
| calc. density/g cm$^{-3}$ | 1.24466(8) |
| μ/mm$^{-1}$ | 0.166 |
| absorption correction | multi-scan |
| transmission factor range | 0.9045–0.9585 |
| refls. measured | 26927 |
| $R_{int}$ | 0.0416 |
| mean σ($I$)/$I$ | 0.0408 |
| θ range | 3.28–27.52 |

| | |
|---|---|
| observed refls. | 4046 |
| *x, y* (weighting scheme) | 0.0742, 2.2726 |
| hydrogen refinement | mixed |
| refls in refinement | 5578 |
| parameters | 299 |
| restraints | 0 |
| $R(F_{obs})$ | 0.0601 |
| $R_w(F^2)$ | 0.1664 |
| $S$ | 1.049 |
| shift/error$_{max}$ | 0.001 |
| max electron density/e Å$^{-3}$ | 1.022 |
| min electron density/e Å$^{-3}$ | −0.402 |

### 8.8.2 (*E*)-*N*-(Butylcarbamoyl)-4-((4-(diethylamino)phenyl)diazenyl) benzenesulfonamide (JB386)

**Supplementary Table 18: Crystallographic data of JB386.**

| | **JB386** |
|---|---|
| net formula | $C_{21}H_{30}CsN_5O_4S$ |
| $M_r$/g mol$^{-1}$ | 581.466 |
| crystal size/mm | 0.130 × 0.100 × 0.060 |
| $T$/K | 173(2) |
| radiation | 'Mo Kα |
| diffractometer | 'Bruker D8Venture' |
| crystal system | triclinic |
| space group | *P*1bar |
| $a$/Å | 9.0002(3) |
| $b$/Å | 12.1776(4) |
| $c$/Å | 23.3502(8) |
| α/° | 79.5295(10) |
| β/° | 88.6369(10) |
| γ/° | 81.6337(10) |

| | |
|---|---|
| $V$/Å$^3$ | 2489.80(14) |
| $Z$ | 4 |
| calc. density/g cm$^{-3}$ | 1.55123(9) |
| μ/mm$^{-1}$ | 1.607 |
| absorption correction | multi-scan |
| transmission factor range | 0.9101–0.9585 |
| refls. measured | 43925 |
| $R_{int}$ | 0.0239 |
| mean σ($I$)/$I$ | 0.0221 |
| θ range | 2.68–26.41 |
| observed refls. | 8946 |
| $x$, $y$ (weighting scheme) | 0.0203, 6.4900 |
| hydrogen refinement | mixed |
| refls in refinement | 10180 |
| parameters | 592 |
| restraints | 8 |
| $R(F_{obs})$ | 0.0393 |
| $R_w(F^2)$ | 0.0892 |
| $S$ | 1.193 |
| shift/error$_{max}$ | 0.001 |
| max electron density/e Å$^{-3}$ | 1.239 |
| min electron density/e Å$^{-3}$ | −0.771 |

### 8.8.3 (*E*)-5-((4-morpholinophenyl)diazenyl)-1,3,4-thiadiazole-2-sulfonamide (8.5)

**Supplementary Table 19: Crystallographic data of 8.5**

| | **8.5** |
|---|---|
| net formula | $C_{40}H_{54}N_{18}O_{11}S_8$ |
| $M_r$/g mol$^{-1}$ | 1219.500 |
| crystal size/mm | 0.250 × 0.233 × 0.066 |
| $T$/K | 173(2) |

| | |
|---|---|
| radiation | MoKα |
| diffractometer | 'Oxford XCalibur' |
| crystal system | monoclinic |
| space group | $P2_1/c$ |
| $a$/Å | 11.1228(5) |
| $b$/Å | 35.4529(17) |
| $c$/Å | 13.5819(7) |
| α/° | 90 |
| β/° | 91.285(4) |
| γ/° | 90 |
| $V$/Å$^3$ | 5354.4(4) |
| $Z$ | 4 |
| calc. density/g cm$^{-3}$ | 1.51282(11) |
| μ/mm$^{-1}$ | 0.408 |
| absorption correction | 'multi-scan' |
| transmission factor range | 0.98457–1.00000 |
| refls. measured | 17634 |
| $R_{\mathrm{int}}$ | 0.0280 |
| mean σ($I$)/$I$ | 0.0502 |
| θ range | 4.17–25.35 |
| observed refls. | 7356 |
| $x$, $y$ (weighting scheme) | 0.0373, 2.3251 |
| hydrogen refinement | mixed |
| refls in refinement | 9709 |
| parameters | 746 |
| restraints | 0 |
| $R(F_{\mathrm{obs}})$ | 0.0412 |
| $R_{\mathrm{w}}(F^2)$ | 0.0994 |

| | |
|---|---|
| $S$ | 1.019 |
| shift/error$_{max}$ | 0.001 |
| max electron density/e Å$^{-3}$ | 0.427 |
| min electron density/e Å$^{-3}$ | −0.433 |

C-H: constr, N-H: refall, disorder of a dmso described by a split model, sof ratio 0.68/0.32, C and O of less occupied part refined isotropically.

# *9 Photochromic Tethered Dimerizers (PTDs) and a Second Generation of Photochromic Tethered Ligands (PTLs)*

## 9.1 Introduction

Several (transmembrane) proteins have been successfully remote-controlled with light with the PTL approach.[162] However, this approach still bears some disadvantages, such as i) possible cross-reactivity with other free cysteines, ii) the creation of a stereocenter after attachment and iii) the possible hydrolysis and ring-opening of the generated succinimide,[80,81] which liberates more degrees of freedom. Furthermore, introduced "free" cysteines cost proteins quite an amount of energy and have to be made sometimes accessible with the help of other chemical reagents – for instance DTT or TCEP – as they tend to form more stable disulfide bonds *via* for instance dimerization.[163] A genetically encoded system (ideally with photochromic ligands) would therefore be advantageous, which can easily be diversified late-stage by chemical synthesis for a large number of biological targets. For this purpose, the SNAP-tag labeling technology can be employed. The SNAP-tag originates from the human DNA-repair protein $O^6$-alkylguanine-DNA-alkyltransferase and reacts with $O^6$-alkylated guanines (when benzylated termed **BG**) in a highly specific way therefore being tagged by a label of interest (Figure 51a).[164] Furthermore, it can be fused to a variety of proteins without loss of native activity.[165,166] Therefore, azobenzene-containing ligands with a benzyl-guanine moiety for attachment, and furthermore azobenzene-containing bis-benzyl-guanines for dimerizing SNAP-tag (fused) targets, would be advantageous. Thus, the concept of a second generation of a photochromic tethered ligand (PTL') (Figure 51b) and a novel photochromic tethered dimerizer (PTD) (Figure 51c) for the labeling of SNAP-tags with the ability to photoswitch the tether reversibly with light is introduced. Although dimerization of SNAP-fusion proteins has been described before.[167], this system can be envisioned as an advanced version for photopharmacology, which can be applied by research groups based on the ease of chemical synthesis. This results described in this chapter might pave the way for a cleaner photocontrol of

biological targets as it neglects the introduction of cysteines and thiol-maleimide chemistry.

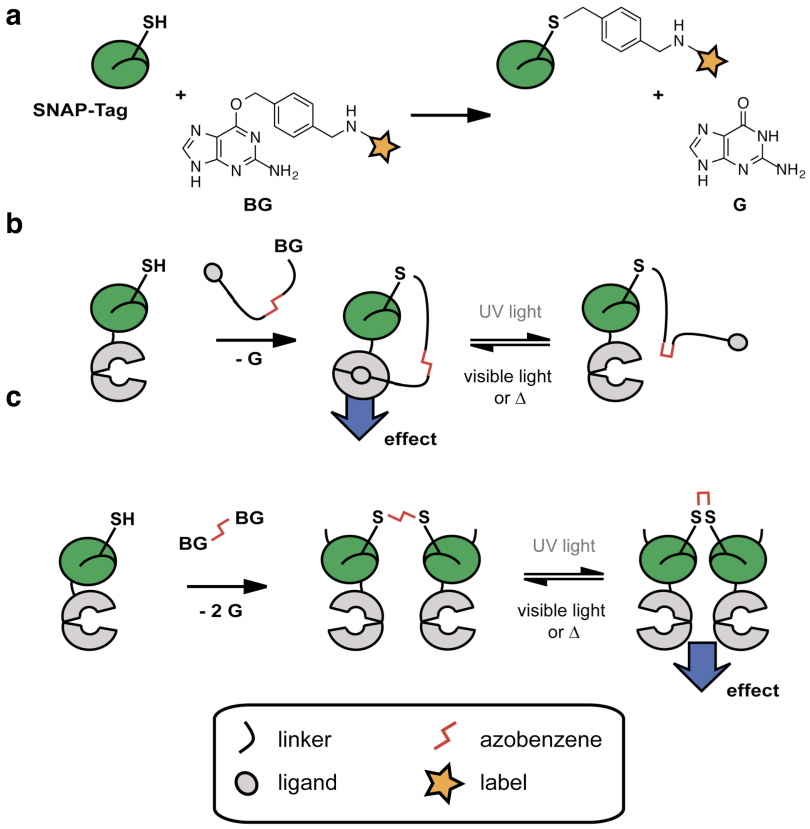


**Figure 51: The logic of the SNAP-tag technology and the PTL' and PTD approach for photopharmacology. a)** SNAP-tag labeling with an $O^6$-alkylated guanine (BG); the high specificity for the guanine substrate allows clean labeling, while guanine (G) serves as a leaving group. **b)** The genetically encoded photochromic tethered ligand (PTL') approach, where a ligand and a BG are fused to an azobenzene for SNAP-tag labeling and it can then bind in one state, triggering an effect, while not in the other. **c)** The photochromic tethered dimerizer (PTD) approach: SNAP-tag fused protein can be homodimerized with two BG linked to an azobenzene, thus being able to pull both proteins in closer proximity under UV light and eventually triggering an effect by dimerization.

## 9.2 Results and Discussion

*O*$^6$-Benzylated guanine (**BG**) is the indispensable precursor for utilizing the SNAP-tag technology as it combines the specific recognition pattern for labeling and a free amine, which can be coupled to the desired labeling agent. Therefore, **BG** synthesis was performed in a five-step procedure according to Johnsson and co-workers[164] with slight modifications to improve the yield of certain steps (see Experimental) and additional characterization of each compound by high-resolution mass spectrometry, $^{13}$C NMR and UV/Vis spectroscopy.

The first aim was to employ azide-alkyne click chemistry to build up the PTL' and PTD as the copper catalyzed Huisgen reaction is known to work under mild conditions in high yields.[94] In order to be synthetically flexible, an alkyne or an azide was installed on the **BG** by HBTU coupling (Scheme 11). Alkyne acid **9.2**, which was obtained from its corresponding alcohol **9.1** using a Jones oxidation protocol[168] with modified work-up procedure was coupled to **BG** (**9.4**) (in 43% yield) to give alkyne-BG **9.6**, while azide acid[169] **9.5** was coupled to **BG** (in 35% yield) to give azide-BG **9.7**, both after HPLC purification. Although complete conversion was observed, it is hypothesized that undesired side couplings have taken place, for instance on the aromatic amine. Nevertheless, the two novel compounds alkyne-BG **9.6** and azide-BG **9.7**, were obtained, which both are intended for alkyne-azide click chemistry and can serve as powerful intermediates for the derivatization of **BG** towards novel SNAP-tag labels..

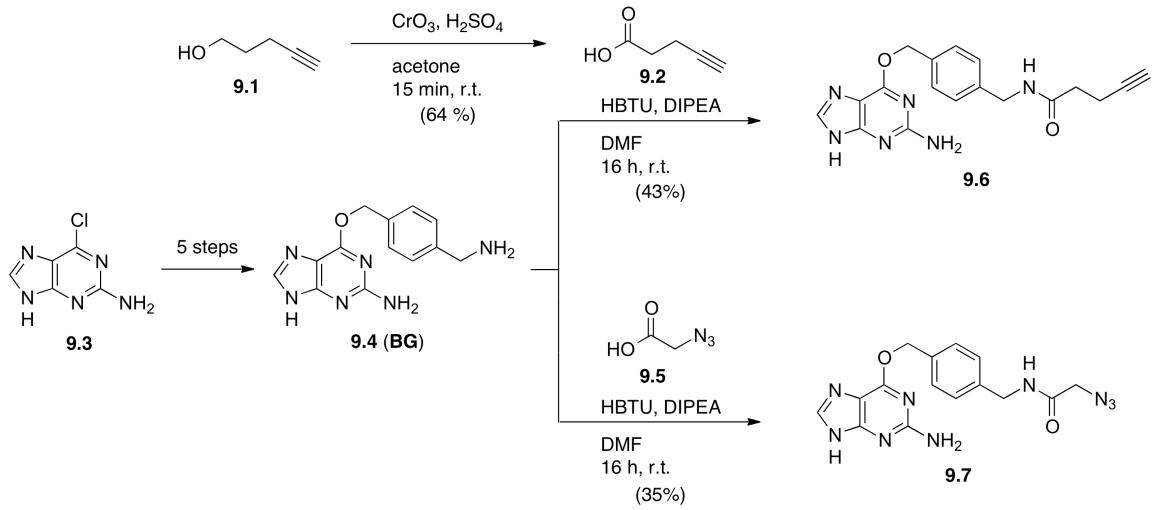


**Scheme 11: Diversification of BG for alkyne-azide click chemistry. BG** is synthesized according to Johnsson and co-workers[164] and then coupled to alkyne acid **9.2** (obtained via Jones oxidation from its corresponding alcohol **9.1**) or azide acid **9.5** to yield alkyne-BG **9.6** and azide-BG **9.7**, respectively.

The stage was set to build the first PTL' based on *D*-MAG0, which has successfully been used to photocontrol metabotropic glutamate receptors.[42] A long PEG-linker was chosen for solubility reasons and the activated $N_3$-$PEG_{12}$-NHS ester[170] was coupled to **9.8** to give protected glutamate containing amine **9.9**[42] (also see Chapter 5), a known intermediate in the synthesis of *D*-MAG0 in 80% yield to afford azide glutamate **9.10**. Click reaction of **9.10** with BG-alkyne **9.6** (under elevated temperatures) to form triazole **9.11**, and subsequent treatment with neat TFA yielded the desired PTL' (**9.12**) in 65% yield over two steps (Scheme 12). This fast route should be applicable for the synthesis of other PTL' as long as they bear a free amine that can be connected *via* an azide-containing PEG-linker and can then be "clicked" to the newly introduced alkyne-BG **9.6**.

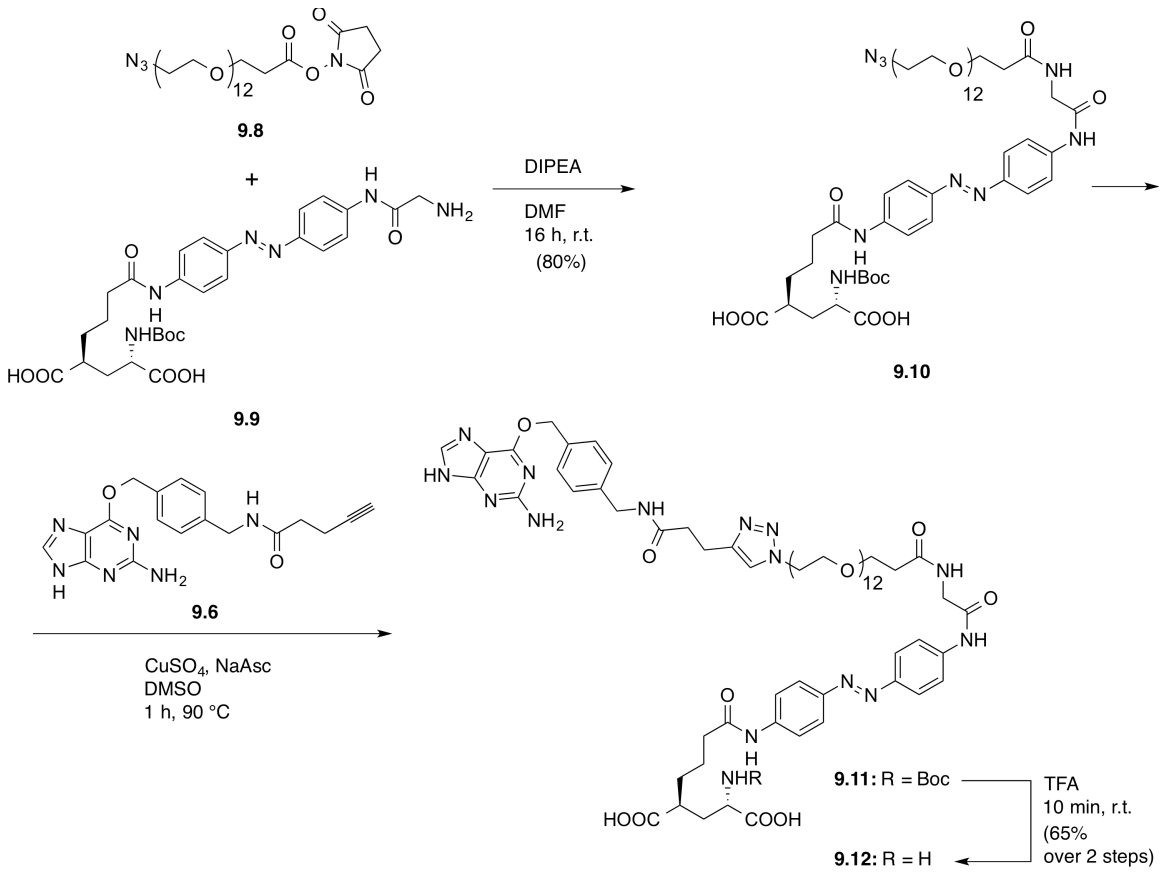


**Scheme 12: Synthesis of the second generation photochromic tethered ligand (PTL').** Amine **9.9**[42] was linked to an azide containing $PEG_{12}$ chain *via* activated NHS ester **9.8** to obtain azide glutamate **9.10**. Click-chemistry with alkyne-BG **9.6** tand triazole **9.11**, followed by Boc-deprotection, yielded the PTL' (**9.12**) for SNAP-tag labeling over two steps.

Initial UV/Vis spectroscopic experiments (the spectrometer being equipped with a monochromator to apply light orthogonally for switching) in aqueous Ringer solution showed the switchability of PTL' **9.12** from its dark adapted state (Figure 52a, black) to its photostationary *trans*-state under 440 nm (Figure 52a, blue) and its *cis*-state under 365 nm (Figure 52a, gray). Switching was reversible over five cycles, and **9.12** showed a tendency towards bi-stability when it was allowed to relax in the dark (Figure 52b). When fitting the slopes from Figure 52b exponentially, the τ-values were determined to be $\tau_{cis}$ = 26.9 ± 1.97 seconds and $\tau_{trans}$ = 28.0 ± 2.45 seconds (N≥4, mean±S.D.). It should be noted that the good solubility in water is highly advantageous for the testing of biological systems, a characteristic that small PCLs for instance do not share. Further

examination included the labeling of SNAP-tag protein, which was performed and analyzed using SDS-PAGE (Figure 52c). According to the manufacturer (see Experimental for details), the SNAP-tag's molecular weight is 19.7 kDa, which should be increased by 1.25 kDa upon binding to **9.12** following the loss of guanine. Indeed, when the protein was incubated for 30 minutes at 37 °C with **9.12** (stochiometry = 1/2), a shift in molecular weight of the expected size was observed (Figure 52c, left lane versus middle lane). In a control experiment, incubating **9.12** alone under the same reaction conditions was not detectable. Therefore, the PTL' **9.12** is fully functional with regards to photoswitching, solubility and reactivity towards SNAP-tag protein.

In preliminary electrophysiological experiments on HEK293t cells that were co-transfected with a N-terminal fused SNAP-tag to mGluR2 and GIRK1/2 photodependent currents could be recorded (Figure 52d). After incubation of the transfected cells with 9.12 for 1 h and extensive wash-out with buffer, GIRK currents could be evoked by illuminating the sample with UV-light. A wavelength screen was performed ranging from 330 to 430 nm in 20 nm steps, and the best currents could be triggered with 370 nm. Even more, all currents could be reversibly muted by illumination with green light (500 nm).

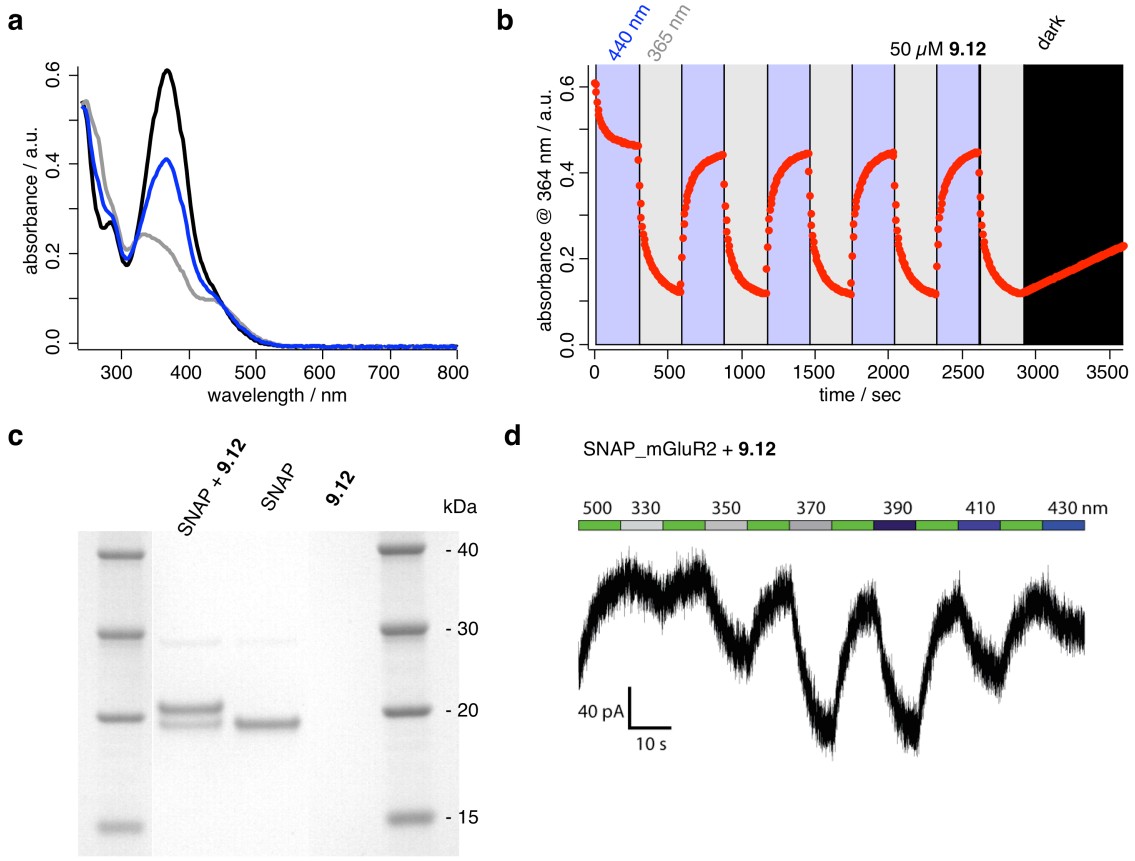


**Figure 52: UV/Vis spectroscopy of 50 µM of 9.12 in Ringer solution and SNAP-tag labeling including function *in vivo*. a)** UV/Vis spectra of the dark-adapted state (black), and illuminated with λ = 440 nm (blue) and λ = 365 nm (gray). **b)** Kinetic trace recorded at the 364 nm while switching **9.12** with blue light (λ = 440 nm, blue) and UV light (λ = 365 nm, gray) including slow dark relaxation at the end of the experiment. **c)** SDS-PAGE of SNAP-tag with **9.12** shows a shift of approximately 1 kDa (left lane) with respect to pure SNAP-tag (middle) lane. **9.12** alone served as a control (right lane). Note that gel was modified: bands of compounds irrelevant for this study were cut. **d)** HEK293t cells co-transfected with a SNAP_mGluR2 construct together with GIRK1/2 and labeled with **9.12** gave reversible photodependent currents in a wavelength screen. Optimal wavelength for GIRK activation is 370 nm, while 500 nm was able to reverse the current.

The second goal, the synthesis of a PTD was anticipated for by click chemistry between alkyne-BG **9.6** or azide-BG **9.7** with their respective azobenzene counterparts. Therefore, the same acids used before to diversify **BG** (*i.e.* **9.2** and **9.5**) were coupled under HBTU conditions to 4,4'-bisamino azobenzene **9.13** to obtain bis-alkyne azobenzene **9.14** and bis-azide-azobenzene **9.15** in 55% and

35% yield, respectively (Scheme 13a). Unfortunately, and albeit multiple attempts using different Cu(I) sources (*i.e.* $CuSO_4$ and NaAsc or CuBr) in different solvent systems (*i.e.* DMSO, MeCN, *tert*-BuOH, THF) and using elevated temperatures up to 100 °C, formation of either triazoles could not be accomplished (Scheme 13b).

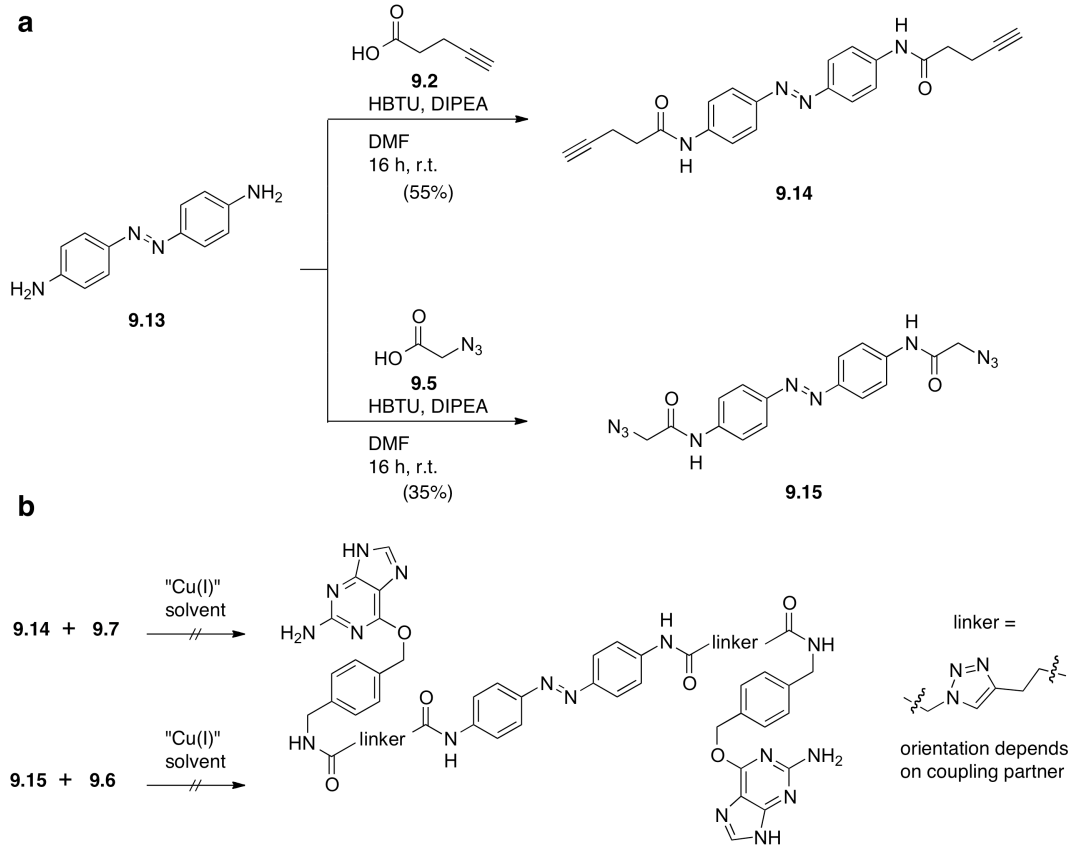


**Scheme 13: First synthetic attempt to obtain the PTD via click-chemistry. a)** Bis-amino azobenzene **9.13** was coupled to alkyne acid **9.2** and azide acid **9.5** to yield the corresponding bis-alkyne azobenzene **9.14** and bis-azide azobenzene 15. **b)** Click chemistry failed, albeit multiple attempts for both substrates (**9.14** and **9.7**; **9.15** and **9.6**) and screening different Cu(I) sources and solvents systems.

Consequently, looking back at the successful amide couplings, the strategy was redesigned. Bis-amino azobenzene **9.13** was again functionalized on both amines this time by opening succinic anhydride (**9.18**) to obtain the corresponding bis-acid azobenzene **9.19** in 84% yield. Although HBTU coupling to **BG** was achieved

with complete conversion according to LCMS, it proved impossible to isolate the desired product **9.20** (Scheme 14). Instead, either starting material or decomposition products were recovered.

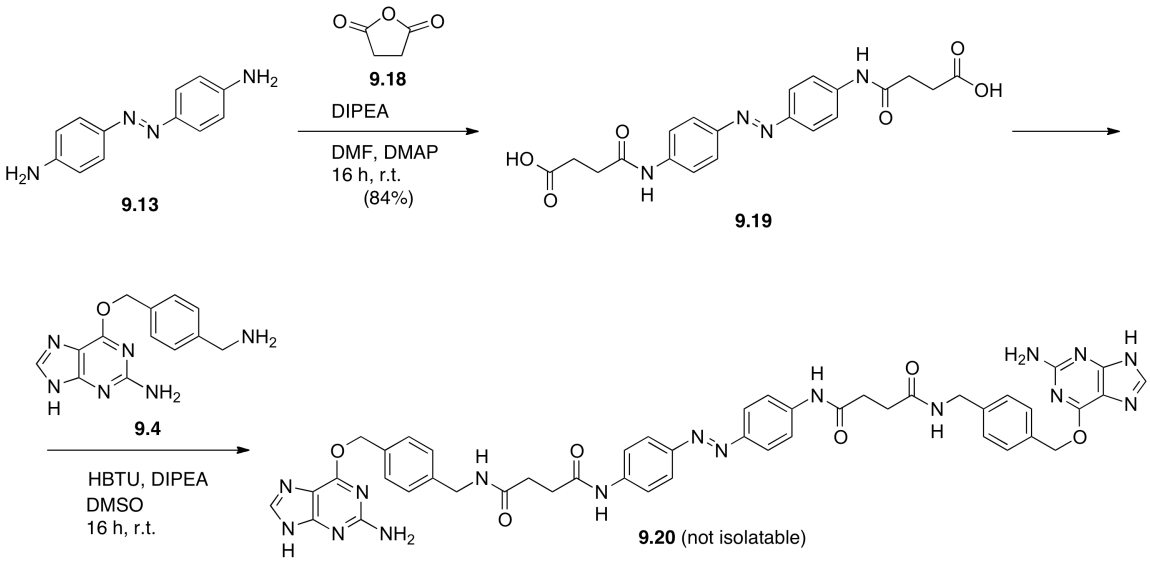


**Scheme 14: Second attempt toward the PTD synthesis.** After succinic anhydride opening of bis-amine **9.13** to obtain the azobenzene bis-acid **9.19**, **BG** was HBTU coupled with HBTU to this precursor. Although conversion was complete according to LCMS, **9.20** could not be isolated albeit multiple attempts.

As a last resort, and with the knowledge that alkyne-BG **6** does successfully undergo click reactions, a three-component one-pot synthesis was developed to finally access a PTD. A highly reactive and commercially available cyclooctyne[171] **9.21**, which also bears an activated NHS ester was used for copper-free click conditions. Bis-azide azobenzene **9.15**, **BG** and linker **9.21** were combined in DMF and, after 6 hours at room temperature, PTD **9.22** was isolated in 46% yield after HPLC purification as a mixture of regioisomers (Scheme 15). However, the end-to-end distance should not be affected considerably by the possible 1,4-1,4-, 1,4-1,5- or 1,5-1,5-regioisomers as it exhibits degrees of freedom among the succinate chain. Furthermore, by eliminating copper from the reaction mixture, the time-consuming work-up procedures to separate the metal from the PTD, which have been described to be difficult before and is not compatible with biological systems due to its toxicity were circumvented.[98]

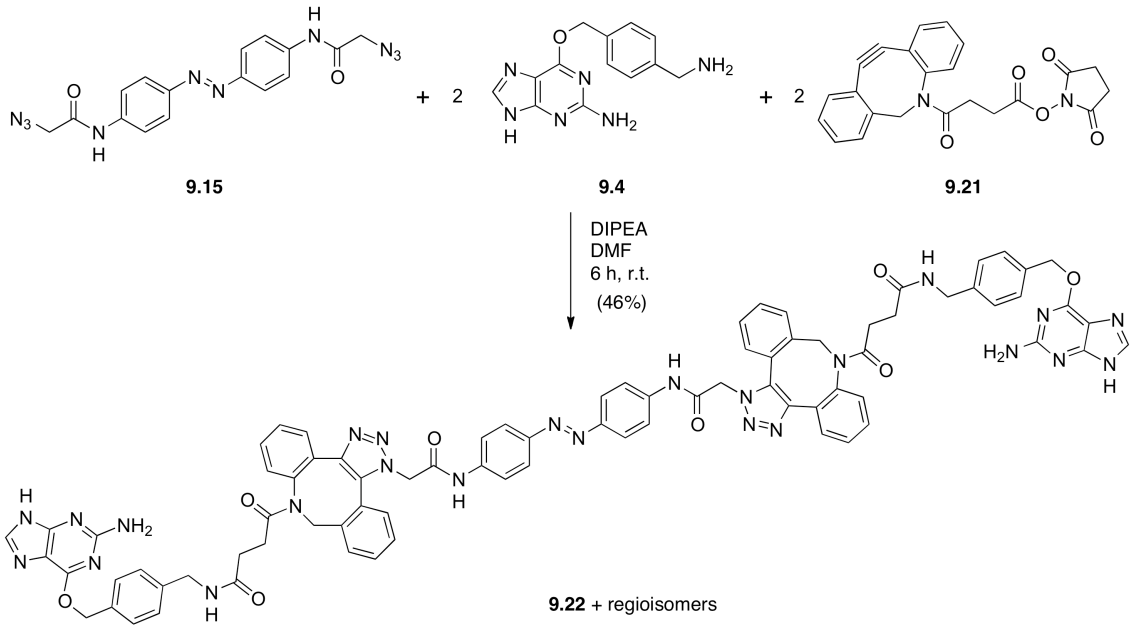


**Scheme 15: Synthesis of the photochromic tethered dimerizer (PTD).** A three-component-one-pot reaction was employed for building the PTD **9.22** at room temperature. Linker **9.21** combined azide **9.15** by strain-promoted copper-free click chemistry to yield the triazole, while the activated NHS ester of **9.21** reacted with **BG** to form an amide bond. Only one obtained regioisomer (1,4-1,4) is shown for clarity.

The UV/Vis spectral analysis of **9.22** in aqueous Ringer solution shows switching capability from the dark-adapted state (Figure 53a, black) to its photostationary *trans*-isomer under blue light irradiation (λ = 440 nm) (Figure 53a, blue) and to its *cis*-isomer under UV-light (λ = 375 nm) (Figure 53a, gray). Switching can be reversibly achieved for at least five cycles, while some bi-stability was observed when **9.22** was allowed to thermally relax (Figure 53b). Kinetics were obtained by exponential fit of the switching experiments and were determined to be $\tau_{cis}$ = 75.4 ± 6.04 seconds and $\tau_{trans}$ = 37.2 ± 1.52 seconds (N≥4, mean±S.D.). With respect to PTL' **9.12**, PTD **9.22** was only soluble up to 25 µM in buffer, which still is high enough to avoid limitations for SNAP-tag labeling (*in vivo* labeling of an Alexa488-dye is performed with 5 µM of labeling reagent as in the manufacturer's instructions[172]). However, when subjected to SNAP-tag labeling, only one site was attached to the protein albeit different concentrations (Figure 53c). While control experiments of solely **9.22** or SNAP-tag (lane 1 and 2) proved

to be consistent with previous experiments, incubation of increasing **9.22** with the SNAP-tag always yielded a shift of ~1 kDa (lane 3-6), which is expected for single attachment (calculated: 1.36 kDa). A possible explanation is that the linker length is too short, *i.e.* after first attachment the chain interacts with the protein and is therefore not accessible for a second labeling reaction.

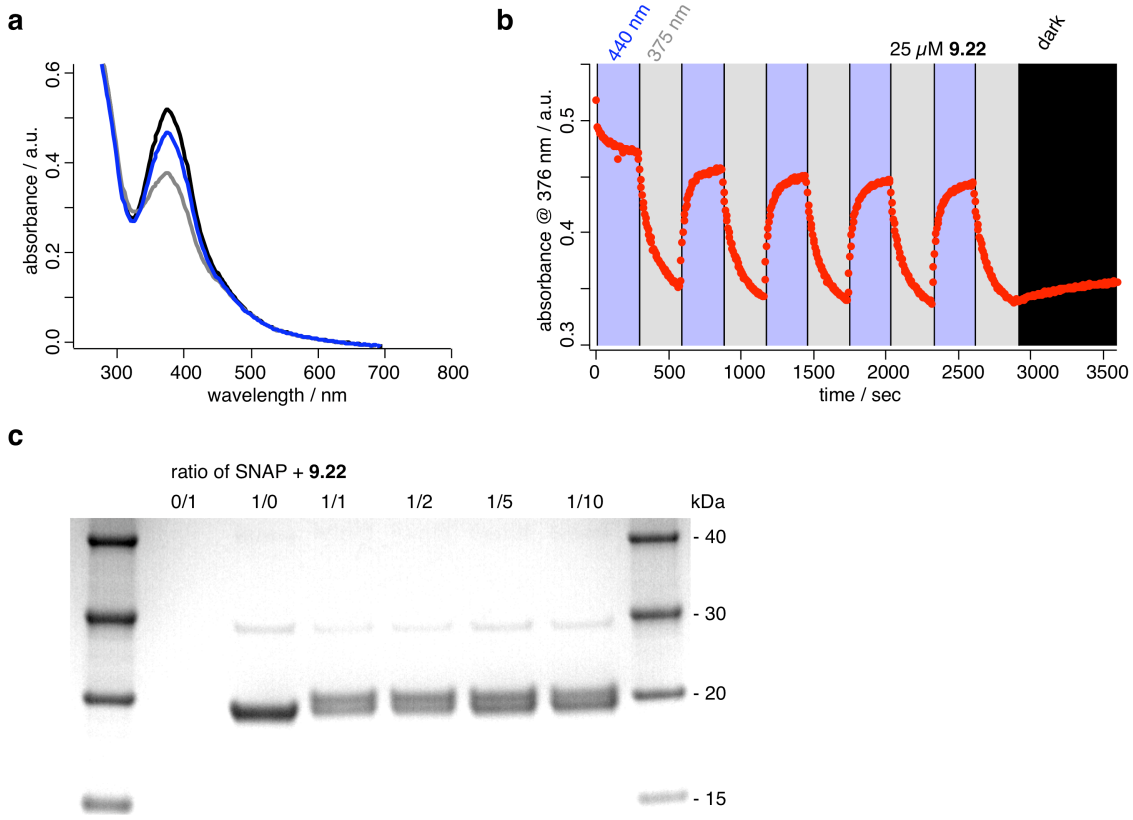


**Figure 53: UV/Vis spectroscopy of 25 µM of 9.22 in Ringer solution and SNAP-tag labeling. a)** UV/Vis spectra of the dark adapted state (black), and illuminated with λ = 440 nm (blue) and λ = 375 nm (gray). **b)** Kinetic traces recorded at the 376 nm while switching **9.22** with blue light (λ = 440 nm, blue) and UV light (λ = 375 nm, gray) including slow dark relaxation at the end of the experiment. **c)** SDS-PAGE after reaction of SNAP-tag with increasing concentration of **9.22** does not lead to enhanced double labeling.

Another G-protein coupled receptor has been SNAP-tagged, *viz*. the µ-opioid receptor.[173] Together with recent findings that led to the optical control over this receptor,[174] another PTL' can be envisioned that is based on fentanyl with a similar approach as described above. Therefore a synthetic route was started commencing with *N*,*N*-diallylaniline (**9.23**)[175] and diazonium salt **9.24**[176] to give

the bis-allyl protected nitro azobenzene **9.25** in 81% yield. Subsequent reduction of **9.25** to amine **9.26** was achieved in quantitative yield with sodium sulfide. Reductive amination with ketone **9.27** gave access to azobenzene **9.28** in 85% yield based on recovered starting material (brsm) (Scheme 16).

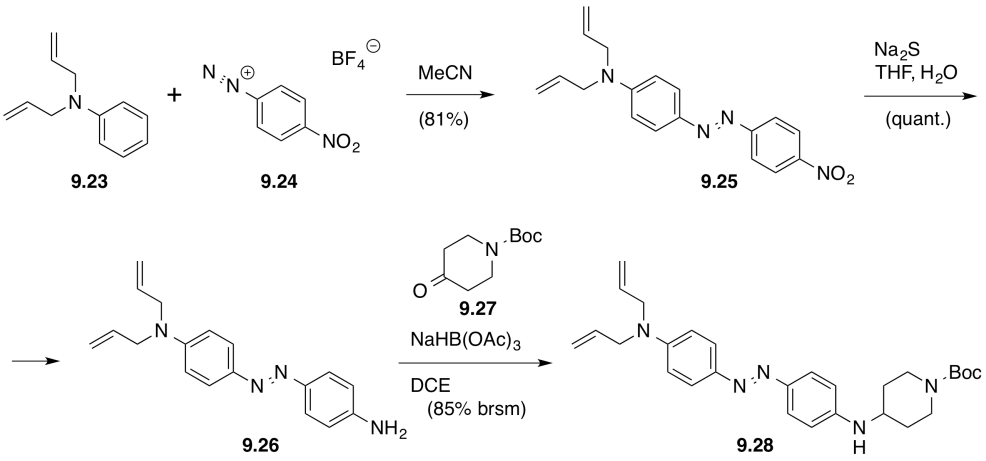


**Scheme 16: Synthesis of 9.28.** Literature reported aniline and diazonium (**9.23** and **9.24**) were reacted to give nitro azobenzene **9.25**, which was reduced to its corresponsing amine 9.26. Reductive amination with ketone **9.27** led to **9.28**.

Further derivatization of **9.28** included acylation of the aniline with propionyl chloride to its corresponding anilide **9.29**, which was deproteteced in neat TFA to give the free amine **9.30**. The latter underwent reductive amination with 2-phenyl acetaldehyde in order to obtain fenanyl based scaffold **9.31** (Scheme 17).

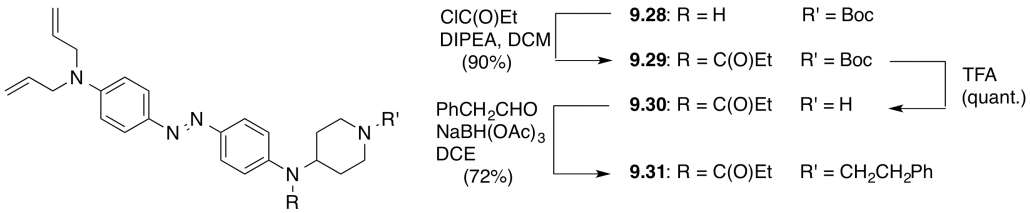


**Scheme 17: Derivatization of 9.28 to 9.31.** Acylation, deprotection and reductive amination yielded **9.31** in 65% over three steps.

Bis-allyl amino fentanyl **9.31** has to be deprotected to its corresponsing amine, which can be further reacted with a linker containing **BG** (Scheme 18). First, deprotection could be achieved with $^{t}$BuOK in DMSO and the corresponding

amine reacted with Fmoc-glycine. After Fmoc-deprotection, and according to the procedures described for **9.12** (*vide supra*), benzyl guanine azobenzene fentanyl (**BGAF**) could be obtained for PTL' photocontrol over the μ-opioid receptor.

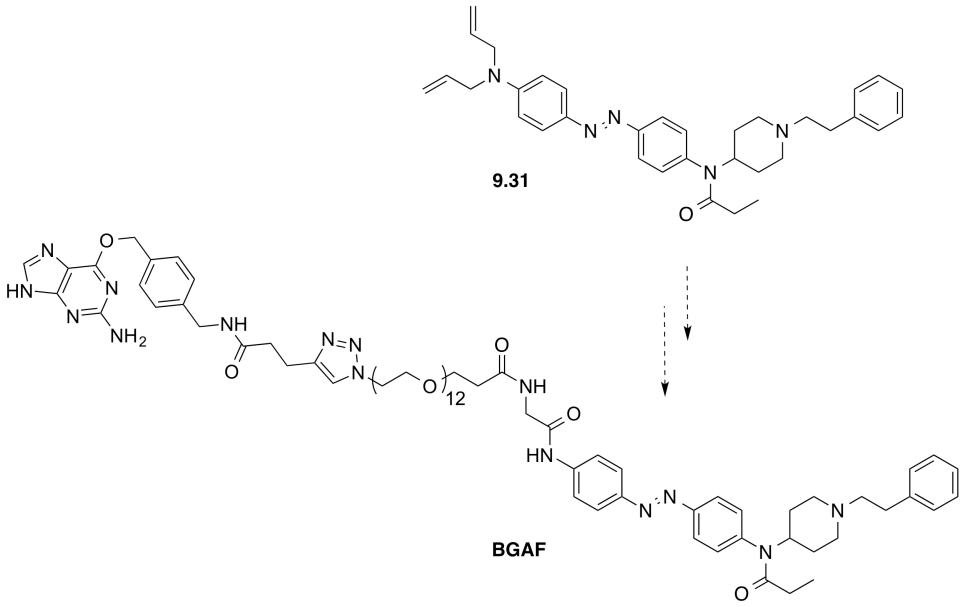


**Scheme 18: 9.31 has to be further derivatized to give BGAF.**

## 9.3 Conclusion and Outlook

It should be noted, after all these attempts that different linker lengths would have resulted in different desired PTDs. However, from a proof-of-principle point of view, we were rather interested in synthesizing a bis-**BG** linked by an azobenzene for SNAP-tag dimerization rather than optimizing the length. This subject will have to be addressed when specific targets are chosen for homodimerization and await further experimentation.

Thus far, novel **BG**- and azobenzene-derivatives for click chemistry have been synthesized. Furthermore, two molecules for SNAP-tag labeling are presented to ultimately control biological function with light by a genetically encodable labeling technique. Ultimately, it is shown that labeling of the photochromic molecules can be achieved with short reaction times *in vitro*, paving the way for more photopharmacological control of biological functions in a genetically encoded way. The PTL' can be accessed easily with commercially available $N_3$-$PEG_{12}$-NHS ester, of which other PEG-linker lengths are available. Most importantly, PTL' **9.12** does work on HEK293t cells that co-express a SNAP-tagged mGluR2 and GIRK1/2. The optical control over these potassium channels via a GPCR could open new avenues for the elucidation of for instance heteromultimers of mGluRs by selective labeling and activation.

The PTD is synthesized in a three-component-one-pot synthesis, linking the azobenzene to **BG** via an amide coupling and strain-promoted, copper-free click chemistry with a commercially available cyclooctyne.

Both, the PTD and the PTL' molecules can be switched reversibly over many cycles and dark relaxation is slow, which is beneficial as not to irradiate living systems with UV light for an extended period of time and induce phototoxic reactions. Employing the synthetic route described herein will lead to more PTL' and PTD in the future, likely with different linker lengths, which will be tested for biological activity in the Trauner laboratories. Lastly, coupling of both, PTL' **12** and PTD **22** to pure and recombinant SNAP-protein were successful *in vitro*.

Therefore, the stage is set to further explore labeling and functionality in living systems.

Furthermore, **BGAF** synthesis has to be completed in order to perform similar experiments that have been carried out for **9.12** on the μ-opioid receptor.

## 9.4 Experimental

### 9.4.1 Synthesis of BG

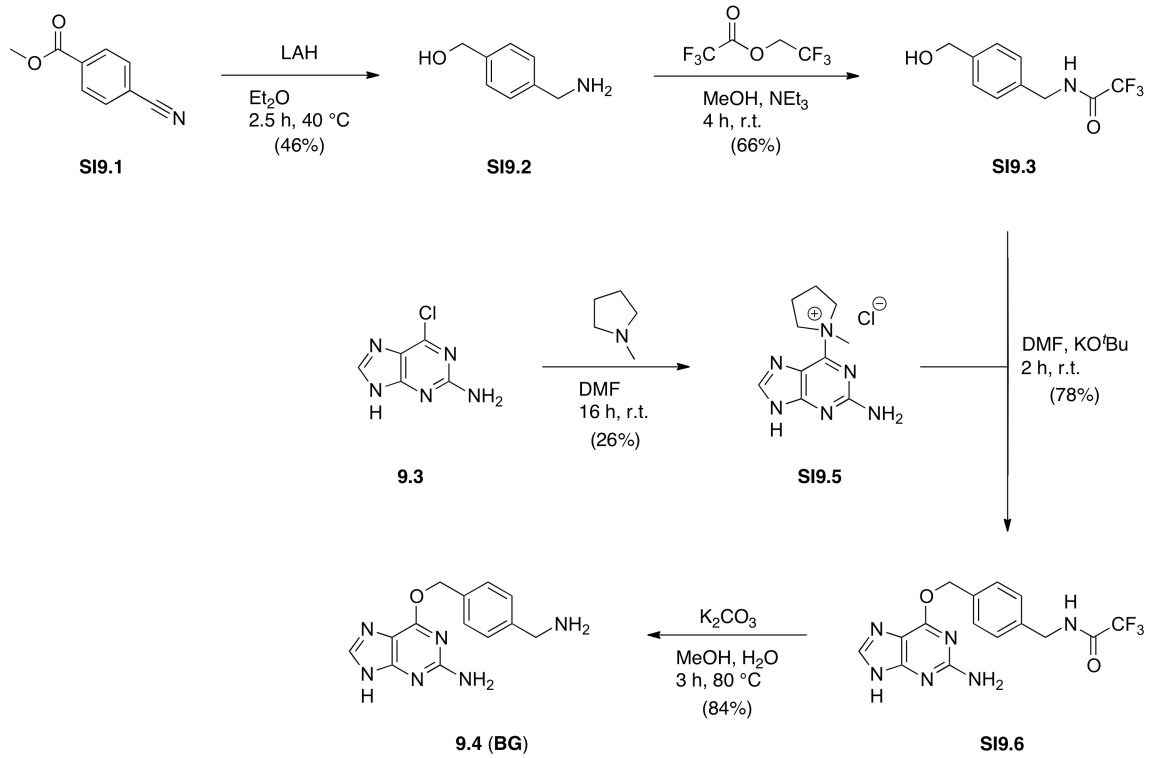


**Supplementary Scheme 2: Synthesis of benzyl guanine BG. SI9.1** is completely reduced by LAH and the resulting free amine **SI9.2** is protected as its trifluoro acetate **SI9.3**. In parallel, chloro-guanine SI9.4 is activated with N-methyl pyrrolidine to give **SI9.5**. Aromatic substitution between **SI9.3** and **SI9.5** afforded protected **BG SI9.6**, which is deprotected under basic conditions to yield **BG**.

#### 9.4.1.1 (4-(Aminomethyl)-phenyl)-methanol (SI9.2)

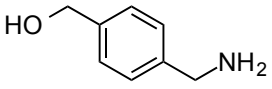

LAH (7.40 g, 195 mmol, 6.4 eq.) was suspended in $Et_2O$ (375 mL). To this suspension a solution of methyl 4-cyanobenzoate (**SI9.1**) (4.92 mg, 30.5 mmol, 1.0 eq.) in $Et_2O$ (30 mL) was added dropwise. The reaction was refluxed for 2.5 h at 40 °C. The reaction mixture was cooled to -4 °C and $H_2O$ (7.40 mL),

NaOH (15%, 7.40 mL) and $H_2O$ (22.2 mL) was added sequentially drop-wise. The solution was filtered through a pore III frit and the filtrate was purified by flash column chromatography (DCM/MeOH = 0.95/0.05 → 0.925/0.075). All solvents were removed *in vacuo* and 1.91 g (13.9 mmol) of the desired product was obtained in 46% yield.

**$^1$H NMR** (400 MHz, $CDCl_3$): $\delta$ [ppm] = 7.28 (d, $J$ = 8.2, 2H), 7.22 (d, $J$ = 8.1 Hz, 2H), 4.60 (s, 2H), 3.76 (s, 2H), 2.28 (br s, 3H).

**$^{13}$C NMR** (101 MHz, $CDCl_3$): $\delta$ [ppm] = 141.8, 140.1, 127.1, 127.1, 64.3, 45.9.

**HRMS (ESI)**: calc. for $C_8H_{11}NO^+$ $(M+H)^+$: 138.0913, found: 138.0913.

### 9.4.1.2 2,2,2-Trifluoro-N-(4-(hydroxymethyl)benzyl)acetamide (SI9.3)

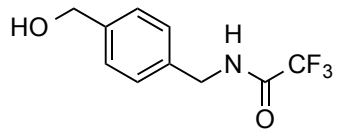


(4-(aminomethyl)-phenyl)-methanol (**SI9.2**) (1.90 g, 13.8 mmol, 1.0 eq.) was dissolved in dry MeOH (23 mL) and $NEt_3$ (5.9 mL, 42.6 mmol, 3.1 eq.). 2,2,2-trifluoroethyl 2,2,2-trifluoroacetate (6.0 mL, 44.7 mmol, 3.2eq.) was added drop-wise. The mixture was stirred for 4 h at r.t., before the mixture was diluted with $H_2O$ (50 ml) and EtOAc (50 mL), the organic layer was washed with brine and concentrated *in vacuo*. The crude product was purified by flash column chromatography (DCM/MeOH = 0.95/0.05) and purified once more by flash column chromatography (EtOAc/pentane = 1/5 → 1/1). All solvents were removed *in vacuo* and 2.11 g (9.05 mmol) of the desired product was obtained in 66% yield.

**$^1$H NMR** (400 MHz, DMSO-$d_6$): $\delta$ [ppm] = 9.98 (s, 1 H), 7.29 (d, $J$ = 8.4 Hz, 2H), 7.23 (d, $J$ = 8.4, 2H), 5.16 (t, $J$ = 5.6 Hz, 1H), 4.47 (d, $J$ = 5.6 Hz, 2H), 4.37 (d, $J$ = 6.0 Hz, 2H).

**$^{13}$C NMR** (101 MHz, DMSO-$d_6$): $\delta$ [ppm] = 156.3 (q, $J$ = 36.0 Hz), 141.7, 135.8, 127.2, 126.6, 116.0 (q, $J$ = 286.5 Hz), 62.6, 42.4.

**HRMS (EI)**: calc. for $C_{10}H_9F_3NO_2^{\cdot+}$ ($M^{\cdot+}$): 233.0664, found: 233.0662.

### 9.4.1.3 (1-(2-Amino-9*H*-purin-6-yl)-1-methylpyrrolidin-1-ium-2-ylium) chloride (SI9.5)

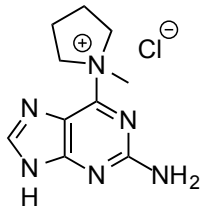


6-chloro-9*H*-purin-2-amine (**SI9.4**) (5.00 g, 29.5 mmol, 1.0 eq.) was dissolved in DMF (250 mL). The suspension was heated until the solution was clear. 1-methylpyrrolidine (7.00 mL, 64.9 mmol, 2.2 eq.) was added and the reaction mixture was stirred o.n. at r.t.. Acetone (20 mL) was added and the solution was filtered through a pore III frit. Acetone (70 mL) was added to the filtrate and filtered through a pore III frit again. The residue was washed with $Et_2O$ (20 mL) and dried under HV conditions. 1.95 g (7.66 mmol) of the desired product was obtained in 26% yield.

**$^{1}$H NMR** (400 MHz, DMSO-$d_6$): $\delta$ [ppm] = 13.32 (br s, 1H), 8.34 (br s, 1H), 7.11 (br s, 2H), 4.60–4.58 (m, 2H), 3.97–3.94 (m, 2H), 3.64 (s, 3H), 2.24–2.23 (m, 2H), 2.07–2.05 (m, 2H).

**$^{13}$C NMR** (101 MHz, DMSO-$d_6$): $\delta$ [ppm] = 159.1, 158.6, 151.7, 142.9, 116.0, 64.1, 51.6, 21.4.

**HRMS (ESI)**: calc. for $C_{10}H_{15}N_6^+$ $(M)^+$: 219.1353, found: 219.1353.

### 9.4.1.4 *N*-(4-(((2-Amino-7*H*-purin-6-yl)oxy)methyl)benzyl)-2,2,2-trifluoroacetamide (SI9.6)

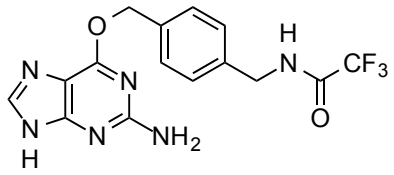

(1-(2-amino-9*H*-purin-6-yl)-1-methylpyrrolidin-1-ium-2-ylium) chloride (**SI9.5**) (2.00 g, 8.58 mmol, 2.2 eq.) was dissolved in dry DMF under $N_2$ atmosphere and KO$^t$Bu (1.98 g, 17.6 mmol, 4.5 eq.) was added. 2,2,2-trifluoro-N-(4-(hydroxymethyl)benzyl)acetamide (**SI9.3**) (992 mg, 3.90 mmol, 1.0 eq.) was added and the solution was stirred for 2 h at r.t.. Solvents were removed *in vacuo* and the crude product was purified by flash column chromatography (MeOH/DCM = 1/50 → 1/10). All solvents were removed under HV conditions and 1.12 g (3.06 mmol) of the desired product was obtained in 78% yield.

**$^1$H NMR** (400 MHz, DMSO-$d_6$): $\delta$ [ppm] = 12.42 (s, 1H), 10.01 (s, 1H), 7.81 (s, 1H), 7.49 (d, $J$ = 8.0 Hz, 2H), 7.30 (d, $J$ = 8.0 Hz, 2H), 6.28 (s, 2H), 5.46 (s, 2H), 4.39(s, 2H).

**$^{13}$C NMR** (101 MHz, DMSO-$d_6$): $\delta$ [ppm] = 174.4, 163.9, 160.1, 157.2 (q, $J$ = 36.5 Hz, -$CF_3$), 137.7, 136.4, 129.2, 128.0, 118.8, 117.9, 100.1, 67.1, 42.9.

**HRMS (ESI)**: calc. for $C_{15}H_{14}F_3N_6O_2^+$ $(M+H)^+$: 367.1125, found: 367.1123.

**UV/Vis** (LCMS): $\lambda$ ($\pi \rightarrow \pi^*$) = 286 nm.

**$R_t$** (LCMS; MeCN/$H_2O$/formic acid = 10/90/0.1 → 90/10/0.1 over 7 min) = 2.999 min.

### 9.4.1.5 6-((4-(Aminomethyl)benzyl)oxy)-7*H*-purin-2-amine (9.4, BG)

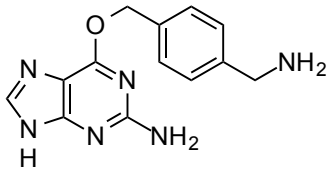

*N*-(4-(((2-amino-7*H*-purin-6-yl)oxy)methyl)benzyl)-2,2,2-trifluoroacetamide (**SI9.6**) (1.11 g, 3.03 mmol, 1.0 eq.) was suspended in MeOH (136 mL) and $H_2O$ (8 mL). $K_2CO_3$ (2.18 g, 15.8 mmol, 5.2 eq.) was added and the reaction mixture was refluxed for 3 h at 80 °C. The mixture was concentrated *in vacuo* and the crude product was purified by flash column chromatography (DCM/$NEt_3$/MeOH = 5/0.05/1) and subjected to RP-HPLC (MeCN/$H_2O$/formic acid = 10/80/0.1 → 80/20/0.1 over 40 min). All solvents were removed and the product was dried under HV-conditions. 68.6 mg (2.54 mmol) of the desired product was obtained in 84% yield.

**$^1$H NMR** (400 MHz, DMSO-$d_6$): $\delta$ [ppm] = 8.58 (s, 1H), 7.74 (s, 1H) 7.22 (d, *J* = 8.0 Hz, 2H), 7.31 (d, *J* = 8.0 Hz, 2H), 6.01 (s, 2H), 5.45 (s, 2H), 3.70 (s, 2H), 4.50 – 3.80 (br s, 6H, 2 $H_2O$ and $-NH_2$).

**$^{13}$C NMR** (101 MHz, DMSO-$d_6$): $\delta$ [ppm] = 165.8, 159.3, 159.1, 144.1, 140.6, 134.8, 128.3, 127.0, 113.3, 66.5, 45.5.

**HRMS (ESI)**: calc. for $C_{13}H_{15}N_6O^+$ $(M+H)^+$: 271.1302, found: 271.1299.

**UV/Vis** (LCMS): λ (π → π*) = 287 nm.

**$R_t$** (LCMS; MeCN/$H_2O$/formic acid = 10/90/0.1 → 90/10/0.1 over 7 min) = 0.741 min.

## 9.4.2 Synthesis of Photochromic Tethered Dimerizers and Second Generation Photochromic Tethered Ligands

### 9.4.2.1 Amide Coupling Procedure

Acid (1.2–2.0 eq. / amine group) and amine (1.0 eq.) were combined in a round bottom flask equipped with a stirring bar and HBTU was added in one portion. The solids were dissolved in DMF and cooled to 0 °C. DIPEA was added dropwise and the solution was allowed to warm to r.t. and stirred o.n.. The crude reaction mixture was filtered through a PTFE filter (CHROMAFIL® Xtra PTFE 0.45) and

subjected to RP-HPLC (MeCN/$H_2O$/formic acid = 10/80/0.1 → 80/20/0.1 over 40 min). All solvents were removed *in vacuo*.

#### 9.4.2.2 Click Chemistry Protocol

Stock solutions of $CuSO_4$ x 5 $H_2O$ (100 mg, 3.8 mL, 105 mM) and sodium ascorbate (100 mg, 3.8 mL, 131 mM) were prepared in $N_2$ sat. $H_2O$. Equal volumes of the stock solutions were combined to obtain the catalytic $Cu^I$ species. Azide (1.0 eq.) and alkyne (1.1 eq.) were combined in a Schlenk flask and dissolved in DMSO. The $Cu^I$ solution was added and the reaction mixture was stirred at 90 °C. Reaction progress was monitored using LCMS until all starting material was consumed. The reaction was allowed to cool to r.t. and filtered through a PTFE filter (CHROMAFIL® Xtra PTFE 0.45) and subjected to RP-HPLC (MeCN/$H_2O$/formic acid = 10/80/0.1 → 80/20/0.1 over 40 min).

#### 9.4.2.3 Pent-4-ynoic acid (9.2)

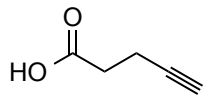


105 mmol of Jones reagent was freshly prepared according to the literature procedure of Eisenbraun.[168] To the freshly prepared chromic acid solution, pent-4-yn-1-ol (**9.1**) (4.00 g, 47.6 mmol, 1.0 eq.) was dissolved in 200 mL acetone and added drop-wise submerged in an ice bath. After 15 min, the reaction was diluted with 250 mL $H_2O$ and extracted with $Et_2O$ (3 x 200 mL). The combined organic layers were washed with $H_2O$, extracted with 3 M NaOH (3 x 100 mL) and the combined aqueous washed again with $Et_2O$ (3 x 100 mL). The basic aqueous solution was carefully acidified under ice-cooling with cHCl (100 mL) and extracted with $Et_2O$ (4 x 150 mL). The combined organic layers were dried over $MgSO_4$ and 3.00 g (30.6 mmol) of the title compound (**9.2**) was isolated after removal of all volatiles in 64% yield as a white solid.

**$^1$H NMR** (400 MHz, DMSO-$d_6$): $\delta$ [ppm] = 12.26 (s, 1H), 2.75 (t, $J$ = 2.5 Hz, 1H), 2.43–2.30 (m, 4H).

**$^{13}$C NMR** (101 MHz, DMSO-$d_6$): $\delta$ [ppm] = 83.5, 72.9, 71.4, 32.9, 13.9.

### 9.4.2.4 *N*-(4-(((2-Amino-9*H*-purin-6-yl)oxy)methyl)benzyl)pent-4-ynamide (9.6)

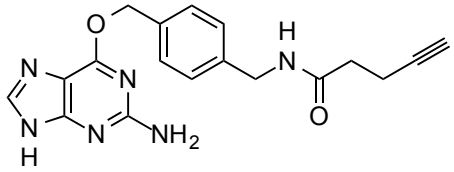

Amide coupling procedure was performed according to amide coupling protocol A (chapter 9.4.2.1). **9.4** (382 mg, 1.41 mmol, 1.2 eq.), **9.2** (115 mg, 1.17 mmol, 1.0 eq.), HBTU (489 mg, 1.29 mmol, 1.1 mmol), DIPEA (302 mg, 2.34 mmol, 409 µL, 2.0 eq.) in DMF (5mL). Completion of the reaction was observed with LCMS, and the crude was subjected to RP-HPLC (MeCN/H2O/formic acid = 10/90/0.1 → 80/20/0.1 over 40 min). The collected fractions were combined and dried under HV conditions. 178 mg (508 mmol) of the desired product was obtained in 43% yield as a white powder.

**$^1$H NMR** (400 MHz, DMSO-$d_6$): $\delta$ [ppm] = 8.45–8.34 (m, 1H), 8.13 (s, 1H), 8.10 (s, 1H), 7.47 (d, $J$ = 8.4 Hz, 2H), 7.29 (d, $J$ = 8.4 Hz, 2H), 6.59 (br s, 2H), 5.48 (s, 2H), 4.32–4.21 (m, 2H), 2.78 (m, 1H), 2.43–2.28 (m, 4H).

**$^{13}$C NMR** (101 MHz, DMSO-$d_6$): $\delta$ [ppm] = 170.8, 159.1, 158.5, 153.7, 141.3, 140.4, 134.3, 129.4, 127.7, 126.8, 84.3, 71.8, 68.7, 42.3, 34.6, 14.7.

**HRMS (ESI)**: calc. for $C_{18}H_{19}N_6O_2^+$ $(M+H)^+$: 351.1564, found: 351.1562.

**UV/Vis** (LCMS): $\lambda_{max1}$ = 196 nm, $\lambda_{max2}$ = 212 nm, $\lambda_{max3}$ = 287 nm.

**$R_t$** (LCMS; MeCN/$H_2O$/formic acid = 10/90/0.1 → 90/10/0.1 over 7 min) = 1.955 min.

### 9.4.2.5 *N*-(4-(((2-Amino-9*H*-purin-6-yl)oxy)methyl)benzyl)-2-azidoacetamide (9.7)

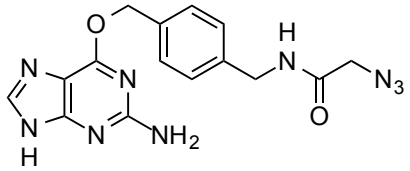

Amide coupling procedure was performed according to amide coupling protocol A (chapter 9.4.2.1). **9.4** (40.0 mg, 0.148 mmol, 1.1 eq.), 2-azidoacetic acid (**9.5**) (13.6 mg, 0.135 mmol, 1.0 eq.), HBTU (51.2 mg, 0.135 mmol, 1.0 eq.), DIPEA (47.1 µL, 0.270 mmol, 2.0 eq.) in DMF (1 mL). Completion of the reaction was observed with LCMS, and the crude was subjected to RP-HPLC (MeCN/H2O/formic acid = 10/90/0.1 → 80/20/0.1 over 40 min). The collected fractions were combined and dried under HV conditions. 16.9 mg (47.8 µmol) of the desired product was obtained in 35% yield.

**$^{1}$H NMR** (400 MHz, DMSO-$d_6$): $\delta$ [ppm] = 8.62 (t, *J* = 5.6, 1H), 8.05 (s, 1H), 7.48 (d, *J* = 8.0, 2H), 7.29 (d, *J* = 8.0, 2H), 6.58 (br s, 2H), 5.48 (s, 2H), 4.31 (d, 2H), 3.88 (s, 2H).

**$^{13}$C NMR** (101 MHz, DMSO-$d_6$): $\delta$ [ppm] = 167.4, 163.1, 159.4, 155.6, 153.7 138.9, 135.2, 128.7, 127.5, 126.5, 66.8, 50.8, 42.1.

**HRMS (ESI)**: calc. for $C_{15}H_{16}N_9O_2^+$ $(M+H)^+$: 354.1421, found: 354.1419.

**UV/Vis** (LCMS): λ = 287 nm.

**$R_t$** (LCMS; MeCN/$H_2O$/formic acid = 10/90/0.1 → 90/10/0.1 over 7 min) = 1.926 min.

### 9.4.2.6 (2*S*,4*S*)-2-(4-((4-((*E*)-(4-(1-Azido-39-oxo-3,6,9,12,15,18,21,24,27,30,33,36-dodecaoxa-40-azadotetracontan-42-amido)phenyl)diazenyl)phenyl)amino)-4-oxobutyl)-4-((*tert*-butoxycarbonyl)amino)pentanedioic acid, $N_3$-$PEG_{12}$-D-AG0-Boc (9.10)

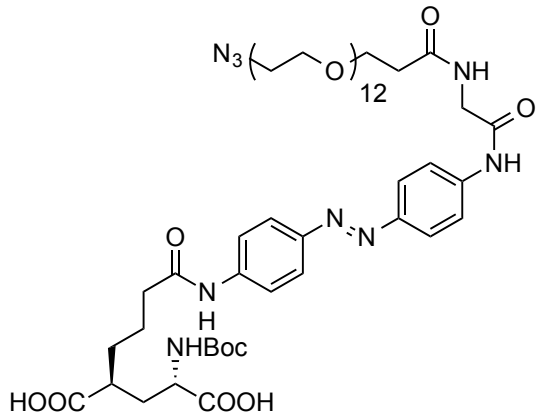


A round bottom flask was charged with $N_3$-PEG12-CO-*N*-succinimide (**9.8**) (Jena Bioscience CLK-L033-10, 10.0 mg, 13.5 µmol, 1.0 eq.) and *N*-Boc-*D*-AG0 (**9.9**) (8.7 mg, 14.8 µmol, 1.1 eq.) and dissolved in DMF (500 µL). DIPEA (3.5 mg, 27.0 µmol, 4.7 µL, 2.0 eq.) was added and the mixture was stirred o.n. at r.t. before being diluted with $H_2O$ (1 mL). RP flash column chromatography (MeCN/$H_2O$/formic acid = 0/100/0.1 → 10/90/0.1 → 20/80/0.1 → 40/60/0.1) yielded 13.0 mg (10.8 µmol) of the desired product as a yellow solid in 80% yield.

**HRMS (ESI)**: calc. for $C_{55}H_{86}N_9O_{21}^-$ $(M-H)^-$: 1208.5944, found: 1208.5921.

**UV/Vis** (LCMS): λ (π → π*) = 366 nm.

**$R_t$** (LCMS; MeCN/$H_2O$/formic acid = 10/90/0.1 → 90/10/0.1 over 7 min) = 3.232 min.

### 9.4.2.7 (2*S*,4*S*)-2-Amino-4-(4-((4-((*E*)-(4-(1-(4-(3-((4-(((2-amino-9*H*-purin-6-yl)oxy)methyl)benzyl)amino)-3-oxopropyl)-1*H*-1,2,3-triazol-1-yl)-39-oxo-3,6,9,12,15,18,21,24,27,30,33,36-dodecaoxa-40-azadotetracontan-42-amido)phenyl)diazenyl)phenyl)amino)-4-oxobutyl)pentanedioic acid, PTL' (9.12)

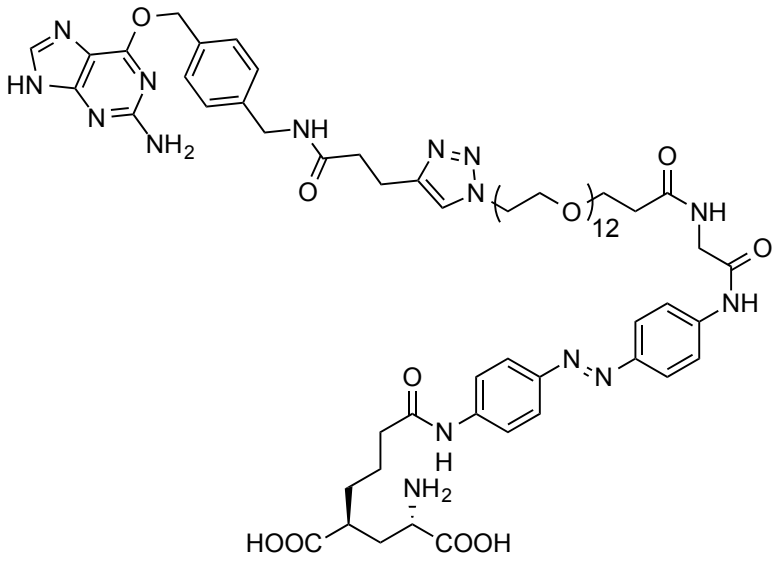

Click chemistry was performed according to click chemistry protocol B (chapter 9.4.2.2.). **9.6** (4.2 mg, 11.9 µmol, 1.2 eq.), **9.10** (12.0 mg, 9.9 µmol, 1.0 eq.) were combined in a mixture of stock solutions of $CuSO_4$ and NaAsc (50/50 µL) in DMSO (2 mL). Completion of the reaction was observed with LCMS ($\mathbf{R_t}$ (LCMS; MeCN/$H_2O$/formic acid = 10/90/0.1 → 90/10/0.1 over 7 min) = 2.926 min, $\lambda_{max}$ ($\pi \rightarrow \pi^*$) = 369 nm) and the crude was subjected to RP-HPLC (MeCN/H2O/formic acid = 10/90/0.1 → 80/20/0.1). The collected yellow fractions were combined, dried to obtain **9.11** as a yellow solid and used without further purification for the next step. **9.11** was treated with neat TFA (250 µL) for 10 min at r.t., before $Et_2O$ (100 mL) was added and the cloudy solution was centrifuged for 20 min at 4000 rpm. 6.8 mg (7.06 µmol) of the orange precipitate were collected as the desired product **9.12** in 65% yield (over 2 steps).

**$^1$H NMR** (400 MHz, DMSO-$d_6$): $\delta$ [ppm] =.10.30 (s, 1H), 10.26 (s, 1H), 8.47 (br s, 1H), 8.81 (t, $J$ = 6.0 Hz, 1H), 8.36–8.16 (m, 3H), 7.93–7.68 (m, 8H), 7.48 (d, $J$ = 6.0 Hz, 2H), 7.24 (d, $J$ = 6.0 Hz, 2H), 6.88–6.74 (m, 1H), 5.53 (br s, 2H), 4.44 (t,

*J* = 5.2 Hz, 2H), 4.27 (d, *J* = 6.0 Hz, 2H), 3.94 (d, *J* = 5.6 Hz, 2H), 3.87–3.78 (m, 1H), 3.76 (t, *J* = 5.2 Hz, 2H), 3.63 (t, *J* = 6.8 Hz, 2H), 3.56–3.41 (m, 44H), 2.86 (t, *J* = 8.0 Hz, 2H), 2.62–2.55 (m, 2H), 2.46–2.28 (m, 7H), 2.16–1.91 (m, 2H), 1.90–1.74 (m, 1H), 1.66–1.51 (m, 4H), 1.48–1.28 (m, 2H).

**$^{13}$C NMR** (101 MHz, DMSO-$d_6$): $\delta$ [ppm] = 175.5, 171.3, 171.2, 170.8, 170.7, 168.2, 158.8, 158.3, 158.0, 147.7, 147.5, 145.8, 141.9, 141.5, 140.0 137.5, 134.0 128.9, 127.2, 123.4, 122.3, 119.3, 119.2, 69.9, 69.8, 69.7, 69.6, 69.5, 68.8, 68.1, 66.7, 50.4, 49.2, 42.8, 41.8, 40.4, 36.2, 35.9, 34.8, 31.7, 31.1, 28.2, 22.2, 21.3.

**HRMS (ESI)**: calc. for $C_{68}H_{99}N_{15}O_{21}^{2+}$ $(M+2H)^{2+}$: 730.8565, found: 730.8564.

**UV/Vis** (LCMS): $\lambda_{max}$ ($\pi \rightarrow \pi^*$) = 369 nm.

**$R_t$** (LCMS; MeCN/$H_2O$/formic acid = 10/90/0.1 → 90/10/0.1 over 7 min) = 2.463 min.

### 9.4.2.8 (*E*)-*N*,*N*'-(Diazene-1,2-diylbis(4,1-phenylene))bis(pent-4-ynamide) (9.14)

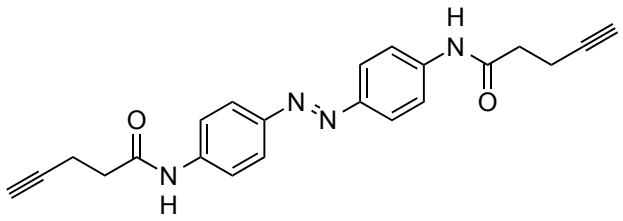

Amide coupling procedure was performed according to amide coupling protocol A (chapter 9.4.2.2.). **9.13** (50.0 mg, 0.236 mmol, 1.0 eq.), **9.2** (50.9 mg, 0.519 mmol, 2.2 eq.), HBTU (197 mg, 0.519 mmol, 2.2 eq.) and DIPEA (330 µL, 1.89 mmol, 8.0 eq.) in DMF (5 mL). Completion of the reaction was observed with LCMS, and the reaction mixture was diluted with $H_2O$ (30 mL) and EtOAc (100 mL). The organic layer was washed with HCl (50 mL, 1 M). The product was extracted with NaOH (100 mL, 1 M) and the aqueous layer was acidified with HCl (150 mL, 1 M) and extracted with EtOAc (3 x 100 mL). The organic layers were washed with brine, dried over $MgSO_4$, concentrated *in vacuo* and purified by

flash column chromatography (DCM/MeOH = 0.95/0.05). All solvents were removed under HV conditions and 48.0 mg (0.129 mmol) of the desired product was obtained in 55% yield.

**$^{1}$H NMR** (400 MHz, DMSO-$d_6$): $\delta$ [ppm] = 10.52–10.08 (m, 2H), 7.85 (d, $J$ = 8.8 Hz, 4H), 7.81 (d, $J$ = 8.8 Hz, 4H), 2.94 (s, 2H), 2.64–2.53 (m, 8H).

**$^{13}$C NMR** (101 MHz, DMSO-$d_6$): $\delta$ [ppm] = 169.8, 147.6, 141.8, 124.8, 123.4, 122.5, 119.2, 83.5, 71.6, 35.3, 14.0.

**HRMS (ESI)**: calc. for $C_{22}H_{21}N_4O_2^+$ $(M+H)^+$: 373.1659, found: 373.1660.

**UV/Vis** (LCMS): $\lambda$ ($\pi \rightarrow \pi^*$) = 368 nm.

**$R_t$** (LCMS; MeCN/$H_2O$/formic acid = 10/90/0.1 → 90/10/0.1 over 7 min) = 3.949 min.

### 9.4.2.9 (*E*)-*N,N'*-(Diazene-1,2-diylbis(4,1-phenylene))bis(2-azidoacetamide) (9.15)

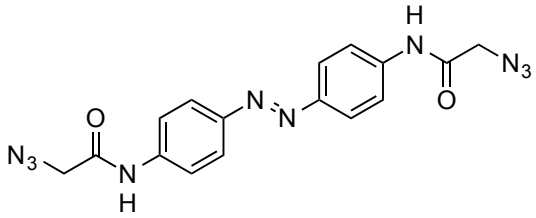

Amide coupling procedure was performed according to amide coupling protocol A (chapter 9.4.2.2). **9.13** (250 mg, 1.18 mmol, 1.0 eq.), **9.5** (477 mg, 4.72 mmol, 4.0 eq.), HBTU (1.79 g, 4.72 mmol, 4.0 eq.) and DIPEA (1.65 mL, 9.44 mmol, 8.0 eq.) in DMF (25 mL). Completion of the reaction was observed with LCMS, and the reaction mixture was diluted $H_2O$ (5 mL) and extracted with EtOAc (3x 100 mL), the organic layers were washed with brine, dried over $MgSO_4$ and concentrated *in vacuo*. The crude was subjected to RP-HPLC (MeCN/H2O/formic acid = 10/90/0.1 → 80/20/0.1). The collected fractions were combined and

dried under HV conditions. 155 mg (0.410 mmol) of the desired product was obtained.

**$^1$H NMR** (400 MHz, DMSO-$d_6$): $\delta$ [ppm] = 10.50 (s, 2H), 7.87 (d, $J$ = 8.8 Hz, 4H), 7.81 (d, $J$ = 9.2 Hz, 4H), 4.11 (s, 4H).

**$^{13}$C NMR** (101 MHz, DMSO-$d_6$): $\delta$ [ppm] = 166.8, 147.9, 141.1, 123.5, 119.6, 51.4.

**HRMS (ESI)**: calc. for $C_{16}H_{13}N_{10}O_2^-$ $(M-H)^-$: 377.1228, found: 377.1228.

**UV/Vis** (LCMS): $\lambda$ ($\pi \rightarrow \pi^*$) = 364 nm.

**$R_t$** (LCMS; MeCN/$H_2O$/formic acid = 10/90/0.1 → 90/10/0.1 over 7 min) = 3.138 min.

### 9.4.2.10 (*E*)-4,4'-((Diazene-1,2-diylbis(4,1-phenylene))bis(azanediyl))-bis(4-oxobutanoic acid) (9.19)

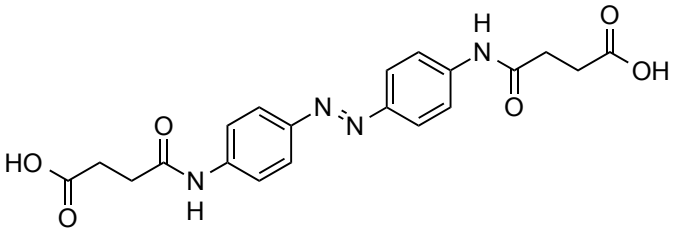


**9.13** (450 mg, 2.12 mmol, 1.0 eq.), succinic anhydride (**9.18**) (1.27 g, 12.7 mmol, 6.0 eq.), DMAP (3 grains) and DIPEA (1.85 mL, 10.6 mmol, 5.0 eq.) were dissolved in dry DMF (10 mL) and stirred o.n. at r.t.. The mixture was diluted with $H_2O$ (100 mL) and acidified with 1 M HCl (40 mL). The resulting solid was aggraded in $H_2O$ and centrifuged at 4000 rpm for 20 min. The $H_2O$ was decanted and the procedure was repeated two more times. 737 mg (1.79 mmol) of the product was obtained in 84% yield.

**$^1$H NMR** (400 MHz, DMSO-$d_6$): $\delta$ [ppm] = 12.16 (s, 2H), 10.30 (s, 2H), 7.83 (d, $J$ = 9.2 Hz, 4H), 7.79 (d, $J$ = 9.2 Hz, 4H), 2.62 (t, $J$ = 6.4 Hz, 4H), 2.55 (t, $J$ = 6.0 Hz, 4H).

**$^{13}$C NMR** (101 MHz, DMSO-$d_6$): $\delta$ [ppm] = 173.8, 170.8, 147.5, 141.9, 123.4, 119.1, 31.2, 28.7.

**HRMS (ESI)**: calc. for $C_{20}H_{21}N_4O_6^+$ $(M+H)^+$: 413.1456, found: 413.1456.

**UV/Vis** (LCMS): nm; $\lambda$ ($\pi \rightarrow \pi^*$) = 368 nm.

**$R_t$** (LCMS; MeCN/$H_2O$/formic acid = 10/90/0.1 → 90/10/0.1 over 7 min) = 2.687 min.

### 9.4.2.11 (*E*)-4,4'-((((Diazene-1,2-diylbis(4,1-phenylene))bis(azanediyl))bis(2-oxoethane-2,1-diyl))bis(1,9-dihydro-8*H*-dibenzo[*b,f*][1,2,3]triazolo-[4,5-*d*]azocine-1,8-diyl))bis(*N*-(4-(((2-amino-9*H*-purin-6-yl)oxy)methyl)benzyl)-4-oxobutanamide) (9.22)

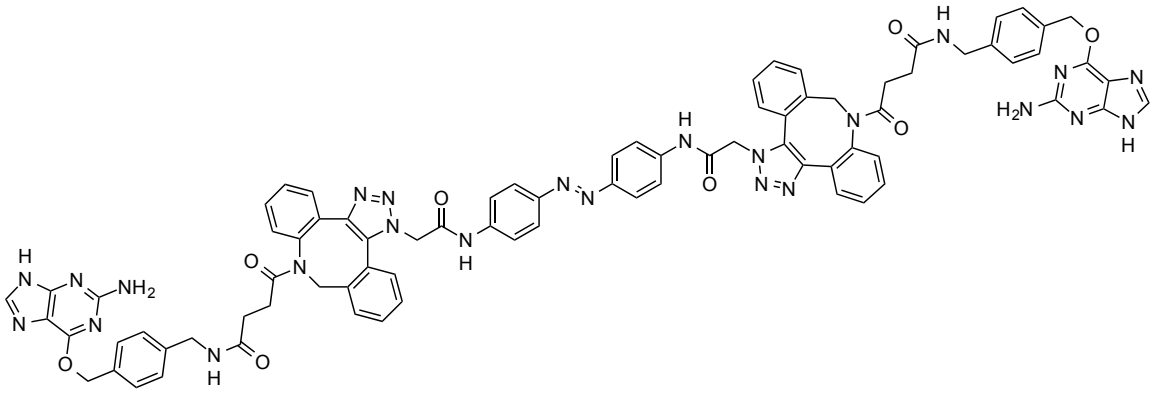

DBCO-NHS ester (**9.21**) (Jena Bioscience CLK-A133-25, 10.0 mg, 24.9 µmol, 2.0 eq.) and **9.4** (6.7 mg, 24.9 µmol, 2.0eq.) were dissolved in dry DMF (1.00 mL) and cooled to 0 °C. DIPEA (4.73 µL, 24.9 µmol, 2.0 eq.) was added before the mixture was allowed to warm up to r.t. and stirred for 2.5 h at r.t.. **9.15** (4.7 mg, 12.5 µmol, 1.0 eq.) was added and stirred for further 2 h at r.t.. The reaction mixture was filtered through a PTFE filter (CHROMAFIL® Xtra PTFE 0.45) and subjected to RP-HPLC (MeCN/$H_2O$/formic acid = 10/80/0.1 → 60/40/0.1 over 45 min). All solvents were removed under HV conditions and 8.6 mg (5.76 µmol) of the desired product was obtained in 46% yield.

**$^1$H NMR** (400 MHz, DMSO-$d_6$): $\delta$ [ppm] = 12.44 (s, 2H), 11.06 (s, 1H), 10.91 (s, 1H), 8.25 (m, 2H), 7.88–7.20 (m, 32H), 6.26 (br s, 2H), 5.89–5.74 (m, 2H), 5.55–5.32 (m, 6H), 5.18–5.14 (m, 2H), 4.53–4.49 (m, 2H), 4.25–4.03 (m, 4H), 2.33–2.03 (m, 8H), 1.73–1.55 (m, 4H).

**HRMS (ESI)**: calc. for $C_{80}H_{70}N_{24}O_8^{2+}$ $(M+2H)^{2+}$: 747.2899, found: 747.2896.

### 9.4.2.12 (*E*)-*N,N*-Diallyl-4-((4-nitrophenyl)diazenyl)aniline (9.25)

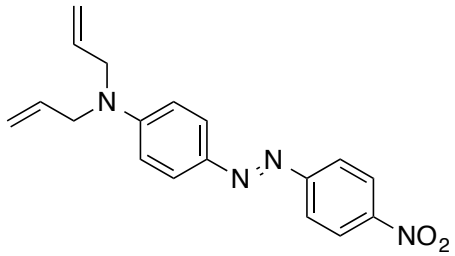


4-nitrobenzenediazonium tetrafluoroborate (**9.24**) (160 mg, 0.670 mmol, 1.0 eq.) was dissolved in MeCN (10 mL) and cooled down to 0 °C. A solution of *N*,*N*-diallylaniline (**9.23**) (116 mg, 0670 mmol, 1.0 eq.) in MeCN/1 M NaOAc (5 mL /5 mL) was added dropwise. The resulting reaction mixture was allowed to warm up to r.t. and was diluted with $H_2O$ (5 mL) and DCM (3 x 25 mL). The organic layers were washed with brine, dried over $MgSO_4$ and concentrated *in vacuo*. The crude product was purified by flash column chromatography (DCM). All solvents were removed under HV conditions and 175 mg (0.542 mmol) of the desired product was obtained in 81% yield.

**$^1$H NMR** (400 MHz, $CDCl_3$): $\delta$ [ppm] = 8.32 (d, *J* = 9.2, 2H), 7.91 (d, *J* = 9.2, 2H), 7.88 (d, *J* = 9.2, 2H), 6.77 (d, *J* = 9.6, 2H), 5.93–5.84 (m, 2H), 5.25–5.17 (m.,4H), 4.06–4.04 (m, 4H).

**$^{13}$C NMR** (101 MHz, $CDCl_3$): $\delta$ [ppm] = 156.9, 152.3, 147.5, 144.1, 132.5, 126.1, 124.8, 122.8, 116.9, 112.0, 53.0.

**HRMS (ESI)**: calc. for $C_{18}H_{19}N_4O_2^+$ $(M+H)^+$: 323.1503, found: 323.1499.

**UV/Vis** (LCMS): nm; $\lambda$ ($\pi \rightarrow \pi^*$) = 475 nm.

**$R_t$** (LCMS; MeCN/$H_2O$/formic acid = 10/90/0.1 → 90/10/0.1 over 7 min) = 5.749 min.

### 9.4.2.13 (*E*)-*N,N*-Diallyl-4-((4-aminophenyl)diazenyl)aniline (9.26)

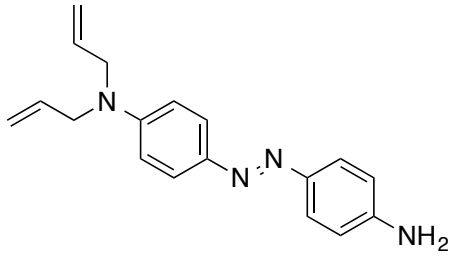


**9.25** (174 mg, 0.540 mmol, 1.0 eq.) was dissolved in THF (10 mL). A solution of sodium sulfide (65%, 262 mg, 2.16 mmol, 4.0 eq.) in $H_2O$ was added und the resulting solution was refluxed for 3 h at 80 °C. The reaction mixture was extracted with EtOAc (3 x 100 mL) and $H_2O$/$NaHCO_3$ (200 mL), washed with brine, dried over $MgSO_4$, concentrated *in vacuo* and the crude product was purified by flash column chromatography (DCM/pentane = 50/50 → 100/0). All Solvents were removed and 172 mg (0.588 mmol) of the desired product were obtained in quant. yield.

**$^1$H NMR** (400 MHz, $CDCl_3$): $\delta$ [ppm] = 7.77 (d, $J$ = 9.2, 2H), 7.72 (d, $J$ = 8.8, 2H), 6.75–6.72 (m, 4H), 5.92–5.83 (m, 2H), 5.21 (m, 2H), 5.18–5.16 (m, 2H), 4.00–3.99 (m, 4H), 3.91 (br s, 2H).

**$^{13}$C NMR** (101 MHz, $CDCl_3$): $\delta$ [ppm] = 150.4, 148.3, 146.2, 144.2, 133.3, 124.3, 124.3, 116.5, 115.0, 112.0, 53.2.

**HRMS (ESI)**: calc. for $C_{18}H_{21}N_4^+$ $(M+H)^+$: 293.1761, found: 293.1761.

### 9.4.2.14 *tert*-Butyl-(*E*)-4-((4-((4-(diallylamino)phenyl)diazenyl)-phenyl)amino)-piperidine-1-carboxylate (9.28)

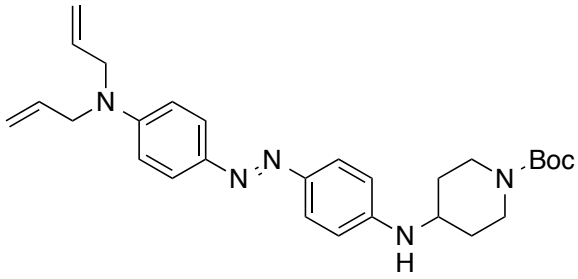


**9.26** (60.0 mg, 0.205 mmol, 1.1 eq.) was dissolved in 1,2-dichloroethane (1.00 mL). *tert*-Butyl 4-oxopiperidine-1-carboxylate (**9.27**) (38.8 mg, 0.195 mmol, 1.0 eq.) and AcOH (11.1 µL, 0.195 mmol, 1.0 eq.) and $NaHB(OAc)_3$ (51.6 mg, 0.274 mmol, 1.4 eq.) were added sequentially and the mixture was stirred o.n. at r.t.. The crude product was purified by flash column chromatography (DCM/MeOH = 100/0 → 99/1). All solvents were removed under HV conditions and 75.2 mg (0.158 mmol) of the desired product were obtained in 85% yield brsm.

**$^1$H NMR** (400 MHz, $CDCl_3$): $\delta$ [ppm] = 7.77–7.73 (m, 4H), 7.74 (d, $J$ = 8.8, 2H), 6.63 (d, $J$ = 8.8, 2H), 5.92–5.82 (m, 2H), 5.21–5.20 (m, 2H), 5.18–5.16 (m, 2H), 4.14–4.02 (br s, 2H) 4.01–3.97 (m, 4H), 3.94–3.78 (br s, 1H), 3.62–3.47 (m, 1H), 3.02–2.84 (m, 2H), 2.09–2.01 (m, 2H), 1.48 (s, 9H), 1.42–1.28 (m, 2H).

**$^{13}$C NMR** (101 MHz, $CDCl_3$): $\delta$ [ppm] = 173.5, 154.9, 150.2, 148.4, 145.3, 144.2, 133.3, 124.4, 124.1, 116.5, 112.8, 112.0, 79.8, 52.9, 50.1, 32.4, 28.6.

**HRMS (ESI)**: calc. for $C_{28}H_{38}N_5O_2^+$ $(M+H)^+$: 476.3020, found: 476.3019.

**UV/Vis** (LCMS): nm; $\lambda$ ($\pi \rightarrow \pi^*$) = 449 nm.

**$R_t$** (LCMS; MeCN/$H_2O$/formic acid = 10/90/0.1 → 90/10/0.1 over 7 min) = 6.114 min.

### 9.4.2.15 *tert*-Butyl-(*E*)-4-(*N*-(4-((4-(diallylamino)phenyl)diazenyl)phenyl)-propionamido)piperidine-1-carboxylate (9.29)

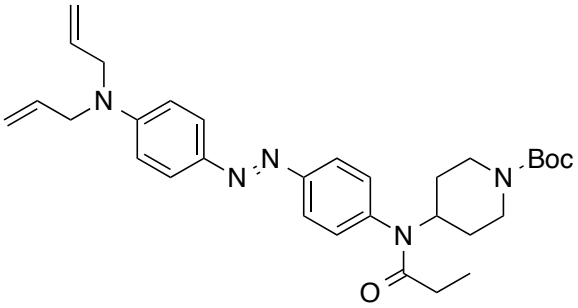


**9.28** (75.0 mg, 0.158 mmol, 1.0 eq.) was dissolved in dry DCM (1.5 mL) under a $N_2$-atmosphere. Propionyl chloride (15.2 µL, 0.174 mmol, 1.1 eq.) and $NEt_3$ (32.9 µL, 0.237 mmol, 1.5 eq.) were added. The reaction mixture was stirred o.n. at r.t.. More propionyl chloride (15.2 µL, 0.174 mmol, 1.1 eq.) was added and stirred for further 2 h. MeOH (few drops) were added and the crude product was purified by flash column chromatography (DCM/MeOH = 100/0 → 99/1). All Solvents were removed under HV conditions and 75.5 mg (0.142 mmol) of the desired product were obtained in 90% yield.

**$^1$H NMR** (400 MHz, $CDCl_3$): $\delta$ [ppm] = 7.85–7.81 (m, 4H), 7.27 (d, *J* = 8.4, 2H), 6.75 (d, *J* = 9.2, 2H), 5.91–5.82 (m, 2H), 5.22-5.16 (m, 4H), 4.78 (t, *J* = 12.4, 1H), 4.26–4.06 (br s, 2H), 4.05–3.97 (m, 4H), 2.79 (t, *J* = 11.6, 2H), 1.98 (q, *J* = 7.2, 2H), 1.37 (s, 9H), 1.31–1.19 (m, 4H) 1.02 (t, *J* = 7.2, 3H).

**$^{13}$C NMR** (101 MHz, $CDCl_3$): $\delta$ [ppm] = 173.5, 154.6, 153.0, 151.6, 143.9, 139.4, 132.8, 130.9, 125.4, 123.0, 116.7, 111.9, 79.6, 52.9, 52.5, 30.7, 29.4, 28.7, 28.5, 9.7.

**HRMS (ESI)**: calc. for $C_{31}H_{42}N_5O_3^+$ $(M+H)^+$: 532.3282, found: 532.3286.

**UV/Vis** (LCMS): nm; $\lambda$ ($\pi \rightarrow \pi^*$) = 421 nm.

**$R_t$** (LCMS; MeCN/$H_2O$/formic acid = 10/90/0.1 → 90/10/0.1 over 7 min) = 6.225 min.

### 9.4.2.16 (*E*)-*N*-(4-((4-(Diallylamino)phenyl)diazenyl)phenyl)-*N*-(piperidin-4-yl)propionamide (9.30)

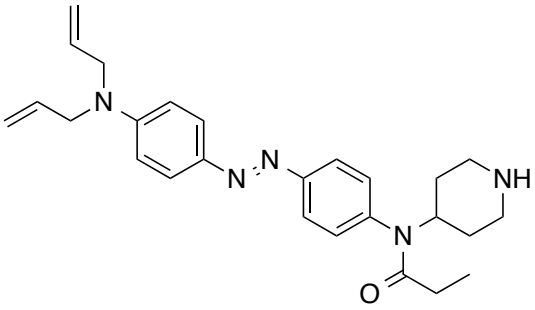

**9.29** (58.8 mg, 0.111 mmol, 1.0 eq.) was treated with neat TFA (2.00 mL) and stirred for 10 min at r.t.. The reaction mixture was diluted with $NaHCO_3$ and extracted with EtOAc (3 x 100 mL), washed with brine, dried over $MgSO_4$ and concentrated *in vacuo*. The crude product was purified by flash column chromatography (DCM/MeOH = 100/0 → 90/10). All solvents were removed under HV conditions. The presumption of a quantitative reaction was made and 47.9 mg (0.111 mmol) were obtained.

**$^1$H NMR** (400 MHz, $CDCl_3$): $\delta$ [ppm] = 7.95–7.70 (m, 4H), 7.10 (d, $J$ = 7.2, 2H), 6.75(d, $J$ = 9.2, 2H), 5.94–5.76 (m, 2H), 5.30–5.11 (m, 4H), 4.71 (br s, 1H), 4.01 (s, 4H), 3.49–3.24 (m, 2H), 3.01–2.77 (m, 2H), 2.10–1.82 (m, 2H), 1.43 (s, 1H), 1.30–1.18 (m, 2H), 1.02–0.86 (m, 3H).

**$^{13}$C NMR** (101 MHz, $CDCl_3$): $\delta$ [ppm] = 153.2, 151.6, 143.9, 132.8, 130.4, 125.5, 123.4, 116.7, 111.9, 77.4, 60.5, 52.9, 43.7, 30.4, 29.4, 28.5, 27.5.

**UV/Vis** (LCMS): nm; $\lambda$ ($\pi \rightarrow \pi^*$) = 426 nm.

**$R_t$** (LCMS; MeCN/$H_2O$/formic acid = 10/90/0.1 → 90/10/0.1 over 7 min) = 3.794 min.

### 9.4.2.17 (*E*)-*N*-(4-((4-(Diallylamino)phenyl)diazenyl)phenyl)-*N*-(1-phenethylpiperidin-4-yl)propionamide (9.31)

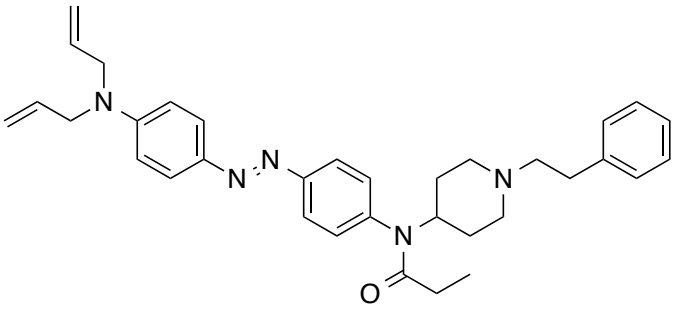

**26** (47.9 mg, 0.111, 1.1 eq.) was dissolved in 1,2-dichloroethane (2.00 mL). 2-phenylacetaldehyde (12.7 mg, 106 mmol, 1.0 eq.) and AcOH (6.07 µL, 0.106 mmol, 1.0 eq.) and $NaHB(OAc)_3$ (30.0 mg, 0.148 mmol, 1.4 eq.) were added sequentially and the mixture was stirred o.n. at r.t.. More of 2-phenylacetaldehyde (25.4 mg, 212 mmol, 2.0 eq.), AcOH (12.1 µL, 0.212 mmol, 2.0 eq.) and $NaHB(OAc)_3$ (40.1 mg, 0.212 mmol, 2.0 eq.) were added and the reaction mixture was stirred o.n. at r.t.. Even more 2-phenylacetaldehyde (12.7 mg, 106 mmol, 1.0 eq.) and AcOH (6.07 µL, 106 mmol, 1.0 eq.) and $NaHB(OAc)_3$ (20.0 mg, 106 mmol, 1.0 eq.) were added and stirred o.n. at r.t.. The reaction mixture was diluted with MeOH (500 µL) and the crude product was purified by flash column chromatography (pentane/DCM/MeOH = 50/50/0 → 0/90/10). All solvents were removed under HV conditions and 42.6 mg (79.5 µmol) of the desired product was obtained in 72% yield.

**$^1$H NMR** (400 MHz,$CD_3OD$): $\delta$ [ppm] = 7.88 (d, $J$ = 8.4 Hz, 2H), 7.83 (d, $J$ = 9.2 Hz,2H), 7.32–7.11 (m, 7H), 6.81 (d, $J$ = 9.2 Hz, 2H), 5.97–5.82 (m, 2H), 5.22–5.11 (m, 4H), 4.64–4.51 (br m, 1H), 4.11–4.00 (m, 4H), 3.07–2.95 (m, 2H), 2.75–2.63 (m, 2H), 2.54–2.46 (m, 2H), 2.16 (m, 2H), 2.01 (q, $J$ = 7.6 Hz, 2H), 1.90–1.76 (m, 2H), 1.54–1.43 (m, 2H), 1.01 (t, $J$ = 7.6 Hz, 3H).

**$^{13}$C NMR** (101 MHz, $CD_3OD$): $\delta$ [ppm] = 175.7, 154.2, 153.1, 144.9, 141.1, 140.5, 134.3, 132.1, 129.6, 129.5, 127.1, 126.3, 124.0, 116.7, 113.0, 61.3, 54.1, 54.0, 53.9, 34.1, 31.2, 29.5, 10.0.

**HRMS (ESI)**: calc. for $C_{34}H_{42}N_5O^+$ $(M+H)^+$: 536.3384, found: 536.3383.

**UV/Vis** (LCMS): nm; λ (π → π*) = 425 nm.

**$R_t$** (LCMS; MeCN/$H_2O$/formic acid = 10/90/0.1 → 90/10/0.1 over 7 min) = 4.475 min.

### 9.4.3 *in vitro* SNAP-tag Labeling

Recombinant and purified SNAP-tag protein was commercially available (NEB, #P9312S) and the labeling reaction was performed according to the manufacturer's instructions. Briefly, the reaction mixture contained 2 µL of SNAP-tag, 4 µL of 5 mM DTT, appropriate amount of labeling agent diluted with PBS to a final volume of 20 µL and was incubated at 37 °C. After 30 minutes to 2 hours, 6 µL of and 3 µL of Redox buffer (10x) was added and the reaction mixture was warmed to 70 °C for 10 minutes. After cooling to r.t., the whole sample was subjected to SDS-PAGE, which was developed by Coomassie staining o.n..

### 9.4.4 *in cellulo* SNAP-tag Labeling

HEK293t cells were labeled with **9.12** 18-24 hours after transfection with either SNAP-mGluR2-GFP[165] or cotransfected with SNAP-mGluR2[165] and YFP. **9.12** was diluted in PBS to a final concentration of 100 µM and pre-illuminated with 370 nm of light for 15 minutes. After removal of the medium and rinsing the cells with PBS, **9.12** in PBS was applied and incubated over 60 minutes, while every 15 minutes light at 370 nm was applied for 1 minute. After removal of the labeling solution, cells were washed with PBS and were harvested for IP or used for electrophysiological measurements.

## 9.5 Spectral Data

### 9.5.1 Pent-4-ynoic acid (9.2)

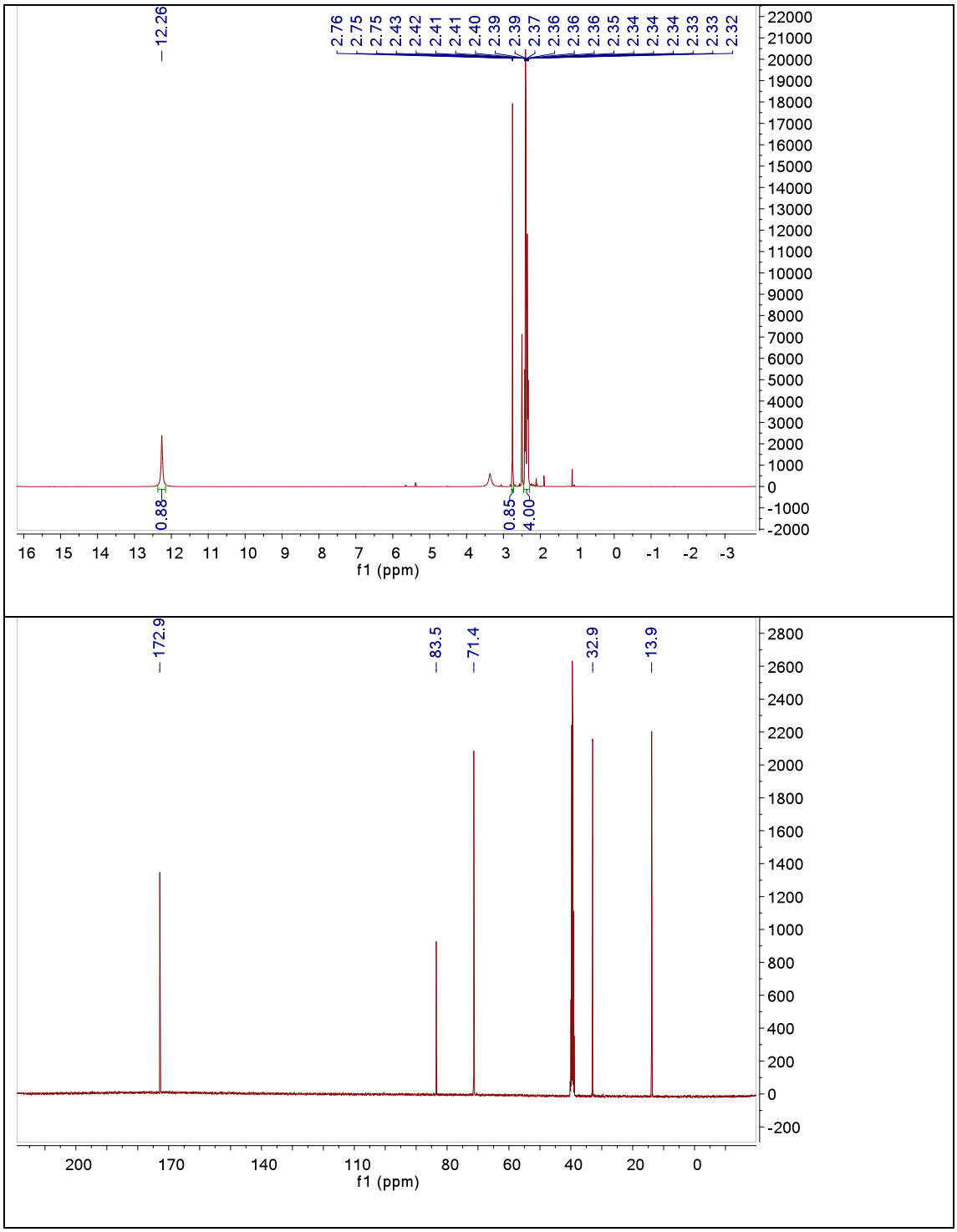

### 9.5.2 (4-(Aminomethyl)-phenyl)-methanol (SI9.2)

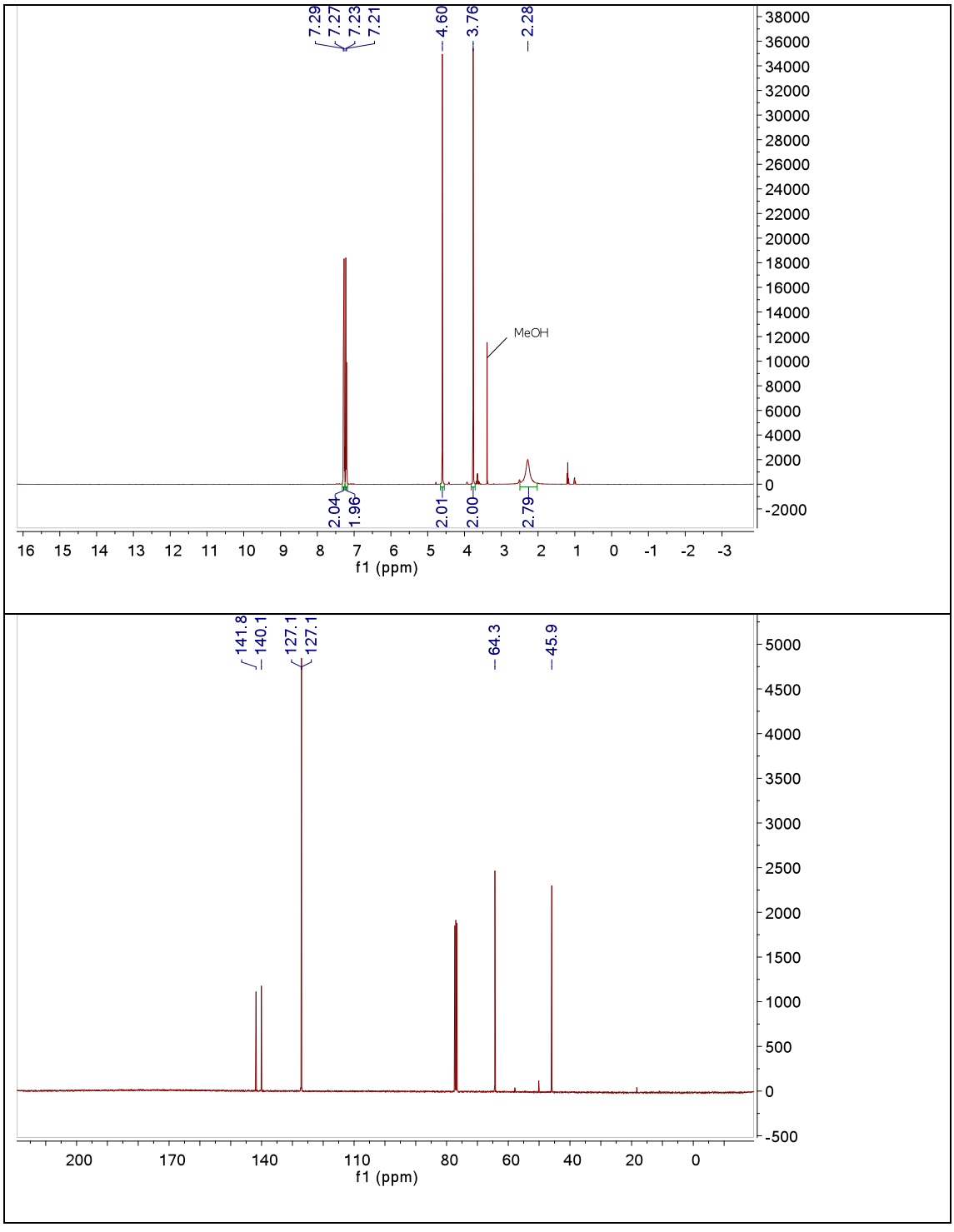

### 9.5.3 2,2,2-Trifluoro-*N*-(4-(hydroxymethyl)benzyl)acetamide (SI9.3)

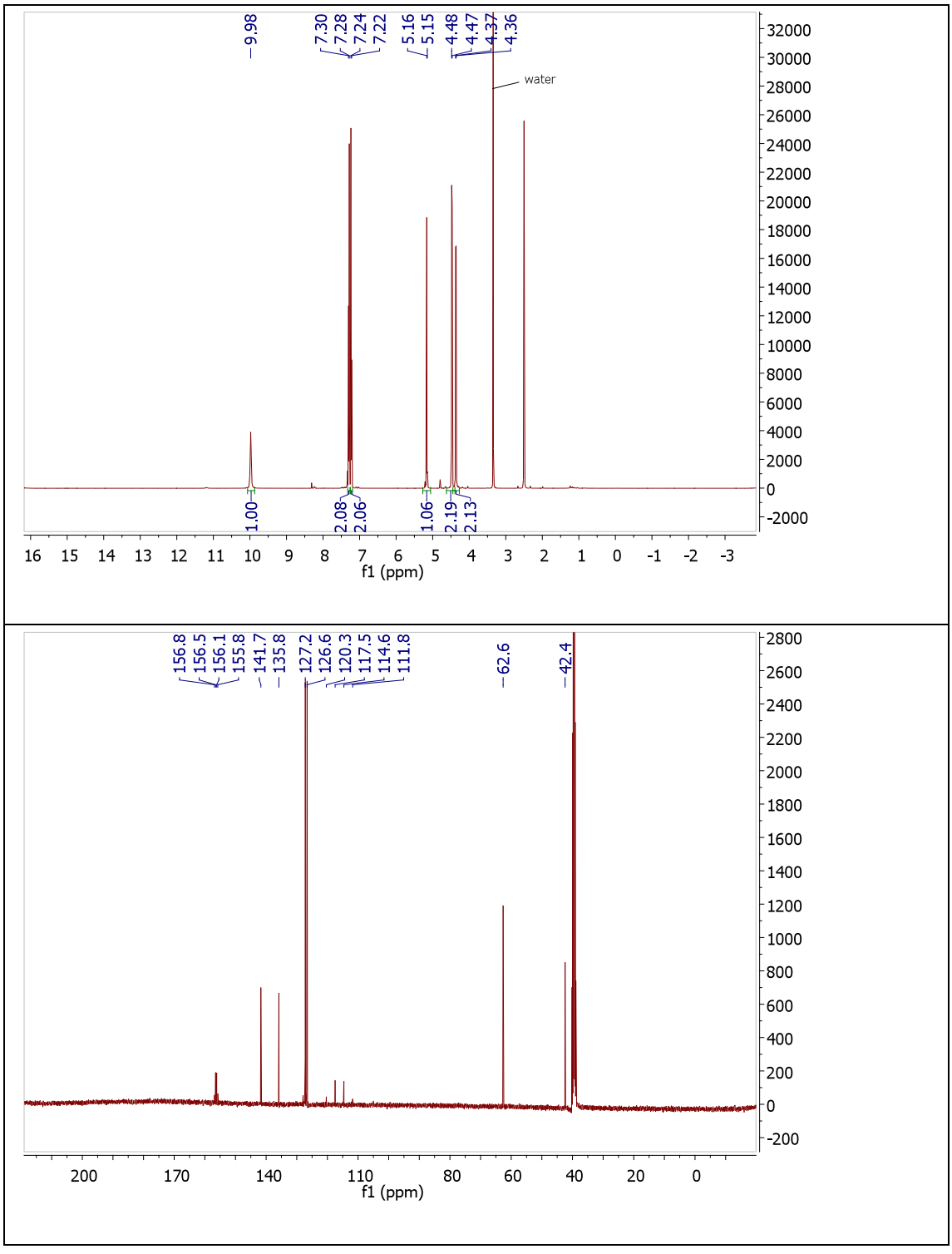

### 9.5.4 (1-(2-Amino-9*H*-purin-6-yl)-1-methylpyrrolidin-1-ium-2-ylium) chloride (SI9.5)

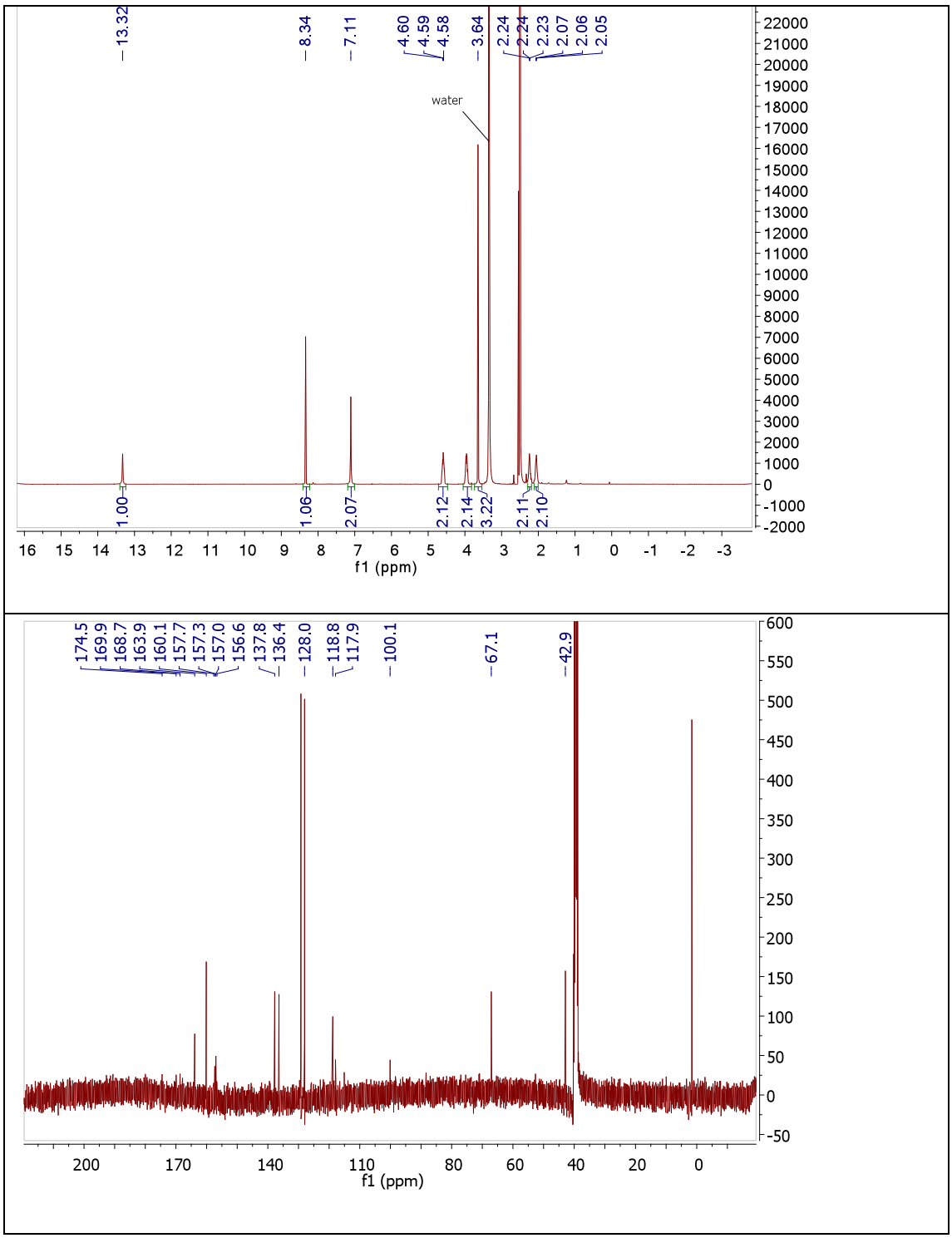

### 9.5.5 *N*-(4-(((2-Amino-7*H*-purin-6-yl)oxy)methyl)benzyl)-2,2,2-trifluoroacetamide (SI9.6)

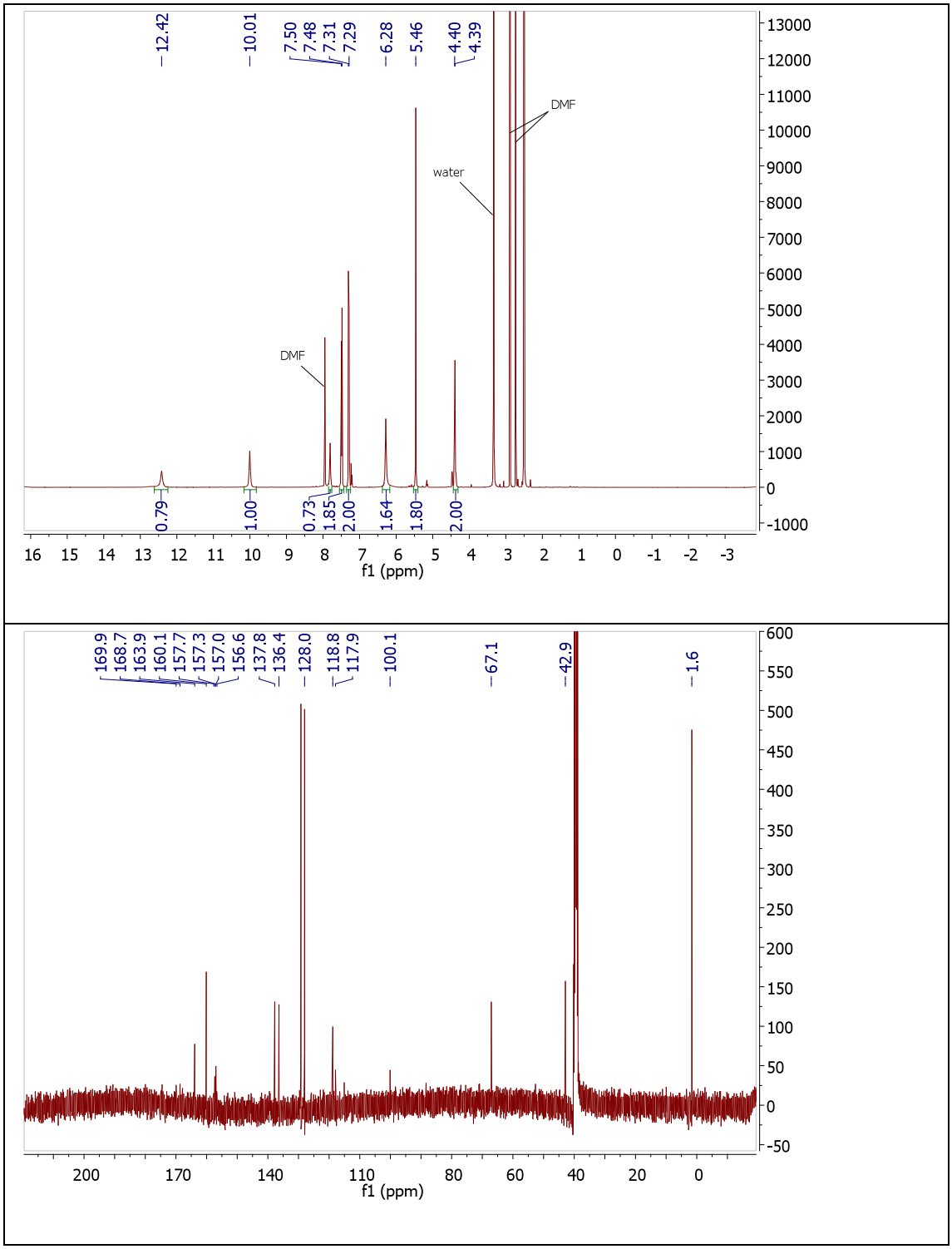

### 9.5.6 6-((4-(Aminomethyl)benzyl)oxy)-7*H*-purin-2-amine (9.4, BG)

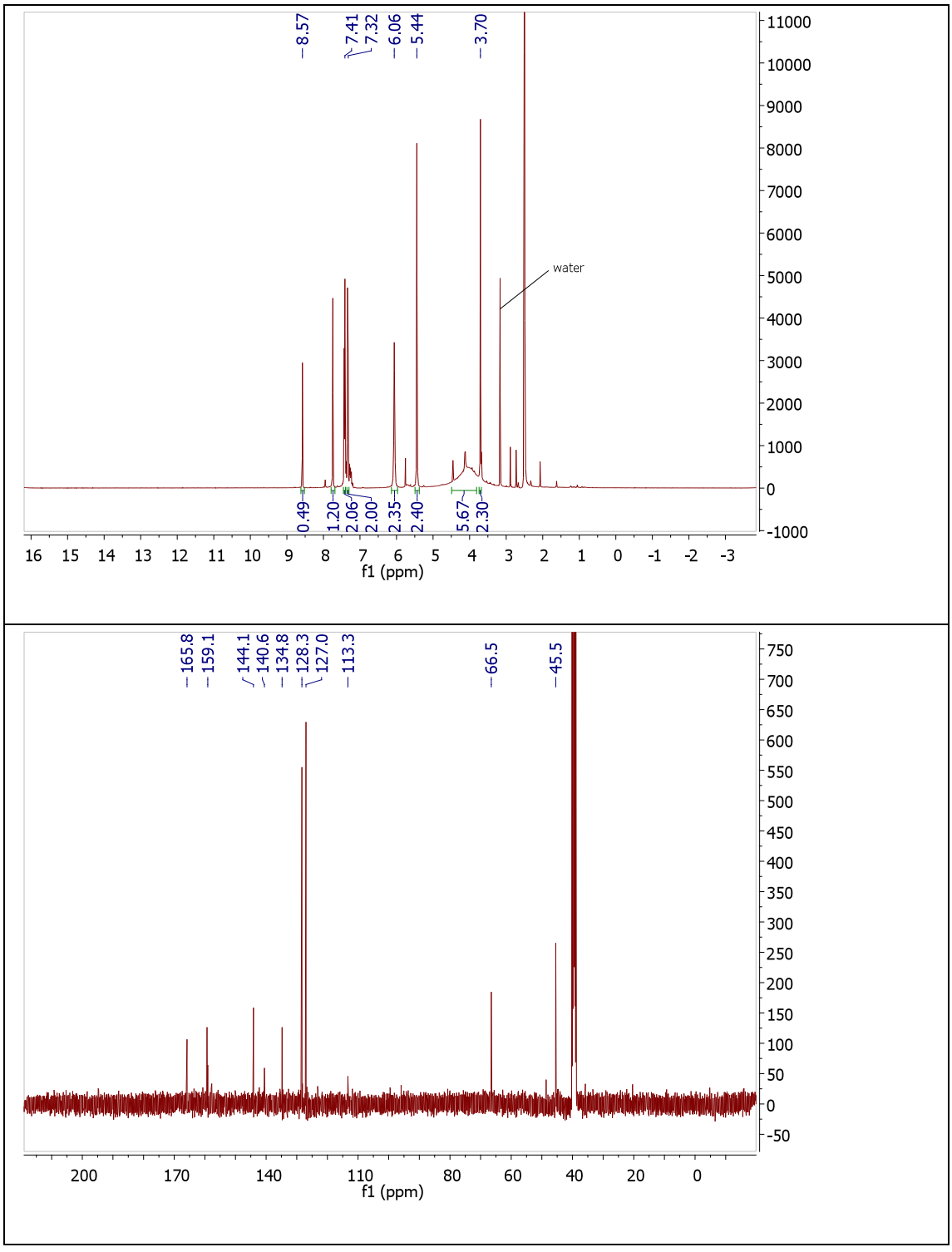

### 9.5.7 *N*-(4-(((2-Amino-9*H*-purin-6-yl)oxy)methyl)benzyl)pent-4-ynamide (9.6)

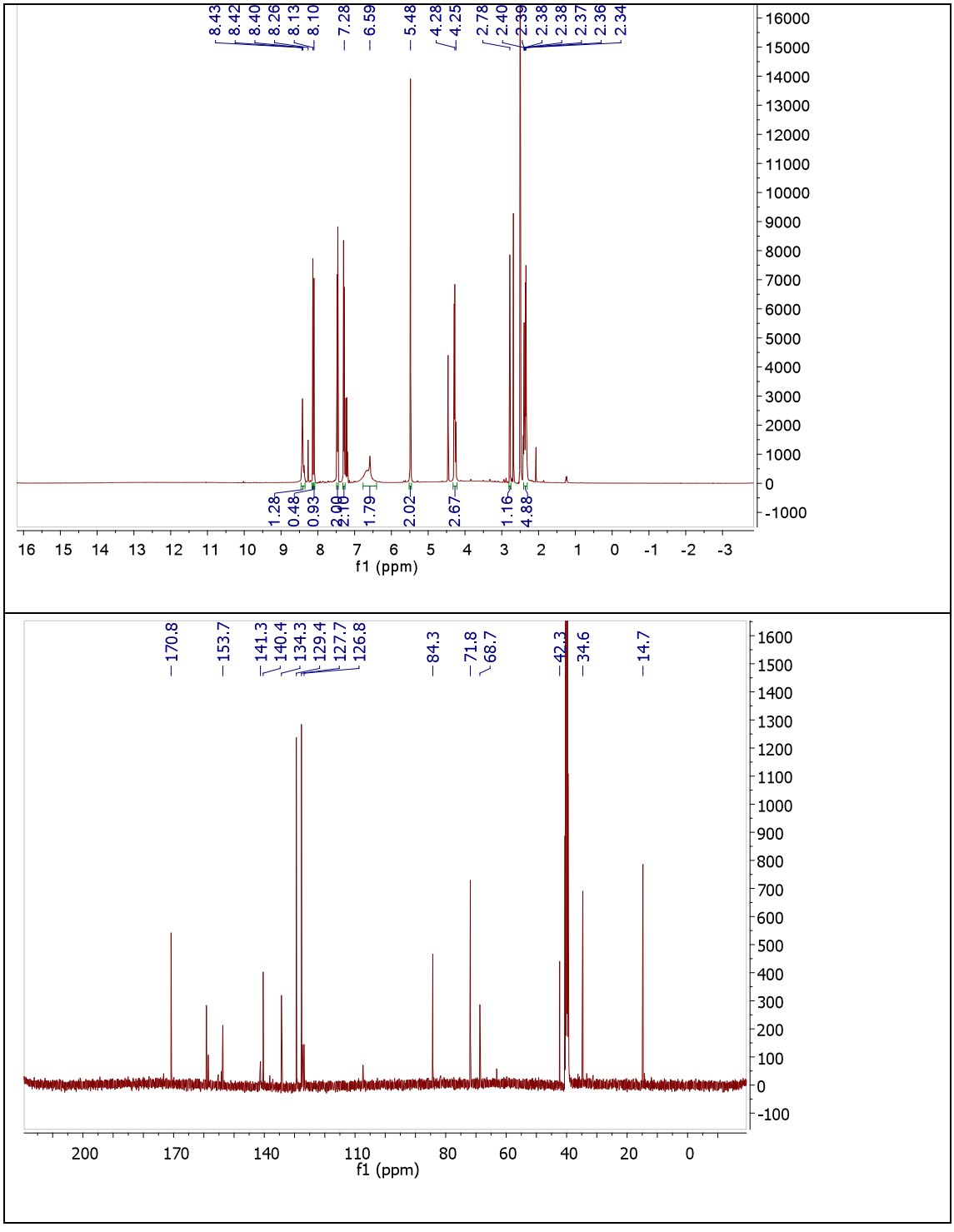

### 9.5.8 *N*-(4-(((2-Amino-9*H*-purin-6-yl)oxy)methyl)benzyl)-2-azidoacetamide (9.7)

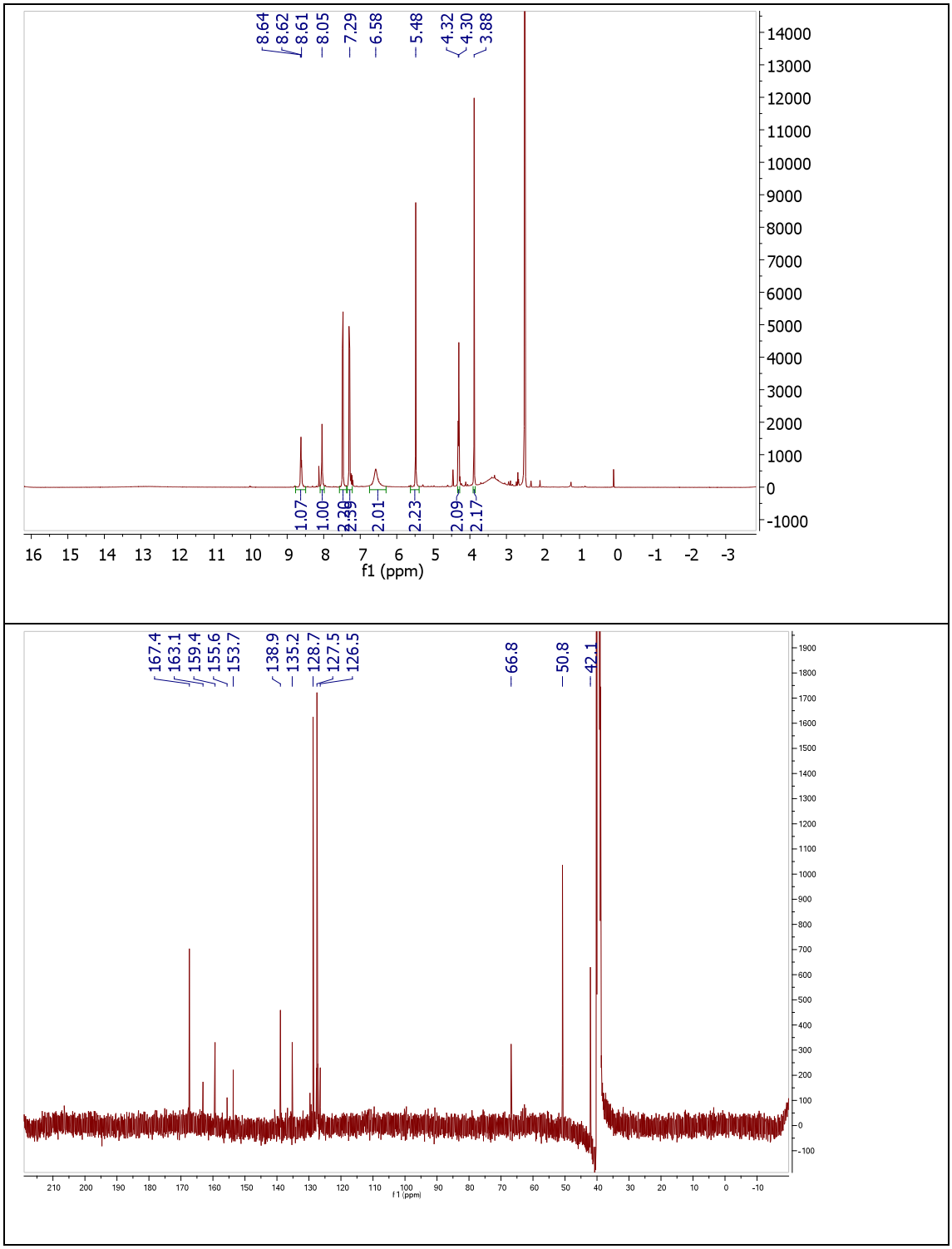

### 9.5.9 (2*S*,4*S*)-2-Amino-4-(4-((4-((*E*)-(4-(1-(4-(3-((4-(((2-amino-9*H*-purin-6-yl)oxy)methyl)benzyl)amino)-3-oxopropyl)-1*H*-1,2,3-triazol-1-yl)-39-oxo-3,6,9,12,15,18,21,24,27,30,33,36-dodecaoxa-40-azadotetracontan-42-amido)phenyl)diazenyl)phenyl)amino)-4-oxobutyl)pentanedioic acid, PTL' (9.12)

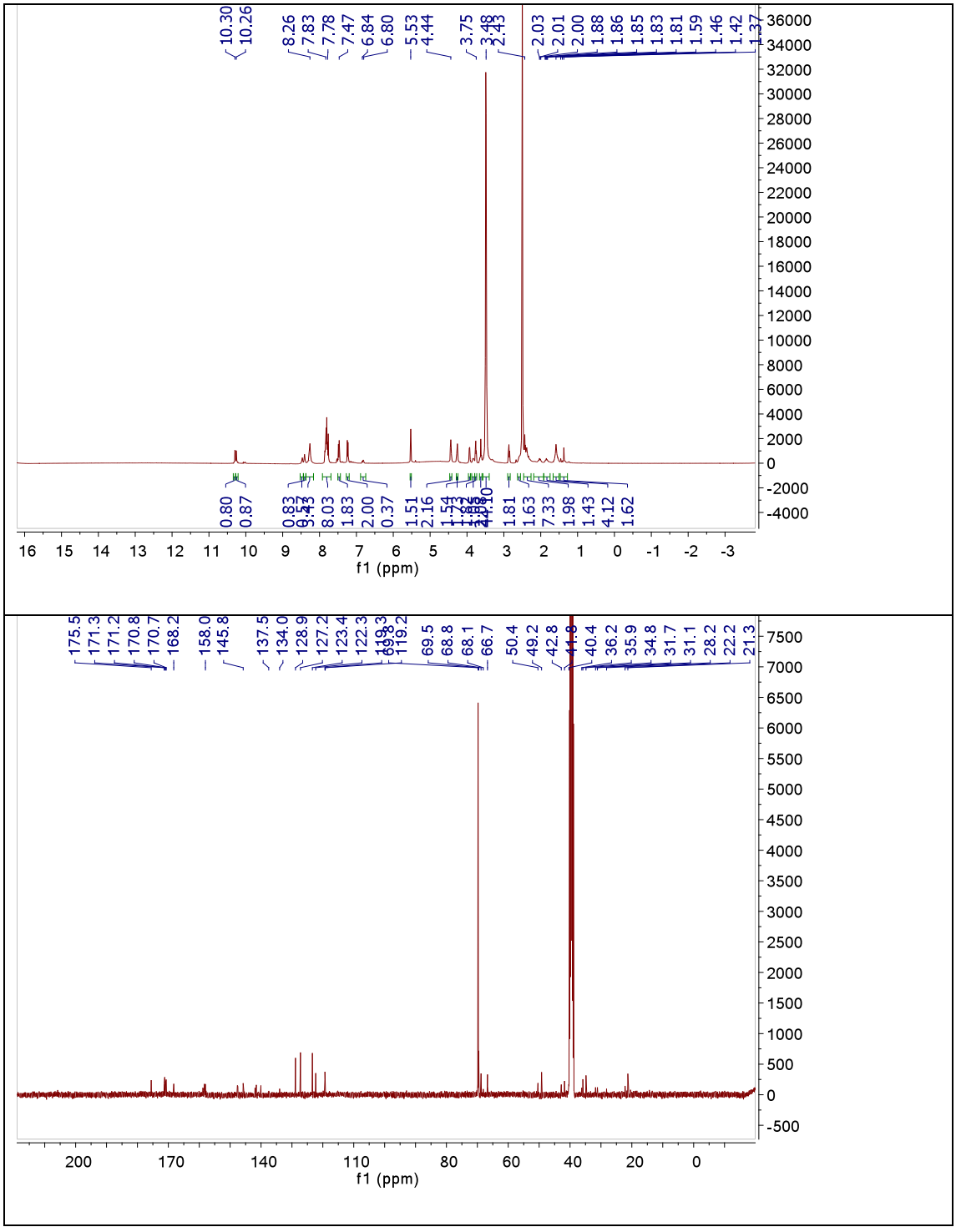

### 9.5.10 (*E*)-*N*,*N*'-(Diazene-1,2-diylbis(4,1-phenylene))bis(pent-4-ynamide) (9.14)

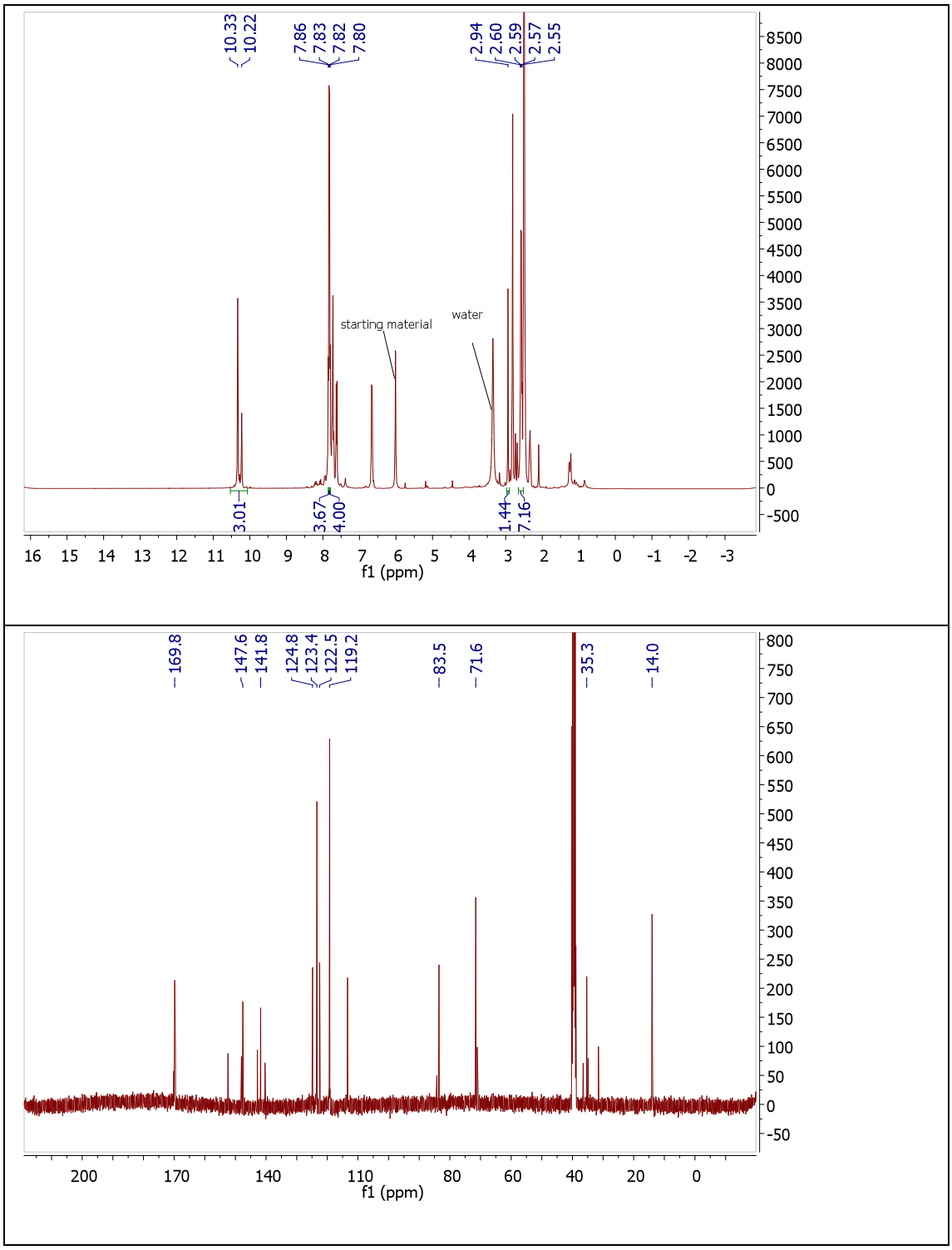

### 9.5.11 (*E*)-*N*,*N*′-(Diazene-1,2-diylbis(4,1-phenylene))bis(2-azidoacetamide) (9.15)

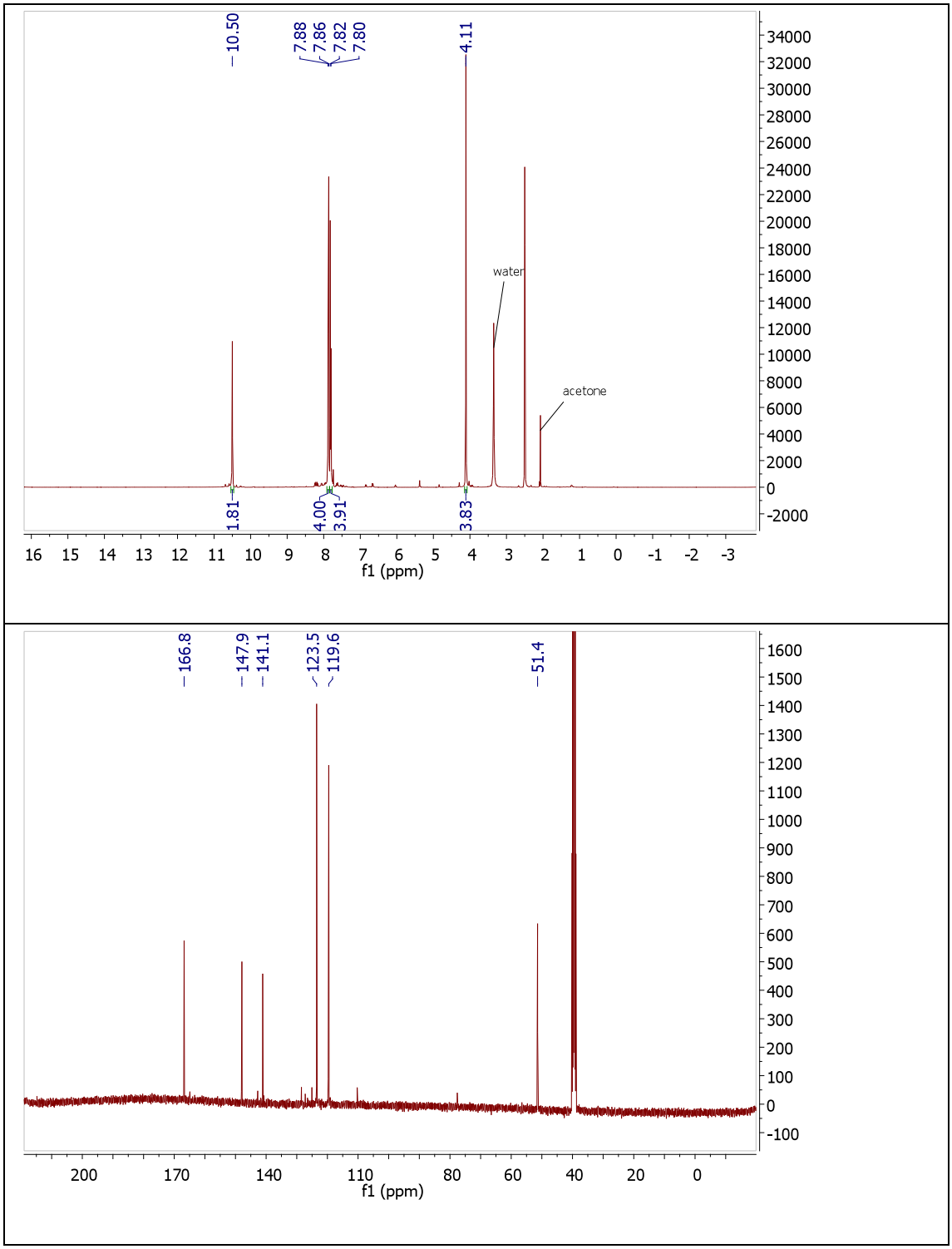

### 9.5.12 (*E*)-4,4'-((Diazene-1,2-diylbis(4,1-phenylene))bis(azanediyl))bis(4-oxobutanoic acid) (9.19)

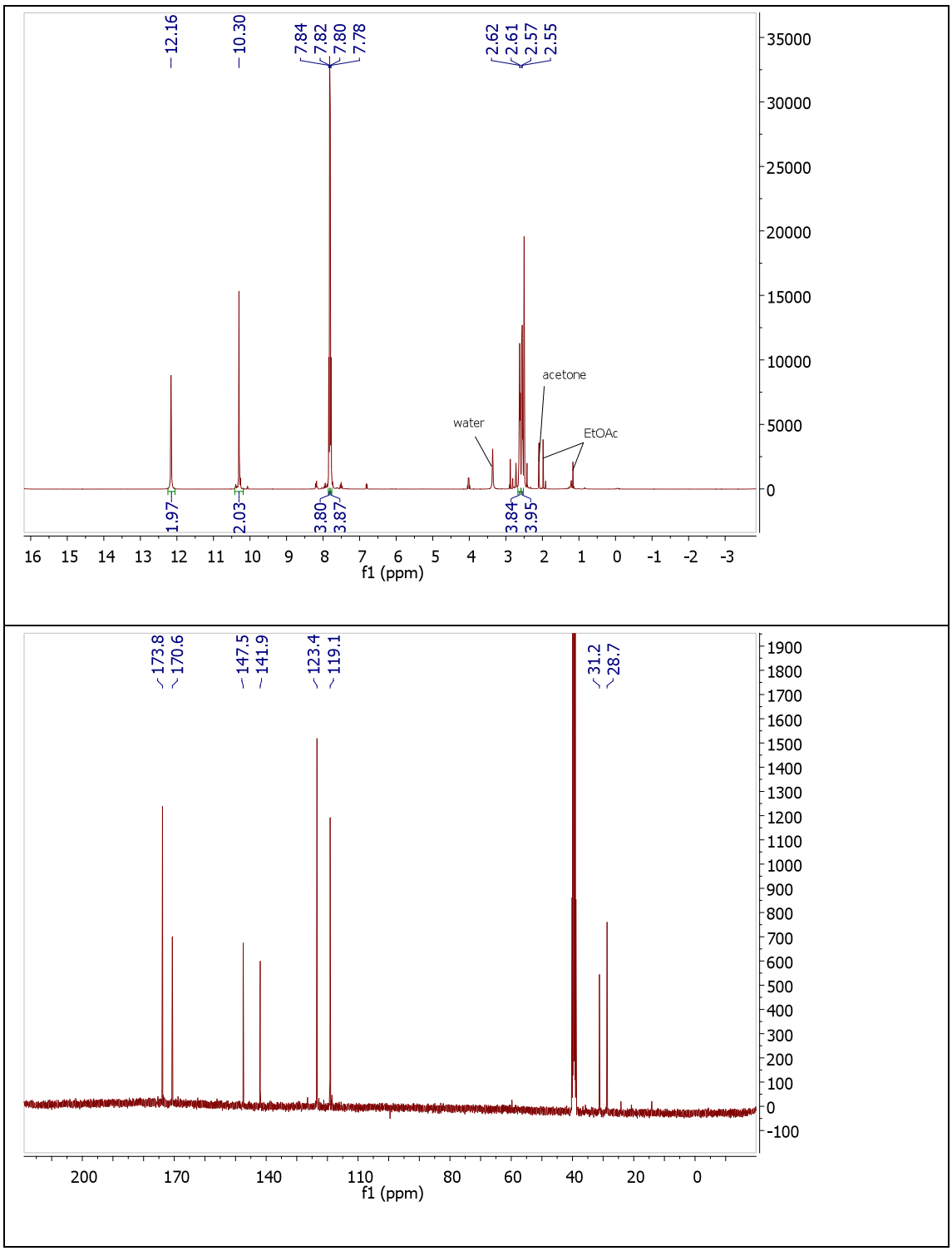

**9.5.13 (*E*)-4,4'-((((Diazene-1,2-diylbis(4,1-phenylene))bis(azanediyl))bis(2-oxoethane-2,1-diyl))bis(1,9-dihydro-8*H*-dibenzo[*b,f*][1,2,3]triazolo-[4,5-*d*]azocine-1,8-diyl))bis(*N*-(4-(((2-amino-9*H*-purin-6-yl)oxy)methyl)benzyl)-4-oxobutanamide) (9.22)**

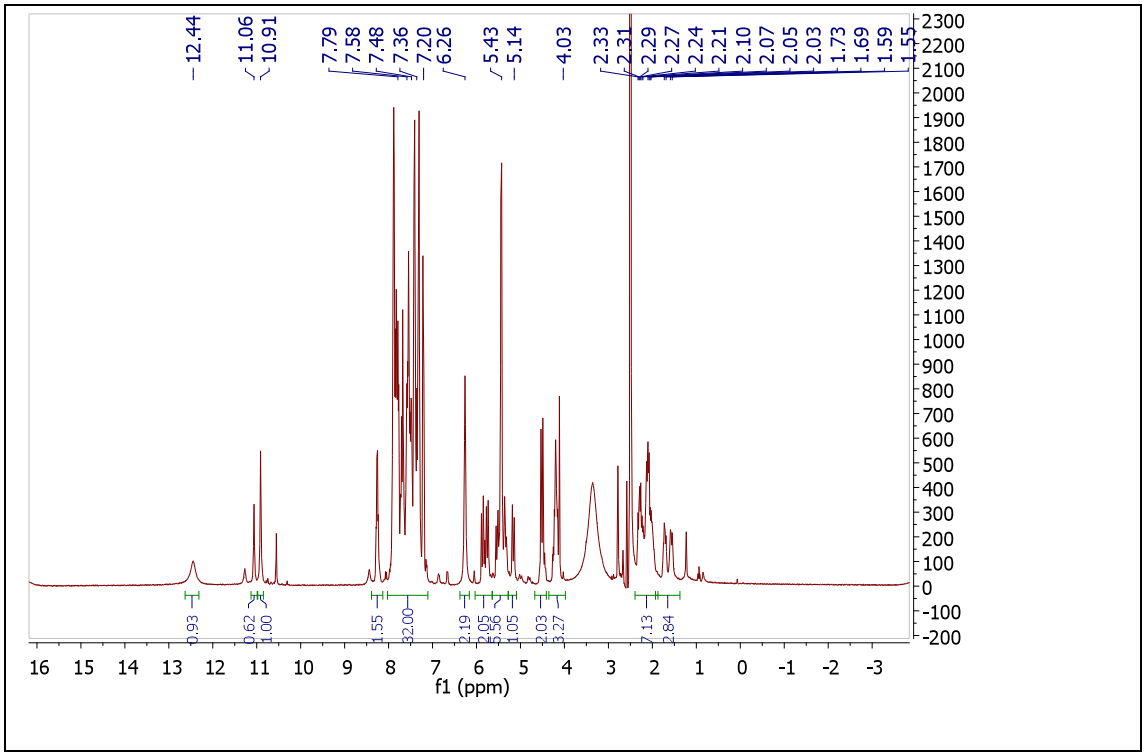

### 9.5.14 (*E*)-*N*,*N*-Diallyl-4-((4-nitrophenyl)diazenyl)aniline (9.25)

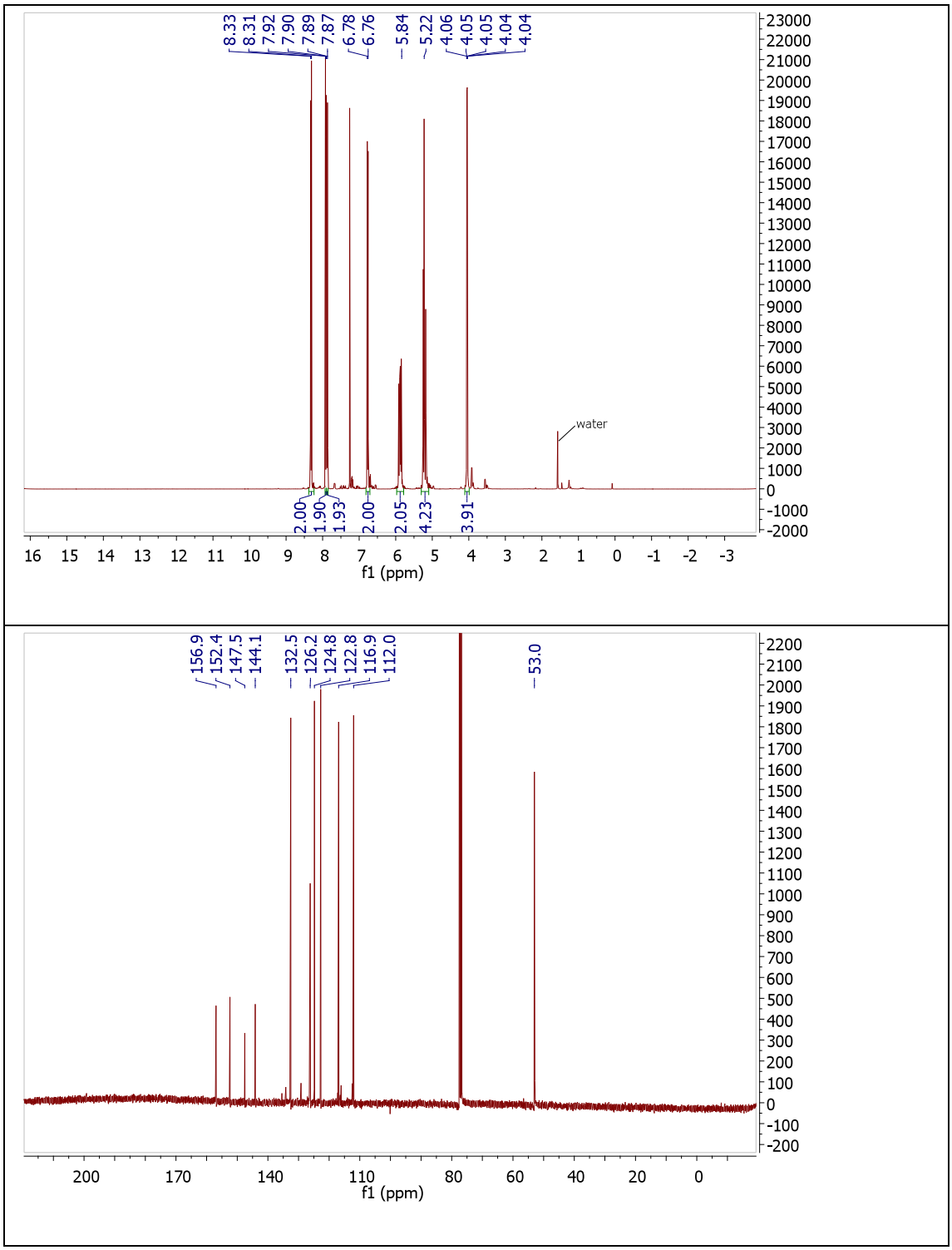

## 9.5.15 (*E*)-*N,N*-Diallyl-4-((4-aminophenyl)diazenyl)aniline (9.26)

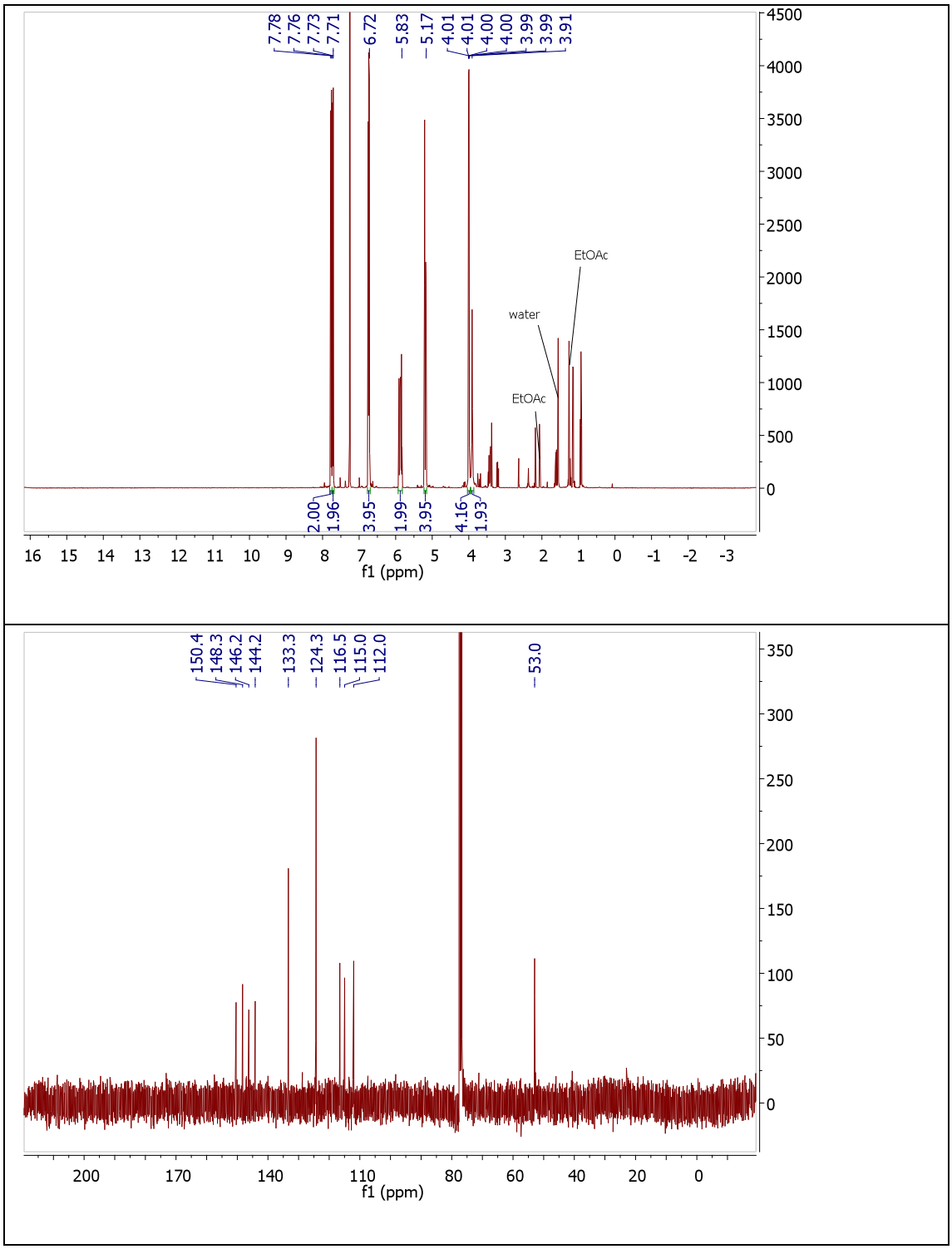

### 9.5.16 *tert*-Butyl-(*E*)-4-((4-((4-(diallylamino)phenyl)diazenyl)-phenyl)amino)-piperidine-1-carboxylate (9.28)

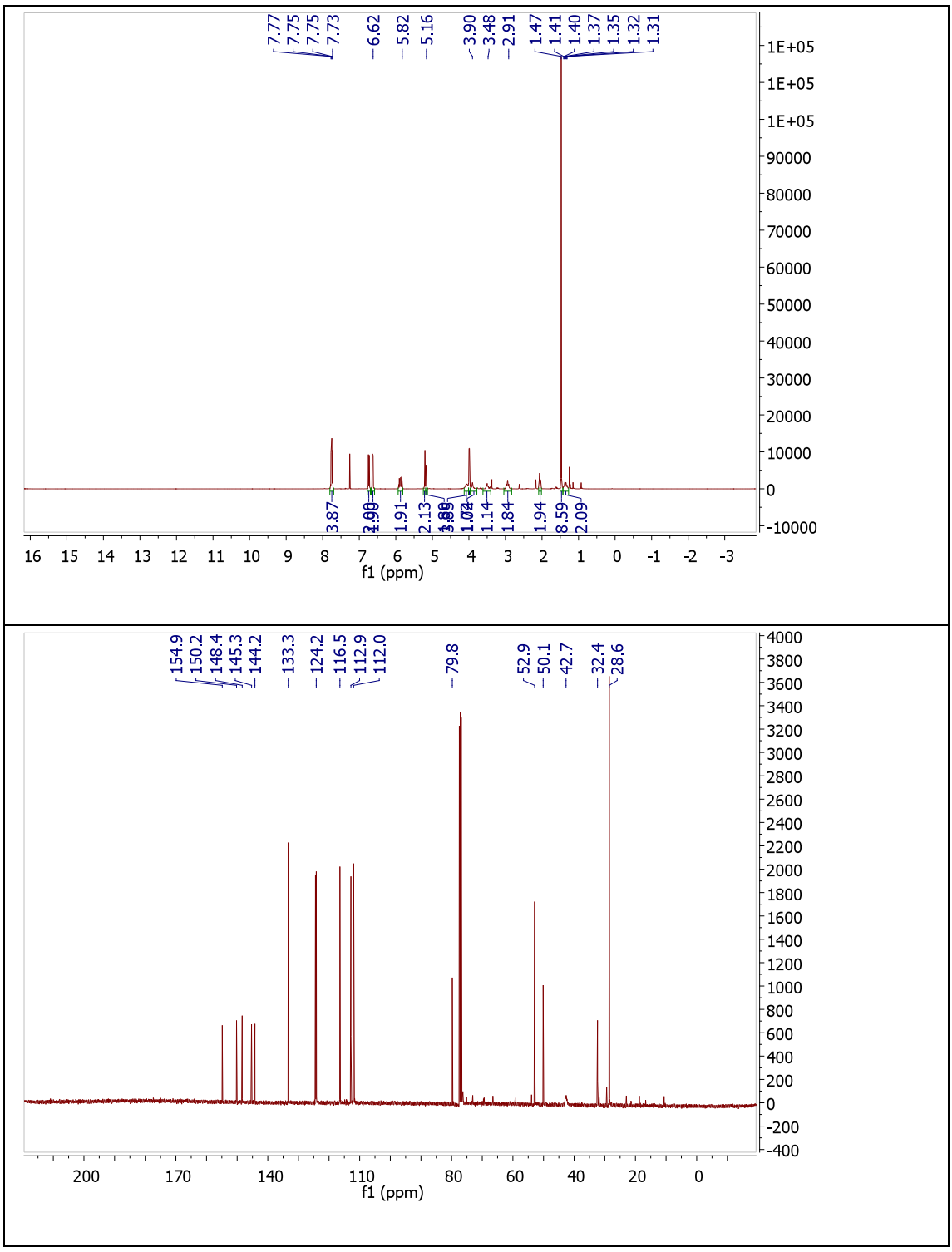

### 9.5.17 *tert*-Butyl-(*E*)-4-(*N*-(4-((4-(diallylamino)phenyl)diazenyl)phenyl)-propionamido)piperidine-1-carboxylate (9.29)

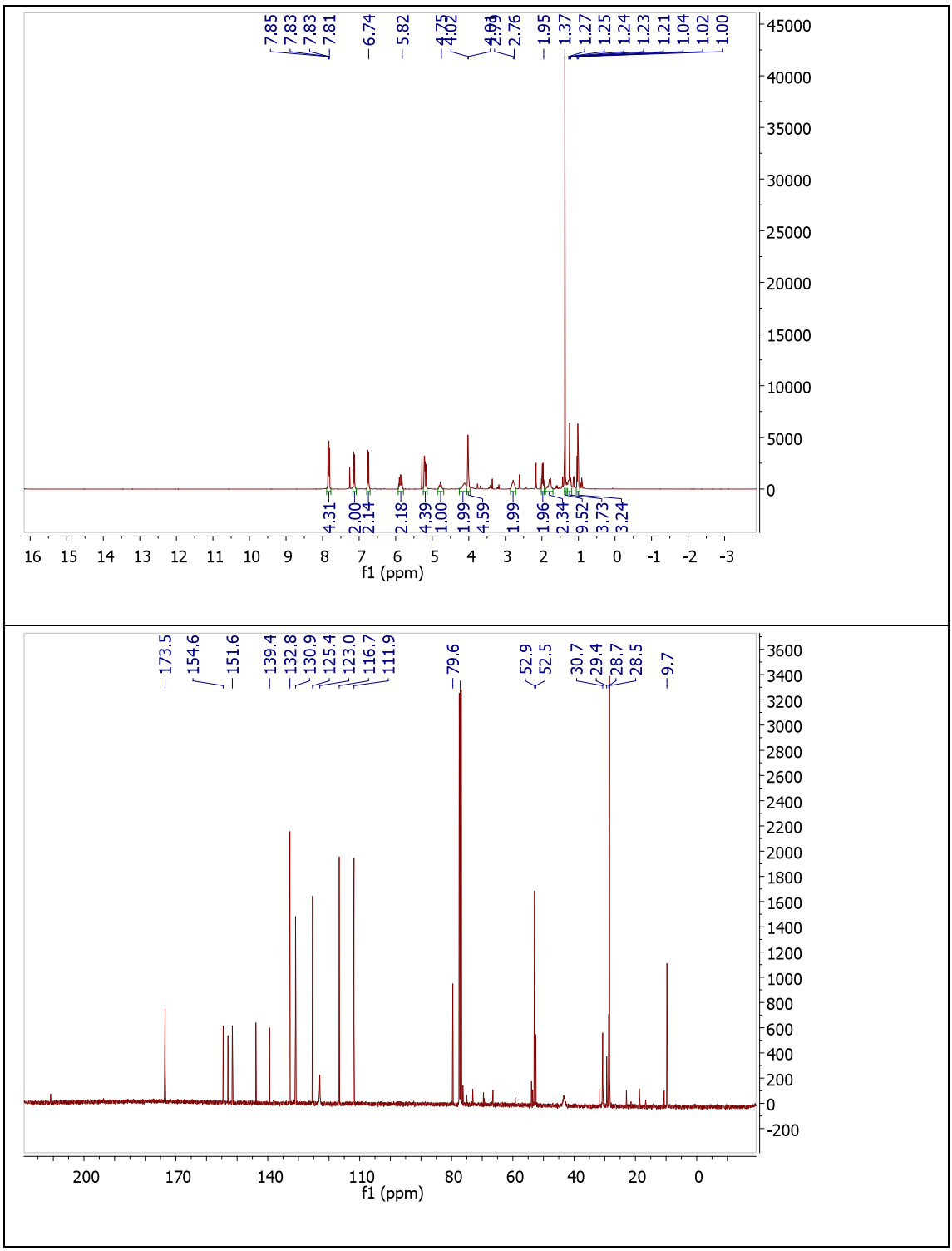

### 9.5.18 (*E*)-*N*-(4-((4-(Diallylamino)phenyl)diazenyl)phenyl)-*N*-(piperidin-4-yl)propionamide (9.30)

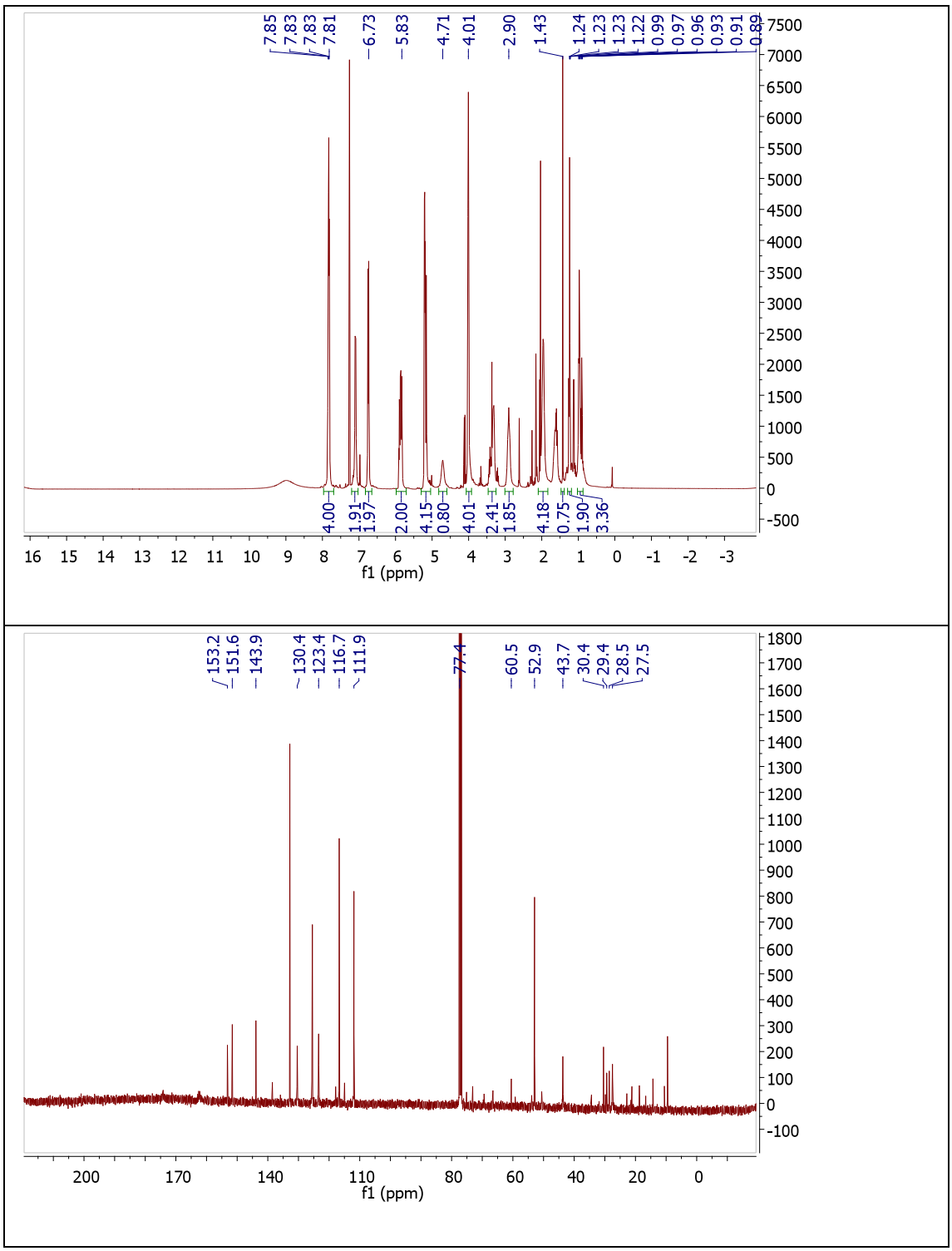

### 9.5.19 (*E*)-*N*-(4-((4-(diallylamino)phenyl)diazenyl)phenyl)-*N*-(1-phenethylpiperidin-4-yl)propionamide (9.31)

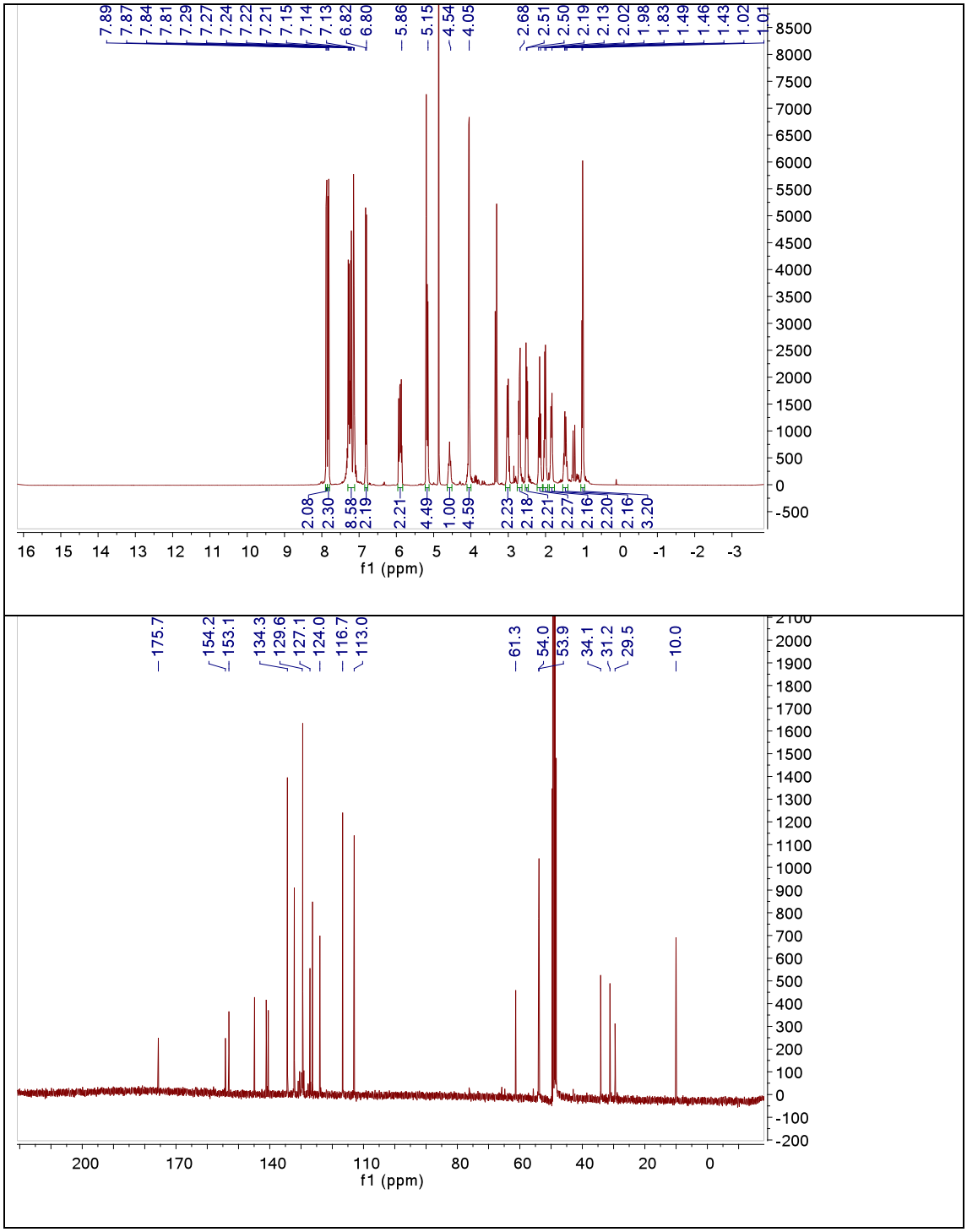

# *10 Photochromic Molecules for Various Biological Targets*

## 10.1 General Introduction

In the course of the experimental work described herein, several other azobenzene-based pharmacophores have been synthesized for a variety of different biological targets. These targets include enzymes (such as glutathione S-tranferase (GST), ion-channels (*e.g.* nicotinic Acetylcholine receptors (nAChRs), voltage-gated potassium channels, the $GABA_A$ receptor and the transient receptor potential channel ML3 (TRPML3)) as well as metabotropic receptor (such as the metabotropic glutamate recptor (mGluR), muscarinic acetylcholine receptor (mAChR) and the $GABA_B$ receptor). The synthesis of photochromic molecules including their chemical and physical characterization and if available their biological activity will be described herein.

The compounds described herein range from commercially available sulfasalazine (SSZ) to simple pharmacophores, such as ammonium ions and more complex ones, such as AzoGABA. The latter was synthesized with the aid of an enantioselective Jørgensen-Hiyashi organocatalyst. Most compounds have undergone preliminary testing that is not described herein and await full (photo-)pharmacological characterization towards theur specific targets.

## 10.2 Glutathione S-Transferase

Glutathione S-transferases (GSTs) (Figure 54a) are a family of detoxifying enzymes found in many organism ranging from prokaryotes to metazoans, which catalyze the reaction between the reduced form of glutathione (GSH) and a second substance for decreasing its toxicity, and increasing its solubility to ultimately remove the product from the organism via excretion.[177] Sulfasalazine (Figure 54b) is a sulfa drug, which is known to block GST activity.[178] Furthermore, the structure of SSZ consists of a sulfapyridine and a salicylate, connected *via* a diazene unit. With the resulting azobenzene structure, it can be reasoned that it might serve as a PCL for GST catalysis. Maximal absorbance was determined to be $\lambda_{max}$ = 360 nm and although no switching was detectable with UV/Vis spectroscopy (Figure 54c) for SSZ, this does not exclude switching properties. For a fast assay, a commercial kit (Sigma, #CS0410) was used to assess light-dependent inhibitory constants of SSZ towards GST with a platereader. In order to assess light dependent affinity, SSZ was pre-irradiated with a hand-held UV lamp ($\lambda$ = 366 nm) (VWR, #732-0859) prior to measurement. Endpoint catalytical activity was recorded and subtracted from background absorption to obtain GST activity. Indeed, this measurement proves SSZ to have blocking abilities in the micromolar range. However, over a range from 10 nM SSZ to 10 mM, no significant light-dependency could be observed (Figure 54d).

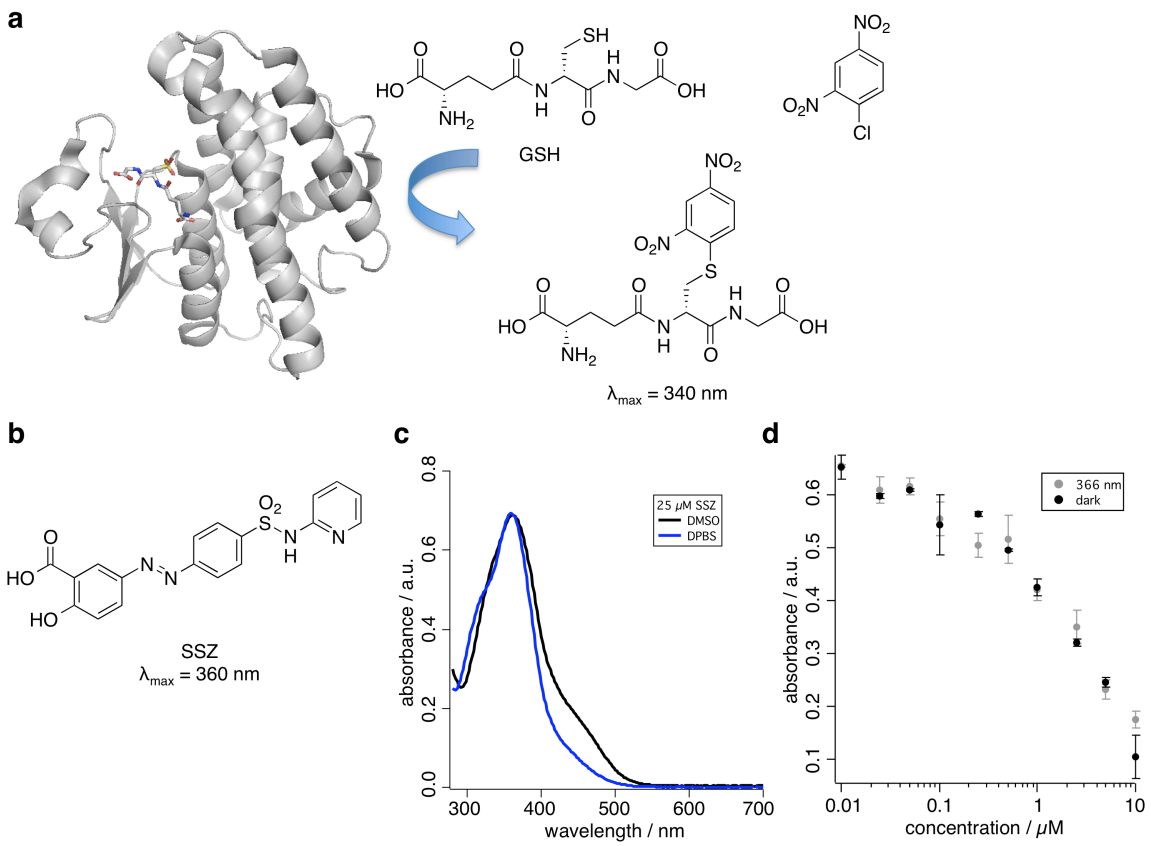


**Figure 54: Attempts towards photocontrolled glutathione S-transferase (GST). a)** GST (pdb: 1R5A[179]) catalyzes the reaction between glutathione (GSH) and chloro-2,4-dinitrobenzene to give a reaction product with an maximal absorbance at λ = 340 nm, which can be followed by UV/Vis spectroscopy. **b)** The structure of sulfasalazine (SSZ) and its **c)** UV/Vis spectrum in DMSO (black) and DPBS (blue); both 25 μM. **d)** GST assay with different SSZ concentrations under pre-irradiated conditions (λ = 366 nm, gray) and in the dark (black) shows no significant difference in blocking capabilities.

Although no difference in pre-irradiated samples toward GST could be observed, the switching kinetics of SSZ have so far not been fully evaluated. It would therefore be beneficial to obtain these parameters, for instance by $^{1}$H NMR as described before,[180] especially to obtain thermal relaxation kinetics. If these are fast, the assay performed would indeed give the same results for pre-irradiated samples and samples that have been kept in the dark, as only the *trans*-isomer would be present. To conclude, further investigations would be interesting to target GST for photopharmacology. This can also be envisioned by further

derivatizing sulfonamide containing azobenzenes that have been described in chapter 7 to their pyridine-sulfonamide counterparts.

## 10.3 TRPML3 Channel

Transient receptor potential channels are a large family of at least 28 ion channels, which share structural similarity and are subdivided into two groups: group I consists of TRPA, TRPC, TRPM, TRPN and TRPV channels, while group II consists of TRP and TRPML.[181] Their versatility and function is broad and reaches among other functions from heat and cold sensation to taste sensors and nociception.[1] Not much is known about the TRPML family, which is divided into TRPML1, TRPML2 and TRPML3 in terms of their function and cellular responsiblities.[182] However, research has been ongoing to find and design selective inhibitors to target these channels, resulting in a library of pharmacophores being previously described.[182] For instance, the TRPML3 channel activator SF-23 has been described with an $EC_{50}$ = 1.1 µM (Figure 55a). From a structural perspective, an aryl sulfonamide is *N*-linked to a phenyl-2-morpholine moiety, and furthermore the aryl ring is a thiophene with a substitued chlorine in the 5-position. Therefore, an "azologization" can be carried out at two different positions. Firtsly, on the thiophene ring replacing the chloride atom, and secondly, on the phenyl ring that is connected to the sulfonamide (Figure 55a, right side). For the ease of synthesis and furthermore to gain access to a first possible TRPML3 photoactivator, the route was chosen for displacement of the chlorine atom with the phenzyl diazene unit to yield **JB556** in a one step procedure from commercially available substrates (Figure 55b). Sulfonylchloride **10.1** was derivatized to sulfonamide **JB556** by reaction with aniline **10.2** in DCM under basic conditions (DIPEA, cat. DMAP) in 59% yield. The substitution of the thiophene to a phenyl ring should be tolerated, as these are regarded as bioisosters of each other (*i.e.* isopharmacological). The fact that the sulfonyl chloride containing azobenzene is substituted with a *N*,*N*-dimethylamine in the 4'-position results in a red-shift of the π-π*-band, which is a fastidious side-effect in this synthetic route; shifting the maximal absorbance into the visible range: $\lambda_{max}$ = 462 nm in DMSO and $\lambda_{max}$ = 454 nm in PBS (both 50 µM) (Figure 55c). Even more, crystals suitable for X-ray diffractometry were obtained for **JB556** and the solved structure is displayed in Figure 55d.

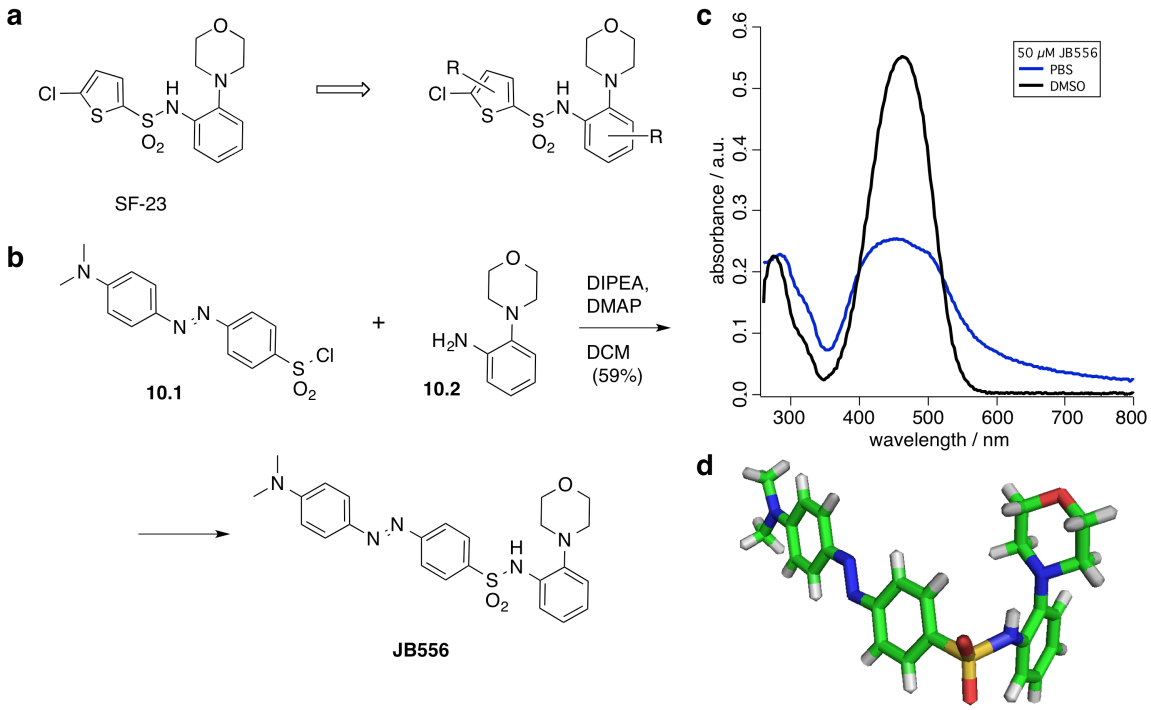


**Figure 55: Azologization of SF-23 to yield JB556 as a photoswitchable TRPML3 channel activator. a)** The channel activator SF-23, which can be "azologued" with respect to its two aromatic rings. **b)** Synthesis of **JB556** in a one-step procedure. **c)** UV/Vis spectra in DMSO (λ = 462 nm, black) and PBS (λ = 454 nm, blue). **d)** Crystal structure of **JB556**.

In summary, sulfonamide **JB556** was synthesized in a one-step procedure from commercially available substrates in good yields including its crystal structure. The ability to activate TRPML3 channels (in a photodependent manner) with **JB556** will be tested in due course, alongside its switching characteristics that are exhibited in the visible range, which is beneficial for deeper tissue penetration and reducing phototoxicity.

## 10.4 Acetylcholine Receptors

In a cold winter night in 1921, Otto Loewi woke up dreaming about a crucial experiment.[183] He went to his laboratory to electrically stimulate a frog heart and taking a fluid sample to add it to a second heart. Amazingly, the heart rate of the second heart decreased. With this finding, Loewi answered a long-standing question about synaptical communication: information is transmitted electrically and chemically, the latter by the so-called "Vagusstoff", today known as acetylcholine.[184] This earned him together with Sir Henry Dale the Nobel Prize in Physiology and Medicine in 1936.[184]

Acetylcholine is the main player in synaptic communication.[1] Once released from vesicles into the synapse, it stimulates nicotinic and muscarinic acetylcholine receptors, which propagate the signal in the postsynapse. Nicotinic acetylcholine receptors are pentameric ligand-gated ion-channels, while muscarinic receptors are G-protein coupled receptors. The first has been optically controlled before by Erlanger and co-workers in the early 1970's with a compound named **BisQ**.[57] As they were able to reversibly control the behaviour of explanted neurons from *Electrophoros electroplax*, the exact target remained elusive until today. Ever since, molecular biology has advanced rapidly in terms of cloning, heterologous expression systems and the possibility to study proteins on a molecular level by means of X-ray crystallography. Therefore, a reinvestigate of this molecule in order to gain a deeper knowledge of the exact effect of **BisQ** in neuronal communication would be beneficial.

### 10.4.1 Nicotinic Acetylcholine Receptors (nAChRs)

Nicotinic acetylcholine receptors (nAChRs) are pentameric ligand gated ion channels found in the synapse that sense acetylcholine (ACh) once this neurotransmitter is released into it. When bound, ACh triggers channel opening and depolarization occurs, the entry point for the creation of action potentials. Therefore, nAChR are the main stimulatory receptors in the nervous system and their malfunction is associated with many severe diseases, such as schizophrenia, epilepsy, Parkinson's and Alzheimer's disease.[185,186] Controlling

nAChRs in a fast manner with high temporal and spatial resolution could elucidate its role further for various pathological states. An engineered PTL light-gated nAChR has been previously described.[84] However, as usual for a PTL approach, this channel would have to be introduced genetically. More importantly would be the optical control of nAChRs subtypes with a drug-like, freely diffusible PCL. This subchapter describes the design and synthesis of photochromic nAChR ligands beginning with the synthesis of a benchmark activator (**phenylcholine**) towards a new synthesis of **BisQ** culminating in the development of **AzoCholine**.

In order to perform initial studies on nicotinic acetylcholine receptors, the known agonist **phenylcholine** was synthesized.[187] Starting synthetic work from phenol (**10.3**), the amine was installed by substitution with 2-chloro-*N*,*N*-dimethylethan-1-aminium chloride under basic conditions with catalytic amounts of potassium iodide in DMF at elevated temperatures to give **norphenylcholine** in 40% yield. Quarternization of the amine with MeI in THF yielded 68% of **phenylcholine** as its iodide salt after filtration without the need for column chromatographic purification procedures (Scheme 19).

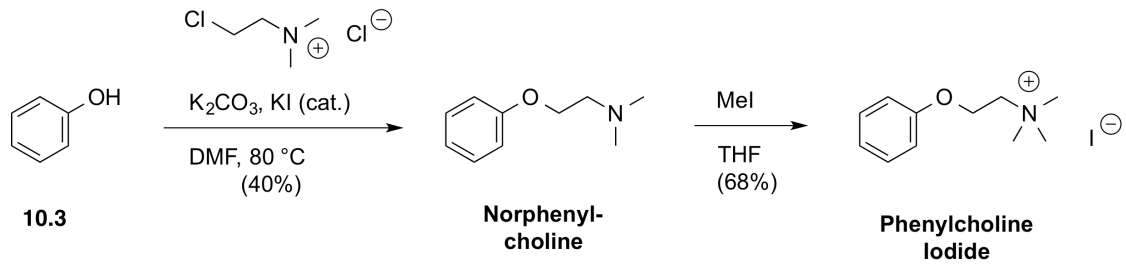


**Scheme 19: Synthesis of Phenylcholine.** Starting form phenol (**10.3**), **Norphenylcholine** was obtained *via* nucleophilic substitution and the quartenary ammonium ion was installed with MeI to yield **Phenylcholine** as its iodide salt.

**BisQ** has previously been synthesized by Wohl-Ziegler bromination of *m*-azotoluene in refluxing carbon tetrachloride with installment of the quarternary ammonium ion by benzylic displacement with trimethylamine.[57] However, due

to the toxicity of carbon tetrachloride a different, more environmentally friendly route was chosen. First, benzylic amine **10.4** was protected with a Boc-group in quantitative yield (*i.e.* aniline **10.5**) in order to be subjected to oxidation of its aniline group to a nitroso species **10.6**, which was not isolated. Instead, the nitroso compound **10.6** was reacted with aniline **10.5** to give access to the protected azobenzene **10.7** in a Mills reaction in 39% yield. After deprotection of the Boc-group, which proceeded in 86% to give free bis-amine **10.8**, the quartenary ammonium moiety was installed with MeI in 67% yield to give access to **BisQ** (Scheme 20a). Switching between its *cis*- and *trans*-states was achieved by illumination with UV- ($\lambda$ = 360 nm) and blue light ($\lambda$ = 440 nm) (Scheme 20b) and monitored by UV/Vis spectroscopy (Scheme 20c). Although **BisQ** shows it maximal absorbance at 320 nm (Scheme 20c), switching with 360 nm is favorable due to less energized photons at this wavelength. Ultimately, crystals suitable for X-ray diffractometry were obtained by letting a solution of EtOH/water slowly evaporate at 4 °C over several days (Scheme 20d).

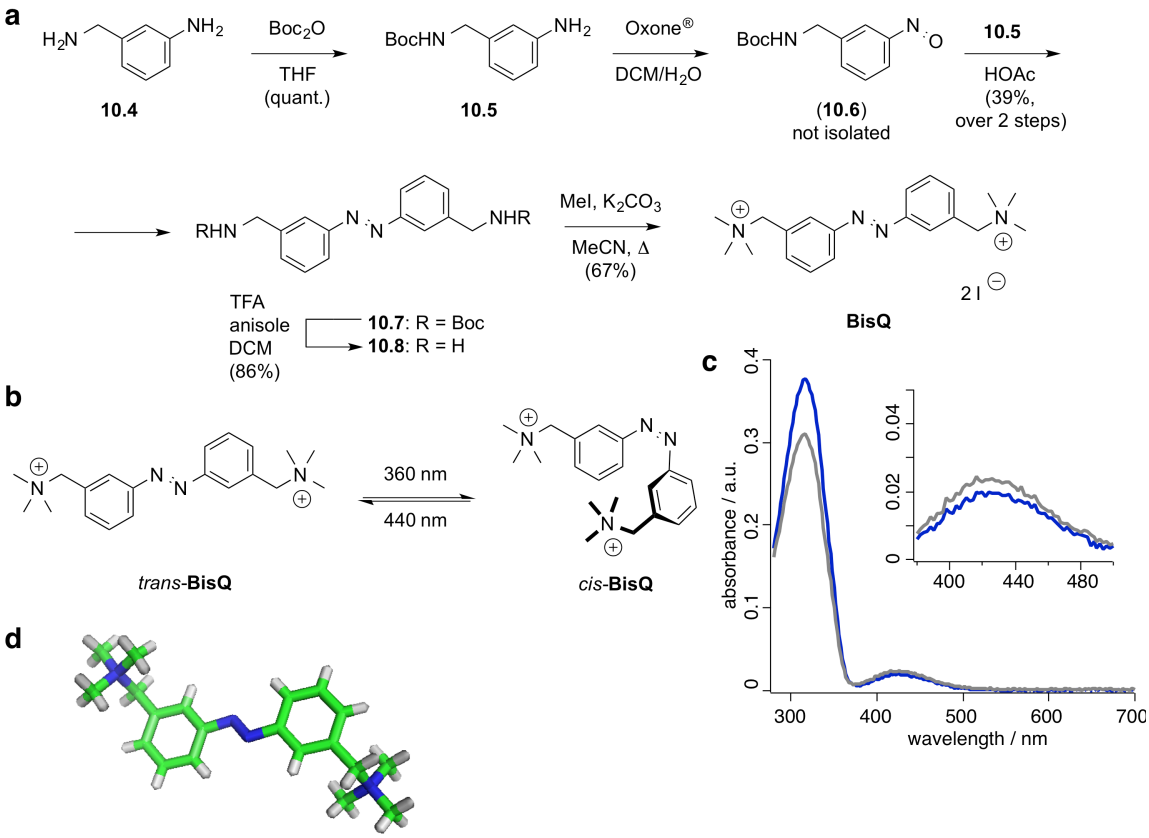


**Scheme 20: Novel synthesis, switching and X-ray diffractometry of BisQ. a)** Alternative and environmentally friendly four-step synthesis. **b)** *cis*-/*trans*-Isomerism. **c)** UV/Vis spectra of *trans*- (blue) under blue light (λ = 440 nm) and *cis*-isomer (gray) under UV-light (λ = 360 nm) (insert shows n-π*-band). **d)** Crystal structure of **BisQ** (counterions are omitted for clarity).

Another AChR molecule was synthesized based on the structure of ACh, *viz* **AzoCholine** according to protocols developed by Dr. Tatsuya Urushima. This ligand is merged to an azobenzene directly at its oxygen atom of choline thereby lacking the structural composition of the acetate moiety in Ach rather resembling an extension to **phenylcholine**. Starting from 4-hydroxy azobenzene (**10.9**) the ethylene-connected amine **10.10** was installed by a $S_N2$ reaction in 73% yield. Final quarternization was achieved with MeI in THF to obtain **AzoCholine** in 87% yield as its iodide salt in a highly pure form without the needs for column chromatography (Scheme 21a). **AzoCholine** could be switched back and forth from its *trans*- to its *cis*-state by reversible irradiation with blue (λ = 440 nm) and UV-light (λ = 360 nm) (Scheme 21b) while following switching

by UV/Vis spectroscopy (Scheme 21c). Crystals suitable for X-ray diffractometry were obtained to solve the molecular structure of **AzoCholine** (Scheme 21d).

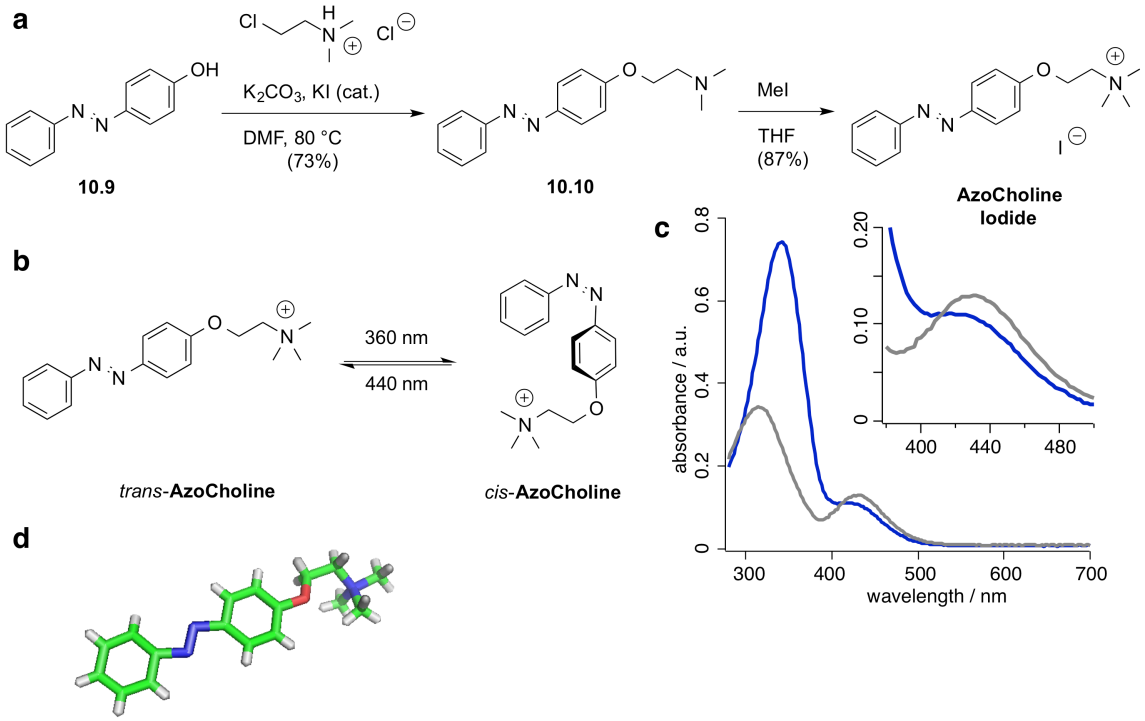


**Scheme 21: Synthesis, switching and X-ray diffractometry of Azocholine. a)** Convenient two step synthesis of **AzoCholine**. **b)** *cis*-/*trans*-Isomerism. **c)** UV/Vis spectra of *trans* (blue) under blue light (λ = 440 nm) and *cis*- **AzoCholine** (gray) under UV light (λ = 360 nm) (insert shows n-π*-band). **d)** Crystal structure of **AzoCholine** (counterion is omitted for clarity).

In summary, **phenylcholine** has been synthesized as a nAChR agonist, together with a newly developed synthetic protocol that is more environmental friendly for **BisQ** in a four-step protocol. **AzoCholine** has been synthesized and crystal structures have been obtained for both PCLs and can be photoisomerized with UV-light to their *cis*- and with blue light to their *trans*-states. Initial testing exhibited photoagonism of **BisQ** towards muscle nAChR subtype and of **AzoCholine** towards an α7/Gly chimera that resembles the α7-homopentamer subtype (electrophysiological data recorded by Arunas Damijonaitis, data not shown). Concluding, both PCLs are interesting nAChR subtype selective activators that will be fully evaluated *in vitro* and *in vivo* in ongoing studies.

### 10.4.2 Muscarinic Acetylcholine Receptors (mAChRs)

Muscarinic acetylcholine receptors (mAChRs) are G-protein coupled receptors also found in the synapse. They are activated by ACh and respond slower with respect to their nicotinic counterpart. Found in the heart, trachea, eye and elsewhere, they are for instance responsible for heartbeat, tracheal contraction and pupil dilation. Best to our knowledge, no selective mAChR photoligands have been described so far although n/mAChRs are a prime example for receptor selectivity (therefore their name based on the selective agonism). A muscarinic selective agonist that is photoswitchable would be beneficial to elucidate the role of these receptors, which are found together with nicotinic receptors in the synapse selectively. Accordingly, two molecules have been synthesized, namely **AzoIperoxo** and **AzoCarbachol**. The former was synthesized in four steps but did not show any activity towards muscarinic receptors. Therefore it was discarded for further studies towards this target. The latter was synthesized in a two-step protocol (Supporting Figure 8), which does not activate the muscle or the $\alpha$7/Gly nAChRs (electrophysiology performed by Arunas Damijonaitis, data not shown). Accordingly, this focus lies on this molecule for further investigation as described in here.

Commencing with 4-amino azobenzene (**10.11**), an isocyanate was installed on the amine moiety by treatment with triphosgene to give **10.12**, which could be purified by flash column chromatography and stored in a desiccator. It was then trapped with choline to yield **AzoCarbachol** in quantitative yield (brsm **10.11**), proving its reactivity (Scheme 22a). It therefore resembles the native ligand ACh but the non-hydrolyzable version of ACh, carbachol (Scheme 22b) that is used for instance for protein co-crystallography or for biological testing as it is not cleared by acetylcholinesterase (AChE). **AzoCarbachol** could be switched reversibly between its *cis*- and *trans*-state by applying UV ($\lambda$ = 350 nm) or blue light ($\lambda$ = 440 nm) (Scheme 22c) while isomerization was followed by UV/Vis spectroscopy (Scheme 22d). The measuremtn of repeated cis-trans-isomerization was recorded in order to obtain the $\tau$-values (Scheme 22e). The

sloped were fitted exponentially and *cis*-isomerization was slightly faster ($\tau_{cis}$ = 41.9 ± 6.9 seconds) with respect to *trans*-isomerization ($\tau_{trans}$ = 48.0 ± 3.1 seconds) with the applied wavelengths as described above. Furthermore, and as expected in a side-experiment, **AzoCarbachol** does block AChE catalyzed degradation of ACh with a $K_i$ = 2.16 µM ($IC_{50}$ = 21.6 µM) (Scheme 22f) (see Chapter 6, Experimental for AChE assay and further details).

**AzoCarbachol** proved to remote control the heart rate in explanted mice hearts reversibly (Scheme 22g). After perfusion of 100 µM **AzoCarbachol**, the heart rate could be controlled reversible between 240 and 160 beats per minutes (bpm) by application of blue light (λ = 470 nm) or shutting the light source of and UV light (λ = 360 nm). This gives optical control in an *ex vivo* system presumably on the mAChR2, which is expressed in the heart and responsible for the heart rate via G-protein coupled inward rectifying potassium channels (GIRKs).[188] However, with the action of **AzoCarbachol** also towards AChE further testings have to be conducted in order to focus on optically controlled pacemakers.

Crystals suitable for X-ray diffractometry of **AzoCarbachol** have been obtained by the slow vapor diffusion technique (Scheme 22h). Briefly, a concentrated solution of **AzoCarbachol** in methanol was exposed to an ether atmosphere in a sealed scintillation vial and crystal growth took four days. After the first seed crystals were detectable by the naked eye, more ether was added carefully on top of the solution and crystallization was allowed to proceed for another two days to obtain single crystals of appropriate size.

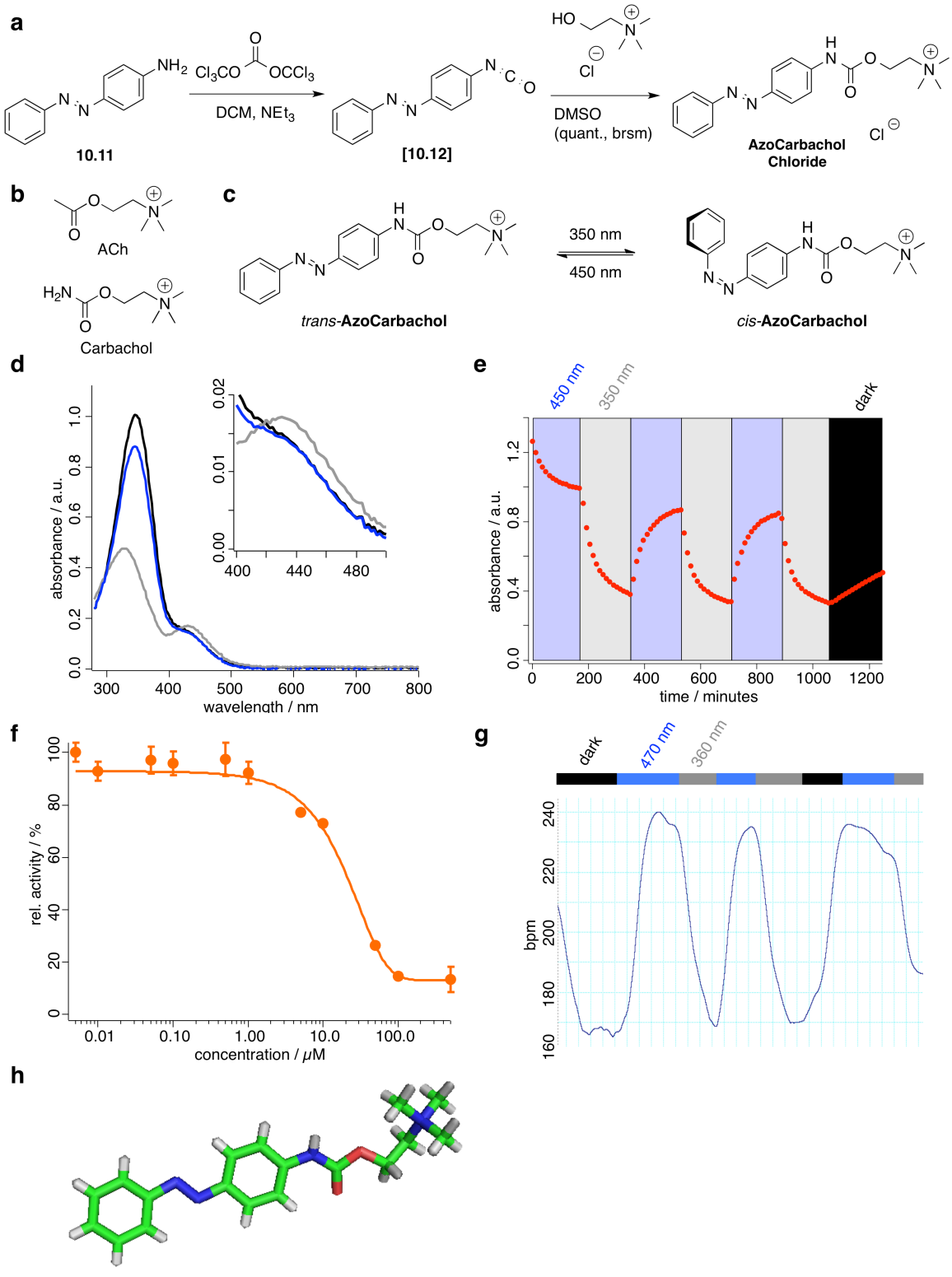


**Scheme 22: Synthesis and characterization of AzoCarbachol. a)** Synthesis of **AzoCarbachol** *via* an isolatable isocyanate containing azobenzene, **b)** acetylcholine receptor agonists acetylcholine (ACh) and carbachol, **c)** switching between the *cis*- and *trans*-states of **AzoCharbachol** is achieved with λ = 350 nm and λ = 450 nm, respectively, **d)** UV/Vis spectra of 50 µM **AzoCarbachol** in Ringer solution in its dark-adapted state (black), *trans*- (blue) and *cis*-isomer (gray) (insert shows n-π*-band), **e)** reversible kinetics of **AzoCarbachol**. **f)**

Acetylcholinesterase (AChE) endpoint assay proves **AzoCarbachol** as an inhibitor with an $IC_{50}$ = 21.6 µM. **g)** Optical control of the heartbeat in explanted mice hearts with 100 µM **AzoCarbachol**. The heart rate could be slowed down with application of UV-light (λ = 360 nm) and recovered under illumination with blue light (λ = 470 nm) or in the dark (bpm = beats per minute). **h)** Crystal structure of AzoCarbachol (counterion is omitted for clarity).

Interestingly, and on a side note, ethyl (*E*)-(4-(phenyldiazenyl)phenyl)carbamate (see Experimental) was isolated as a product, presumably due to a Hofmann elimination of trimethylamine that can serve as a reductant for the intermediate vinyl carbamate.

In summary, **AzoCarbachol** was synthesized in a two-step procedure in quantitative yield based on the recovered starting material **10.11**. The isocyanate intermediate can be purified and stored to synthesize other PCLs or PTLs in the future. Its highly reactive isocyanate makes it a good electrophile to for instance label more complex molecules bearing an alcohol or a free amine. Therefore, azologization can be envisioned more easily to commercially available drugs on the market bearing such residues. **AzoCarbachol** can be switched with UV- and blue light and is also a blocker with no photodependence of AChE. Consequently, this should be taken into consideration for *in vivo* studies, as ACh clearing will take longer due to this inhibitory property. *Ex vivo* studies on explanted hearts were successfully performed to control the heart rate, most probably *via* the M2 receptor. Indeed, this could have an impact on translational medicine for the treatment of patients with for instance cardiac arrhythmia. One can envision an optical pacemaker in order to set the heart beat frequency to physiological levels when needed in a fast, reversible and reliable manner.

## 10.5 Voltage-gated Potassium Channels

Voltage-gated potassium channel play a crucial role in the central nervous system where they open upon depolarization of the cellular membrane to terminate an action potential ultimately setting the membrane potential back to its resting state. The concept of photopharmacology started with these kind of channels by engineering a synthetic photoisomerizable azobenzene-regulated $K^+$ (SPARK) channel about a decade ago.[9] A PTL, MAQ (maleimide-azobenzene-quartenary) (Figure 56a) was used to block channel currents with an attached quartenary ammonium ion upon photoisomerization. Later, PCLs followed that had two attached quartenary ammonium ions on the 4- and 4'-position of the azobenzene through an amide linker. Due to their structural motifs they were called QAQ's (quartenary-azobenzene-quartenary) (Figure 56b) and were able to control nociception with light.[50] In order to find new PCLs with intereseting switching characteristics and different geometrical demand, a dual azobenzene core could be used (Figure 56c). Besides the bigger change in its end-to-end distance when isomerized, the switching wavelength of the two azobenzenes remains the same as they are unable to electronically communicate due to their methylation pattern (Figure 56d).[189]

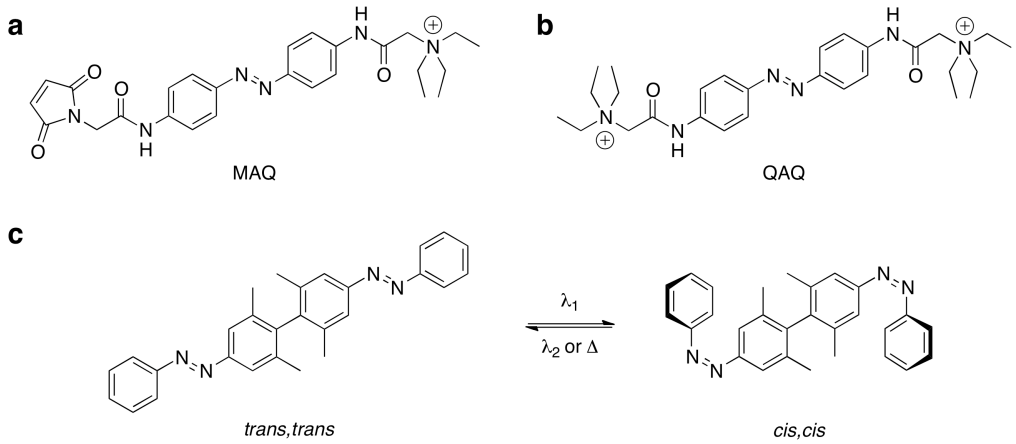


**Figure 56: Photochromic potassium channel blockers and dual azobenzene.** **a)** MAQ (maleimide-azobenzene-quarternary) is a potassium channel PTL blocker. **b)** QAQ (quarternary-azobenzene-quartnary) is a potassium channel

PCL blocker. **c)** Dual azobenzene that can not communicate electronically *via* their biphenyl connection exhibit large geometrical spanwide when isomerized from their *trans*,*trans*- to their *cis*,*cis*-isomer.

The synthesis is depicted in Scheme 23 and started with 3,5-dimethylaniline (**10.13**), which was oxidized to its nitro counterpart **10.14** in 62% yield with Oxone® in a DCM, MeOH and water mixture for a monophasic system. Interestingly, a side-product **10.14'** was obtained that proved to be the corresponding quinone[190] by X-ray diffractometry. Indeed, and on a side note, this reaction would be a convenient way to synthesize such functional groups, especially because anilines and Oxone® are cheap bulk chemicals.

Dimerization of the nitro group under reductive conditions with metallic zinc in an EtOH/$NaOH_{aq}$ mixture[191] yielded the corresponding azobenzene **10.15** and the desired hydrazine **10.16** in 18% and 17% yield, respectively. However, **10.15** (for which crystals suitable for X-ray diffractometry were obtained) could also be converted to **10.16** by diimine reduction with catalytic amounts of Pd/C in ice-cold ethanol in high yields (92%), therefore increasing the total amount of **10.16** to roughly 34%.

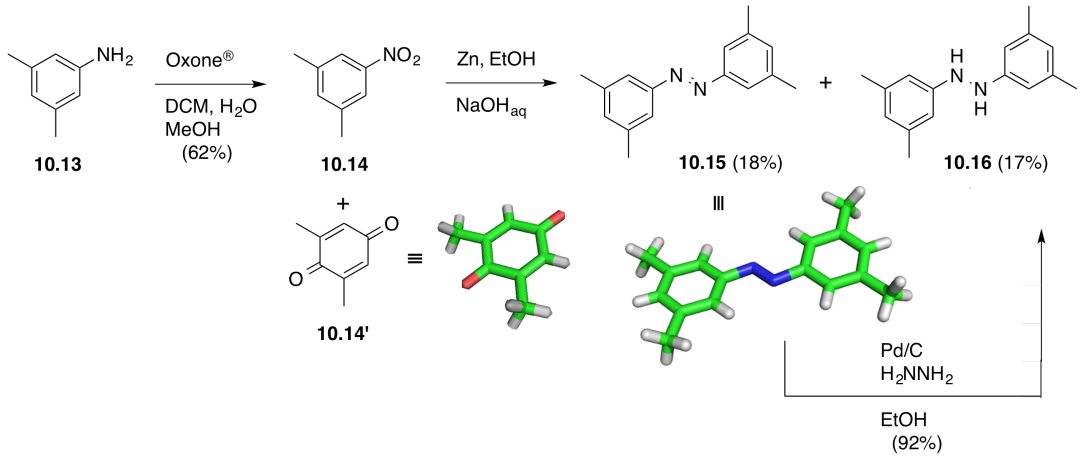


**Scheme 23: Synthesis of the hydrazine precursor.** Aniline **10.13** is oxidized to nitrobenzene **10.14** (and quinone **10.14'** as a side-product proved by X-ray diffractometry), which is dimerized under reductive conditions to hydrazine

**10.16**. Azobenzene side product **10.15** (for which a crystal structure was obtained) can also be reduced to hydrazine **10.16** with diimine and Pd/C.

Hydrazine **10.16** was subjected to acidic conditions in refluxing aqueous HCl to undergo a 5,5-sigmatropic Benzidine rearrangement to give the biphenyl core **10.17** [191] in 80%, which was condensed twice to 4-nitro-nitrosobenzene (**10.18**) in a Mills reaction that only gave 30% yield (Scheme 24a). The resulting dual azobenzene **10.19** was obtained as crystals suitable for X-ray diffractometry that nicely displays the conformation of the two azobenzenes: due to the four methyl groups the two phenyl rings are oriented orthogonally. As a consequence, electronic communication between these is abolished, as their π-system is not overlapping resulting to the observation that the first azobenzene isomerization does not alter the wavelength needed for the second azobenzene. **10.19** was further reduced with sodium sulfide in a refluxing mixture of THF/water to give the respective bis-amine **10.20** in a satisfying yield of 79%. Installing the quartenary ammonium salt was achieved by acylation with the acyl chloride of betaine **10.21**[50] to obtain the desired **QAAQ** molecule in 33% yield (Scheme 24a). With the extended dual azobezene, **QAAQ** is the acronym closely related to QAQ and stands for quartenary-azobenzene-azobenzene-quartenary. Due to its doubly charged character, **QAAQ** shows good solubility in water. UV/Vis spectroscopy was employed to follow switching from the dark-adapted state of **QAAQ** (Scheme 24b, black) to the *cis*-isomer with UV- (Scheme 24b, gray, λ = 358 nm) and to the *trans*-isomer with blue light (Scheme 24b, blue, λ = 434 nm). It should be noted that this investigation does not include the proof for *trans*,*trans*-, *cis*,*trans*-, *trans*,*cis*- or *cis*,*cis*-isomerization.

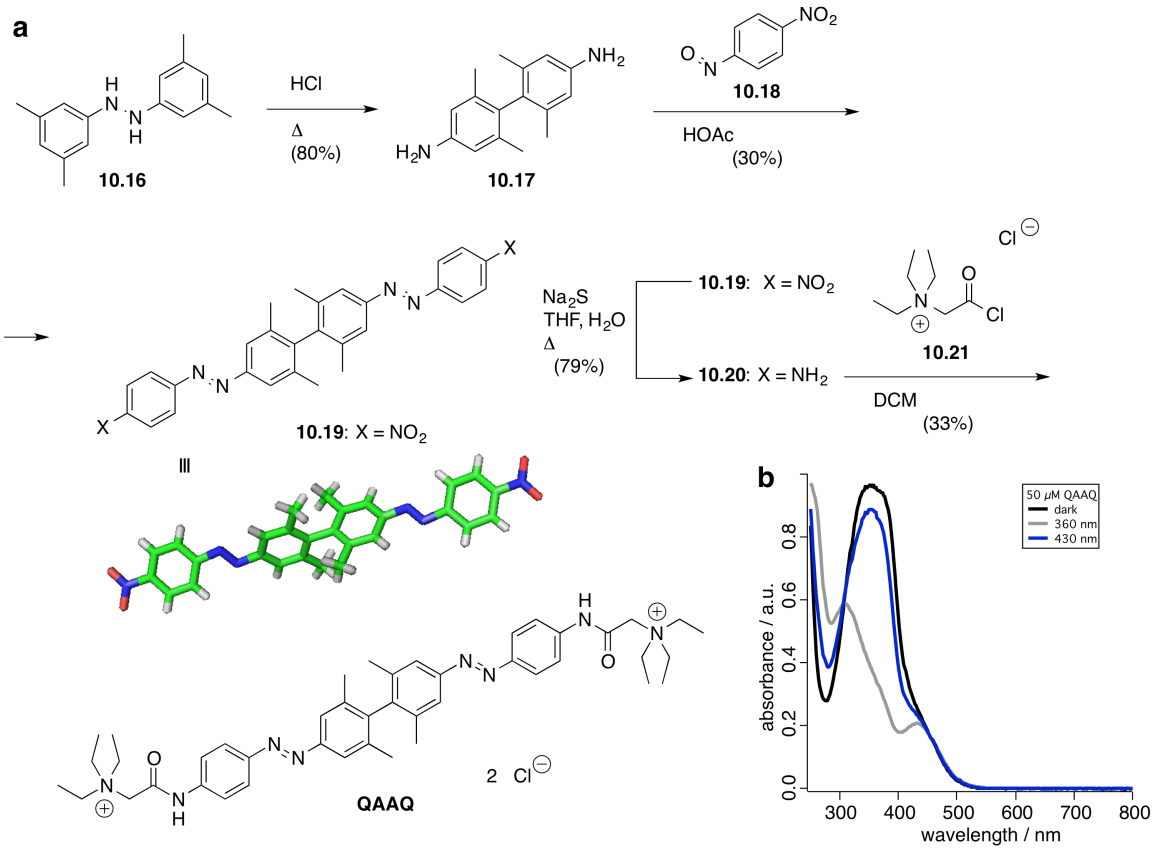


**Scheme 24: Synthesis and UV/Vis spectra of QAAQ. a)** Hydrazine **10.16** undergoes [5,5]-sigmatropic Benzidine rearrangement to yield biphenyl **10.17**, which is subsequently condensed with nitrosobenzene 10.18 to obtain bis-nitro azobenzene **10.19**. A crystal structure was solved for **10.19**. Reduction of **10.19** with sulfide gives access to bis-amine **10.20** and final installment of the quartenary ammonium ion is achieved by betaine acyl chloride **10.21** to obtain **QAAQ**. **b)** UV/Vis spectra of **QAAQ** in its dark adapted state (black), under 430 nm illumination (blue) and under 360 nm illumination (gray).

In summary, the novel dual cationic PCL **QAAQ** has been synthesized that has to be tested for its isomeric states and toward potassium channel blocking capabilities. Furthermore, bis-aniline **10.20** could serve as a good precursor for more PTL, PTL' and PTD molecules (see Chapter 9), as their end-to-end-distance will be affected in a more pronounced manner than bearing a single azobenzene. Taken together the pharmacological and synthetic promises, one can imagine many possible applications for the molecules described herein.

## 10.6 GABA Receptors

γ-Aminobuturic acid (GABA) is a neurotransmitter and the main player in the inihibitory nervous system.[1] When released into the synapse in vertebrates, it binds to transmembrane receptors located in the pre- and postsynapse causing hyperpolarization. This can be mediated by two different type of GABA receptors: once activated, $GABA_A$, a ligand-gated ion channel causes the flow of chloride ions into the neuron and $GABA_B$, a GPCR that is linked to inward-rectifying potassium channels causing the outflow of potassium ions. Consequently, both receptors exhibit hyperpolarizing properties causing an inhibitory effect towards action potential firing. The inhibition has to be tightly controlled as too little inhibition results in seizures, while too much inhibition can result in coma. All in all, GABA receptors are important drug targets for anxiety disorders and their photocontrol may lead to deeper insights in how the brain balances excitement and inhibition to function properly. Furthermore, the ligand-binding domain is a so-called clamshell (or VFT) domain (see chapter 5 for further details), a motif that the Trauner group successfully photocontrolled on ionotropic and metabotropic glutamate receptors.

### 10.6.1 $GABA_A$ Receptor

$GABA_A$ receptors are pentameric ligand-gated ion channels that conduct chloride ions across the lipid bilayer in neurons and mediate fast inhibitory post-synaptic potentiation (IPSP). With its inhibitory function it is an excellent target to treat anxietiy disorders (for instance with methaqualone, Scheme 25a), especially when counseling and psychotherapy fails. As mentioned above, the inhibitory action has to be tightly controlled, and again photopharmacology may contribute to this with its non-invasive and precise chracteristics to control protein function.

Methaqualone (Scheme 25a) is an anti-depressant that is not marketed anymore because of its side-effects, such as addictiveness. However, it is still in use as a recreational drug and exhibits binding and stimulation to $GABA_A$ receptors. The

simplicity of the molecule together with its strong effects on $GABA_A$ made it a good candidate for azologization (Scheme 25b). In one step, an azologed version of methaqualone, *viz.* **JB420** was synthesized by one-pot acylation and condensation between *N*-acetylanthranilic acid (**10.22**, synthesized according to ref[192] of which also a crystal structure was obtained and triboluminescence was not tested) and 4-aminoazobenzene (**10.11**) in refluxing $POCl_3$ in 21% isolated yield. *cis*/*trans*-Isomerization was achieved reversibly by illumination with 320 nm (Scheme 25c, gray) and 433 nm (Scheme 25c, blue) of light from its dark-adapted state (Scheme 25c, black).

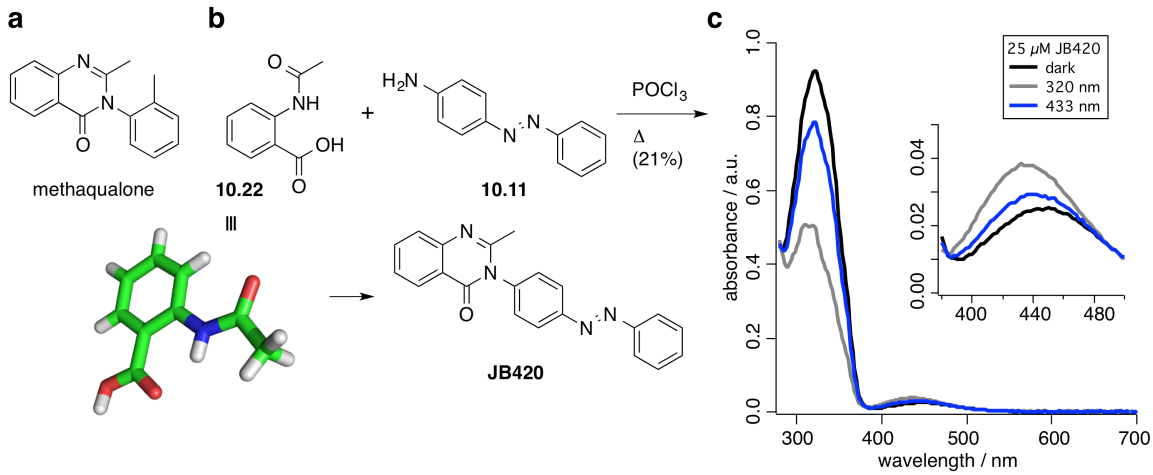


**Scheme 25: Synthesis of methaqualone-based $GABA_A$ inhibitor JB420. a)** The structure of methaqualone. **b)** One-step synthesis of **JB420** by one-pot acylation and condensation between *N*-acetylanthranilic acid (**10.22**, with crystal structure) and 4-aminoazobenzene (**10.11**). **c)** UV/Vis spectra of **JB420** in its dark adapted state (black), under 433 nm illumination (blue) and under 320 nm illumination (gray).

**JB420** will be tested towards $GABA_A$ receptors in a light dependent manner. With the synthetic route established, more congeners can be synthesized. Two major things should be performed: first, a red-shifted version would be desirable by implementing electron-donating groups on the azobenzene, such as an alkylated amine in the 4'-position and secondly, installation of the methyl group in the 3-position that is present in methaqualone but not in **JB420**. The latter

could have pharmacological effects and would hint for permutations according to structure-activity-relationships (SARs).

### 10.6.2 $GABA_B$ Receptor

$GABA_B$ receptors are the metabotropic counterparts to $GABA_A$ receptors therefore, when they are activated the exhibit a longer lasting inhibition and a more negative IPSP. To complete the synthesis of PCLs for the inihibitory VFT receptors, baclofen (*rac*-4-amino-3-(4-chlorophenyl)butanoic acid) was chosen to be azologed to give **AzoGABA**. Because baclofen is marketed as a racemic mixture and both enantiomers show activity towards $GABA_B$, the goal herein was to synthesize both **AzoGABA**s in a enantiopure manner to confirm the SARs of this modification on the β-carbon. For clarity, only the synthesis of **(*R*)-AzoGABA** is discussed and described in detail although the (*S*)-enantiomer has been obtained in parallel.

The synthetic route started with cinnamic aldehyde **10.23** that was reacted with nitromethane catalyzed by a Jørgensen-Hiyashi organocatalyst (i.e. (*R*)-2-(bis(3,5-bis(trifluoromethyl)-phenyl)((trimethylsilyl)oxy)methyl)pyrrolidine) to give a Michael-adduct (not shown), which is oxidized *in situ* with NBS to the corresponding methyl ester **10.24** in 61% yield (Scheme 26a). Subsequent reduction achieves three transformations in one pot: the reduction of both nitro groups with the aliphatic one leading to ring closure when 4M NaOH is added to give γ-lactam **10.25** in 37% yield, from which a crystal structure was obtained proving the correct configuration of the product. Further treatment with commercially available nitrosobenzene installed the azobenzene unit in 42% to obtain **10.26**, which was hydrolyzed to the desired **(*R*)-AzoGABA** in refluxing 4M HCl in 29% yield. It should be noted that lactams are usually opened with 6M HCl, but this caused compound **10.26** to degrade during the reaction.

A red-shifted version was obtained by diazotation of **10.25** and *in situ* trapping of the diazonium salt with *N*,*N*-diethylaniline in 22% yield, followed by lactam opening as described above to yield **red-AzoGABA** with a maximal absorbance wavelength at λ = 460 nm (see Experimental) in 70% yield (Scheme 26b).

Therefore, many congeners of **AzoGABA** can be envisioned that are accessible from **10.25** by either Mills or diazonium coupling reactions; a fact that will be explored further in the future.

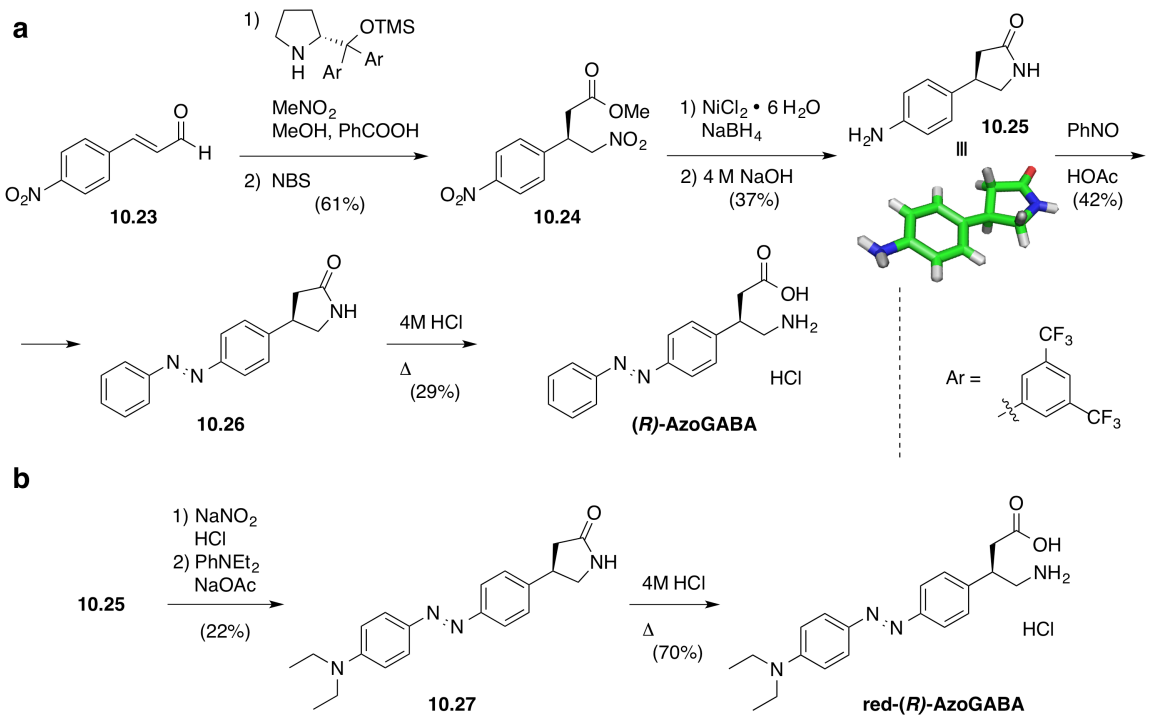


**Scheme 26: Synthesis of AzoGABA and red-AzoGABA (only (*R*)-enantionmers are shown). a)** Synthesis of **AzoGABA**: cinnamic aldehyde undergoes enantioselective Michael-addition and the aldehyde is oxidized with NBS to give ester **10.24**, which is reduced with lactam ring closure to give lactam **10.25**. The azobenzene is installed via a Mills reaction to access **10.26**, and the lactam is hydrolyzed under acidic conditions to give **AzoGABA**. A crystal structure was obtained for **10.25** proving the correct configuration. **b)** Synthesis of **red-AzoGABA**. Aniline **10.25** is diazotized and trapped with *N*,*N*-diethylaniline to give lactam **10.26** that is hydrolyzed in the same way as in **a)** to obtained the red-shifted version **red-AzoGABA**.

### 10.6.3 Summary and Outlook

The optical control of GABA receptors has been reported in the ionotropic receptor, $GABA_A$ with a PTL.[6,193] However, small diffusible molecules are beneficial for pharmacology (*vide supra*). Therefore, with **JB420** and **AzoGABA**

in hand, testing on both $GABA_A$ and $GABA_B$ receptors can be conducted in a light-dependent manner with azologues of methaqualone and baclofen, respectively.

## 10.7 Glucagon-like Peptide-1 Receptor (GLP-1R)

As a proof-of-principle, an azosulfonylurea for the optical control of ATP-sensitive $K^+$ ($K_{ATP}$) channel activity and insulin secretion is described in this work (see chapter 8). It is envisioned to build upon these findings by extending photopharmacology to the incretin axis. Following nutrient transit, glucagon inhibitory peptide (GIP) and glucagon-like peptide-1 (GLP-1) are released from enteroendocrine K and L cells, respectively[194-196]. These incretins bind their cognate receptors in the pancreas and stimulate insulin release in a glucose-dependent manner[197,198], accounting for around 70% of the hormone secreted in response to oral glucose[199]. Glucose concentrations are further normalized by the effects of the incretins to suppress food intake[200], gastrointestinal transit time[197] and glucagon release[201], although GIP has been reported to elevate the latter[202]. While GIP is limited as a therapy due to diminished GIP signaling during type 2 diabetes mellitus (T2DM)[199,203], GLP-1 receptor (GLP-1R) agonists[117,204,205] and modulators[204,206,207] are set to become widely used in the clinic. However, side effects have already been associated with the prescription use of GLP-1 agonists, including an increased risk of developing pancreatitis (although causality is not defined in humans)[153,204,208,209], nausea and gastrointestinal disturbances[205,210]. Thus, methods of targeting receptor activity to the tissue of interest, as well as switching off receptor signaling when not required (*e.g.* after a meal), would provide a desirable refinement to the treatment of T2DM with incretin mimetics and related GLP-1R potentiators. To this end, azobenzenes are well-suited to creating drugs which rely on the spatiotemporal properties of light for activation. Hence, azobenzenes are applicable to the generation of GLP-1R photoswitches for the optical manipulation of the incretin axis (Figure 57). Finally, GLP-1 action and GLP-1R signaling are still not fully understood. A GLP-1R photoswitch would provide a valuable research tool by allowing previously out-of-reach experiments or questions to be addressed. For example: 1) reversible single cell manipulation of cAMP; 2) precise manipulation of GLP-1-regulated connectivity, a signalling mode recently described by us to contribute to incretin-stimulated insulin

secretion in humans[140,141,160]; and 3) targeting of GLP-1R-expressing neural populations involved in glucose homeostasis[211].

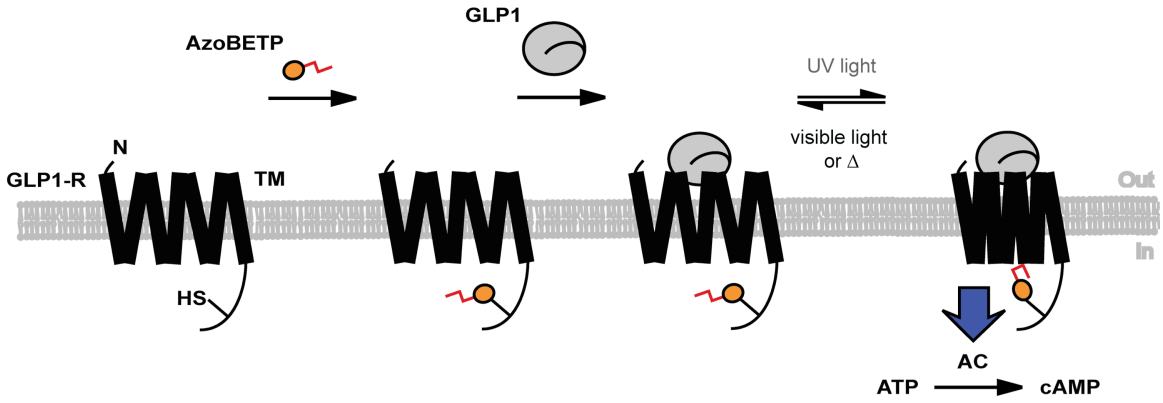


**Figure 57: The logic of a GLP-1R photoswitch.** GLP-1R can be labeled with **AzoBETP**, which then responds to GLP-1 only under illumination with UV light to couple to adenylyl cyclase (AC) and the formation of cAMP.

A six-step synthetic route for the production of a GLP-1R photoswitch (**AzoBETP**), using the recently described ligand-dependent positive allosteric modulator (PAM) 4-(3-(benzyloxy)phenyl)-2-ethylsulfinyl-6-(trifluoromethyl)pyrimidine (**BETP**)[204] as a template (Fig. 58). This PAM presents an ideal scaffold for an azoincretin *versus* other exogenous regulators, since: 1) allosteric ligands are more receptor selective than their orthosteric counterparts[212]; 2) activity is restricted to the site(s) of endogenous GLP1 action[206,207]; and 3) azobenzene installation is synthetically straightforward.

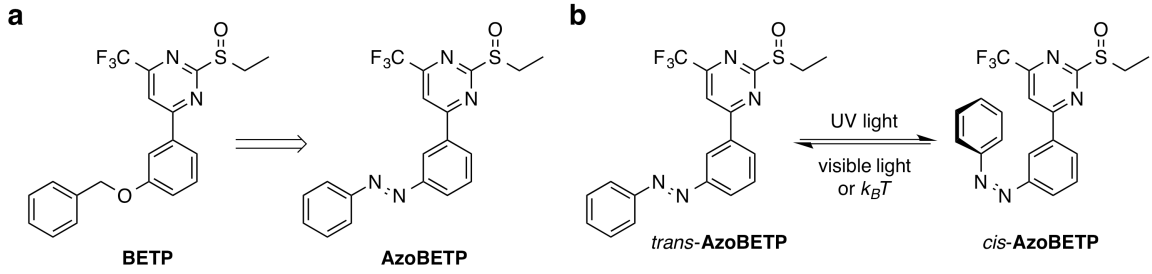


**Figure 58: Azologization of BETP to AzoBETP and its switching principle. a)** The benzylether of **BETP** is replaced by a phenyldiazene, culminating in the design of **AzoBETP**. **b) AzoBETP** as a singly substituted *meta*-azobenzene most probably undergoes switching to its cis-state under UV irradition, while backswitching may occur with visible light or by thermal relaxation in the dark.

Accordingly, AzoBETP was synthesized following the reaction sequence set out in Scheme 27. Starting with a Suzuki coupling between commercially available thioether **10.28** and boronic acid **10.29**, the biphenyl product **10.30** was obtained in excellent 95% yield. Oxidation of **10.30** with *m*CPBA gave access to the sulfone **10.31**, which was immediately subjected to aromatic substitution with mercaptoethanol under microwave irradiation to give ethyl thioether **10.32**. Oxidation of **10.32** with one equivalent of *m*CPBA yielded the sulfoxide **10.33** in 96% yield. Installation of the azobenzene was achieved by Boc-deprotection and an *in situ* Mills reaction with nitrosobenzene in order to obtain **AzoBETP** in 54% yield.

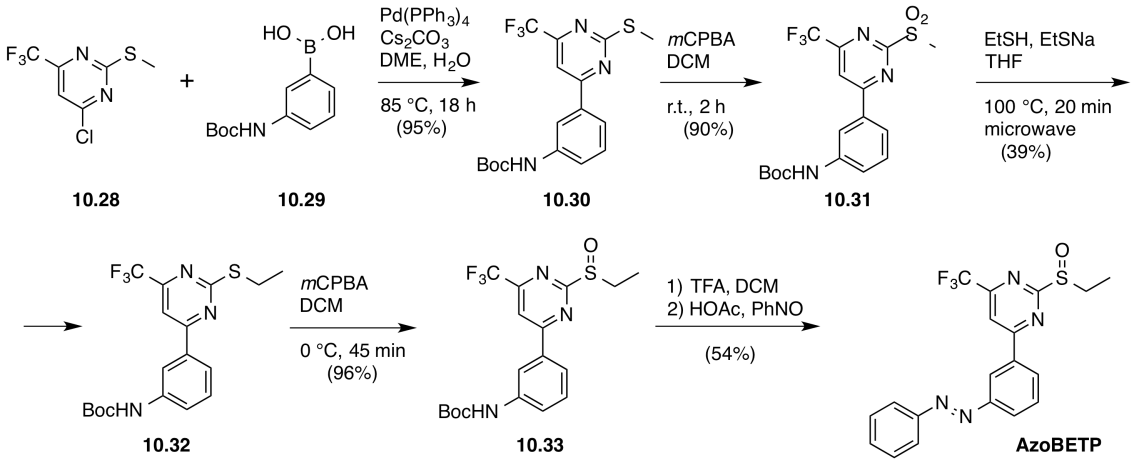


**Scheme 27: Syntheis of AzoBETP.** A six-step sequence gave access to **AzoBETP** from starting materials that can be obtained commercially.

In order to make a re-shifted version, **10.33** was deprotected with TFA in MeCN before cooling and treating the obtained aniline *in situ* with *tert*-butyl nitrite to give the diazonium salt. The latter was trapped with *N*,*N*-dimethylaniline to give **redAzoBETP** in poor 5% yield. (Scheme 28). However, all this was performed in one sequence without purification after each Stepp, which might optimize the overall yield. This proves that the route for **AzoBETP** can be diversified late stage, which is an advantage for the screening of **AzoBETP**s.

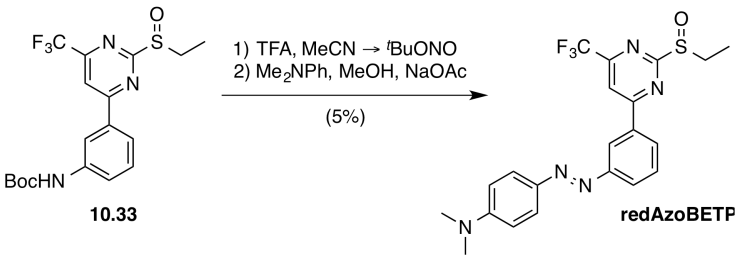


**Scheme 28: A red-shifted version of AzoBETP is obtained by one-pot deprotection, diazotization and reaction with *N*,*N*-dimethylaniline.**

Another route can be enviosioned to circumvent the oxidation/displacement chemitry, one of which proceeding in moderate yield (**10.32**, 39%) by building the ethyl thioether in an entrance step and proceed with the Suzuki reaction, deproctection and Mills reaction accordingly (Scheme 29). This would also render the expensive methylthioether **10.28** redundant. Initial studies have been carried out starting with thiourea (**10.34**) to yield alkylated isothiourea **10.35**. **10.35** co-crystallized with thiourea, of which a crystal structure was obtained. Although this route can be accomplished in the future, as of now there was no need to perform the synthetic sequence as the final **AzoBETP** was obtained in reasonable quantities (10.4 mg) for characterization and first testing.

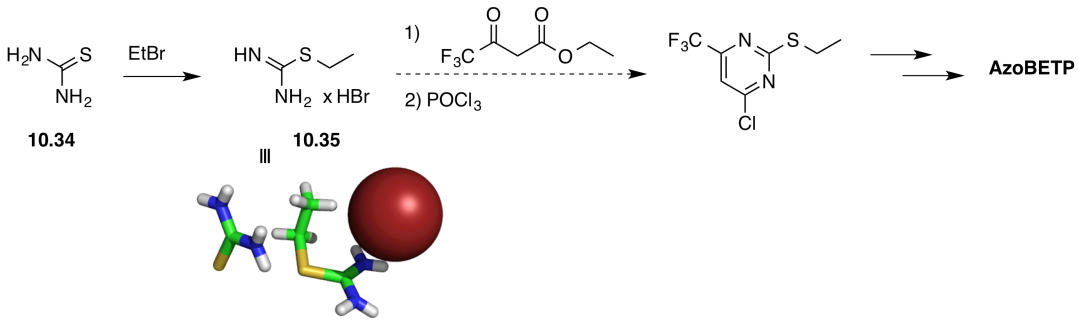


**Scheme 29: Alternative synthesis for AzoBETP.** Thiorea (**10.34**) is ethylated at its sulfur atom, and the resulting ethyl isothiourea **10.35** could be condensed with a 1,3-dione and subsequently treated with $POCl_3$ to give the chlorinated pyrimidine. This could be further converted to **AzoBETP** according to chemistry shown in Scheme 23.

In summary, **AzoBETP** was designed and synthesized as a photoswitchable PAM of GLP-1R. It may be used to investigate photoswitching of GLP-1R signaling using a heterologous expression system, to demonstrate photoswitching of beta cell function and insulin release in rodent islets and to glucose-lowering effects of **AzoBETP** *in vivo* in anaesthetised rodents.

## 10.8 Synthesis

### 10.8.1 (*E*)-4-((4-(Dimethylamino)phenyl)diazenyl)-*N*-(2-morpholinophenyl) benzenesulfonamide (JB556)

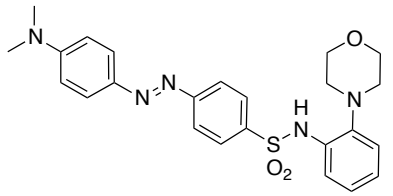

A round bottom flask was charged with 100 mg (0.31 mmol, 1.0 eq.) of (*E*)-4-((4-(dimethylamino)phenyl)diazenyl)benzenesulfonyl chloride (**10.1**) and 55.0 mg (0.31 mmol, 1.0 eq.) 2-morpholinoaniline (**10.2**) dissolved in 10 mL of DCM. A grain of DMAP was added together with 107 µL (0.62 mmol, 2.0 eq.) DIPEA and the resulting mixture was stirred for 2 h at r.t. before the reaction mixture was directly submitted to flash column chromatography (100% DCM) to yield 80.5 mg (0.17 mmol) of **JB556** in 59% yield as a crystalline red solid.

**$^1$H NMR** (400 MHz, $CDCl_3$): $\delta$ [ppm] = 8.03 (s, 1H), 7.92–7.78 (m, 6H), 7.66 (dd, *J* = 8.1, 1.4 Hz, 1H), 7.19–7.02 (m, 3H), 6.73 (d, *J* = 9.2 Hz, 2H), 3.76 (s, 4H), 3.11 (s, 6H), 2.53 (d, *J* = 1.7 Hz, 4H).

**$^{13}$C NMR** (101 MHz, $CDCl_3$): $\delta$ [ppm] = 155.8, 153.1, 143.5, 141.7, 138.7, 133.1, 127.9, 126.4, 125.8, 124.7, 122.4, 122.1, 119.0, 111.4, 67.4, 52.9, 40.3.

**HRMS (ESI)**: calc. for $C_{24}H_{28}N_5O_2S^+$ $(M+H)^+$: 466.1907, found: 466.1905.

**UV/Vis** (LCMS): $\lambda$ ($\pi \rightarrow \pi^*$) = 454 nm.

**$R_t$** (LCMS; MeCN/$H_2O$/formic acid = 10/90/0.1 → 90/10/0.1 over 7 min) = 5.276 min.

### 10.8.2 *N,N*-Dimethyl-2-phenoxyethanamine, Norphenylcholine

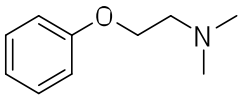

2-Chloro-*N,N*-dimethylethylamine hydrochloride (2.18 g, 15.1 mmol, 3.0 eq.) was added to a mixture of phenol (**10.3**) (470 mg, 5.04 mmol, 1.0 eq.), $K_2CO_3$ (5.56 g, 40.2 mmol, 8.0 eq.) and KI (83.0 mg, 500 µmol, 0.1 eq.) in DMF (50 mL). The reaction mixture was stirred at 80 °C for 3 h. After removal of the solvent *in vacuo*, water was added to the residue and organic material was extracted with DCM. The combined organic layers were dried over $Na_2SO_4$ and concentrated to yield 331 mg (2.01 mmol) of **Norphenylcholine** in 40% yield as a yellow oil.

**$^1$H NMR** (400 MHz, DMSO-$d_6$): $\delta$ [ppm] = 7.35–7.22 (m, 2H), 7.00–6.87 (m, 3H), 4.07 (t, $J$ = 5.8 Hz, 2H), 2.73 (t, $J$ = 5.8 Hz, 2H), 2.34 (s, 6H).

**$^{13}$C NMR** (101 MHz, DMSO-$d_6$): $\delta$ [ppm] = 158.8, 129.4, 120.7, 114.5, 65.8, 58.3, 45.9.

**HRMS (ESI)**: calcd. for $C_{10}H_{16}NO^+$ $(M+H)^+$: 166.1226, found: 166.1224.

**UV/Vis** (LCMS): $\lambda_{max}$ = 267 nm.

**$R_t$** (LCMS; MeCN/$H_2O$/formic acid = 10/90/0.1 → 90/10/0.1 over 7 min) = 1.580 min.

### 10.8.3 *N,N,N*-Trimethyl-2-phenoxyethanaminium iodide, Phenylcholine iodide

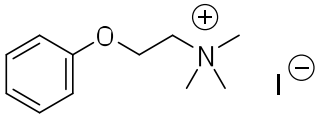

A round bottom flask was charged with *N,N*-dimethyl-2-phenoxyethanamine (165 mg, 1.00 mmol, 10 eq.) and dissolved in 3 mL THF. MeI (142 mg, 210 µL, 3.0 mmol, 3.0 eq.) was added drop-wise and the solution was stirred for 3 h. The

precipitate was collected using a PorIII frit and washed with DCM prior to drying to yield **Phenylcholine iodide** (209 mg, 0.68 mmol, 68%) as a white powder.

**$^1$H NMR** (400 MHz, DMSO-$d_6$): $\delta$ [ppm] = 7.34 (dd, $J$ = 8.7, 7.1 Hz, 2H), 7.03–6.99 (m, 3H), 4.46 (dd, $J$ = 4.9, 2.5 Hz, 2H), 3.81 (dd, $J$ = 5.8, 3.9 Hz, 2H), 3.20 (s, 9H).

**$^{13}$C NMR** (101 MHz, DMSO-$d_6$): $\delta$ [ppm] = 157.3, 129.6, 121.4, 114.7, 64.1 (t, $J$ = 2.9), 61.5, 53.2 (t, $J$ = 3.5 Hz).

**HRMS (ESI)**: calcd. for $C_{11}H_{18}NO^+$ $(M)^+$: 180.1383, found: 180.1381.

**UV/Vis** (LCMS): $\lambda_{max}$ = 276 nm.

**$R_t$** (LCMS; MeCN/$H_2O$/formic acid = 10/90/0.1 → 90/10/0.1 over 7 min) = 1.920 min.

### 10.8.4 *tert*-Butyl 4-aminobenzylcarbamate (10.5)

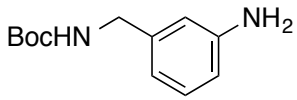


*tert*-Butyl 4-aminobenzylcarbamate was synthesized as previously reported before[213] and the spectra matched those reported.

Briefly, 4-(Aminomethyl)aniline (1.00 g, 8.18 mmol, 1.0 eq.) was dissolved in THF (10 mL) and $(Boc)_2O$ (1.95 g, 8.94 mmol, 1.1 eq.) was added in one portion and stirred at r.t. for 2 h before the volatiles were removed *in vacuo*. Flash column chromatography (30% EtOAc/*i*-hexanes) yielded 1.82 g (8.17 mmol) of the desired product as a white solid in quantitative yield.

### 10.8.5 (*E*)-Di-*tert*-butyl ((diazene-1,2-diylbis(4,1-phenylene))bis(methylene))-dicarbamate (10.7)

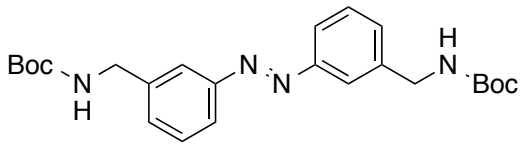


*tert*-Butyl-4-aminobenzylcarbamate (500 mg, 2.25 mmol, 1.0 eq.) was dissolved in 100 mL DCM and poured into a 100 mL aqueous solution of Oxone® (3.46 g, 5.62 mmol, 2.5 eq.) and stirred vigorously for 4 h at r.t.. After separation of the phases, the green organic layer was concentrated and 10 mL of HOAc was added. To this solution, *tert*-butyl-4-aminobenzylcarbamate (**10.5**) (500 mg, 2.25 mmol, 1.0 eq.) was added in one portion and the reaction mixture was stirred o.n.. After neutralizing with sat. aqueous $NaHCO_3$ and extraction with EtOAc, the combined organic layers were washed again with sat. aqueous $NaHCO_3$ and brine. After removal of all solvents, the crude product was subjected to flash column chromatography (30% EtOAc/*i*-hexanes) to yield the desired product (384 mg, 0.87 mmol, 39% over two steps) as an orange solid.

**$^1$H NMR** (300 MHz, $CDCl_3$): $\delta$ [ppm] = 7.83–7.79 (m, 4H), 7.51–7.39 (m, 4H), 4.98 (br s, 2H), 4.42 (d, $J$ = 6.0 Hz, 4H), 1.47 (s, 18H).

**$^{13}$C NMR** (75 MHz, $CDCl_3$): $\delta$ [ppm] = 152.8, 140.2, 130.0, 129.3, 122.3, 121.3, 79.7, 44.4, 28.4.

**HRMS (ESI)**: calcd. for $C_{24}H_{32}N_4NaO_4^+$ $(M+Na)^+$: 463.2316, found: 463.2317.

**UV/Vis** (LCMS): $\lambda_{max}$ ($\pi \rightarrow \pi^*$) = 322 nm.

**$R_t$** (LCMS; MeCN/$H_2O$/formic acid = 10/90/0.1 → 90/10/0.1 over 7 min) = 5.107 min.

### 10.8.6 (*E*)-(Diazene-1,2-diylbis(4,1-phenylene))dimethanamine (10.8)

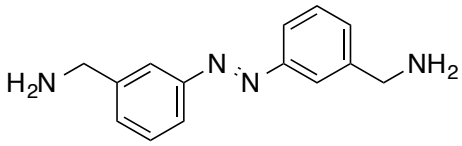

(*E*)-Di-*tert*-Butyl-((diazene-1,2-diylbis(4,1-phenylene))bis(methylene))dicarbamate (**10.7**) (30.0 mg, 68.1 µmol, 1.0 eq.) was dissolved in 6.0 mL DCM with the addition of anisole (1.0 mL) before 2.0 mL of TFA was added. The reaction mixture was stirred at r.t. for 1.5 h until $Et_2O$ was added and the resulting precipitate collected by centrifugation. The solid was resuspended in $Et_2O$ and centrifuged again to remove remaining solvents and finally dried under HV to yield (17.0 mg. 48.0 µmol. 70%) of the desired product as its TFA salt as an orange solid.

**$^1$H NMR** (400 MHz, MeOD-$d_4$): $\delta$ [ppm] = 8.07 (s, 2H), 8.00 (dt, $J$ = 6.9, 2.2 Hz, 2H), 7.71–7.61 (m, 4H), 4.26 (s, 4H).

**$^{13}$C NMR** (101 MHz, MeOD-$d_4$): $\delta$ [ppm] = 154.2, 136.0, 132.9, 131.3, 124.8, 124.1, 44.0.

**HRMS (ESI)**: calcd. for $C_{15}H_{17}N_4O_2^+$ $(M+H+CO_2)^+$: 285.1346, found: 285.1348.

### 10.8.7 (*E*)-1,1'-(Diazene-1,2-diylbis(4,1-phenylene))bis(*N*,*N*,*N*-trimethylmethanaminium) iodide, BisQ

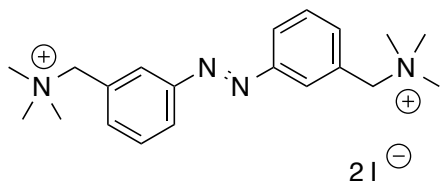

*(E*)-(Diazene-1,2-diylbis(4,1-phenylene))dimethanamine (**10.8**) (70.0 mg, 0.292 mmol, 1.0 eq.) was heated to 80 °C with $K_2CO_3$ (202 mg, 1.46 mmol, 5.0 eq.) in 40 mL MeCN for 45 min before MeI (331 mg, 2.33 mmol, 145 µL, 8.0 eq.) in 1 mL MeCN was added dropwise to the warm solution. The reaction

mixture was heated to reflux for another 2 h before it was allowed to cool to r.t., filtered and the solvent removed *in vacuo*. RP column chromatography (0.1% formic acid in $H_2O$) yielded of the desired product (112 mg, 0.193 mmol, 66%) as an orange solid.

**$^1$H NMR** (400 MHz, DMSO-$d_6$): $\delta$ [ppm] = 8.11–8.09 (m, 2H), 8.07–8.04 (m, 2H), 7.80–7.78 (m, 4H), 4.77 (s, 4H), 3.13 (s, 18H).

**$^{13}$C NMR** (101 MHz, DMSO-$d_6$): $\delta$ [ppm] = 151.9, 135.9, 130.3, 129.9, 127.1, 124.0, 67.0, 51.9.

**HRMS (ESI)**: calcd. for $C_{20}H_{30}IN_4^+$ $(M+I)^+$: 453.1510, found: 453.1511.

**UV/Vis** (100 µM in DMSO): $\lambda_{max}$ (trans, $\pi \rightarrow \pi^*$) = 324 nm; $\lambda_{max}$ (cis, $\pi \rightarrow \pi^*$) = 304 nm; $\lambda_{max}$ (cis, $n \rightarrow \pi^*$) = 440 nm.

**UV/Vis** (LCMS): $\lambda_{max}$ ($\pi \rightarrow \pi^*$) = 318 nm.

**$R_t$** (LCMS; MeCN/$H_2O$/formic acid = 10/90/0.1 → 90/10/0.1 over 7 min) = 1.374 min.

## 10.8.8 Synthesis of AzoIperoxo

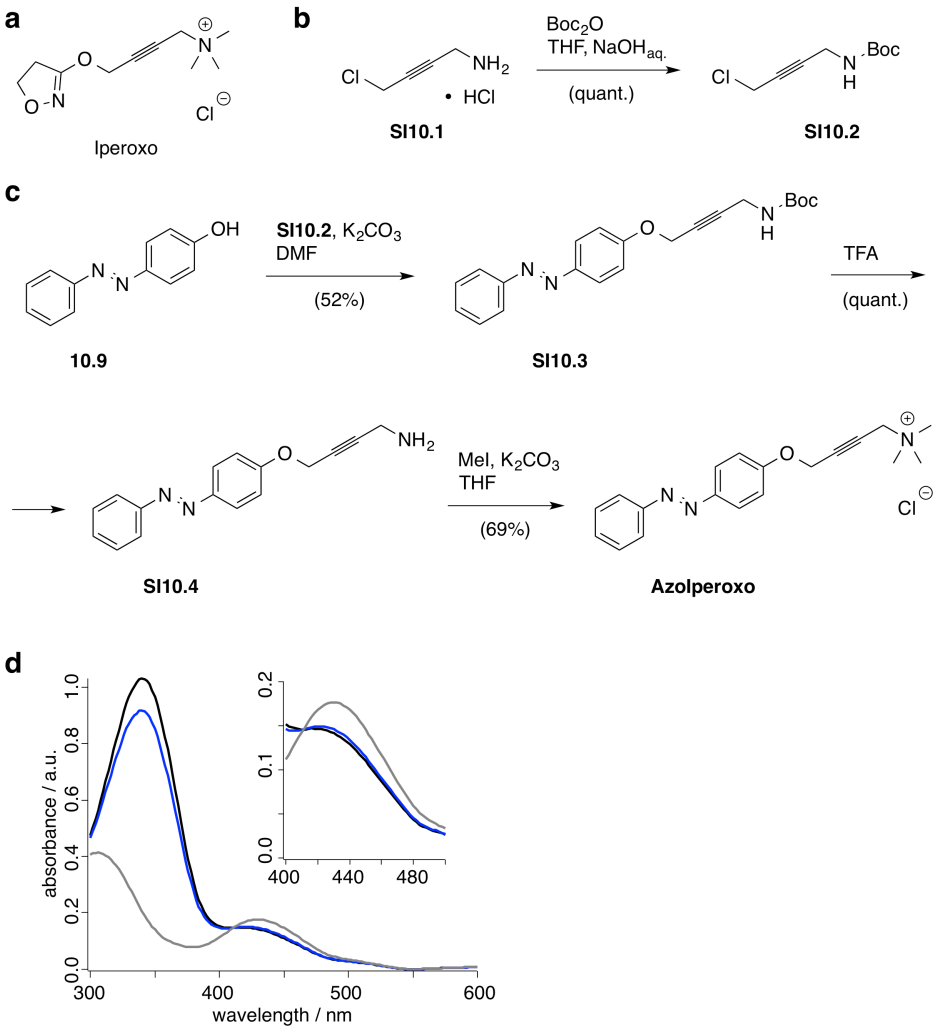


**Supplementary Figure 8: Synthesis and spectroscopy of AzoIperoxo. a)** The structure of Iperoxo. **b)** Synthesis of Boc-protected alkyne **SI10.2** that is used in the synthesis of AzoIperoxo (**c**). **d)** UV/Vis spectra of 50 µM **AzoIperoxo** in Ringer solution in its dark adapted state (black) and under illumination with λ = 440 nm (*trans*-isomer, blue) and λ = 360 nm (*cis*-isomer, gray). Insert shows n-π-band.

## 10.8.9 *tert*-Butyl (4-chlorobut-2-yn-1-yl)carbamate (SI10.2)

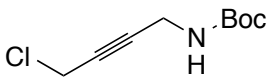

A round bottom flask was charged with 500 mg (3.57 mmol, 1.0 eq.) of 4-chlorobut-2-yn-1-amine dissolved in 50 mL THF. $Boc_2O$ was added in one portion (924 mg, 4.28 mmol, 1.2 eq.) and the resulting mixture was stirred at r.t. upon the drop-wise addition of 4.28 mL 1 M NaOH. The reaction was stirred o.n. before it was diluted with water and extracted with EtOAc (3x). The combined organic layers were dried over $MgSO_4$ and all volatiles were removed *in vacuo* to obtain 727 mg (3.57 mmol) of the desired compound in quantitative yield as a yellow oil.

**$^1$H NMR** (400 MHz, DMSO-$d_6$): $\delta$ [ppm] = 4.73 (br s, 1H), 4.16–4.10 (m, 2H), 3.98–3.96 (m, 2H), 1.44 (s, 9H).

**$^{13}$C NMR** (101 MHz, DMSO-$d_6$): $\delta$ [ppm] = 155.2, 82.9, 77.7, 77.2, 30.4, 28.3, 27.4.

**LRMS (ESI)**: calc. for $C_9H_{14}ClNNaO_2^+$ $(M+Na)^+$: 226.1 and 228.1, found: 226.0 and 228.1.

**UV/Vis** (LCMS): $\lambda_{max}$ = 262 nm.

**$R_t$** (LCMS; MeCN/$H_2O$/formic acid = 10/90/0.1 → 90/10/0.1 over 7 min) = min.

### 10.8.10 *tert*-Butyl (*E*)-(4-(4-(phenyldiazenyl)phenoxy)but-2-yn-1-yl)carbamate (SI10.3)

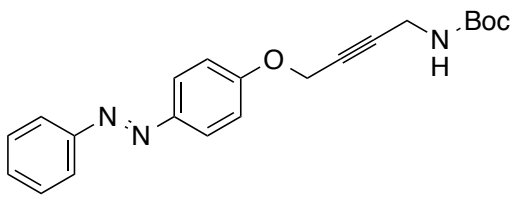


A round bottom flask was charged with 308 mg (1.51 mmol, 1.2 eq.) of *tert*-butyl (4-chlorobut-2-yn-1-yl)carbamate that was dissolved in 15 mL DMF. 4-Hydroxyazobenzene (250 mg, 1.26 mmol, 1.0 eq.) and $K_2CO_3$ (174 mg, 1.26 mmol, 1.0 eq.) were added in one portion and the resulting reaction mixture was stirred at 80 °C for 4 h before it was quenched with the addition of water and extracted with EtOAc (3x). The combined organic layers were dried over $MgSO_4$

and the crude was subjected to flash column chromatography on silica gel (100% DCM) to obtain 240 mg (0.66 mmol) of the desired product in 52% yield as an orange solid.

**$^1$H NMR** (400 MHz, DMSO-$d_6$): $\delta$ [ppm] = 7.94–7.87 (m, 4H), 7.56–7.40 (m, 3H), 7.06 (d, $J$ = 8.9 Hz, 2H), 4.76 (s, 2H), 3.98 (s, 2H), 1.45 (s, 9H).

**$^{13}$C NMR** (101 MHz, DMSO-$d_6$): $\delta$ [ppm] = 159.9, 155.2, 152.6, 147.4, 130.5, 129.0, 124.6, 122.6, 115.0, 84.2, 80.1, 77.2, 56.2, 30.6, 28.3.

**LRMS (ESI)**: calc. for $C_{21}H_{24}N_3O_3^+$ $(M+H)^+$: 366.2, found: 366.2.

**UV/Vis** (LCMS): λ (trans, π → π*) = 342 nm.

**$R_t$** (LCMS; MeCN/$H_2O$/formic acid = 10/90/0.1 → 90/10/0.1 over 7 min) = 5.282 min.

### 10.8.11 (*E*)-4-(4-(Phenyldiazenyl)phenoxy)but-2-yn-1-amine (SI10.4)

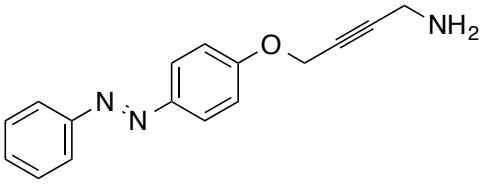


A round bottom flask was charged with 240 mg (0.66 mmol) of *tert*-butyl (*E*)-(4-(4-(phenyldiazenyl)phenoxy)but-2-yn-1-yl)carbamate and cooled to 0 °C before it was dissolved in neat TFA. The reaction mixture was stirred for 10 min before it was allowed to warm to r.t. and all volatiles were removed *in vacuo* to obtain 326 mg (0.66 mmol) of the desired product in quantitative yield as its double TFA salt as a yellow solid.

**$^1$H NMR** (400 MHz, $CDCl_3$): $\delta$ [ppm] = 10.15 (br s, 2H), 8.01–7.81 (m, 7H), 7.58–7.42 (m, 3H), 7.00 (d, $J$ = 8.9 Hz, 2H), 4.71 (s, 2H), 3.86 (s, 2H).

**$^{13}$C NMR** (101 MHz, $CDCl_3$): $\delta$ [ppm] = 161.3 (q, $J$ = 39.5 Hz), 160.2, 151.5, 146.9, 131.1, 129.2, 125.2, 122.5, 115.3 (q, $J$ = 287.5 Hz) 115.2, 82.9, 77.5, 55.7, 30.2.

**HRMS (ESI)**: calc. for $C_{16}H_{16}N_3O^+$ $(M+H)^+$: 266.1288, found: XXX.

**UV/Vis** (LCMS): λ (trans, π → π*) = 342 nm.

**$R_t$** (LCMS; MeCN/$H_2O$/formic acid = 10/90/0.1 → 90/10/0.1 over 7 min) = 2.701 min.

### 10.8.12 (*E*)-*N*,*N*,*N*-Trimethyl-4-(4-(phenyldiazenyl)phenoxy)but-2-yn-1-aminium chloride (AzoIperoxo Chloride)

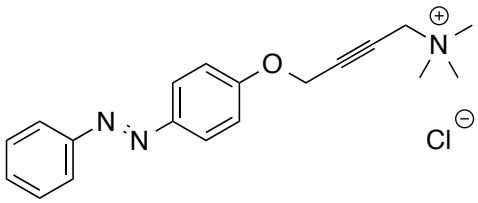


A round bottom flask was charged with 100 mg (0.26 mmol, 1.0 eq.) of (*E*)-4-(4-(phenyldiazenyl)phenoxy)but-2-yn-1-amine (x 2 TFA) dissolved in 15 mL dry THF. $K_2CO_3$ (182 mg, 1.32 mmol, 5.0 eq.) was added in one potion and the resulting suspension was stirred vigorously upon the addition of 200 µL (456 mg, 3.21 mmol, 12.4 eq.) of MeI. The reaction mixture was stirred at r.t. for 4 h before all volatiles were removed *in vacuo* and the crude was subjected to RP flash column chromatography on C18-functionalized silica gel (aq. 1 mM HCl/MeCN = 100/0 → 90/10 → 80/20 → 70/30 → 60/40 → 50/50 → 40/60) to obtain 61.5 mg (0.18 mmol) of the desired compund as its chloride salt in 69% yield as a crystalline orange solid.

**$^1$H NMR** (400 MHz, DMSO-$d_6$): $\delta$ [ppm] = 7.93 (d, *J* = 8.9 Hz, 2H), 7.85 (dd, *J* = 7.3, 1.8 Hz, 2H), 7.64 – 7.50 (m, 3H), 7.26 (d, *J* = 8.9 Hz, 2H), 5.19–5.10 (m, 2H), 4.47 (s, 2H), 3.11 (s, 9H).

**$^{13}$C NMR** (101 MHz, DMSO-$d_6$): $\delta$ [ppm] = 159.6, 151.9, 146.7, 131.1, 129.4, 124.5, 122.3, 115.6, 86.6, 76.3, 55.9, 55.1, 51.9.

**HRMS (ESI)**: calc. for $C_{19}H_{22}N_3O^+$ $(M)^+$: 308.1757, found: 308.1755.

**UV/Vis** (LCMS): λ (trans, π → π*) = 324 nm.

**$R_t$** (LCMS; MeCN/$H_2O$/formic acid = 10/90/0.1 → 90/10/0.1 over 7 min) = 3.038 min.

### 10.8.13 (*E*)-*N*,*N*-Dimethyl-2-(4-(phenyldiazenyl)phenoxy)ethanamine (10.10)

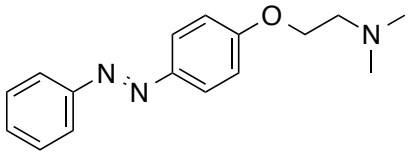

2-Chloro-*N*,*N*-dimethylethylamine hydrochloride (2.18 g, 15.1 mmol, 3.0 eq.) was added to the mixture of 4-hydroxyazobenzene (**10.9**) (1.00 g, 5.04 mmol, 1.0 eq.), $K_2CO_3$ (5.60 g, 40.2 mmol, 8.0 eq.) and KI (83.0 mg, 500 µmol, 0.1 eq.) in DMF (50 mL). The reaction mixture was stirred at 80 °C for 12 h. After removal of the solvent *in vacuo*, water was added to the residue and the organic material was extracted with DCM. The combined organic layers were dried over $Na_2SO_4$, concentrated and the crude material was subjected to flash column chromatography (DCM → 5% MeOH/DCM) to yield (990 mg 3.70 mmol, 74%) of the desired product as a red solid.

**$^1$H NMR** (400 MHz, DMSO-$d_6$): $\delta$ [ppm] = 7.89 (d, $J$ = 8.9 Hz, 2H), 7.84 (d, $J$ = 8.0 Hz, 2H), 7.55 (m, 3H), 7.14 (d, $J$ = 8.9 Hz, 2H), 4.18 (t, $J$ = 5.6 Hz, 2H), 2.73 (t, $J$ = 5.7 Hz, 2H), 2.28 (s, 6H).

**$^{13}$C NMR** (101 MHz, DMSO-$d_6$): $\delta$ [ppm] = 161.2, 152.0, 146.1, 130.8, 129.4, 124.6, 122.2, 115.1, 66.0, 57.4, 45.3.

**HRMS (ESI)**: calcd. for $C_{16}H_{20}N_3O^+$ $(M+H)^+$: 270.1601, found: 270.1599.

**UV/Vis** (LCMS): $\lambda_{max}$ (π → π*) = 342 nm.

**$R_t$** (LCMS; MeCN/$H_2O$/formic acid = 10/90/0.1 → 90/10/0.1 over 7 min) = 2.675 min.

### 10.8.14 (*E*)-*N*,*N*,*N*-Trimethyl-2-(4-(phenyldiazenyl)phenoxy)ethanaminium iodide, AzoCholine

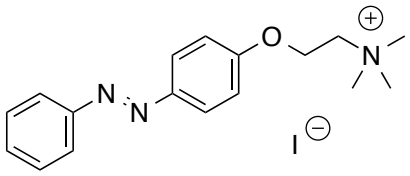

(*E*)-*N*,*N*-Dimethyl-2-(4-(phenyldiazenyl)phenoxy)ethanamine (**10.10**) (269 mg, 1.00 mmol, 1.0 eq.) was dissolved in THF (2 mL). MeI (187 µL, 3.00 mmol, 3.0 eq.) was added to this solution at r.t.. The reaction mixture was stirred at the same temperature for 12 h. The precipitate was collected by filtration and washed with DCM to afford the desired product (358 mg, 0.870 mmol, 87%) as a yellow solid.

**$^1$H NMR** (400 MHz, DMSO-$d_6$): $\delta$ [ppm] = 7.94 (d, $J$ = 8.9 Hz, 2H), 7.89–7.83 (m, 2H), 7.64–7.49 (m, 3H), 7.22 (d, $J$ = 9.0 Hz, 2H), 4.67–4.55 (m, 2H), 3.85 (m, 2H), 3.22 (s, 9H).

**$^{13}$C NMR** (101 MHz, DMSO-$d_6$): $\delta$ [ppm] = 160.0, 151.9, 146.6, 131.0, 129.4, 124.5, 122.3, 115.4, 64.0, 62.1, 53.2.

**HRMS (ESI)**: calcd. for $C_{17}H_{22}N_3O^+$ $(M)^+$: 284.1757, found 284.1756.

**UV/Vis** (LCMS): $\lambda_{max}$ ($\pi \rightarrow \pi^*$) = 342 nm.

**$R_t$** (LCMS; MeCN/$H_2O$/formic acid = 10/90/0.1 → 90/10/0.1 over 7 min) = 2.684 min.

### 10.8.15 (*E*)-1-(4-Isocyanatophenyl)-2-phenyldiazene (10.12)

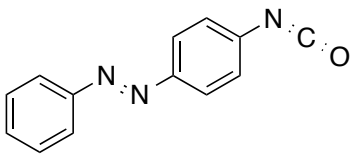

A round bottom flask equipped with a stirring bar was charged with (*E*)-4-(phenyldiazenyl)aniline (**10.11**) (1.00 g, 5.05 mmol, 1.0 eq.) and dissolved in $NEt_3$ (15.15 mmol, 2.1 mL, 3.0 eq.) and DCM (150 mL). The mixture was cooled to 0 °C and triphosgene (1.66 g, 5.60 mmol, 1.1 eq.) was added spatula-wise under vigorous stirring. The solution turned from orange to dark red within minutes and was stirred for another hour before the mixture was concentrated to ~1/10 of the initial volume and purified by flash column chromatography on deactivated silica with DCM (100%) to yield 680 mg of the desired compound as brown-grayish plates, which were used subsequently in the next step.

### 10.8.16 (*E*)-*N*,*N*,*N*-Trimethyl-2-(((4-(phenyldiazenyl)phenyl)-carbamoyl)oxy) ethanaminium chloride, AzoCarbachol Chloride

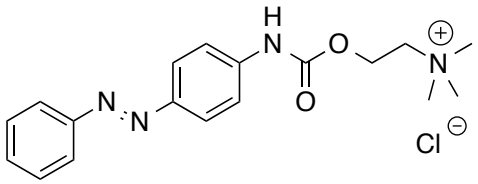

In a round bottom flask, 100 mg (0.45 mmol, 1.0 eq.) of (*E*)-1-(4-isocyanatophenyl)-2-phenyldiazene were dissolved in dry DMSO and choline chloride (125 mg, 0.90 mmol, 2.0 eq., dried under HV at an elevated temperature prior to use) was added in one portion. The reaction was stirred o.n. at r.t. before water (6 mL) was added and the mixture was directly purified by RP C18 flash column chromatography (MeCN/1 mM aq. HCl = 0/100 → 10/100→ 20/100→ 40/100→ 50/50) to yield 23.6 mg (quant., brsm) of the desired product as its chloride salt as an orange solid.

**$^1$H NMR** (400 MHz, $D_2O$): $\delta$ [ppm] = 8.37 (s, 1H), 7.58–7.51 (m, 2H), 7.48 (d, $J$ = 8.4 Hz, 2H), 7.37–7.30 (m, 3H), 7.27 (d, $J$ = 8.4 Hz, 2H), 4.40 (d, $J$ = 4.1 Hz, 2H), 3.81 – 3.53 (m, 2H), 3.13 (s, 9H).

**$^{13}$C NMR** (101 MHz, $D_2O$): $\delta$ [ppm] = 153.1, 151.7, 147.4, 140.5, 131.0, 129.2, 123.7, 122.3, 118.8, 64.6, 58.5, 53.7.

**HRMS (ESI)**: calc. for $C_{18}H_{23}N_4O_2^+$ $(M)^+$: 327.1816, found: 327.1816.

**UV/Vis** (LCMS): $\lambda_{max}$ (trans, $\pi \rightarrow \pi^*$) = 350 nm

**$R_t$** (LCMS; MeCN/$H_2O$/formic acid = 10/90/0.1 → 90/10/0.1 over 7 min) = 2.874 min.

**UV/Vis** (50 µM in $H_2O$): $\lambda_{max}$ (trans, $\pi \rightarrow \pi^*$) = 352 nm; $\lambda_{max}$ (cis, $\pi \rightarrow \pi^*$) = 340 nm; $\lambda_{max}$ (cis, $n \rightarrow \pi^*$) = 454 nm.

**Spectral data for ethyl (*E*)-(4-(phenyldiazenyl)phenyl)carbamate**

**$^1$H NMR** (400 MHz, $CDCl_3$): $\delta$ [ppm] = 8.13–7.76 (m, 4H), 7.76–7.30 (m, 5H), 6.78 (s, 1H), 4.26 (q, $J$ = 7.1 Hz, 2H), 1.34 (t, $J$ = 7.1 Hz, 3H).

**$^{13}$C NMR** (101 MHz, $CDCl_3$): $\delta$ [ppm] = 153.2, 152.7, 148.4, 140.6, 130.6, 129.0, 124.1, 122.7, 118.4, 77.2, 61.6, 14.5.

### 10.8.17 1,3-Dimethyl-5-nitrobenzene (10.14)

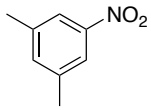


3,5-Dimethylaniline (19.4 g, 160 mmol, 10. eq.) was dissolved in 450 mL DCM and 100 mL MeOH. A solution of Oxone® (197 g, 320 mmol, 2.0 eq.) in 450 mL of water was added and the mixture was vigorously stirred for 3 days. After separating the organic layer, drying over $MgSO_4$ and concentrating the crude was submitted to flash column chromatography (100% DCM) to obtain 15.0 g (0.99 mol) of the desired compound in 62% yield as a pale yellow solid.

**$^1$H NMR** (400 MHz, $CDCl_3$) δ [ppm] = 7.81 ($m_c$, 2H), 7.29 ($m_c$,, 1H), 2.39 (dd, $J$ = 1.3, 0.6 Hz, 6H).

**$^{13}$C NMR** (101 MHz, $CDCl_3$) δ [ppm] = 139.4, 136.1, 121.1, 21.1. One carbon could not be observed by 1D NMR.

### 10.8.18 1,2-Bis(3,5-dimethylphenyl)hydrazine (10.16)

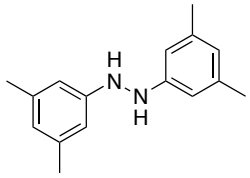

1,2-bis(3,5-dimethylphenyl)hydrazine (**10.16**) was prepared according to literature procedure by Helms *et al.* downscaled by a factor of 0.78 with small modifications. [191] The workup procedure was changed to flash column chromatography (DCM/hexanes = 1/2 → DCM/hexanes = 1/1) instead of precipitation in order to obtain 883 mg (3.6 mmol) of hydrazine **10.16** and 1.00 g (4.2 mmol) of the corresponding azobenzene **10.15** in 17% and 18% yield, respectively. **10.15** was converted into **10.16** by dissolving the whole amount in 200 mL EtOH and 15 mL of hydrazine hydrate (100%) at -10 °C and adding 3 spatula tips of 10 mol% of Pd/C to it. After stirring for 30 minutes, the reaction was allowed to warm to r.t. and filtered over a plug of Celite. Water was added (400 mL) and the hydrazine was extracted into DCM, which was dried over $MgSO_4$. Concentration *in vacuo* and filtration over silica gel in DCM afforded 925 mg (3.9 mmol) of the hydrazine in 92% yield in this transformation, giving an overall yield of 1,2-bis(3,5-dimethylphenyl)hydrazine of 29%.

**$^1$H NMR** (400 MHz, $CDCl_3$) δ [ppm] = 6.51 (m, 6H), 5.46 (br s, 2H), 2.27 (s, 12H).

**$^{13}$C NMR** (101 MHz, $CDCl_3$) δ [ppm] = 149.2, 139.1, 121.7, 110.1, 21.5.

**HRMS (ESI)**: calc. for $C_{16}H_{21}N_2^+$ $(M+H)^+$: 241.1699, found: 241.1697.

**UV/Vis** (LCMS): $\lambda_{max1}$ = 254 nm, $\lambda_{max2}$ = 294 nm.

**$R_t$** (LCMS; MeCN/$H_2O$/formic acid = 10/90/0.1 → 90/10/0.1 over 7 min) = 3.048 min.

### 10.8.19 2,2',6,6'-Tetramethyl-[1,1'-biphenyl]-4,4'-diamine (10.17)

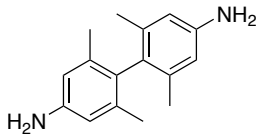


2,2',6,6'-Tetramethyl-[1,1'-biphenyl]-4,4'-diamine (**10.17**) was prepared from **10.16** according to literature procedure by Helms *et al.* [191] downscaled by a factor of 0.16 with slight modifications. After 5 hours of reflux, the workup procedure was changed to washing the aqueous layer with hexanes, basifying the aqueous layer with 4 M NaOH to pH = 12 and extraction with EtOAc. After removal of the solvent *in vacuo*, 714 mg (3.0 mmol) of the desired product of sufficent purity for the next step was obtained in 80% yield as a white solid.

**$^{1}$H NMR** (400 MHz, $CDCl_3$) δ [ppm] = 6.46 (s, 4H), 3.49 (br s, 4H), 1.80 (s, 12H).

**$^{13}$C NMR** (101 MHz, $CDCl_3$) δ [ppm] = 144.6, 137.2, 130.7, 114.3, 20.0.

**HRMS (ESI)**: calc. for $C_{16}H_{21}N_2^+$ $(M+H)^+$: 241.1699, found: 241.1698

### 10.8.20 2,2'-(2,2',6,6'-Tetramethyl-[1,1'-biphenyl]-4,4'-diyl)bis(1-(4-nitrophenyl)diazene) (10.19)

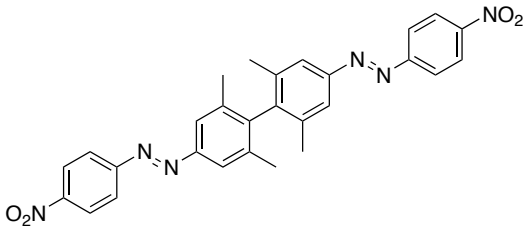


2,2',6,6'-Tetramethyl-[1,1'-biphenyl]-4,4'-diamine (**10.17**) (1.0 eq., 410 mg, 1.71 mmol) was dissolved in 20 mL glacial acetic acid and 20 mL DCM and 1-nitro-4-nitrosobenzene (**10.18**) (3.0 eq., 780 mg, 5.13 mmol) was added in one portion. After stirring for 60 minutes at r.t. TLC indicated complete consumption of the starting material. The reaction mixture was quenched by addition of sat. aqueous $NaHCO_3$ solution and extracted with DCM. The organic layers were combined and concentrated *in vacuo* and the crude product was submitted to flash column

chromatography on silica gel (DCM/hexanes = 1/1 → 100% DCM → MeOH/DCM = 0.25/100) to obtain 290 mg (0.57 mmol) of the bis-azobenzene and 165 mg (0.47 mmol) of the mono-azobenzene in 33% and 28% yield, respectively, both isolated as deep red solids.

**$^1$H NMR** (599 MHz, $CDCl_3$) δ [ppm] = 8.40 (d, *J* = 9.0 Hz, 4H), 8.04 (d, *J* = 9.0 Hz, 4H), 7.79 (s, 4H), 2.06 (s, 12H).

**$^{13}$C NMR** (151 MHz, $CDCl_3$) δ [ppm] = 155.8, 151.7, 148.6, 143.8, 136.8, 124.8, 123.3, 122.8, 19.9.

**HRMS (EI)**: calc. for $C_{28}H_{24}N_6O^{\cdot+}$ $(M^{\cdot})^+$: 508.1854, found: 508.1843.

**UV/Vis** (LCMS): $\lambda_{max}$ ($\pi \rightarrow \pi^*$) = 347 nm.

**$R_t$** (LCMS; MeCN/$H_2O$/formic acid = 10/90/0.1 → 90/10/0.1 over 7 min) = 4.720 min.

### 10.8.21 4,4'-(2,2',6,6'-Tetramethyl-[1,1'-biphenyl]-4,4'-diyl)bis(diazene-2,1-diyl))dianiline (10.20)

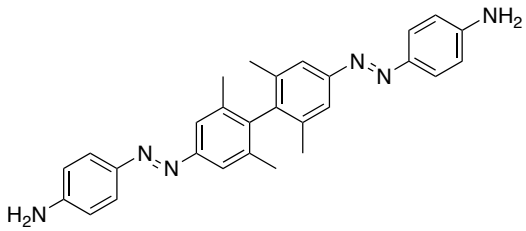


2,2'-(2,2',6,6'-Tetramethyl-[1,1'-biphenyl]-4,4'-diyl)bis(1-(4-nitrophenyl)diazene) (**10.19**) (120 mg, 0.24 mmol, 1.0 eq.) was dissolved in a mixture of dioxane/water (20 mL / 20 mL) under a nitrogen atmosphere and 65% $Na_2S$ • x $H_2O$ (150 mg) was added in one portion. The mixture was stirred under reflux for 1 h and another 180 mg of 65% $Na_2S$ • x $H_2O$ was added. TLC indicated complete conversion after another 1.5 h of reflux. The mixutre was basified with sat. aqueous $NaHCO_3$ and extracted with EtOAc. After separation of the organic layer, it was washed with brine and concentrated *in vauo*. Flash

column chromatography on silica gel (EtOAc/hexanes = 1/1) yielded 85 mg (0.19 mmol) of the desired product in 79% yield as a deep red solid.

**$^{1}$H NMR** (599 MHz, $CDCl_3$) δ [ppm] = 7.81 (d, *J* = 8.7 Hz, 4H), 7.63 (s, 4H), 6.75 (d, *J* = 8.8 Hz, 4H), 2.00 (s, 12 H).

**$^{13}$C NMR** (151 MHz, $CDCl_3$) δ [ppm] = 152.1, 149.4, 145.7, 141.6, 136.5, 125.0, 121.5, 114.6, 19.9.

**HRMS (ESI)**: calc. for $C_{28}H_{29}N_6^+$ $(M+H)^+$: 449.2448, found: 449.2446.

**UV/Vis** (LCMS): $\lambda_{max}$ ($\pi \rightarrow \pi^*$) = 388 nm.

**$R_t$** (LCMS; MeCN/$H_2O$/formic acid = 10/90/0.1 → 90/10/0.1 over 7 min) = 2.949 min.

### 10.8.22 2,2'-((((1*E*,1'*E*)-(2,2',6,6'-Tetramethyl-[1,1'-biphenyl]-4,4'-diyl)bis(diazene-2,1-diyl))bis(4,1-phenylene))bis(azanediyl))bis(*N*,*N*,*N*-triethyl-2-oxoethanaminium) chloride (QAAQ)

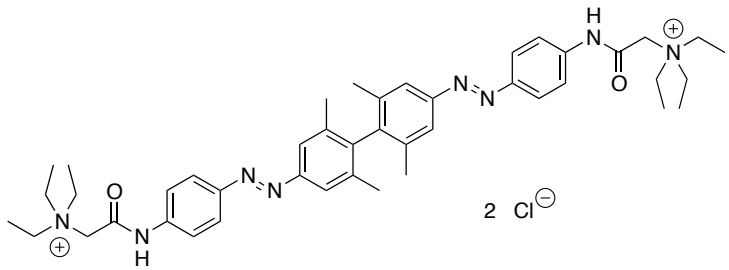


4,4'-(2,2',6,6'-Tetramethyl-[1,1'-biphenyl]-4,4'-diyl)bis(diazene-2,1-diyl))dianiline (**10.20**) (1.0 eq., 40 mg, 0.089 mmol) was dissolved in a mixture of DMF and DIPEA (1.5 mL / 0.2 mL) under a nitrogen atmosphere and 2-chloro-*N*,*N*,*N*-triethyl-2-oxoethanaminium chloride (**10.21**)[50] (4.0 eq., 76 mg, 0.357 mmol) was added in one portion. After 4 h of stirring a precipitate formed, and the reaction was quenched by the addition of water. The crude material was submitted to flash column chromatography on C18-silica gel (0.1% formic acid in

$H_2O$ → 10% MeCN / 0.1% formic acid in $H_2O$) to obtain 24 mg (0.030 mmol) of the desired product in 33% yield as an orange solid.

**$^1$H NMR** (599 MHz, DMSO-$d_6$) δ [ppm] = 11.94 (s, 2H), 7.94 (d, *J* = 3.1 Hz, 8H), 7.74 (d, *J* = 0.7 Hz, 4H), 4.45 (s, 4H), 3.55 (q, *J* = 7.3 Hz, 12H), 2.00 (s, 12H), 1.31 (t, *J* = 7.3 Hz, 18H).

**$^{13}$C NMR** (151 MHz, DMSO-$d_6$) δ [ppm] = 162.7, 151.4, 148.7, 142.3, 141.1, 136.6, 123.8, 122.0, 120.4, 56.8, 54.5, 19.8, 7.9.

**HRMS (ESI)**: calc. for $C_{44}H_{60}N_8O_2^{2+}$ $(M)^{2+}$: 366.2414, found: 366.2413.

**UV/Vis** (LCMS): $\lambda_{max}$ ($\pi \rightarrow \pi^*$) = 366 nm.

**$R_t$** (LCMS; MeCN/$H_2O$/formic acid = 10/90/0.1 → 90/10/0.1 over 7 min) = 3.048 min.

### 10.8.23 (*E*)-2-Methyl-3-(4-(phenyldiazenyl)phenyl)quinazolin-4(3*H*)-one (JB420)

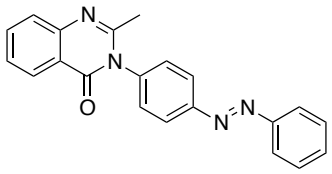


In a round bottom flask, azobenzene **10.11** (55 mg, 0.279 mmol, 1.0 eq.) and *N*-acetyl anthranilic acid (10.22) (50 mg, 0.279 mmol, 1.0 eq.) were dissolved in neat $POCl_3$ and heated to reflux for 3 h. The reaction was allowed to cool to r.t. and was carefully quenched with sat. aq. $NaHCO_3$ and extracted with EtOAc. Flash column chromatography (EtOAc/pentane) yielded 19.9 mg (0.058 mmol) of **JB420** in 21% yield as an orange solid.

**$^1$H NMR** (400 MHz, $CDCl_3$): *δ* [ppm] = 8.29 (dd, *J* = 8.1, 1.5 Hz, 1H), 8.11 (d, *J* = 8.6 Hz, 2H), 7.96 (dd, *J* = 8.1, 1.7 Hz, 2H), 7.79 (ddd, *J* = 8.5, 7.1, 1.5 Hz, 1H), 7.73–7.69 (m, 1H), 7.58–7.41 (m, 6H), 2.30 (s, 3H).

**$^{13}$C NMR** (101 MHz, $CDCl_3$): $\delta$ [ppm] = 162.2, 153.7, 152.6, 152.5, 147.4, 139.7, 134.7, 131.6, 129.2, 129.0, 127.1, 126.8, 126.8, 124.3, 123.1, 120.7, 24.4.

**HRMS (ESI)**: calc. for $C_{21}H_{17}N_4O^+$ $(M+H)^+$: 341.1397, found: 341.1396.

### 10.8.24 (*R*)-Methyl 4-nitro-3-(4-nitrophenyl)butanoate (10.24)

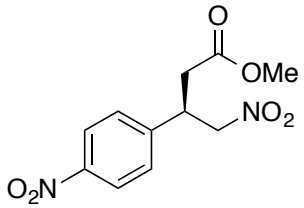


(*R*)-Methyl 4-nitro-3-(4-nitrophenyl)butanoate was synthesized as reported before[214] using (*R*)-2-(bis(3,5-bis(trifluoromethyl)phenyl)((trimethylsilyl)oxy)-methyl)pyrrolidine as a catalyst and scaling up the reaction by a factor of 15.

The workup procedure was simplified by diluting the crude reaction with the addition of DCM and subsequent filtering the mixture over a plug of silica gel, washing several times with DCM. Flash column chromatography (100% DCM) yielded the desired product in 61% yield (492 mg, 1.83 mmol) as a pale yellow wax.

**$^{1}$H NMR** (599 MHz, $CDCl_3$) δ [ppm] = 8.20 (d, *J* = 8.8 Hz, 2H), 7.43 (d, *J* = 8.6 Hz, 2H), 4.78 (dd, *J* = 13.0, 6.4 Hz, 1H), 4.68 (dd, *J* = 13.0, 8.4 Hz, 1H), 4.16–4.07 (m, 1H), 3.62 (s, 3H), 2.82 (dd, *J* = 16.6, 7.0 Hz, 1H), 2.77 (dd, *J* = 16.6, 7.6 Hz, 1H).

**$^{13}$C NMR** (151 MHz, $CDCl_3$) δ [ppm] = 170.4, 147.6, 145.6, 128.5, 124.3, 78.5, 52.2, 39.8, 37.0.

### 10.8.25 (*R*)-4-(4-Aminophenyl)pyrrolidin-2-one (10.25)

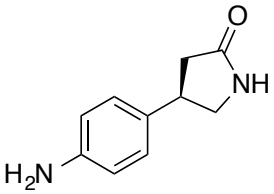

(*R*)-4-(4-Aminophenyl)pyrrolidin-2-one was prepared according to a modified procedure from Jensen *et al.*.[214] (*R*)-Methyl 4-nitro-3-(4-nitrophenyl)butanoate (**10.24**) (1.0 eq., 492 mg, 1.83 mmol) and $NiCl_2 \bullet 6\ H_2O$ (2.0 eq., 870 mg, 3.66 mmol) were dissolved in EtOH (25 mL) and cooled to 0 °C. $NaBH_4$ (22.0 eq., 1.52 g, 40.3 mmol) was added portionwise to the vigorously stirred reaction mixture and stirring was continued for 1 h. 20 mL of 4 M NaOH was added and the reaction was allowed to warm to r.t. and stirred for another 2 h before it was quenched with saturated $NH_4Cl$ (20 mL) and extracted with DCM (3 × 30 mL). The combined organic layers were dried over $MgSO_4$, filtered and concentrated *in vacuo* to afford 120 mg (0.68 mmol) of the desired product in 37% yield as colorless needles.

**$^1$H NMR** (599 MHz, $CDCl_3$) δ [ppm] = 7.01 (d, *J* = 8.5 Hz, 2H), 6.64 (d, *J* = 8.4 Hz, 2H), 6.34 (br s, 1H), 3.74–3.66 (m, *J* = 8.8 Hz, 1H), 3.63 (br s, 2H), 3.62–3.52 ($m_c$, 1H), 3.32 (dd, *J* = 9.4, 7.7 Hz, 1H), 2.65 (dd, *J* = 16.9, 8.9 Hz, 1H), 2.42 (dd, *J* = 16.9, 9.1 Hz, 1H).

**$^{13}$C NMR** (151 MHz, $CDCl_3$) δ [ppm] = 177.9, 145.4, 131.8, 127.6, 115.3, 49.8, 39.7, 38.1.

**HRMS (ESI)**: calc. for $C_{10}H_{13}N_2O^+$ $(M+H)^+$: 177.1022, found: 177.1021.

### 10.8.26 (*R*)-4-(4-(Phenyldiazenyl)phenyl)pyrrolidin-2-one (10.26)

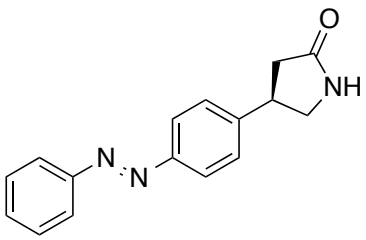


(*R*)-4-(4-Aminophenyl)pyrrolidin-2-one (**10.25**) (1.0 eq., 100 mg, 0.57 mmol) was dissolved in glacial acetic acid (10 mL) and nitrosobenzene (1.2 eq., 73 mg, 0.68 mmol) was added to it in one portion. The reaction was stirred at r.t. for 24 hours before it was quenched with sat. aqueous $NaHCO_3$ and extracted into DCM. The organic layer was dried over $MgSO_4$, filtered and concentrated *in vacuo*

before it was submitted to flash column chromatography on silica gel (100% EtOAc → 5% MeOH/EtOAc) to afford 63 mg (0.24 mmol) of (*R*)-4-(4-(phenyldiazenyl)phenyl)pyrrolidin-2-one in 42% yield as an orange solid.

**$^1$H NMR** (599 MHz, $CDCl_3$) δ [ppm] = 7.93–7.87 (m, 4H), 7.54–7.49 (m, 2H), 7.49–7.44 (m, 1H), 7.39 (d, *J* = 8.3 Hz, 2H), 6.10 (br s, 1H), 3.87–3.73 (m, 2H), 3.46 (dd, *J* = 9.1, 6.8 Hz, 1H), 2.78 (dd, *J* = 16.9, 8.9 Hz, 1H), 2.54 (dd, *J* = 17.1, 8.4 Hz, 1H).

**$^{13}$C NMR** (151 MHz, $CDCl_3$) δ [ppm] = 177.2, 152.6, 151.8, 145.1, 131.1, 129.1, 127.5, 123.3, 122.8, 49.2, 40.2, 30.9.

**HRMS (ESI)**: calc. for $C_{16}H_{16}N_3O^+$ $(M+H)^+$: 266.1288, found: 266.1287.

### 10.8.27 (*R*)-4-Amino-3-(4-(phenyldiazenyl)phenyl)butanoic acid hydro-chloride, AzoGABA hydrochloride salt

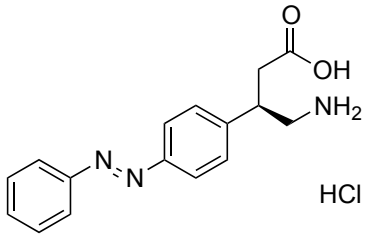


A round-bottom flask was charged with (*R*)-4-(4-(phenyldiazenyl)phenyl)pyrrolidin-2-one (**10.26**) (15.5 mg, 58.5 µmol) under a nitrogen atmosphere and dissolved in degassed 4M HCl. The solution was refluxed for 3 h before it was allowed to cool to r.t. and subsequently filtered over a C18 silica plug. The crude was washed with HCl (1 mM) and eluted with a mixture of MeCN/1 mM HCl = 1/4 to obtain **AzoGABA**. Final drying was performed by freeze-drying over night to yield 4.8 mg (17.0 µmol) of the desired product as a yellow powder in 29% yield.

**$^1$H NMR** (400 MHz, DMSO-$d_6$) δ [ppm] = 8.08 (br s, 2H), 7.88 (td, *J* = 6.0, 3.2 Hz, 4H), 7.63–7.54 (m, 5H), 3.52–3.44 (m, 1H), 3.18 (dd, *J* = 12.8, 6.6 Hz, 1H), 3.06 (dd, *J* = 12.8, 8.3 Hz, 1H), 2.92 (dd, *J* = 16.5, 5.4 Hz, 1H), 2.65 (dd, *J* = 16.4, 9.2 Hz, 1H).

**$^{13}$C NMR** (101 MHz, DMSO-$d_6$) δ [ppm] = 172.4, 152.0, 151.2, 144.1, 131.6, 129.5, 129.2, 122.8, 122.5, 43.1, 39.6, 37.8.

**HRMS (ESI)**: calc. for $C_{16}H_{18}N_3O_2^+$ $(M+H)^+$: 284.1394, found: 284.1390.

**$R_t$** (LCMS; MeCN/$H_2O$/formic acid = 10/90/0.1 → 90/10/0.1 over 7 min) = 2.474 min.

**UV/Vis** (LCMS) = 324 nm.

### 10.8.28 (*R*,*E*)-4-(4-((4-(Diethylamino)phenyl)diazenyl)phenyl)-pyrrolidin-2-one (10.27)

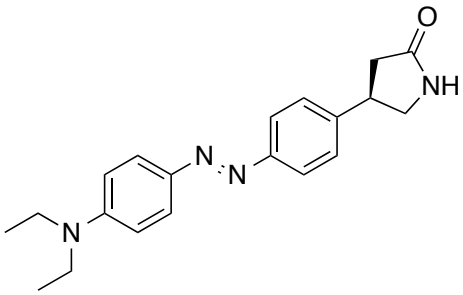


A round-bottom flask was charged with **10.25** (40.0 mg, 0.23 mmol, 1.0 eq.) in 10 mL 2.4 M HCl and cooled to 0 °C. An aqueous solution of $NaNO_2$ (19.3 mg, 0.28 mmol, 1.2 eq.) in 10 mL water was added drop-wise. The reaction mixture turned pale yellow, was stirred for 10 minutes at 0 °C before it was transferred to a pre-cooled flask containing *N*,*N*-diethylaniline (34.0 mg, 0.23 mmol, 304 µL, 1.0 eq.) dissolved in 10 mL of 1 M NaOAc (water/MeOH = 1/1). The reaction mixture turned red and was allowed to warm to r.t. before it was extracted three times with EtOAc with the help of sat. $NaHCO_3$. The combined organic layers were dried over $MgSO_4$ and after filtration and removal of all volatiles the crude product was further purified by flash column chromatography (EtOAc/MeOH = 10/0 → 9/1) to yield 16.3 mg (0.05 mmol) of **10.27** as an red solid in 21% yield.

**$^1$H NMR** (400 MHz, DMSO-$d_6$) $\delta$ [ppm] = 7.80–7.75 (m, 4H), 7.43 (d, $J$ = 8.4 Hz, 2H), 6.79 (d, $J$ = 9.2 Hz, 2H), 3.80 (td, $J$ = 8.2, 7.6, 3.5 Hz, 2H), 2.83–2.68 (m, 2H),

3.50 (q, *J* = 7.0 Hz, 4H), 2.80–2.69 (m, 1H), 2.52 (dd, *J* = 16.6, 8.5 Hz, 1H), 1.22 (t, *J* = 7.0 Hz, 6H).

**$^{13}$C NMR** (101 MHz, DMSO-$d_6$) $\delta$ [ppm] = 180.0, 153.5, 151.8, 145.1, 144.2, 128.6, 126.3, 123.4, 112.1, 50.7, 45.6, 41.3, 39.2, 12.9.

**HRMS (ESI)**: calc. for $C_{20}H_{25}N_4O^+$ $(M+H)^+$: 337.2023, found: 337.2020.

**$R_t$** (LCMS; MeCN/$H_2O$/formic acid = 10/90/0.1 → 90/10/0.1 over 7 min) = 4.136 min.

**UV/Vis** (LCMS) = 437 nm.

### 10.8.29 (*R*,*E*)-4-Amino-3-(4-((4-(diethylamino)phenyl)diazenyl)phenyl) butanoic acid hydrochloride salt, red-AzoGABA hydrochloride salt

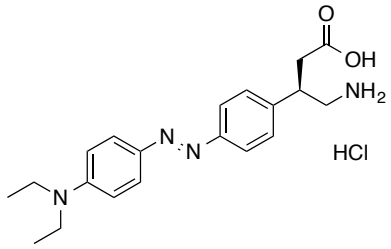


13.6 mg (0.035 mmol) **Red-AzoGABA** was obtained in 70% yield from 16.6 mg (0.050 mmol) **10.27** according to the procedure used for **AzoGABA**.

**$^1$H NMR** (400 MHz, $CD_3OD$) $\delta$ [ppm] = 7.83–7.75 (m, 4H), 7.41 (d, *J* = 8.4 Hz, 2H), 7.11–6.92 (m, 2H), 3.50 (q, *J* = 7.1 Hz, 4H), 3.44–3.39 (m, 1H), 3.29 (dd, *J* = 12.8, 5.7 Hz, 1H), 3.16 (dd, *J* = 12.8, 9.5 Hz, 1H), 2.77 (dd, *J* = 16.5, 6.8 Hz, 1H), 2.64 (dd, *J* = 16.5, 7.7 Hz, 1H), 1.14 (t, *J* = 7.1 Hz, 6H).

**HRMS (ESI)**: calc. for $C_{20}H_{27}N_4O_2^+$ $(M+H)^+$: 355.2129, found: 355.2125.

**$R_t$** (LCMS; MeCN/$H_2O$/formic acid = 10/90/0.1 → 90/10/0.1 over 7 min) = 2.704 min.

**UV/Vis** (LCMS) = 460 nm.

### 10.8.30 *tert*-Butyl (3-(2-(methylthio)-6-(trifluoromethyl)pyrimidin-4-yl)phenyl)-carbamate (10.30)

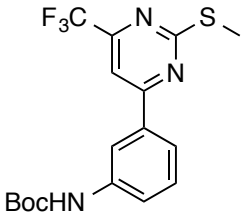


A round bottom flask was charged under a nitrogen atmosphere with 500 mg (2.19 mmol, 1.0 eq.) of 4-chloro-2-(methylthio)-6-(trifluoromethyl)pyrimidine (**10.28**), 519 mg (2.19 mmol, 1.0 eq.) of (3-((*tert*-butoxycarbonyl)amino)phenyl)boronic acid (**10.29**) and 714 mg (2.19 mmol, 1.0 eq.) of $Cs_2CO_3$. The solids were dissolved in a degassed mixture of DME (16 mL) and $H_2O$ (4 mL) before the addition of 254 mg (0.219 mmol, 0.1 eq.) of $Pd(PPh_3)_4$. The reaction was heated to 85 °C for 18 hours, before the volatiles were removed *in vacuo* and the crude material was subjected to FCC (pentane/DCM = 1/1 → 0/1) to obtain 805 mg (2.09 mmol) of the desired compound in 95% yield as a white powder.

**$^1$H NMR** (400 MHz, $CDCl_3$): $\delta$ [ppm] = 8.11 (t, $J$ = 1.9 Hz, 1H), 7.76 (dt, $J$ = 7.7, 1.2 Hz, 1H), 7.61 (m, 2H), 7.43 (t, $J$ = 8.0 Hz, 1H), 6.70 (br s, 1H), 2.66 (s, 3H), 1.54 (s, 9H).

**$^{13}$C NMR** (101 MHz, $CDCl_3$): $\delta$ [ppm] = 174.2, 165.9, 156.3 (q, $J$ = 35.8 Hz), 152.6, 139.3, 136.1, 129.8, 128.5, 121.9, 121.9, 120.5 (q, $J$ = 275.5 Hz), 117.1, 107.4 (q, $J$ = 2.8 Hz), 81.0, 28.3, 14.4.

**HRMS (ESI)**: calc. for $C_{17}H_{19}F_3N_3O_2S^+$ $(M+H)^+$: 386.1145, found: 386.1143.

**UV/Vis** (LCMS): $\lambda_{max1}$ = 260 nm; $\lambda_{max2}$ = 325 nm.

**$R_t$** (LCMS; MeCN/$H_2O$/formic acid = 10/90/0.1 → 90/10/0.1 over 7 min) = 5.585 min.

### 10.8.31 *tert*-Butyl (3-(2-(methylsulfonyl)-6-(trifluoromethyl)pyrimidin-4-yl)-phenyl)carbamate (10.31)

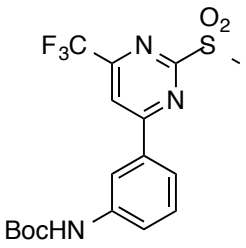


A round bottom flask was charged with 200 mg (0.52 mmol, 1.0 eq.) of *tert*-Butyl (3-(2-(methylthio)-6-(trifluoromethyl)pyrimidin-4-yl)phenyl)carbamate (**10.30**) dissolved in DCM (10 mL) before the addition of 349 mg (1.56 mmol, 3.0 eq.) of *m*CPBA (77%). The reaction was stirred for 2 h at r.t. before the crude material was subjected to FCC (100% DCM) to obtain 195 mg (0.47 mmol) of the desired product in 90% yield as a yellow foam.

**$^{1}$H NMR** (400 MHz, $CDCl_3$): $\delta$ [ppm] = 8.26 (t, $J$ = 1.9 Hz, 1H), 8.18 (s, 1H), 7.91–7.84 (m, 1H), 7.71–7.67 (m, 1H), 7.48 (t, $J$ = 8.0 Hz, 1H), 6.82 (br s, 1H), 3.48 (s, 3H), 1.54 (s, 9H).

**$^{13}$C NMR** (101 MHz, $CDCl_3$): $\delta$ [ppm] = 169.1, 167.1, 157.6 (q, $J$ = 35.8 Hz), 152.9, 140.1, 134.5, 130.5, 123.6, 122.7, 120.2 (q, $J$ = 275.5 Hz), 117.7, 115.1 (q, $J$ = 2.8 Hz), 81.6, 39.4, 28.6.

**HRMS (ESI)**: calc. for $C_{17}H_{17}F_3N_3O_4S^-$ $(M-H)^-$: 416.0897, found: 416.0898.

**UV/Vis** (LCMS): $\lambda_{max1}$ = 234 nm; $\lambda_{max2}$ = 287 nm.

**$R_t$** (LCMS; MeCN/$H_2O$/formic acid = 10/90/0.1 → 90/10/0.1 over 7 min) = 4.591 min.

### 10.8.32 *tert*-Butyl (3-(2-(ethylthio)-6-(trifluoromethyl)pyrimidin-4-yl)phenyl)-carbamate (10.32)

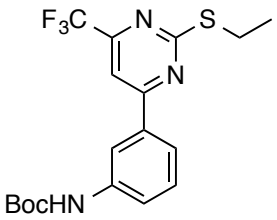


A microwave vial was charged with 130 mg (0.31 mmol, 1.0 eq.) of *tert*-butyl (3-(2-(methylsulfonyl)-6-(trifluoromethyl)pyrimidin-4-yl)-phenyl)carbamate (**10.31**) dissolved in a mixture of THF (3 mL) and EtSH (170 µL) before the addition of 13.5 mg (0.16 mmol, 0.5 eq.) of EtSNa. The reaction was heated in a microwave for 20 min at 100 °C before the crude material was subjected to FCC (pentane/DCM = 1/1) to obtain 48.5 mg (0.12 mmol) of the desired product in 39% yield as a yellow wax.

**$^{1}$H NMR** (400 MHz, $CDCl_3$): $\delta$ [ppm] = 8.12 (d, *J* = 2.0 Hz, 1H), 7.80–7.72 (m, 1H), 7.61 (m, 2H), 7.44 (t, *J* = 7.9 Hz, 1H), 6.67 (br s, 1H), 3.26 (q, *J* = 7.3 Hz, 2H), 1.54 (s, 9H), 1.46 (t, *J* = 7.3 Hz, 3H).

**$^{13}$C NMR** (101 MHz, $CDCl_3$): $\delta$ [ppm] = 174.0, 165.9, 156.4 (q, *J* = 35.8 Hz), 152.6, 139.3, 136.2, 129.8, 121.9, 121.8, 120.5 (q, *J* = 274.4 Hz), 117.1, 107.4 (q, *J* = 2.8 Hz), 81.0, 28.3, 25.6, 14.2.

**HRMS (ESI)**: calc. for $C_{18}H_{21}F_3N_3O_2S^+$ $(M+H)^+$: 400.1301, found: 400.1301.

**UV/Vis** (LCMS): $\lambda_{max1}$ = 264 nm; $\lambda_{max2}$ = 326 nm.

**$R_t$** (LCMS; MeCN/$H_2O$/formic acid = 10/90/0.1 → 90/10/0.1 over 7 min) = 5.821 min.

### 10.8.33 *tert*-Butyl (3-(2-(ethylsulfinyl)-6-(trifluoromethyl)pyrimidin-4-yl)-phenyl)carbamate (10.33)

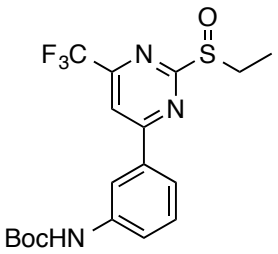


A round bottom flask was charged with 30.5 mg (0.076 mmol, 1.0 eq.) of *tert*-butyl (3-(2-(ethylthio)-6-(trifluoromethyl)pyrimidin-4-yl)phenyl)carbamate (**10.32**) dissolved in DCM (4 mL). The reaction mixture was cooled to 0 °C before the addition of 17.1 mg (0.076 mmol, 1.0 eq.) of *m*CPBA (77%). The reaction was stirred for 45 min while allowing to warm to r.t. before the crude material was subjected to FCC (DCM/MeOH = 100/0 → 100/3) to obtain 30.4 mg (0.073 mmol) of the desired product in 96% yield as a yellow foam.

**$^1$H NMR** (400 MHz, $CDCl_3$): $\delta$ [ppm] = 8.25 (s, 1H), 8.04 (s, 1H), 7.90–7.83 (m, 1H), 7.75–7.67 (m, 1H), 7.45 (t, *J* = 8.0 Hz, 1H), 6.96 (s, 1H), 3.31 (dt, *J* = 14.7, 7.4 Hz, 1H), 3.19 (dd, *J* = 13.5, 7.3 Hz, 1H), 1.52 (s, 9H), 1.35 (t, *J* = 7.4 Hz, 3H).

**$^{13}$C NMR** (101 MHz, $CDCl_3$): $\delta$ [ppm] = 174.4, 167.9, 157.2 (q, *J* = 36.9 Hz), 152.7, 139.8, 134.7, 130.0, 122.9, 122.2, 120.2 (q, *J* = 275.8 Hz), 116.0, 112.7 (q, *J* = 2.7 Hz), 81.0, 47.6, 28.3, 6.4.

**HRMS (ESI)**: calc. for $C_{18}H_{20}F_3N_3NaO_3S^+$ $(M+H)^+$: 438.1070, found: 438.1073.

**UV/Vis** (LCMS): $\lambda_{max1}$ = 236 nm; $\lambda_{max2}$ = 278 nm, $\lambda_{max3}$ = 340 nm.

**$R_t$** (LCMS; MeCN/$H_2O$/formic acid = 10/90/0.1 → 90/10/0.1 over 7 min) = 4.531 min.

### 10.8.34 (*E*)-2-(Ethylsulfinyl)-4-(3-(phenyldiazenyl)phenyl)-6-(trifluoro-methyl)pyrimidine (AzoBETP)

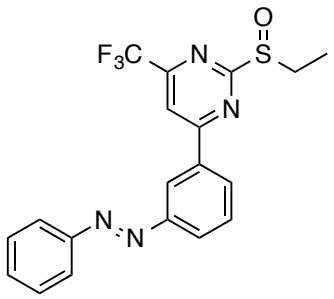

A round bottom flask was charged with 20.0 mg (48.2 µmol, 1.0 eq.) of *tert*-butyl (3-(2-(ethylsulfinyl)-6-(trifluoromethyl)pyrimidin-4-yl)-phenyl)carbamate (**10.33**) dissolved in a mixture of DCM (2 mL) and TFA (2 mL). The reaction was stirred for 1 hour before all volatiles were removed *in vacuo* and the resulting material was dissolved in HOAc (2 mL) and DCM (2 mL) and 15.0 mg (140 µmol, 2.9 eq.) of PhNO was added in one portion. The mixture was stirred for 18 h at r.t. before it was quenched with an aqueous sat. solution of $NaHCO_3$ and extracted with DCM. The organic layer was dried over $MgSO_4$ and the crude material was subjected to FCC (pentane/DCM = 50/50 → 0/100) to obtain 10.6 mg (26.2 µmol) of the desired product in 54% yield over two steps as an orange solid.

**$^1$H NMR** (400 MHz, $CDCl_3$): $\delta$ [ppm] = 8.68 (s, 1H), 8.44–8.39 (m, 1H), 8.19–8.12 (m, 2H), 8.00–7.94 (m, 2H), 7.72 (t, $J$ = 7.8 Hz, 1H), 7.58–7.49 (m, 3H), 7.24 (s, 1H), 3.41–3.29 ($m_c$, $J$ = 13.3 Hz, 7.2 Hz, 1H), 3.29–3.14 ($m_c$, $J$ = 13.3 Hz, 7.2 Hz, 1H), 1.37 (t, $J$ = 7.4 Hz, 3H).

**$^{13}$C NMR** (101 MHz, $CDCl_3$): $\delta$ [ppm] = 175.0, 167.6, 157.6 (q, $J$ = 37.4 Hz), 153.2, 152.4, 135.3, 131.7, 130.3, 130.1, 129.2, 126.7, 123.1, 122.5, 120.2 (q, $J$ = 276 Hz) 112.8 (q, $J$ = 1.0 Hz), 47.7, 6.5.

**$^{19}$F NMR** (376 MHz, $CDCl_3$): $\delta$ [ppm] = –69.4.

**HRMS (ESI)**: calc. for $C_{19}H_{16}F_3N_4OS^+$ $(M+H)^+$: 405.0991, found: 405.0993.

**LRMS (ESI)**: calc. for $C_{19}H_{16}F_3N_4OS^+$ $(M+H)^+$: 405.1, found: 405.1.

**UV/Vis** (LCMS): λ (*trans*-**AzoBETP**, π → π*) = 302 nm; λ (*cis*-**AzoBETP**, n → π*) = 428 nm.

**$R_t$** (LCMS; MeCN/$H_2O$/formic acid = 10/90/0.1 → 90/10/0.1 over 7 min) = 4.149 min (*cis*-AzoBETP), 4.979 min (*trans*-**AzoBETP**).

### 10.8.35 (*E*)-4-((3-(2-(Ethylsulfinyl)-6-(trifluoromethyl)pyrimidin-4-yl)-phenyl)diazenyl)-*N*,*N*-dimethylaniline (redAzoBETP)

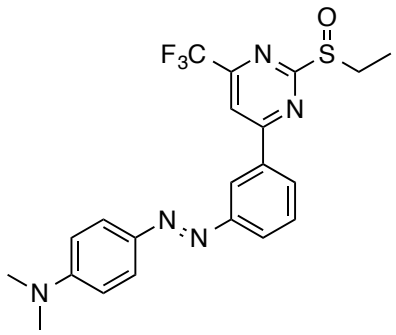

**10.33** (20.0 mg, 48.2 µmol, 1.0 eq.) was dissolved in a mixture of TFA (5 drops) and MeCN (2 mL) and stirred at r.t. for 30 min. The reaction mixture was cooled to 0 °C and $^t$BuONO (12.0 mg, 115.6 µmol, 13.7 µL, 2.4 eq.) were added and the diazotization was stirred for an additional 10 min before it was transferred drop-wise to a flask containing *N*,*N*-dimethylaniline (5.8 mg, 48.2 µmol, 6.15 µL, 1.0 eq.) dissolved in MeOH (5 mL) and 1 M aqueous NaOAc (1 mL). The mixture turned orange immediately upon addition and was stirred for additional 30 min before it was extracted into DCM (3 x) and the combined organic layers were washed with sat. aqueous $NaHCO_3$, water and brine. The crude material was subjected to preparative thin-layer chromatography (100% DCM) after drying over $MgSO_4$ in order to yield 1.1 mg (2.4 µmol) of the desired product in 5% yield.

**$^1$H NMR** (400 MHz, $CDCl_3$): $\delta$ [ppm] = 8.60 (s, 1H), 8.36–8.30 (m, 1H), 8.17 (s, 1H), 8.08 (dt, *J* = 7.8, 1.4 Hz, 1H), 7.94 (d, *J* = 9.0 Hz, 2H), 7.67 (t, *J* = 7.9 Hz, 1H), 6.78 (d, *J* = 9.0 Hz, 2H), 3.36 (dq, *J* = 13.6, 7.2 Hz, 1H), 3.24 (dq, *J* = 14.3, 7.3 Hz, 1H), 3.13 (s, 6H), 1.39 (t, *J* = 7.4 Hz, 3H).

**$^{13}$C NMR** (101 MHz, $CDCl_3$): $\delta$ [ppm] = .

**$^{19}$F NMR** (376 MHz, $CDCl_3$): $\delta$ [ppm] = –69.4.

**HRMS (ESI)**: calc. for $C_{19}H_{16}F_3N_4OS^+$ $(M+H)^+$: 448.1413, found: 448.1417.

**UV/Vis** (LCMS): $\lambda_{max1}$ = 278 nm; $\lambda_{max2}$ = 430 nm.

**$R_t$** (LCMS; MeCN/$H_2O$/formic acid = 10/90/0.1 → 90/10/0.1 over 7 min) = 5.204 min.

## 10.9 Spectral Data

### 10.9.1 (*E*)-4-((4-(Dimethylamino)phenyl)diazenyl)-*N*-(2-morpholinophenyl) benzenesulfonamide (JB556)

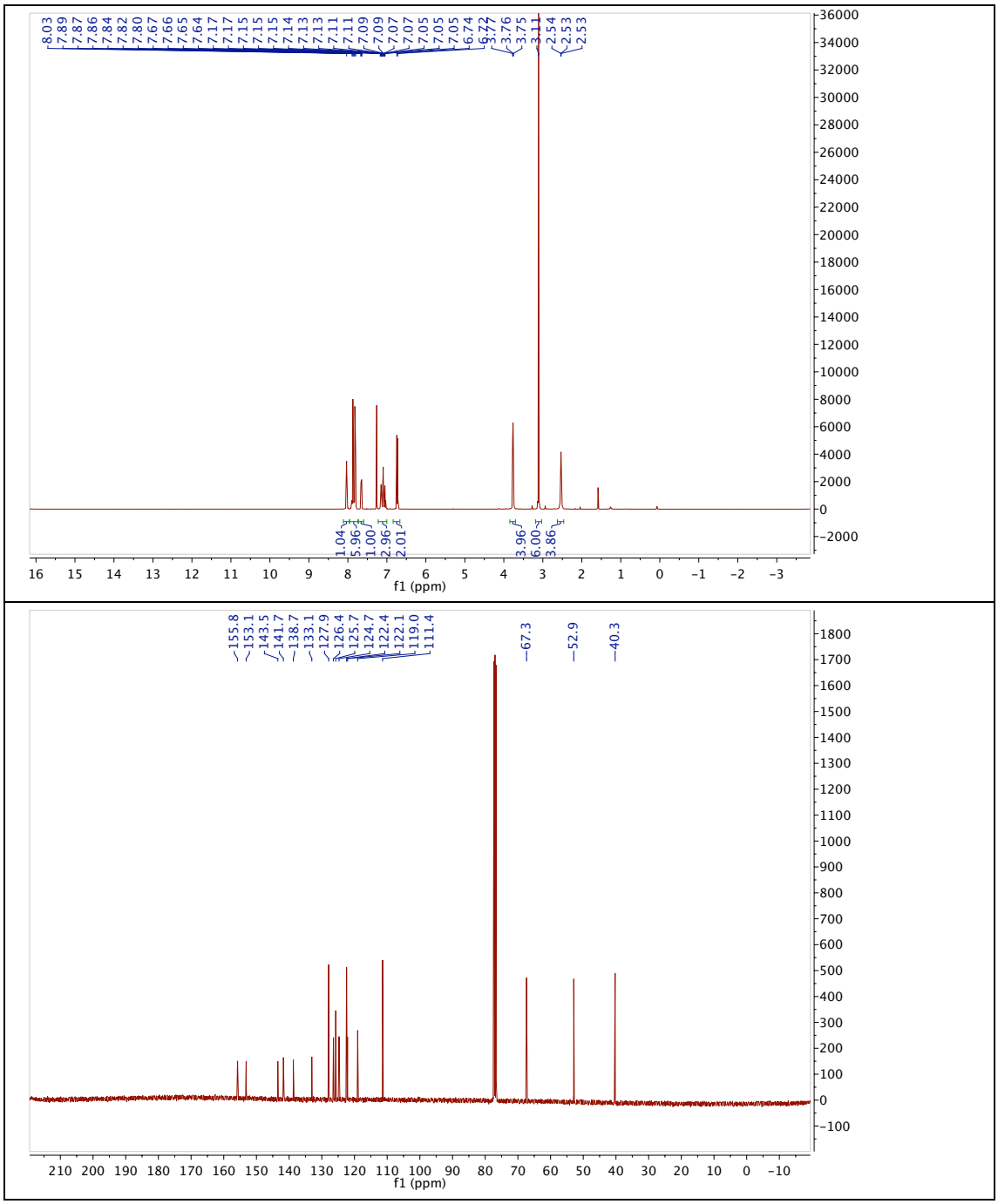

## 10.9.2 *N,N*-dimethyl-2-phenoxyethan-1-amine, Norphenylcholine

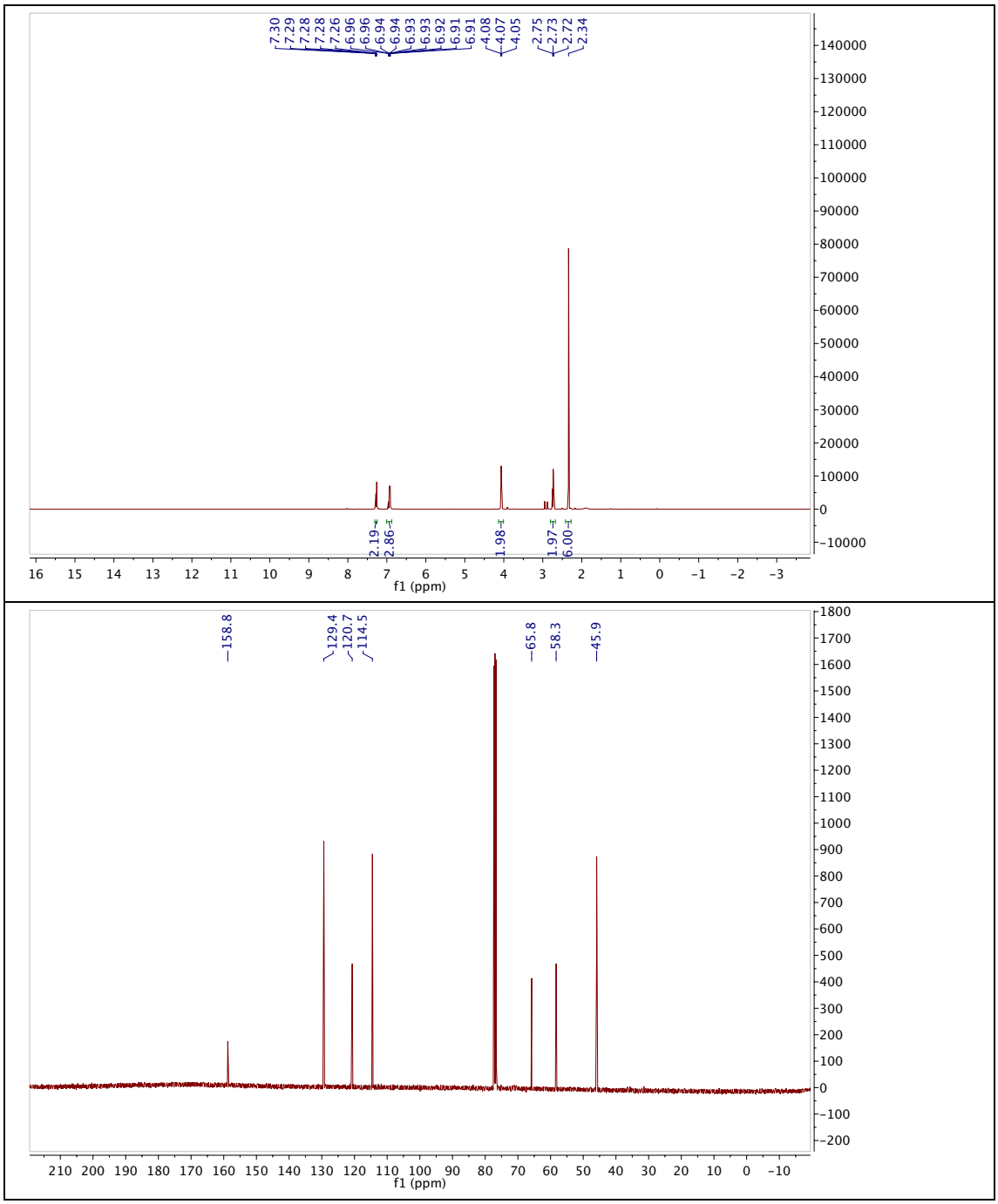

### 10.9.3 *N,N,N*-trimethyl-2-phenoxyethan-1-aminium iodide, Phenylcholine Iodide

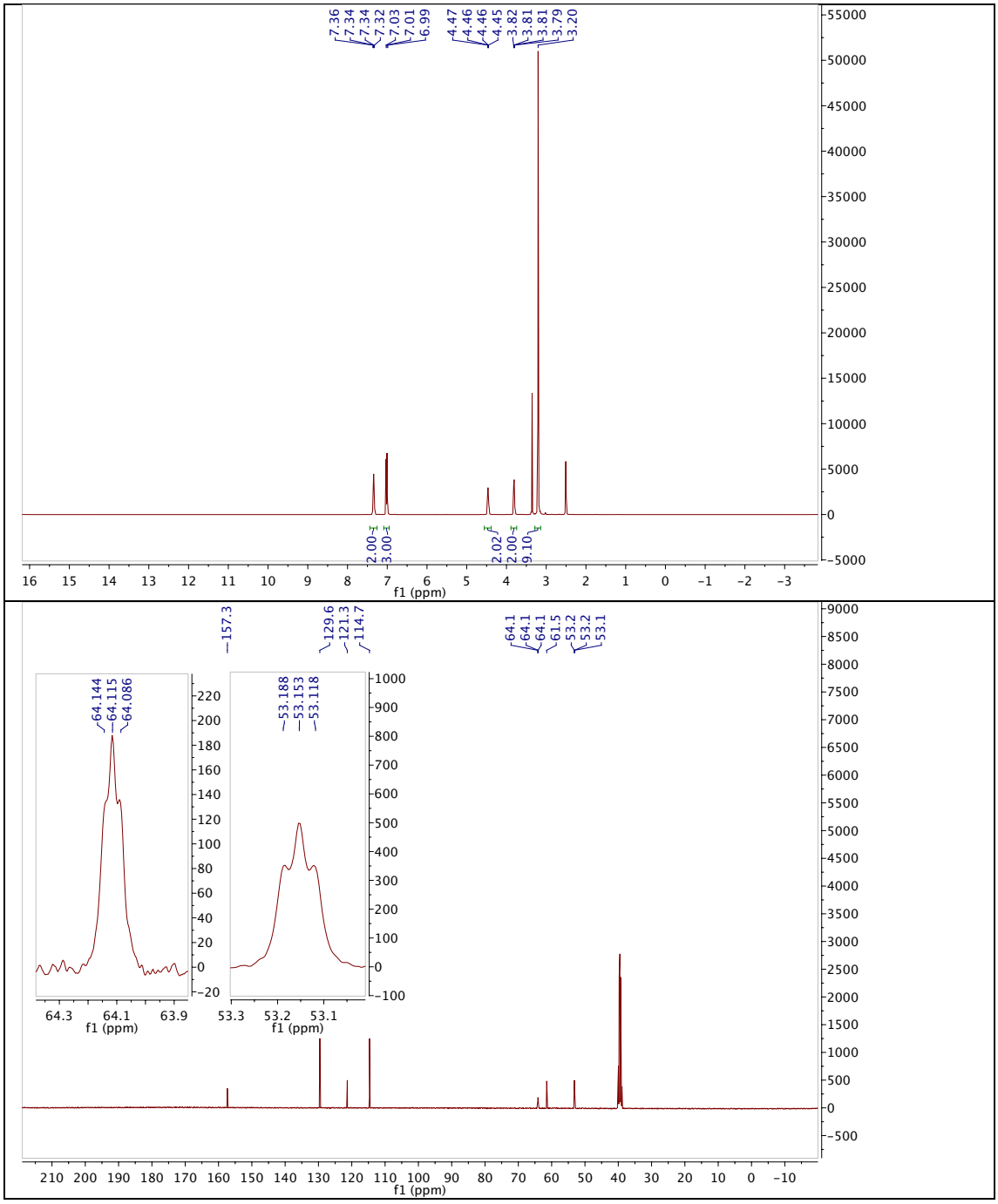

### 10.9.4 (*E*)-Di-*tert*-butyl ((diazene-1,2-diylbis(4,1-phenylene))bis(methylene))-dicarbamate (10.7)

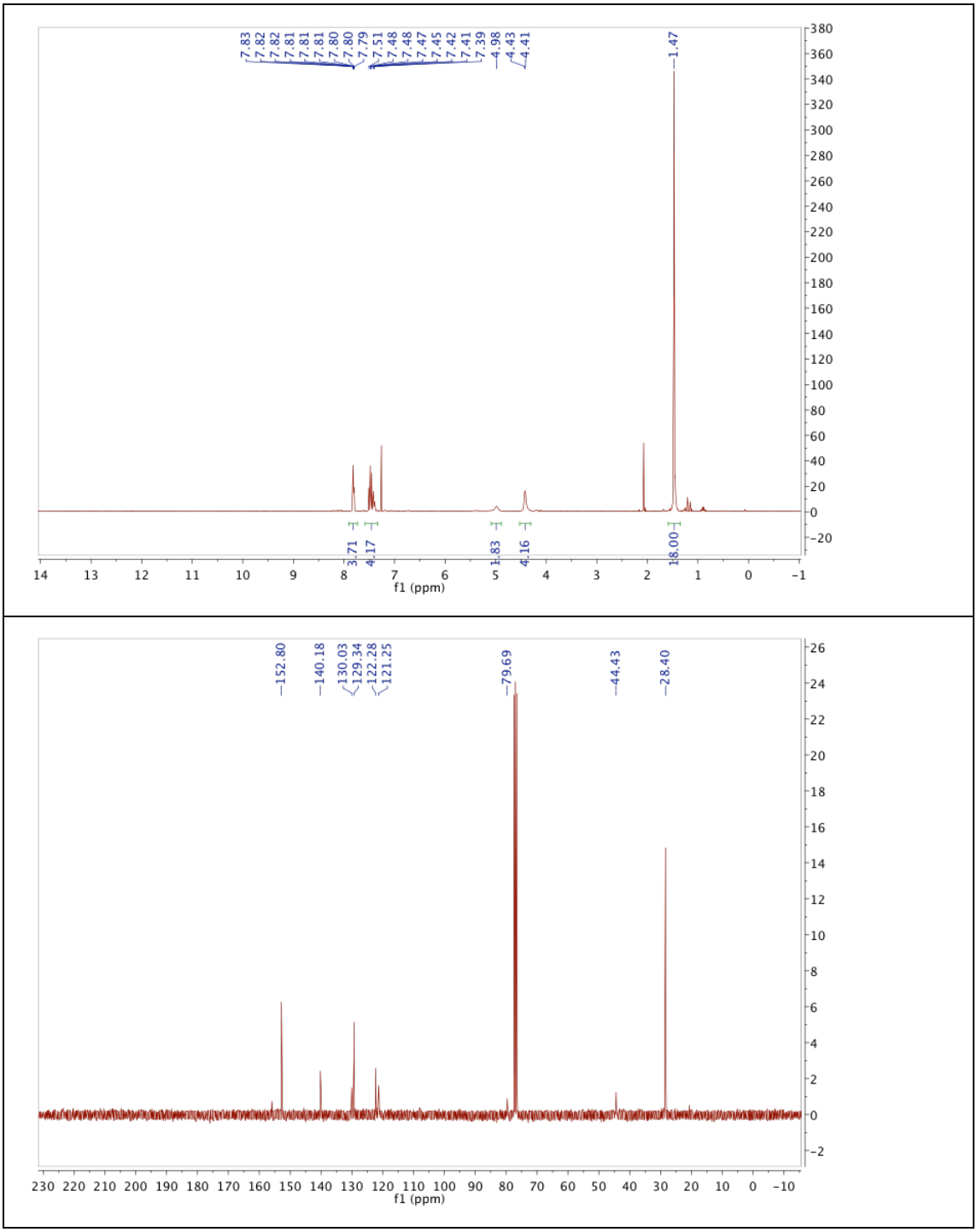

### 10.9.5 (*E*)-(Diazene-1,2-diylbis(4,1-phenylene))dimethanamine (10.8)

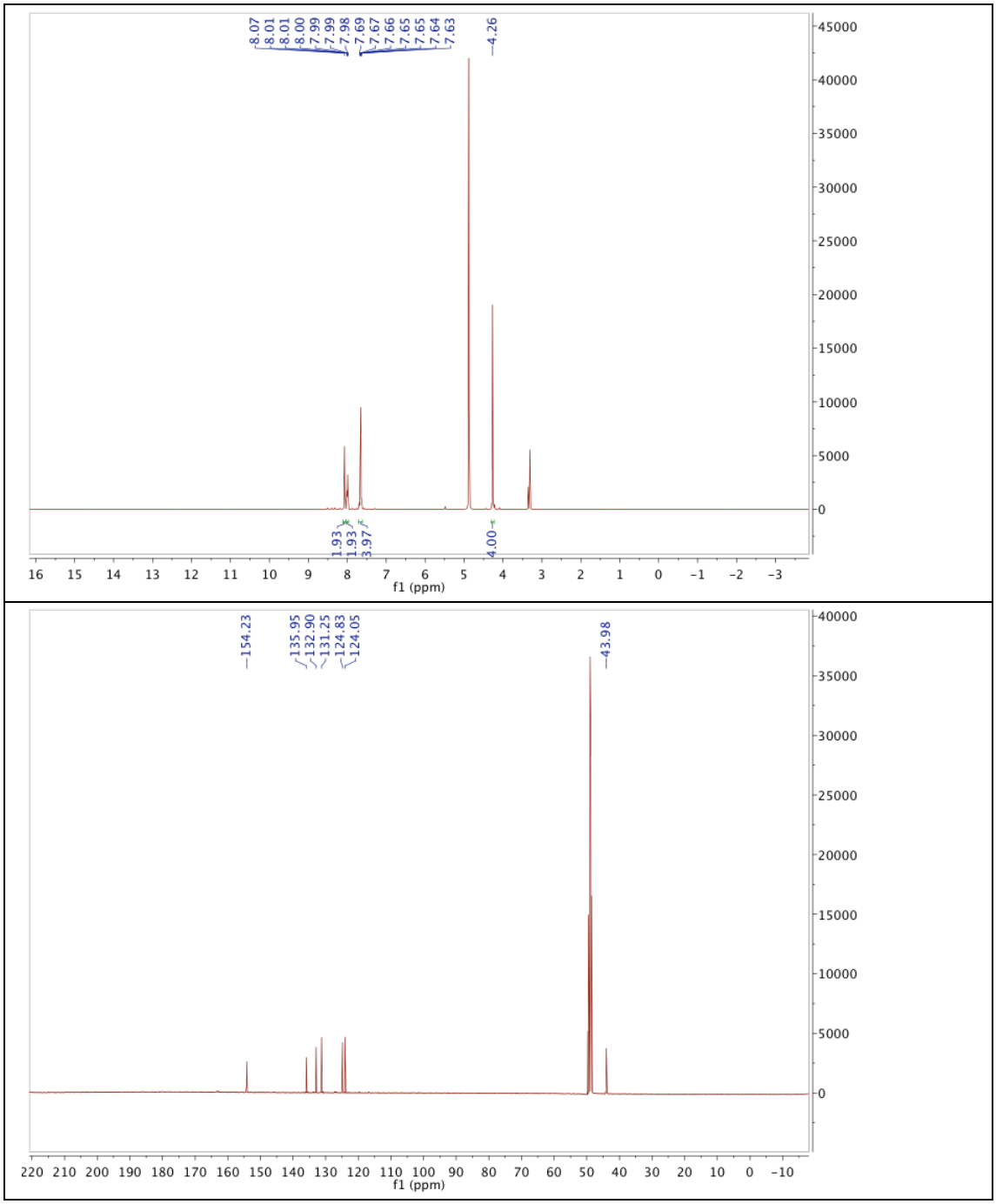

### 10.9.6 (*E*)-1,1'-(Diazene-1,2-diylbis(4,1-phenylene))bis(*N*,*N*,*N*-trimethylmethanaminium) iodide, BisQ

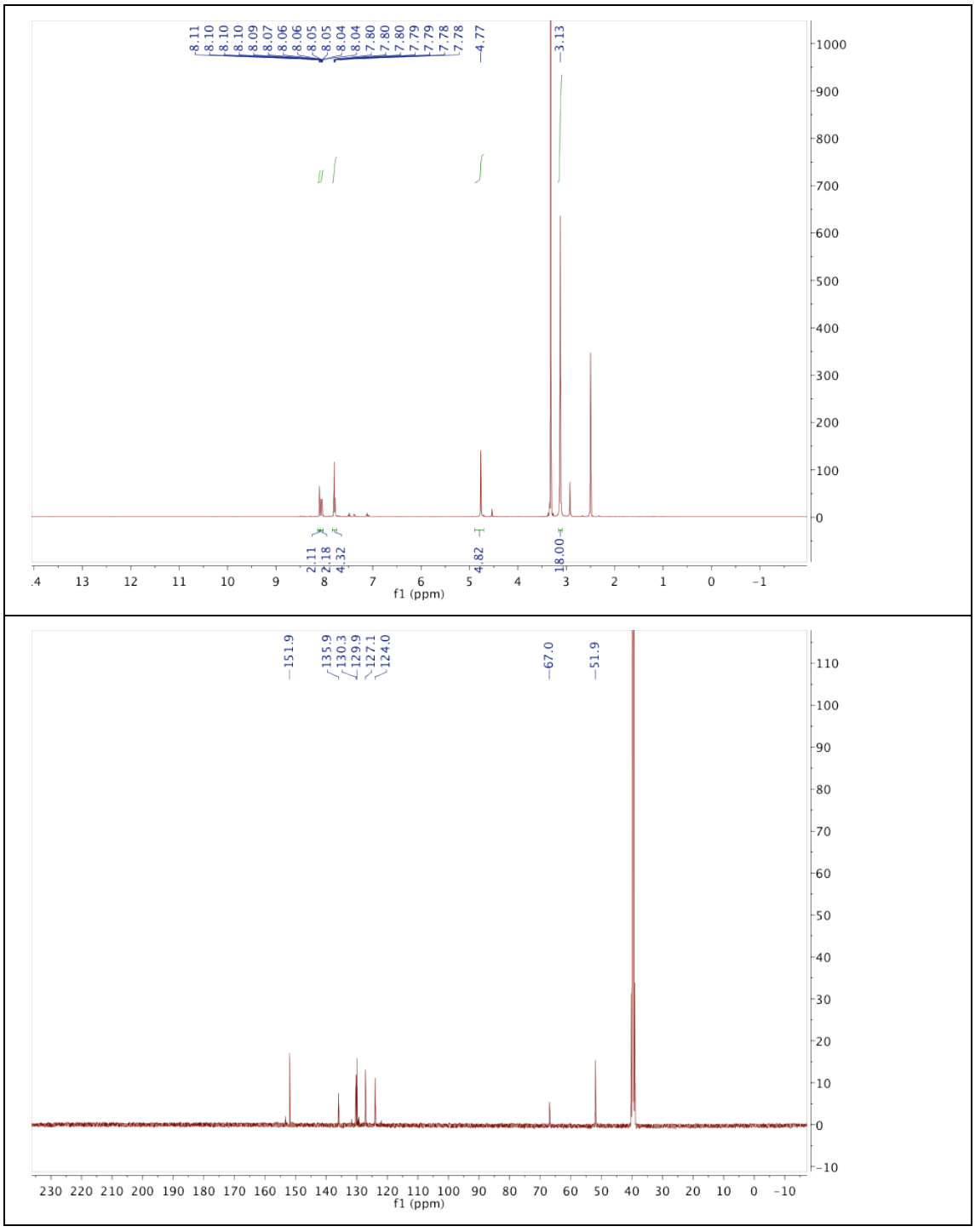

### 10.9.7 (*E*)-*N*,*N*-Dimethyl-2-(4-(phenyldiazenyl)phenoxy)ethanamine (10.10)

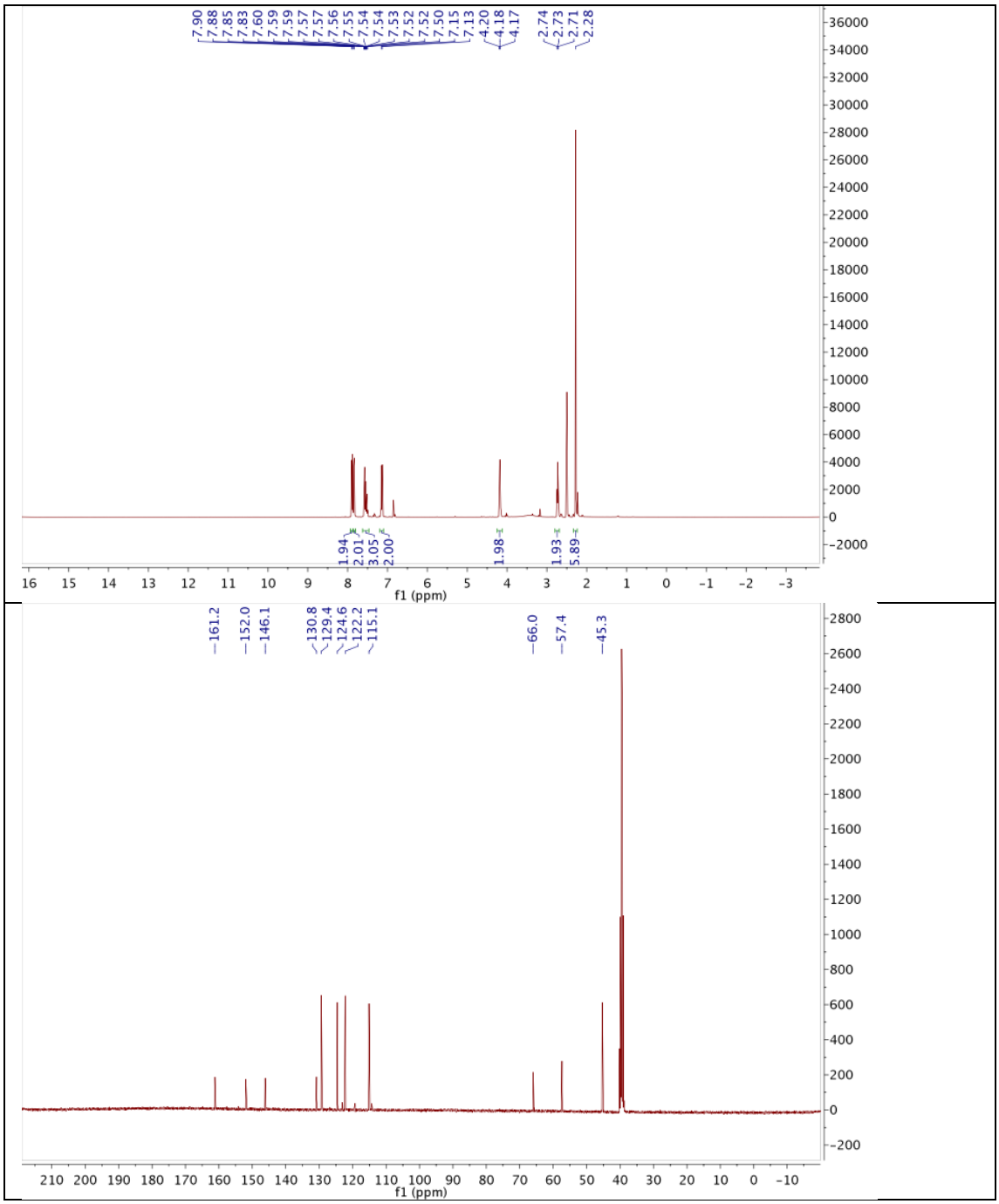

## 10.9.8 (*E*)-*N*,*N*,*N*-Trimethyl-2-(4-(phenyldiazenyl)phenoxy)ethanaminium iodide, AzoCholine

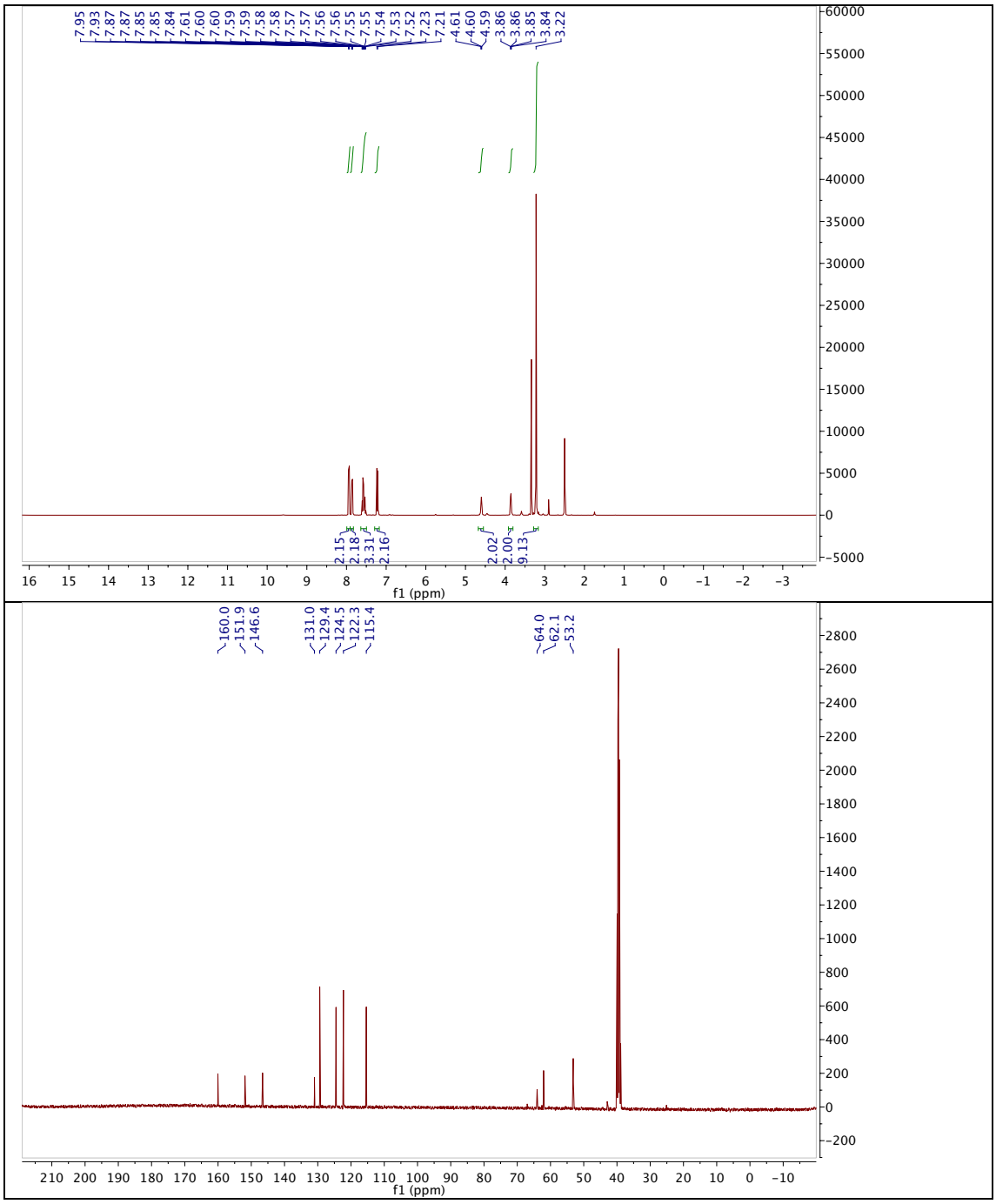

### 10.9.9 *tert*-Butyl (4-chlorobut-2-yn-1-yl)carbamate (SI10.2)

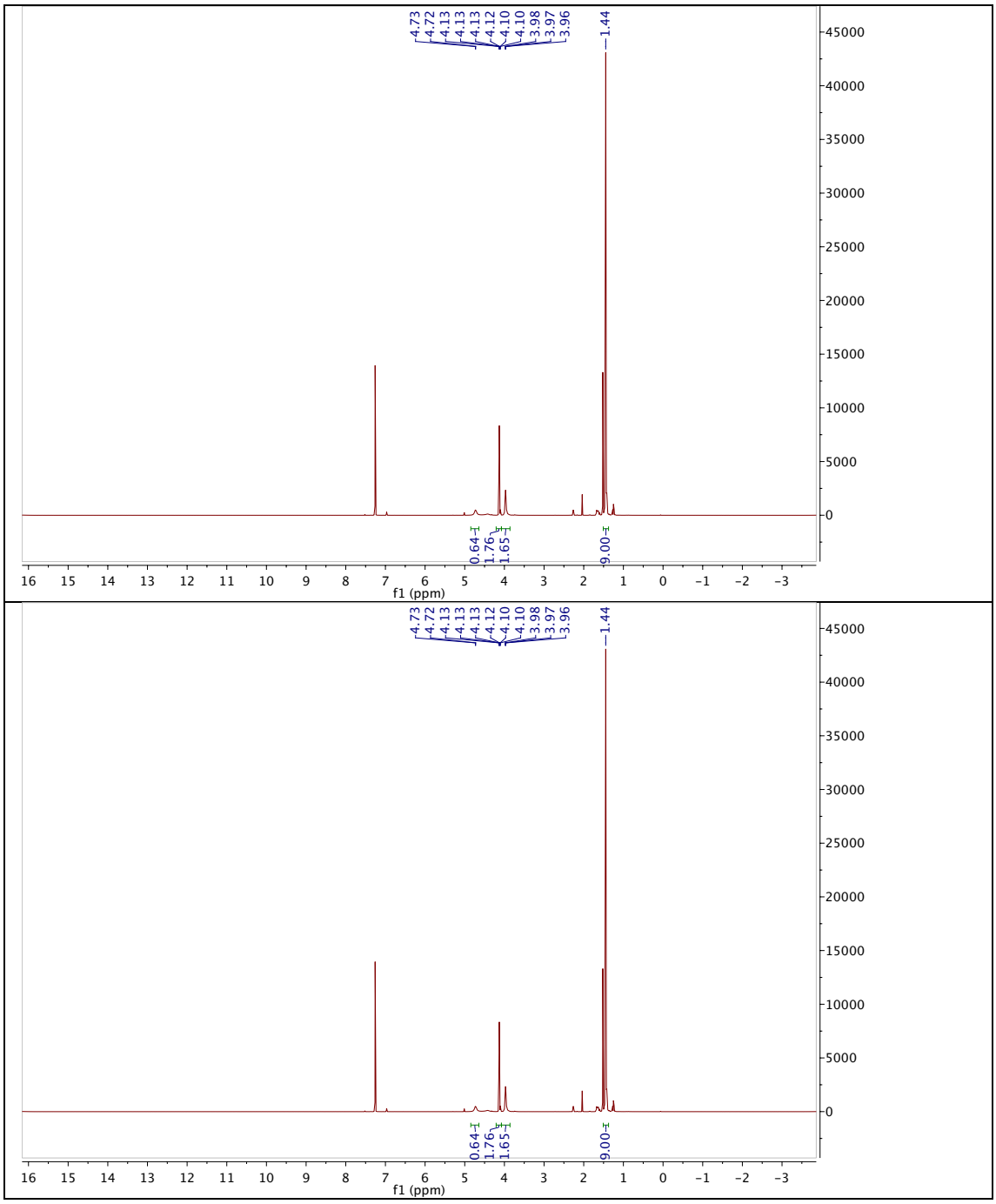

### 10.9.10 *tert*-Butyl (*E*)-(4-(4-(phenyldiazenyl)phenoxy)but-2-yn-1-yl)carbamate (SI10.3)

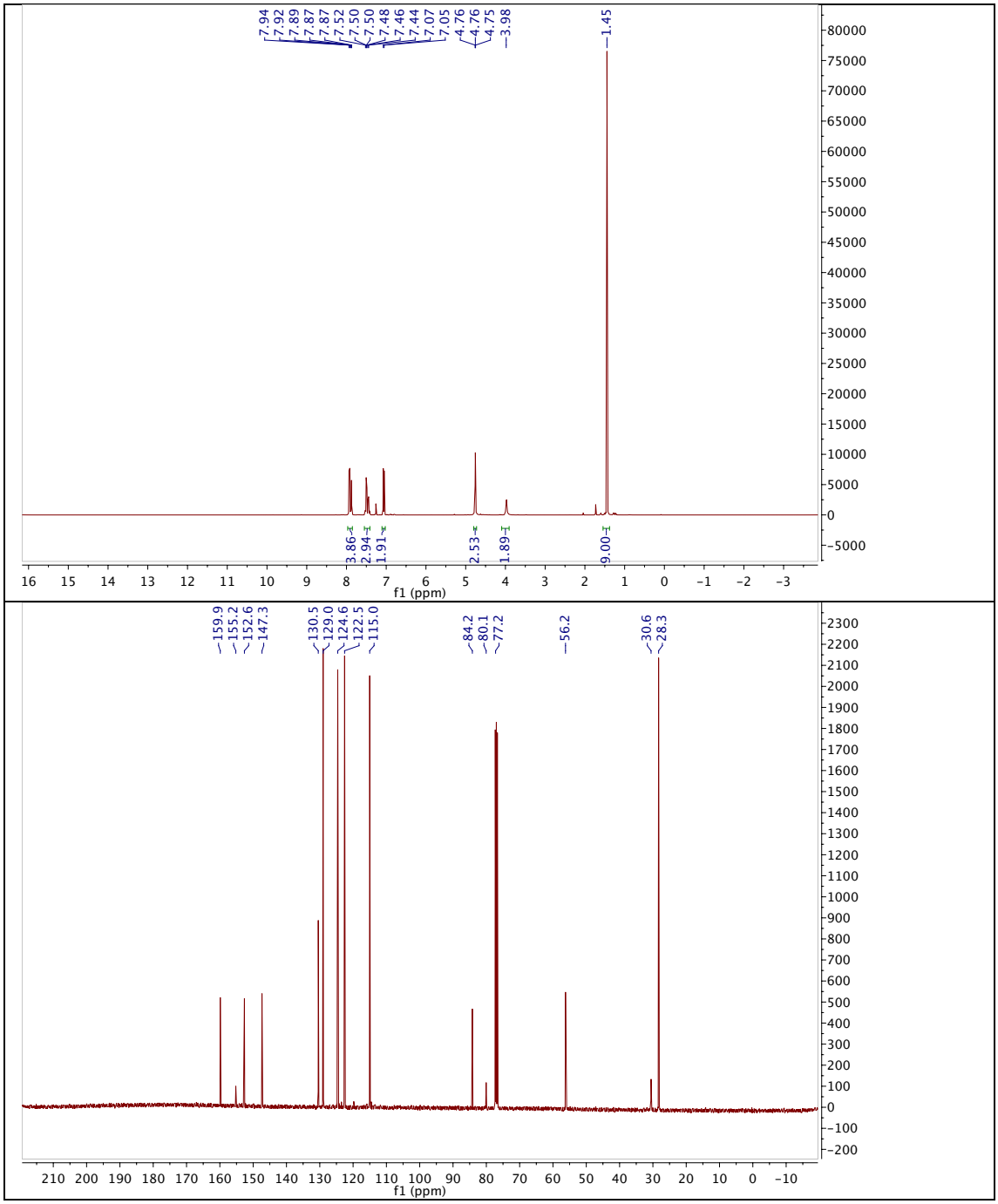

## 10.9.11 (*E*)-4-(4-(Phenyldiazenyl)phenoxy)but-2-yn-1-amine (SI10.4)

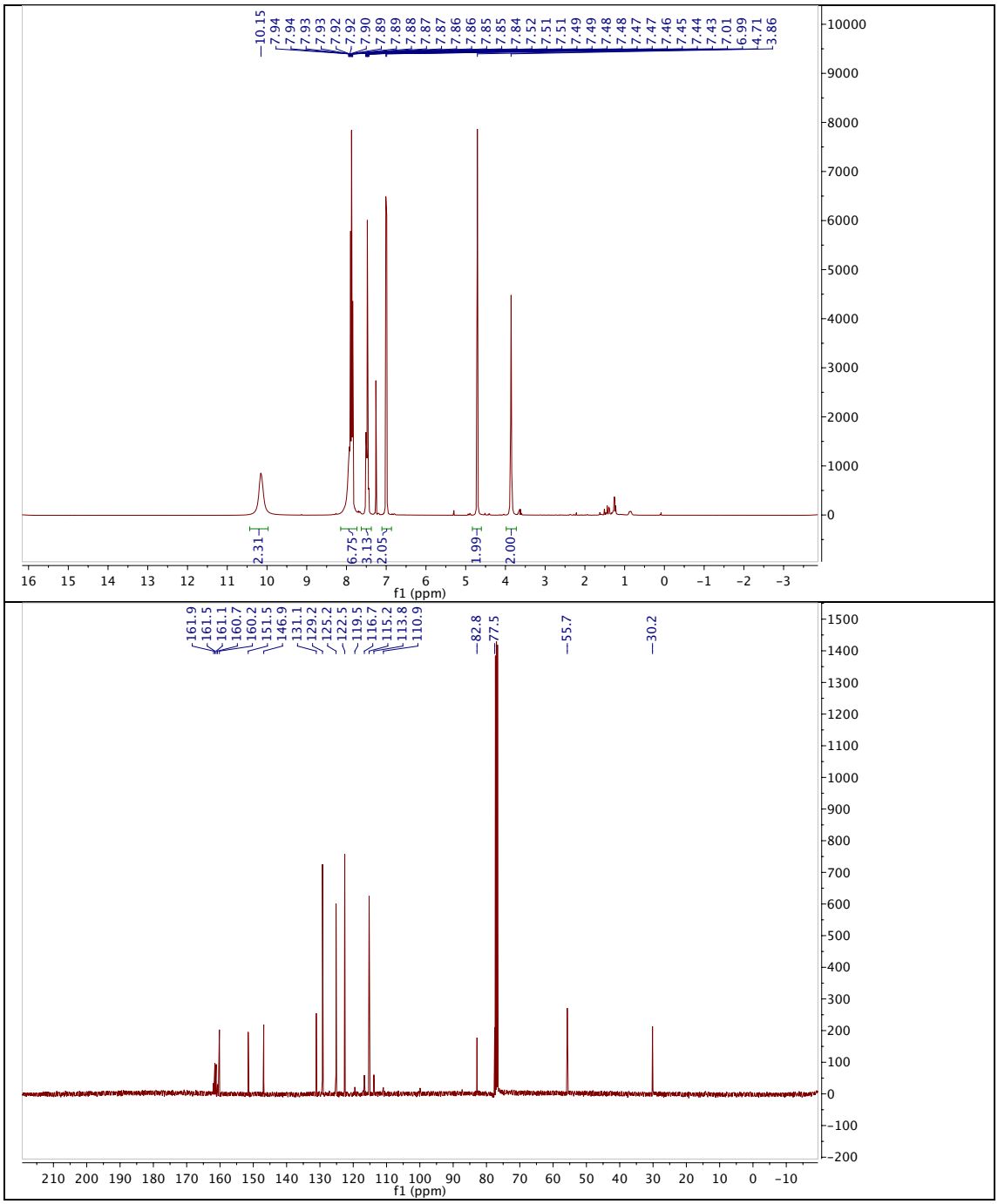

### 10.9.12 (*E*)-*N*,*N*,*N*-Trimethyl-4-(4-(phenyldiazenyl)phenoxy)but-2-yn-1-aminium chloride (AzoIperoxo Chloride)

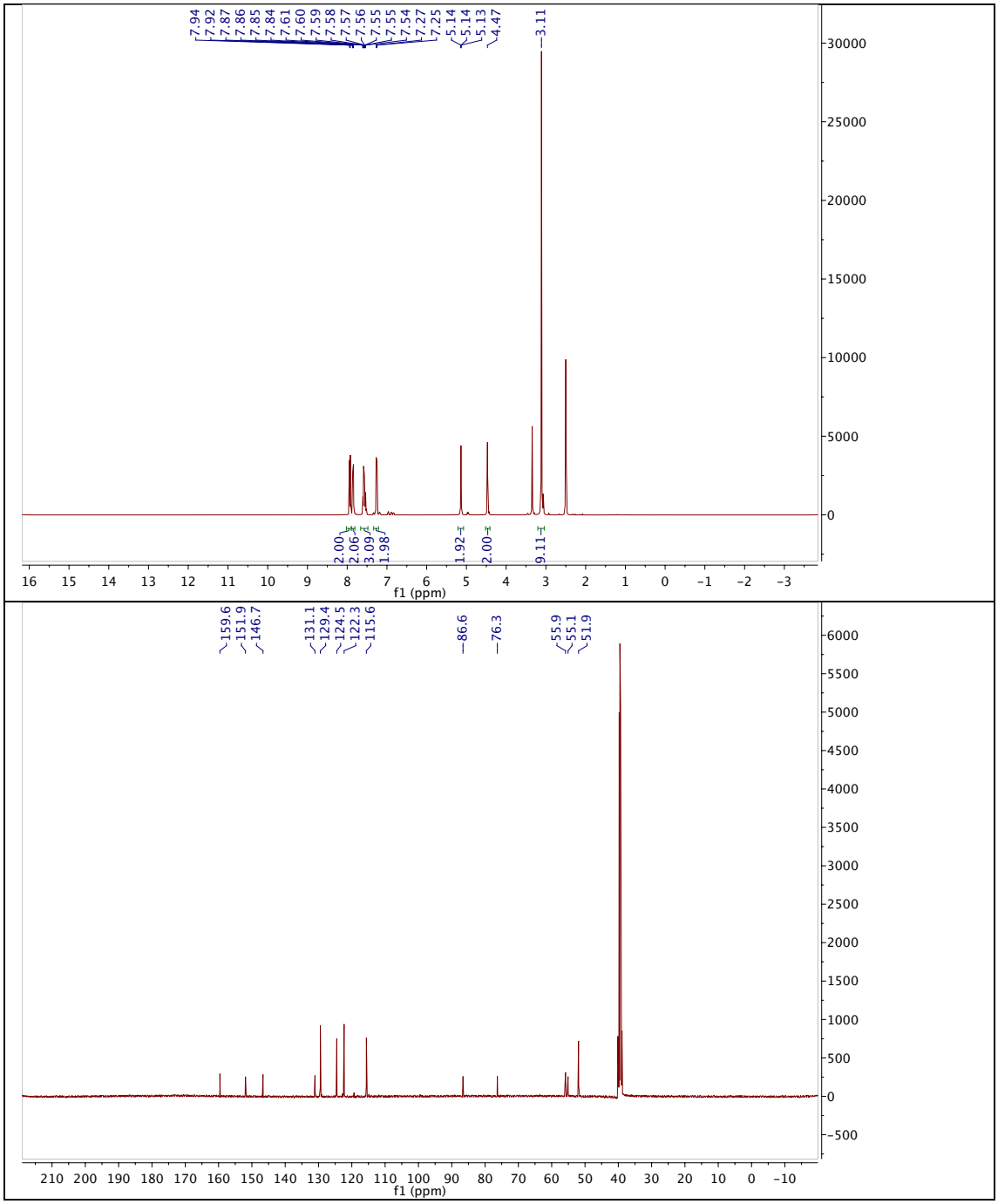

### 10.9.13 1,3-Dimethyl-5-nitrobenzene (10.14)

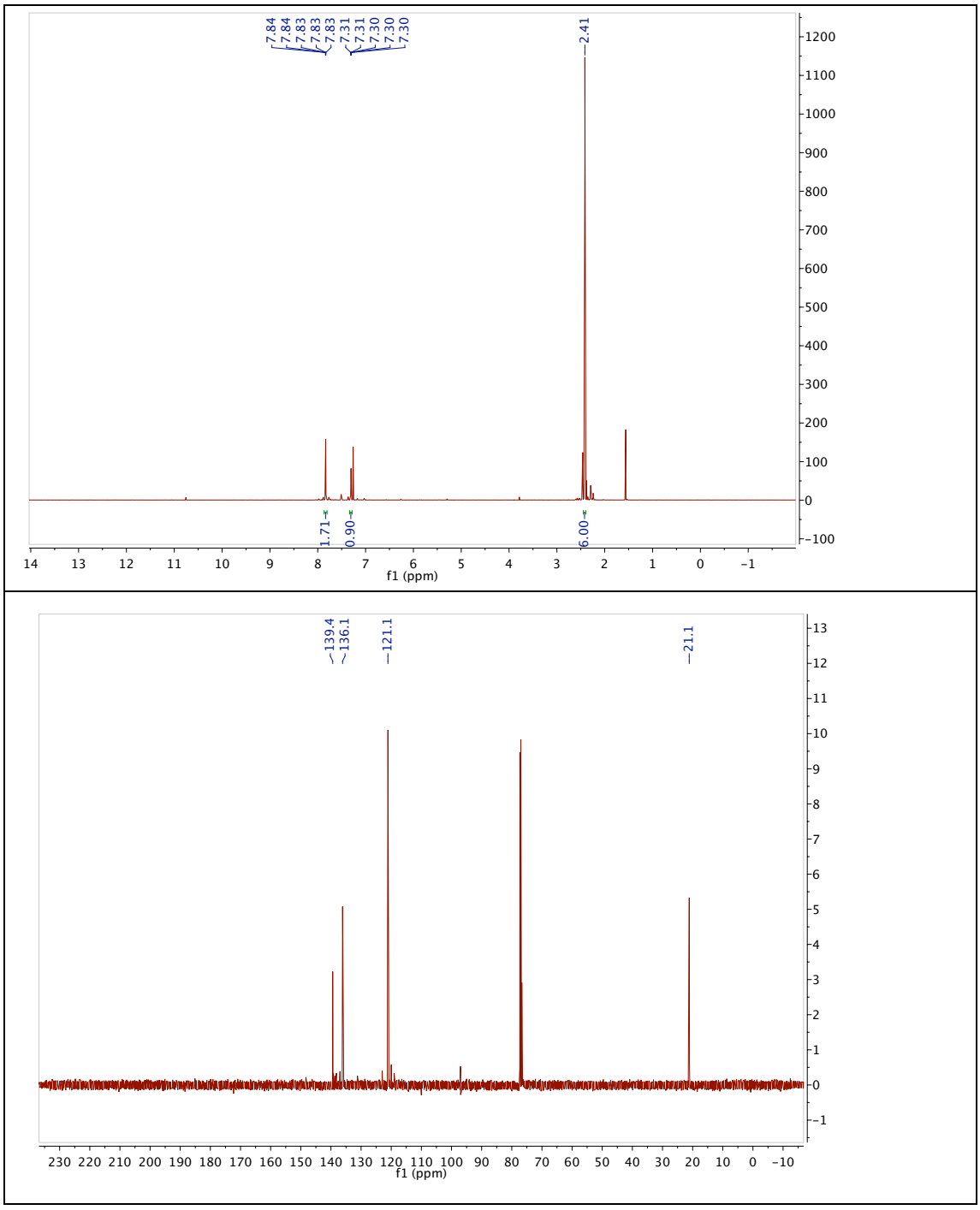

### 10.9.14 1,2-Bis(3,5-dimethylphenyl)hydrazine (10.16)

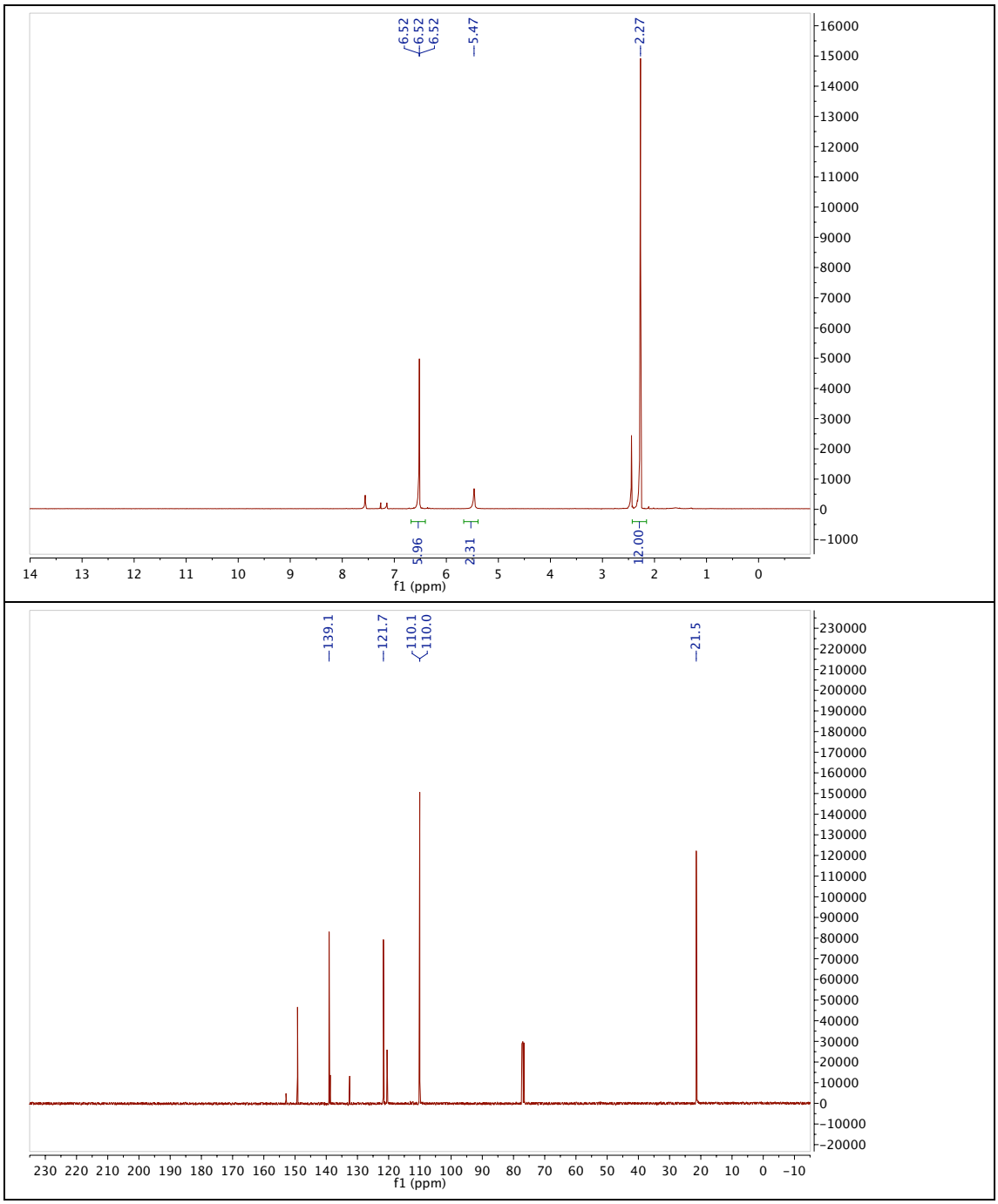

### 10.9.15 2,2',6,6'-Tetramethyl-[1,1'-biphenyl]-4,4'-diamine (10.17)

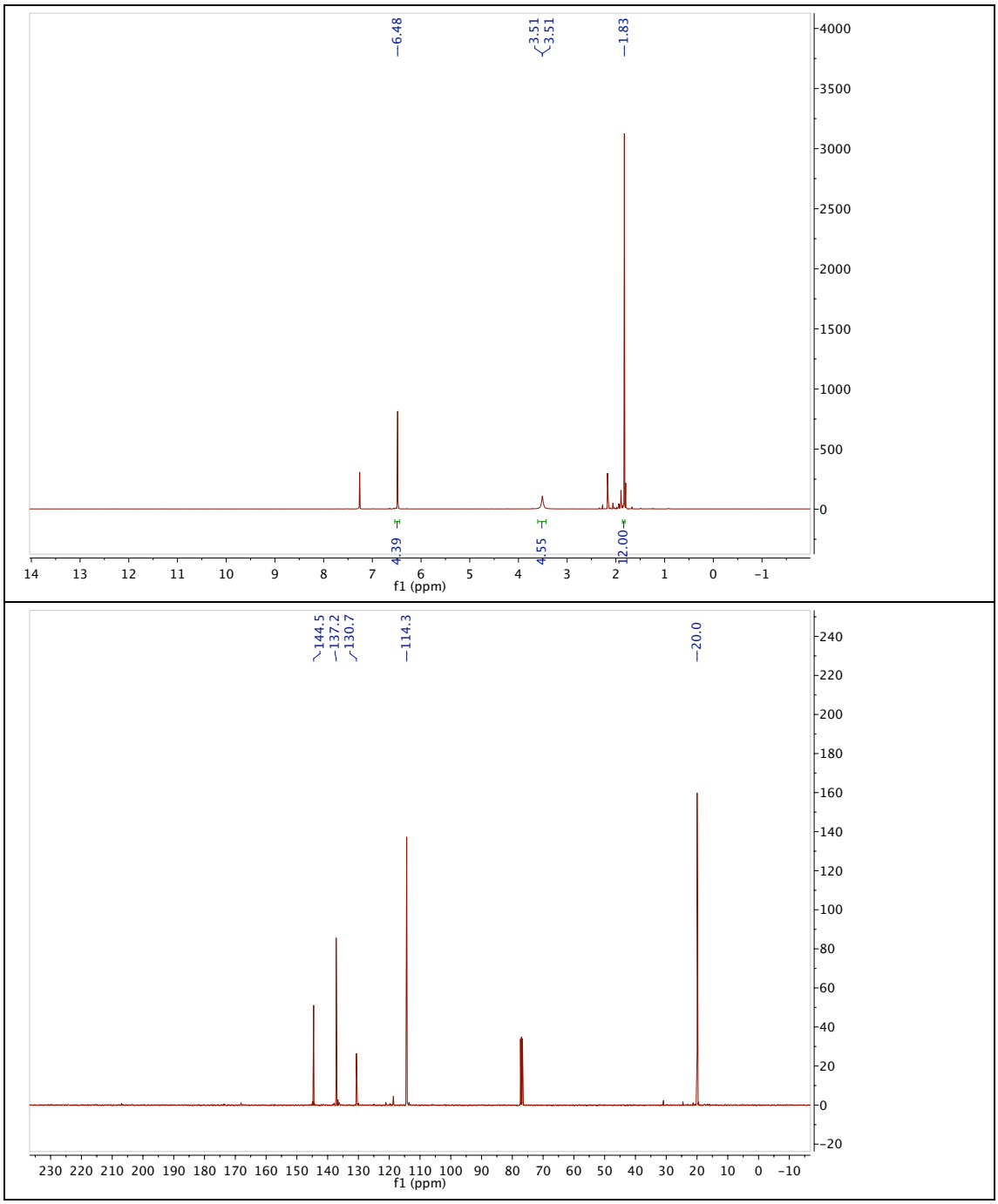

### 10.9.16 2,2'-(2,2',6,6'-Tetramethyl-[1,1'-biphenyl]-4,4'-diyl)bis(1-(4-nitrophenyl)diazene) (10.19)

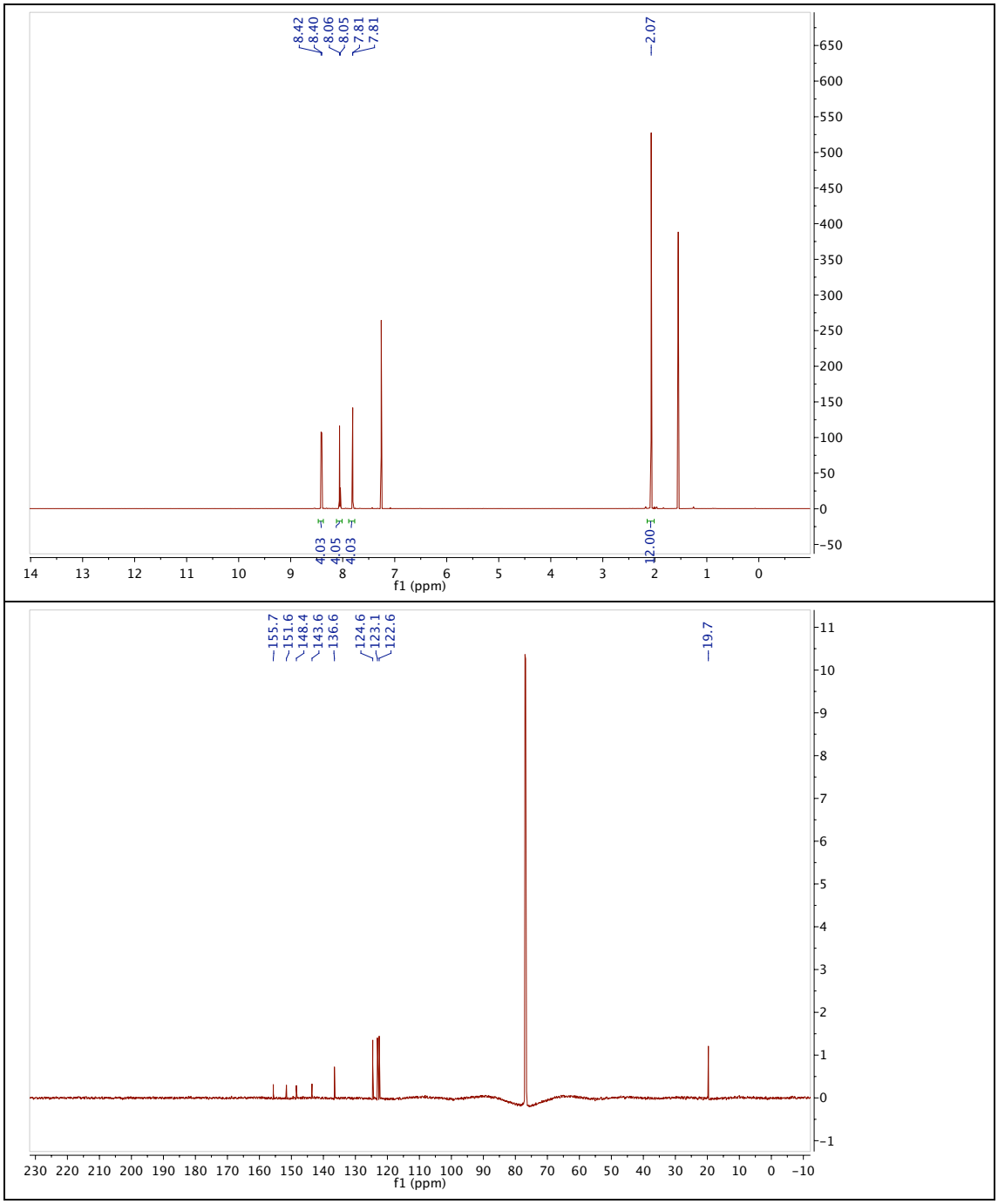

### 10.9.17 4,4'-(2,2',6,6'-Tetramethyl-[1,1'-biphenyl]-4,4'-diyl)bis(diazene-2,1-diyl))dianiline (10.20)

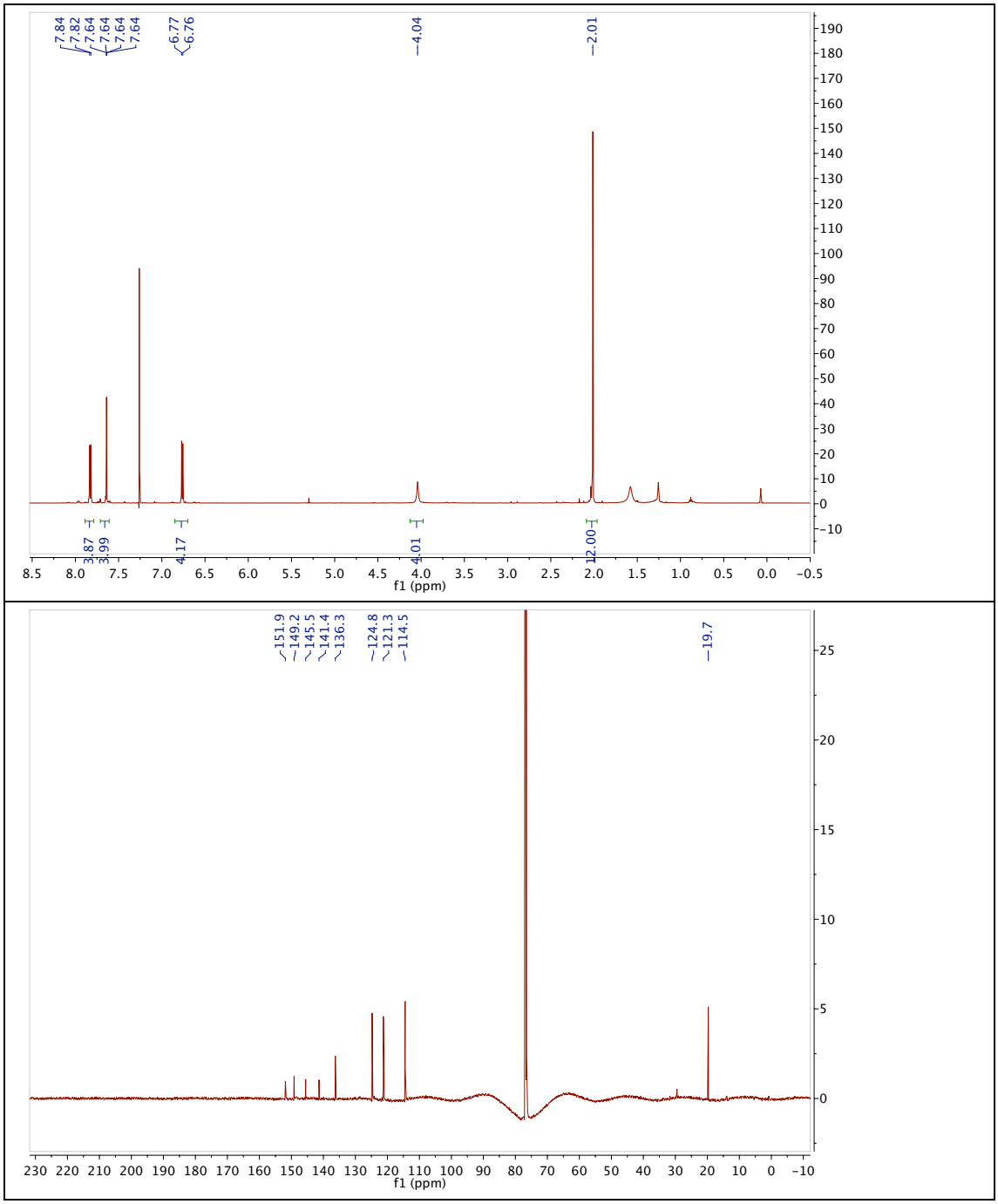

### 10.9.18 2,2'-((((1*E*,1'*E*)-(2,2',6,6'-Tetramethyl-[1,1'-biphenyl]-4,4'-diyl)bis-(diazene-2,1-diyl))bis(4,1-phenylene))bis(azanediyl))bis(*N*,*N*,*N*-triethyl-2-oxoethanaminium) chloride (QAAQ)

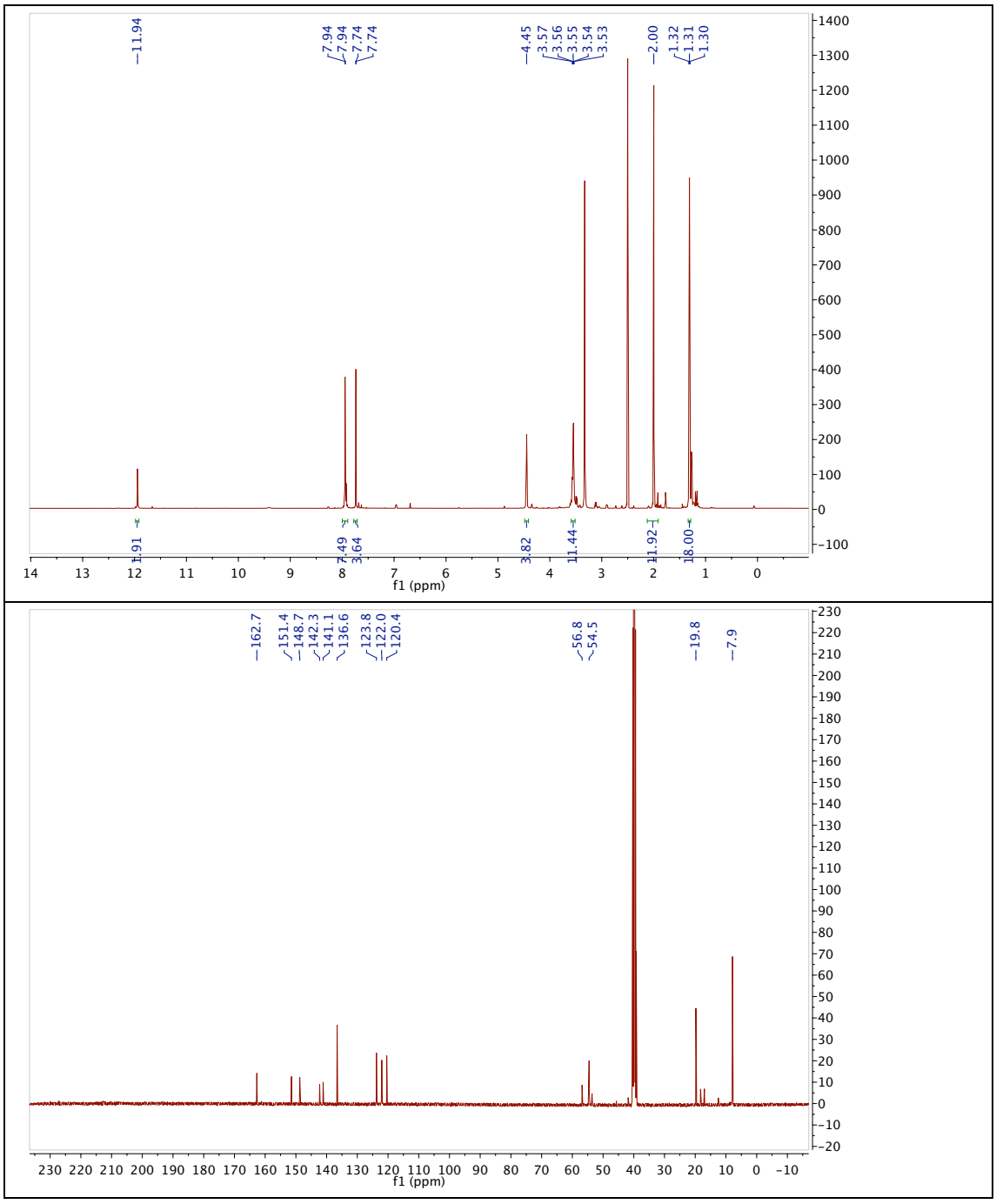

### 10.9.19 (*E*)-2-Methyl-3-(4-(phenyldiazenyl)phenyl)quinazolin-4(3*H*)-one (JB420)

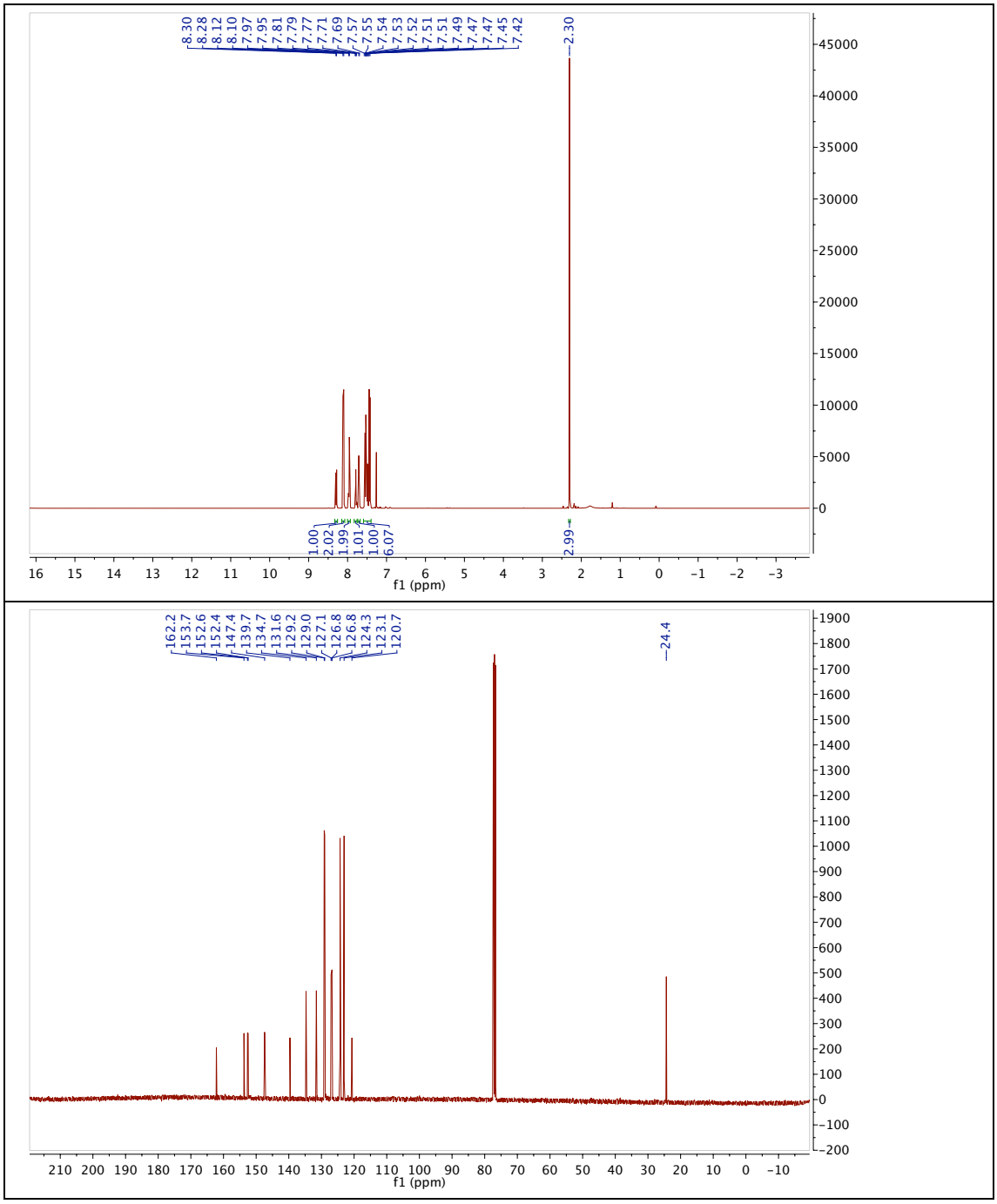

### 10.9.20 (*E*)-*N*,*N*,*N*-Trimethyl-2-(((4-(phenyldiazenyl)phenyl)carbamoyl)-oxy) ethanaminium chloride, AzoCarbachol Chloride

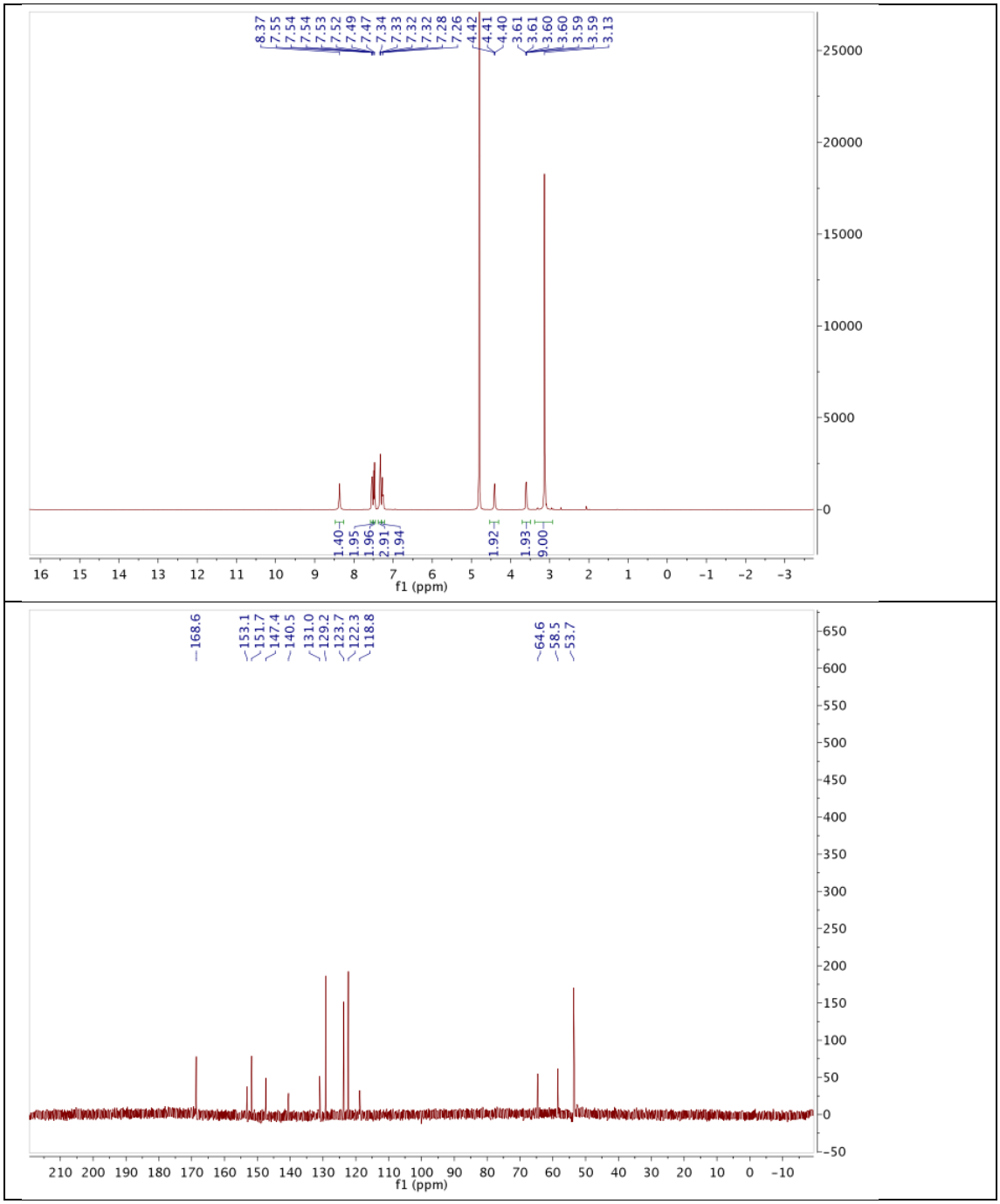

## 10.9.21 Ethyl (*E*)-(4-(phenyldiazenyl)phenyl)carbamate

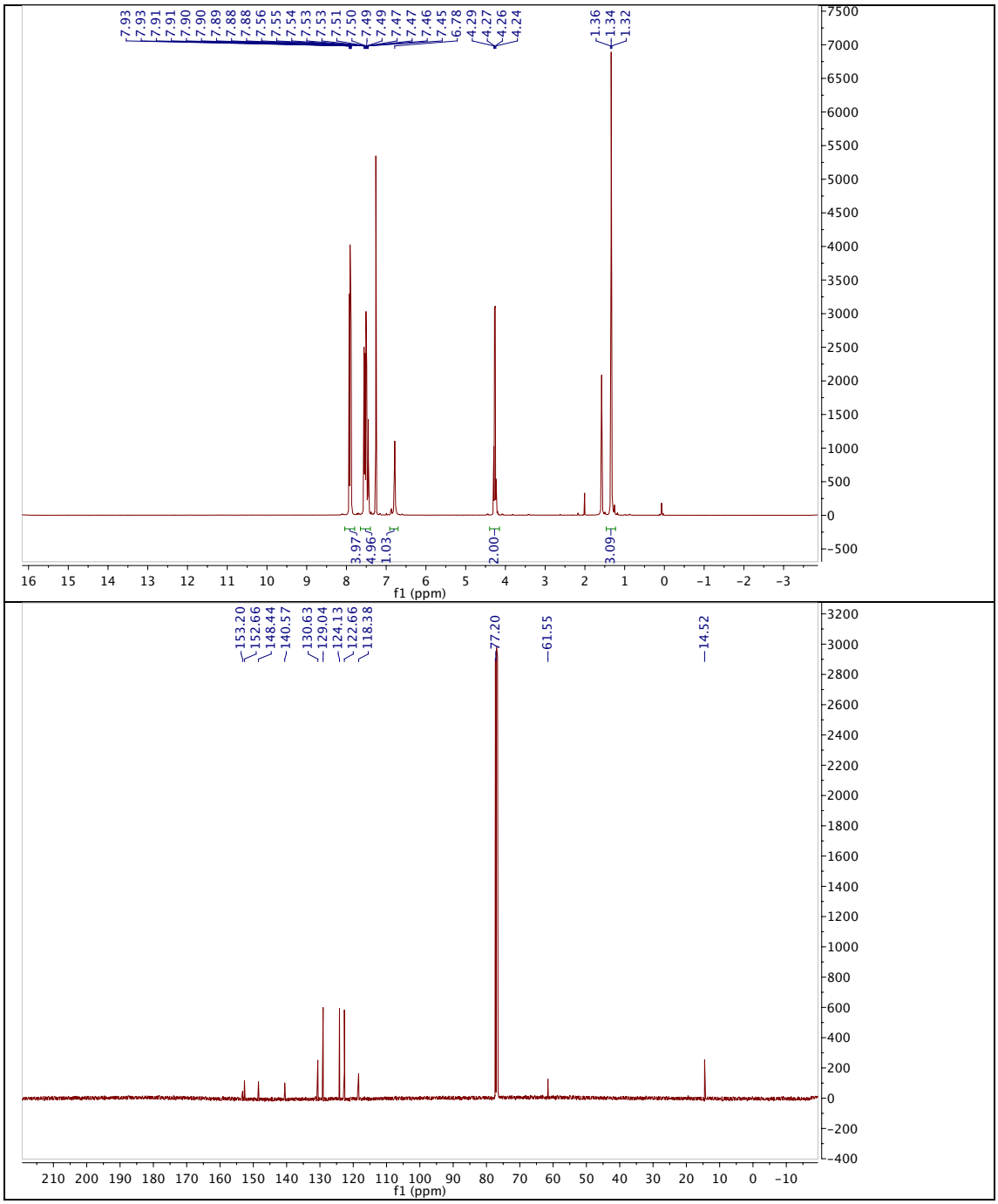

## 10.9.22 (*R*)-Methyl 4-nitro-3-(4-nitrophenyl)butanoate (10.24)

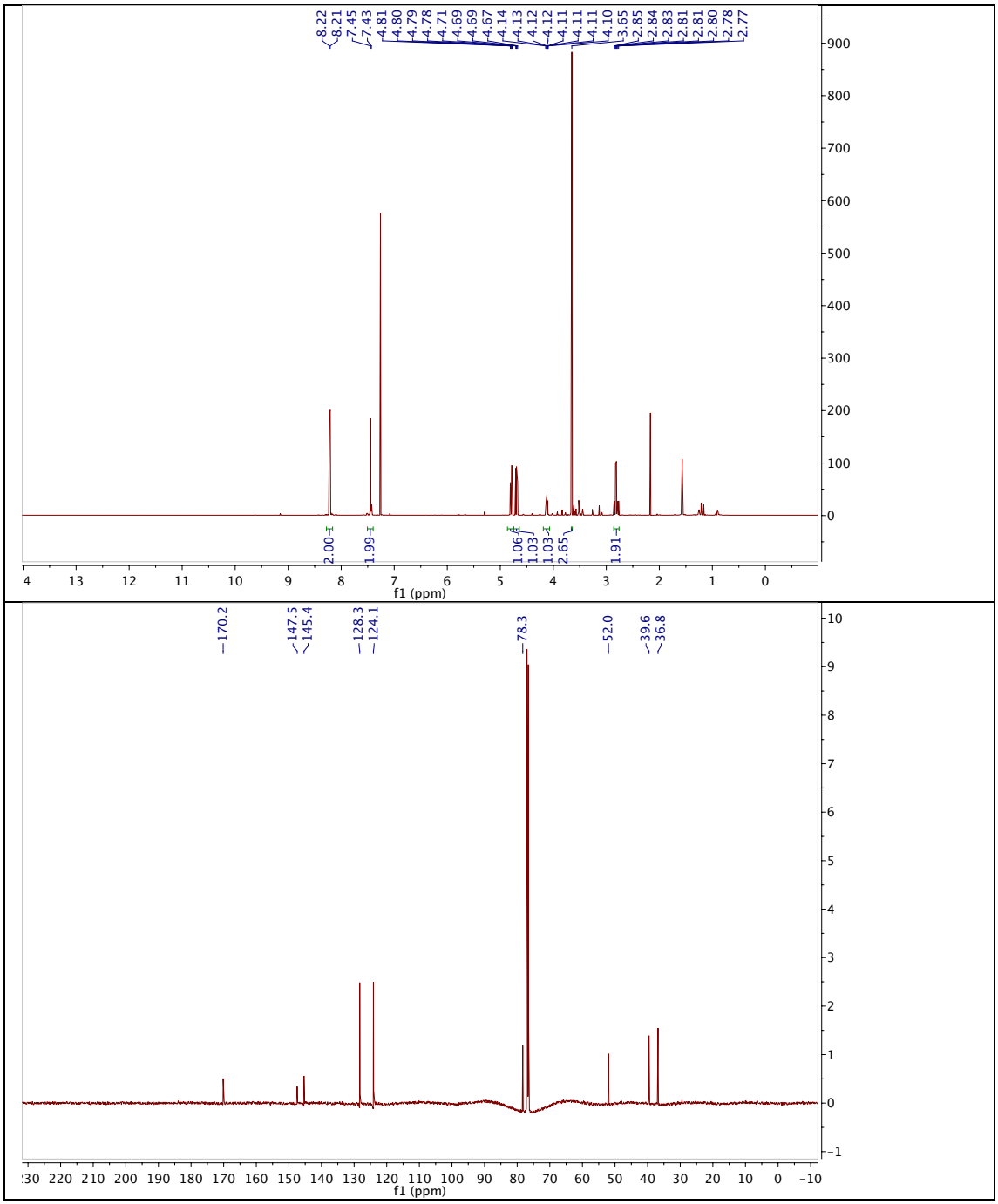

### 10.9.23 (*R*)-4-(4-Aminophenyl)pyrrolidin-2-one (10.25)

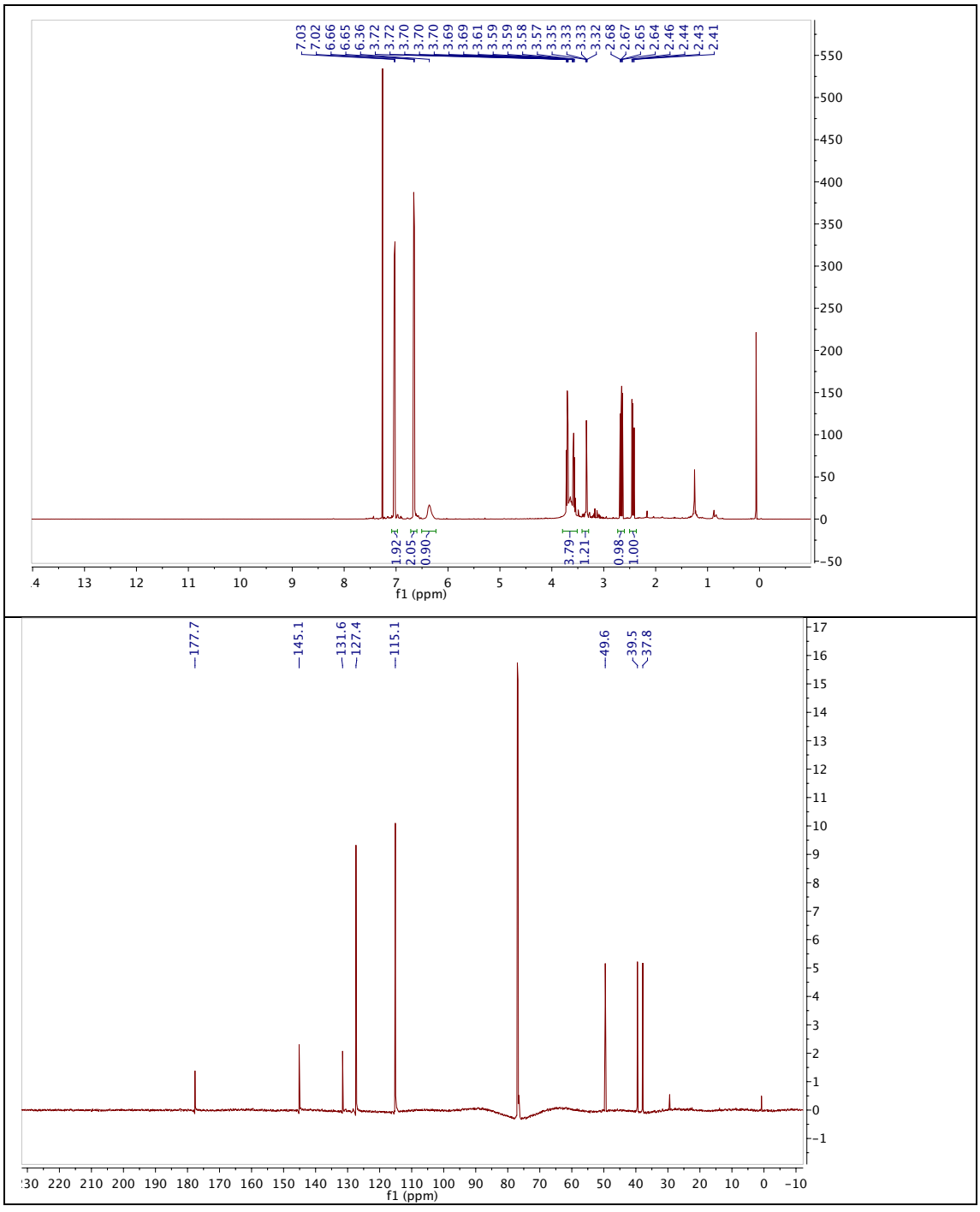

### 10.9.24 (*R*)-4-(4-(Phenyldiazenyl)phenyl)pyrrolidin-2-one (10.26)

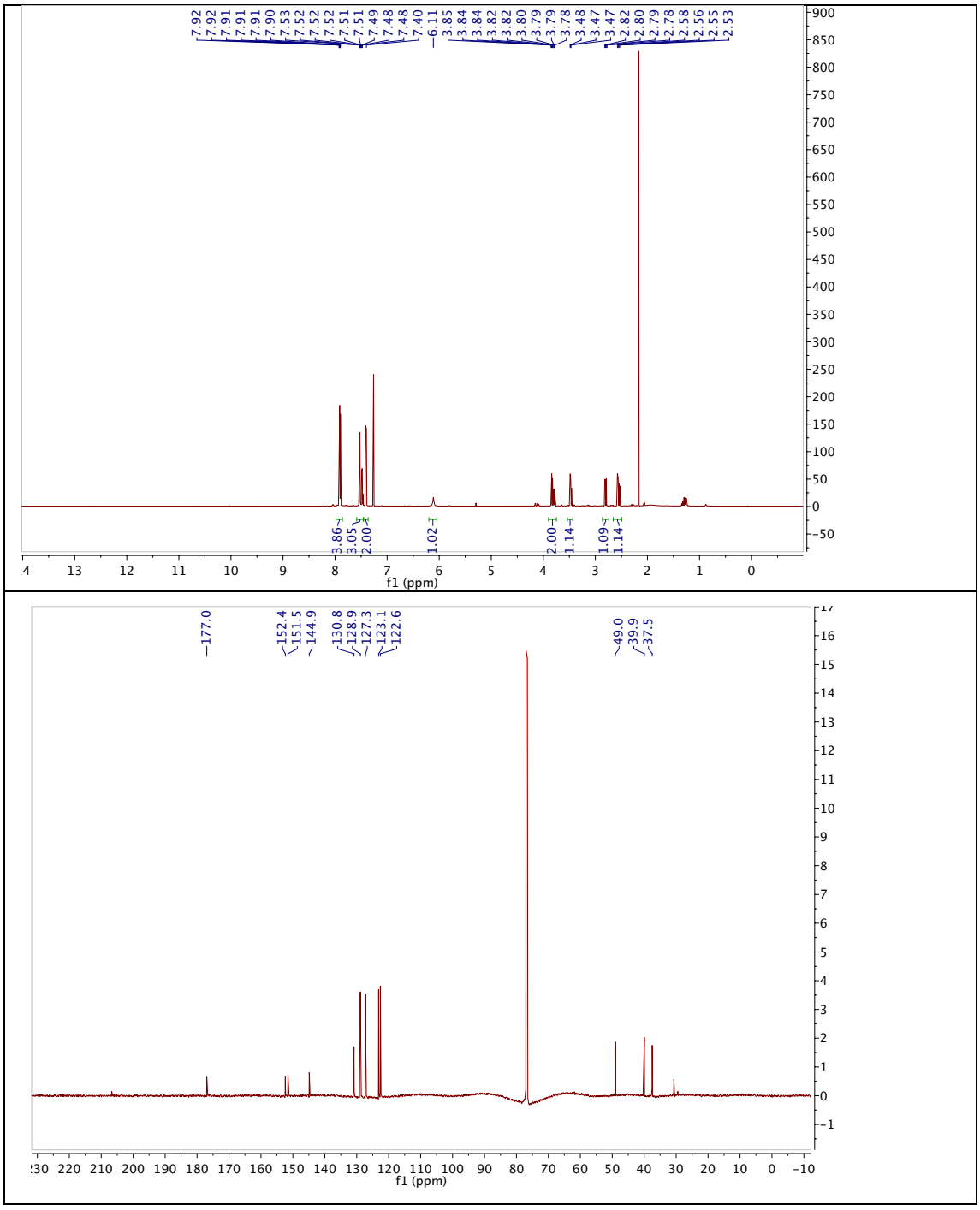

### 10.9.25 (*R*)-4-Amino-3-(4-(phenyldiazenyl)phenyl)butanoic acid hydro-chloride, AzoGABA HCl

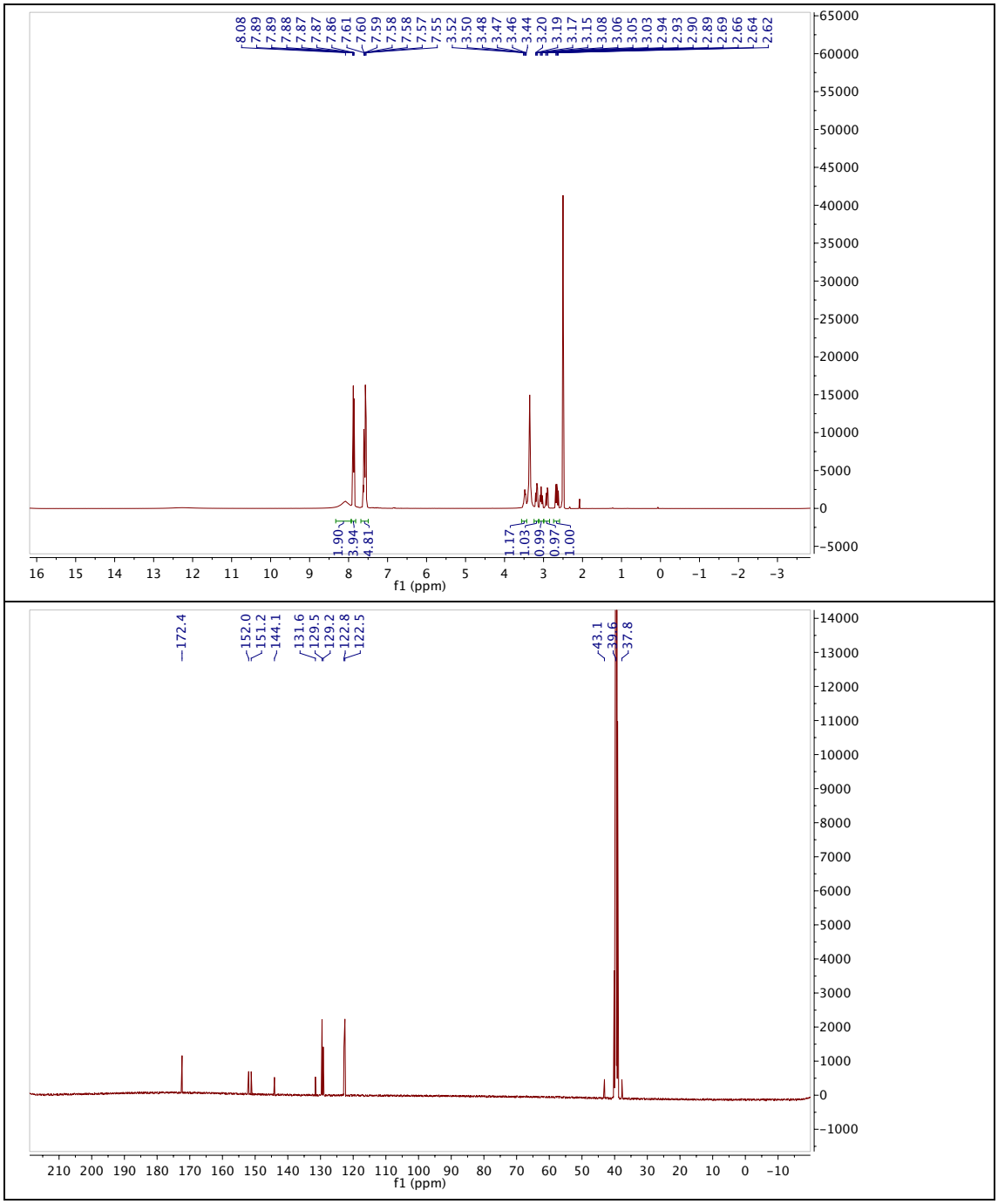

### 10.9.26 (*R*,*E*)-4-(4-((4-(Diethylamino)phenyl)diazenyl)phenyl)-pyrrolidin-2-one (10.27)

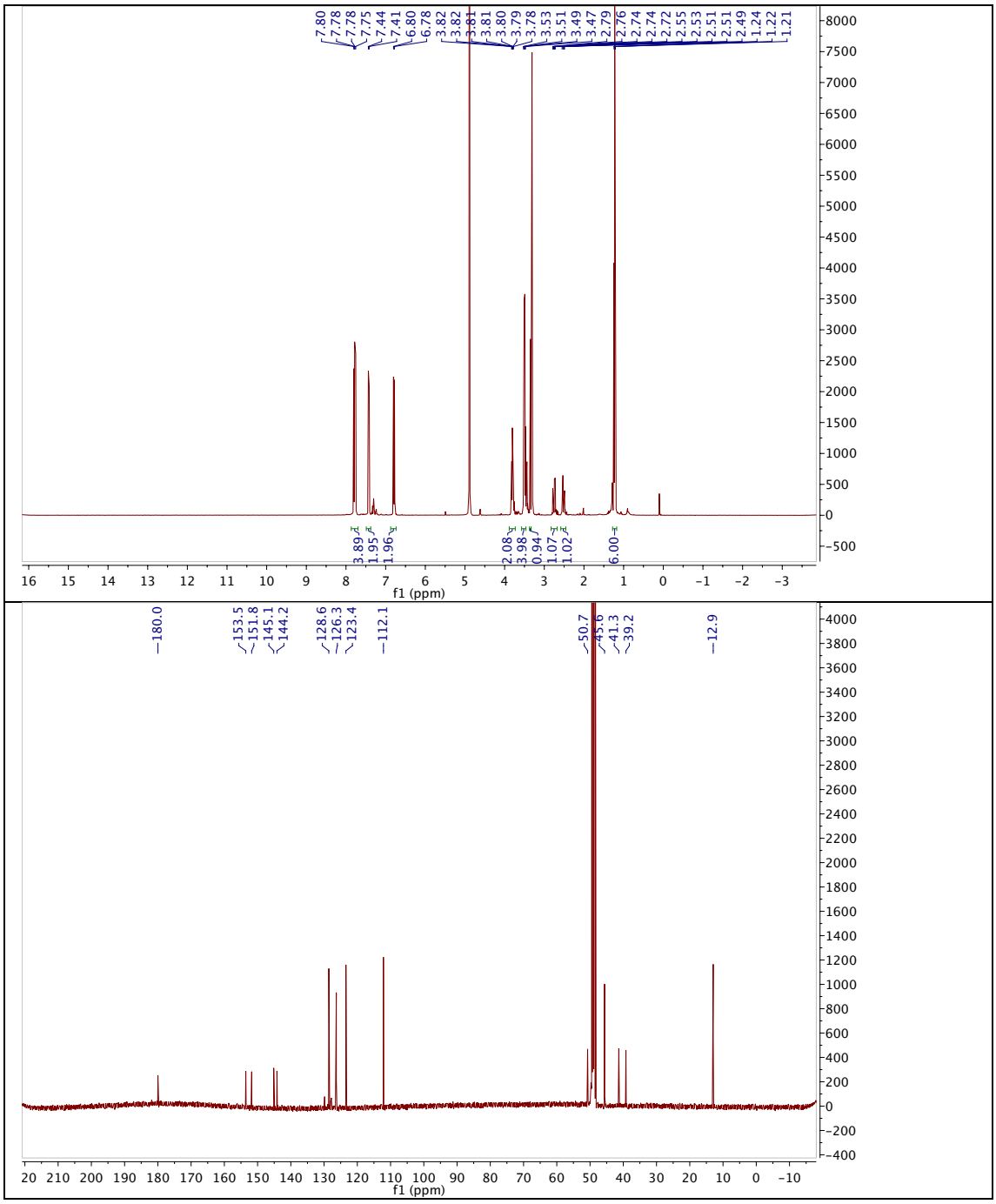

### 10.9.27 (*R*,*E*)-4-Amino-3-(4-((4-(diethylamino)phenyl)diazenyl)phenyl) butanoic acid hydrochloride salt, Red-AzoGABA HCl

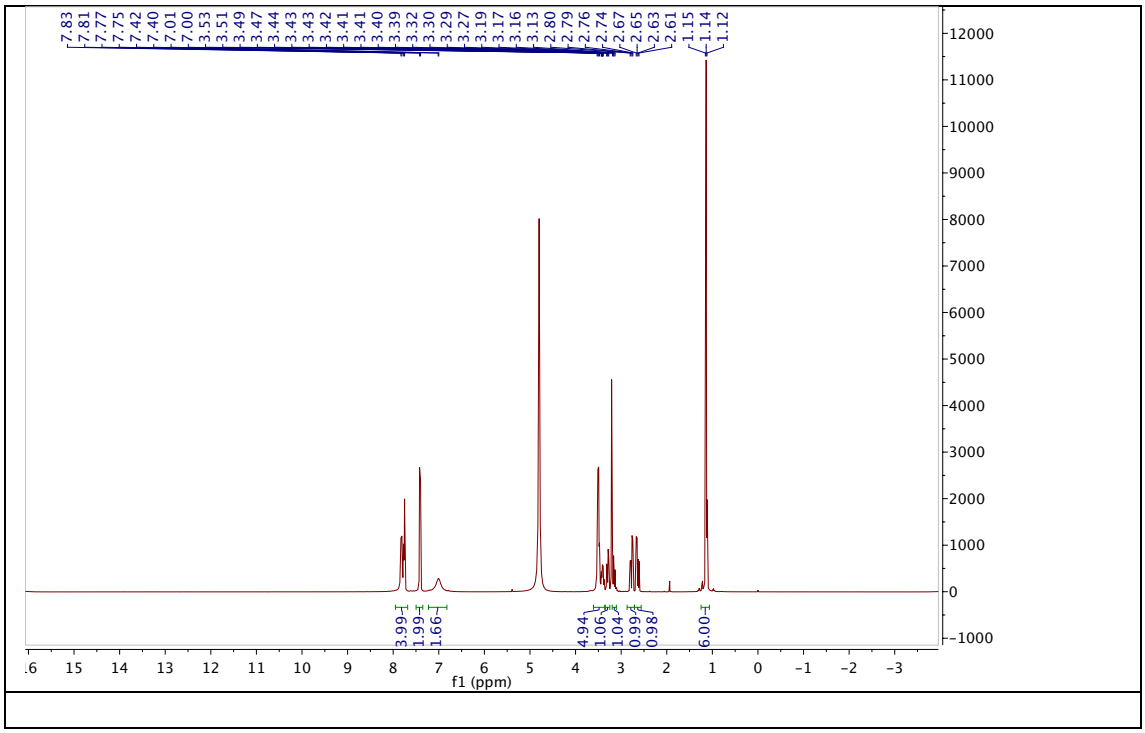

### 10.9.28 *tert*-Butyl (3-(2-(methylthio)-6-(trifluoromethyl)pyrimidin-4-yl)phenyl)-carbamate (10.30)

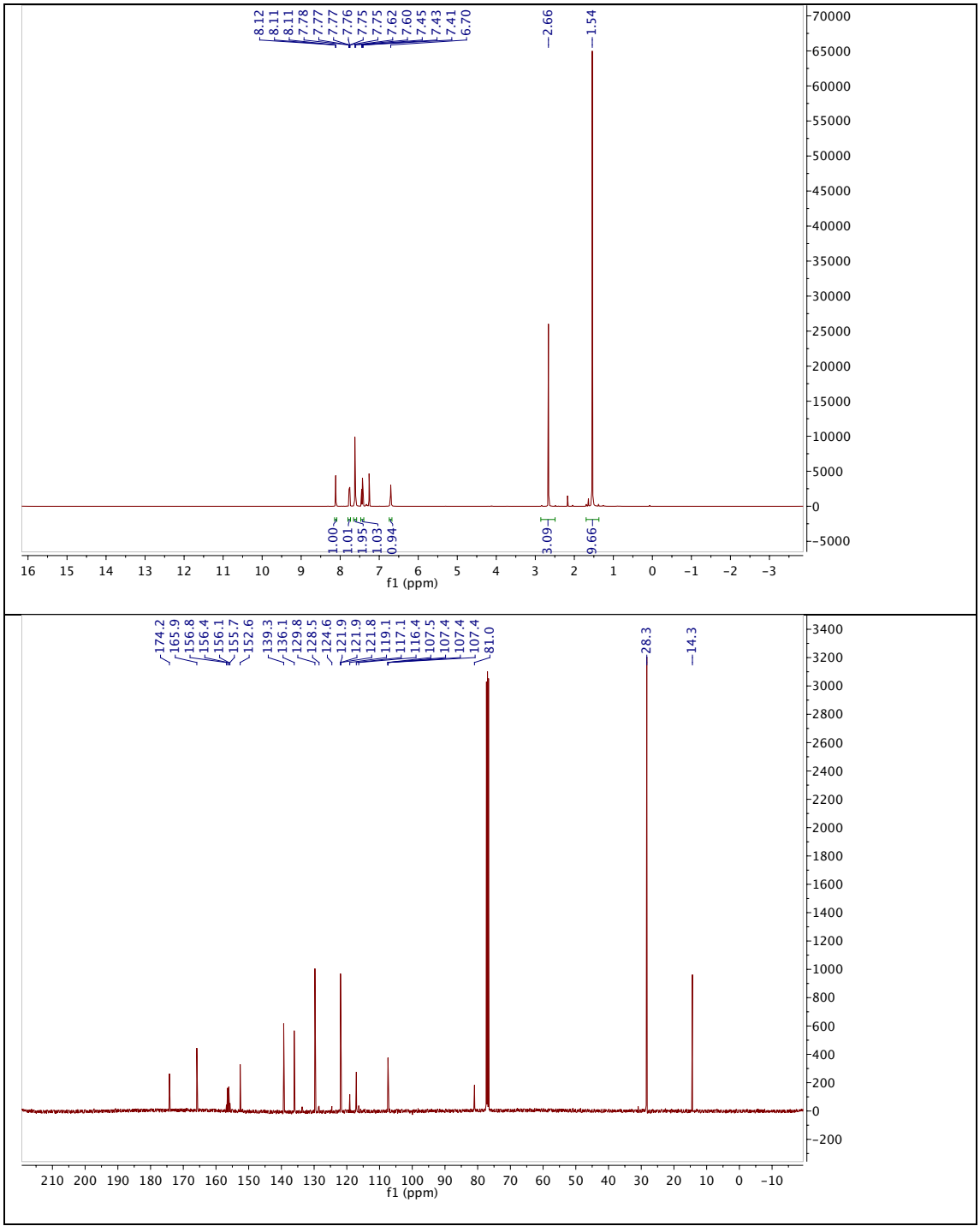

### 10.9.29 *tert*-Butyl (3-(2-(methylsulfonyl)-6-(trifluoromethyl)pyrimidin-4-yl)-phenyl)carbamate (10.31)

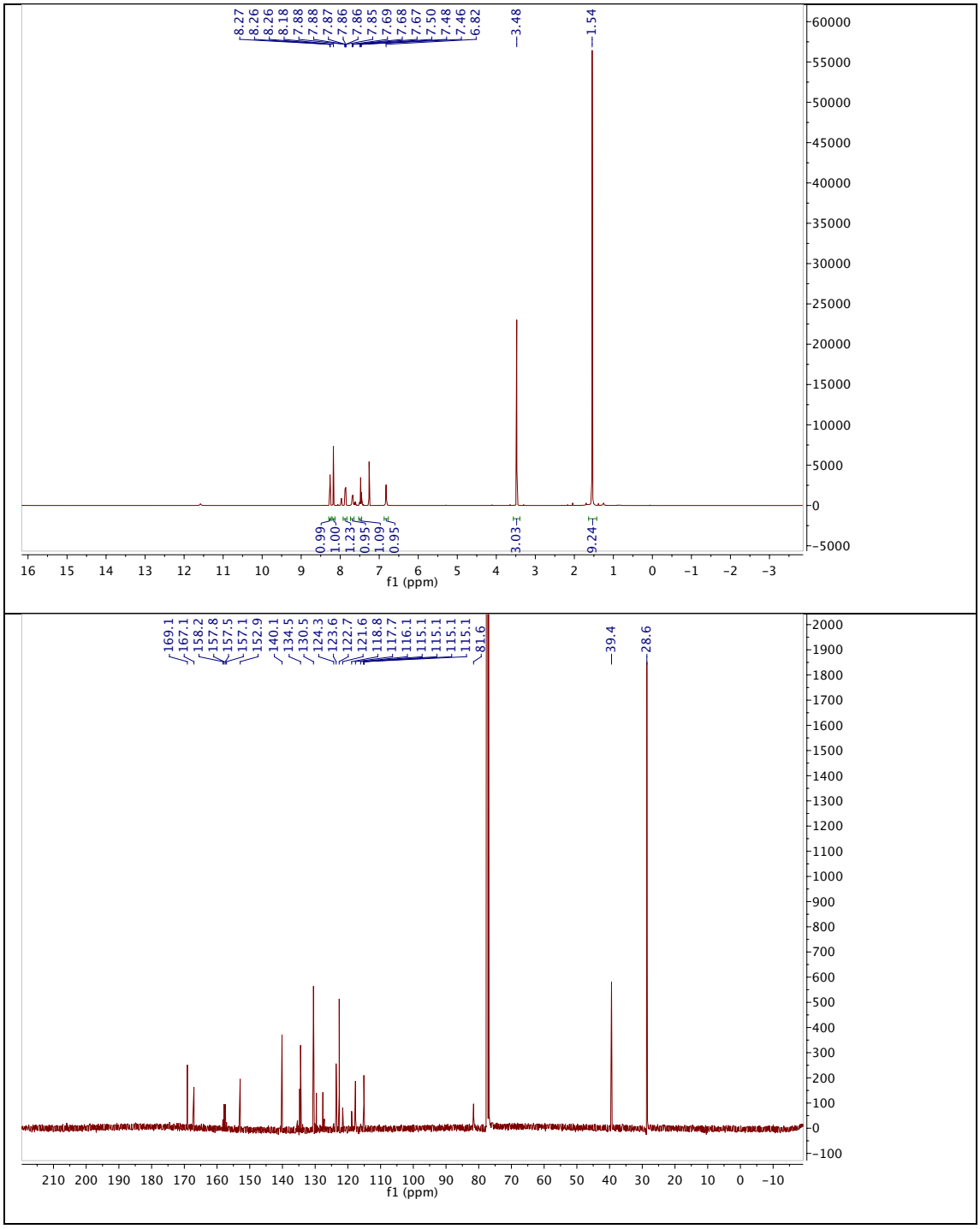

### 10.9.30 *tert*-Butyl (3-(2-(ethylthio)-6-(trifluoromethyl)pyrimidin-4-yl)phenyl)-carbamate (10.32)

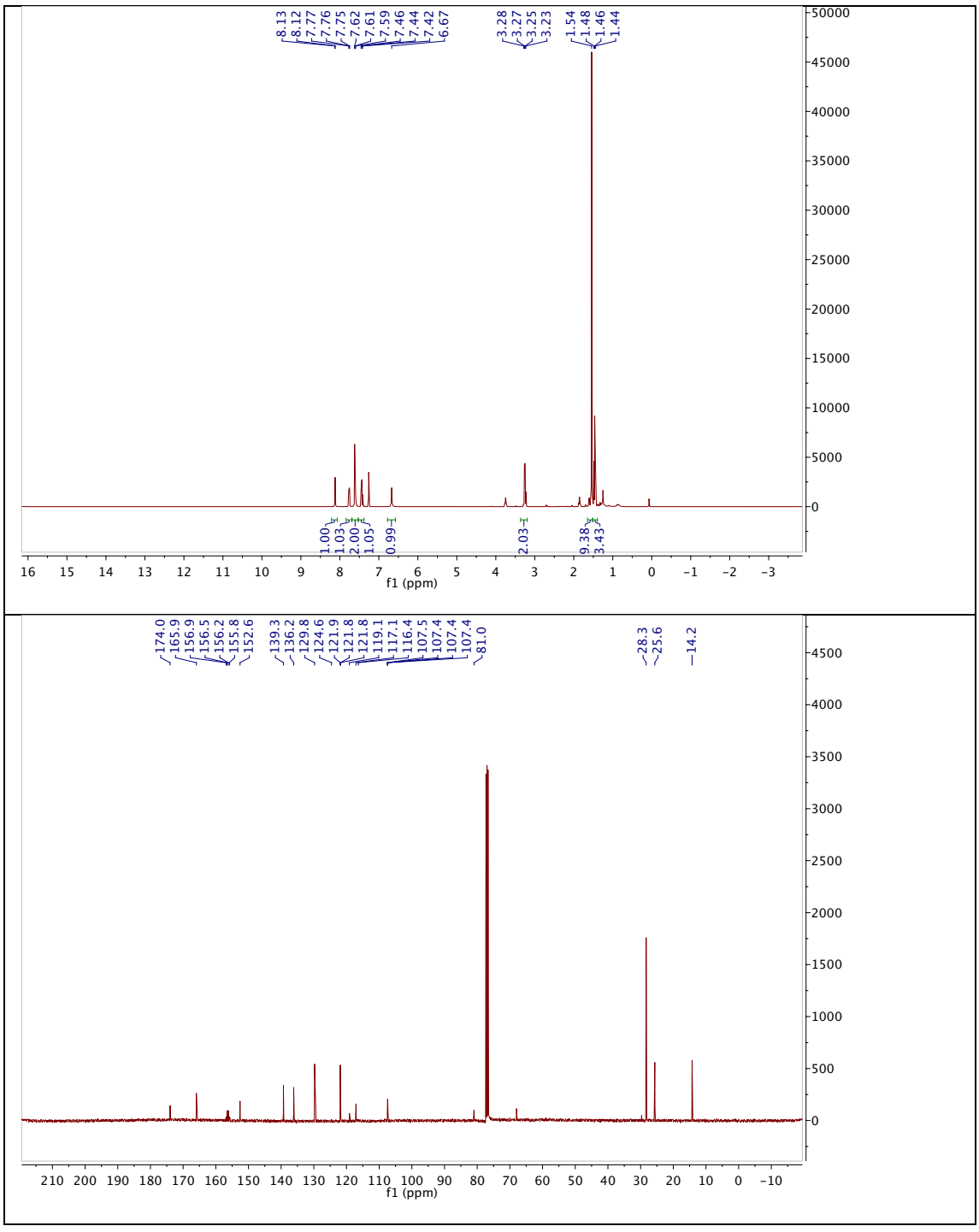

### 10.9.31 *tert*-Butyl (3-(2-(ethylsulfinyl)-6-(trifluoromethyl)pyrimidin-4-yl)-phenyl)carbamate (10.33)

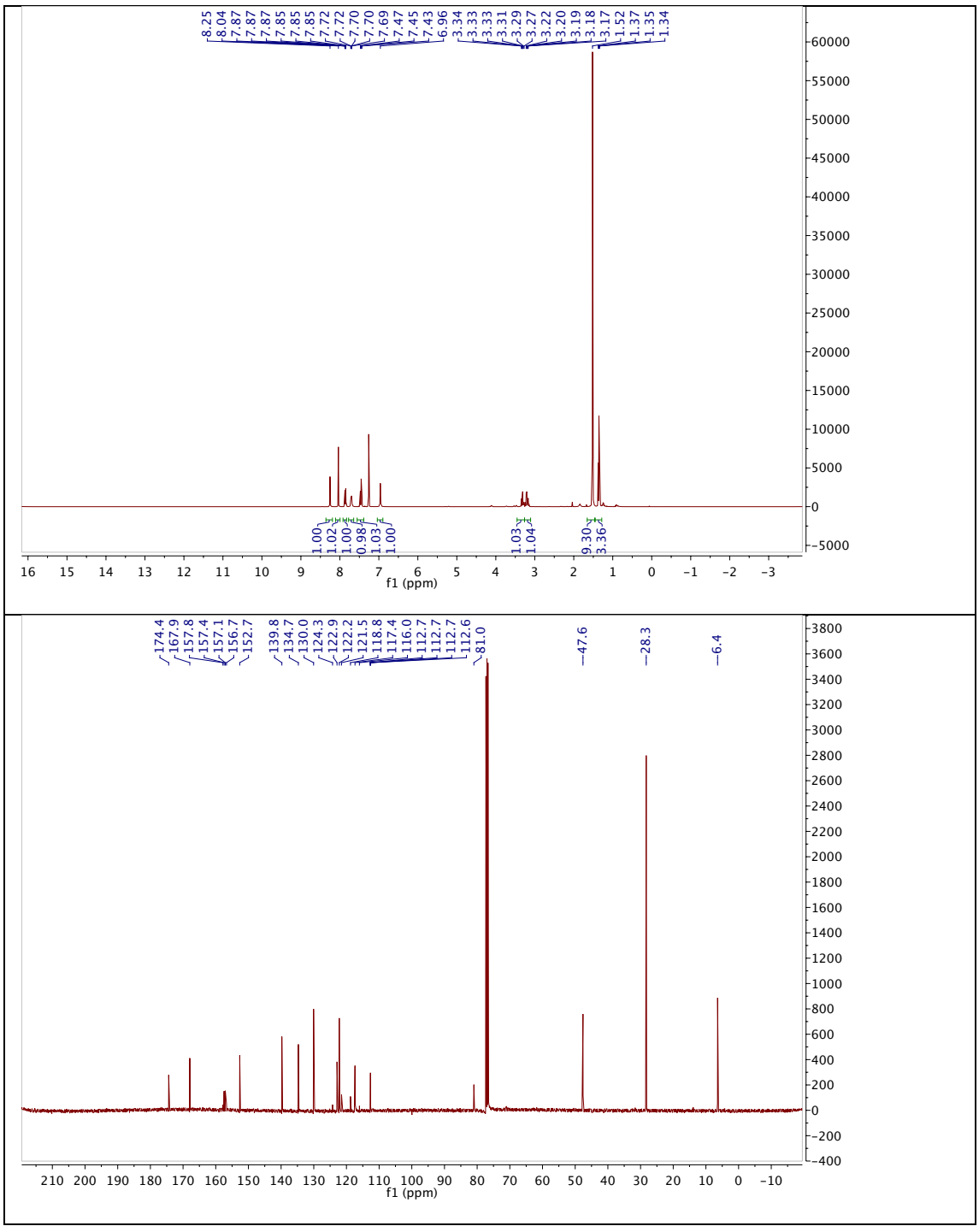

### 10.9.32 (*E*)-2-(Ethylsulfinyl)-4-(3-(phenyldiazenyl)phenyl)-6-(trifluoro-methyl)pyrimidine (AzoBETP)

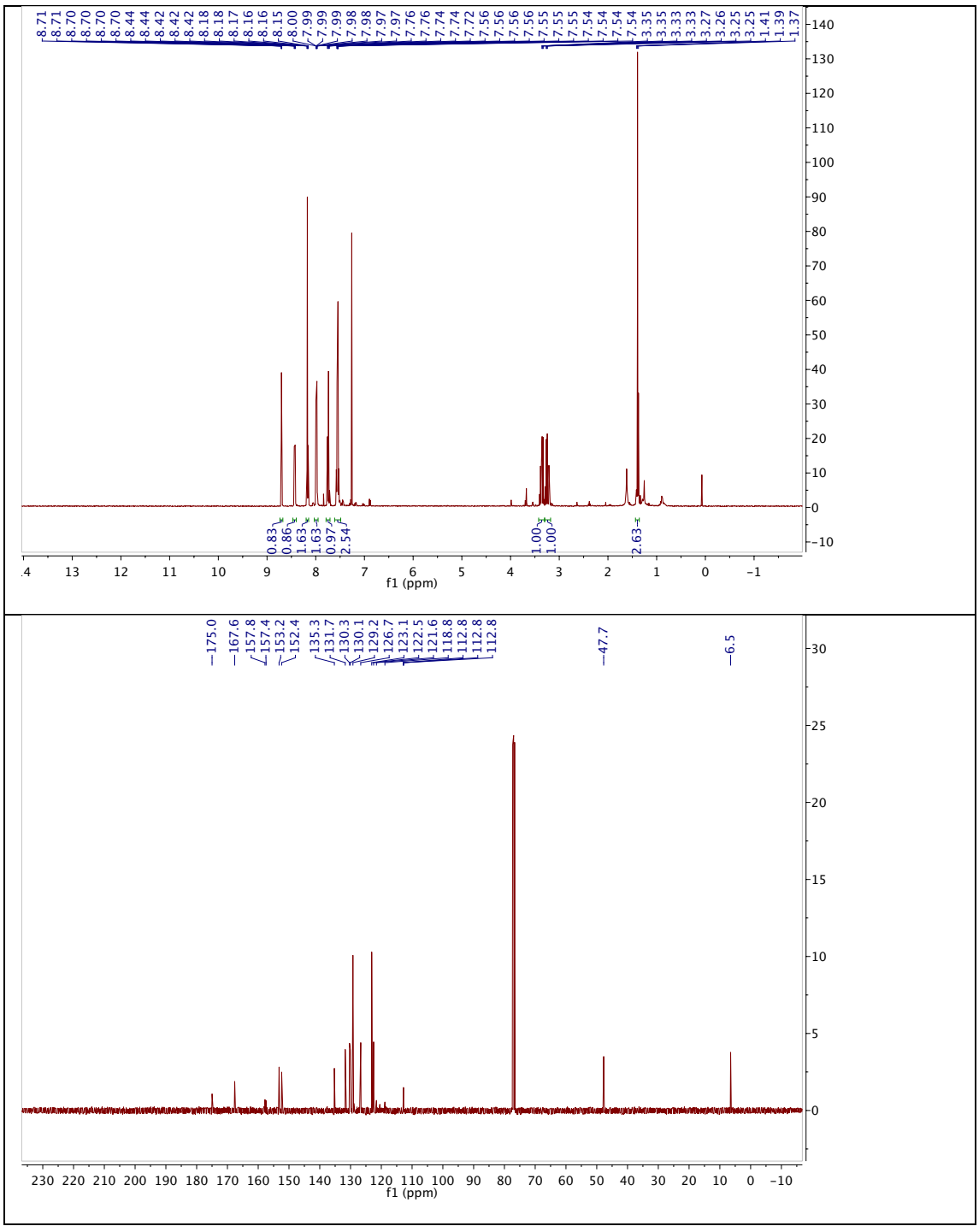

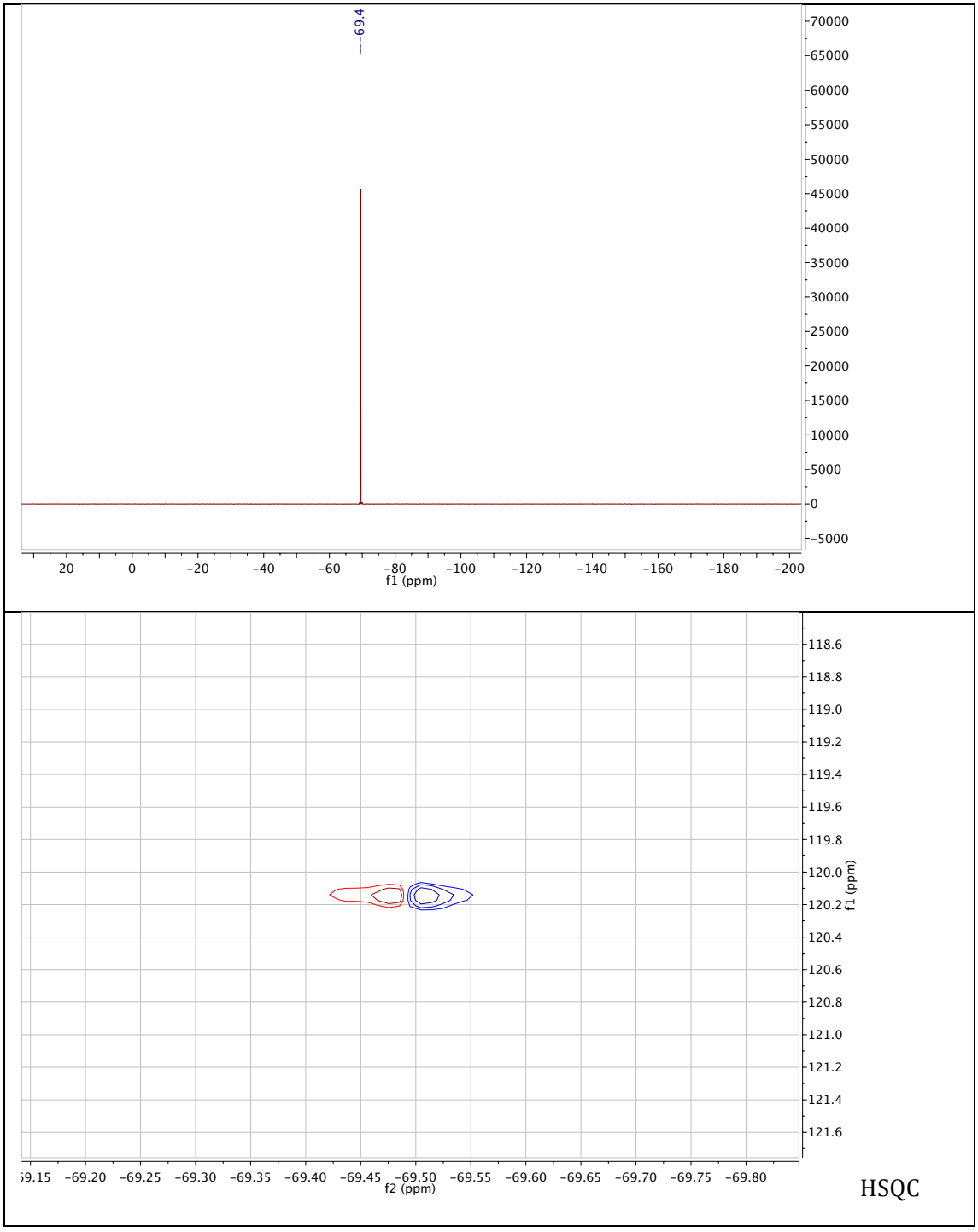
-69.4
70000
65000
60000
55000
50000
45000
40000
35000
30000
25000
20000
15000
10000
5000
0
-5000
20
0
-20
-40
-60
-80
-100
-120
-140
-160
-180
-200
f1 (ppm)
118.6
118.8
119.0
119.2
119.4
119.6
119.8
120.0
120.2
120.4
120.6
120.8
121.0
121.2
121.4
121.6
f1 (ppm)
-69.15
-69.20
-69.25
-69.30
-69.35
-69.40
-69.45
-69.50
-69.55
-69.60
-69.65
-69.70
-69.75
-69.80
f2 (ppm)
HSQC

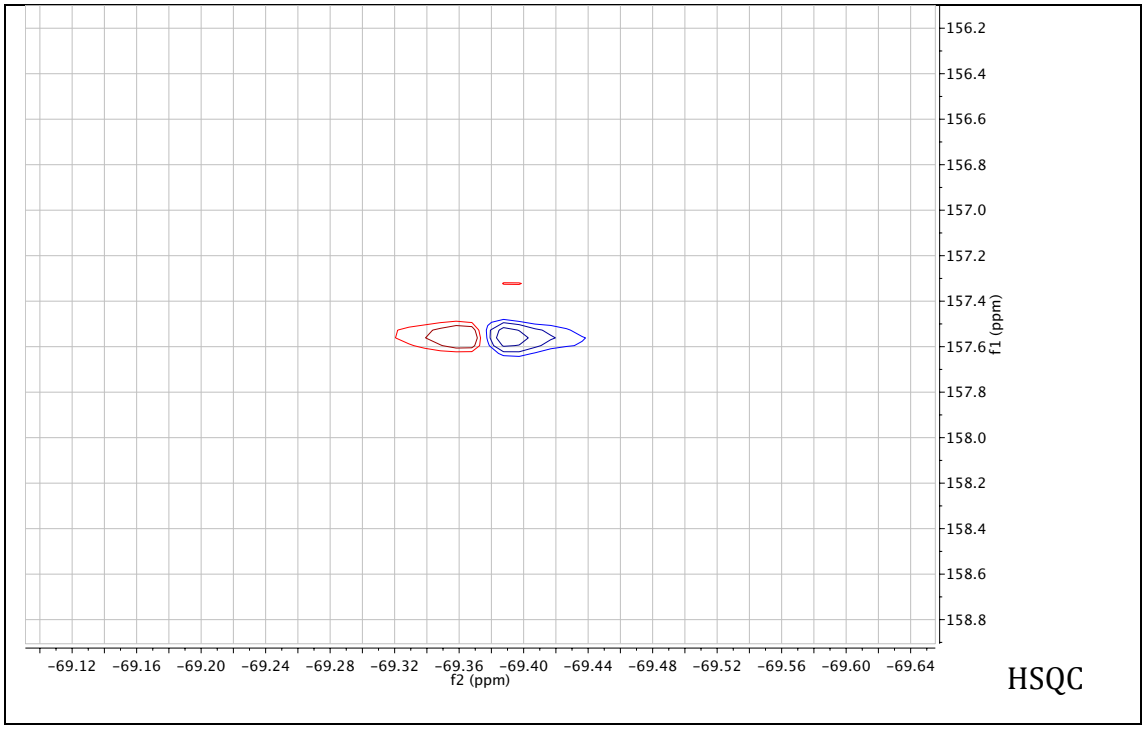
156.2
156.4
156.6
156.8
157.0
157.2
157.4
157.6
157.8
158.0
158.2
158.4
158.6
158.8
f1 (ppm)
-69.12
-69.16
-69.20
-69.24
-69.28
-69.32
-69.36
-69.40
-69.44
-69.48
-69.52
-69.56
-69.60
-69.64
f2 (ppm)
HSQC

### 10.9.33 (*E*)-4-((3-(2-(Ethylsulfinyl)-6-(trifluoromethyl)pyrimidin-4-yl)-phenyl)diazenyl)-*N*,*N*-dimethylaniline (redAzoBETP)

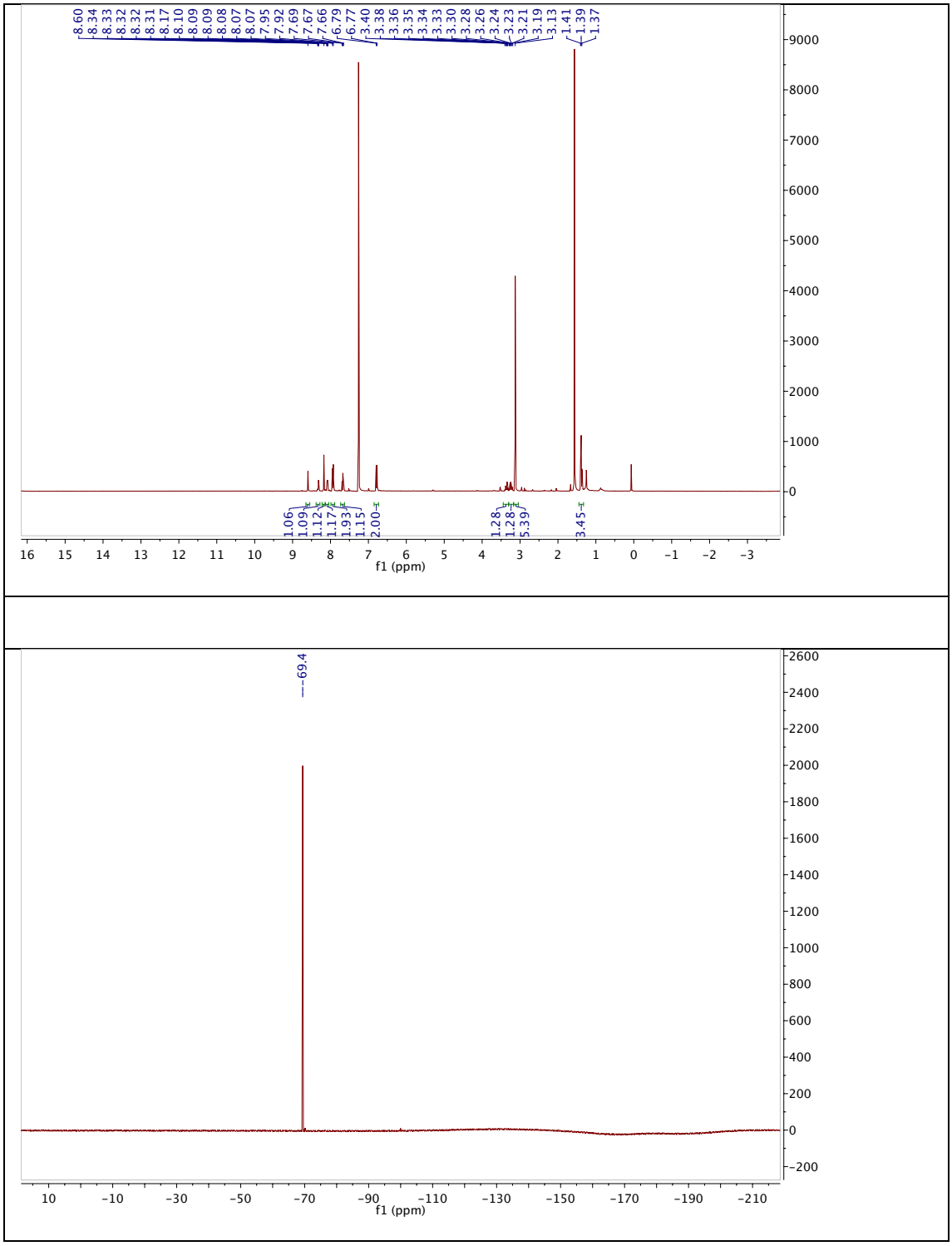

## 10.10 X-ray Crystallographic Data

### 10.10.1 (*E*)-4-((4-(Dimethylamino)phenyl)diazenyl)-*N*-(2-morpholinophenyl) benzenesulfonamide (JB556)

**Supplementary Table 20: Crystallographic data of JB556.**

| | **JB556** |
|---|---|
| net formula | $C_{24}H_{27}N_5O_3S$ |
| $M_r$/g mol$^{-1}$ | 465.569 |
| crystal size/mm | 0.140 × 0.100 × 0.080 |
| $T$/K | 173(2) |
| radiation | 'Mo Kα |
| diffractometer | 'Bruker D8Venture' |
| crystal system | triclinic |
| space group | $P$1bar |
| $a$/Å | 10.0027(5) |
| $b$/Å | 15.3126(7) |
| $c$/Å | 15.6965(7) |
| α/° | 75.0450(13) |
| β/° | 89.5183(14) |
| γ/° | 88.9895(13) |
| $V$/Å$^3$ | 2322.38(19) |
| $Z$ | 4 |
| calc. density/g cm$^{-3}$ | 1.33158(11) |
| μ/mm$^{-1}$ | 0.176 |
| absorption correction | multi-scan |
| transmission factor range | 0.9206–0.9585 |
| refls. measured | 60667 |
| $R_{int}$ | 0.0342 |
| mean σ($I$)/$I$ | 0.0250 |

| | |
|---|---|
| θ range | 2.43–26.42 |
| observed refls. | 6994 |
| *x, y* (weighting scheme) | 0.0658, 0.9527 |
| hydrogen refinement | mixed |
| refls in refinement | 9530 |
| parameters | 607 |
| restraints | 0 |
| $R(F_{obs})$ | 0.0427 |
| $R_w(F^2)$ | 0.1280 |
| $S$ | 1.034 |
| shift/error$_{max}$ | 0.001 |
| max electron density/e Å$^{-3}$ | 0.386 |
| min electron density/e Å$^{-3}$ | −0.329 |

### 10.10.2 (*E*)-1,1'-(Diazene-1,2-diylbis(4,1-phenylene))bis(*N*,*N*,*N*-trimethylmethanaminium) iodide, BisQ

**Supplementary Table 21: Crystallographic data of BisQ.**

| | **BisQ** |
|---|---|
| net formula | $C_{20}H_{30}I_6N_4$ |
| $M_r$/g mol$^{-1}$ | 1087.906 |
| crystal size/mm | 0.067 × 0.044 × 0.011 |
| $T$/K | 100(2) |
| radiation | 'Mo Kα |
| diffractometer | 'Bruker D8Venture' |
| crystal system | monoclinic |
| space group | $P2_1/n$ |
| $a$/Å | 8.6169(5) |
| $b$/Å | 21.6556(11) |
| $c$/Å | 9.0042(5) |
| α/° | 90 |
| β/° | 114.3280(15) |

| | |
|---|---|
| γ/° | 90 |
| $V$/Å$^3$ | 1531.02(15) |
| $Z$ | 2 |
| calc. density/g cm$^{-3}$ | 2.3599(2) |
| μ/mm$^{-1}$ | 6.101 |
| absorption correction | multi-scan |
| transmission factor range | 0.6537–0.7454 |
| refls. measured | 33124 |
| $R_{int}$ | 0.0528 |
| mean σ($I$)/$I$ | 0.0242 |
| θ range | 2.75–26.41 |
| observed refls. | 2609 |
| $x$, $y$ (weighting scheme) | 0.0307, 7.3926 |
| hydrogen refinement | constr |
| refls in refinement | 3134 |
| parameters | 139 |
| restraints | 0 |
| $R(F_{obs})$ | 0.0281 |
| $R_w(F^2)$ | 0.0699 |
| $S$ | 1.038 |
| shift/error$_{max}$ | 0.001 |
| max electron density/e Å$^{-3}$ | 1.854 |
| min electron density/e Å$^{-3}$ | −0.691 |

Symmetry code i = 1−$x$, 1−$y$, 1−$z$.

### 10.10.3 (*E*)-*N*,*N*,*N*-Trimethyl-2-(4-(phenyldiazenyl)phenoxy)ethanaminium iodide, AzoCholine

**Supplementary Table 22: Crystallographic data of AzoCholine.**

| | **AzoCholine** |
|---|---|

| | |
|---|---|
| net formula | $C_{17}H_{22}IN_3O$ |
| $M_r$/g mol$^{-1}$ | 411.281 |
| crystal size/mm | 0.120 × 0.110 × 0.020 |
| $T$/K | 293(2) |
| radiation | 'Mo Kα |
| diffractometer | 'Bruker D8Quest' |
| crystal system | monoclinic |
| space group | $P2_1$ |
| $a$/Å | 5.9981(4) |
| $b$/Å | 7.7485(5) |
| $c$/Å | 19.4519(13) |
| α/° | 90 |
| β/° | 93.6786(18) |
| γ/° | 90 |
| $V$/Å$^3$ | 902.19(10) |
| $Z$ | 2 |
| calc. density/g cm$^{-3}$ | 1.51400(17) |
| μ/mm$^{-1}$ | 1.780 |
| absorption correction | multi-scan |
| transmission factor range | 0.6595–0.7452 |
| refls. measured | 16166 |
| $R_{int}$ | 0.0424 |
| mean σ($I$)/$I$ | 0.0375 |
| θ range | 2.83–25.38 |
| observed refls. | 2633 |
| *x, y* (weighting scheme) | 0.0541, 0.5108 |
| hydrogen refinement | constr |
| Flack parameter | 0.00(17) |
| refls in refinement | 3303 |
| parameters | 202 |
| restraints | 1 |
| $R(F_{obs})$ | 0.0424 |
| $R_w(F^2)$ | 0.1026 |

| | |
|---|---|
| $S$ | 1.087 |
| shift/error$_{max}$ | 0.001 |
| max electron density/e Å$^{-3}$ | 0.748 |
| min electron density/e Å$^{-3}$ | −0.370 |

Verfeinert als racemischer Zwilling, -N=N-Fragment fehlgeordnet, Splitmodell, Besetzungsverhältnis 0.45/0.44, isotrope Verfeinerung der fehlgeordneten Atome.

### 10.10.4 AzoCarbachol Chloride

**Supplementary Table 23: Crystallographic data of AzoCarbachol chloride**

| | **AzoCarbachol chloride** |
|---|---|
| net formula | C18H23ClN4O2 |
| Mr/g mol−1 | 362.854 |
| crystal size/mm | 0.120 × 0.100 × 0.080 |
| T/K | 100(2) |
| radiation | 'Mo Kα |
| diffractometer | 'Bruker D8Venture' |
| crystal system | monoclinic |
| space group | P21/c |
| a/Å | 7.0840(3) |
| b/Å | 9.0991(4) |
| c/Å | 28.2695(13) |
| α/° | 90 |
| β/° | 91.7903(12) |
| γ/° | 90 |
| V/Å3 | 1821.31(14) |
| Z | 4 |
| calc. density/g cm−3 | 1.32331(10) |
| μ/mm−1 | 0.229 |
| absorption correction | multi-scan |

| | |
|---|---|
| transmission factor range | 0.7999–0.8620 |
| refls. measured | 19303 |
| Rint | 0.0258 |
| mean σ(I)/I | 0.0225 |
| θ range | 2.88–26.44 |
| observed refls. | 3286 |
| x, y (weighting scheme) | 0.0282, 1.1130 |
| hydrogen refinement | mixed |
| refls in refinement | 3725 |
| parameters | 233 |
| restraints | 0 |
| R(Fobs) | 0.0350 |
| Rw(F2) | 0.0810 |
| S | 1.082 |
| shift/errormax | 0.001 |
| max electron density/e Å−3 | 0.298 |
| min electron density/e Å−3 | −0.213 |

### 10.10.5 (*E*)-1,2-bis(3,5-dimethylphenyl)diazene (10.15)

**Supplementary Table 24: Crystallographic data of 10.15**

| | **10.15** |
|---|---|
| net formula | $C_{16}H_{18}N_2$ |
| $M_r$/g mol$^{-1}$ | 238.328 |
| crystal size/mm | 0.419 × 0.141 × 0.079 |
| $T$/K | 173(2) |
| radiation | MoKα |
| diffractometer | 'Oxford XCalibur' |
| crystal system | monoclinic |
| space group | 'P 21/c' |

| | |
|---|---|
| $a$/Å | 8.1737(5) |
| $b$/Å | 13.5359(8) |
| $c$/Å | 12.4775(11) |
| α/° | 90 |
| β/° | 104.116(8) |
| γ/° | 90 |
| $V$/Å$^3$ | 1338.80(17) |
| $Z$ | 4 |
| calc. density/g cm$^{-3}$ | 1.18243(15) |
| μ/mm$^{-1}$ | 0.070 |
| absorption correction | 'multi-scan' |
| transmission factor range | 0.97085–1.00000 |
| refls. measured | 4885 |
| $R_{\rm int}$ | ? |
| mean σ($I$)/$I$ | 0.0876 |
| θ range | 4.519–29.057 |
| observed refls. | 1614 |
| *x, y* (weighting scheme) | 0.0696, |
| hydrogen refinement | constr |
| refls in refinement | 4885 |
| parameters | 168 |
| restraints | 0 |
| $R(F_{\rm obs})$ | 0.0498 |
| $R_{\rm w}(F^2)$ | 0.1462 |
| $S$ | 0.758 |
| shift/error$_{\rm max}$ | 0.001 |
| max electron density/e Å$^{-3}$ | 0.589 |
| min electron density/e Å$^{-3}$ | −0.754 |

Poor quality data set. Refined as two-component twin, BASF 0.02.

### 10.10.6 2,2'-(2,2',6,6'-Tetramethyl-[1,1'-biphenyl]-4,4'-diyl)bis(1-(4-nitrophenyl)diazene) (10.19)

**Supplementary Table 25: Crystallographic data of 10.19.**

| | **10.19** |
|---|---|
| net formula | $C_{28}H_{24}N_6O_4$ |
| $M_r$/g mol$^{-1}$ | 508.528 |
| crystal size/mm | 0.120 × 0.080 × 0.060 |
| $T$/K | 173(2) |
| radiation | 'Mo Kα |
| diffractometer | 'Bruker D8Venture' |
| crystal system | monoclinic |
| space group | $P2_1$ |
| $a$/Å | 14.8429(8) |
| $b$/Å | 7.3293(4) |
| $c$/Å | 23.3459(11) |
| α/° | 90 |
| β/° | 95.5969(16) |
| γ/° | 90 |
| $V$/Å$^3$ | 2527.6(2) |
| $Z$ | 4 |
| calc. density/g cm$^{-3}$ | 1.33636(11) |
| μ/mm$^{-1}$ | 0.093 |
| absorption correction | multi-scan |
| transmission factor range | 0.9045–0.9585 |
| refls. measured | 29719 |
| $R_{int}$ | 0.0458 |
| mean σ($I$)/$I$ | 0.0519 |
| θ range | 2.85–26.43 |

| | |
|---|---|
| observed refls. | 6796 |
| *x, y* (weighting scheme) | 0.0424, 0.4506 |
| hydrogen refinement | constr |
| Flack parameter | 0.9(11) |
| refls in refinement | 9499 |
| parameters | 702 |
| restraints | 1 |
| $R(F_{obs})$ | 0.0449 |
| $R_w(F^2)$ | 0.1035 |
| $S$ | 1.029 |
| shift/error$_{max}$ | 0.001 |
| max electron density/e Å$^{-3}$ | 0.270 |
| min electron density/e Å$^{-3}$ | −0.214 |

### 10.10.7 *N*-Acetylanthranilic acid (10.22)

**Supplementary Table 26: Crystallographic data of 10.22.**

| | **10.22** |
|---|---|
| net formula | $C_9H_9NO_3$ |
| $M_r$/g mol$^{-1}$ | 179.173 |
| crystal size/mm | 0.303 × 0.185 × 0.155 |
| $T$/K | 173(2) |
| radiation | MoKα |
| diffractometer | 'Oxford XCalibur' |
| crystal system | monoclinic |
| space group | 'C 2/c' |
| $a$/Å | 14.1697(8) |
| $b$/Å | 18.7838(11) |
| $c$/Å | 7.5134(5) |
| α/° | 90 |

| | |
|---|---|
| β/° | 93.088(6) |
| γ/° | 90 |
| $V$/Å$^3$ | 1996.9(2) |
| $Z$ | 8 |
| calc. density/g cm$^{-3}$ | 1.19196(12) |
| μ/mm$^{-1}$ | 0.091 |
| absorption correction | 'multi-scan' |
| transmission factor range | 0.98314–1.00000 |
| refls. measured | 5560 |
| $R_{int}$ | ? |
| mean σ($I$)/$I$ | 0.0515 |
| θ range | 4.340–26.368 |
| observed refls. | 1381 |
| $x$, $y$ (weighting scheme) | 0.0882, |
| hydrogen refinement | constr |
| refls in refinement | 2036 |
| parameters | 120 |
| restraints | 0 |
| $R(F_{obs})$ | 0.0584 |
| $R_w(F^2)$ | 0.1720 |
| $S$ | 1.066 |
| shift/error$_{max}$ | 0.001 |
| max electron density/e Å$^{-3}$ | 0.252 |
| min electron density/e Å$^{-3}$ | –0.247 |

SQUEEZE applied to solve the problem with the remaining electron densities in two voids.

### 10.10.8 (*R*)-4-(4-Aminophenyl)pyrrolidin-2-one (10.25)

**Supplementary Table 27: Crystallographic data of 10.25.**

| | **10.25** |
|---|---|
| net formula | $C_{20}H_{40}Cl_2MgN_4O_{10}$ |
| $M_r$/g mol$^{-1}$ | 591.763 |
| crystal size/mm | 0.090 × 0.070 × 0.050 |
| $T$/K | 173(2) |
| radiation | 'Mo Kα |
| diffractometer | 'Bruker D8Venture' |
| crystal system | triclinic |
| space group | $P$1 |
| $a$/Å | 6.3479(3) |
| $b$/Å | 8.4811(4) |
| $c$/Å | 14.4047(6) |
| α/° | 85.0471(12) |
| β/° | 79.6607(12) |
| γ/° | 74.4087(13) |
| $V$/Å$^3$ | 734.25(6) |
| $Z$ | 1 |
| calc. density/g cm$^{-3}$ | 1.33832(11) |
| μ/mm$^{-1}$ | 0.297 |
| absorption correction | multi-scan |
| transmission factor range | 0.9008–0.9585 |
| refls. measured | 29380 |
| $R_{int}$ | 0.0421 |
| mean σ($I$)/$I$ | 0.0364 |
| θ range | 3.38–26.43 |
| observed refls. | 4850 |
| $x$, $y$ (weighting scheme) | 0.0472, 0.2190 |
| hydrogen refinement | mixed |

| | |
|---|---|
| Flack parameter | −0.49(6) |
| refls in refinement | 5810 |
| parameters | 400 |
| restraints | 25 |
| $R(F_{obs})$ | 0.0359 |
| $R_w(F^2)$ | 0.0900 |
| $S$ | 1.030 |
| shift/error$_{max}$ | 0.001 |
| max electron density/e Å$^{-3}$ | 0.312 |
| min electron density/e Å$^{-3}$ | −0.244 |

### 10.10.9 Ethyl carbamimidothioate hydrobromide(10.35)

**Supplementary Table 28: Crystallographic data of 10.35**

| | **10.35** |
|---|---|
| net formula | $C_4H_{13}BrN_4S_2$ |
| $M_r$/g mol$^{-1}$ | 261.209 |
| crystal size/mm | 0.230 × 0.184 × 0.087 |
| $T$/K | 173(2) |
| radiation | MoKα |
| diffractometer | 'Oxford XCalibur' |
| crystal system | monoclinic |
| space group | 'P 21/c' |
| $a$/Å | 7.7771(3) |
| $b$/Å | 6.0981(2) |
| $c$/Å | 21.8868(8) |
| α/° | 90 |
| β/° | 91.206(3) |
| γ/° | 90 |
| $V$/Å$^3$ | 1037.77(6) |

| | |
|---|---|
| $Z$ | 4 |
| calc. density/g cm$^{-3}$ | 1.67187(10) |
| μ/mm$^{-1}$ | 4.316 |
| absorption correction | 'multi-scan' |
| transmission factor range | 0.88337–1.00000 |
| refls. measured | 5504 |
| $R_{int}$ | 0.0347 |
| mean σ($I$)/$I$ | 0.0411 |
| θ range | 4.247–26.369 |
| observed refls. | 1842 |
| $x$, $y$ (weighting scheme) | 0.0243, 0.000 |
| hydrogen refinement | mixed |
| refls in refinement | 2109 |
| parameters | 133 |
| restraints | 0 |
| $R(F_{obs})$ | 0.0267 |
| $R_w(F^2)$ | 0.0611 |
| $S$ | 1.054 |
| shift/error$_{max}$ | 0.001 |
| max electron density/e Å$^{-3}$ | 0.348 |
| min electron density/e Å$^{-3}$ | −0.401 |

C-H: constr, N-H: refall.

# *11 Azobenzene Core Structures for Further Derivatization*

## 11.1 Azobenzene Building Blocks

Since azobenzenes are widely used in photopharmacology and the Trauner group is targeting more and more classes of proteins and lipids for photocontrol, sharing synthetic knowledge and synthesized compounds is essential for fast progress. Therefore, some azobenzene core structures that can be used for further derivatization are reported herein. Until now, and QAQ (see Chapter 10, Figure 56) being a prime example, azobenzenes are often derivatized symmetrically in their 4,4'-positions. However, in order to enable the preparation of unsymmetrical azobenzenes, a short route has been carried out to obtain a free amine moiety in the 4-position, while an amine in the 4'-position is Boc-protected. With this molecule, functionalizing one end, for instance, by acylation or reductive amination is possible, when the other end can be deprotected and reacted with a different substrate.

This was achieved starting from 1,4-phenylenediamine (**11.1**) by mono-Boc protection according to Togashi *et al.* to give **11.2** in 91% yield (Scheme 30).[215] The azobenzene was obtained by Mills reaction with 4-nitro-1-nitrosobenzene (**11.3**) to give nitro azobenzene **11.4** in 41% yield, which was reduced with $Na_2S$ in a mixture of THF/water at elevated temperatures to ultimately gain access to **11.5** in quantitative yield.

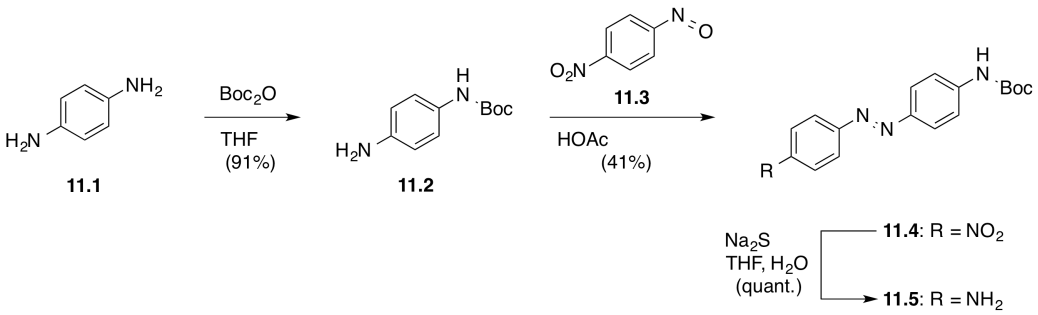


**Scheme 30: Synthesis of 11.5.** Boc-protection of phenylene diamine (**11.1**) yields **11.2**, which is condensed with **11.3** to nitro azobenzene **11.4**. Final reduction employinf sodium sulfide yields **11.5** in quantitative yield.

Further exploration remains to be conducted with this building block. Furthermore, studies could be made to access **11.5** form 4,4'-diamino azobenzene directly. However, as this compound proved difficult to obtain from *via* commercial sources, the reported route might stand to be useful in the future.

## 11.2 Tetrafluoro-substituted Azobenzenes

The fact that azobenzenes do thermally relax can be either an advantage or a drawback, depending on their application. The benefit is the potential self-deactivation without a second wavelength of light if the photopharmaceutical is acitve in its less stable *cis*-form, therefore circumventing longer exposure of tissue or biological samples to light. However, one then has to irraditate the sample continuously to keep it in the *cis*-form, which can be considered a disadvantage. Ideally, an azobenzene should be converted from one to the other state by a brief pulse of light in a quantitative manner while showing bistability. This issue has been addressed by Woolley and co-workers[216] and Hecht and co-workers[217] by two different approaches. The Woolley group linked the aryl group of an azobenzene with an ethylene bridge (Figure 57a), which makes the it *cis*-form the most stable, while the Hecht group installed fluoride substituents in all four ortho positions *ortho*- to the diazene unit (Figure 57b). Following the procedure from the Hecht laboratory, a precursor (**11.7**) was synthesized as reported before (Figure 57c).[217] This molecule can then be further derivatized by for instance Buchwald-Hartwig couplings on the 4- and 4'-position to give symmetric azobenzenes with pharmacophores on each side.[217] As the obtained material proved to be highly crystalline, suitable crystals were obtained by slowly evaporating the solvent from a solution of **11.7** in chloroform (Figure 57d). X-ray diffractometric analyses was performed as the X-ray derived structure has not been reported to date.

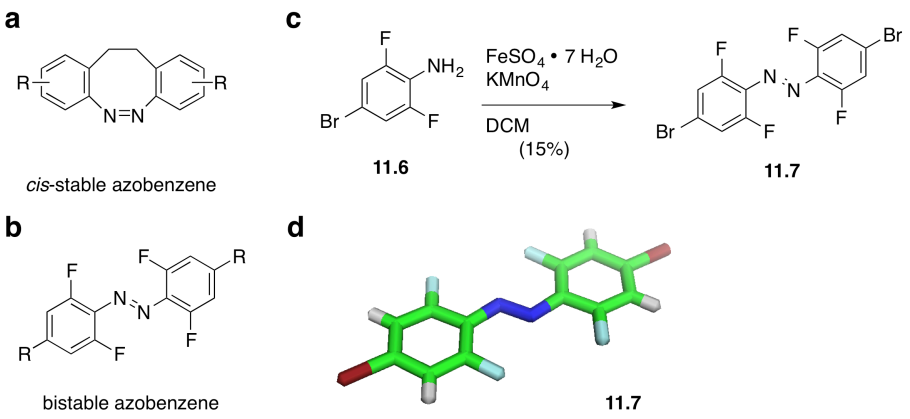


**Figure 59: *Cis*- and bi-stable azobenzenes. a)** A *cis*-stable azobenzene made by ethylene bridging. **b)** A bistable azobenzene made by fluorine atom introduction. **c)** Synthesis of bistable azobenzene **11.7** by oxidative dimerization of aniline **11.6** and **d)** its crystal structure.

It should be noted that **11.7** was obtained as a mixture of *cis*-/*trans*-isomers, of which only the *trans*-isomer is described in the spectral data section. Bistable azobenzene **11.7** is a versatile precursor for further synthesis as Pd(II) coupling procedures have been described for this compound.[217] For instance, it can be envisioned to synthesize tetrafluoro QAQ (Figure 56, see Chapter 10) that can be employed to optically control nociception. With this derivatization, less irradiation times would be necessary in order to apply any isomeric state. Indeed, that can be beneficial when light application seems to be difficult (e.g, the spinal cord) and phototoxicity should be circumvented.

## 11.3 *para*-"Handle" Azobenzenes

One way of azologization is the simple addition of an azobenzene (see for instance chapter 9). Therefore, more structures are reported herein that all consist of an azobenzene that bears a carbon in various oxidation states in the *para*-position. As such, an alcohol (**11.9**) was obtained by a Mills reaction between benzyl alcohol **11.8** and nitrosobenzene that could be oxidized with manganese dioxide to its corresponding aldehyde **11.10** (Scheme 31a). In addition, an azobenzene ester **11.12** has been obtained by a Mills reaction between ester **11.11** and nitrosobenzene that could be saponified by the "magic mixture" aqueous LiOH in THF and MeOH to acid **11.13** (Scheme 31b).

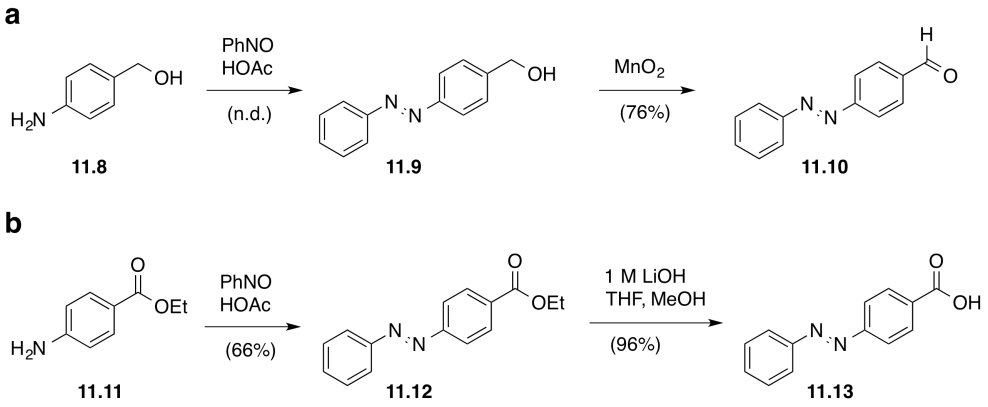


**Scheme 31: Azobenzenes with "handles". a)** Azobenzene containing alcohol **11.9** and aldehyde **11.10**. **b)** Azobenzene containing ester **11.12** and acid **11.13**.

The structures reported in this chapter can be covalently attached to other chemicals. As such, **11.9** can be employed in a Mitsonobu reaction, while **11.10** can be used for reductive aminations. Furthermore, **11.12** can be used with amines activated by for instance $AlMe_3$ and acid **11.13** can be peptide coupled to amines. In summary, these structures are accessible easily and straightforward and can be used with their handles in different reaction types to introduce azobenzenes late-stage in synthetic protocols.

## 11.4 Synthesis

### 11.4.1 *tert*-Butyl (4-aminophenyl)carbamate (11.2)

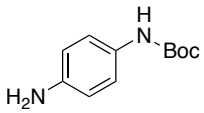

**11.2** was synthesized according to a procedure from Togashi *et al.*.[215]

In a round bottom flask 11.5 g (106.1 mmol, 5.0 eq.) of phenylenediamine (**11.1**) were dissolved in 500 mL DCM and cooled to 0 °C. $Boc_2O$ dissolved in 50 mL DCM was added drop-wise and the resulting mixture was allowed to warm to r.t. and stirred o.n.. The crude was concentrated to roughly 20% of the initial volume and filtered over a plug of silica with EtOAc/pentane = 1/1 as an eluent to obtain 4.03 g (19.3 mmol) of the desired product in 91% yield.

**$^1$H NMR** (400 MHz, $CDCl_3$) δ [ppm] = 7.12 (d, *J* = 7.8 Hz, 2H), 6.62 (d, *J* = 8.7 Hz, 2H), 6.32 (br s, 1H), 3.52 (br s, 2H), 1.49 (s, 9H).

**$^{13}$C NMR** (101 MHz, $CDCl_3$) δ [ppm] = 153.3, 142.4, 129.7, 120.9, 115.6, 80.0 28.4.

### 11.4.2 *tert*-Butyl (4-((4-nitrophenyl)diazenyl)phenyl)carbamate (11.4)

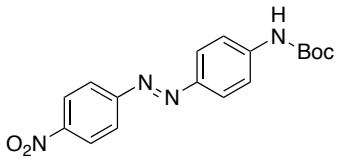

In a round bottom flask, 585 mg (1.2 eq., 3.85 mmol) of 1-nitro-4-nitrosobenzene (**11.3**) was dissolved in 50 mL HOAc, and *tert*-butyl (4-aminophenyl)carbamate (**11.2**) was added in one portion. The reaction mixture was stirred for 24 hours before it was quenched with sat. aqueous $NaHCO_3$, diluted with water and extracted with EtOAc. Flash column chromatography on silica gel (100% DCM) yielded 415 mg (1.33 mmol) of the desired comound as an orange solid in 41% yield.

**$^1$H NMR** (300 MHz, $CDCl_3$) δ [ppm] = 8.36 (d, *J* = 8.8 Hz, 2H), 7.99 (d, *J* = 8.8 Hz, 2H), 7.95 (d, *J* = 9.0 Hz, 2H), 7.56 (d, *J* = 8.9 Hz, 2H), 6.74 (s, 1H), 1.55 (s, 9H).

**$^{13}$C NMR** (75 MHz, $CDCl_3$) δ [ppm] = 155.9, 152.1, 148.4, 148.1, 142.5, 124.9, 124.7, 123.2, 118.2, 81.4, 28.3.

**HRMS (ESI)**: calc. for $C_{17}H_{17}N_4O_4^-$ $(M-H)^-$: 341.1255, found: 341.1260.

### 11.4.3 (*E*)-*tert*-Butyl (4-((4-aminophenyl)diazenyl)phenyl)carbamate (11.5)

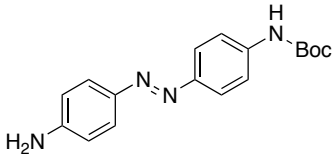


A round bottom flask was charged with 440 mg of *tert*-butyl (4-((4-nitrophenyl)diazenyl)phenyl)carbamate (**11.4**) (1.29 mmol, 1.0 eq.) and dissolved in a mixture of THF/water (75/50 mL). Then 1.54 g (12.85 mmol, 10.0 eq.) of $Na_2S$ (65%) was added as a solid. The reaction mixture was refluxed at 100 °C for 3 h before it was allowed to cool to r.t. and extracted with EtOAc against 4 M NaOH. The combined organic layers were washed with water and brine before the crude was subjected to flash column chromatography (100% EtOAc) to obtain 401 mg (1.28 mmol) of the desired product in quantitative yield.

**$^1$H NMR** (300 MHz, $CDCl_3$) δ [ppm] = 7.82 (d, *J* = 8.8 Hz, 2H), 7.77 (d, *J* = 8.9 Hz, 2H), 7.47 (d, *J* = 8.9 Hz, 2H), 6.73 (d, *J* = 8.9 Hz, 2H), 6.65 (br s, 1H), 4.00 (br s, 2H), 1.54 (s, 9H).

**$^{13}$C NMR** (75 MHz, $CDCl_3$) δ [ppm] = 152.4, 149.2, 148.6, 145.6, 139.9, 124.8, 123.4, 118.3, 114.7, 80.9, 28.3.

**HRMS (ESI)**: calc. for $C_{17}H_{21}N_4O_2^+$ $(M+H)^+$: 313.1659, found: 313.1659.

### 11.4.4 (*E*)-1,2-Bis(4-bromo-2,6-difluorophenyl)diazene (11.7)

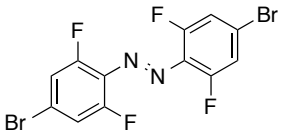


**11.7** was synthesized according to a literature procedure from Hecht and co-workers[217] and was isolated in 15% yield as deep red needles.

Spectral data is reported for the major isomer.

**$^{1}$H NMR** (600 MHz, $CDCl_3$) δ [ppm] = 7.27 (d, *J* = 8.2 Hz, 1H).

**$^{13}$C NMR** (151 MHz, $CDCl_3$) δ [ppm] = 155.45 (d, *J* = 266.3 Hz), 130.69 (t, *J* = 9.7 Hz), 124.37 (t, *J* = 12.0 Hz), 116.70 (d, *J* = 22.7 Hz).

**$^{19}$F NMR** (282 MHz, $CDCl_3$) δ [ppm] = 118.60 (d, *J* = 8.4 Hz).

**HRMS (ESI)**: calc. for $(M-H)^-$: 313.1659, found: 313.1659.

### 11.4.5 (*E*)-(4-(Phenyldiazenyl)phenyl)methanol (11.9)

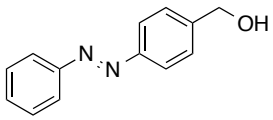


A round bottom flask was charged with 500 mg (4.06 mmol, 1.0 eq.) of alcohol **10.8** and 435 mg (4.06 mmol, 1.0 eq.) of nitrosobenzene dissolved in HOAc (20 mL). The reaction mixture was stiired o.n. at 40 °C. The reaction was quenched with sat. aqueous $NaHCO_3$ and extracted in EtOAc (3 x). The combined organic layers were washed with brine and dried over $MgSO_4$ before the crude material was subjected to flash column chromatography (MeOH/DCM = 0/100 → 4/100) to obtain the desired compound as a orange solid.

**$^{1}$H NMR** (400 MHz, DMSO-$d_6$): *δ* [ppm] = 7.88 (td, *J* = 5.6, 2.9 Hz, 4H), 7.65–7.49 (m, 5H), 5.41 (t, *J* = 5.7 Hz, 1H), 4.61 (d, *J* = 5.5 Hz, 2H).

**$^{13}$C NMR** (101 MHz, DMSO-$d_6$): $\delta$ [ppm] = 151.9, 150.8, 146.5, 131.4, 129.5, 127.2, 122.5, 62.5.

**LRMS (ESI)**: calc. for $C_{13}H_{13}N_2O^+$ $(M+H)^+$: 213.1, found: 213.1.

**UV/Vis** (LCMS): $\lambda_{max1}$ (*cis*-**10.9**) = 244 nm, $\lambda_{max2}$ (*cis*-**10.9**) = 290 nm; $\lambda_{max1}$ (*trans*-**10.9**) = 230 nm, $\lambda_{max2}$ (*trans*-**10.9**) = 324 nm.

**$R_t$** (LCMS; MeCN/$H_2O$/formic acid = 10/90/0.1 → 90/10/0.1 over 7 min) = 3.325 min (*cis*-**10.9**) , 4.229 (*trans*-**10.9**).

### 11.4.6 (*E*)-4-(Phenyldiazenyl)benzaldehyde(11.10)

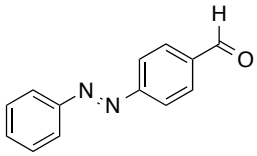


A round bottom flask was charged with 100 mg (0.471 mmol, 1.0 eq.) of **10.9** and 819 mg (9.43 mmol, 20 eq.) of $MnO_2$ in DCM. The reaction was stirred for 3 min before it was filtered over Celite. The crude material was subjected to flash column chromatography (100% DCM) to obtain 75 mg (0.36 mmol) of the desired compound in 76% yield as an orange solid.

**$^1$H NMR** (400 MHz, DMSO-$d_6$): $\delta$ [ppm] = 10.12 (s, 1H), 8.13 (d, *J* = 8.3 Hz, 2H), 8.06 (d, *J* = 8.2 Hz, 2H), 7.95 (dd, *J* = 6.8, 3.0 Hz, 2H), 7.68–7.61 (m, 3H).

**$^{13}$C NMR** (101 MHz, DMSO-$d_6$): $\delta$ [ppm] = 192.8, 155.0, 151.9, 137.6, 132.5, 130.9, 129.7, 123.2, 123.0.

**HRMS (ESI)**: calc. for $C_{13}H_{11}N_2O^+$ $(M+H)^+$: 211.1, found: 211.1.

**UV/Vis** (LCMS): $\lambda_{max1}$ (*cis*-**10.10**) = 230 nm, $\lambda_{max2}$ (*cis*-**10.10**) = 280 nm; $\lambda_{max1}$ (*trans*-**10.10**) = 229 nm, $\lambda_{max2}$ (*trans*-**10.10**) = 327 nm.

**$R_t$** (LCMS; MeCN/$H_2O$/formic acid = 10/90/0.1 → 90/10/0.1 over 7 min) = 4.008 min (*cis*-**10.10**) , 4.987 (*trans*-**10.10**).

### 11.4.7 Ethyl (*E*)-4-(phenyldiazenyl)benzoate(11.12)

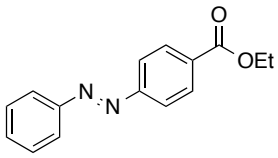


A round bottom flask was charged with 500 mg (3.00 mmol, 1.0 eq.) of ester **10.11** and 324 mg (3.00 mmol, 1.0 eq.) of nitrosobenzene dissolved in HOAc (20 mL). The reaction mixture was stiired o.n. at r.t.. The reaction was quenched with sat. aqueous $NaHCO_3$ and extracted in EtOAc (3 x). The combined organic layers were washed with brine and dried over $MgSO_4$ before the crude material was subjected to flash column chromatography (*i*-hexanes/DCM = 50/50) to obtain 500 mg (1.97 mmol) of the desired compound as a orange solid in 66% yield.

**$^1$H NMR** (400 MHz, DMSO-$d_6$): $\delta$ [ppm] = 8.19–8.10 (m, 2H), 8.04–7.88 (m, 4H), 7.62 (dd, *J* = 4.9, 1.9 Hz, 3H), 4.35 (q, *J* = 7.1 Hz, 2H), 1.34 (t, *J* = 7.1 Hz, 3H).

**$^{13}$C NMR** (101 MHz, DMSO-$d_6$): $\delta$ [ppm] = 165.1, 154.4, 151.9, 132.3, 131.8, 130.5, 129.6, 122.9, 122.7, 61.1, 14.2.

**HRMS (ESI)**: calc. for $C_{15}H_{15}N_2O_2^+$ $(M+H)^+$: 255.1, found: 255.1.

**UV/Vis** (LCMS): $\lambda_{max1}$ (*cis*-**10.12**) = 260 nm; $\lambda_{max1}$ (*trans*-**10.12**) = 229 nm, $\lambda_{max2}$ (*trans*-**10.12**) = 322 nm.

**$R_t$** (LCMS; MeCN/$H_2O$/formic acid = 10/90/0.1 → 90/10/0.1 over 7 min) = 4.661 min (*cis*-**10.12**) ,5.686 (*trans*-**10.12**).

### 11.4.8 (*E*)-4-(Phenyldiazenyl)benzoic acid (11.13)

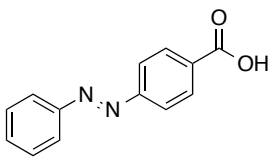

A round bottom flask was charged with 100 mg (0.39 mmol, 1.0 eq.) of **11.12** dissolved in 1 M aqueous LiOH (3.9 mL), THF (8 mL) and MeOH (8 mL). The reaction mixture was stirred for 2 h at r.t. before it was neutralized with cHCl and extracted with EtOAc. The crude material was subjected to flash column chromatography (100% DCM) to obtain 85.0 mg (0.38 mmol) of the desired compound in 96% yield as an orange solid.

**$^{1}$H NMR** (400 MHz, DMSO-$d_6$): $\delta$ [ppm] = 8.12 (d, $J$ = 8.5 Hz, 2H), 7.96–7.88 (m, 4H), 7.67–7.55 (m, 3H).

**$^{13}$C NMR** (101 MHz, DMSO-$d_6$): $\delta$ [ppm] = 167.3, 153.3, 152.0, 131.8, 130.3, 129.5, 122.7, 122.1.

## 11.5 Spectral Data

### 11.5.1 *tert*-Butyl (4-aminophenyl)carbamate (11.2)

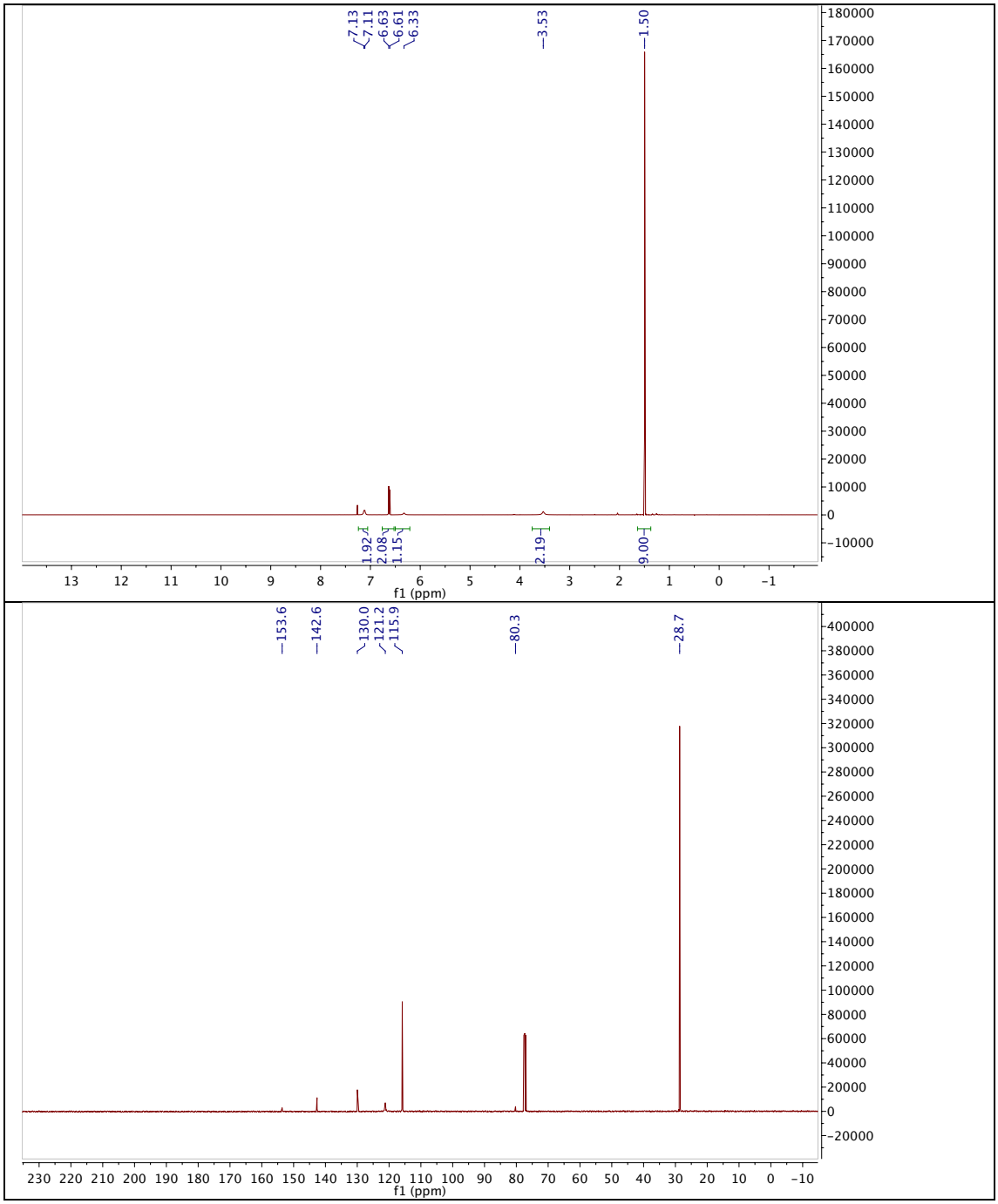

## 11.5.2 *tert*-Butyl (4-((4-nitrophenyl)diazenyl)phenyl)carbamate (11.4)

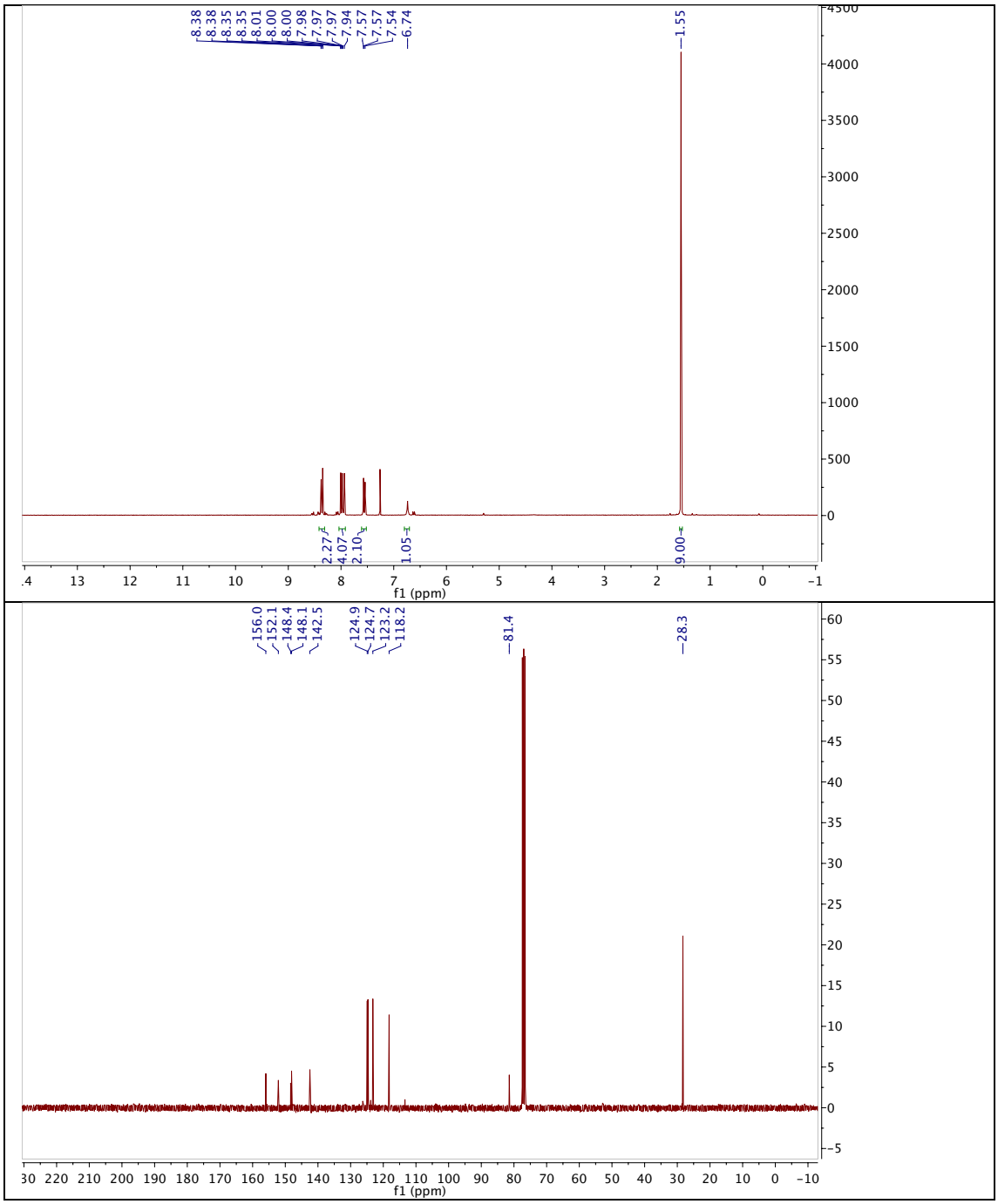

### 11.5.3 (*E*)-*tert*-Butyl (4-((4-aminophenyl)diazenyl)phenyl)carbamate (11.5)

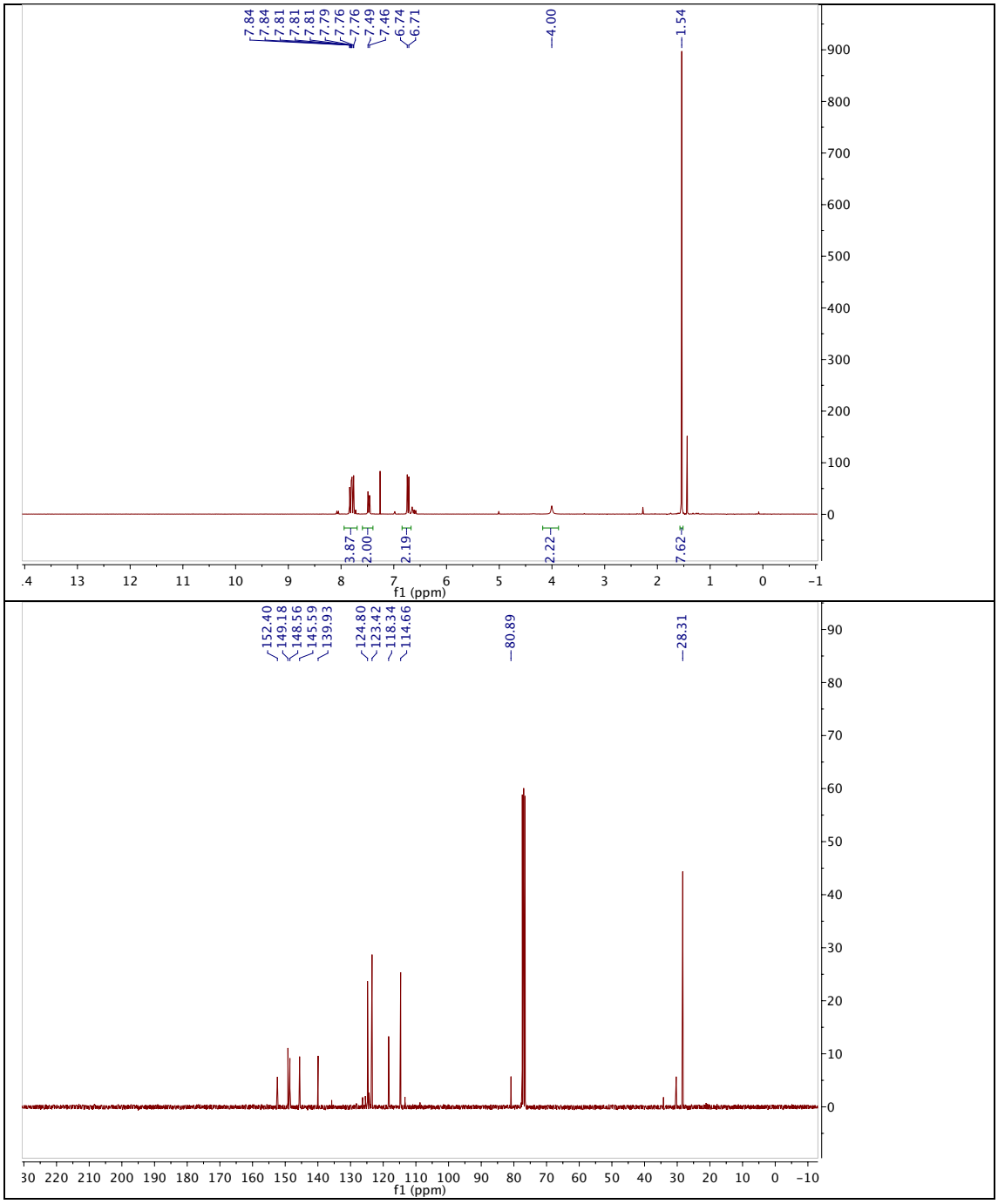

## 11.5.4 (*E*)-1,2-Bis(4-bromo-2,6-difluorophenyl)diazene (11.7)

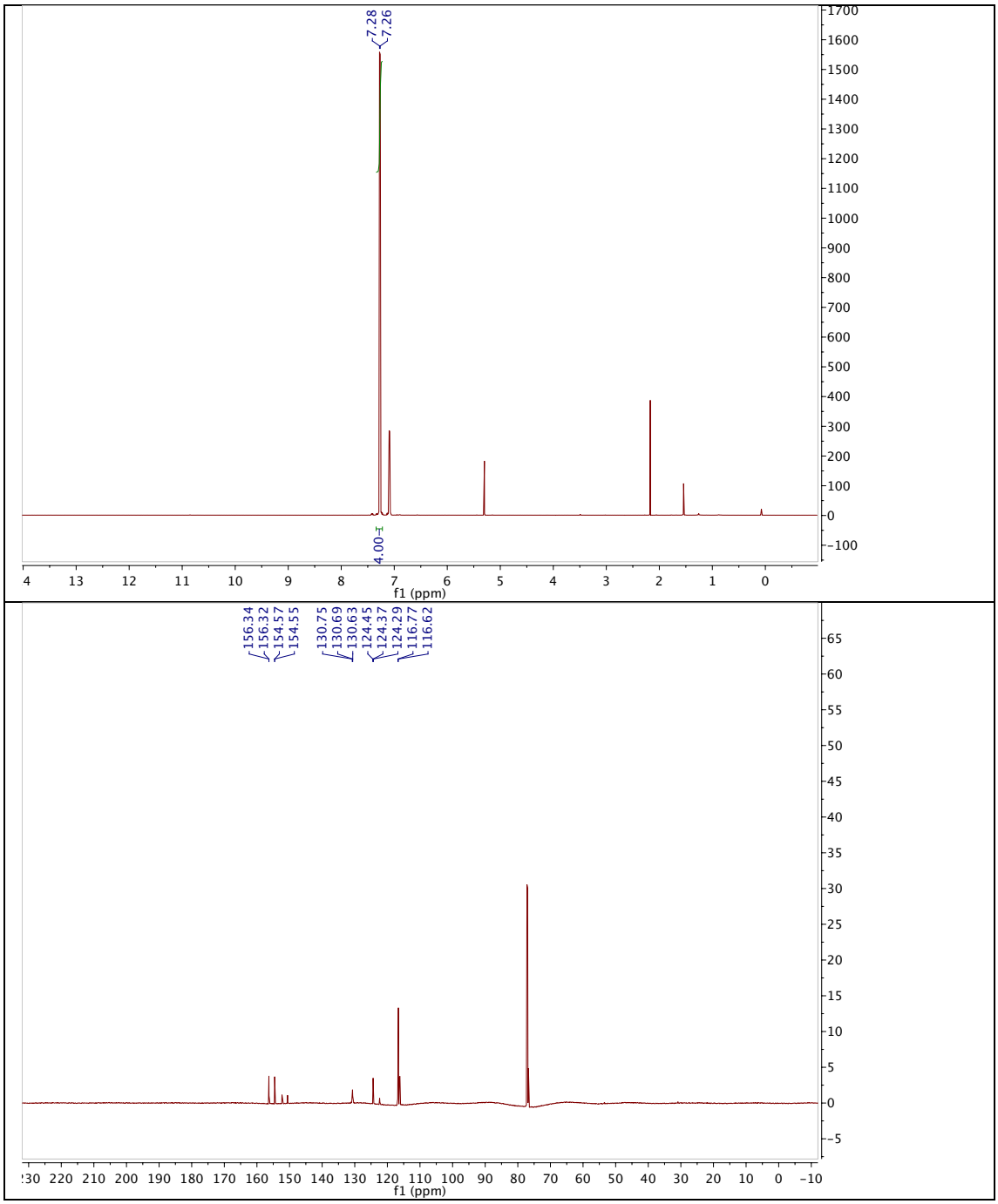

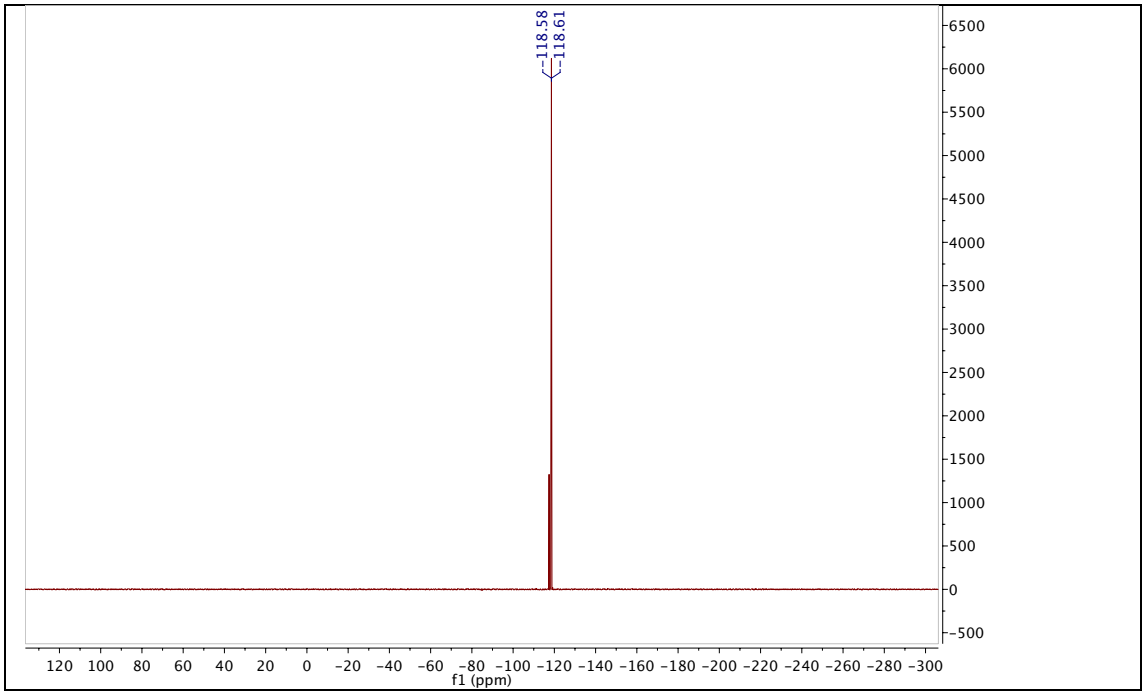
-118.58
-118.61
6500
6000
5500
5000
4500
4000
3500
3000
2500
2000
1500
1000
500
0
-500
120 100 80 60 40 20 0 -20 -40 -60 -80 -100 -120 -140 -160 -180 -200 -220 -240 -260 -280 -300
f1 (ppm)

## 11.5.5 (*E*)-(4-(Phenyldiazenyl)phenyl)methanol (11.9)

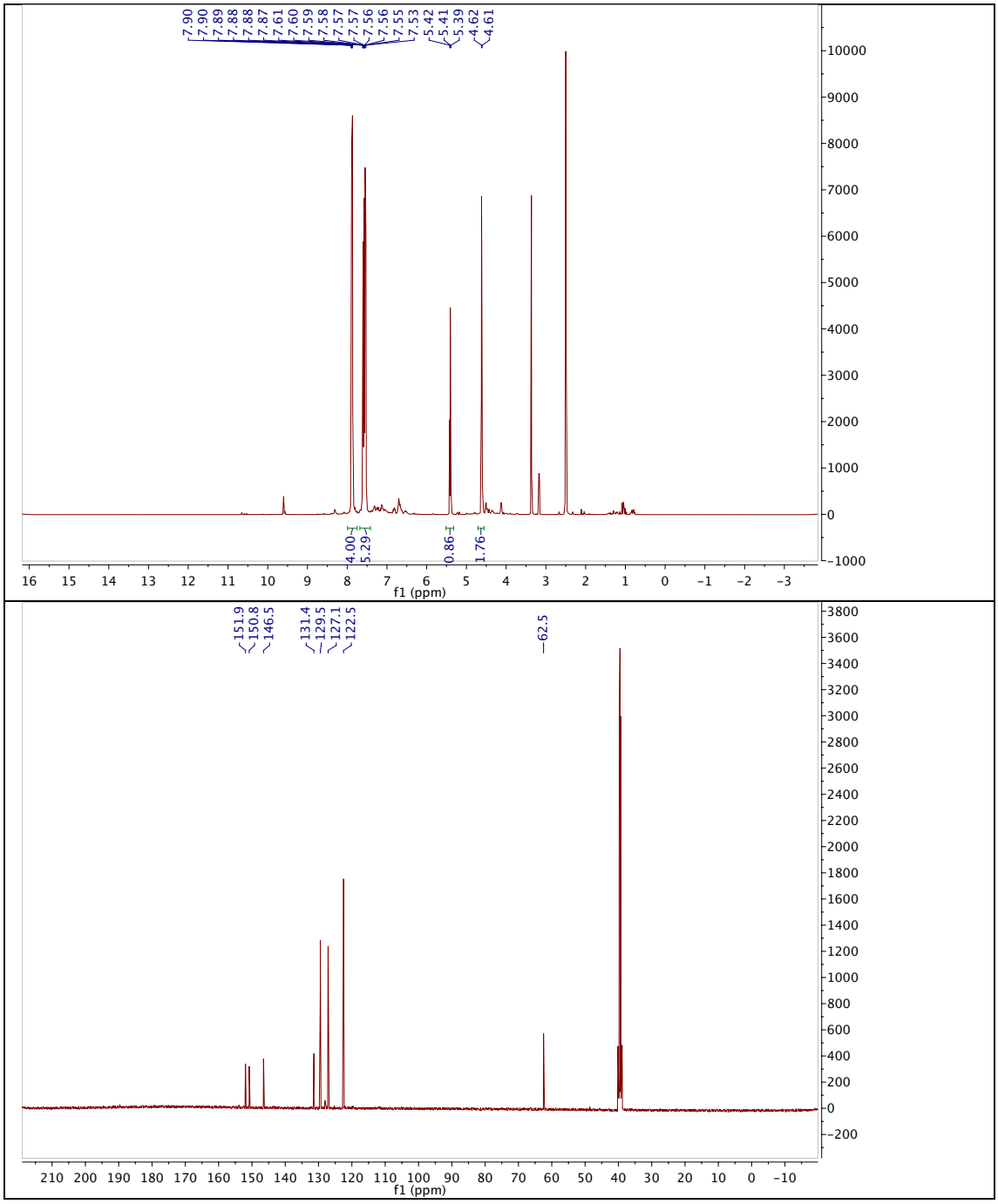

## 11.5.6 (*E*)-4-(Phenyldiazenyl)benzaldehyde(11.10)

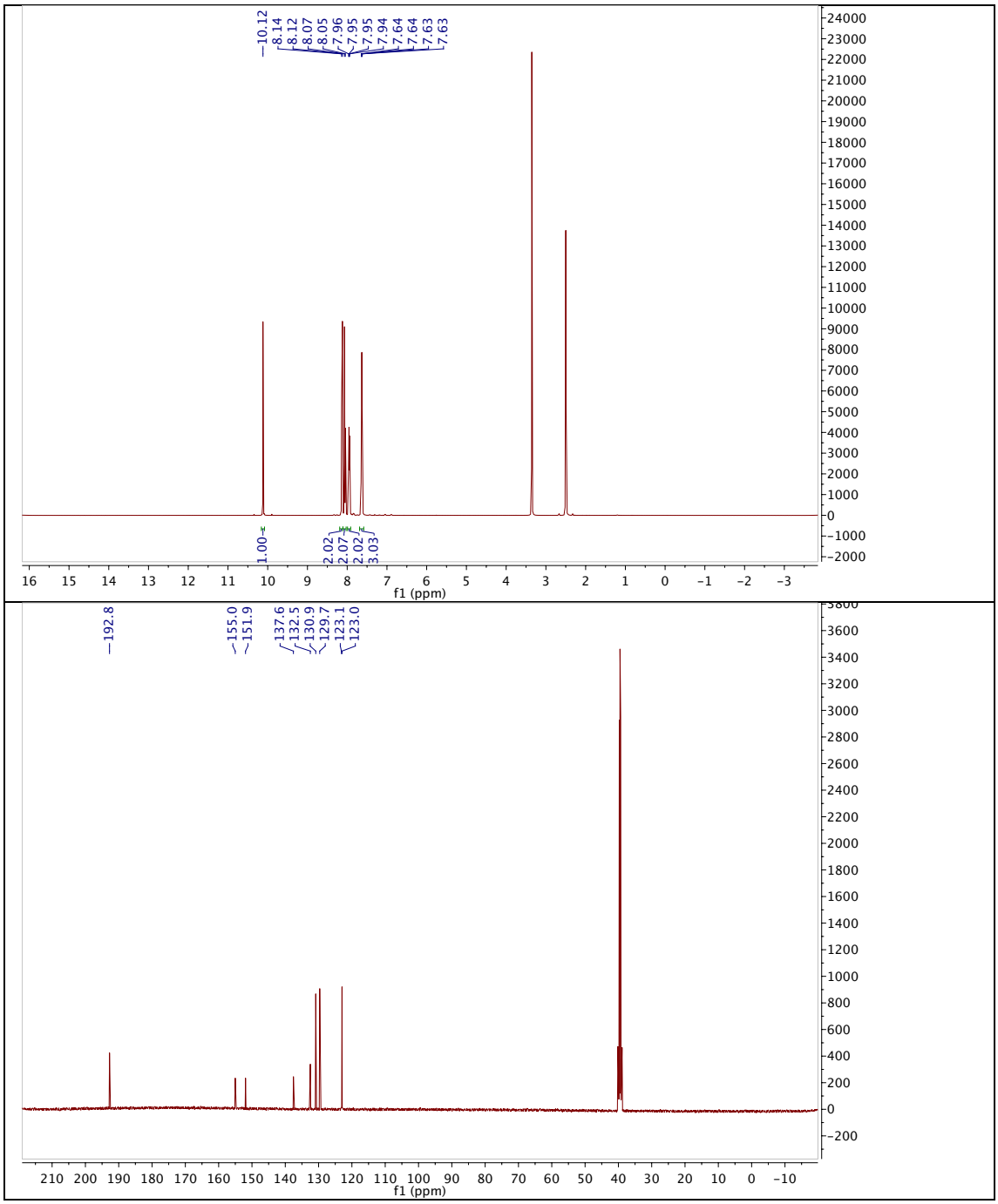

## 11.5.7 Ethyl (*E*)-4-(phenyldiazenyl)benzoate (11.12)

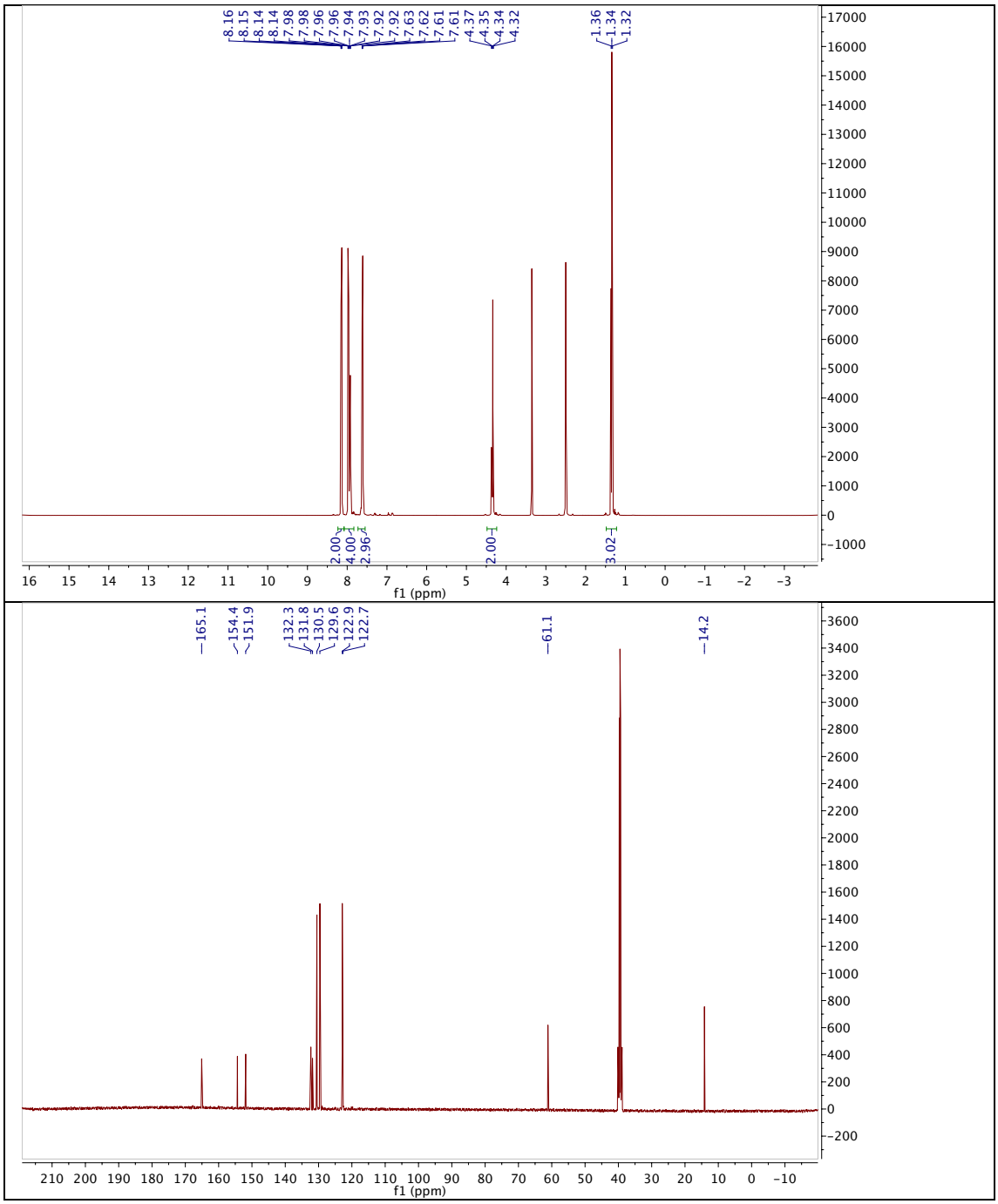

## 11.5.8 (*E*)-4-(Phenyldiazenyl)benzoic acid (11.13)

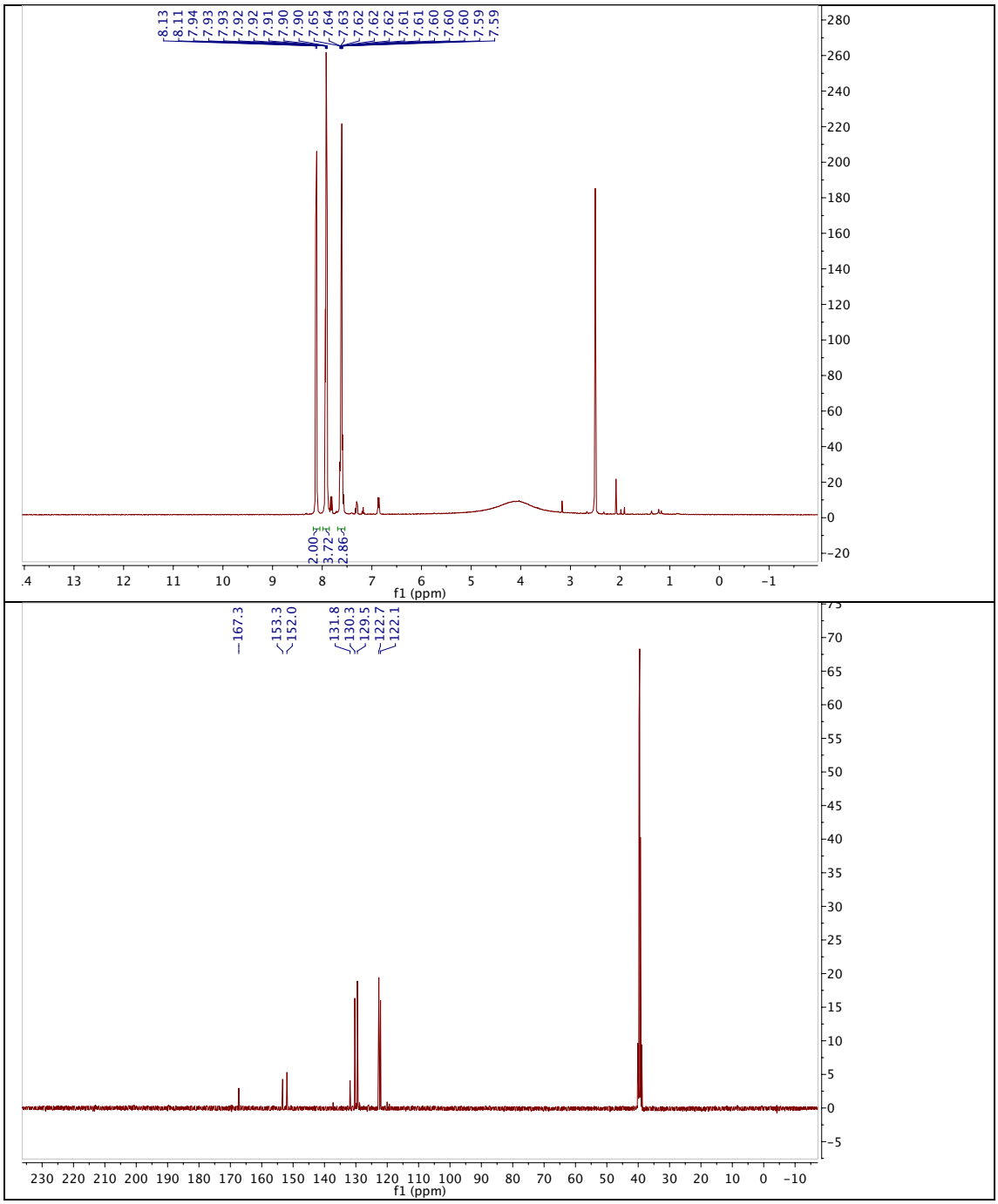

## 11.6 X-ray Crystallographic Data

**Supplementary Table 29: Crystallographic data of 11.7.**

| | **11.7** |
|---|---|
| net formula | $C_{12}H_4Br_2F_4N_2$ |
| $M_r$/g mol$^{-1}$ | 411.975 |
| crystal size/mm | 0.137 × 0.066 × 0.023 |
| $T$/K | 173(2) |
| radiation | 'Mo Kα |
| diffractometer | 'Bruker D8Quest' |
| crystal system | monoclinic |
| space group | $P2_1/c$ |
| $a$/Å | 10.3274(5) |
| $b$/Å | 4.5667(2) |
| $c$/Å | 13.1039(6) |
| α/° | 90 |
| β/° | 90.340(3) |
| γ/° | 90 |
| $V$/Å$^3$ | 618.00(5) |
| $Z$ | 2 |
| calc. density/g cm$^{-3}$ | 2.21395(18) |
| μ/mm$^{-1}$ | 6.597 |
| absorption correction | multi-scan |
| transmission factor range | 0.5716–0.7457 |
| refls. measured | 9803 |
| $R_{int}$ | 0.0512 |
| mean σ($I$)/$I$ | 0.0371 |
| θ range | 3.11–28.36 |
| observed refls. | 1218 |
| $x$, $y$ (weighting scheme) | 0.0231, 0.2317 |

| | |
|---|---|
| hydrogen refinement | constr |
| refls in refinement | 1523 |
| parameters | 91 |
| restraints | 0 |
| $R(F_{obs})$ | 0.0266 |
| $R_w(F^2)$ | 0.0547 |
| $S$ | 1.016 |
| shift/error$_{max}$ | 0.001 |
| max electron density/e Å$^{-3}$ | 0.358 |
| min electron density/e Å$^{-3}$ | −0.298 |

Symmetry code i = 1−*x*, 2−*y*, 1−*z*.

# *12 Appendix*

## 12.1 Abbreviations

| | |
|---|---|
| ° | degree |
| A | adenine, ampere |
| Å | angstrom |
| AAZ | acetazolamide |
| Ac | acetyl |
| ACh | acetylcholine |
| AChE | acetylcholinesterase |
| AG | azobenzene glutamate |
| Amp | ampicillin |
| Asc | ascorbate |
| a.u. | arbitrary units |
| B | base(s) |
| BETP | 2-(Ethylsulfinyl)-4-[3-(phenylmethoxy)phenyl]-6-(trifluoromethyl)-pyrimidine |
| BG | 6-((4-(aminomethyl)benzyl)oxy)-7*H*-purin-2-amine |
| BME | β-mercaptoethanol |
| Bn | benzyl |
| Boc | *tert*-butyloxycarbonyl |
| brsm | based on recovered starting material |
| br | broad |
| BSA | bovine serum albumin |
| Bu | butyl |
| c | centi |
| C | Celsius, cytosine |
| CA | carbonic anhydrase |
| COSY | correlation spectroscopy |
| CPBA | chlorperbenzoic acid |
| CRD | cysteine-rich domain |
| $\delta$ | chemical shift |
| d | doublet, desoxy, deionized |
| Δ | difference, heat |
| Da | dalton |
| DBCO | dibenzocyclooctyne |
| DCC | dicyclohexylcarbodiimide |
| DCM | dichloromethane |
| DDQ | dichlorodicyanoquinone |
| DIPEA | ethyldiisopropylamine |
| DMAP | 4-dimethylaminopyridin |
| DME | dimethoxy ethylene |
| DMEM | Dulbecco's modified eagle medium |
| DMF | *N,N*-dimethylformamide |

| | |
|---|---|
| DMSO | dimethylsulfoxide |
| DNA | desoxyribonucleic acid |
| DTT | dithiothreitol |
| EDCI | 1-ethyl-3-(3-aminopropyl)carbodiimide |
| EDTA | ethylenediamine tetraacetic acid |
| EI | electron impact |
| ESI | electrospray ionization |
| Et | ethyl |
| eq. | equivalents |
| *F* | fluorescence |
| FA | formic acid |
| FBS | fetal bovine serum |
| FCS | fetal calf serum |
| Fmoc | fluorenylmethoxycarbonyl |
| g | gram |
| G | guanine, 2-amino-1*H*-purin-6(9*H*)-one |
| GFP | green fluorescent protein |
| GIP | glucagon inhibitory peptide |
| GIRK | G-protein coupled inward rectifying potassium channel |
| GLP | glucagon-like peptide |
| GVBD | germinal vesicle breakdown |
| GPCR | G-protein coupled receptors |
| GSH | glutathione (reduced form) |
| GSSG | glutathione (oxidized form) |
| GST | glutathione *S*-transferase |
| h | hour, human, Planck constant |
| HBTU | *N,N,N′,N′*-Tetramethyl-*O*-(1*H*-benzotriazol-1-yl)uronium hexafluorophosphate |
| HEK | human embryonic kidney |
| HEPES | 4-(2-Hydroxyethyl)-1-piperazineethanesulfonic acid |
| HMBC | heteronuclear multipl-bond correlation spectroscopy |
| HOBt | hydroxybenzotriazole |
| HPLC | high-performance liquid chromatography |
| HRMS | high-resolution mass spectrometry |
| HSQC | heteronuclear single-quantum correlation spectroscopy |
| HV | high vacuum |
| Hz | hertz |
| $IC_{50}$ | half-maximal inhibitory constant |
| *i* | iso |
| Ins | insulin |
| IPTG | *i*-propyl thiogalactoside |
| IR | infrared, insulin receptor |
| *J* | coupling constant |
| k | kilo |
| Kan | kanamycin |
| $k_B$ | Boltzmann constant |
| $K_i$ | inhibitory constant |
| $K_M$ | Michaelis-Menten constant |
| LAH | lithium aluminum hydride |

| | |
|---|---|
| λ | wavelength |
| L | liter |
| LB | Luria Broth |
| LBD | ligand binding domain |
| LCMS | liquid chromatography mass spectrometry |
| LF | Lipofectamine® 2000 |
| LRMS | low resolution mass spectrometry |
| μ | micro |
| m | milli, meter, multiplet |
| *m* | meta |
| $m_c$ | centrosymmetric multiplet |
| M | mega, molar |
| MAG | maleimide azobenzene glutamate |
| MAPK | mitogen activated protein kinase |
| MAQ | maleimide azobenzene quarternary |
| Me | methyl |
| mGluR | metabotropic glutamate receptor |
| min | minute(s) |
| mRNA | messenger ribonucleic acid |
| $M_w$ | molecular weight |
| MWCO | molecular weight cut-off |
| m.p. | melting point |
| n | nano |
| ν | wavenumber |
| NBS | *N*-bromosuccinimid |
| NHS | *N*-hydroxysuccinimid |
| NMR | nuclear magnetic resonance |
| NPA | nitrophenyl acetate |
| NTP | nucleoside triphosphate |
| OD | optical density |
| o.n. | over night |
| p | pico, pressure, phosphorylated |
| *p* | para |
| PAGE | polyacrylamide gel electrophoresis |
| PBS | phosphate buffered saline |
| PCL | photochromic ligand |
| PCMB | *p*-chloromercuribenzoic acid |
| PCR | polymerase chain reaction |
| PEG | polyethylene glycol |
| Ph | phenyl |
| ppm | parts per million |
| Pr | propyl |
| PS | penicillin/streptomycine |
| psi | pounds per square inch |
| PTD | photochromic tethered dimerizer |
| PTL | photochromic tethered ligand |
| PTL' | photochromic tethered ligand (second generation) |
| q | quartet |
| QAQ | quarternary azobenzene quarternary |

| | |
|---|---|
| qu | quintet |
| rel. | relative |
| RP | reverse phase |
| rpm | rounds per minute |
| r.t. | room temperature |
| s | second, singlett |
| sat. | saturated |
| *S* | substrate |
| SDS | sodium dodecylsulfate |
| SEM | standard error of the mean |
| SSZ | sulfasalazine |
| S.D. | standard deviation |
| t | triplet |
| *t* | tert |
| T | temperature, thymine |
| T2DM | type 2 diabetes mellitus |
| TCEP | tris-(2-carboxyethyl)phosphine |
| TFA | trifluoroacetic acid |
| TK | tyrosine kinase |
| TLC | thin layer chromatography |
| TM | transmembrane |
| TMS | trimethylsilyl |
| Tris | tris(hydroxymtehyl)aminomethane |
| UV | ultra-violett |
| VFT | venus flytrap |
| VKR | venus kinase receptor |

## 12.2 General Remarks for Synthetic Procedures including Spectroscopy and Spectrometry

Solvents for chromatography and reactions were purchased in HPLC grade or distilled over an appropriate drying reagent prior to use. If necessary, solvents were degassed either by freeze-pump-thaw or by bubbling $N_2$ through the vigorously stirred solution for several minutes. Unless otherwise stated, all other reagents were used without further purification from commercial sources.

Flash column chromatography was carried out on silica gel 60 (0.040–0.063 mm) purchased from Merck. Reactions and chromatography fractions were monitored by thin layer chromatography (TLC) on Merck silica gel 60 F254 glass plates. The spots were visualized either under UV light at 254 nm or with appropriate staining method (iodine, *para*-anisaldehyde, $KMnO_4$) followed by heating.

NMR spectra were recorded in deuterated solvents on VARIAN Mercury 200, BRUKER AXR 300, VARIAN VXR 400 S, BRUKER AMX 600 and BRUKER Avance III HD 400 (equipped with a CryoProbe™) instruments and calibrated to residual solvent peaks ($^1H/^{13}C$ in ppm): $CDCl_3$ (7.26/77.16), DMSO-$d_6$ (2.50/39.52), $CD_3OD$ (3.31/49.00), MeCN-$d_3$ (1.94/1.32), DMF-$d_7$ (2.88/162.62). Multiplicities are abbreviated as follows: s = singlet, d = doublet, t = triplet, q = quartet, p = pentet, br = broad, m = multiplet. Spectra are reported based on appearance, not on theoretical multiplicities derived from structural information.

A Varian MAT CH7A mass spectrometer was used to obtain low- and high-resolution electron impact (EI) mass spectra. Low- and high-resolution electrospray (ESI) mass spectra were obtained on a Varian MAT 711 MS instrument operating in either positive or negative ionization modes.

UV/Vis spectra and time-resolved light-dependent AChE activity were recorded on a Varian Cary 50 Bio UV-Visible Spectrophotometer using Helma SUPRASIL precision cuvettes (10 mm light path) equipped with a Polychrome V (Till Photonics) monochromator (intensity vs. wavelength screen, Figure XX).

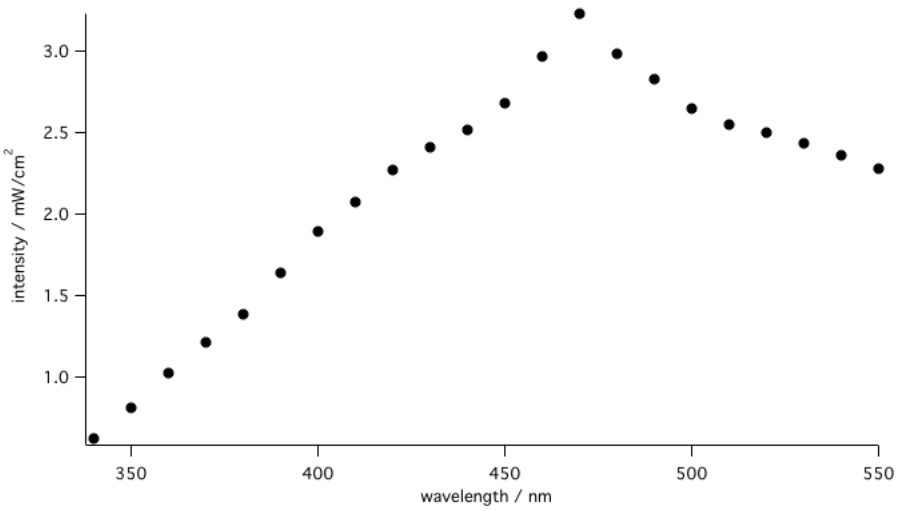


Figure 60: Wavelength versus intensity screen of the Till Photonics Polychrome V.

LC-MS was performed on an Agilent 1260 Infinity HPLC System, MS-Agilent 1100 Series, Type: 1946D, Model: SL, equipped with a Agilent Zorbax Eclipse Plus C18 (100 x 4.6 mm, particle size 3.5 micron) RP column with a constant flow-rate of 2 mL/min.

Melting points were measured on the apparatus BÜCHI Melting Point B-540 from *BÜCHI Labortechnik AG* or on an EZ-Melt apparatus form *Stanford Research Systems* and are uncorrected.

Infrared spectra (IR) were recorded on a PERKIN ELMER Spectrum BX-59343 instrument as neat materials. For detection a SMITHS DETECTION DuraSam-plIR II Diamond ATR sensor was used. The measured wave numbers are reported in $cm^{-1}$.

X-ray data collections were performed either on an Oxford Diffraction Xcalibur diffractometer, on a Bruker D8Quest diffractometer or on a Bruker D8Venture at 100 K or at 173 K using MoKα-radiation (λ = 0.71073 Å, graphite monochromator). The CrysAlisPro software (version 1.171.33.41)[CrysAlisPro, Oxford Diffraction Ltd., Version 1.171.33.41 (release 06-05-2009 CrysAlis171.NET)] was applied for the integration, scaling and multi-scan absorption correction of the data. The structures were solved by direct methods with SIR97[218] and refined by least-squares methods against F2 with SHELXL-

97.[219] All non-hydrogen atoms were refined anisotropically. The hydrogen atoms were placed in ideal geometry riding on their parent atoms.

## 12.3 Buffer Recipes

**Supplementary Table 30: Buffer recipes.**

| name | recipe |
|---|---|
| RIPA | 20 mM HEPES<br>1% NP-40<br>0.1% SDS<br>5% glycerol<br>142 mM KCl<br>5 mM $MgCl_2$<br>1 mM EDTA<br>pH = 7.45 |
| blocking buffer | 2 g/L caseine<br>0.05% Tween<br>in PBS |
| primary antibody buffer | 5% BSA<br>0.1% $NaN_3$<br>in PBS |
| Redox buffer (10x) | 2.45 M BME<br>2.45 M DTT |
| lysis buffer | 50 mM Tris<br>50 mM NaCl<br>10 mM BME<br>200 uM $ZnSO_4$<br>5 mM $MgCl_2$<br>2 EDTA-free protease inhibitor tablets (Roche, #04 693 132 001)<br>50 uM lysozyme<br>50 uM DNAse<br>pH = 8.0 |
| activation buffer A | 50 mM Tris<br>pH = 8.5 |
| washing buffer B | 25 mM Tris<br>50 mM $Na_2SO_4$<br>50 mM $NaClO_4$<br>pH = 8.8 |
| elution buffer C | 0.1 M NaOAc<br>0.2 M $NaClO_4$<br>pH = 5.6 |
| transfer buffer | 10% MeOH<br>10% Tris/Gly (10x) (Jena Bioscience, #BU-122)<br>0.00025% SDS (20%) |
| gel filtration buffer | 150 mM NaCl<br>50 mM Tris<br>pH = 7.4 |
| Gibson | 3 mL 1M Tris-HCl pH 7.5 |

| | |
|---|---|
| assembly buffer (5x) | 150 uL 2M $MgCl_2$<br>60 uL 100 mM dATP<br>60 uL 100 mM dGTP<br>60 uL 100 mM dCTP<br>60 uL 100 mM dTTP<br>300 uL 1M DTT<br>1.5 g PEG-8000<br>300 uL 100 mM NAD |
| Gibson master mix | 320 uL 5X Gibson assembly buffer<br>1 uL T5 Exonuclease<br>20 uL Phusion polymerase (Not Hotstart)<br>160 uL Taq ligase<br>700 uL $H_2O$ |
| Collecting Gel | 3.4 mL $dH_2O$<br>0.83 mL 30% acrylamide<br>0.63 mL Tris (1 M, pH = 6.8)<br>50 µL 10% SDS<br>50 µL 10% APS<br>5 µL TEMED |
| Separation Gel | 3.95 mL $dH_2O$<br>3.35 mL 30% acrylamide<br>2.5 mL Tris (1.5 M, pH = 8.8)<br>100 µL 10% SDS<br>100 µL 10% APS<br>10 µL TEMED |
| TEA buffer | 10 mM Tris<br>1 mM EDTA<br>pH = 8.0 |
| Coomassie staining | 103.75 mL MeOH<br>20.75 mL HOAc<br>125 mL $dH_2O$<br>0.5 g coomassie |
| 5x LAEMLI | 30 mL Tris (1 M, pH = 6.8)<br>10 g SDS<br>50 mL gkycerol<br>20 mL BME<br>250 mg bromophenolblue |
| 10x SDS running buffer | 30 g Tris (0.25 M)<br>144 g glycine (1.92 M)<br>10 g SDS (1%)<br>fill up to 1 L with $dH_2O$ |

## 12.4 Gibson Cloning

Restriction enzyme free cloning was performed according to Gibson *et al.*.[37] Briefly, primers were constructed with 40 bp overhangs complementary to the desired fusion DNA. PCR was performed with the PfuX protocol (*vide infra*) and DNA-fragments were analyzed on agarose gel and used after purification with a plasmid purification kit (Jena Bioscience, #PP-204L) and incubated in Gibson master mix for 1 h at 50 °C. DNA was transformed into E. coli XL10 Gold cells and growed at 37 °C o.n., before colonies were picked and grown for sequencing and further use.

## 12.5 Curve Fitting

To obtain kinetic parameters for azobenzene isomerization, data points were fitted exponentially (eq. 1, $x_0$ being a constant, not a fitting coefficient) using IgorPro (version 6.22A) and values are given as mean±S.D..

$$y = y_0 + A^*\exp[-(x-x_0)/\tau] \quad \text{(eq. 1)}$$

To obtain IC50 values data points were fitted sigmoidal (eq. 2) or using the Hill equation (eq. 3) using IgorPro (version 6.22A) and the resulting equation was solved to obtain the $IC_{50}$ by using $y = 0.5$.

$$y = base + [max / (1 + \exp[(xhalf - x)/rate)]] \quad \text{(eq. 2)}$$

$$y = base + (max - base)/(1 + (xhalf / x)^{rate}) \quad \text{(eq. 3)}$$

### 12.6 Converting $IC_{50}$ to $K_i$

Inhibitory constants were determined using the Cheng-Prussow equation (eq. 4) with the measured half-maximal inibitory constants ($IC_{50}$).

$$K_i = IC_{50} / (1 + [S]/K_M) \quad \text{(eq. 4)}$$

## 12.7 Full DNA Sequences

### 12.7.1 AmVKR

AAAATCGTGATCTCAAATCGATGTCTGACCATGCTCGAAGATGTGAATCCAAAGAGG
GTAATCCATTTGGACGGGCAACCATTGAACATAAATTTCGAGGTGTCTCGTAGAGTG
ACTCAGAGGCTGGCTACTATAATCATGAAAATATTCTTGACAGAGGTGCTCGGTTAT
TCGAAAGTGTCTATCTATGAAAAGGAGGATGAGTTCAGGGCGGAGGAAACTTTCAGC
AGATTGTCCGACGACATTATGTTTAGTAGCAAACTTCCAATGGTGAATATGGAGGTG
TGGATCCCGCCGCACCTAGACACAATGCCACTGCTAAATTCGCATGAAGTGAAAGAA
TGCGGATCCATCGCTCCCCCGGGCCGTTTCGGTTGGTTCGTTCCTACTGCGTTATCC
AGGCGCAACGACAATTGGATAATCTTCACGGAGCTTGAAAAAGCTTCCCGCTTCGAG
ATGGACGAATCCACGTTGGACAGCATTCGGAATTTTACCATAGACCCGAAAACCAGT
ACCTATTACTGCCAGGAATCGTATTGCCAACAGGGAATGTACATTCCGGAATGGTGC
CAAGGGAAACCGTGCGCTTTATTGTTGACCAGTTACATCGATGTTACCAATCTTGTC
AAGGATCGCATAGATCAAATGAAACTGTACGTGAACGTGATCTGGTTCGGGCCGAAT
TTGAAACACGTGATCAAACTTGCTGAAGAGCTGATGTTCGATCGAAACTCGTCTACT
TCCATCGATAGATCGTTGGTATTTCTGCATTGGACTCCCAGCACCGTGATACCTAAC
GAGAGGGATTTCGTCAGCATCGACTTCCCCCGATGCGGCGCCACGAGCTCGGAGATC
GGTTGCAAGTACGAATCCAACAGGTTGACCAAACTCGTCTGGGCCAGGCTCGAATAC
GCCGCCAAATTGGCCTACGAGGCGATCAATCGCGCGAAATTCACGCGCGAGATGTAC
GAGGATCTGATCGACAGGCGCAACCGCGATTCATCCATGAACGAAGAAGAGATCGCG
TGCGACTGGTTGAGGGAGAATCTCAACTACACTCTCGATGCGTGGATGCCGAATACC
GCCGACAAGAACATTCTCTACGTCGGCGGGATATTTCCTATGAGCGAGACGTTTTAT
TCGGGGAAAGCGATATTGGTCGCGGCCATGATGGCAAAGGAGGCGATCAACGTGAAC
AACACCATCCTCAGGGATTACAATTTCACCCTGCTGGTGAATGACGGCCAATGCAAA
TCGGATATGGTGATGAGATCGTTCATCAATTACATAGTGCACAATCAGTACGAGAAG
CTTGTCGGCGTTTTGGGGCCCGCTTGTTCGGAGACCGTCGAGCCTTTGGTCGGCGTT
TCCAAGCATTACAAGACGGTGGTGATCAGTTACAGCGCCGAGGGATCCAGCTTCAAC
GATCGCACTAAGTATCCTTACTTCTTTCGGACTATCGGCGAGAACAAGCAGTACAAG
CACGTTTATTTGCAATTGTTGAAGAAACTCGGATGGAAGAGGGTGGCTTCGTTGACG
GAGGATGGACAGAAATACACCGAGTACATATCTTACATGCAAGATTTGTTCAGGGAC
AATGGAATCGTGTTCGTGGCGAATGCAAAGTTTCCAAGGGAACGGGAACCCATTGTG
ATGACCAAGTATTTGCAAGATTTCAAGCAGAAGAAGGCAAAGATCATCATCGCTGAT
GTATACGATCAAGCAGCCCGTCAAGTTATGTGCAACGCGTACAAATTAGAAATGACA
GCGGTTCAGGGCTACGTGTGGTTCTTGCCTCTTTGGCTACGACCAGAATGGTACGAT
ACGGATCGATACAATCAGGAAGGGGAACAGGTTCCGTGTACCACGGCAGAAATGAGC
AAAGCGATAAACGGATATCTCGGTTTATCTCACGCGTACTTTGCACCGGATAACGAC
ATCATGCAAGAAGGGATAACGGTGCGTCAATGGCGCGATCGTTACGAGCTTCAGTGC
CAGAATAAGGAACAACCGCCGTCTAATTACGCTGGTTACGCGTATGACGCTATGTGG
ACTTACGCCTACGCGATGGACAGGCTGCTTCGCGAGAATCAGAGTTACGTTTTCGAT
CTGCATAGCAATCATACTATCAATCGATTAACGGACATCATCGGTGAAACGGATTTT
TACGGGGTGTCTGGGAGAATAAAATTCTTCGGTGGCCCTTCGAGATATTCTGTTATC
AATATCGTTCAGCATGTTAATAACGAAACTCGATTGGTCGGTAATTTTTACCCCAAC
GTGTCAGAAAAGCAGCACGAAGTGGCGGGTGGTAAATTGGATTTGAATGTCTCTTCC
TTGGTCTGGCTATCGAAAAGCATGCCAGACGATGGCTCCGAACCACCTCAACGATGT
GTCATCGGTGGATTCGCAGATTTCATAAACGTGTCTTGCGAAGTAGCTTTCGTGATC
GTCAATATCATTGGTTTCACATTACTCGGGATATTCTTGATCATTGGTTTCCTCATC
ATCAAACAAAGATACGAAAGAAAAGTACGCGAGCAGAGAGAGTATCTGAAGTCTATG

GGCATATCCTACGCCTGTGACGACTCGTCTGATCTGGACAAATGGGAGATTCCTCGA
CACAGGGTGGTTATTAACCGAAAATTGGGGGAGGGTGCTTTTGGAACGGTTTACGGT
GGCGAGGCGTTCTTCCCTGAAAAGGGTTGGCTAGCCGTGGCCGTGAAGACTCTGAAG
ATTGGAAGTTCCACCGAGGAAAAATTAGACTTTCTGAGCGAGGTGGAAGTGATGAAA
CAGTTCGAGCACAAGAATATAATCAAACTGTTAGGGGTTTGCATCAAGAGCGAACCA
GTCTTAACCGTGATGGAATTCATGCTTTACGGCGATCTGAAGACGTATCTTCTCGCC
AGAAGGCATCTCGTCAACGACAACAGTTACGAAGATTCGGACGAGATCTCTAACAAA
AAGTTAACCGCAATGGCGTTAGATGTAGCTAGGGCGCTCAGCTATTTGGCTCAGTCA
AAATATGTTCATAGGGATATTGCCTCGCGTAATTGTCTGGTGAACGCGCAACGTGTA
GTGAAGCTTGGAGATTTTGGTATGACGAGGTTGATGTACGAGAACGATTACTACAAG
TTCAATCGAAGACGTATGCTACCTGTAAGATGGATGGCACCAGAATCCTTGGGACTG
GGTATCTTCAGTCCAGCTTCGGATGTGTGGTCCTATGGCGTTCTTTTGTACGAGATT
ATCACGTTCGGTAGCTTCCCTTTCCAGGGTATGAGCAATATCGAAGTACTGRATCAC
GTTAAGAGTGGAAACTCGTTGATGGTTCCCAAAGGAGTGAAGATACAATTAGAAAAC
TTGATGTACTCTTGTTGGAGGCTAGATCACATAAAGAGGCCAACTGCTCCGGAGATC
GTCGAGTTTCTAGCCACGAATCCTCGAATTTTATCTCCCTGTTTAGACGTTCCTTTG
GCCAGTGTGCAGRTCGAGCATACCGGACAATTAGACATAGAGTTACCAGAGAATTTG
AGGAAGTTTTCATTGTCGTGGTCACCTCAGAATTCCACGACTCGACCCGCGTCCACG
TCCAGCCCTTTCGGTGTACCGTATCCATCTTTGCTAGACATCAATGATCACGACGAT
AAGCCGATTCAAAACTCGATTATGGGCAACGGAATCGCCGACGCAGAGAGTTCCAGG
CCACTTTTGTTGAACGCCAACGAACCTTTGTCGGGTTTACCTATGATTCTTCAAAGC
TTCAAGCAGAAAGAGGAGTCGCCGCATAAATACGTCAACATTCAGCCGGGGATATCG
AATAATTGCGATTACTCGAGCGATCAGAACGGCGGTGGCAGCATTCAGATGGAGGAA
AGAAGGGCCATATTGCCGGAAAATAGAAAGTCGGAGGACGTGTCGATTCTTTGA

### 12.7.2 VFT$^{mGluR2}$-TK$^{AmVKR}$ Chimera A

GAGGGCCCGGCCAAGAAGGTGCTGACCCTGGAGGGGGACCTGGTGCTGGGTGGGCTG
TTCCCAGTGCACCAGAAGGGTGGCCCAGCCGAGGAGTGTGGACCTGTTAATGAGCAC
CGAGGCATACAGCGCCTAGAGGCTATGCTTTTTGCACTGGACCGCATCAACCGCGAC
CCCCACCTGCTGCCTGGTGTGCGCTTGGGTGCGCACATCCTCGACAGCTGCTCCAAG
GATACACACGCCCTGGAGCAGGCGCTGGACTTTGTGCGTGCCTCACTCAGTCGTGGC
GCTGACGGCTCACGCCACATCTGTCCTGATGGCTCCTATGCCACCCACAGTGATGCT
CCTACAGCTGTCACCGGTGTCATTGGTGGCTCCTACAGTGATGTCTCCATCCAGGTG
GCCAATCTCCTGCGGCTGTTCCAGATCCCACAGATCAGCTATGCCTCCACCAGTGCC
AAGCTGAGTGACAAGTCCCGTTACGATTACTTTGCTCGCACTGTGCCCCCAGACTTC
TTCCAAGCCAAGGCCATGGCTGAGATTCTCCGCTTTTTCAACTGGACATATGTGTCT
ACGGTGGCATCTGAGGGTGACTATGGTGAGACAGGCATTGAGGCTTTCGAGCTCGAG
GCTCGGGCACGCAACATCTGCGTGGCCACTTCTGAGAAGGTGGGCCGTGCCATGAGC
CGCGCTGCCTTCGAGGGCGTGGTGCGAGCCCTGTTGCAGAAACCCAGTGCCCGTGTG
GCTGTGCTCTTCACCCGGTCCGAGGATGCCCGTGAGCTGCTTGCAGCCACCCAGCGC
CTCAACGCCAGCTTCACATGGGTGGCCAGCGACGGCTGGGGGGCCCTGGAGAGCGTG
GTGGCAGGCAGTGAAAGGGCTGCTGAGGGCGCCATCACCATTGAACTGGCCTCCTAC
CCCATCAGTGACTTTGCTTCCTACTTCCAGAGCTTGGATCCCTGGAACAACAGCAGA
AACCCTTGGTTCCGTGAGTTCTGGGAGGAGAGGTTCCATTGCAGCTTCCGGCAGCGA
GACTGTGCCGCCCACTCTCTGCGGGCCGTGCCCTTTGAACAGGAGTCAAAGATCATG
TTTGTGGTTAATGCCGTCTATGCCATGGCCCACGCTCTACACAACATGCACCGTGCC
CTCTGTCCCAACACCACCCACCTCTGCGATGCTATGAGGCCTGTCAATGGGCGCCGC
CTCTACAAAGACTTCGTGCTCAATGTCAAGTTTGACGCCCCCTTTCGCCCAGCAGAT
ACTGACGATGAGGTCCGCTTCGACCGCTTTGGTGACGGTATTGGCCGCTACAACATC
TTCACCTATCTGCGGGCAGGCAGTGGGCGCTATCGCTACCAGAAGGTAGGCTACTGG
GCAGAAGGTCTGACTCTGGACACTAGCTTCATTCCATGGGCCTCCCCATCAGCCGGA

CCTCTTCCTGCCTCTCGCTTCGTGATCGTCAATATCATTGGTTTCACATTACTCGGG
ATATTCTTGATCATTGGTTTCCTCATCATCAAACAAAGATACGAAAGAAAAGTACGC
GAGCAGAGAGAGTATCTGAAGTCTATGGGCATATCCTACGCCTGTGACGACTCGTCT
GATCTGGACAAATGGGAGATTCCTCGACACAGGGTGGTTATTAACCGAAAATTGGGG
GAGGGTGCTTTTGGAACGGTTTACGGTGGCGAGGCGTTCTTCCCTGAAAAGGGTTGG
CTAGCCGTGGCCGTGAAGACTCTGAAGATTGGAAGTTCCACCGAGGAAAAATTAGAC
TTTCTGAGCGAGGTGGAAGTGATGAAACAGTTCGAGCACAAGAATATAATCAAACTG
TTAGGGGTTTGCATCAAGAGCGAACCAGTCTTAACCGTGATGGAATTCATGCTTTAC
GGCGATCTGAAGACGTATCTTCTCGCCAGAAGGCATCTCGTCAACGACAACAGTTAC
GAAGATTCGGACGAGATCTCTAACAAAAAGTTAACCGCAATGGCGTTAGATGTAGCT
AGGGCGCTCAGCTATTTGGCTCAGTCAAAATATGTTCATAGGGATATTGCCTCGCGT
AATTGTCTGGTGAACGCGCAACGTGTAGTGAAGCTTGGAGATTTTGGTATGACGAGG
TTGATGTACGAGAACGATTACTACAAGTTCAATCGAAGAGGTATGCTACCTGTAAGA
TGGATGGCACCAGAATCCTTGGGACTGGGTATCTTCAGTCCAGCTTCGGATGTGTGG
TCCTATGGCGTTCTTTTGTACGAGATTATCACGTTCGGTAGCTTCCCTTTCCAGGGT
ATGAGCAATATCGAAGTACTGAATCACGTTAAGAGTGGAAACTCGTTGATGGTTCCC
AAAGGAGTGAAGATACAATTAGAAAACTTGATGTACTCTTGTTGGAGGCTAGATCAC
ATAAAGAGGCCAACTGCTCCGGAGATCGTCGAGTTTCTAGCCACGAATCCTCGAATT
TTATCTCCCTGTTTAGACGTTCCTTTGGCCAGTGTGCAGGTCGAGCATACCGGACAA
TTAGACTTAGAGTTACCAGAGAATTTGAGGAAGTTTTCATTGTCGTGGTCACCTCAG
AATTCCACGACTCGACCCGCGTCCACGTCCAGCCCTTTCGGTGTACCGTATCCATCT
TTGCTAGACATCAATGATCACGACGATAAGCCGATTCAAAACTCGATTATGGGCAAC
GGAATCGCCGACACGGAGAGTTCCAGGCCACTTTTGTTGAACGCCAACGAACCTTTG
TCGGGTTTACCTATGATTCTTCAAAGCTTCAAGCAGAAAGAGGAGTCGCCGCATAAA
TACGTCAACATTCAGCCGGGGATATCGAATAATTGCGATTACTCGAGCGATCAGAAC
GGCGGTGGCAGCATTCAGATGGAGGAAAGAAGGGCCATATTGCCGGAAAATAGAAAG
TCGGAGGACGTGTCGATTCTTTCTAAATGA

### 12.7.3 VFT$^{mGluR2}$-TK$^{AmVKR}$ Chimera B

GAGGGCCCGGCCAAGAAGGTGCTGACCCTGGAGGGGGACCTGGTGCTGGGTGGGCTG
TTCCCAGTGCACCAGAAGGGTGGCCCAGCCGAGGAGTGTGGACCTGTTAATGAGCAC
CGAGGCATACAGCGCCTAGAGGCTATGCTTTTTGCACTGGACCGCATCAACCGCGAC
CCCCACCTGCTGCCTGGTGTGCGCTTGGGTGCGCACATCCTCGACAGCTGCTCCAAG
GATACACACGCCCTGGAGCAGGCGCTGGACTTTGTGCGTGCCTCACTCAGTCGTGGC
GCTGACGGCTCACGCCACATCTGTCCTGATGGCTCCTATGCCACCCACAGTGATGCT
CCTACAGCTGTCACCGGTGTCATTGGTGGCTCCTACAGTGATGTCTCCATCCAGGTG
GCCAATCTCCTGCGGCTGTTCCAGATCCCACAGATCAGCTATGCCTCCACCAGTGCC
AAGCTGAGTGACAAGTCCCGTTACGATTACTTTGCTCGCACTGTGCCCCCAGACTTC
TTCCAAGCCAAGGCCATGGCTGAGATTCTCCGCTTTTTCAACTGGACATATGTGTCT
ACGGTGGCATCTGAGGGTGACTATGGTGAGACAGGCATTGAGGCTTTCGAGCTCGAG
GCTCGGGCACGCAACATCTGCGTGGCCACTTCTGAGAAGGTGGGCCGTGCCATGAGC
CGCGCTGCCTTCGAGGGCGTGGTGCGAGCCCTGTTGCAGAAACCCAGTGCCCGTGTG
GCTGTGCTCTTCACCCGGTCCGAGGATGCCCGTGAGCTGCTTGCAGCCACCCAGCGC
CTCAACGCCAGCTTCACATGGGTGGCCAGCGACGGCTGGGGGGCCCTGGAGAGCGTG
GTGGCAGGCAGTGAAAGGGCTGCTGAGGGCGCCATCACCATTGAACTGGCCTCCTAC
CCCATCAGTGACTTTGCTTCCTACTTCCAGAGCTTGGATCCCTGGAACAACAGCAGA
AACCCTTGGTTCCGTGAGTTCTGGGAGGAGAGGTTCCATTGCAGCTTCCGGCAGCGA
GACTGTGCCGCCCACTCTCTGCGGGCCGTGCCCTTTGAACAGGAGTCAAAGATCATG
TTTGTGGTTAATGCCGTCTATGCCATGGCCCACGCTCTACACAACATGCACCGTGCC
CTCTGTCCCAACACCACCCACCTCTGCGATGCTATGAGGCCTGTCAATGGGCGCCGC
CTCTACAAAGACTTCGTGCTCAATGTCAAGTTTGACGCCCCCTTTCGCCCAGCAGAT

ACTGACGATGAGGTCCGCTTCGACCGCTTTGGTGACGGTATTGGCCGCTACAACATC
TTCACCTATCTGCGGGCAGGCAGTGGGCGCTATCGCTACCAGAAGGTAGGCTACTGG
GCAGAAGGTCTGACTCTGGACACTAGCTTCATTCCATGGGCCTCCCCATCAGCCGGA
CCTCTTCCTGCCTCTCGCGAAACTCGATTGGTCGGTAATTTTTACCCCAACGTGTCA
GAAAAGCAGCACGAAGTGGCGGGTGGTAAATTGGATTTGAATGTCTCTTCCTTGGTC
TGGCTATCGAAAAGCATGCCAGACGATGGCTCCGAACCACCTCAACGATGTGTCATC
GGTGGATTCGCAGATTTCATAAACGTGTCTTGCGAAGTAGCTTTCGTGATCGTCAAT
ATCATTGGTTTCACATTACTCGGGATATTCTTGATCATTGGTTTCCTCATCATCAAA
CAAAGATACGAAAGAAAAGTACGCGAGCAGAGAGAGTATCTGAAGTCTATGGGCATA
TCCTACGCCTGTGACGACTCGTCTGATCTGGACAAATGGGAGATTCCTCGACACAGG
GTGGTTATTAACCGAAAATTGGGGGAGGGTGCTTTTGGAACGGTTTACGGTGGCGAG
GCGTTCTTCCCTGAAAAGGGTTGGCTAGCCGTGGCCGTGAAGACTCTGAAGATTGGA
AGTTCCACCGAGGAAAAATTAGACTTTCTGAGCGAGGTGGAAGTGATGAAACAGTTC
GAGCACAAGAATATAATCAAACTGTTAGGGGTTTGCATCAAGAGCGAACCAGTCTTA
ACCGTGATGGAATTCATGCTTTACGGCGATCTGAAGACGTATCTTCTCGCCAGAAGG
CATCTCGTCAACGACAACAGTTACGAAGATTCGGACGAGATCTCTAACAAAAAGTTA
ACCGCAATGGCGTTAGATGTAGCTAGGGCGCTCAGCTATTTGGCTCAGTCAAAATAT
GTTCATAGGGATATTGCCTCGCGTAATTGTCTGGTGAACGCGCAACGTGTAGTGAAG
CTTGGAGATTTTGGTATGACGAGGTTGATGTACGAGAACGATTACTACAAGTTCAAT
CGAAGAGGTATGCTACCTGTAAGATGGATGGCACCAGAATCCTTGGGACTGGGTATC
TTCAGTCCAGCTTCGGATGTGTGGTCCTATGGCGTTCTTTTGTACGAGATTATCACG
TTCGGTAGCTTCCCTTTCCAGGGTATGAGCAATATCGAAGTACTGAATCACGTTAAG
AGTGGAAACTCGTTGATGGTTCCCAAAGGAGTGAAGATACAATTAGAAAACTTGATG
TACTCTTGTTGGAGGCTAGATCACATAAAGAGGCCAACTGCTCCGGAGATCGTCGAG
TTTCTAGCCACGAATCCTCGAATTTTATCTCCCTGTTTAGACGTTCCTTTGGCCAGT
GTGCAGGTCGAGCATACCGGACAATTAGACATAGAGTTACCAGAGAATTTGAGGAAG
TTTTCATTGTCGTGGTCACCTCAGAATTCCACGACTCGACCCGCGTCCACGTCCAGC
CCTTTCGGTGTACCGTATCCATCTTTGCTAGACATCAATGATCACGACGATAAGCCG
ATTCAAAACTCGATTATGGGCAACGGAATCGCCGACACGGAGAGTTCCAGGCCACTT
TTGTTGAACGCCAACGAACCTTTGTCGGGTTTACCTATGATTCTTCAAAGCTTCAAG
CAGAAAGAGGAGTCGCCGCATAAATACGTCAACATTCAGCCGGGGATATCGAATAAT
TGCGATTACTCGAGCGATCAGAACGGCGGTGGCAGCATTCAGATGGAGGAAAGAAGG
GCCATATTGCCGGAAAATAGAAAGTCGGAGGACGTGTCGATTCTTTCTAAATGA

### 12.7.4 VFT$^{mGluR2}$-TK$^{AmVKR}$ Chimera C

AGGCATACAGCGCCTAGAGGCTATGCTTTTTGCACTGGACCGCATCAACCGCGACCC
CCACCTGCTGCCTGGTGTGCGCTTGGGTGCGCACATCCTCGACAGCTGCTCCAAGGA
TACACACGCCCTGGAGCAGGCGCTGGACTTTGTGCGTGCCTCACTCAGTCGTGGCGC
TGACGGCTCACGCCACATCTGTCCTGATGGCTCCTATGCCACCCACAGTGATGCTCC
TACAGCTGTCACCGGTGTCATTGGTGGCTCCTACAGTGATGTCTCCATCCAGGTGGC
CAATCTCCTGCGGCTGTTCCAGATCCCACAGATCAGCTATGCCTCCACCAGTGCCAA
GCTGAGTGACAAGTCCCGTTACGATTACTTTGCTCGCACTGTGCCCCCAGACTTCTT
CCAAGCCAAGGCCATGGCTGAGATTCTCCGCTTTTTCAACTGGACATATGTGTCTAC
GGTGGCATCTGAGGGTGACTATGGTGAGACAGGCATTGAGGCTTTCGAGCTCGAGGC
TCGGGCACGCAACATCTGCGTGGCCACTTCTGAGAAGGTGGGCCGTGCCATGAGCCG
CGCTGCCTTCGAGGGCGTGGTGCGAGCCCTGTTGCAGAAACCCAGTGCCCGTGTGGC
TGTGCTCTTCACCCGGTCCGAGGATGCCCGTGAGCTGCTTGCAGCCACCCAGCGCCT
CAACGCCAGCTTCACATGGGTGGCCAGCGACGGCTGGGGGGCCCTGGAGAGCGTGGT
GGCAGGCAGTGAAAGGGCTGCTGAGGGCGCCATCACCATTGAACTGGCCTCCTACCC
CATCAGTGACTTTGCTTCCTACTTCCAGAGCTTGGATCCCTGGAACAACAGCAGAAA
CCCTTGGTTCCGTGAGTTCTGGGAGGAGAGGTTCCATTGCAGCTTCCGGCAGCGAGA

CTGTGCCGCCCACTCTCTGCGGGCCGTGCCCTTTGAACAGGAGTCAAAGATCATGTT
TGTGGTTAATGCCGTCTATGCCATGGCCCACGCTCTACACAACATGCACCGTGCCCT
CTGTCCCAACACCACCCACCTCTGCGATGCTATGAGGCCTGTCAATGGGCGCCGCCT
CTACAAAGACTTCGTGCTCAATGTCAAGTTTGACGCCCCCTTTCGCCCAGCAGATAC
TGACGATGAGGTCCGCTTCGACCGCTTTGGTGACGGTATTGGCCGCTACAACATCTT
CACCTATCTGCGGGCAGGCAGTGGGCGCTATCGCTACCAGAAGGTAGGCTACTGGGC
AGAAGGTCTGACTCTGGACACTAGCTTCATTCCATGGGCCTCCCCATCAGCCGGACC
TCTTCCTGCCTCTCGCTGTAGCGAGCCCTGCCTTCAGAACGAGGTGAAGAGCGTGCA
GCCGGGCGAGGTCTGCTGTTGGCTCTGCATTCCCTGTCAGCCCTATGAGTACAGGCT
GGATGAGTTCACCTGCGCTGACTGTGGCCTGGGCTACTGGCCTAATGCCAGTCTGAC
TGGCTGCTTTGAGCTGCCCCAGGAGTACATCCGCTGGGGTGATGCCTGGTTCGTGAT
CGTCAATATCATTGGTTTCACATTACTCGGGATATTCTTGATCATTGGTTTCCTCAT
CATCAAACAAAGATACGAAAGAAAAGTACGCGAGCAGAGAGAGTATCTGAAGTCTAT
GGGCATATCCTACGCCTGTGACGACTCGTCTGATCTGGACAAATGGGAGATTCCTCG
ACACAGGGTGGTTATTAACCGAAAATTGGGGGAGGGTGCTTTTGGAACGGTTTACGG
TGGCGAGGCGTTCTTCCCTGAAAAGGGTTGGCTAGCCGTGGCCGTGAAGACTCTGAA
GATTGGAAGTTCCACCGAGGAAAAATTAGACTTTCTGAGCGAGGTGGAAGTGATGAA
ACAGTTCGAGCACAAGAATATAATCAAACTGTTAGGGGTTTGCATCAAGAGCGAACC
AGTCTTAACCGTGATGGAATTCATGCTTTACGGCGATCTGAAGACGTATCTTCTCGC
CAGAAGGCATCTCGTCAACGACAACAGTTACGAAGATTCGGACGAGATCTCTAACAA
AAAGTTAACCGCAATGGCGTTAGATGTAGCTAGGGCGCTCAGCTATTTGGCTCAGTC
AAAATATGTTCATAGGGATATTGCCTCGCGTAATTGTCTGGTGAACGCGCAACGTGT
AGTGAAGCTTGGAGATTTTGGTATGACGAGGTTGATGTACGAGAACGATTACTACAA
GTTCAATCGAAGAGGTATGCTACCTGTAAGATGGATGGCACCAGAATCCTTGGGACT
GGGTATCTTCAGTCCAGCTTCGGATGTGTGGTCCTATGGCGTTCTTTTGTACGAGAT
TATCACGTTCGGTAGCTTCCCTTTCCAGGGTATGAGCAATATCGAAGTACTGAATCA
CGTTAAGAGTGGAAACTCGTTGATGGTTCCCAAAGGAGTGAAGATACAATTAGAAAA
CTTGATGTACTCTTGTTGGAGGCTAGATCACATAAAGAGGCCAACTGCTCCGGAGAT
CGTCGAGTTTCTAGCCACGAATCCTCGAATTTTATCTCCCTGTTTAGACGTTCCTTT
GGCCAGTGTGCAGGTCGAGCATACCGGACAATTAGACATAGAGTTACCAGAGAATTT
GAGGAAGTTTTCATTGTCGTGGTCACCTCAGAATTCCACGACTCGACCCGCGTCCAC
GTCCAGCCCTTTCGGTGTACCGTATCCATCTTTGCTAGACATCAATGATCACGACGA
TAAGCCGATTCAAAACTCGATTATGGGCAACGGAATCGCCGACACGGAGAGTTCCAG
GCCACTTTTGTTGAACGCCAACGAACCTTTGTCGGGTTTACCTATGATTCTTCAAAG
CTTCAAGCAGAAAGAGGAGTCGCCGCATAAATACGTCAACATTCAGCCGGGGATATC
GAATAATTGCGATTACTCGAGCGATCAGAACGGCGGTGGCAGCATTCAGATGGAGGA
AAGAAGGGCCATATTGCCGGAAAATAGAAAGTCGGAGGACGTGTCGATTCTTTCTAA
ATGA

### 12.7.5 VFT$^{mGluR2}$-TK$^{AmVKR}$ Chimera D

AGGCATACAGCGCCTAGAGGCTATGCTTTTTGCACTGGACCGCATCAACCGCGACCC
CCACCTGCTGCCTGGTGTGCGCTTGGGTGCGCACATCCTCGACAGCTGCTCCAAGGA
TACACACGCCCTGGAGCAGGCGCTGGACTTTGTGCGTGCCTCACTCAGTCGTGGCGC
TGACGGCTCACGCCACATCTGTCCTGATGGCTCCTATGCCACCCACAGTGATGCTCC
TACAGCTGTCACCGGTGTCATTGGTGGCTCCTACAGTGATGTCTCCATCCAGGTGGC
CAATCTCCTGCGGCTGTTCCAGATCCCACAGATCAGCTATGCCTCCACCAGTGCCAA
GCTGAGTGACAAGTCCCGTTACGATTACTTTGCTCGCACTGTGCCCCCAGACTTCTT
CCAAGCCAAGGCCATGGCTGAGATTCTCCGCTTTTTCAACTGGACATATGTGTCTAC
GGTGGCATCTGAGGGTGACTATGGTGAGACAGGCATTGAGGCTTTCGAGCTCGAGGC
TCGGGCACGCAACATCTGCGTGGCCACTTCTGAGAAGGTGGGCCGTGCCATGAGCCG
CGCTGCCTTCGAGGGCGTGGTGCGAGCCCTGTTGCAGAAACCCAGTGCCCGTGTGGC

TGTGCTCTTCACCCGGTCCGAGGATGCCCGTGAGCTGCTTGCAGCCACCCAGCGCCT
CAACGCCAGCTTCACATGGGTGGCCAGCGACGGCTGGGGGGCCCTGGAGAGCGTGGT
GGCAGGCAGTGAAAGGGCTGCTGAGGGCGCCATCACCATTGAACTGGCCTCCTACCC
CATCAGTGACTTTGCTTCCTACTTCCAGAGCTTGGATCCCTGGAACAACAGCAGAAA
CCCTTGGTTCCGTGAGTTCTGGGAGGAGAGGTTCCATTGCAGCTTCCGGCAGCGAGA
CTGTGCCGCCCACTCTCTGCGGGCCGTGCCCTTTGAACAGGAGTCAAAGATCATGTT
TGTGGTTAATGCCGTCTATGCCATGGCCCACGCTCTACACAACATGCACCGTGCCCT
CTGTCCCAACACCACCCACCTCTGCGATGCTATGAGGCCTGTCAATGGGCGCCGCCT
CTACAAAGACTTCGTGCTCAATGTCAAGTTTGACGCCCCCTTTCGCCCAGCAGATAC
TGACGATGAGGTCCGCTTCGACCGCTTTGGTGACGGTATTGGCCGCTACAACATCTT
CACCTATCTGCGGGCAGGCAGTGGGCGCTATCGCTACCAGAAGGTAGGCTACTGGGC
AGAAGGTCTGACTCTGGACACTAGCTTCATTCCATGGGCCTCCCCATCAGCCGGACC
TCTTCCTGCCTCTCGCTGTAGCGAGCCCTGCCTTCAGAACGAGGTGAAGAGCGTGCA
GCCGGGCGAGGTCTGCTGTTGGCTCTGCATTCCCTGTCAGCCCTATGAGTACAGGCT
GGATGAGTTCACCTGCGCTGACTGTGGCCTGGGCTACTGGCCTAATGCCAGTCTGAC
TGGCTGCTTTGAGCTGCCCCAGGAGTACATCCGCTGGGGTGATGCCTGGGAAACTCG
ATTGGTCGGTAATTTTTACCCCAACGTGTCAGAAAAGCAGCACGAAGTGGCGGGTGG
TAAATTGGATTTGAATGTCTCTTCCTTGGTCTGGCTATCGAAAAGCATGCCAGACGA
TGGCTCCGAACCACCTCAACGATGTGTCATCGGTGGATTCGCAGATTTCATAAACGT
GTCTTGCGAAGTAGCTTTCGTGATCGTCAATATCATTGGTTTCACATTACTCGGGAT
ATTCTTGATCATTGGTTTCCTCATCATCAAACAAAGATACGAAAGAAAAGTACGCGA
GCAGAGAGAGTATCTGAAGTCTATGGGCATATCCTACGCCTGTGACGACTCGTCTGA
TCTGGACAAATGGGAGATTCCTCGACACAGGGTGGTTATTAACCGAAAATTGGGGGA
GGGTGCTTTTGGAACGGTTTACGGTGGCGAGGCGTTCTTCCCTGAAAAGGGTTGGCT
AGCCGTGGCCGTGAAGACTCTGAAGATTGGAAGTTCCACCGAGGAAAAATTAGACTT
TCTGAGCGAGGTGGAAGTGATGAAACAGTTCGAGCACAAGAATATAATCAAACTGTT
AGGGGTTTGCATCAAGAGCGAACCAGTCTTAACCGTGATGGAATTCATGCTTTACGG
CGATCTGAAGACGTATCTTCTCGCCAGAAGGCATCTCGTCAACGACAACAGTTACGA
AGATTCGGACGAGATCTCTAACAAAAAGTTAACCGCAATGGCGTTAGATGTAGCTAG
GGCGCTCAGCTATTTGGCTCAGTCAAAATATGTTCATAGGGATATTGCCTCGCGTAA
TTGTCTGGTGAACGCGCAACGTGTAGTGAAGCTTGGAGATTTTGGTATGACGAGGTT
GATGTACGAGAACGATTACTACAAGTTCAATCGAAGAGGTATGCTACCTGTAAGATG
GATGGCACCAGAATCCTTGGGACTGGGTATCTTCAGTCCAGCTTCGGATGTGTGGTC
CTATGGCGTTCTTTTGTACGAGATTATCACGTTCGGTAGCTTCCCTTTCCAGGGTAT
GAGCAATATCGAAGTACTGAATCACGTTAAGAGTGGAAACTCGTTGATGGTTCCCAA
AGGAGTGAAGATACAATTAGAAAACTTGATGTACTCTTGTTGGAGGCTAGATCACAT
AAAGAGGCCAACTGCTCCGGAGATCGTCGAGTTTCTAGCCACGAATCCTCGAATTTT
ATCTCCCTGTTTAGACGTTCCTTTGGCCAGTGTGCAGGTCGAGCATACCGGACAATT
AGACATAGAGTTACCAGAGAATTTGAGGAAGTTTTCATTGTCGTGGTCACCTCAGAA
TTCCACGACTCGACCCGCGTCCACGTCCAGCCCTTTCGGTGTACCGTATCCATCTTT
GCTAGACATCAATGATCACGACGATAAGCCGATTCAAAACTCGATTATGGGCAACGG
AATCGCCGACACGGAGAGTTCCAGGCCACTTTTGTTGAACGCCAACGAACCTTTGTC
GGGTTTACCTATGATTCTTCAAAGCTTCAAGCAGAAAGAGGAGTCGCCGCATAAATA
CGTCAACATTCAGCCGGGGATATCGAATAATTGCGATTACTCGAGCGATCAGAACGG
CGGTGGCAGCATTCAGATGGAGGAAAGAAGGGCCATATTGCCGGAAAATAGAAAGTC
GGAGGACGTGTCGATTCTTTCTAAATGA

### 12.7.6 VFT$^{mGluR2}$-TK$^{Met}$ (mGluR2_Met construct)

ATGGTCCTTCTGTTGATCCTGTCAGTCCTACTTCTGAAAGAAGATGTACGAGGGAGT
GCACAGTCCACGCGATACCCCTACGACGTGCCCGACTACGCCACGCGTGGATCCGAC
AAAGACTGCGAAATGAAGCGCACCACCCTGGATAGCCCTCTGGGCAAGCTGGAACTG

TCTGGGTGCGAACAGGGCCTGCACGAGATCAAGCTGCTGGGCAAAGGAACATCTGCC
GCCGACGCCGTGGAAGTGCCTGCCCCAGCCGCCGTGCTGGGCGGACCAGAGCCACTG
ATGCAGGCCACCGCCTGGCTCAACGCCTACTTTCACCAGCCTGAGGCCATCGAGGAG
TTCCCTGTGCCAGCCCTGCACCACCCAGTGTTCCAGCAGGAGAGCTTTACCCGCCAG
GTGCTGTGGAAACTGCTGAAAGTGGTGAAGTTCGGAGAGGTCATCAGCTACCAGCAG
CTGGCCGCCCTGGCCGGCAATCCCGCCGCCACCGCCGCCGTGAAAACCGCCCTGAGC
GGAAATCCCGTGCCCATTCTGATCCCCTGCCACCGGGTGGTGTCTAGCTCTGGCGCC
GTGGGGGGCTACGAGGGCGGGCTCGCCGTGAAAGAGTGGCTGCTGGCCCACGAGGGC
CACAGACTGGGCAAGCCTGGGCTGGGCACGCGTAAGAAGGTGCTGACCCTGGAGGGG
GACCTGGTGCTGGGTGGGCTGTTCCCAGTGCACCAGAAGGGTGGCCCAGCCGAGGAG
TGTGGACCTGTTAATGAGCACCGAGGCATACAGCGCCTAGAGGCTATGCTTTTTGCA
CTGGACCGCATCAACCGCGACCCCCACCTGCTGCCTGGTGTGCGCTTGGGTGCGCAC
ATCCTCGACAGCTGCTCCAAGGATACACACGCCCTGGAGCAGGCGCTGGACTTTGTG
CGTGCCTCACTCAGTCGTGGCGCTGACGGCTCACGCCACATCTGTCCTGATGGCTCC
TATGCCACCCACAGTGATGCTCCTACAGCTGTCACCGGTGTCATTGGTGGCTCCTAC
AGTGATGTCTCCATCCAGGTGGCCAATCTCCTGCGGCTGTTCCAGATCCCACAGATC
AGCTATGCCTCCACCAGTGCCAAGCTGAGTGACAAGTCCCGTTACGATTACTTTGCT
CGCACTGTGCCCCCAGACTTCTTCCAAGCCAAGGCCATGGCTGAGATTCTCCGCTTT
TTCAACTGGACATATGTGTCTACGGTGGCATCTGAGGGTGACTATGGTGAGACAGGC
ATTGAGGCTTTCGAGCTCGAGGCTCGGGCACGCAACATCTGCGTGGCCACTTCTGAG
AAGGTGGGCCGTGCCATGAGCCGCGCTGCCTTCGAGGGCGTGGTGCGAGCCCTGTTG
CAGAAACCCAGTGCCCGTGTGGCTGTGCTCTTCACCCGGTCCGAGGATGCCCGTGAG
CTGCTTGCAGCCACCCAGCGCCTCAACGCCAGCTTCACATGGGTGGCCAGCGACGGC
TGGGGGGCCCTGGAGAGCGTGGTGGCAGGCAGTGAAAGGGCTGCTGAGGGCGCCATC
ACCATTGAACTGGCCTCCTACCCCATCAGTGACTTTGCTTCCTACTTCCAGAGCTTG
GATCCCTGGAACAACAGCAGAAACCCTTGGTTCCGTGAGTTCTGGGAGGAGAGGTTC
CATTGCAGCTTCCGGCAGCGAGACTGTGCCGCCCACTCTCTGCGGGCCGTGCCCTTT
GAACAGGAGTCAAAGATCATGTTTGTGGTTAATGCCGTCTATGCCATGGCCCACGCT
CTACACAACATGCACCGTGCCCTCTGTCCCAACACCACCCACCTCTGCGATGCTATG
AGGCCTGTCAATGGGCGCCGCCTCTACAAAGACTTCGTGCTCAATGTCAAGTTTGAC
GCCCCCTTTCGCCCAGCAGATACTGACGATGAGGTCCGCTTCGACCGCTTTGGTGAC
GGTATTGGCCGCTACAACATCTTCACCTATCTGCGGGCAGGCAGTGGGCGCTATCGC
TACCAGAAGGTAGGCTACTGGGCAGAAGGTCTGACTCTGGACACTAGCTTCATTCCA
TGGGCCTCCCCATCAGCCGGACCTCTTCCTGCCTCTCGCTGTAGCGAGCCCTGCCTT
CAGAACGAGGTGAAGAGCGTGCAGCCGGGCGAGGTCTGCTGTTGGCTCTGCATTCCC
TGTCAGCCCTATGAGTACAGGCTGGATGAGTTCACCTGCGCTGACTGTGGCCTGGGC
TACTGGCCTAATGCCAGTCTGACTGGCTGCTTTGAGCTGCCCCAGGAGTACATCCGC
TGGGGTGATCCTGAGCGGCCGCAAGTAATAGTTCAACCAGATCAGAATTTCACAGGA
TTGATTGCTGGTGTTGTCTCAATATCAACAGCACTGTTATTACTACTTGGGTTTTTC
CTGTGGCTGAAAAAGAGAAAGCAAATTAAAGATCTGGGCAGTGAATTAGTTCGCTAC
GATGCAAGAGTACACACTCCTCATTTGGATAGGCTTGTAAGTGCCCGAAGTGTAAGC
CCAACTACAGAAATGGTTTCAAATGAATCTGTAGACTACCGAGCTACTTTTCCAGAA
GATCAGTTTCCTAATTCATCTCAAAACGGTTCATGCCGACAAGTGCAATATCCTCTG
ACAGACATGTCCCCCATCCTAACTAGTGGGGACTCTGATATATCCAGTCCATTACTG
CAAAATACTGTCCACATTGACCTCAGTGCTCTAAATCCAGAGCTGGTCCAGGCAGTG
CAGCATGTAGTGATTGGGCCCAGTAGCCTGATTGTGCATTTCAATGAAGTCATAGGA
AGAGGGCATTTTGGTTGTGTATATCATGGGACTTTGTTGGACAATGATGGCAAGAAA
ATTCACTGTGCTGTGAAATCCTTGAACAGAATCACTGACATAGGAGAAGTTTCCCAA
TTTCTGACCGAGGGAATCATCATGAAAGATTTTAGTCATCCCAATGTCCTCTCGCTC
CTGGGAATCTGCCTGCGAAGTGAAGGGTCTCCGCTGGTGGTCCTACCATACATGAAA
CATGGAGATCTTCGAAATTTCATTCGAAATGAGACTCATAATCCAACTGTAAAAGAT
CTTATTGGCTTTGGTCTTCAAGTAGCCAAAGGCATGAAATATCTTGCAAGCAAAAAG

TTTGTCCACAGAGACTTGGCTGCAAGAAACTGTATGCTGGATGAAAAATTCACAGTC
AAGGTTGCTGATTTTGGTCTTGCCAGAGACATGTATGATAAAGAATACTATAGTGTA
CACAACAAAACAGGTGCAAAGCTGCCAGTGAAGTGGATGGCTTTGGAAAGTCTGCAA
ACTCAAAAGTTTACCACCAAGTCAGATGTGTGGTCCTTTGGCGTGCTCCTCTGGGAG
CTGATGACAAGAGGAGCCCCACCTTATCCTGACGTAAACACCTTTGATATAACTGTT
TACTTGTTGCAAGGGAGAAGACTCCTACAACCCGAATACTGCCCAGACCCCTTATAT
GAAGTAATGCTAAAATGCTGGCACCCTAAAGCCGAAATGCGCCCATCCTTTTCTGAA
CTGGTGTCCCGGATATCAGCGATCTTCTCTACTTTCATTGGGGAGCACTATGTCCAT
GTGAACGCTACTTATGTGAACGTAAAATGTGTCGCTCCGTATCCTTCTCTGTTGTCA
TCAGAAGATAACGCTGATGATGAGGTGGACACACGACCAGCCTCCTTCTGGGAGACA
TCATAA

### 12.7.7 VFT$^{mGluR2}$-TK$^{hIR}$ (mGluR2_hIR construct LL1)

ATGGTCCTTCTGTTGATCCTGTCAGTCCTACTTCTGAAAGAAGATGTACGAGGGAGT
GCACAGTCCACGCGATACCCCTACGACGTGCCCGACTACGCCACGCGTGGATCCGAC
AAAGACTGCGAAATGAAGCGCACCACCCTGGATAGCCCTCTGGGCAAGCTGGAACTG
TCTGGGTGCGAACAGGGCCTGCACGAGATCAAGCTGCTGGGCAAAGGAACATCTGCC
GCCGACGCCGTGGAAGTGCCTGCCCCAGCCGCCGTGCTGGGCGGACCAGAGCCACTG
ATGCAGGCCACCGCCTGGCTCAACGCCTACTTTCACCAGCCTGAGGCCATCGAGGAG
TTCCCTGTGCCAGCCCTGCACCACCCAGTGTTCCAGCAGGAGAGCTTTACCCGCCAG
GTGCTGTGGAAACTGCTGAAAGTGGTGAAGTTCGGAGAGGTCATCAGCTACCAGCAG
CTGGCCGCCCTGGCCGGCAATCCCGCCGCCACCGCCGCCGTGAAAACCGCCCTGAGC
GGAAATCCCGTGCCCATTCTGATCCCCTGCCACCGGGTGGTGTCTAGCTCTGGCGCC
GTGGGGGGCTACGAGGGCGGGCTCGCCGTGAAAGAGTGGCTGCTGGCCCACGAGGGC
CACAGACTGGGCAAGCCTGGGCTGGGCACGCGTAAGAAGGTGCTGACCCTGGAGGGG
GACCTGGTGCTGGGTGGGCTGTTCCCAGTGCACCAGAAGGGTGGCCCAGCCGAGGAG
TGTGGACCTGTTAATGAGCACCGAGGCATACAGCGCCTAGAGGCTATGCTTTTTGCA
CTGGACCGCATCAACCGCGACCCCCACCTGCTGCCTGGTGTGCGCTTGGGTGCGCAC
ATCCTCGACAGCTGCTCCAAGGATACACACGCCCTGGAGCAGGCGCTGGACTTTGTG
CGTGCCTCACTCAGTCGTGGCGCTGACGGCTCACGCCACATCTGTCCTGATGGCTCC
TATGCCACCCACAGTGATGCTCCTACAGCTGTCACCGGTGTCATTGGTGGCTCCTAC
AGTGATGTCTCCATCCAGGTGGCCAATCTCCTGCGGCTGTTCCAGATCCCACAGATC
AGCTATGCCTCCACCAGTGCCAAGCTGAGTGACAAGTCCCGTTACGATTACTTTGCT
CGCACTGTGCCCCCAGACTTCTTCCAAGCCAAGGCCATGGCTGAGATTCTCCGCTTT
TTCAACTGGACATATGTGTCTACGGTGGCATCTGAGGGTGACTATGGTGAGACAGGC
ATTGAGGCTTTCGAGCTCGAGGCTCGGGCACGCAACATCTGCGTGGCCACTTCTGAG
AAGGTGGGCCGTGCCATGAGCCGCGCTGCCTTCGAGGGCGTGGTGCGAGCCCTGTTG
CAGAAACCCAGTGCCCGTGTGGCTGTGCTCTTCACCCGGTCCGAGGATGCCCGTGAG
CTGCTTGCAGCCACCCAGCGCCTCAACGCCAGCTTCACATGGGTGGCCAGCGACGGC
TGGGGGGCCCTGGAGAGCGTGGTGGCAGGCAGTGAAAGGGCTGCTGAGGGCGCCATC
ACCATTGAACTGGCCTCCTACCCCATCAGTGACTTTGCTTCCTACTTCCAGAGCTTG
GATCCCTGGAACAACAGCAGAAACCCTTGGTTCCGTGAGTTCTGGGAGGAGAGGTTC
CATTGCAGCTTCCGGCAGCGAGACTGTGCCGCCCACTCTCTGCGGGCCGTGCCCTTT
GAACAGGAGTCAAAGATCATGTTTGTGGTTAATGCCGTCTATGCCATGGCCCACGCT
CTACACAACATGCACCGTGCCCTCTGTCCCAACACCACCCACCTCTGCGATGCTATG
AGGCCTGTCAATGGGCGCCGCCTCTACAAAGACTTCGTGCTCAATGTCAAGTTTGAC
GCCCCCTTTCGCCCAGCAGATACTGACGATGAGGTCCGCTTCGACCGCTTTGGTGAC
GGTATTGGCCGCTACAACATCTTCACCTATCTGCGGGCAGGCAGTGGGCGCTATCGC
TACCAGAAGGTAGGCTACTGGGCAGAAGGTCTGACTCTGGACACTAGCTTCATTCCA
TGGGCCTCCCCATCAGCCGGACCTCTTCCTGCCTCTCGCTGTAGCGAGCCCTGCCTT
CAGAACGAGGTGAAGAGCGTGCAGCCGGGCGAGGTCTGCTGTTGGCTCTGCATTCCC

TGTCAGCCCTATGAGTACAGGCTGGATGAGTTCACCTGCGCTGACTGTGGCCTGGGC
TACTGGCCTAATGCCAGTCTGACTGGCTGCTTTGAGCTGCCCCAGGAGTACATCCGC
TGGGGTGATCCTGAGCGGCCGCTCCCGTCAAATATTGCAAAAATTATCATCGGCCCC
CTCATCTTTGTCTTTCTCTTCAGTGTTGTGATTGGAAGTATTTATCTATTCCTGAGA
AAGAGGCAGCCAGATGGGCCGCTGGGACCGCTTTACGCTTCTTCAAACCCTGAGTAT
CTCAGTGCCAGTGATGTGTTTCCATGCTCTGTGTACGTGCCGGACGAGTGGGAGGTG
TCTCGAGAGAAGATCACCCTCCTTCGAGAGCTGGGGCAGGGCTCCTTCGGCATGGTG
TATGAGGGCAATGCCAGGGACATCATCAAGGGTGAGGCAGAGACCCGCGTGGCGGTG
AAGACGGTCAACGAGTCAGCCAGTCTCCGAGAGCGGATTGAGTTCCTCAATGAGGCC
TCGGTCATGAAGGGCTTCACCTGCCATCACGTGGTGCGCCTCCTGGGAGTGGTGTCC
AAGGGCCAGCCCACGCTGGTGGTGATGGAGCTGATGGCTCACGGAGACCTGAAGAGC
TACCTCCGTTCTCTGCGGCCAGAGGCTGAGAATAATCCTGGCCGCCCTCCCCCTACC
CTTCAAGAGATGATTCAGATGGCGGCAGAGATTGCTGACGGGATGGCCTACCTGAAC
GCCAAGAAGTTTGTGCATCGGGACCTGGCAGCGAGAAACTGCATGGTCGCCCATGAT
TTTACTGTCAAAATTGGAGACTTTGGAATGACCAGAGACATCTATGAAACGGATTAC
TACCGGAAAGGGGGCAAGGGTCTGCTCCCTGTACGGTGGATGGCACCGGAGTCCCTG
AAGGATGGGGTCTTCACCACTTCTTCTGACATGTGGTCCTTTGGCGTGGTCCTTTGG
GAAATCACCAGCTTGGCAGAACAGCCTTACCAAGGCCTGTCTAATGAACAGGTGTTG
AAATTTGTCATGGATGGAGGGTATCTGGATCAACCCGACAACTGTCCAGAGAGAGTC
ACTGACCTCATGCGCATGTGCTGGCAATTCAACCCCAAGATGAGGCCAACCTTCCTG
GAGATTGTCAACCTGCTCAAGGACGACCTGCACCCCAGCTTTCCAGAGGTGTCGTTC
TTCCACAGCGAGGAGAACAAGGCTCCCGAGAGTGAGGAGCTGGAGATGGAGTTTGAG
GACATGGAGAATGTGCCCCTGGACCGTTCCTCGCACTGTCAGAGGGAGGAGGCGGGG
GGCCGGGATGGAGGGTCCTCGCTGGGTTTCAAGCGGAGCTACGAGGAACACATCCCT
TACACACACATGAACGGAGGCAAGAAAAACGGGCGGATTCTGACCTTGCCTCGGTCC
AATCCTTCCTAA

### 12.7.8 wild-type hCAII

ATGGCCCATCACTGGGGGTACGGCAAANACAACGGACCTGAGCACTGGCATAAGGAC
TTCCCCATTGCCAAGGGAGAGCGCCAGTCCCCTGTTGACATCGACACTCATACAGCC
AAGTATGACCCTTCCCTGAAGCCCCTGTCTGTTTCCTATGATCAAGCAACTTCCCTG
AGGATCCTCAACAATGGTCATGCTTTCAACGTGGAGTTTGATGACTCTCAGGACAAA
GCAGTGCTCAAGGGAGGACCCCTGGATGGCACTTACAGATTGATTCAGTTTCACTTT
CACTGGGGTTCACTTGATGGACAAGGTTCAGAGCATACTGTGGATAAAAAGAAATAT
GCTGCAGAACTTCACTTGGTTCACTGGAACACCAAATATGGGGATTTTGGGAAAGCT
GTGCAGCAACCTGATGGACTGGCCGTTCTAGGTATTTTTTTGAAGGTTGGCAGCGCT
AAACCGGGCCTTCAGAAAGTTGTTGATGTGCTGGATTCCATTAAAACAAAGGGCAAG
AGTGCTGACTTCACTAACTTCGATCCTCGTGGCCTCCTTCCTGAATCCCTGGATTAC
TGGACCTACCCAGGCTCACTGACCACCCCTCCTCTTCTGGAATGTGTGACCTGGATT
GTGCTCAAGGAACCCATCAGCGTCAGCAGCGAGCAGGTGTTGAAATTCCGTAAACTT
AACTTCAATGGGGAGGGTGAACCCGAAGAACTGATGGTGGACAACTGGCGCCCAGCT
CAGCCACTGAAGAACAGGCAAATCAAAGCTTCCTTCAAATAA

### 12.7.9 hCAII (G129C)

ATGGCCCATCACTGGGGGTACGGCAAACACAACGGACCTGAGCACTGGCATAAGGAC
TTCCCCATTGCCAAGGGAGAGCGCCAGTCCCCTGTTGACATCGACACTCATACAGCC
AAGTATGACCCTTCCCTGAAGCCCCTGTCTGTTTCCTATGATCAAGCAACTTCCCTG
AGGATCCTCAACAATGGTCATGCTTTCAACGTGGAGTTTGATGACTCTCAGGACAAA
GCAGTGCTCAAGGGAGGACCCCTGGATGGCACTTACAGATTGATTCAGTTTCACTTT
CACTGGGGTTCACTTGATGGACAAGGTTCAGAGCATACTGTGGATAAAAAGAAATAT

GCTGCAGAACTTCACTTGGTTCACTGGAACACCAAATATTGTGATTTTGGGAAAGCT
GTGCAGCAACCTGATGGACTGGCCGTTCTAGGTATTTTTTTGAAGGTTGGCAGCGCT
AAACCGGGCCTTCAGAAAGTTGTTGATGTGCTGGATTCCATTAAAACAAAGGGCAAG
AGTGCTGACTTCACTAACTTCGATCCTCGTGGCCTCCTTCCTGAATCCCTGGATTAC
TGGACCTACCCAGGCTCACTGACCACCCCTCCTCTTCTGGAATGTGTGACCTGGATT
GTGCTCAAGGAACCCATCAGCGTCAGCAGCGAGCAGGTGTTGAAATTCCGTAAACTT
AACTTCAATGGGGAGGGTGAACCCGAAGAACTGATGGTGGACAACTGGCGCCCAGCT
CAGCCACTGAAGAACAGGCAAATCAAAGCTTCCTTCAAATAA

### 12.7.10 hCAII (D130C)

ATGGCCCATCACTGGGGGTACGGCAAACACAACGGACCTGAGCACTGGCATAAGGAC
TTCCCCATTGCCAAGGGAGAGCGCCAGTCCCCTGTTGACATCGACACTCATACAGCC
AAGTATGACCCTTCCCTGAAGCCCCTGTCTGTTTCCTATGATCAAGCAACTTCCCTG
AGGATCCTCAACAATGGTCATGCTTTCAACGTGGAGTTTGATGACTCTCAGGACAAA
GCAGTGCTCAAGGGAGGACCCCTGGATGGCACTTACAGATTGATTCAGTTTCACTTT
CACTGGGGTTCACTTGATGGACAAGGTTCAGAGCATACTGTGGATAAAAAGAAATAT
GCTGCAGAACTTCACTTGGTTCACTGGAACACCAAATATGGGTGTTTTGGGAAAGCT
GTGCAGCAACCTGATGGACTGGCCGTTCTAGGTATTTTTTTGAAGGTTGGCAGCGCT
AAACCGGGCCTTCAGAAAGTTGTTGATGTGCTGGATTCCATTAAAACAAAGGGCAAG
AGTGCTGACTTCACTAACTTCGATCCTCGTGGCCTCCTTCCTGAATCCCTGGATTAC
TGGACCTACCCAGGCTCACTGACCACCCCTCCTCTTCTGGAATGTGTGACCTGGATT
GTGCTCAAGGAACCCATCAGCGTCAGCAGCGAGCAGGTGTTGAAATTCCGTAAACTT
AACTTCAATGGGGAGGGTGAACCCGAAGAACTGATGGTGGACAACTGGCGCCCAGCT
CAGCCACTGAAGAACAGGCAAATCAAAGCTTCCTTCAAATAA

### 12.7.11 hCAII (F131C)

ATGGCCCATCACTGGGGGTACGGCAAACACAACGGACCTGAGCACTGGCATAAGGAC
TTCCCCATTGCCAAGGGAGAGCGCCAGTCCCCTGTTGACATCGACACTCATACAGCC
AAGTATGACCCTTCCCTGAAGCCCCTGTCTGTTTCCTATGATCAAGCAACTTCCCTG
AGGATCCTCAACAATGGTCATGCTTTCAACGTGGAGTTTGATGACTCTCAGGACAAA
GCAGTGCTCAAGGGAGGACCCCTGGATGGCACTTACAGATTGATTCAGTTTCACTTT
CACTGGGGTTCACTTGATGGACAAGGTTCAGAGCATACTGTGGATAAAAAGAAATAT
GCTGCAGAACTTCACTTGGTTCACTGGAACACCAAATATGGGGATTGTGGGAAAGCT
GTGCAGCAACCTGATGGACTGGCCGTTCTAGGTATTTTTTTGAAGGTTGGCAGCGCT
AAACCGGGCCTTCAGAAAGTTGTTGATGTGCTGGATTCCATTAAAACAAAGGGCAAG
AGTGCTGACTTCACTAACTTCGATCCTCGTGGCCTCCTTCCTGAATCCCTGGATTAC
TGGACCTACCCAGGCTCACTGACCACCCCTCCTCTTCTGGAATGTGTGACCTGGATT
GTGCTCAAGGAACCCATCAGCGTCAGCAGCGAGCAGGTGTTGAAATTCCGTAAACTT
AACTTCAATGGGGAGGGTGAACCCGAAGAACTGATGGTGGACAACTGGCGCCCAGCT
CAGCCACTGAAGAACAGGCAAATCAAAGCTTCCTTCAAATAA

### 12.7.12 hCAII (G132C)

ATGGCCCATCACTGGGGGTACGGCAAACACAACGGACCTGAGCACTGGCATAAGGAC
TTCCCCATTGCCAAGGGAGAGCGCCAGTCCCCTGTTGACATCGACACTCATACAGCC
AAGTATGACCCTTCCCTGAAGCCCCTGTCTGTTTCCTATGATCAAGCAACTTCCCTG
AGGATCCTCAACAATGGTCATGCTTTCAACGTGGAGTTTGATGACTCTCAGGACAAA
GCAGTGCTCAAGGGAGGACCCCTGGATGGCACTTACAGATTGATTCAGTTTCACTTT
CACTGGGGTTCACTTGATGGACAAGGTTCAGAGCATACTGTGGATAAAAAGAAATAT
GCTGCAGAACTTCACTTGGTTCACTGGAACACCAAATATGGGGATTTTTGCAAAGCT
GTGCAGCAACCTGATGGACTGGCCGTTCTAGGTATTTTTTTGAAGGTTGGCAGCGCT

AAACCGGGCCTTCAGAAAGTTGTTGATGTGCTGGATTCCATTAAAACAAAGGGCAAG
AGTGCTGACTTCACTAACTTCGATCCTCGTGGCCTCCTTCCTGAATCCCTGGATTAC
TGGACCTACCCAGGCTCACTGACCACCCCTCCTCTTCTGGAATGTGTGACCTGGATT
GTGCTCAAGGAACCCATCAGCGTCAGCAGCGAGCAGGTGTTGAAATTCCGTAAACTT
AACTTCAATGGGGAGGGTGAACCCGAAGAACTGATGGTGGACAACTGGCGCCCAGCT
CAGCCACTGAAGAACAGGCAAATCAAAGCTTCCTTCAAATAA

### 12.7.13 hCAII (K133C)

ATGGCCCATCACTGGGGGTACGGCAAANACAACGGACCTGAGCACTGGCATAAGGAC
TTCCCCATTGCCAAGGGAGAGCGCCAGTCCCCTGTTGACATCGACACTCATACAGCC
AAGTATGACCCTTCCCTGAAGCCCCTGTCTGTTTCCTATGATCAAGCAACTTCCCTG
AGGATCCTCAACAATGGTCATGCTTTCAACGTGGAGTTTGATGACTCTCAGGACAAA
GCAGTGCTCAAGGGAGGACCCCTGGATGGCACTTACAGATTGATTCAGTTTCACTTT
CACTGGGGTTCACTTGATGGACAAGGTTCAGAGCATACTGTGGATAAAAAGAAATAT
GCTGCAGAACTTCACTTGGTTCACTGGAACACCAAATATGGGGATTTTGGGTGCGCT
GTGCAGCAACCTGATGGACTGGCCGTTCTAGGTATTTTTTTGAAGGTTGGCAGCGCT
AAACCGGGCCTTCAGAAAGTTGTTGATGTGCTGGATTCCATTAAAACAAAGGGCAAG
AGTGCTGACTTCACTAACTTCGATCCTCGTGGCCTCCTTCCTGAATCCCTGGATTAC
TGGACCTACCCAGGCTCACTGACCACCCCTCCTCTTCTGGAATGTGTGACCTGGATT
GTGCTCAAGGAACCCATCAGCGTCAGCAGCGAGCAGGTGTTGAAATTCCGTAAACTT
AACTTCAATGGGGAGGGTGAACCCGAAGAACTGATGGTGGACAACTGGCGCCCAGCT
CAGCCACTGAAGAACAGGCAAATCAAAGCTTCCTTCAAATAA

### 12.7.14 hCAII (G129C, C206S)

ATGGCCCATCACTGGGGGTACGGCAAACACAACGGACCTGAGCACTGGCATAAGGAC
TTCCCCATTGCCAAGGGAGAGCGCCAGTCCCCTGTTGACATCGACACTCATACAGCC
AAGTATGACCCTTCCCTGAAGCCCCTGTCTGTTTCCTATGATCAAGCAACTTCCCTG
AGGATCCTCAACAATGGTCATGCTTTCAACGTGGAGTTTGATGACTCTCAGGACAAA
GCAGTGCTCAAGGGAGGACCCCTGGATGGCACTTACAGATTGATTCAGTTTCACTTT
CACTGGGGTTCACTTGATGGACAAGGTTCAGAGCATACTGTGGATAAAAAGAAATAT
GCTGCAGAACTTCACTTGGTTCACTGGAACACCAAATATTGTGATTTTGGGAAAGCT
GTGCAGCAACCTGATGGACTGGCCGTTCTAGGTATTTTTTTGAAGGTTGGCAGCGCT
AAACCGGGCCTTCAGAAAGTTGTTGATGTGCTGGATTCCATTAAAACAAAGGGCAAG
AGTGCTGACTTCACTAACTTCGATCCTCGTGGCCTCCTTCCTGAATCCCTGGATTAC
TGGACCTACCCAGGCTCACTGACCACCCCTCCTCTTCTGGAATCTGTGACCTGGATT
GTGCTCAAGGAACCCATCAGCGTCAGCAGCGAGCAGGTGTTGAAATTCCGTAAACTT
AACTTCAATGGGGAGGGTGAACCCGAAGAACTGATGGTGGACAACTGGCGCCCAGCT
CAGCCACTGAAGAACAGGCAAATCAAAGCTTCCTTCAAATAA

### 12.7.15 hCAII (D130C, C206S)

ATGGCCCATCACTGGGGGTACGGCAAACACAACGGACCTGAGCACTGGCATAAGGAC
TTCCCCATTGCCAAGGGAGAGCGCCAGTCCCCTGTTGACATCGACACTCATACAGCC
AAGTATGACCCTTCCCTGAAGCCCCTGTCTGTTTCCTATGATCAAGCAACTTCCCTG
AGGATCCTCAACAATGGTCATGCTTTCAACGTGGAGTTTGATGACTCTCAGGACAAA
GCAGTGCTCAAGGGAGGACCCCTGGATGGCACTTACAGATTGATTCAGTTTCACTTT
CACTGGGGTTCACTTGATGGACAAGGTTCAGAGCATACTGTGGATAAAAAGAAATAT
GCTGCAGAACTTCACTTGGTTCACTGGAACACCAAATATGGGTGTTTTGGGAAAGCT
GTGCAGCAACCTGATGGACTGGCCGTTCTAGGTATTTTTTTGAAGGTTGGCAGCGCT
AAACCGGGCCTTCAGAAAGTTGTTGATGTGCTGGATTCCATTAAAACAAAGGGCAAG
AGTGCTGACTTCACTAACTTCGATCCTCGTGGCCTCCTTCCTGAATCCCTGGATTAC

TGGACCTACCCAGGCTCACTGACCACCCCTCCTCTTCTGGAATCTGTGACCTGGATT
GTGCTCAAGGAACCCATCAGCGTCAGCAGCGAGCAGGTGTTGAAATTCCGTAAACTT
AACTTCAATGGGGAGGGTGAACCCGAAGAACTGATGGTGGACAACTGGCGCCCAGCT
CAGCCACTGAAGAACAGGCAAATCAAAGCTTCCTTCAAATAA

### 12.7.16 hCAII (F131C, C206S)

ATGGCCCATCACTGGGGGTACGGCAAACACAACGGACCTGAGCACTGGCATAAGGAC
TTCCCCATTGCCAAGGGAGAGCGCCAGTCCCCTGTTGACATCGACACTCATACAGCC
AAGTATGACCCTTCCCTGAAGCCCCTGTCTGTTTCCTATGATCAAGCAACTTCCCTG
AGGATCCTCAACAATGGTCATGCTTTCAACGTGGAGTTTGATGACTCTCAGGACAAA
GCAGTGCTCAAGGGAGGACCCCTGGATGGCACTTACAGATTGATTCAGTTTCACTTT
CACTGGGGTTCACTTGATGGACAAGGTTCAGAGCATACTGTGGATAAAAAGAAATAT
GCTGCAGAACTTCACTTGGTTCACTGGAACACCAAATATGGGGATTGTGGGAAAGCT
GTGCAGCAACCTGATGGACTGGCCGTTCTAGGTATTTTTTTGAAGGTTGGCAGCGCT
AAACCGGGCCTTCAGAAAGTTGTTGATGTGCTGGATTCCATTAAAACAAAGGGCAAG
AGTGCTGACTTCACTAACTTCGATCCTCGTGGCCTCCTTCCTGAATCCCTGGATTAC
TGGACCTACCCAGGCTCACTGACCACCCCTCCTCTTCTGGAATCTGTGACCTGGATT
GTGCTCAAGGAACCCATCAGCGTCAGCAGCGAGCAGGTGTTGAAATTCCGTAAACTT
AACTTCAATGGGGAGGGTGAACCCGAAGAACTGATGGTGGACAACTGGCGCCCAGCT
CAGCCACTGAAGAACAGGCAAATCAAAGCTTCCTTCAAATAA

### 12.7.17 hCAII (G132C, C206S)

ATGGCCCATCACTGGGGGTACGGCAAACACAACGGACCTGAGCACTGGCATAAGGAC
TTCCCCATTGCCAAGGGAGAGCGCCAGTCCCCTGTTGACATCGACACTCATACAGCC
AAGTATGACCCTTCCCTGAAGCCCCTGTCTGTTTCCTATGATCAAGCAACTTCCCTG
AGGATCCTCAACAATGGTCATGCTTTCAACGTGGAGTTTGATGACTCTCAGGACAAA
GCAGTGCTCAAGGGAGGACCCCTGGATGGCACTTACAGATTGATTCAGTTTCACTTT
CACTGGGGTTCACTTGATGGACAAGGTTCAGAGCATACTGTGGATAAAAAGAAATAT
GCTGCAGAACTTCACTTGGTTCACTGGAACACCAAATATGGGGATTTTTGCAAAGCT
GTGCAGCAACCTGATGGACTGGCCGTTCTAGGTATTTTTTTGAAGGTTGGCAGCGCT
AAACCGGGCCTTCAGAAAGTTGTTGATGTGCTGGATTCCATTAAAACAAAGGGCAAG
AGTGCTGACTTCACTAACTTCGATCCTCGTGGCCTCCTTCCTGAATCCCTGGATTAC
TGGACCTACCCAGGCTCACTGACCACCCCTCCTCTTCTGGAATCTGTGACCTGGATT
GTGCTCAAGGAACCCATCAGCGTCAGCAGCGAGCAGGTGTTGAAATTCCGTAAACTT
AACTTCAATGGGGAGGGTGAACCCGAAGAACTGATGGTGGACAACTGGCGCCCAGCT
CAGCCACTGAAGAACAGGCAAATCAAAGCTTCCTTCAAATAA

### 12.7.18 hCAII (K133C, C206S)

ATGGCCCATCACTGGGGGTACGGCAAANACAACGGACCTGAGCACTGGCATAAGGAC
TTCCCCATTGCCAAGGGAGAGCGCCAGTCCCCTGTTGACATCGACACTCATACAGCC
AAGTATGACCCTTCCCTGAAGCCCCTGTCTGTTTCCTATGATCAAGCAACTTCCCTG
AGGATCCTCAACAATGGTCATGCTTTCAACGTGGAGTTTGATGACTCTCAGGACAAA
GCAGTGCTCAAGGGAGGACCCCTGGATGGCACTTACAGATTGATTCAGTTTCACTTT
CACTGGGGTTCACTTGATGGACAAGGTTCAGAGCATACTGTGGATAAAAAGAAATAT
GCTGCAGAACTTCACTTGGTTCACTGGAACACCAAATATGGGGATTTTGGGTGCGCT
GTGCAGCAACCTGATGGACTGGCCGTTCTAGGTATTTTTTTGAAGGTTGGCAGCGCT
AAACCGGGCCTTCAGAAAGTTGTTGATGTGCTGGATTCCATTAAAACAAAGGGCAAG
AGTGCTGACTTCACTAACTTCGATCCTCGTGGCCTCCTTCCTGAATCCCTGGATTAC
TGGACCTACCCAGGCTCACTGACCACCCCTCCTCTTCTGGAATCTGTGACCTGGATT
GTGCTCAAGGAACCCATCAGCGTCAGCAGCGAGCAGGTGTTGAAATTCCGTAAACTT

AACTTCAATGGGGAGGGTGAACCCGAAGAACTGATGGTGGACAACTGGCGCCCAGCT
CAGCCACTGAAGAACAGGCAAATCAAAGCTTCCTTCAAATAA

### 12.7.19 hCAII (C206S)

ATGGCCCATCACTGGGGGTACGGCAAANACAACGGACCTGAGCACTGGCATAAGGAC
TTCCCCATTGCCAAGGGAGAGCGCCAGTCCCCTGTTGACATCGACACTCATACAGCC
AAGTATGACCCTTCCCTGAAGCCCCTGTCTGTTTCCTATGATCAAGCAACTTCCCTG
AGGATCCTCAACAATGGTCATGCTTTCAACGTGGAGTTTGATGACTCTCAGGACAAA
GCAGTGCTCAAGGGAGGACCCCTGGATGGCACTTACAGATTGATTCAGTTTCACTTT
CACTGGGGTTCACTTGATGGACAAGGTTCAGAGCATACTGTGGATAAAAAGAAATAT
GCTGCAGAACTTCACTTGGTTCACTGGAACACCAAATATGGGGATTTTGGGAAAGCT
GTGCAGCAACCTGATGGACTGGCCGTTCTAGGTATTTTTTTGAAGGTTGGCAGCGCT
AAACCGGGCCTTCAGAAAGTTGTTGATGTGCTGGATTCCATTAAAACAAAGGGCAAG
AGTGCTGACTTCACTAACTTCGATCCTCGTGGCCTCCTTCCTGAATCCCTGGATTAC
TGGACCTACCCAGGCTCACTGACCACCCCTCCTCTTCTGGAATCTGTGACCTGGATT
GTGCTCAAGGAACCCATCAGCGTCAGCAGCGAGCAGGTGTTGAAATTCCGTAAACTT
AACTTCAATGGGGAGGGTGAACCCGAAGAACTGATGGTGGACAACTGGCGCCCAGCT
CAGCCACTGAAGAACAGGCAAATCAAAGCTTCCTTCAAATAA

### 12.7.20 hCAII (L198A)

ATGGCCCATCACTGGGGGTACGGCAAANACAACGGACCTGAGCACTGGCATAAGGAC
TTCCCCATTGCCAAGGGAGAGCGCCAGTCCCCTGTTGACATCGACACTCATACAGCC
AAGTATGACCCTTCCCTGAAGCCCCTGTCTGTTTCCTATGATCAAGCAACTTCCCTG
AGGATCCTCAACAATGGTCATGCTTTCAACGTGGAGTTTGATGACTCTCAGGACAAA
GCAGTGCTCAAGGGAGGACCCCTGGATGGCACTTACAGATTGATTCAGTTTCACTTT
CACTGGGGTTCACTTGATGGACAAGGTTCAGAGCATACTGTGGATAAAAAGAAATAT
GCTGCAGAACTTCACTTGGTTCACTGGAACACCAAATATGGGGATTTTGGGAAAGCT
GTGCAGCAACCTGATGGACTGGCCGTTCTAGGTATTTTTTTGAAGGTTGGCAGCGCT
AAACCGGGCCTTCAGAAAGTTGTTGATGTGCTGGATTCCATTAAAACAAAGGGCAAG
AGTGCTGACTTCACTAACTTCGATCCTCGTGGCCTCCTTCCTGAATCCCTGGATTAC
TGGACCTACCCAGGCTCAGCGACCACCCCTCCTCTTCTGGAATGTGTGACCTGGATT
GTGCTCAAGGAACCCATCAGCGTCAGCAGCGAGCAGGTGTTGAAATTCCGTAAACTT
AACTTCAATGGGGAGGGTGAACCCGAAGAACTGATGGTGGACAACTGGCGCCCAGCT
CAGCCACTGAAGAACAGGCAAATCAAAGCTTCCTTCAAATAA

## 12.8 HEK293 Cell Transfection

### 12.8.1 Normal Transfection Protocol

Cells were seeded at the appropriate density one day prior to transfection. Transfectio was performed with Lipofectamine® 2000 (LF) according to the manufacturer's instructions. Briefly, DNA and LF was mixed in OptiMEM at r.t. in the dark and incubated for 30 minutes. Cells were washed with PBS and OptiMEM was added. In addition, the DNA/LF mixture was added and the cells were incubated for 4-5 hours at 37 °C. Final removal of OptiMEM and outgrow in DMEM/10% FBS was performed.

### 12.8.2 Reverse Transfection Protocol

Before transfection calculate needed DNA/Lipofectamine 2000® (LF) mixtures for

- 96 well-plate:
  - 0.5 µL LF/well
  - 100 ng DNA/well
- 24 well-plate:
  - 2 µL LF/well
  - 50-350 ng DNA/well

Mix DNA/LF in OptiMEM in an Eppendorf tube and transfer into wells before placing the plate in the incubator for 20 minutes. Add appropriate amount of cells to each well:

- Ephys: 40,000 cells/well for 24 well-plate
- Confluent: 100,000 cells/well for 24 well-plate
- Confluent: 50,000 cells/well for 96 well-plate

Incubate for 3-6h at 37 °C before removing OptiMEM and the subsequent addition of 500 uL 10%FCS/DMEM. Expression should take between 24-48 hours o.n. at 37 °C.

## 12.9 Western Blotting

Medium was aspirated and the cell-containing 6-well plate was put on ice and washed with ice-cold PBS (1 mL/well). 50-75 µL of pre-cooled RIPA buffer including 0.25vol% protease inhibitors (Sigma, #P8340) and 0.5vol% phosphatase inhibitors (Sigma, #P5726-5mL) was added to each well and cells were collected separately in an Eppendorf tube. After centrifugation for 10 minutes at 14.000 rpm at 4 °C, the supernatant was collected and protein concentration was measured either with a BCA protein assay kit (Thermo Scientific, #23225) on a colorimetric platereader (Thermo Scientific, MultiscanEX) according to the manufacturer's instructions. For each sample, 20 µg of protein was incubated with 5 µL of NuPAGE® blue (life technologies, #NP0007) and 2 µL of Redox buffer (10x) and $dH_2O$ to a total volume of 35 µL for 10 minutes at 70 °C prior to SDS-PAGE (4-12% NuPAGE® Bis-Tris Plus Gel, life technologies, #BG04120BOX or #WG1401BOX; or self-made gels, see buffer recipes). Protein was transferred onto a PVDF membrane (1.5 h, 55 V, 4 °C), which was subsequently blocked for 2 hours at r.t. with blocking buffer. After washing with $dH_2O$, the membrane was incubated with the primary antibody (diluted according to the manufaturer's recommendations in primary antibody buffer) at 4 °C o.n.. The membrane was washed 5 times (5 minutes each) with PBS (including 0.05% Tween-20), incubated with the secondary antibody (1/30.000 dilution in blocking buffer) for 40 minutes at r.t., and again washed 5 times (5 minutes each) with PBS (+ 0.05% Tween-20) and rinsed twice with $dH_2O$. After removal of washing buffer, the membrane was treated with chemiluminiscent substrate (Pico, Thermo Scientific, #34080 or Dura, Thermo Scientific, #34076F) according to the manufacturer's instructions. CL-XPosure™ X-ray film (Thermo Scientific, #OK196129) was exposed to luminiscence signal between 30 seconds and 8 minutes prior to development. Blots were scanned and processed with ImageJ for integration of signals.

## 12.10 mRNA Preparation for *Xenopus* oocyte Injection

mRNA was prepared by first digesting 5 µg of the DNA by the FastDigest® (Thermoe Scientific, #00151181) protocol with MssI (Thermo Scientific, #FD1344) for 1.5 h at 37 °C. Afterwards, subsequent addition of 250 µL absolute EtOH followed by 10 µL of 3 M NaOAc was carried out before storing the solution at -20 °C o.n. in order to precipitate the linearized plasmid, which was centrifuged for 20 minutes at 12,000 rpm at 4 °C. After removal of the supernatant, DNA was dissolved in 15 µL $dH_2O$ and 1 µg was reverse-transcribed by using the mMessage mMachine® T7 transcription Kit (life technologies, #AM1344) according to the manufacturer's instructions. Pure mRNA was taken up in nuclease-free water aliquoted and stored at -20 °C.

## *13 References*


1 Bear, M. F., Connors, B. W., Paradiso, M. A. *Neuroscience*. 3rd edn, (Lippincott Williams & Wilkins, 2007).

2 Fehrentz, T., Schonberger, M. & Trauner, D. Optochemical genetics. *Angew Chem Int Ed Engl* **50**, 12156-12182, doi:10.1002/anie.201103236 (2011).

3 Velema, W. A., Szymanski, W. & Feringa, B. L. Photopharmacology: beyond proof of principle. *J Am Chem Soc* **136**, 2178-2191, doi:10.1021/ja413063e (2014).

4 Deisseroth, K. Optogenetics. *Nat Methods* **8**, 26-29, doi:10.1038/nmeth.f.324 (2011).

5 Kramer, R. H., Mourot, A. & Adesnik, H. Optogenetic pharmacology for control of native neuronal signaling proteins. *Nat Neurosci* **16**, 816-823, doi:10.1038/nn.3424 (2013).

6 Broichhagen, J. & Trauner, D. The in vivo chemistry of photochromic tethered ligands. *Current Opinion in Chemical Biology* **21**, 121-127 (2014).

7 Kruse, K. & Julicher, F. Oscillations in cell biology. *Curr Opin Cell Biol* **17**, 20-26, doi:10.1016/j.ceb.2004.12.007 (2005).

8 Reiner, A. & Isacoff, E. Y. Tethered ligands reveal glutamate receptor desensitization depends on subunit occupancy. *Nat Chem Biol* **10**, 273-280, doi:10.1038/nchembio.1458 (2014).

9 Banghart, M., Borges, K., Isacoff, E., Trauner, D. & Kramer, R. H. Light-activated ion channels for remote control of neuronal firing. *Nat Neurosci* **7**, 1381-1386, doi:10.1038/nn1356 (2004).

10 Janovjak, H., Szobota, S., Wyart, C., Trauner, D. & Isacoff, E. Y. A light-gated, potassium-selective glutamate receptor for the optical inhibition of neuronal firing. *Nat Neurosci* **13**, 1027-1032, doi:10.1038/nn.2589 (2010).

11 Lemoine, D. *et al.* Optical control of an ion channel gate. *Proc Natl Acad Sci U S A* **110**, 20813-20818, doi:10.1073/pnas.1318715110 (2013).

12 Wyart, C. *et al.* Optogenetic dissection of a behavioural module in the vertebrate spinal cord. *Nature* **461**, 407-410, doi:10.1038/nature08323 (2009).

13 Szobota, S. *et al.* Remote control of neuronal activity with a light-gated glutamate receptor. *Neuron* **54**, 535-545, doi:10.1016/j.neuron.2007.05.010 (2007).

14 Caporale, N. *et al.* LiGluR restores visual responses in rodent models of inherited blindness. *Mol Ther* **19**, 1212-1219, doi:10.1038/mt.2011.103 (2011).

15 Kienzler, M. A. *et al.* A red-shifted, fast-relaxing azobenzene photoswitch for visible light control of an ionotropic glutamate receptor. *J Am Chem Soc* **135**, 17683-17686, doi:10.1021/ja408104w (2013).

16 Izquierdo-Serra, M. *et al.* Two-Photon Neuronal and Astrocytic Stimulation with Azobenzene-Based Photoswitches. *J Am Chem Soc*, doi:10.1021/ja5026326 (2014).

17 Schoenberger, M., Damijonaitis, A., Zhang, Z., Nagel, D. & Trauner, D. Development of a New Photochromic Ion Channel Blocker via Azologization of Fomocaine. *ACS Chem Neurosci* **5**, 514-518, doi:10.1021/cn500070w (2014).
18 Barretto, R. P. *et al.* Time-lapse imaging of disease progression in deep brain areas using fluorescence microendoscopy. *Nature Medicine* **17**, 223-228, doi:10.1038/nm.2292 (2011).
19 Kim, T. I. *et al.* Injectable, cellular-scale optoelectronics with applications for wireless optogenetics. *Science* **340**, 211-216, doi:10.1126/science.1232437 (2013).
20 Marks, F., Klingmüller, U. & Müller-Decker, K. *Cellular signaling processing*. (Garland Science, Taylor and Francis Group, LLC, 2009).
21 Alberts, B. *et al. Molecular Biology of the Cell*. 5. edn, (Garland Science, 2007).
22 O'Hara, P. J. *et al.* The ligand-binding domain in metabotropic glutamate receptors is related to bacterial periplasmic binding proteins. *Neuron* **11**, 41-52 (1993).
23 Vicogne, J. *et al.* An unusual receptor tyrosine kinase of Schistosoma mansoni contains a Venus Flytrap module. *Mol Biochem Parasitol* **126**, 51-62, doi:S0166685102002499 [pii] (2003).
24 Pin, J. P., Galvez, T. & Prezeau, L. Evolution, structure, and activation mechanism of family 3/C G-protein-coupled receptors. *Pharmacol Ther* **98**, 325-354 (2003).
25 Volgraf, M. *et al.* Allosteric control of an ionotropic glutamate receptor with an optical switch. *Nature chemical biology* **2**, 47-52, doi:10.1038/nchembio756 (2006).
26 Levitz, J. *unpublished* (2010).
27 Olcese, J., Middendorff, R., Munker, M., Schmidt, C. & McArdle, C. A. Natriuretic peptides stimulate cyclic GMP production in an immortalized LHRH neuronal cell line. *Journal of Neuroendocrinology* **6**, 127-130 (1994).
28 Ahier, A. *et al.* A new family of receptor tyrosine kinases with a venus flytrap binding domain in insects and other invertebrates activated by aminoacids. *PLoS One* **4**, e5651, doi:10.1371/journal.pone.0005651 (2009).
29 Hynes, N. E. & MacDonald, G. ErbB receptors and signaling pathways in cancer. *Curr Opin Cell Biol* **21**, 177-184, doi:10.1016/j.ceb.2008.12.010 (2009).
30 Citri, A. & Yarden, Y. EGF-ERBB signalling: towards the systems level. *Nat Rev Mol Cell Biol* **7**, 505-516, doi:10.1038/nrm1962 (2006).
31 Lemmon, M. A. & Schlessinger, J. Cell signaling by receptor tyrosine kinases. *Cell* **141**, 1117-1134, doi:10.1016/j.cell.2010.06.011 (2010).
32 Alberts, B. *et al. Molekularbiologie der Zelle*. 4 edn, (WILEY-VCH Verlag GmbH, 2004).
33 Weinberg, R. A. *The Biology of Cancer*. 2 edn, (Garland Science, 2013).
34 Anastassiadis, T. *et al.* A highly selective dual insulin receptor (IR)/insulin-like growth factor 1 receptor (IGF-1R) inhibitor derived from an extracellular signal-regulated kinase (ERK) inhibitor. *J Biol Chem* **288**, 28068-28077, doi:10.1074/jbc.M113.505032 (2013).

35 Gilmore, T. D. Introduction to NF-kappaB: players, pathways, perspectives. *Oncogene* **25**, 6680-6684, doi:10.1038/sj.onc.1209954 (2006).
36 Brasier, A. R. The NF-kappaB regulatory network. *Cardiovascular toxicology* **6**, 111-130 (2006).
37 Gibson, D. G. *et al.* Enzymatic assembly of DNA molecules up to several hundred kilobases. *Nat Methods* **6**, 343-345, doi:10.1038/nmeth.1318 (2009).
38 Wang, D., Li, Z., Messing, E. M. & Wu, G. Activation of Ras/Erk pathway by a novel MET-interacting protein RanBPM. *J Biol Chem* **277**, 36216-36222, doi:10.1074/jbc.M205111200 (2002).
39 Maun, H. R., Kirchhofer, D. & Lazarus, R. A. Pseudo-active sites of protease domains: HGF/Met and Sonic hedgehog signaling in cancer. *Biol Chem* **391**, 881-892, doi:10.1515/BC.2010.098 (2010).
40 El Moustaine, D. *et al.* Distinct roles of metabotropic glutamate receptor dimerization in agonist activation and G-protein coupling. *Proc Natl Acad Sci U S A* **109**, 16342-16347, doi:10.1073/pnas.1205838109 (2012).
41 Ullman, E. F. *et al.* Luminescent oxygen channeling immunoassay: measurement of particle binding kinetics by chemiluminescence. *Proc Natl Acad Sci U S A* **91**, 5426-5430 (1994).
42 Levitz, J. *et al.* Optical control of metabotropic glutamate receptors. *Nat Neurosci* **16**, 507-516, doi:10.1038/nn.3346 (2013).
43 Broichhagen, J., Jurastow, I., Iwan, K., Kummer, W. & Trauner, D. Optical control of acetylcholinesterase with a tacrine switch. *Angew Chem Int Ed Engl* **53**, 7657-7660, doi:10.1002/anie.201403666 (2014).
44 Bear, M. F., Connors, B. W., Paradiso, M. A. *Neuroscience*. 2nd edn, (Lippincott Williams & Wilkins, 2001).
45 Taylor, P. The cholinesterases. *J Biol Chem* **266**, 4025-4028 (1991).
46 Soreq, H. & Seidman, S. Acetylcholinesterase--new roles for an old actor. *Nat Rev Neurosci* **2**, 294-302, doi:10.1038/35067589 (2001).
47 Millard, C. B. & Broomfield, C. A. Anticholinesterases: medical applications of neurochemical principles. *J Neurochem* **64**, 1909-1918 (1995).
48 Method of the Year 2010. *Nat Methods* **8**, 1 (2011).
49 Polosukhina, A. *et al.* Photochemical restoration of visual responses in blind mice. *Neuron* **75**, 271-282, doi:10.1016/j.neuron.2012.05.022 (2012).
50 Mourot, A. *et al.* Rapid optical control of nociception with an ion-channel photoswitch. *Nat Methods* **9**, 396-402, doi:10.1038/nmeth.1897 (2012).
51 Bieth, J., Vratsanos, S. M., Wassermann, N. & Erlanger, B. F. Photoregulation of biological activity by photocromic reagents. II. Inhibitors of acetylcholinesterase. *Proc Natl Acad Sci U S A* **64**, 1103-1106 (1969).
52 Bieth, J., Wassermann, N., Vratsanos, S. M. & Erlanger, B. F. Photoregulation of biological activity by photochromic reagents, IV. A model for diurnal variation of enzymic activity. *Proc Natl Acad Sci U S A* **66**, 850-854 (1970).
53 Bieth, J., Vratsanos, S. M., Wassermann, N. H., Cooper, A. G. & Erlanger, B. F. Photoregulation of biological activity by photochromic reagents. Inactivators of acetylcholinesterase. *Biochemistry* **12**, 3023-3027 (1973).

54 Hestrin, S. The reaction of acetylcholine and other carboxylic acid derivatives with hydroxylamine, and its analytical application. *J Biol Chem* **180**, 249-261 (1949).
55 Harel, M. *et al.* Quaternary ligand binding to aromatic residues in the active-site gorge of acetylcholinesterase. *Proc Natl Acad Sci U S A* **90**, 9031-9035 (1993).
56 Conn, P. M. *et al.* Mechanism of action of gonadotropin releasing hormone. *Annual Review of Physiology* **48**, 495-513, doi:10.1146/annurev.ph.48.030186.002431 (1986).
57 Bartels, E., Wassermann, N. H. & Erlanger, B. F. Photochromic activators of the acetylcholine receptor. *Proc Natl Acad Sci U S A* **68**, 1820-1823 (1971).
58 Harel, M. *et al.* Three-dimensional structures of Drosophila melanogaster acetylcholinesterase and of its complexes with two potent inhibitors. *Protein Sci* **9**, 1063-1072, doi:10.1110/ps.9.6.1063 (2000).
59 Hu, M. K., Wu, L. J., Hsiao, G. & Yen, M. H. Homodimeric tacrine congeners as acetylcholinesterase inhibitors. *Journal of Medicinal Chemistry* **45**, 2277-2282, doi:Doi 10.1021/Jm010308g (2002).
60 Carlyle, R. F. The Responses of the Guinea-Pig Isolated Intact Trachea to Transmural Stimulation and the Release of an Acetylcholine-Like Substance under Conditions of Rest and Stimulation. *British journal of pharmacology and chemotherapy* **22**, 126-136 (1964).
61 Carlyle, R. F. The Mode of Action of Neostigmine and Physostigmine on the Guinea-Pig Trachealis Muscle. *British journal of pharmacology and chemotherapy* **21**, 137-149 (1963).
62 Chen, X. *et al.* Acetylcholinesterase Inhibitors with Photoswitchable Inhibition of beta-Amyloid Aggregation. *ACS Chem Neurosci*, doi:10.1021/cn500016p (2014).
63 Harvey, J. H. & Trauner, D. Regulating enzymatic activity with a photoswitchable affinity label. *Chembiochem* **9**, 191-193, doi:10.1002/cbic.200700570 (2008).
64 Vomasta, D., Hogner, C., Branda, N. R. & Konig, B. Regulation of human carbonic anhydrase I (hCAI) activity by using a photochromic inhibitor. *Angew Chem Int Ed Engl* **47**, 7644-7647, doi:10.1002/anie.200802242 (2008).
65 Krishnamurthy, V. M. *et al.* Carbonic anhydrase as a model for biophysical and physical-organic studies of proteins and protein-ligand binding. *Chemical Reviews* **108**, 946-1051, doi:Doi 10.1021/Cr050262p (2008).
66 Pocker, Y. & Stone, J. T. The catalytic versatility of erythrocyte carbonic anhydrase. VI. Kinetic studies of noncompetitive inhibition of enzyme-catalyzed hydrolysis of p-nitrophenyl acetate. *Biochemistry* **7**, 2936-2945 (1968).
67 Supuran, C. T. Carbonic anhydrases: novel therapeutic applications for inhibitors and activators. *Nat Rev Drug Discov* **7**, 168-181, doi:10.1038/nrd2467 (2008).
68 Boriack-Sjodin, P. A. *et al.* Structural analysis of inhibitor binding to human carbonic anhydrase II. *Protein Sci* **7**, 2483-2489, doi:10.1002/pro.5560071201 (1998).

69 Masini, E., Carta, F., Scozzafava, A. & Supuran, C. T. Antiglaucoma carbonic anhydrase inhibitors: a patent review. *Expert Opin Ther Pat* **23**, 705-716, doi:10.1517/13543776.2013.794788 (2013).
70 Maresca, A., Carta, F., Vullo, D., Scozzafava, A. & Supuran, C. T. Carbonic anhydrase inhibitors. Inhibition of the Rv1284 and Rv3273 beta-carbonic anhydrases from Mycobacterium tuberculosis with diazenylbenzenesulfonamides. *Bioorg Med Chem Lett* **19**, 4929-4932, doi:10.1016/j.bmcl.2009.07.088 (2009).
71 Sjoblom, B., Polentarutti, M. & Djinovic-Carugo, K. Structural study of X-ray induced activation of carbonic anhydrase. *Proc Natl Acad Sci U S A* **106**, 10609-10613, doi:10.1073/pnas.0904184106 (2009).
72 Merino, E. Synthesis of azobenzenes: the coloured pieces of molecular materials. *Chem Soc Rev* **40**, 3835-3853, doi:10.1039/c0cs00183j (2011).
73 Barral, K., Moorhouse, A. D. & Moses, J. E. Efficient conversion of aromatic amines into azides: a one-pot synthesis of triazole linkages. *Org Lett* **9**, 1809-1811, doi:10.1021/ol070527h (2007).
74 Birnbaum, P. P., Linford, J. H. & Style, D. W. G. The absorption spectra of azobenzene and some derivatives. *Trans. Faraday Soc.*, 735-744 (1953).
75 Leffler, J. E. & Grunwald, E. *Rates and equilibria of organic reactions as treated by statistical, thermodynamic, and extrathermodynamic methods*. (Wiley, 1963).
76 Chen, R. F. & Kernohan, J. C. Combination of bovine carbonic anhydrase with a fluorescent sulfonamide. *J Biol Chem* **242**, 5813-5823 (1967).
77 Vogtle, F. *et al.* Photochemical and photophysical properties of poly(propylene amine) dendrimers with peripheral naphthalene and azobenzene groups. *Photochem Photobiol Sci* **1**, 45-51 (2002).
78 Cheng, Y. & Prusoff, W. H. Relationship between the inhibition constant (KI) and the concentration of inhibitor which causes 50 per cent inhibition (I50) of an enzymatic reaction. *Biochem Pharmacol* **22**, 3099-3108 (1973).
79 Nimmo, C. M. & Shoichet, M. S. Regenerative Biomaterials that "Click": Simple, Aqueous-Based Protocols for Hydrogel Synthesis, Surface Immobilization, and 3D Patterning. *Bioconjugate Chemistry* **22**, 2199-2209, doi:Doi 10.1021/Bc200281k (2011).
80 Kalia, J. & Raines, R. T. Catalysis of imido group hydrolysis in a maleimide conjugate. *Bioorg Med Chem Lett* **17**, 6286-6289, doi:10.1016/j.bmcl.2007.09.002 (2007).
81 Shen, B. Q. *et al.* Conjugation site modulates the in vivo stability and therapeutic activity of antibody-drug conjugates. *Nat Biotechnol* **30**, 184-189, doi:10.1038/nbt.2108 (2012).
82 Carta, F., Maresca, A., Scozzafava, A., Vullo, D. & Supuran, C. T. Carbonic anhydrase inhibitors. Diazenylbenzenesulfonamides are potent and selective inhibitors of the tumor-associated isozymes IX and XII over the cytosolic isoforms I and II. *Bioorganic & Medicinal Chemistry* **17**, 7093-7099, doi:10.1016/J.Bmc.2009.09.003 (2009).
83 Jeganathan, A., Richardson, S. K., Mani, R. S., Haley, B. E. & Watt, D. S. Selective Reactions of Azide-Substituted Alpha-Diazo Amides with Olefins and Alcohols Using Rhodium(Ii) Catalysts. *Journal of Organic Chemistry* **51**, 5362-5367, doi:Doi 10.1021/Jo00376a057 (1986).

84 Tochitsky, I. *et al.* Optochemical control of genetically engineered neuronal nicotinic acetylcholine receptors. *Nature Chemistry* **4**, 105-111, doi:Doi 10.1038/Nchem.1234 (2012).
85 Reich, N. W. *Synthesis of Photoswitchable Tethered Maltose Derivatives for Ultrafast Control of Protein Folding*, UC Berkeley, (2008).
86 Barral, K., Moorhouse, A. D. & Moses, J. E. Efficient conversion of aromatic amines into azides: A one-pot synthesis of triazole linkages. *Organic Letters* **9**, 1809-1811, doi:Doi 10.1021/Ol070527h (2007).
87 Hakansson, K., Carlsson, M., Svensson, L. A. & Liljas, A. Structure of native and apo carbonic anhydrase II and structure of some of its anion-ligand complexes. *J Mol Biol* **227**, 1192-1204 (1992).
88 Pocker, Y. & Stone, J. T. The catalytic versatility of erythrocyte carbonic anhydrase. 3. Kinetic studies of the enzyme-catalyzed hydrolysis of p-nitrophenyl acetate. *Biochemistry* **6**, 668-678 (1967).
89 Kiefer, L. L., Paterno, S. A. & Fierke, C. A. Hydrogen-Bond Network in the Metal-Binding Site of Carbonic-Anhydrase Enhances Zinc Affinity and Catalytic Efficiency. *Journal of the American Chemical Society* **117**, 6831-6837, doi:Doi 10.1021/Ja00131a004 (1995).
90 Huang, S., Sjoblom, B., Sauer-Eriksson, A. E. & Jonsson, B. H. Organization of an efficient carbonic anhydrase: Implications for the mechanism based on structure-function studies of a T199P/C206S mutant. *Biochemistry* **41**, 7628-7635, doi:Doi 10.1021/Bi020053o (2002).
91 Nair, S. K. & Christianson, D. W. Structural consequences of hydrophilic amino acid substitutions in the hydrophobic pocket of human carbonic anhydrase II. *Biochemistry* **32**, 4506-4514 (1993).
92 Goodman, H. M., Abelson, J., Landy, A., Brenner, S. & Smith, J. D. Amber suppression: a nucleotide change in the anticodon of a tyrosine transfer RNA. *Nature* **217**, 1019-1024 (1968).
93 Kaya, E. *et al.* A Genetically Encoded Norbornene Amino Acid for the Mild and Selective Modification of Proteins in a Copper-Free Click Reaction. *Angewandte Chemie International Edition* **51**, 4466-4469, doi:10.1002/anie.201109252 (2012).
94 Kolb, H. C., Finn, M. G. & Sharpless, K. B. Click Chemistry: Diverse Chemical Function from a Few Good Reactions. *Angew Chem Int Ed Engl* **40**, 2004-2021 (2001).
95 Rostovtsev, V. V., Green, L. G., Fokin, V. V. & Sharpless, K. B. A stepwise huisgen cycloaddition process: copper(I)-catalyzed regioselective "ligation" of azides and terminal alkynes. *Angew Chem Int Ed Engl* **41**, 2596-2599, doi:10.1002/1521-3773(20020715)41:14<2596::AID-ANIE2596>3.0.CO;2-4 (2002).
96 Tornoe, C. W., Christensen, C. & Meldal, M. Peptidotriazoles on solid phase: [1,2,3]-triazoles by regiospecific copper(i)-catalyzed 1,3-dipolar cycloadditions of terminal alkynes to azides. *J Org Chem* **67**, 3057-3064 (2002).
97 Soriano del Amo, D. *et al.* Chemoenzymatic synthesis of the sialyl Lewis X glycan and its derivatives. *Carbohydrate research* **345**, 1107-1113, doi:10.1016/j.carres.2010.03.032 (2010).
98 Ornelas, C., Broichhagen, J. & Weck, M. Strain-promoted alkyne azide cycloaddition for the functionalization of poly(amide)-based dendrons

and dendrimers. *J Am Chem Soc* **132**, 3923-3931, doi:10.1021/ja910581d (2010).
99 Vrabel, M. *et al.* Norbornenes in inverse electron-demand Diels-Alder reactions. *Chemistry* **19**, 13309-13312, doi:10.1002/chem.201301838 (2013).
100 Karver, M. R., Weissleder, R. & Hilderbrand, S. A. Synthesis and evaluation of a series of 1,2,4,5-tetrazines for bioorthogonal conjugation. *Bioconjug Chem* **22**, 2263-2270, doi:10.1021/bc200295y (2011).
101 Hansell, C. F. *et al.* Additive-free clicking for polymer functionalization and coupling by tetrazine-norbornene chemistry. *J Am Chem Soc* **133**, 13828-13831, doi:10.1021/ja203957h (2011).
102 Carta, F., Maresca, A., Scozzafava, A., Vullo, D. & Supuran, C. T. Carbonic anhydrase inhibitors. Diazenylbenzenesulfonamides are potent and selective inhibitors of the tumor-associated isozymes IX and XII over the cytosolic isoforms I and II. *Bioorg Med Chem* **17**, 7093-7099, doi:10.1016/j.bmc.2009.09.003 (2009).
103 Lesburg, C. A., Huang, C., Christianson, D. W. & Fierke, C. A. Histidine --> carboxamide ligand substitutions in the zinc binding site of carbonic anhydrase II alter metal coordination geometry but retain catalytic activity. *Biochemistry* **36**, 15780-15791, doi:10.1021/bi971296x (1997).
104 McCoy, A. J. *et al.* Phaser crystallographic software. *Journal of applied crystallography* **40**, 658-674, doi:10.1107/S0021889807021206 (2007).
105 Murshudov, G. N., Vagin, A. A. & Dodson, E. J. Refinement of macromolecular structures by the maximum-likelihood method. *Acta Crystallogr D Biol Crystallogr* **53**, 240-255, doi:10.1107/S0907444996012255 (1997).
106 Emsley, P. & Cowtan, K. Coot: model-building tools for molecular graphics. *Acta Crystallogr D Biol Crystallogr* **60**, 2126-2132, doi:10.1107/S0907444904019158 (2004).
107 Perrakis, A., Morris, R. & Lamzin, V. S. Automated protein model building combined with iterative structure refinement. *Nature structural biology* **6**, 458-463, doi:10.1038/8263 (1999).
108 Laskowski, R. A., Rullmannn, J. A., MacArthur, M. W., Kaptein, R. & Thornton, J. M. AQUA and PROCHECK-NMR: programs for checking the quality of protein structures solved by NMR. *Journal of biomolecular NMR* **8**, 477-486 (1996).
109 Schroedinger (LLC, New York, NY).
110 DuBay, K. H. & Geissler, P. L. Calculation of proteins' total side-chain torsional entropy and its influence on protein-ligand interactions. *J Mol Biol* **391**, 484-497, doi:10.1016/j.jmb.2009.05.068 (2009).
111 Metropolis, N., Rosenbluth, A. W., Rosenbluth, M. N., Teller, A. H. & Teller, E. Equation of state calculations by fast computing machines. *J Chem Phys* **21**, 1087 (1953).
112 Stitt, A. W. AGEs and diabetic retinopathy. *Investigative Ophthalmology and Visual Science* **51**, 4867-4874, doi:10.1167/iovs.10-5881 (2010).
113 Currie, C. J., Poole, C. D. & Gale, E. A. The influence of glucose-lowering therapies on cancer risk in type 2 diabetes. *Diabetologia* **52**, 1766-1777, doi:10.1007/s00125-009-1440-6 (2009).

114 Prentki, M. & Nolan, C. J. Islet beta cell failure in type 2 diabetes. *Journal of Clinical Investigation* **116**, 1802-1812, doi:10.1172/JCI29103 (2006).
115 Turner, R. C., Cull, C. A., Frighi, V. & Holman, R. R. Glycemic control with diet, sulfonylurea, metformin, or insulin in patients with type 2 diabetes mellitus: progressive requirement for multiple therapies (UKPDS 49). UK Prospective Diabetes Study (UKPDS) Group. *JAMA* **281**, 2005-2012 (1999).
116 Inzucchi, S. E. *et al.* Management of hyperglycemia in type 2 diabetes: a patient-centered approach: position statement of the American Diabetes Association (ADA) and the European Association for the Study of Diabetes (EASD). *Diabetes Care* **35**, 1364-1379, doi:10.2337/dc12-0413 (2012).
117 Fineman, M. S. *et al.* Effect on glycemic control of exenatide (synthetic exendin-4) additive to existing metformin and/or sulfonylurea treatment in patients with type 2 diabetes. *Diabetes Care* **26**, 2370-2377 (2003).
118 Miki, T., Nagashima, K. & Seino, S. The structure and function of the ATP-sensitive K+ channel in insulin-secreting pancreatic beta-cells. *Journal of Molecular Endocrinology* **22**, 113-123 (1999).
119 Ashcroft, F. M. & Gribble, F. M. Correlating structure and function in ATP-sensitive K+ channels. *Trends in Neurosciences* **21**, 288-294 (1998).
120 Aguilar-Bryan, L. *et al.* Toward understanding the assembly and structure of KATP channels. *Physiol Rev* **78**, 227-245 (1998).
121 Ashcroft, F. M. & Gribble, F. M. ATP-sensitive K+ channels and insulin secretion: their role in health and disease. *Diabetologia* **42**, 903-919, doi:10.1007/s001250051247 (1999).
122 Seino, S. & Miki, T. Physiological and pathophysiological roles of ATP-sensitive K+ channels. *Prog Biophys Mol Biol* **81**, 133-176 (2003).
123 Rorsman, P., Braun, M. & Zhang, Q. Regulation of calcium in pancreatic alpha- and beta-cells in health and disease. *Cell Calcium* **51**, 300-308, doi:10.1016/j.ceca.2011.11.006 (2012).
124 Rutter, G. A. Nutrient-secretion coupling in the pancreatic islet beta-cell: recent advances. *Molecular Aspects of Medicine* **22**, 247-284 (2001).
125 Henquin, J. C. Regulation of insulin secretion: a matter of phase control and amplitude modulation. *Diabetologia* **52**, 739-751, doi:10.1007/s00125-009-1314-y (2009).
126 Tsuboi, T. & Rutter, G. A. Multiple forms of "kiss-and-run" exocytosis revealed by evanescent wave microscopy. *Current biology : CB* **13**, 563-567 (2003).
127 Cheatham, B. & Kahn, C. R. Insulin action and the insulin signaling network. *Endocrine Reviews* **16**, 117-142 (1995).
128 Jennings, A. M., Wilson, R. M. & Ward, J. D. Symptomatic hypoglycemia in NIDDM patients treated with oral hypoglycemic agents. *Diabetes Care* **12**, 203-208 (1989).
129 Evans, J. M., Ogston, S. A., Emslie-Smith, A. & Morris, A. D. Risk of mortality and adverse cardiovascular outcomes in type 2 diabetes: a comparison of patients treated with sulfonylureas and metformin. *Diabetologia* **49**, 930-936, doi:10.1007/s00125-006-0176-9 (2006).
130 Nathan, D. M. *et al.* Management of hyperglycemia in type 2 diabetes: A consensus algorithm for the initiation and adjustment of therapy: a consensus statement from the American Diabetes Association and the

European Association for the Study of Diabetes. *Diabetes Care* **29**, 1963-1972, doi:10.2337/dc06-9912 (2006).
131 Engler, R. L. & Yellon, D. M. Sulfonylurea KATP blockade in type II diabetes and preconditioning in cardiovascular disease. Time for reconsideration. *Circulation* **94**, 2297-2301 (1996).
132 Hernandez-Sanchez, C. *et al.* Mice transgenically overexpressing sulfonylurea receptor 1 in forebrain resist seizure induction and excitotoxic neuron death. *Proceedings of the National Academy of Sciences of the United States of America* **98**, 3549-3554, doi:10.1073/pnas.051012898 (2001).
133 Lam, T. K. Neuronal regulation of homeostasis by nutrient sensing. *Nature Medicine* **16**, 392-395, doi:10.1038/nm0410-392 (2010).
134 Quayle, J. M., Nelson, M. T. & Standen, N. B. ATP-sensitive and inwardly rectifying potassium channels in smooth muscle. *Physiological Reviews* **77**, 1165-1232 (1997).
135 Fortin, D. L. *et al.* Photochemical control of endogenous ion channels and cellular excitability. *Nat Methods* **5**, 331-338, doi:10.1038/nmeth.1187 (2008).
136 Grell, W. *et al.* Repaglinide and related hypoglycemic benzoic acid derivatives. *J. Med. Chem.* **41**, 5219-5246, doi:10.1021/jm9810349 (1998).
137 Takahashi, T. *et al.* Antidiabetic sulfonylureas and cAMP cooperatively activate Epac2A. *Science signaling* **6**, ra94, doi:10.1126/scisignal.2004581 (2013).
138 Herbst, K. J., Coltharp, C., Amzel, L. M. & Zhang, J. Direct activation of Epac by sulfonylurea is isoform selective. *Chemistry & biology* **18**, 243-251, doi:10.1016/j.chembiol.2010.12.007 (2011).
139 Zhang, C. L. *et al.* The cAMP sensor Epac2 is a direct target of antidiabetic sulfonylurea drugs. *Science* **325**, 607-610, doi:10.1126/science.1172256 (2009).
140 Hodson, D. J. *et al.* Lipotoxicity disrupts incretin-regulated human beta cell connectivity. *Journal of Clinical Investigation* **123**, 4182-4194, doi:10.1172/JCI68459 (2013).
141 Rutter, G. A. & Hodson, D. J. Minireview: intraislet regulation of insulin secretion in humans. *Mol. Endocrinol.* **27**, 1984-1995, doi:10.1210/me.2013-1278 (2013).
142 Quesada, I., Nadal, A. & Soria, B. Different effects of tolbutamide and diazoxide in alpha, beta-, and delta-cells within intact islets of Langerhans. *Diabetes* **48**, 2390-2397 (1999).
143 Head, W. S. *et al.* Connexin-36 gap junctions regulate in vivo first- and second-phase insulin secretion dynamics and glucose tolerance in the conscious mouse. *Diabetes* **61**, 1700-1707, doi:10.2337/db11-1312 (2012).
144 Santos, R. M. *et al.* Widespread synchronous [Ca2+]i oscillations due to bursting electrical activity in single pancreatic islets. *Pflugers Archiv (European Journal of Physiology)* **418**, 417-422 (1991).
145 Jonkers, F. C., Guiot, Y., Rahier, J. & Henquin, J. C. Tolbutamide stimulation of pancreatic beta-cells involves both cell recruitment and increase in the

individual Ca(2+) response. *British Journal of Pharmacology* **133**, 575-585, doi:10.1038/sj.bjp.0704108 (2001).
146 Gorostiza, P. & Isacoff, E. Y. Optical switches for remote and noninvasive control of cell signaling. *Science* **322**, 395-399, doi:10.1126/science.1166022 (2008).
147 Stein, M. *et al.* Azo-propofols: photochromic potentiators of GABA(A) receptors. *Angewandte Chemie. International Ed. In English* **51**, 10500-10504, doi:10.1002/anie.201205475 (2012).
148 Velema, W. A. *et al.* Optical control of antibacterial activity. *Nat Chem* **5**, 924-928, doi:10.1038/nchem.1750 (2013).
149 Kramer, W., Muller, G. & Geisen, K. Characterization of the molecular mode of action of the sulfonylurea, glimepiride, at beta-cells. *Hormone and Metabolic Research* **28**, 464-468, doi:10.1055/s-2007-979838 (1996).
150 Caro, L. N., Moreau, C. J., Estrada-Mondragon, A., Ernst, O. P. & Vivaudou, M. Engineering of an artificial light-modulated potassium channel. *PLoS One* **7**, e43766, doi:10.1371/journal.pone.0043766 (2012).
151 Reinbothe, T. M., Safi, F., Axelsson, A. S., Mollet, I. G. & Rosengren, A. H. Optogenetic control of insulin secretion in intact pancreatic islets with beta-cell-specific expression of Channelrhodopsin-2. *Islets* **6** (2014).
152 Ye, H., Daoud-El Baba, M., Peng, R. W. & Fussenegger, M. A synthetic optogenetic transcription device enhances blood-glucose homeostasis in mice. *Science* **332**, 1565-1568, doi:10.1126/science.1203535 (2011).
153 Butler, P. C., Dry, S. & Elashoff, R. GLP-1-based therapy for diabetes: what you do not know can hurt you. *Diabetes Care* **33**, 453-455, doi:10.2337/dc09-1902 (2010).
154 Nauck, M. A. & Friedrich, N. Do GLP-1-based therapies increase cancer risk? *Diabetes Care* **36 Suppl 2**, S245-252, doi:10.2337/dcS13-2004 (2013).
155 Rossger, K., Charpin-El-Hamri, G. & Fussenegger, M. A closed-loop synthetic gene circuit for the treatment of diet-induced obesity in mice. *Nat Commun* **4**, 2825, doi:10.1038/ncomms3825 (2013).
156 Grossweiner, L. I., Jones, L. R., Grossweiner, J. B. & Rogers, B. H. G. *The science of phototherapy : an introduction*. (Springer, 2005).
157 Seino, S., Shibasaki, T. & Minami, K. Dynamics of insulin secretion and the clinical implications for obesity and diabetes. *Journal of Clinical Investigation* **121**, 2118-2125, doi:10.1172/JCI45680 (2011).
158 Pocai, A. *et al.* Hypothalamic K(ATP) channels control hepatic glucose production. *Nature* **434**, 1026-1031, doi:10.1038/nature03439 (2005).
159 Martinez, C. H. & Dardonville, C. Rapid Determination of Ionization Constants (*pKa*) by UV Spectroscopy Using 96-Well Microtiter Plates. *ACS medicinal chemistry letters* **4**, 142-145, doi:10.1021/ml300326v (2013).
160 Hodson, D. J. *et al.* ADCY5 couples glucose to insulin secretion in human islets *Diabetes* **In press** (2014).
161 Ravier, M. A. & Rutter, G. A. Glucose or insulin, but not zinc ions, inhibit glucagon secretion from mouse pancreatic alpha-cells. *Diabetes* **54**, 1789-1797 (2005).
162 Broichhagen, J. & Trauner, D. The in vivo chemistry of photochromic tethered ligands. *Curr Opin Chem Biol* **21**, 121-127 (2014).

163 Trivedi, M. V., Laurence, J. S. & Siahaan, T. J. The role of thiols and disulfides on protein stability. *Curr Protein Pept Sci* **10**, 614-625, doi:CPPS-17 [pii] (2009).
164 Keppler, A. *et al.* A general method for the covalent labeling of fusion proteins with small molecules in vivo. *Nat Biotechnol* **21**, 86-89, doi:10.1038/nbt765 (2003).
165 Doumazane, E. *et al.* A new approach to analyze cell surface protein complexes reveals specific heterodimeric metabotropic glutamate receptors. *Faseb J* **25**, 66-77, doi:10.1096/fj.10-163147 (2011).
166 Maurel, D. *et al.* Cell-surface protein-protein interaction analysis with time-resolved FRET and snap-tag technologies: application to GPCR oligomerization. *Nat Methods* **5**, 561-567, doi:10.1038/nmeth.1213 (2008).
167 Lemercier, G., Gendreizig, S., Kindermann, M. & Johnsson, K. Inducing and sensing protein--protein interactions in living cells by selective cross-linking. *Angew Chem Int Ed Engl* **46**, 4281-4284, doi:10.1002/anie.200700408 (2007).
168 Eisenbraun, E. J. Cycloöctanone. *Org. Synth.* **45**, 28, doi:10.15227/orgsyn.045.0028 (1965).
169 Wang, H., Zhuang, J. & Thayumanavan, S. Functionalizable Amine-Based Polymer Nanoparticles. *ACS Macro Lett.* **2**, 948−951 (2013).
170 Ben-Ari, Y. & Cossart, R. Kainate, a double agent that generates seizures: two decades of progress. *Trends in Neurosciences* **23**, 580-587, doi:S0166-2236(00)01659-3 [pii] (2000).
171 Bernard, C., Cossart, R., Hirsch, J. C., Esclapez, M. & Ben-Ari, Y. What is GABAergic inhibition? How is it modified in epilepsy? *Epilepsia* **41 Suppl 6**, S90-95 (2000).
172 Cossart, R. *et al.* Distribution of spontaneous currents along the somato-dendritic axis of rat hippocampal CA1 pyramidal neurons. *Neuroscience* **99**, 593-603, doi:S0306-4522(00)00231-1 [pii] (2000).
173 Perez-Aguilar, J. M. *et al.* A computationally designed water-soluble variant of a G-protein-coupled receptor: the human mu opioid receptor. *PLoS One* **8**, e66009, doi:10.1371/journal.pone.0066009 (2013).
174 Schonberger, M. & Trauner, D. A photochromic agonist for mu-opioid receptors. *Angew Chem Int Ed Engl* **53**, 3264-3267, doi:10.1002/anie.201309633 (2014).
175 Sawadjoon, S. & Samec, J. S. An atom efficient route to N-aryl and N-alkyl pyrrolines by transition metal catalysis. *Organic & biomolecular chemistry* **9**, 2548-2554, doi:10.1039/c0ob00383b (2011).
176 Starkey, E. B., Smith, L. I. & Ungnade, H. E. *p*-Nitrophenylarsonic acid. *Org. Synth.* **19**, 40, doi:10.15227/orgsyn.045.0028 (1939).
177 Schnekenburger, M., Karius, T. & Diederich, M. Regulation of epigenetic traits of the glutathione S-transferase P1 gene: from detoxification toward cancer prevention and diagnosis. *Frontiers in pharmacology* **5**, 170, doi:10.3389/fphar.2014.00170 (2014).
178 He, N. G., Awasthi, S., Singhal, S. S., Trent, M. B. & Boor, P. J. The role of glutathione S-transferases as a defense against reactive electrophiles in the blood vessel wall. *Toxicol Appl Pharmacol* **152**, 83-89, doi:10.1006/taap.1998.8511 (1998).

179 Udomsinprasert, R. *et al.* Identification, characterization and structure of a new Delta class glutathione transferase isoenzyme. *Biochem J* **388**, 763-771, doi:10.1042/BJ20042015 (2005).
180 Banghart, M. R. & Trauner, D. A 1H NMR assay for measuring the photostationary States of photoswitchable ligands. *Methods Mol Biol* **995**, 107-120, doi:10.1007/978-1-62703-345-9_8 (2013).
181 Hellmich, U. A. & Gaudet, R. Structural Biology of TRP Channels. *Handbook of experimental pharmacology* **223**, 963-990, doi:10.1007/978-3-319-05161-1_10 (2014).
182 Grimm, C. *et al.* Small molecule activators of TRPML3. *Chemistry & biology* **17**, 135-148, doi:10.1016/j.chembiol.2009.12.016 (2010).
183 Friedman, A. H. Circumstances influencing Otto Loewi's discovery of chemical transmission in the nervous system. *Pflugers Arch* **325**, 85-86 (1971).
184 Bennett, M. R. The concept of transmitter receptors: 100 years on. *Neuropharmacology* **39**, 523-546 (2000).
185 Lemoine, D. *et al.* Ligand-gated ion channels: new insights into neurological disorders and ligand recognition. *Chem Rev* **112**, 6285-6318, doi:10.1021/cr3000829 (2012).
186 Kalamida, D. *et al.* Muscle and neuronal nicotinic acetylcholine receptors. Structure, function and pathogenicity. *FEBS J* **274**, 3799-3845, doi:10.1111/j.1742-4658.2007.05935.x (2007).
187 Coleman, M. E., Hume, A. H. & Holland, W. C. Nicotine-Like Stimulant Actions of Several Substituted Phenylcholine Ethers. *J Pharmacol Exp Ther* **148**, 66-70 (1965).
188 Haga, K. *et al.* Structure of the human M2 muscarinic acetylcholine receptor bound to an antagonist. *Nature* **482**, 547-551, doi:10.1038/nature10753 (2012).
189 Bleger, D. *et al.* Electronic decoupling approach to quantitative photoswitching in linear multiazobenzene architectures. *J Phys Chem B* **115**, 9930-9940, doi:10.1021/jp2044114 (2011).
190 Rabinovich, D. Topochemistry. Part XIV. The crystal structure of 2,3-dimethyl-1,4-benzoquinone. *Journal of the Chemical Society B: Physical Organic* **127**, 140-144 (1967).
191 Helms, A., Heiler, D. & Mclendon, G. Electron transfer in bis-porphyrin donor-acceptor compounds with polyphenylene spacers shows a weak distance dependence. *Journal of the American Chemical Society* **114**, 6227-6238 (1992).
192 Mascarenhas, Y. P., de Almeida, V. N., Lechat, J. R. & Barelli, N. N-Acetylanthranilic acid (o-acetamidobenzoic acid), a strongly triboluminescent material. *Acta Crystallogr B* **36**, 502-504, doi:10.1107/S0567740880003688 (1980).
193 Yue, L. *et al.* Robust photoregulation of GABA(A) receptors by allosteric modulation with a propofol analogue. *Nat Commun* **3**, 1095, doi:10.1038/ncomms2094 (2012).
194 Parker, H. E. *et al.* Molecular mechanisms underlying bile acid-stimulated glucagon-like peptide-1 secretion. *Br. J. Pharmacol.* **165**, 414-423, doi:10.1111/j.1476-5381.2011.01561.x (2012).

195 Parker, H. E., Reimann, F. & Gribble, F. M. Molecular mechanisms underlying nutrient-stimulated incretin secretion. *Expert reviews in molecular medicine* **12**, e1, doi:10.1017/S146239940900132X (2010).
196 Tolhurst, G., Reimann, F. & Gribble, F. M. Nutritional regulation of glucagon-like peptide-1 secretion. *The Journal of physiology* **587**, 27-32, doi:10.1113/jphysiol.2008.164012 (2009).
197 Campbell, J. E. & Drucker, D. J. Pharmacology, physiology, and mechanisms of incretin hormone action. *Cell metabolism* **17**, 819-837, doi:10.1016/j.cmet.2013.04.008 (2013).
198 Baggio, L. L. & Drucker, D. J. Biology of incretins: GLP-1 and GIP. *Gastroenterology* **132**, 2131-2157, doi:10.1053/j.gastro.2007.03.054 (2007).
199 Nauck, M. A. *et al.* Preserved incretin activity of glucagon-like peptide 1 [7-36 amide] but not of synthetic human gastric inhibitory polypeptide in patients with type-2 diabetes mellitus. *Journal of Clinical Investigation* **91**, 301-307, doi:10.1172/JCI116186 (1993).
200 Holst, J. J. Incretin hormones and the satiation signal. *Int J Obes (Lond)* **37**, 1161-1168, doi:10.1038/ijo.2012.208 (2013).
201 De Marinis, Y. Z. *et al.* GLP-1 inhibits and adrenaline stimulates glucagon release by differential modulation of N- and L-type Ca2+ channel-dependent exocytosis. *Cell metabolism* **11**, 543-553, doi:10.1016/j.cmet.2010.04.007 (2010).
202 Chia, C. W. *et al.* Exogenous glucose-dependent insulinotropic polypeptide worsens post prandial hyperglycemia in type 2 diabetes. *Diabetes* **58**, 1342-1349, doi:10.2337/db08-0958 (2009).
203 Xu, G. *et al.* Downregulation of GLP-1 and GIP receptor expression by hyperglycemia: possible contribution to impaired incretin effects in diabetes. *Diabetes* **56**, 1551-1558, doi:10.2337/db06-1033 (2007).
204 Nolte, W. M. *et al.* A potentiator of orthosteric ligand activity at GLP-1R acts via covalent modification. *Nat Chem Biol* **10**, 629-631, doi:10.1038/nchembio.1581 (2014).
205 Buse, J. B. *et al.* Effects of exenatide (exendin-4) on glycemic control over 30 weeks in sulfonylurea-treated patients with type 2 diabetes. *Diabetes Care* **27**, 2628-2635 (2004).
206 Wootten, D. *et al.* Allosteric modulation of endogenous metabolites as an avenue for drug discovery. *Molecular Pharmacology* **82**, 281-290, doi:10.1124/mol.112.079319 (2012).
207 Sloop, K. W. *et al.* Novel small molecule glucagon-like peptide-1 receptor agonist stimulates insulin secretion in rodents and from human islets. *Diabetes* **59**, 3099-3107, doi:10.2337/db10-0689 (2010).
208 Egan, A. G. *et al.* Pancreatic safety of incretin-based drugs--FDA and EMA assessment. *New England Journal of Medicine* **370**, 794-797, doi:10.1056/NEJMp1314078 (2014).
209 Mondragon, A. *et al.* Divergent effects of liraglutide, exendin-4, and sitagliptin on beta-cell mass and indicators of pancreatitis in a mouse model of hyperglycaemia. *PLoS One* **9**, e104873, doi:10.1371/journal.pone.0104873 (2014).

210 Nauck, M. A., Vilsboll, T., Gallwitz, B., Garber, A. & Madsbad, S. Incretin-based therapies: viewpoints on the way to consensus. *Diabetes Care* **32 Suppl 2**, S223-231, doi:10.2337/dc09-S315 (2009).
211 Lockie, S. H. Glucagon-like peptide-1 receptor in the brain: role in neuroendocrine control of energy metabolism and treatment target for obesity. *Journal of Neuroendocrinology* **25**, 597-604, doi:10.1111/jne.12039 (2013).
212 Pittolo, S. *et al.* An allosteric modulator to control endogenous G protein-coupled receptors with light. *Nat Chem Biol*, doi:10.1038/nchembio.1612 (2014).
213 Lee, J. *et al.* N-(3-acyloxy-2-benzylpropyl)-N'-[4-(methylsulfonylamino)benzyl]thiourea analogues: novel potent and high affinity antagonists and partial antagonists of the vanilloid receptor. *J Med Chem* **46**, 3116-3126, doi:10.1021/jm030089u (2003).
214 Jensen, K. L., Poulsen, P. H., Donslund, B. S., Morana, F. & Jorgensen, K. A. Asymmetric Synthesis of gamma-Nitroesters by an Organocatalytic One-Pot Strategy. *Organic Letters* **14**, 1516-1519, doi:Doi 10.1021/Ol3002514 (2012).
215 Togashi, M. *et al.* Sensitive detection of acrolein in serum using time-resolved luminescence. *Org Lett* **12**, 1704-1707, doi:10.1021/ol1002219 (2010).
216 Samanta, S., Qin, C., Lough, A. J. & Woolley, G. A. Bidirectional photocontrol of peptide conformation with a bridged azobenzene derivative. *Angew Chem Int Ed Engl* **51**, 6452-6455, doi:10.1002/anie.201202383 (2012).
217 Bléger, D., Schwarz, J., Brouwer, A. M. & Hecht, S. o-Fluoroazobenzenes as Readily Synthesized Photoswitches Offering Nearly Quantitative Two-Way Isomerization with Visible Light. *Journal of the American Chemical Society* **134**, 20597-20600, doi:10.1021/ja310323y (2012).
218 Altomare, A. *et al. J. Appl. Crystallogr.* **32**, 115–119 (1999).
219 Sheldrick, G. M. A short history of SHELX. *Acta crystallographica. Section A, Foundations of crystallography* **64**, 112-122, doi:10.1107/S0108767307043930 (2008).